DECLARATION

No part of this thesis has been previously submitted for a degree at this or any other university. The work described in this thesis is entirely that of the author, except where reference is made to previously published or unpublished work.

W. R. Bailey

University of Durham

Department of Geological Sciences
February 1997

ABSTRACT

In SW Cyprus, arcuate serpentinite-filled fault zones mark the tectonic suture between two oceanic terranes: the Upper Cretaceous Troodos Complex and the Triassic to Lower Cretaceous Mamonia Complex. Although the processes involved in the seafloor evolution of these two complexes are well documented, the mode of their juxtaposition and the importance of the serpentinite fault zones is poorly understood. Structural field mapping of these fault zones, combined with microstructural (optical and scanning electron microscope) and geochemical (X-ray diffraction and electron microprobe) analyses undertaken as part of this thesis have identified evidence of three main tectonic events of Upper Cretaceous age.

The earliest deformation is recorded by high temperature (>600°C) peridotite mylonites that are associated with amphibolite-facies metamorphic rocks and Mamonia Complex units. These mylonites are interpreted as fragments of Mamonia Complex mantle that were deformed within a transform-related, dextral strike-slip fault zone during Turonian to Santonian times (~90-83Ma). The microstructural chronology displayed by the mylonites suggest that during their formation, heat was supplied by the newly formed Troodos crust. This conclusion is of regional significance, as it suggests that the Mamonia and Troodos Complexes were in close geographical proximity as early as 90Ma, which is at least 8Ma earlier than previously accepted.

Field and microstructural evidence records the retrograde hydration of the fault zones, which was contemporaneous with dextral transtension and extensional tectonism of broadly Campanian age (*c.* 83-73Ma). The geochemistry of chrome spinels indicates that this phase is associated with the protrusion of mantle-derived serpentinites associated with both complexes at low temperatures. The dextral structures described are considered to be associated with the onset of the anticlockwise rotation of the Troodos microplate. The formation of a steep fault zone architecture is thought to have influenced the displacement patterns during subsequent compressional reactivation.

Regional compressional deformation at low temperatures ($\geq$100°C) represents the final tectonic event responsible for the juxtaposition of the two complexes, which ceased by the end of the Maastrichtian (~65Ma). During this event, westerly-directed thrust tectonics in the Northern Region of SW Cyprus formed in response to regional E-W shortening. The structures formed during thrusting suggests the operation of gravity tectonics within the evolving thrust wedges. Pure shear-dominated sinistral transpressional deformation in the Southern Region formed in response to NNE-SSW to NE-SW shortening. The preponderance of conjugate strike-slip faults that formed during this transpressional event suggests that shortening was predominantly accommodated by strike-parallel extension, here termed lateral extrusion. Lateral extrusion is interpreted to have resulted from the compression of a rheologically weak fault zone that possessed a highly irregular, pre-existing structural architecture, and is explained using an unconfined model for transpression. On the scale of SW Cyrpus, local thrust displacements and maximum shortening directions display a radial distribution, indicating near fault-normal compression along the length of the arcuate suture zone.

The microstructural fabrics preserved along the fault zones, suggest the operation of several grain-scale deformation mechanisms that are thought to have caused significant rheological weakening at both high and low temperatures. It is proposed that the influx of chemically active hydrous fluids throughout the deformational history led to significant long term weakening, which resulted in intense crustal-scale strain localisation and reactivation over an approximately 25Ma time-scale. The identification of these weakening mechanisms has profound implications for our understanding of the factors influencing the rheological strength of the lithosphere.

ACKNOWLEDGEMENTS

- First and foremost, I must express my gratitude to my three supervisors, Dick Swarbrick, Bob Holdsworth and Julian Pearce, who, without question, have been first class and inspirational throughout.
- The following people are thanked for their academic input. Without their assistance a great deal of the study undertaken would have been impossible: Ercan Aldamaz for amphibole microprobe analyses; Eric Condliffe and Jonny Imber for advice and guidance on the SEM at Leeds; all the microprobe staff in Edinburgh; Javier Escartín for high quality discussion on serpentinite deformation; Alfonso for advise on peridotites; Gaff for being my field assistant in Akamas; John Freeman for the use his Troodos samples.
- Special thanks are expressed to Richard Jones, whose discussion and literature on transpression has been invaluable.
- My fellow PhD throng in the department have made my time in Durham thoroughly enjoyable. Mikey Curtis, Andy Steele, Jipper, Roberto, Alun, Adam (Bouncy Castle) Styles, (Sporting) Jonny (SJ) Imber, Simon (Molly) Molyneux, Jo (Jugsy-Jug-Jug) Garland, Caroline (Curvey), Ziad (KJ) Ahmadi, Alwyn, Matt, Otter, Toby, Ian, Andy, Paul, Loraine and Rupert have all been excellent company and good friends. Special thanks are expressed to Jo, Jonny, Gail, Roberto, Alun, and Adam for their timely assistance in the past week. Without them, I wouldn't be writing this now.
- The friends I have made during my time in Durham have made the past three years without question the best of my life to date. Shane and Andrea receive a special mention for dragging me, kicking and screaming, to the Woodies in the first year and for visiting me in Cyprus. The lads of Gradsoc. AFC have been great, both on and off the pitch (i.e. in the New Inn), in Durham and on tour.
- The unsung heroes of the geology department are the technical staff; Ron Hardy, Dave, Karen, Julie, Ron Lambert, Carole, Claire, Dick, George, Dave, Gerry and last but not least Alan Carr are all fabulous and have been my saviours on more than one occasion.
- Angela's mummy and daddy are thanked for donating their car (and their daughter), without which I would have taken another year to write up.
- Angela over the last few weeks has been smashing. She has continuously filled me with brain food (bacon and egg butties), washed my clothes, done my shopping, dragged me out of bed, and typed the boring bits. Thanks chuck for keeping me in one piece.
- Finally, to Mum, Dad and Kev, whose support has been invaluable. The scale of their influence on my life and work cannot be overestimated. This thesis would have been dedicated to them had it not been for the loss of my grandmother who sadly passed away whilst I was in Cyprus in 1994.

Dedicated to my Nan,

Annie Pointon B.E.M

TABLE OF CONTENTS

PART ONE - INTRODUCTION

CHAPTER ONE
INTRODUCTION AND TERMINOLOGY

1.1. Introduction: formation and occurrence of serpentinite

Serpentinite is the term for a rock composed of more than 50% serpentine minerals (Coleman, 1971). There are numerous forms of serpentine, but three dominant polymorphs are cited in the literature: lizardite, chrysotile and antigorite (after Whittaker and Zussman, 1956). The process of serpentinisation is a metamorphic reaction whereby a mantle-derived, ultramafic rock is hydrated to produce a rock composed of predominantly serpentine minerals which have the approximate composition $H_4Mg_3Si_2O_9$ (Deer *et al.* 1966). Serpentinisation significantly modifies the physical and chemical properties of the rock; the resultant changes in seismic velocity, magnetic susceptibility, density, volume and rheology of the serpentinised peridotite have profound implications on the evolution of the crust and mantle (e.g. Hess, 1955a, b, 1965; Raleigh and Paterson, 1965; Bonatti, 1976; Cannat, 1993; Reinen *et al.* 1994). Of particular importance is the knowledge of where the parent rock originates, how and where it becomes hydrated, and how and when it is emplaced within the crust.

The purpose of this chapter is to outline the nature and occurrence of serpentinised ultramafic rock and to detail the processes and consequences of serpentinisation. The layout for the rest of the thesis is presented at the end of this chapter.

1.2. Peridotite classification and occurrence

Serpentinites result from the hydration of olivine-dominated peridotites. The ultramafic rocks referred to in the text are classified on the basis of their relative proportions of olivine (OL), orthopyroxene (OPX) and clinopyroxene (CPX) (Figure 1.1). The terms used may be qualified by a prefix of the main accessory phase: plagioclase, spinel, or garnet.

Our understanding of the composition of the deep interior of the Earth is largely constrained by seismic and density models, and by the chemistry of rocks brought to the Earth's surface. Partially to totally serpentinised ultramafic rocks are

associated with oceanic spreading centres, fracture zones, subduction zones, obducted ophiolite complexes, major crustal faults, and as nodules associated with kimberlites and basalts. The following review is sub-divided into three sections; the first two concentrate on 'oceanic' and 'continental' serpentinites, while the third section is used to describe 'sedimentary' serpentinites that crop out on-land and on the sea floor.

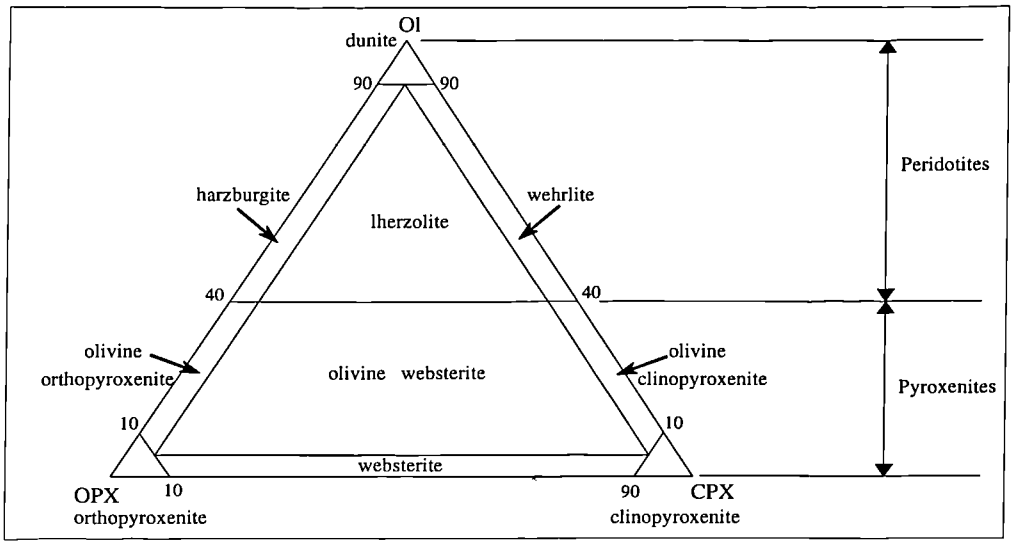

Figure 1.1. Terminology of ultramafic rocks based on the proportions of primary mineralogies.

1.2.1. Oceanic ultramafic rocks

As a generalisation, the oceanic crust may be separated into four layers on the basis of their varied seismic velocities and correlateable changes in composition (Figure 1.2). *Layers 1* and *2* are referred to as the *sedimentary* and *volcanic layers* respectively. Layer 2 is characterised by a variable increase in seismic velocity with depth, which is attributed to a gradation from sediments to basalt to sheeted dykes.

Layer 3, or the *oceanic layer*, is generally assumed to be of either gabbroic or peridotitic composition. Hess (1955a, b, 1965) proposed that layer 3 is largely composed of partially serpentinised peridotite. Hess envisaged that large volumes of partially serpentinised peridotite are generated under mid-oceanic ridges as they pass upwards through the 500°C isotherm. He suggested that Layer 3 migrates laterally from the spreading centre carrying with it the overlying crustal units. On the basis of seismic studies, Christensen (1972) concluded that serpentinite is *not* a major component of the oceanic crust; rather, serpentinites are generated and tectonically emplaced within fracture zones. However, Cannat (1993) favours an alternative model whereby seismic layer 3 is composed of discontinuous intrusions of gabbro within partially serpentinised peridotite. Thus, a number of lithologies have been proposed for layer 3, but the composition of this layer is still uncertain.

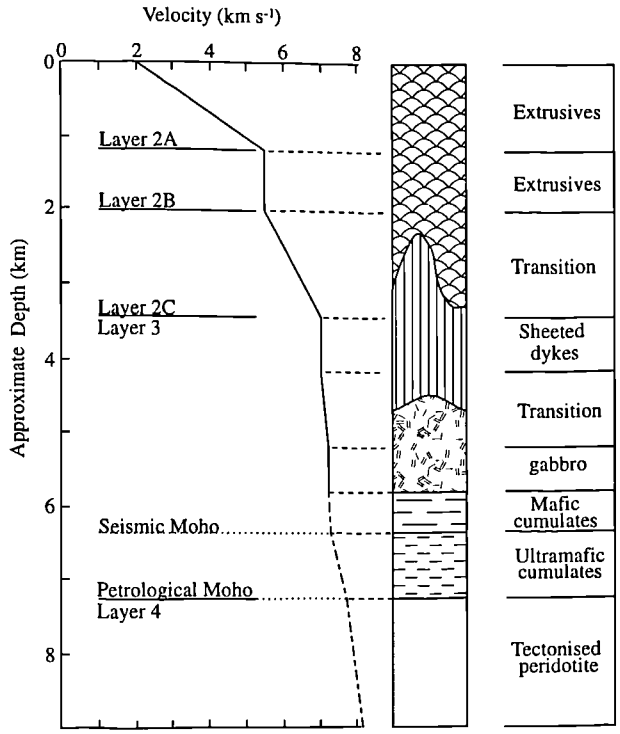

Figure 1.2. Idealised velocity-depth profile for the oceanic crust, adapted from Gass (1980) and Fowler (1993). The lower dashed section of the seismic velocity profile is based on approximations from Fowler (1993).

Layer 4 is the *upper mantle*, which is widely accepted to be composed of peridotite. Most models call for a zone of residual harzburgite overlying lherzolite (Bonatti and Hamlyn, 1981), but complications occur in the vicinity of transforms and slow-spreading ridges. Spinel-bearing +/- minor plagioclase-bearing harzburgite and lherzolite are the most abundant ultramafic lithologies dredged from oceanic environments, with harzburgite being more common. Subordinate dunite, pyroxenites, wehrlite and chromitite samples have also been recovered. Plagioclase peridotites are stable in the shallower zone of the oceanic upper mantle to approximately 25km below the top of the crust (Bonatti and Hamlyn, 1981). Spinel peridotites are in turn stable to 60-70km, whilst garnet peridotites are stable to the base of the lithosphere (>75km). Note that the depth ranges quoted are merely estimates based on geophysical and experimental grounds and that they relate specifically to the oceanic lithosphere; significant differences are expected for continental lithosphere.

The boundary between layers 3 and 4 may be defined on petrological or seismic grounds (Figure 1.2). The *seismic* Moho is a transition from crust to ultramafic mantle, whilst the petrological Moho is the boundary between cumulate ultramafic units, precipitated from melt, and underlying deformed, residual upper mantle (see section 1.2.2a).

Whatever is the dominant component of the oceanic crust, partially to totally serpentinised peridotites are commonly exposed on the sea floor and crop out in one of four geotectonic environments (Bonatti and Hamlyn, 1981).

- In relatively young crust associated with mid-ocean ridges.
- In crustal sections exposed along transform faults with large offsets (>100km).
- In crustal sections exposed in trenches and forearc regions.
- In regions associated with pre-oceanic rifts and continental margins.

1.2.1a. Peridotites associated with mid-ocean ridges

Serpentinised peridotites crop out along the bathymetric highs that parallel mid-ocean ridges, but are located at least 30km away from the spreading centres (Figure 1.3) (Aumento and Loubat, 1971; Bonatti, 1976; Bonatti and Honnorez, 1976; Rona *et al.* 1987). Bonatti (1976) proposed that these are solid, vertical *protrusions* of serpentinised upper mantle emplaced along mid-ocean ridge-parallel faults. 'Protrusion' (after Lockwood, 1971) is used to describe the process of tectonic-assisted, upward transport of serpentinised material in the solid state to reach high structural and stratigraphic levels. With increasing distance from the ridge axis serpentinites are dredged at increasingly shallow depths in the crust. Based on calculations combining spreading rate with the location of the serpentinite relative to the ridge axis, the rate of ascent of these protrusions is estimated to be on the order of 1mm/year. This upward mobility is attributed to a combination of tectonic processes and the decrease in density and increase in volume accompanying serpentinisation.

Mid-ocean ridges with serpentinised peridotite are in most cases characterised by slow spreading rates, and correlate with regions possessing a thin, magmatic crust and thick axial lithosphere (Cannat, 1993). Cannat suggested that if very little magma is supplied to the ridge axis, the uppermost levels of the oceanic lithosphere must at least be partially made of uplifted mantle material. Such magma-starved regions are predicted to be composed of peridotite and gabbro, which may be mutually intrusive. Furthermore, Cannat's predictions, based on geological and geophysical observations, explain the preferential emplacement of serpentinised ultramafic rocks in proximity to ridge-transform intersections where there is a local reduction in magma supply and magmatic crustal thickness (Karson and Dick, 1983; Rona *et al.* 1987). Rates of ascent of serpentinite protrusions at these intersections are estimated to be in the region of 1.1 to 7.5mm/year (Rona *et al.* 1987), which corresponds to 1mm/year estimated for the Indian Ridge (Bonatti and Hamlyn, 1978) and Mid-Atlantic Ridge-parallel protrusions (Bonatti, 1976).

1.2.1b. Fracture Zones

Mantle material is most commonly exposed along fracture zones, including those of the Mid-Atlantic (Christensen, 1972; Bonatti, 1976; Bonatti and Honnorez, 1976; Michael and Bonatti, 1985; Rona *et al.* 1987), Mid-Indian (Engel and Fisher, 1975; Bonatti and Hamlyn, 1978; Hamlyn and Bonatti, 1980), Circum-Atlantic spreading centres (Bonatti and Hamlyn, 1981), and more rarely, the East Pacific Rise (Hébert *et al.* 1983). Ultramafic rocks are the dominant constituent of elongate bathymetric highs (transverse ridges) that parallel the fracture zone (Figure 1.3) (Bonatti, 1973). Variably serpentinised peridotites are recovered in sampling surveys with diverse lithologic units such as basalts, gabbros, plagiogranites, pyroxenites, metabasalts and metagabbros ranging from zeolite-facies to amphibolite-facies, and variably deformed mafic and ultramafic rocks. Lherzolite and harzburgite are the most abundant, but subordinate dunite exists (Bonatti and Hamlyn, 1981).

Fracture zones are the loci of intense vertical tectonic motions, which lead to the uplift of upper mantle and crustal rocks forming transverse ridges (Bonatti, 1978). Variations in compressional and tensional forces and thermal conduction across the transform are two main parameters causing vertical tectonism, which, coupled with the mechanical properties of serpentinite, preferentially exhume serpentinised masses.

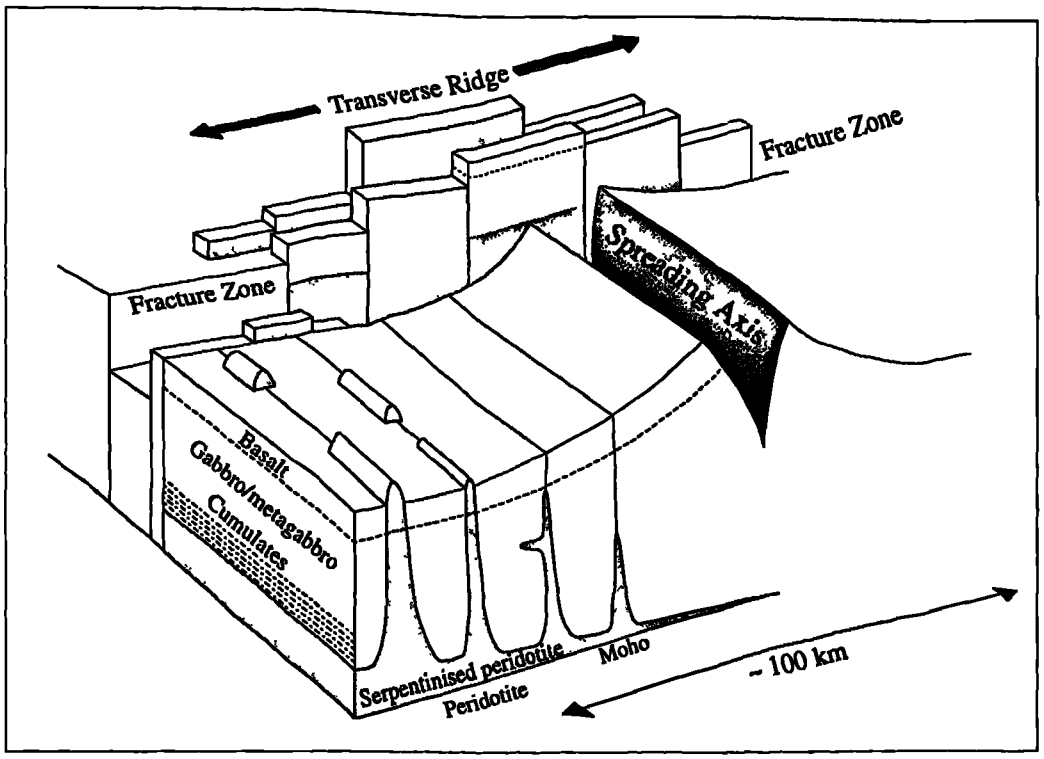

Figure 1.3. Schematic diagram showing the emplacement and distribution of ultramafic material in the oceanic crust in the vicinity of mid-ocean ridges and fracture zones.

1.2.1c. Subduction-related trenches and forearc regions

Peridotites are recovered in areas such as the Puerto Rico Trench (Bowin *et al.* 1966) and the Tonga Trench (Fisher and Engel, 1969), but the best documented ultramafics are the serpentinite seamounts of the Marianas Trench (Fryer *et al.* 1985, 1989). Seamounts composed almost entirely of serpentinite muds and their entrained clasts reach 30km in diameter and 2km in height. They are located between 50 and 150km westward of the trench axis (Fryer *et al.* 1989) lying between the trench and the related island-arc volcanoes. Their restriction to the outer half of the forearc is attributed to the geometry of the subduction zone, its thermal structure, and the rheological properties of the mantle wedge (Fryer *et al.* 1985). The fluids responsible for the hydration of the mantle wedge are thought to originate by dehydration and compaction of the subducting Pacific plate and its sedimentary cover. The reduction in density resulting from hydration of the mantle facilitates diapiric uprise of the serpentinite, which penetrates and entrains fragments of the forearc along pre-existing fractures.

The seamounts commonly deform under their own weight to form sediment gravity flows which are sourced from the central conduits (Fryer, 1992). Fryer *et al.* (1987) document unconsolidated serpentine mud-rich flows supporting clasts of variously serpentinised mafic and ultramafic rocks. Sedimentary serpentinites are detailed in the next section.

1.2.1d. Pre-oceanic rifts and continental margins

Peridotites have been recovered from pre-oceanic rifts and continental margins, but are rarely described in the literature. A 'pre-oceanic rift' is defined as a region undergoing extension that is at a transitional stage between a continental and an oceanic rift. An example is the Red Sea, which is floored by attenuated continental crust injected by basalt dykes (Bonatti and Michael, 1989). A mantle body is exposed in the northern Red Sea, which possesses a relatively undepleted, parent upper mantle composition and is thus considered as an uplifted fragment of pre-oceanic upper mantle, emplaced prior to the extraction of basaltic melt. Mantle peridotites have also been reported from passive margins close to the boundary between thinned continental crust and oceanic crust. Examples reviewed by Bonatti and Michael (1989) include the Iberian and Spitsbergen margins of the North Atlantic and south-western Australian margin in the Pacific-Antarctic ocean. Passive margin peridotites are, in general, more depleted than those sampled from pre-oceanic rifts, which indicates extraction of basaltic melt prior to emplacement.

1.2.2. Continental ultramafic rocks

Two groups of upper mantle rocks are accessible for direct structural and petrofabric studies. The first group include peridotite xenoliths associated with basalt and kimberlites. Schemes proposed in the literature for the classification of peridotitic textures from all tectonic environments are based on petrofabric observations of xenoliths. The terminology adopted in this work is presented in section 1.3. The second group comprise fault-bounded units of peridotite emplaced within the crust during orogenesis. Such serpentinised ultramafics that are exposed in orogenic zones are termed ***Alpine***-type (e.g. Thayer, 1960; Coleman, 1971) and may be grouped into two sub-categories: (1) ultramafic units associated with obducted fragments of oceanic lithosphere (e.g. ophiolites) that preserve evidence of ocean floor processes, and (2) serpentinites situated along fault zones.

1.2.2a. Ophiolitic ultramafic rocks

Ultramafic rocks generally form the lowest parts of obducted ophiolitic complexes. Examples include the Bay of Islands, Newfoundland (Williams, 1973), the Vourinos Complex, Greece (Moores, 1969), and the Semail Complex, Oman (Gealey, 1977). In most ophiolites, the ultramafic section may contain two genetically distinct peridotite subclasses. The first, forming the deepest structural levels of the complex is composed predominantly of tectonised, spinel-bearing harzburgite and/or lherzolite. They are interpreted as residual upper mantle depleted by partial melting and extraction of basic magmas (Dick, 1977). Deformational fabrics preserved in ophiolitic peridotites are analogous to textures frequently observed in oceanic ultramafic rocks (Nicholas *et al.* 1971) and in ultramafic inclusions in kimberlites (e.g. Harte *et al.* 1975) and basalts (e.g. Mercier and Nicholas, 1975). They are deformed to varying degrees under high temperature upper mantle conditions.

The second type of peridotite includes layered cumulate ultramafics, which possess mineral chemistries and textures indicative of crystal accumulation in shallow-level, slowly cooled magma chambers (Bonatti and Hamlyn, 1981). Analogous textures are present in oceanic environments, but are far less abundant than tectonites (Jackson *et al.* 1975).

Variably deformed serpentinites and peridotites are also present in complexes interpreted as fossil fracture zones associated with ophiolites. Examples include Gibbs Island, South Shetland Islands (De Wit *et al.* 1977), the Bogata Penninsula Peridotite Nappe (Prinzhofer and Nicolas, 1980), and the Arakapas Fault Zone, Cyprus (Moores and Vine, 1971).

1.2.2b. Fault zone serpentinites

Serpentinites commonly crop out along many major, active crustal fault zones, such as the San Andreas Fault (Allen, 1968; Irwin and Barnes, 1975), the Alpine Fault, New Zealand (Scholz, 1977), and the Motagua fault zone, Guatemala (Dengo and Logan, 1981). Extinct serpentinite-filled fault zones are also common in many tectono-metamorphic terranes. Ultramafic rocks derived from the upper mantle may be emplaced into the crust either as allochthonous thrust sheets (e.g. the Erro Tobbio Peridotite: Hoogerduijin Strating, 1993) or as intrusions/protrusions along sub vertical crustal fractures (e.g. Stuart-Smith, 1990). Frequently, later metamorphism and deformation obliterates evidence of pre- and syn-emplacement events (van Schalkwyk *et al.* 1993).

1.2.3. Sedimentary serpentinites

Serpentinised peridotite bodies may be formed by sedimentary processes both onland and in marine environments. *'Sedimentary'* is used here in the widest sense to encompass all depositional processes including *extrusion* and gravity sliding of large sheets of serpentinised material. 'Extrusion' is the process of exposing serpentinised bodies on the Earth's surface after their protrusive upward movement from depth. Ultramafic masses exposed on the seafloor are prone to reworking by sedimentary processes, whilst the plastic behaviour of serpentinite, which facilitates serpentinite protrusion, is responsible for the downslope movement of serpentinite extrusions associated with Alpine-type peridotites (e.g. Dickinson, 1966; Cowan and Mansfield, 1970).

1.2.3a. Submarine serpentinite deposits

By far the most abundant sedimentary serpentinites are those deposited in marine environments. Such deposits include variously consolidated mudstones, sandstones, breccias and olistostromes comprising >98% serpentine minerals, which are dominantly lizardite and chrysotile. Many examples preserve sedimentological evidence for rapid deposition from submarine landslides, mudflows or turbidity currents. As most examples are formed in deep water marine environments, normal erosional processes are not expected to supply detritus fast enough. However, the ability of serpentinite to behave plastically at low temperatures coupled with further weakening due to the influx of sea water can allow rapid downslope movement (e.g. serpentine-mud flows from Marianas seamounts: Fryer, 1992). Similar sediments formed in a submarine environment have been documented on-land, such as those

described by Lockwood (1971) and Carlson (1984) associated with Alpine-type ultramafics.

The identification of submarine, sedimentary serpentinite deposits can be difficult as they may possess similar characteristics to serpentinites generated by other processes. For example, carbonate-cemented peridotite breccias are reported from mid-Atlantic fracture zones (e.g. Bonatti *et al.* 1974) and ophiolitic complexes. They may be interpreted as tectonic breccias associated with fluid flow and brecciation along transform faults. However, other mechanisms that may form such breccias include cementation of talus breccia on fault scarps, submarine alteration of serpentinite bodies, shear due to the intrusion/protrusion of ultramafic bodies, shear due to sliding of crustal plates over a zone of stagnant upper mantle, or brecciation in 'vents' caused by volcanic gases (Green, 1961).

Of particular importance is the problem of distinguishing submarine, sedimentary serpentinites from the more massive 'protrusive' bodies, which often constitute upslope source areas for the deposits. Lockwood (1971) suggested numerous criteria to identify a sedimentary serpentinite which include:-

- The occurrence of fossils.
- Sedimentary structures such as graded- and cross-bedding preserved.
- Minerals or rocks foreign to the ultramafic assemblage, such as lithic fragments, are incorporated into the flow.
- A lack of contact metamorphism, which may indicate sedimentary or cold protrusive emplacement.
- Planar bodies of serpentinite possessing conformable contacts are often situated within sedimentary packages (commonly flysch) and extend laterally for large distances.
- Serpentinites which possess chemical characteristics diagnostic of interaction with sea water and subsequent diagenesis.
- Lack of shearing along contacts.
- Common chlorite, but rare brucite.

These criteria are useful except in the case of large coherent bodies emplaced by gravity sliding where few, if any, of the above features may be preserved.

1.2.3b. Continental serpentinite deposits

Dickinson (1966) and Cowan and Mansfield (1970) document sheets of serpentinite breccias that form by downslope flowage from fault-hosted extrusions and protrusive bodies in terrestrial environments. The flows comprise blocks of serpentinised

peridotite in a slickenside-rich foliated matrix. They are interpreted to move downslope to produce deposits morphologically analogous to debris flows. Basal contacts are characteristically angular and unconformable. Cowan and Mansfield (1970) have shown on experimental and theoretical grounds that sheared lizardite-chrysotile serpentinites can have very low shear strengths of a few bars at low temperatures and confining pressures, which explains how they can flow in a plastic manner downslope under the influence of gravity on-land.

1.3. Serpentinite

The term 'serpentine' is used as the family name containing the three main minerals lizardite, chrysotile and antigorite (Figure 1.4), or as a general term when the individual mineralogy is unknown or unspecified (Moody, 1976). This work complies with the terminology of Whittaker and Zussman (1956, 1971) who initially classified the serpentine minerals on structural grounds:-

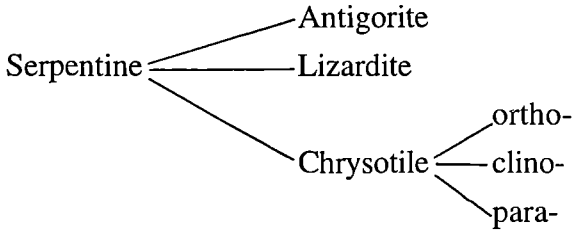

Figure 1.4. Crystal structures of the three main serpentine minerals (from Deer *et al.* 1989).

This was revised by Wicks and Whittaker (1975) on the basis of theoretical polytypic stacking sequences for trioctahedral 1:1 layer silicates. The classification of Wicks and Whittaker is adhered to in this thesis, particularly with respect to X-ray diffraction studies.

Page (1968a) realised that there are pronounced variations from the ideal formula $Mg_3Si_2O_5(OH)$. All three of the main serpentine minerals show distinct substitutions of Fe (2^+ and 3^+) and Al (Wicks and Whittaker, 1975) and, therefore, cannot be considered as true polymorphs. However, in general, most authors (e.g. Wicks and Whittaker, 1975) consider lizardite and chrysotile to be polymorphs, but not antigorite. The compositional variations in antigorite are considered necessary for antigorite's alternating wave structure (Whittaker and Wicks, 1970). To summarise, the main compositional differences between lizardite, chrysotile and antigorite include (from Whittaker and Wicks, 1970):-

- Lizardite and chrysotile contain H_2O^+ in excess of the ideal formula.

- Antigorite has a high wt. % SiO_2, and relatively low wt. % MgO and H_2O^+.
- Lizardite has a large amount of Fe_2O_3 and is relatively low in FeO.
- Chrysotile has a relatively low Al_2O_3 content.
- Antigorite has the highest $FeO/Fe_2O_3 + FeO + Al_2O_3$ contents and lizardite has the lowest.

The most common serpentinisation products derived from an ultramafic protolith are lizardite + chrysotile + magnetite ± brucite ± antigorite (Wicks, 1969; Aumento, 1970; Dietrich and Peters, 1971; Wenner and Taylor, 1971, 1973; Moody, 1976). *Lizardite* is by far the most abundant serpentine mineral and predominantly forms by the hydration of olivine during retrograde serpentinisation of peridotite below 450-600°C (e.g. Wicks and Whittaker, 1977; Rutter and Brodie, 1988a). Lizardite consists of planar layers (O'Hanley and Dyar, 1993) and possesses a platy morphology. Many different structural types of lizardite have been identified using X-ray diffraction studies, including 2-, 3-, and 6-layer serpentines, but the most common is the single layer, 1*T* variety. Lizardite, as with other serpentine minerals, shows a minor degree of substitution with minor amounts of Cr, Al and Fe accommodated in the crystal structure (O'Hanley and Dyar, 1993).

Chrysotile consists of cylindrical layers (O'Hanley and Dyar, 1993) and generally has a fibrous habit. In oceanic serpentinites, chrysotile crystallises when olivine is totally replaced by lizardite (Prichard, 1979). It forms fine fibres characteristically filling veins or replacing lizardite or antigorite.

Antigorite possesses a modulated crystal structure (Guggenheim and Eggleton, 1985) with the layer stacking controlled by direct bonding between layers and not hydrogen bonding as is the case with the other serpentine minerals. Wicks (1969) and Coleman (1971) observed that in most cases, antigorite is found where regional metamorphism or pressure/temperature conditions are significantly different from those in which lizardite and chrysotile form. Antigorite is considered the higher temperature serpentine mineral, whilst lizardite and chrysotile are accepted to be the lower temperature polytypes because: (1) under experimental conditions lizardite/chrysotile serpentinites dehydrate at lower temperatures than antigorite samples (>350°C as opposed to 550-600°C, respectively: Raleigh and Paterson, 1965); (2) oxygen and hydrogen isotopic thermometers and petrographic observations indicate lizardite and chrysotile crystallise at lower temperatures (85-300°C) than antigorite (220-550°C) (Wenner and Taylor, 1971; Coleman, 1971); (3) lizardite and chrysotile may replace antigorite under retrograde metamorphic conditions, whilst the inverse relationship is observed under prograde conditions (e.g. Maltman, 1978).

Other common serpentinisation products include magnetite ($Fe^{2+}Fe_2^{3+}O_4$) and brucite ($Mg(OH)_2$). Brucite is widespread in Alpine-type ultramafics of the circum-

Pacific orogenic belts (Hostetler *et al.* 1966). It weathers readily and alters to mineralogies such as hydromagnesite. *Brucite* is often difficult to distinguish in thin section, but it may be recognised in XRD studies when it occurs with amounts greater than 2 wt.%. *Magnetite* formation generally results from the alteration of chrome spinel, but it *may* also form simply as a consequence of the serpentinisation process. The production of magnetite is frequently correlated with relatively high temperatures, whilst lower temperatures favour Fe substitution into brucite (and lizardite) rather than the formation of magnetite (Moody, 1976; Wenner and Taylor, 1971). However, O'Hanley and Dyar (1993) stress that the production of magnetite is not simply controlled by temperature (also see section 1.2.2c). For example, rocks with high SiO_2 contents, such as serpentinites after harzburgite, contain more magnetite than those with low SiO_2, such as those after dunite, because lizardite can accommodate Fe^{2+} and Fe^{3+}, by substitution of Si.

Spinels may also alter to *ferrit chromite*, which is a spinel of intermediate composition between relict chromite and magnetite. Ferrit chromite is commonly associated with antigorite, chlorite, tremolite, metamorphic olivine and diopside (Evans and Frost, 1975), indicative of upper greenschist to amphibolite facies conditions in ultramafic rocks.

The following text concerns the textural classification adopted in this work, the processes and controls on serpentinisation, the origin of serpentinising fluids with particular reference to Cyprus, and the physical consequences of serpentinisation.

1.3.1. Serpentinite textures

Three dominant pseudomorphic textures after olivine have been documented in the literature. The most common is called *'mesh'* texture, first described by Selfridge (1935) (Figure 1.5), which is recognisable as a pattern of polygonal cells. Mesh textures are most commonly described at microscopic scales, but they are also identifiable on the scale of a hand specimen. The texture results from the direct replacement of olivine by serpentine and comprises two components: (1) irregular, polyhedral areas of serpentine representing the last portions of alteration of olivine called *"cores"* (or mesh cells) (Deer *et al.* 1962); and (2) the enclosing network formed in the cracks and grain boundaries in and between olivine called *"cords"* (or mesh rims) (Lauder *et al.* 1965). Mesh textures are invariably dominated by lizardite and cores commonly comprise isotropic mixtures of lizardite ± a combination of chrysotile and/or antigorite, or preserve relict islands of primary olivine, or display *'hourglass'* textures (see below). Cords are often identifiable by a string of magnetite grains, or by a

central parting, or a by a zone of isotropic or anisotropic serpentine (Wicks, Whittaker and Zussman, 1977).

'Hourglass' textures (Figure 1.6) are another common lizardite-dominated fabric (Selfridge, 1936; Deer *et al.* 1962). Hourglass textures are interpreted to result from the uninterrupted replacement of olivine by lizardite, whilst mesh textures are thought to represent an interrupted or sequential serpentinisation process (Wicks *et al.* 1977).

'Bladed mat' textures (Maltman, 1978) (Figure 1.7) (or, 'flame-like' after Du Rietz, 1935; 'matted-field' of Selfridge, 1936) result from the complete replacement of pre-existing structures by the intergrowth of antigorite blades (± lizardite ± chrysotile). The development of bladed mat textures is indicative of relatively high temperature metamorphic conditions and may result from the retrogression of primary olivine or the prograde replacement of lizardite-dominated textures (Maltman, 1978).

'Disturbed textures' (Maltman, 1978) are those intermediate between the three above and commonly result from replacement of one texture by another and/or the development of a texture under actively deforming conditions. One serpentine assemblages may be replaced by another in response to a change in conditions (see section 1.4.2.). The process is termed *serpentine recrystallisation* and need not be attributable to hydration (O'Hanley and Dyar, 1993).

'Bastite' is the name given to serpentine pseudomorphs after orthopyroxene, most commonly composed of lizardite and chrysotile (Whittaker and Zussman, 1956). Alteration may begin at the edge of the bastite and proceed inward and/or along cleavage planes or intragranular fractures (Bailey, 1984).

1.3.2. Controls on serpentinisation

Several variables have a profound effect on the serpentinisation process and on the mineral assemblages produced. The following sub-sections review the main controls.

1.3.2a. Temperature and pressure

Early experimental studies constrained the upper stability limit for serpentinite at 500° C at 3kb (Bowen and Tuttle, 1948) to 400°C at 3.5kb (Johannes, 1968). Subsequent stable isotope data (see section 1.4.3; Wenner and Taylor, 1974), petrographic and field observations (e.g. Maltman, 1978), and phase equilibrium experiments (e.g. Evans *et al.* 1976) all suggest that antigorite is the high temperature, high pressure serpentine mineral, whilst lizardite and chrysotile are low temperature equivalents. For example, Coleman (1971), using experimental information on the system MgO-SiO_2-FeO-Fe_2O_3-H_2O, inferred temperatures of between 100-300°C for alpine lizardite-

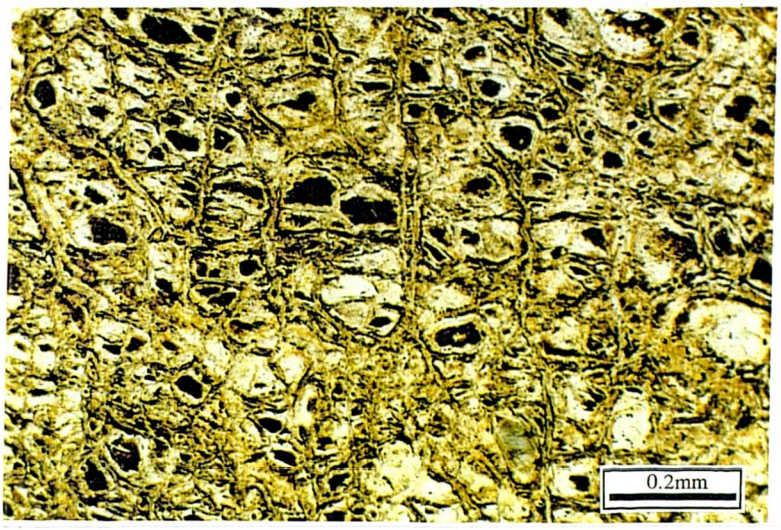

Figure 1.5. Photomicrograph of mesh texture developed in lizardite serpentinite (plane polarised light)

Figure 1.6. Hourglass texture developed in lizardite serpentinite (cross polars; taken from Wicks *et al.* 1977)

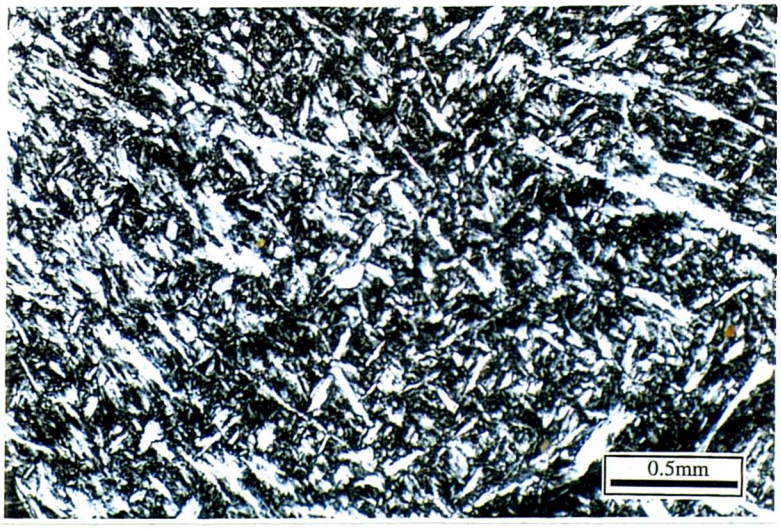

Figure 1.7. Photomicrograph of bladed mat texture developed in antigorite-lizardite serpentinite (cross polars).

clinochrysotile serpentinites and >300-550°C for antigorite samples. Textural observations from natural samples often document a chronology in serpentine mineral development, which directly relate to changing pressure and temperature conditions. Antigorite replaces lizardite and chrysotile during prograde metamorphism at upper greenschist to lower amphibolite facies (Lockwood, 1971; Evans and Frost, 1975; Maltman, 1978). Conversely, during retrogression lizardite and chrysotile replace antigorite (Coleman, 1971; Mumpton and Thompson, 1975). The higher temperatures required for antigorite stability is attributed to the beginning of dehydration and the lower activity of water (Moody, 1976), i.e. lizardite and chrysotile contain H_2O+ in excess of the ideal formula (Whittaker and Wicks, 1970).

Serpentinisation is also reported to be a very low temperature phenomenon. The reduction in the degree of serpentinisation in the Jimberlana intrusive cumulates with depth led Campbell (1975) to suggest that the hydration of olivine by H_2O and CO_2 to form lizardite-serpentinites is a present day, low temperature (20±2°C) process. Also, MacDonald and Fyfe (1985) indicate that serpentinisation occurs in seafloor environments, but note that the rate of serpentine crystallisation is slow because the low temperatures involved (<100°C) are rate limiting. In general, rates of reaction during serpentinisation are controlled by temperature and the access of fluid (MacDonald and Fyfe, 1985). Martin and Fyfe (1970) suggest that at temperatures above 100°C, serpentinisation is a geologically rapid, continuous process controlled by the rate at which water is supplied to the reaction interface. However, at temperatures below 100°C both rates of hydration and diffusion become rate-limiting and serpentinisation is slow.

1.3.2b. Mineral and bulk rock chemistry

Chemistry is frequently cited as a control on the relative stability of the serpentine minerals. For example, O'Hanley and Dyar (1993) suggest that $^{[4]}Fe^{3+}/^{[6]}Fe^{3+}$ and Si/Mg ratios of serpentine minerals are important in their stability. Furthermore, lizardite and chrysotile may be stabilised to higher temperatures by Fe^{3+} and lizardite to higher pressures and temperatures by increasing Al-content. However, Moody (1976) suggests that Al and Fe substitution in the serpentine minerals merely reflects the bulk composition of the parent rock; a view partially supported by O'Hanley and Dyar (1993) who state that the composition of lizardite is more dependant on bulk rock composition than on temperature, pressure and chemical potentials.

1.3.2c. Fluid Chemistry

Janecky and Seyfried, Jnr (1986) demonstrated by experimental studies of sea water interaction with peridotite that the composition of the fluid phase changes greatly during serpentinisation. These changes in fluid chemistry over time may be attributed to the variation in rates of serpentinisation and dissolution of primary mineralogies, which contribute different ionic species to the active fluid phase. For example, magnetite frequently forms late in the serpentinisation process with no change in the P/T conditions (O'Hanley and Dyar, 1993). This late formation may be explained by the relative rates of hydration of initial mineralogies (O'Hanley and Dyar, 1993). Enstatite hydrates more slowly than olivine (Coleman and Keith, 1971) and then the only product of olivine serpentinisation is lizardite (Wicks and Plant, 1979). Later in the hydration process excess Si is expected to be liberated from enstatite. This additional Si would combine with lizardite (± brucite) to generate more lizardite and Fe to form magnetite.

Chrysotile formation also appears to relate to a change in fluid compositions. Many authors (e.g. Wicks, 1969; Mumpton and Thompson, 1975; Prichard, 1979) suggest, on textural grounds, that chrysotile replaces lizardite in the later stages of serpentinisation. This late development of chrysotile may be attributed to the change in the serpentinising fluid composition after olivine is removed from the system (Prichard, 1979). Also, specific fluid chemistries, derived within and/or outside the ultramafic mass, may determine serpentine mineral growth. For instance, experimental studies by Korytkova and Makarova (1971) and Kortkova *et al.* (1972) demonstrate that influx of alkaline and Si-bearing fluids are necessary to form antigorite from olivine.

1.3.2d. Reaction kinetics

As serpentinisation is a metamorphic process it is controlled by reaction kinetics. Samples containing all three serpentine minerals attest to the complex stabilities of these systems (Wicks and Plant, 1979) and the common existence of one serpentine mineral in the experimentally determined stability field of another suggests that the serpentine polytypes are often metastable. Lizardite is rarely synthesised in laboratory experiments, which led Dungan (1977) to suggest it is a metastable product after olivine and enstatite. Phase diagram experiments and observations by O'Hanley (1991) further indicate that the hydration of peridotite proceeds via a metastable reaction. O'Hanley suggested that lizardite is produced as opposed to antigorite, which should be theoretically stable, because it is able to nucleate on olivine due to the correspondence in their crystal structures. Metastability in the serpentine minerals is also demonstrated by antigorite, which is reported to exist at lower temperatures than

experimentally predicted (Mumpton and Thompson, 1975). Conversely, lizardite and chrysotile may exist into prograde metamorphic events (Dietrich and Peters, 1971).

1.3.3. Serpentinising fluids

Important in any study concerning the hydration of a rock mass is the source of the reactant fluids. Trace element geochemistry can be used to determine the source of the fluid phase because it may leave a signature of its composition in the rock during hydration. For example oceanic serpentinites are commonly enriched in Cl, B, U and other elements which suggest alteration by sea water (Moody, 1976; Sanford, 1981). However, the use of oxygen and hydrogen isotopic analyses of serpentine mineral separates is more effective as they characterise the source of the fluids and the temperatures during serpentinisation. Wenner and Taylor (1971) proposed a geothermometer for serpentinisation based on the O^{18}/O^{16} ratio between coexisting magnetite and serpentine minerals. The geothermometer was derived by extrapolating δO^{18} fractionations between chlorites and Fe-Ti oxides in low grade pelitic schists, in which the isotopic equilibration temperatures were known from pre-existing thermometers. Wenner and Taylor assumed that the O^{18} fractionation factor between chlorite and serpentine is equal to one and that isotopic equilibrium is attained in all samples. Their thermometer yielded the following approximate temperatures during serpentinisation:-

- Continental lizardite-chrysotile: 85-115°C
- Oceanic lizardite-chrysotile: 130-185°C
- Oceanic antigorite: 235°C
- Continental antigorite 220-460°C

However, Bottinga and Javoy (1973) suggested that these temperatures are as much as 100°C too low due to the large number of assumptions made in the geothermometer, but the conclusion that antigorite is the higher temperature serpentine mineral is valid.

Wenner and Taylor (1973) demonstrated that serpentinites from on-land ophiolitic complexes possessed significantly different $\delta^{18}O$ and δD values compared to oceanic serpentinites (Figure 1.8). They concluded that if ophiolites represent original oceanic crust, then they must be serpentinised in a continental regime by exchanged groundwaters, mixed meteoric/magmatic and/or meteoric/connate waters, most probably during the deformation accompanying obduction-related processes. However, more specific to the present study, Margaritz and Taylor (1974) indicated lizardite-chrysotile serpentinites from the Troodos Massif are, in general, unusually high in $\delta^{18}O$ compared to all other serpentinites and that they possess D values too low to

have formed from heated ocean waters. They concluded that Troodos serpentinites either formed in contact with large amounts of meteoric, metamorphic, or formation waters at low temperature (<50°C) in a near surface environment, or, more favourably, by reaction at elevated temperatures (75-100°C) with meteoric-hydrothermal waters abnormally enriched in $\delta^{18}O$. Preliminary analyses of five samples from SW Cyprus by H. Margaritz (1981 - *pers comm.* Alistair Robertson and Dick Swarbrick) show a spread of $\delta^{18}O$ data which correlates with the variation observed for Troodos samples. The serpentinising fluids are therefore considered similar to those responsible for the serpentinisation of the Troodos ultramafics.

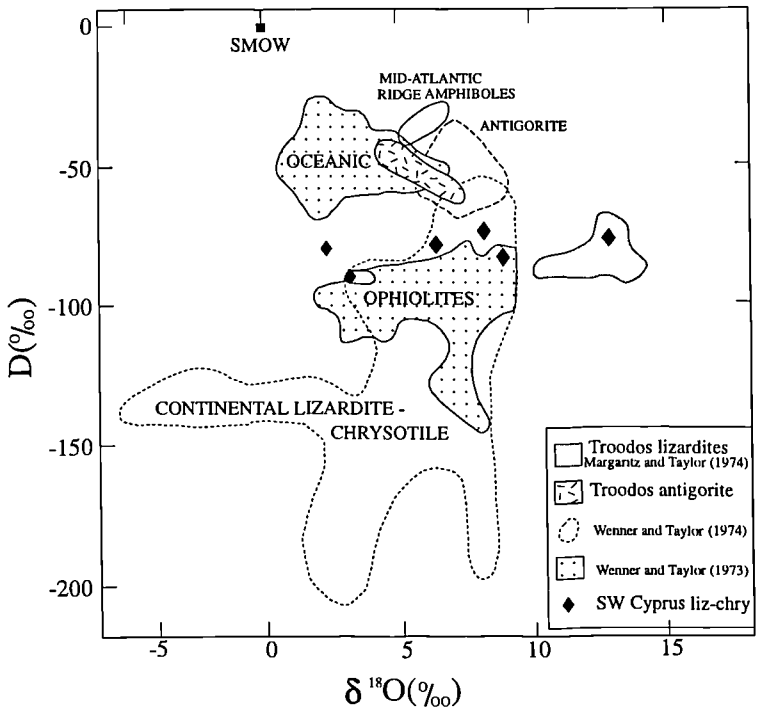

Figure 1.8. $\delta D/\delta^{18}O$ diagram depicting previously constrained isotopic ranges of various types of serpentinite (after Margaritz and Taylor, 1974). Note the isotopic values for SW Cyprus lizardite-chrysotile samples correlate with the range of data from the Troodos ophiolite.

1.3.4. Physical consequences of serpentinisation

Certain physical changes occur during serpentinisation, which have significant geophysical and structural implications. Decreases in *density* and increases in *volume* could facilitate the emplacement of serpentinised masses into the crust along fault zones (e.g. Hostetler *et al.* 1966; Mumpton and Thompson, 1975; Bonatti, 1978). Changes in the *magnetic susceptibility* of serpentinised peridotites are important in geophysical modelling of the oceanic lithosphere, whilst the *rheological properties* of serpentinised fault rocks may have a strong influence on the mechanical behaviour of major fault zones in the lithosphere

1.3.4a. Density

Sink-float techniques in heavy liquids or by pyconometer indicate densities for liz ardite and chrysotile are approximately 2.55g/cm^3 and for antigorite 2.61g/cm^3 (Coleman, 1971). Values of less than 2.55 g/cm^3 are recorded in chrysotile-dominated samples (i.e. 2.19-2.39 g/cm^3; Huggins and Shell, 1965). These values indicate an approximately 20% decrease in density from 3.3g/cm^3, the typical value for unserpentinised peridotite (O'Hanley, 1992). Other products such as brucite (2.39 g/cm^3) also contribute to the decrease in density during serpentinisation.

1.3.4b. Volume

Serpentinisation may be either a constant volume (Thayer, 1966) or volume expansive process (Hostetler, 1966). Recent workers suggest that both processes exist (e.g. Coleman, 1971; Moody, 1976; Wicks and Whittaker, 1977), but the problem with evaluating volume and chemistry changes during serpentinisation is finding an unaltered ultramafic unit and it s serpentinised equivalent.

Constant volume serpentinisation is commonly associated with a change in chemical composition, which implies an open system with free exchange between the fluid phase and the host rock (Moody, 1976). Such conditions may prevail in *dynamic* systems of sheared, fault zone serpentinites (Coleman, 1971). On the other hand, *static* conditions favour volume increase in closed systems.

Constant volume serpentinisation in past literature has been identified by (after Moody, 1976):-

- Perfect pseudomorphic replacement of euhedral olivine by serpentine.
- Mg, Ca and Si removal, which may be deposited far away from the source or involved in metasomatism adjacent to the serpentinised body.

The use of the above criteria, however, may be misleading and are not necessarily indicative of constant volume serpentinisation. For example, Condie and Madison (1969) provide geochemical evidence from a partially (4-45%) serpentinised alpine-dunite body to suggest the hydration reactions should cause a 50% increase in volume. The example is particularly interesting in that Fe and Mg appear to have been removed in solution which suggests open-system conditions leading to a change in bulk composition. Therefore, the rule that constant chemical serpentinisation should be volume increasing may be incorrect, and the process and products of serpentinisation are more complex.

The retention of pre-existing structures, particularly with delicate chromite intergrowths, have been cited as evidence for volume conservation (Thayer, 1966; Cerney, 1967; Wicks and Whittaker, 1977). However, Condie and Madison (1969)

provide geochemical evidence to suggest that volume increasing hydration reactions involved in the serpentinisation of an alpine-dunitic body preserve primary spinel banding. O'Hanley (1992) explained this by a simple calculation; 25-45% volume expansion would result in changes in length of olivine-pseudomorph mesh cells by 0.003-0.05mm. Such changes would obviously be difficult to identify, thus emphasising the importance in the scale of observation. Therefore, preservation of primary layering in serpentinised masses does not appear to constitute evidence for volume-for-volume replacement.

Volume increase may be inferred by a lack of Ca-metasomatism associated with the serpentinised body or constant chemical compositions between protolith and serpentinite (except for the addition of H_2O). However, the most reliable indicator of volume expansion is the existence of *kernel pattern* serpentinites (O'Hanley and Offler, 1992; O'Hanley, 1992). The 'kernel pattern' (Figure 1.9) may be identified at micro- to macroscopic scales and comprises a rim of completely serpentinised material surrounding a core of partly or unserpentinised peridotite. The core-rim boundary is commonly sharp and cut at high angles by cross-fractures filled with chrysotile or apple-green, structureless serpentine termed 'picrolite' (O'Hanley, 1992). Fractures are invariably orthogonal to the core-rim boundary and taper into the core of the kernel. The radial distribution of tapering fractures about the kernel, combined with the observation that they are only located in totally serpentinised peridotite, suggest that they are manifestations of volume increase during serpentinisation. The measured densities of cross-fractures in kernel rims are consistent with values predicted from the magnitude of volume increase (34%, O'Hanley and Offler, 1992; 25-45%, Coleman, 1971). The fractures are interpreted to form as the serpentinisation front penetrates the kernel and the serpentinised material expands. The expansion accompanying each increment of serpentinisation will cause the fracture to propagate into the partially serpentinised core because the totally serpentinised rim cannot accommodate the increase in volume. The size of the fracture is therefore proportional to the degree of serpentinisation and how far the serpentinisation front has propagated into the core.

1.3.4c. Magnetic properties

Previous workers have assumed that magnetite is responsible for the remnant magnetisation in serpentinised peridotites and not spinel (e.g. Cox *et al.* 1964). Coleman (1971) demonstrates that a correlation exists between the degree of serpentinisation, density and the magnetic susceptibility. However, O'Hanley and Dyar (1993) comment that the formation of magnetite is not a necessity in the serpentinisation process and that its generation is a consequence of varying parameters

such as bulk rock chemistry. The magnetic susceptibility of serpentinite is therefore not a reliable method of determining the degree of serpentinisation.

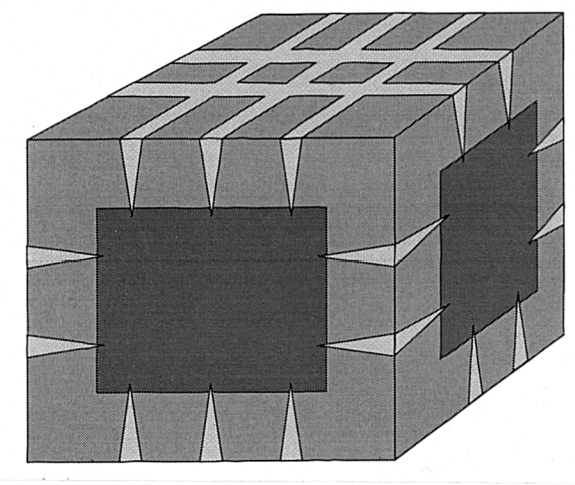

Figure 1.9. Kernel pattern in a cube of peridotite. Cross fractures (light) cut the serpentinised rim (medium) and taper into the partially/unserpentinised core (dark) (after O'Hanley, 1992).

1.3.4d. Strength and ductility

The first noteworthy studies on the mechanical properties of serpentinite were carried out by Raleigh and Paterson (1965). Their experimental investigations were undertaken at constant strain rate (7×10^{-4} s^{-1}), but temperature and confining pressure were varied in order to observe their effects on the brittle-ductile transition in serpentinite. At confining pressures greater than 3kbars and temperatures above 300°C, antigorite-rich (plus minor chrysotile) samples exhibited ductile behaviour (i.e. they displayed uniformly distributed continuous deformation; see section 1.4). However, at all confining pressures, antigorite-rich specimens displayed marked weakening and brittle failure between 500-600°C (Figure 1.10). Lizardite (plus minor chrysotile) serpentinites, exhibited a similar loss in strength, but at considerably lower temperatures (300-350°C) (Figure 1.10). The onset of weakening in both serpentinites was attributed to the dehydration of serpentine to form talc and forsterite. The water vapour released during the dehydration reaction may reduce the effective normal stress and the resistance to frictional sliding. Raleigh and Paterson proposed both antigorite and lizardite serpentinites undergo a transition from a strong ductile rock at low temperatures to a weak brittle one at high temperatures (Figure 1.11). Furthermore, they predicted lizardite serpentinites should fail in a brittle manner at much lower temperatures than antigorite-rich rocks. However, Raleigh and Paterson's conclusions have since been contested. For example, Gates and Kambin (1990) compared naturally deformed antigorite- and lizardite-dominated serpentinites with experimental data.

They suggested that lizardite-rich serpentinites located in retrogressed shear zones deformed in a ductile manner between 490°-320°C at 2-5kbar, whereas contemporaneous antigorite-rich fault rocks experienced brittle deformation. These observations contrast Raleigh and Paterson's (1965) interpretation that antigorite-rich samples should be ductile up to 500°C. Furthermore, experimental studies carried out at room temperature and constant strain rate by Dengo and Logan (1981) suggest that lizardite-rich samples exhibit *ductile* deformation at all confining pressures (up to 200MPa), whereas antigorite-rich serpentinites deform in a *brittle* manner at pressures as low as 10MPa. Dengo and Logan attributed this difference to the fact that lizardite is much weaker than antigorite; lizardite possesses a lower coefficient of friction and requires a much lower shear stress to initiate sliding (up to $0.27\sigma_n$) than antigorite, and lizardite-rich samples have fracture strengths much lower than antigorite-dominated samples. They concluded that the deformation of the two serpentinites is not controlled by pressure and temperature as suggested by Raleigh and Paterson (1965), but imply that the contrasting crystal structures and textures of lizardite and antigorite determine the frictional and mechanical behaviour of the serpentinites. Antigorite is only ever expected to exhibit ductile deformation near its upper temperature stability limit due to dehydration and conversion to forsterite and talc. Talc possesses a lower coefficient of friction than serpentine and would effectively lubricate the system. Therefore, textural and experimental evidence presented by Gates and Kambin (1990) and Dengo and Logan (1981) indicate the poor dependence on temperature and pressure of serpentinite deformation mechanisms

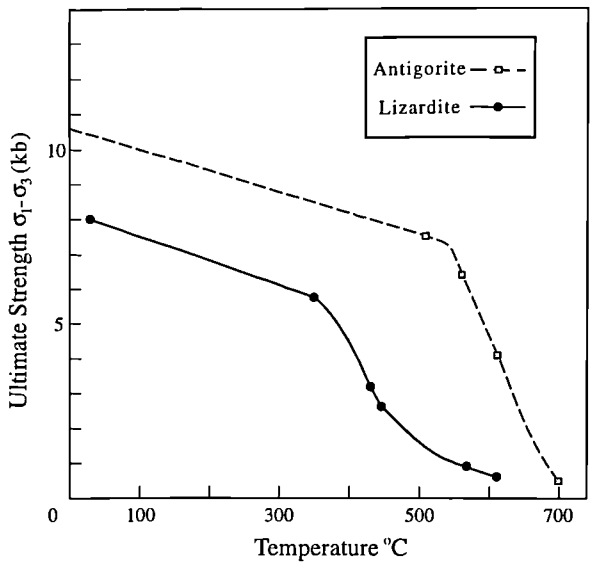

Figure 1.10. Comparison of the ultimate strengths of antigorite and lizardite serpentinites as a function of temperature at constant confining pressure (3.5kbar) (adapted from graphs in Raleigh and Paterson, 1965).

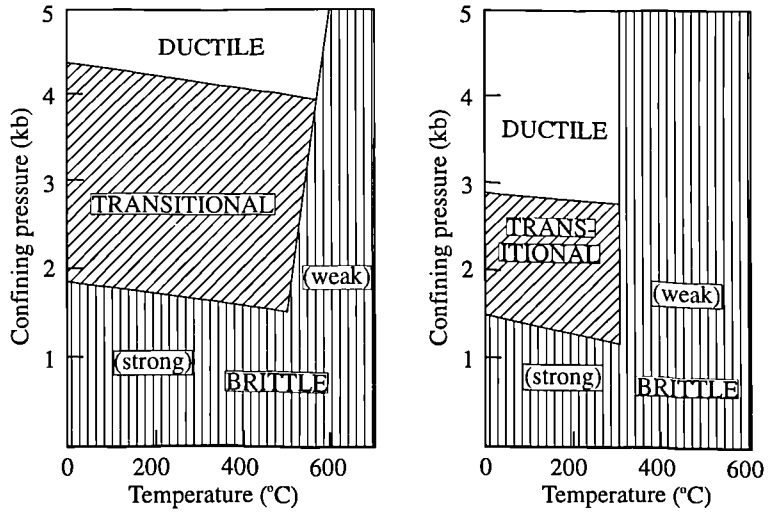

Figure 1.11. Brittle, transitional, and ductile regimes of a pressure-temperature field for antigorite serpentinite (left) and lizardite serpentinite (right) (after Raleigh and Paterson, 1965).

However, these studies were undertaken at constant strain rate and do not address the velocity dependence and consequent slip stability of serpentinite. Reinen *et al.* (1991, 1994) conducted a series of velocity-step tests on lizardite and antigorite gouge. The term *velocity weakening* applies to a rock when the steady-state level of frictional resistance is lower at faster velocity (or strain rate) than at a slower velocity (Reinen *et al.* 1994). Such samples have the potential for unstable, stick-slip motion. *Velocity strengthening* is the opposite case and is usually associated with stable sliding and aseismic creep (Reinen *et al.* 1994). Reinen *et al.* discovered that a transition existed for both lizardite and antigorite from velocity weakening at fast loading velocities to velocity strengthening at slow velocities. Thus, at slower velocities, which are more representative of plate motion rates, both serpentinites are strongly rate strengthening, indicating that stable fault creep should prevail under such conditions. Furthermore, Reinen *et al.* (1991) observed that antigorite serpentinites exhibited an increase in stability at high normal stresses (125MPa), suggesting that an increase in depth would favour stable fault creep. More important to the present study is the recognition that lizardite serpentinites possess a much lower coefficient of friction (0.15-0.35) than antigorite serpentinites (0.50-0.85), which are comparable to other crustal materials (Reinen *et al.* 1994). Small increases in temperature could lower the frictional strength of lizardite below 0.1, which may account for the apparent weakness of continental and oceanic crustal faults (e.g. San Andreas: Rice, 1992; Kane fracture zone: Wilcock *et al.* 1990). Also, the presence of fluid during deformation also appears to be significant as demonstrated by a decrease in the frictional strength with increasing water content (Reinen *et al.* 1994).

The overall conclusion remains that lizardite is substantially weaker than antigorite and other crustal materials. Fault rocks comprising dominantly lizardite are more likely to deform by stable-sliding than antigorite-dominated fault rocks. The weakness of lizardite-dominated samples may be attributed to:-

- Lizardite and antigorite possess contrasting crystal structures (Figure 1.12). Antigorite has a wavy, corrugated structure, whereas lizardite possesses a flat layered platy morphology. The latter structure would more easily facilitate intracrystalline glide (Dengo and Logan, 1981) and grain boundary sliding.
- Si-O bonds connect the corrugated layers within the antigorite crystal lattice at the inflection points. These interlayer bonds are considerably stronger than the corresponding hydrogen bonds in lizardite (Figure 1.12) (Reinen *et al.* 1994).
- Lizardite and chrysotile contain H_2O^+ in excess of the ideal formula (Whittaker and Wicks, 1970). Serpentinites dominated by these two minerals are assumed to have higher porosity than antigorite-dominated samples, because the latter form under prograde metamorphic conditions, whereas the former are normally generated during retrogression where fluid is abundant (Gates and Kambin, 1990). The presence of fluids may further decrease the strength of the serpentinite and enhance ductility (Wicks and Whittaker, 1977).
- Lizardite and antigorite form unique textures with contrasting grain sizes. Previous workers (e.g. Brace, 1961; Friedman, 1975) demonstrated that rocks with a smaller grain size possess a higher fracture strength. Compared to lizardite the smaller grain size for antigorite in interpenetrating, bladed-mat textures suggests a larger area of grain-grain contacts, thus increasing the frictional strength of the rock (Dengo and Logan, 1981).
- Antigorite possesses a higher density (2.6 g/cc) and hardness (up to 3.5 on Moh's scale) than lizardite (2.4g/cc and 2.5 respectively) (Deer *et al.* 1965).

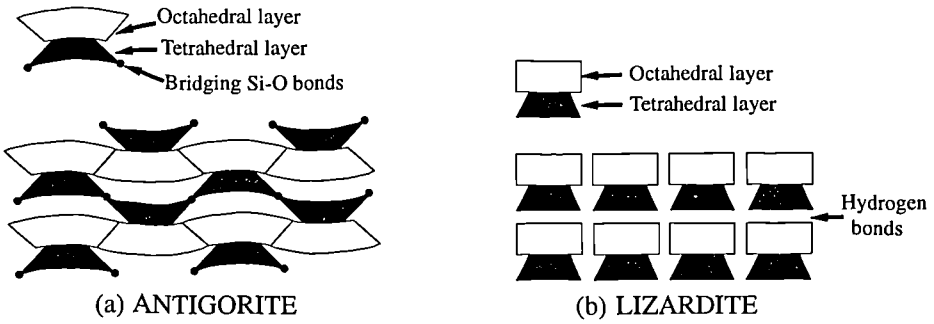

Figure 1.12. Schematic representation contrasting antigorite and lizardite crystal structures (after Reinen *et al.* 1994). (a) Antigorite structure displaying bridging Si-O bonds between alternating layers. (b) Alternating, flat-layered structure of lizardite showing hydrogen bonding between layers.

1.3.5. Identification of the serpentine minerals

The identification of serpentine minerals is best carried out using XRD techniques, since optical petrographic studies generally do not yield satisfactory results. Whittaker and Zussman (1956) provided an initial classification based on powder diffraction techniques, which has been further elaborated by later workers (e.g. Wicks and Zussman, 1975; Wicks, 1979). Where XRD techniques have been used for mineral identification in this thesis the respective trace(s) are displayed with the text. A full description of the techniques applied to the SW Cyprus serpentinites is presented in Appendix 1.

1.4. Structural terminology

Of utmost importance in structural analysis is the understanding of the conditions causing deformation and the identification of the mechanisms that accommodate deformation. However, before the inter-relationships between these parameters and processes are detailed, it is worth outlining the use of the terms ***brittle*** and ***ductile***, which have been used imprecisely in the literature, resulting in confusion. 'Ductile' is used in this thesis to refer to "a permanent, coherent, solid-state deformation in which there is no loss of cohesion on the scale of the crystal grains or larger and there is no evidence of brittle fracturing" (Twiss and Moores, 1992). 'Brittle' is defined as "the breaking of rocks along well defined planes or zones" (Twiss and Moores, 1992). When applying these terms one must be specific about the scale of observation. For example, consider the case of a fine-grained fault rock, in which the macroscopic deformation is accommodated by uniformly distributed flow which may therefore, be termed ductile. However, at microscopic scales or smaller, grain-size reduction and deformation may be accommodated by fracture development and cataclasis. Therefore, any fault rock may be described as ductile if a suitable scale of observation is chosen. In this respect ductility is a *phenomenological* concept. Brittle, on the other hand, describes fracturing and crack development and is thus a *mechanistic* concept (Schmid and Handy, 1991).

1.4.1. Deformation mechanisms

The way in which a deforming rock accommodates strain is controlled by numerous environmental and lithological variables, such as temperature, pressure, strain rate, grain size, fluid activity etc. Combinations of these variables dictate which material processes are activated and, in turn, which deformation mechanisms operate. As

geological conditions, mineral assemblages and microstructure may change over time, strain can be partitioned over space and/or time at all scales. A rock is therefore a dynamic system, sensitive to a number of variables (Knipe, 1989; Williams *et al.* 1994) (Figure 1.13).

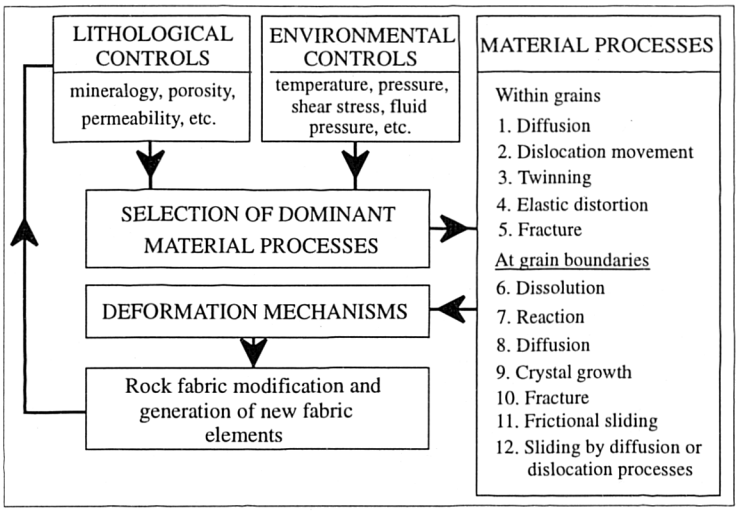

Figure 1.13. Flow diagram showing the inter-relationships between lithological and environmental controls and material behaviour during rock deformation (from Knipe, 1989).

The mechanisms by which deformation is accommodated in rocks may be sub-divided into three broad groups:

- Fracture, frictional grain-boundary sliding and cataclastic flow
- Diffusive mass transfer
- Crystal plastic flow

Mechanisms of fracture and cataclasis dominate faulting at high crustal levels, characteristically generating fault gouges and breccias. These essentially brittle processes involve frictional sliding and dilatancy and, as a consequence, are highly pressure-sensitive. Therefore, the generation of cataclastic fault zones is facilitated at low effective stresses (low confining pressures and/or high pore-fluid pressures), where cohesion between grains is easier to overcome. Temperature and strain-rate are of secondary importance. With increasing depth in the lithosphere, thermally activated deformational mechanisms accommodated by diffusive mass transfer and intracrystalline plasticity, dominate. Temperature, strain-rate and often grain-size control rheology, but effective pressure is of only minor importance. Although the various deformation mechanisms are activated in variable conditions, one must understand that, in general, no single process operates alone and the activation of one mechanism will influence the operation of others (Williams *et al.* 1994).

1.4.1a. Fracture, frictional grain-boundary sliding and cataclastic flow

Deformation of rock by any of these mechanisms involves the creation of new surfaces and a loss of cohesion due to fracturing (Knipe, 1989).

Fracture mechanisms involve the nucleation and propagation of cracks, along which displacement may occur as deformation progresses.

Frictional grain-boundary sliding is the sliding of grains past each other. Sliding takes place when the frictional strength between grains is overcome and cohesion between grains is lost. Frictional grain-boundary sliding contrasts with high temperature grain-boundary sliding (see below) where sliding is accommodated by diffusion or defect motion along grain boundaries and cohesion is maintained.

Cataclasis involves fine-scale fracturing, movement along fractures, frictional grain-boundary sliding, and fragment rotation. Microstructural observations suggest that low-temperature plasticity and low-temperature ductile fracture are important processes in accomodating deformation in cataclasite-filled fracture zones (Lloyd and Knipe, 1992). Cataclasis, as with the above two processes, is a process involving dilatancy and is thus enhanced at low confining pressures. Cataclasis may be localised or may accommodate macroscopically ductile flow over broader areas (cataclastic flow; *cf.* Paterson, 1978).

1.4.1b. Diffusive mass transfer (DMT)

DMT involves the diffusional transport of material away from a source, which is a zone of high intergranular normal stress, to a sink, which is a site of low normal stress (Rutter, 1983; Knipe, 1989 and references therein). The mechanism(s) driving diffusion reflect the presence of a chemical potential gradient, which can occur as a result of existing compositional variations and/or differential stress and/or the strain energy stored in mineral grains (Rutter, 1983; Wheeler, 1993; Williams *et al.* 1994). As this deformational process is controlled by diffusion (intracrystalline and/or intercrystalline) it is facilitated by fine-grain sizes, high temperatures and the presence of a fluid phase. However, due to the significant role of grain size and fluid in the rate of diffusion, deformation mechanisms controlled by DMT are clearly not limited to high temperature regimes (see later).

1.4.1c. Crystal plastic flow

Crystal plasticity involves the accumulation of strain by intracrystalline processes, such as the movement of dislocations (linear lattice defects) and twinning (Barber, 1985). Both these mechanisms accommodate shape change by shear of one section of a crystal

with respect to another. At low temperatures (<0.5 melting temperature), deformation is predominantly accommodated by the confined movement of dislocations along slip planes, termed *dislocation glide* (Knipe, 1989). Deformation at these temperatures is characterised by the build up of dislocations to form dislocation tangles, which restrict further dislocation movement in the crystal lattice. The resulting increase in the resistance to straining during deformation is referred to as *work hardening* and the presence of undulose extinction in thin section is suggestive of this process. At higher temperatures (>0.5 melting temperature) work-hardening is counteracted by thermally activated *recovery* processes, which permit the rearrangement of defects to lower the internal strain energy of a crystal and increase the ductility of the deforming material (Knipe, 1989).

Recovery is achieved predominantly through the process of *dislocation climb*, which involves the diffusive movement of defects to higher or lower slip planes (e.g. Twiss and Moores, 1992; Williams *et al.* 1994, and references therein). Recovery processes are favoured at slow strain rates and/or high temperatures. With sufficient mobility, dislocations may rearrange to form low energy arrays, such as low angle-boundaries and dislocation walls between slightly misoriented regions of a crystal lattice. Such misorientations in the lattice may be identified in thin section as deformation bands and subgrain boundaries respectively. A *subgrain* is a segment of a crystal that has been separated from the main crystal lattice by progressive misorientation (e.g. 3-5° in albite: Williams *et al.* 1994) across a dislocation array. With increased defect mobility the deforming rock may experience *recrystallisation.* 'Recrystallisation' involves the growth of new, relatively strain-free grains (neoblasts), with high-angle boundaries, from old strained grains (paleoblasts), either after (static) or during (dynamic) deformation. The presence of several generations of neoblasts of various sizes growing at the periphery of porphyroclasts indicates dynamic recrystallisation. Two mechanisms of dynamic recrystallisation have been recognised (Drury and Urai, 1990):

- **Rotation recrystallisation**
- **Boundary migration recrystallisation**

'Subgrain rotation recrystallisation' results from the accumulation of an increasing number of dislocations at a subgrain boundary, which causes a progressive misorientation of the subgrain lattice. With increasing rotation (≥10°: Twiss and Moores, 1992; >*c.* 3-5°: Williams *et al.* 1994;), the subgrain boundary becomes a high-angle grain boundary of a newly recrystallised grain. 'Boundary migration recrystallisation' involves the migration of a grain boundary that separates highly strained grains from an unstrained grain of the same mineral. The grain boundary

migrates into the more highly strained grain, leaving the unstrained crystal behind, thus reducing the dislocation density and the strain energy of the strained grain. The resultant microstructures display irregular grain boundaries, indicative of local grain boundary bulging (Ross *et al.* 1980), and abrupt changes in lattice orientation between paleoblasts and neoblasts. Rotation recrystallisation, on the other hand, is a grain-size reducing process that makes independent grains out of subgrains through progressive rotations, and as a result is identifiable by more gradual changes in lattice orientation between paleoblasts and neoblasts.

1.4.2. Strain localisation; effects of grain-size and fluid

The localisation of strain into fault zones results from the development of rheological instabilities. Such instabilities may relate to mineralogical and/or microstructural inhomogeneities, or to a change in physical conditions during deformation. The following discussion reviews the effects of grain-size and fluid activity on deformational processes and, in particular , their role in microstructural change associated with localising strain.

1.4.2a. Grain size effects

Creep is the term used to describe macroscopically ductile, continuous flow, in which the operative deformation mechanisms accommodate a constant stress (Williams *et al.* 1994). Two dominant creep regimes are cited in the literature:

- *Dislocation creep* regime, in which flow is accommodated by the movement of defects in the crystal lattice.
- *Diffusion creep* regime, in which flow is accommodated by intergranular ± intragranular diffusive mass transport.

Some deformation mechanisms, such as dislocation glide, are not affected by variations in grain size. However, mechanisms controlled by diffusion are favoured by a decrease in grain size. Finer-grained rocks not only have a greater volume of grain boundaries that facilitate intergranular diffusion, but they also possess smaller grain-sizes that result in shorter intracrystalline diffusion paths. Deformation mechanisms favoured by a decrease in grain size are termed *grain-size sensitive*, which are invariably associated with diffusion creep processes. On the other hand, mechanisms that are independent of grain-size are referred to as *grain-size insensitive*, which are attributed to dislocation creep. The effect of the variation in grain-size on deformation may be demonstrated on a deformation mechanism map for olivine (Figure 1.14). Note that the strain rate

curves in the dislocation creep regime (blank shading) are horizontal, indicating negligible dependence of grain-size. In contrast, the strain rate curves in the diffusion creep regime (shaded) exhibit a strong dependence on grain size; at constant temperature, an order of magnitude decrease in grain-size results in greater than an order of magnitude increase in strain rate. By comparison, the two deformation mechanism maps in Figure 1.14 illustrate that the diffusion creep field expands with decreasing temperature (800 to 600°C) due to the smaller activation energy for diffusion creep relative to that for dislocation creep. Therefore, even though diffusive processes are enhanced at high temperatures, significant grain-size reduction of a rock deforming in the grain-size sensitive regime can induce a switch to grain-size sensitive creep even at low temperatures (Handy, 1988; Jaroslow *et al.* 1996).

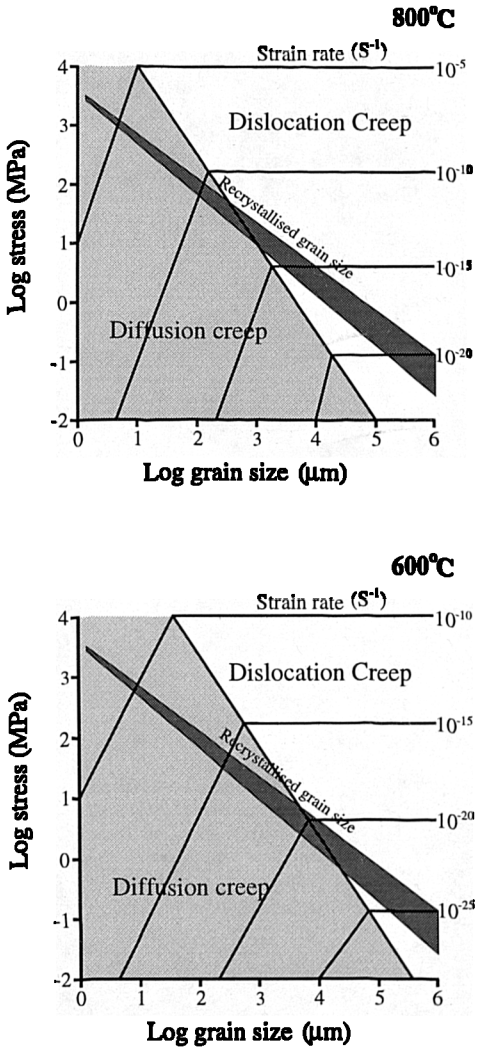

Figure 1.14. Deformation mechanism maps for olivine. Parameters and constitutive flow laws are presented in Rutter and Brodie (1988). Estimates for the dynamic recrystallised grain-size are derived from the piezometer used by Karato *et al.* (1986). Adapted from Rutter and Brodie (1988).

Experimental (e.g. Karato *et al.* 1986; Rutter and Brodie, 1988a) and theoretical (e.g. Rutter and Brodie, 1988b; Handy, 1989; Jaroslow *et al.* 1996) studies suggest rheological weakening and strain localisation in ductile shear zones are enhanced if grain-size reduction (either by cataclasis or recrystallisation) results in a transition to grain-size sensitive diffusion creep. Grain-size sensitive creep processes can accommodate large strains by viscous creep at constant stress, constant strain-rate, and at *constant microstructure* (i.e. *steady-state* flow). Furthermore, rocks deforming by grain-size sensitive creep accommodated by diffusion-assisted grain-boundary sliding will experience a significant increase in strain rate and can effect *superplastic flow*. Superplastic flow was initially described in metals, and refers to materials which can accommodate unusually large strains (c. 1000%) (Ashby and Verral, 1973).

In general, fabrics associated with grain-size insensitive (dislocation) creep are characterised by relatively coarse grain-sizes (>10-20μm) that possess microstructural evidence for recovery and dynamic recrystallisation. Such textures may display strong mineral and crystallographic preferred orientations, dislocation substructures indicative of high intragranular dislocation densities, and highly mobile, sutured grain boundaries. More tentatively, fabrics suggestive of grain size sensitive (diffusion) creep processes are characterised by weak to non-existant crystallographic preferred orientations and fine (<10μm), polygonal grains that possess low dislocation densities (e.g. Handy, 1989; Jaroslow *et al.* 1996).

1.4.2b. Control of fluids on deformation

In general, fluids have a strain softening effect on deforming rocks (Williams *et al.* 1994) for a number of reasons:

- Syn-tectonic metamorphic reactions in polyminerallic fault rocks can have a profound effect on rock strength. Fluids can induce the growth of transient reaction products and influence the rheology of a deforming rock in two ways (Brodie and Rutter, 1985): (a) the reaction products may be weaker or stronger than the pre-existing minerals that constitute the mineral assemblage. If the product(s) are less competent than the reactant(s), the new phase(s) may control the rheology of the deforming rock, and thus cause a *reaction softening* effect. For example, reactions involving fluids generally result in hydration, producing relatively incompetent sheet silicates; (b) a reaction product can act as a pinning-phase, inhibiting growth of the other mineral constituents during recrystallisation, thus facilitating the operation of grain-size sensitive deformation mechanisms (Brodie and Rutter, 1985).

- Fluids accelerate diffusive processes and thus increase the rate of diffusion-controlled deformation mechanisms.
- High pore-fluid pressures decrease the effective stress, enhancing deformation mechanisms such as frictional grain-boundary sliding, cataclasis and fracturing. Also, frictional grain-boundary sliding is facilitated by fluid-assisted diffusion, which accelerates the removal of asperities (Williams *et al.* 1994).
- Crack propagation may be facilitated by the presence of fluids in the crack tip, leading to weakening via sub-critical crack growth processes (Atkinson, 1982).
- The presence of water significantly weakens some minerals such as olivine (Karato *et al.* 1986). The reason for this weakening is not fully understood, but it is considered an intragranular process. Water weakening effects may be attributed to result from water-related defects diffusing through the crystal lattice (e.g. Hobbs, 1981), or to the development and subsequent healing of cracks to incorporate water into the crystal lattice (Rovetta and Holloway, 1986).

1.4.3. Kinematic indicators

Kinematic indicators are formed during non-coaxial strain and comprise a number of structures, microstructures and fabrics that have an asymmetry reflecting the sense of vorticity. To determine the shear sense on a fault, linear structures, which parallel the motion vector, must first be identified. The most common lineations include brittle fault striae, slickenfibres, and ductile mineral stretching lineations. Once the movement direction has been determined, the shear sense may be resolved by utilising the criteria listed below viewed in the plane normal to the shear plane and parallel to the movement vector. However, one must understand that no single shear sense criterion is totally reliable, therefore as many kinematic indicators as possible should be used in conjunction.

1.4.3a. Shear sense indicators - brittle regime

Sets of repeated, secondary brittle (Riedel) fractures which are oriented at an angle to the mean shear plane are invaluable as shear sense criteria, especially when there is an absence of offsets to determine relative movement sense. Figure 1.15 shows the labelling scheme adopted for fracture arrays after Logan *et al.* (1979). Each fracture intersects the slip plane approximately perpendicular to the slip direction.

This classification encompasses relative orientations of fractures, shears and related microstructural fabrics (e.g. mineral preferred orientation) and type (striated shear or non-striated tension fracture) following the work of Riedel (1929), Tchalenko,

(1970), Petit (1987) and Swanson (1988). However, due to the variable parameters that control fracture development and the Riedel angle - including the presence of pre-existing joints, physical properties of the fault rock and deformational conditions, e.g. strain rate, strain magnitudes and temperature (e.g. Moore *et al.* 1989; Moore and Byerlee, 1991) - one must appreciate that the *orientations* of these brittle shears are not always exclusive to any one shear sense. Therefore these structures must be classified by their relative displacement directions and timing before the terminology defined may be applied (Smith and Durney, 1992).

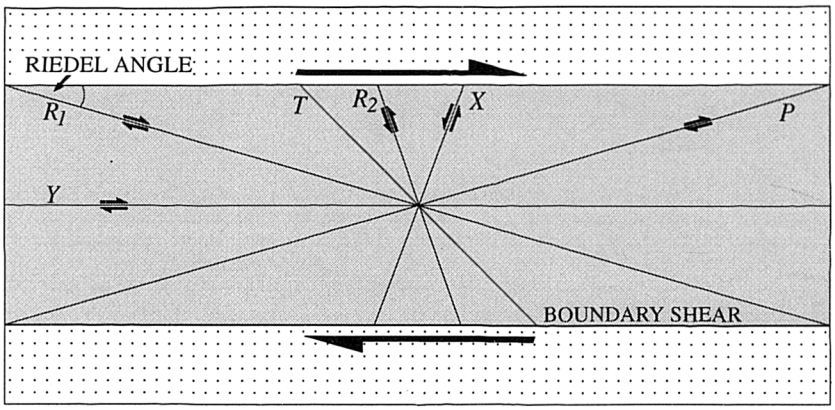

Figure 1.15. Labelling scheme for secondary (Riedel) fracture arrays after Logan *et al.* (1979). The acute angle made by the intersection of a secondary fracture and the trace of the boundary shear is referred to here as the "Riedel angle".

Field and experimental studies show that the most reliable kinematic indicators in brittle fault rocks are the sense of deflection of foliations (S) or synthetic *P*-shears near their intersection with R_1 shears, the obliquity of R_1 shears with respect boundary parallel, *Y* shears, and the sense of offset of *Y* shears by R_1 shears (Logan *et al.* 1979; Rutter *et al.* 1986; Hoogerduijn Strating and Vissers, 1994) (Figure 1.16).

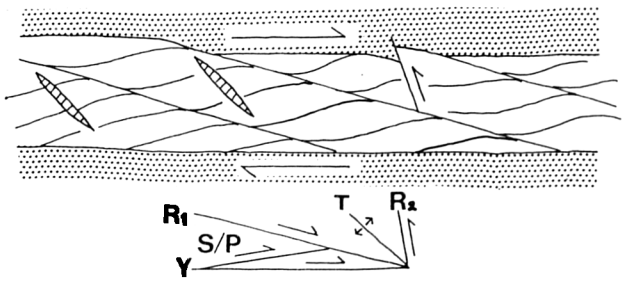

Figure 1.16. Geometrical relationships common in fault gouge. Note the deflection of foliations (S) and *P* shears into *Y* and R_1 synthetic shears, suggesting shear strains increase towards the latter.

The identification of localised deformation along secondary shear fractures has significant implications concerning the palaeoseismology of the host fault zone. Experimental studies (e.g. Moore *et al.* 1989; Moore and Byerlee, 1991) demonstrate that samples which possess a pervasive deformation fabric slide in a stable manner, whereas those containing secondary shears with relative large Riedel angles (>14°) generally exhibit stick-slip motion.

Shear sense criteria in serpentinite gouge

Serpentinised fault rocks commonly comprise cataclastic gouge dominated by oblique synthetic Riedel (R_1) shears and boundary parallel (Y) shears separating zones of massive, poorly foliated gouge (Hoogerduijn Strating and Vissers, 1994). Frequently R_1 shears have a sigmoidal shape which is attributed predominantly to local perturbations in the stress field near heterogeneities on Y or P shears. This geometry may be somewhat misleading as it is similar to the curvature of foliation and P shears into R_1 shears resulting from an opposing sense of shear (compare Figures 1.16 and 1.17). R_1 and P shears may curve asymptotically into Y shears and boundary faults, whilst R_1 shears often bend into parallelism with P shears. Also the sense of curvature of $R_1$and Y shears, and $R_1$and P shears is always opposite to the bending of foliations or P shears into Y shears.

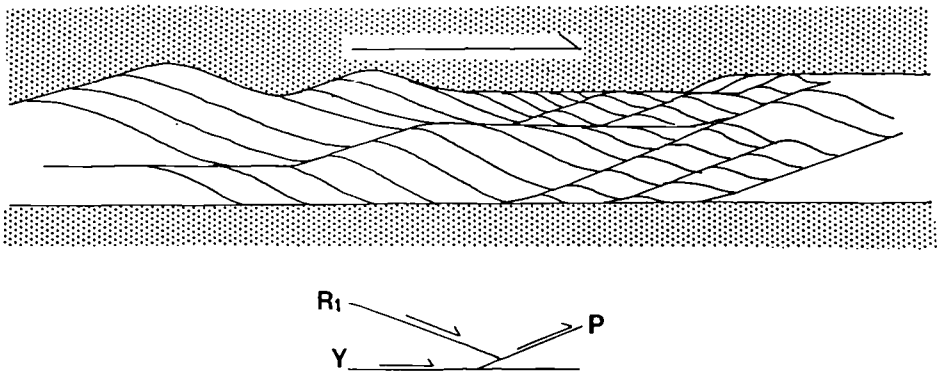

Figure 1.17. Hypothetical Riedel shear assemblage developed in serpentinite gouge (redrawn from Hoogerduijn Strating and Vissers, 1994) comprising R_1, P and Y shears. Note the sigmoidal geometry of R_1 shears between P and Y shears. The anticlockwise curvature of R_1 shears defining the sigmoidal lenses of gouge is opposite to the clockwise sense of curvature of cleavage and P shears against R_1 shears that define geometrical similar phacoids in Figure 1.17.

Another peculiarity in serpentinite deformational fabrics are Riedel angles. For example, the angle between R_1 and Y shears in naturally deformed serpentinite gouge is frequently greater than the 10-20° commonly observed in clay-rich gouges (e.g. Rutter *et al.* 1986; Tanaka, 1992), experimentally deformed serpentinite gouges (Moore *et al.* 1986), and values predicted from (Coulomb-Navier criterion) theory (8° for lizardite gouge and 17° for antigorite). The relatively high angles between R_1 and boundary faults may be indicative of unstable fault sliding behaviour (Moore *et al.* 1989; Moore and Byerlee, 1991).

Coaxial deformation

The above review concerns the case of non-coaxial deformation, principally simple shear, only. However, fracture arrays that form in response to *pure shear* display marked geometrical differences to those formed under simple shear. Pure shear characteristically produces conjugate sets of faults oriented symmetrically about the maximum and minimum compression directions (Figure 1.18). In the brittle regime, the maximum shortening direction commonly bisects the acute angle of the conjugate fault pair (Figure 1.18a). However, where conjugate fault zones are developed in the ductile regime, the angle bisected by maximum compression direction is often greater than 90° (Figure 1.18b; Ramsay, 1980; Casey, 1980)

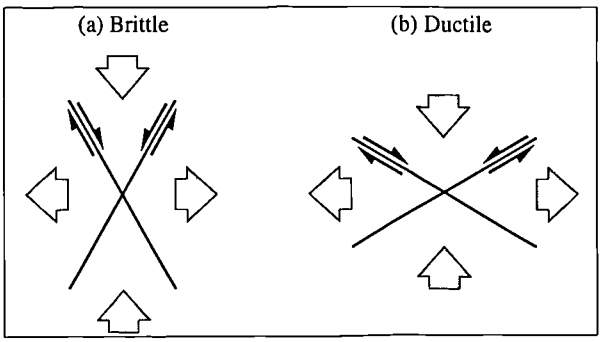

Figure 1.18. Hypothetical orientation of conjugate strike-slip faults formed during pure shear in brittle (a) and ductile (b) regimes.

1.4.3.b. Shear sense indicators - ductile regime

Following the review of Hanmer and Passchier (1991) four main groups of ductile (to brittle-ductile) kinematic indicators are cited:-

- Shape fabrics
- Porphyroclast systems
- Veins
- Folds

Shape Fabrics

Shape fabrics include the rotation and deflection of generated or pre-existing foliation associated with shear zones (Ramsay and Graham, 1970) (Figure 1.19); C/S fabrics (Berthé *et al.* 1979) (Figure 1.20); asymmetrical extensional shear bands (AESBs) (White *et al.* 1980) (Figure 1.21).

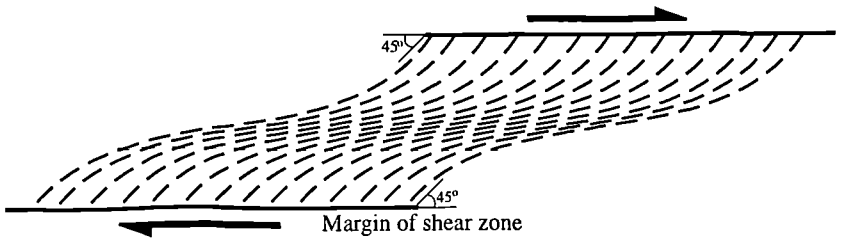

Figure 1.19. Shear zone geometry resulting from progressive simple shear. Schistosity originates at 45° to the shear zone boundary and rotates with increasing strain towards parallelism with the shear zone boundary (redrawn from Ramsay and Graham, 1970).

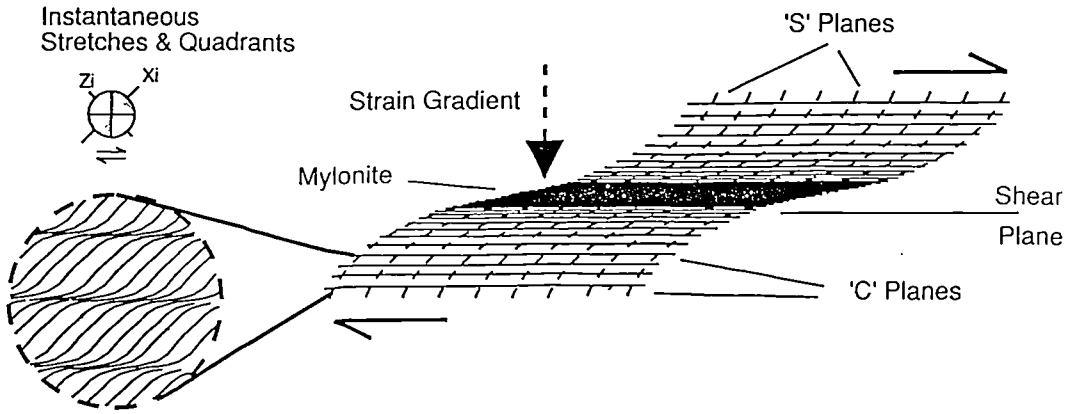

Figure 1.20. Idealised C/S fabric in a general non-coaxial flow. C-planes are discrete shear zones that parallel the bulk shear plane and are bound on either side by strain gradients. The rotation of both S- and C-planes into parallelism with the shear plane results from high finite strains (from Hanmer and Passchier, 1991).

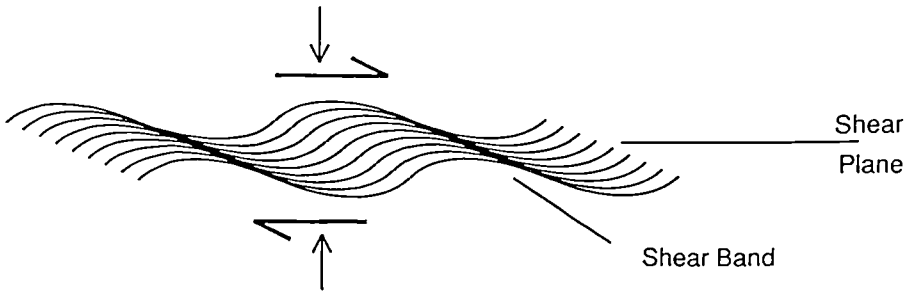

Figure 1.21. Asymmetrical extensional shear bands in a general non-coaxial flow. Note the obliquity between shear bands and the bulk shear plane (from Hanmer and Passchier, 1991).

C/S fabrics of Berthé *et al.* (1979) are composed of shear (Cisaillement) and cleavage (Schistosité) planes. C-planes are discrete shear zones up to tens of cm in length by a mm or more in thickness that tend to form in rocks where the distribution of strain is heterogeneous at the grain scale. S-planes are a flattening fabric that defines sigmoidal microlithons inbetween adjacent C-planes. S-planes are rotated into C-planes in the direction that reflects the sign of the vorticity (shear sense) of the flow.

AESBs have previously been termed shear band foliations (White *et al.* 1980), *C'* (Berthé *et al.* 1979b) and asymmetrical extensional crenulation cleavage (Platt and Vissers, 1980). They are discrete shear zones or 'shear bands' oriented between 15-25° to the bulk flow plane (Hanmer and Passchier, 1991) whose sense of slip is synthetic to the bulk shear sense. However, it is not uncommon for a conjugate, but numerically subordinate antithetic set to occur (Hanmer and Passchier, 1991; Behrman, 1987).

Porphyroclast systems

The geometry of rigid inclusions and their associated appendages resulting from progressive cataclasis or recrystallisation during non-coaxial deformation, may be used as a kinematic indicator. A porphyroclast system, viewed parallel to the rotation axis of the flow, most commonly comprises a monocrystalline core attached to thin, planar, polycrystalline, wing-like appendages referred to as 'tails', often directly derived by deformation of the host porphyroclast. However, inclusions may be polyminerallic themselves and tails may comprise deformed pressure shadows, reaction products or bands of matrix material entrained by the rotating inclusion, all of which extend along foliation planes in the direction of shear (Hanmer and Passchier, 1991). The internal symmetry of a porphyroclast system may be described with respect to a reference plane that passes through the centre of the porphyroclast and parallels foliation and the straight sections of the tails. Two types of porphyroclast systems may be defined using this criteria: σ- and δ-types (Passchier and Simpson, 1986) (Figure 1.22). In both types the 'median lines', which are centrelines drawn through the tails, step up in the direction of shear with respect to the reference plane. σ-type porphyroclast systems comprise a central porphyroclast and two wedge shaped appendages, which thin away from the porphyroclast parallel to the reference plane. δ-type porphyroclast systems, on the other hand, differ in that the tails are of approximately constant thickness and their median lines cross the reference plane adjacent to the porphyroclast. As a result the tails possess characteristic bends.

However, the behaviour of inclusions during shearing and their associated appendages is infinitely more complex than outlined above and additional complexities such as antithetic rotation must be considered (Figure 1.23). Thus, the application of

inclusion geometry in kinematic interpretation must be viewed with caution (Hanmer and Passchier, 1991).

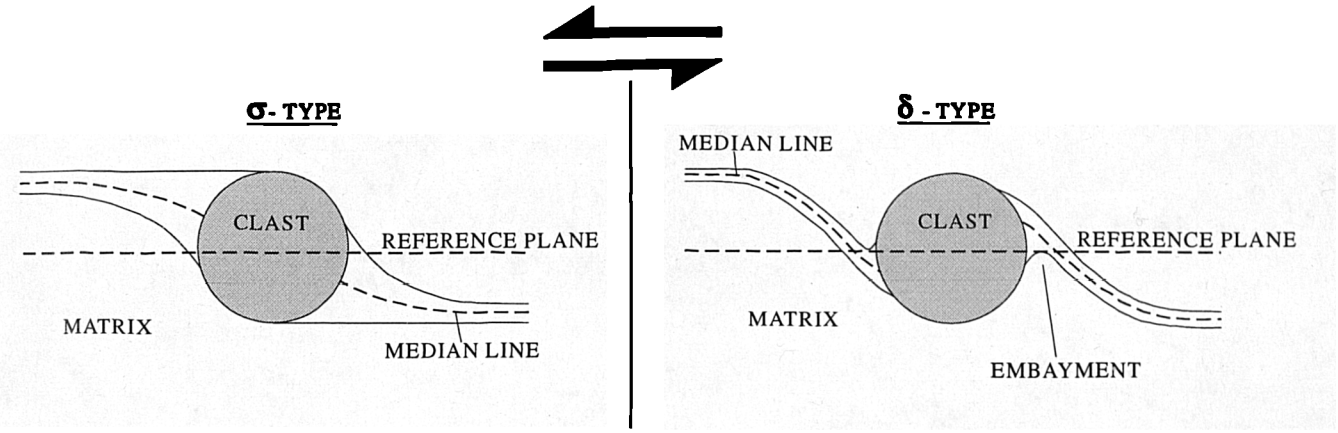

Figure 1.22 Geometries of σ- (a) and δ- (b) type porphyroclast systems in sinistral shear. Note that tails of both types step up to the left with respect to the trace of the reference plane (redrawn from Passchier and Simpson, 1986).

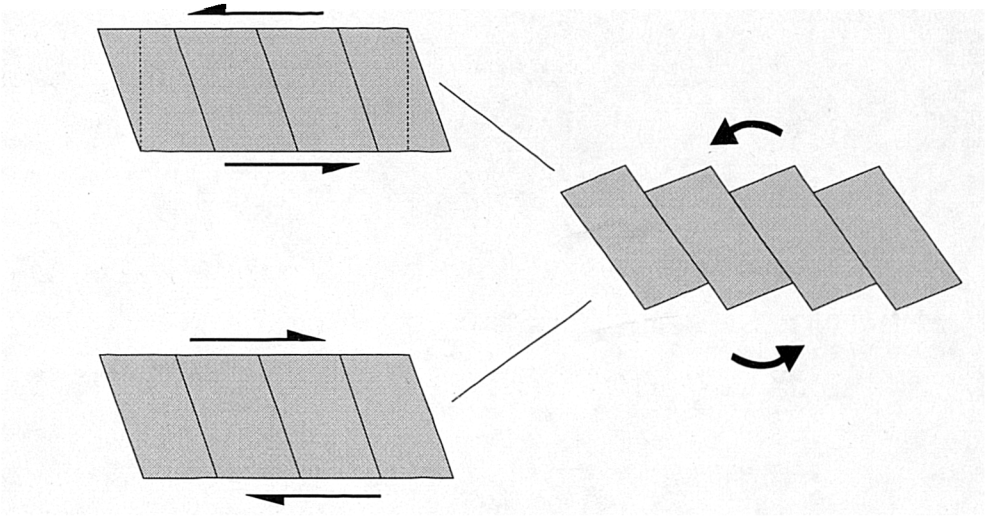

Figure 1.23. Back rotation of fault blocks (a) resulting from *dextral* shear may produce identical geometries as synthetically rotated blocks undergoing sinistral *shear*, and thus cannot be used as shear sense indicators (Hanmer and Passchier, 1991).

Veins

Veins and vein arrays within shear zones may be used to infer the orientation of the instantaneous and finite extensional strain axes. Thus by defining the extension direction one may determine the sense of shear. Figure 1.24 shows such an example; the propagating vein tips of en-echelon gash arrays parallel the minimum instantaneous stretching axis, whilst the mid-sections of each vein, which accumulate greater finite strain than the tips, rotate with the same sense as the vorticity of the flow during progressive deformation (Ramsay and Graham, 1970).

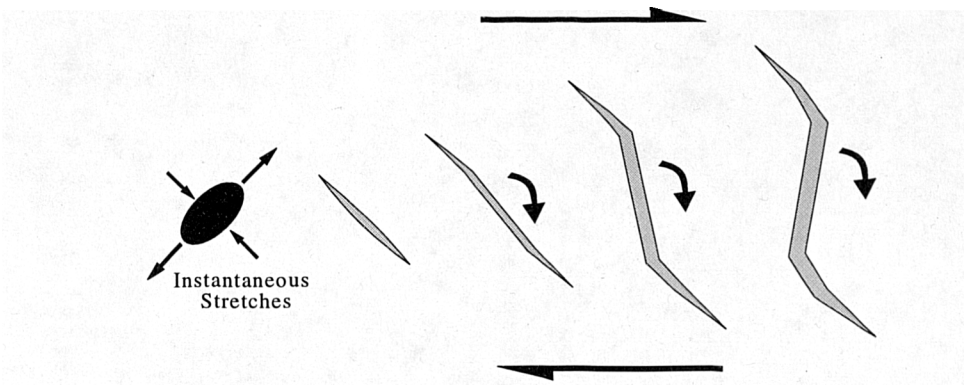

Figure 1.24. Chronology of sigmoidal tension gash development. The older dilational mid-sections of the veins rotate in the same sense as the bulk shear (redrawn from Hanmer and Passchier, 1991).

Fold asymmetry

Folds are dealt with last as they are considered the least reliable kinematic indicator. Fold asymmetry may result from non-coaxial deformation (Figure 1.25), but before shear sense may be inferred one of two conditions must be satisfied (Hanmer and Passchier, 1991): (1) the observed fold must be one of a number of contemporaneous folds that show regionally consistent asymmetry, and/or (2) the progressive development of the fold geometry is observable in the field and the rotation of planar structures results from shear-induced vorticity, which reflects the bulk shear sense.

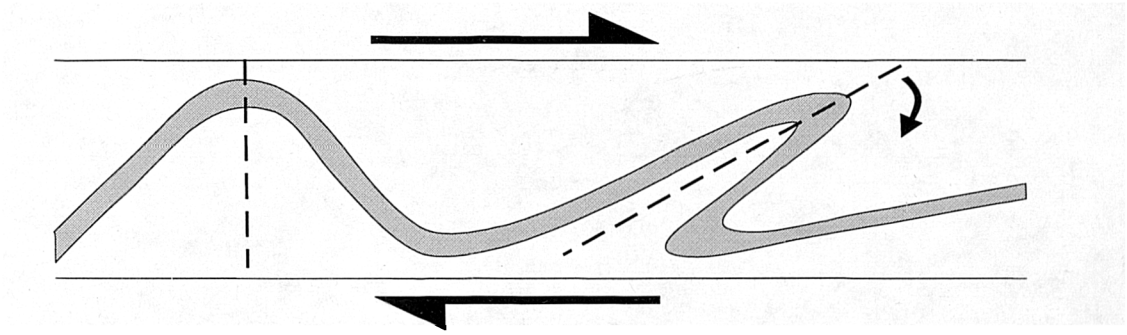

Figure 1.25. Asymmetric (*drag*) fold resulting from dextral shear. Planar constituents of the structure oriented at high angles to the shear direction, such as the fold axial plane and fold limbs, rotate with the same sense as the vorticity of the flow during progressive deformation.

1.4.4. Transpression

The term, transpression, as first defined by Harland (1971), was initially used to describe tectonic regimes that result from the oblique convergence of lithospheric plates. Harland's description, which was mainly conceptual, discussed many of the geometric and kinematic consequences of oblique plate motion. Harland's concept was redefined by Sanderson and Marchini (1984), who considered transpression specifically

as '...a wrench or transcurrent shear accompanied by horizontal shortening across, and vertical lengthening along, the shear plane' (Figure 1.26).

1.4.4a Modelling transpressional strains

Finite strain

In order to model finite transpressional strains, Sanderson and Marchini (1984) imposed a number of mathematically convenient boundary conditions, that were not implicit in Harland's original concept. In their model, they consider a constant volume homogeneous deformation in a vertical zone that is laterally and basally confined, such that the component of shortening across the zone is compensated exactly by vertical extension (Figure 1.26). By choosing to define a set of Cartesian axes with orientations parallel and perpendicular to the shear zone boundaries, Sanderson and Marchini (1984) developed a factorisation scheme in which bulk finite strain could be factorised in to two separate plane strain components; a pure shear shortening and a wrench simple shear.

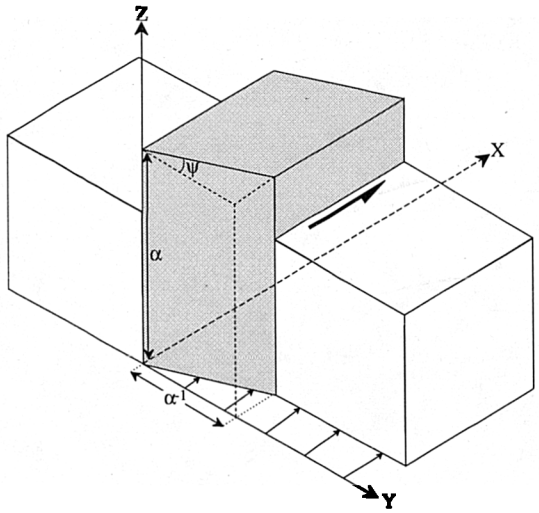

Figure 1.26. Simple homogeneous transpressional strain geometry, with Cartesian axes, after Sanderson and Marchini (1984). The deforming zone (stipple) represents the transformation of a unit cube by shortening parallel to the *Y*-axis, shear parallel to the *X*-axis, and extension parallel to the *Z*-axis, between two obliquely converging, rigid blocks (plates). α^{-1} specifies the shortening across the zone, α represents vertical stretch, γ is shear strain parallel to the zone, and ψ is the angular shear strain.

Instantaneous (or incremental, or infinitesimal) strain

More recent studies consider instantaneous strain as a more suitable quantity to model transpression than finite strain or stress. In the following discussion instantaneous strain axes are referred to as: $s_1 > s_2 > s_3$ (following Tikoff and Teyssier, 1994), which may be inversely correlated with stress, assuming steady-state deformation and rheology (i.e. s_1, s_2, s_3 correlate with σ_3, σ_2, σ_1; Weijermars, 1991; Teyssier *et al.*

1995). Table 1.1 lists the additional terminology and mathematical notations/abbreviations referred to in the text.

Mathematical notation	Description
λ_1, λ_2, and λ_3	Maximum, intermediate and minimum axes of the finite strain ellipse, respectively
α	Angle between the plate margin (or the deformation zone boundary) and the plate motion vector (Tikoff and Teyssier, 1994). Note that this is ***not*** equivalent to α of the Sanderson and Marchini (1984), which represents vertical stretch (see Figure 1.27).
θ	Angle between the plate margin and s_3 (Fossen and Tikoff, 1993)
W_k	The kinematic vorticity number

Table 1.1. Terms and abbreviations used in text.

By adopting the constraints of the Sanderson and Marchini (1984) model, McCoss (1986) proposed a simple geometrical construction that may be used to determine the relative magnitudes and orientations of the principal incremental strain axes. The McCoss construction permits the rapid determination of the orientation of the principal strain axes of the incremental sectional strain ellipse if the zone boundary displacement vector (S) is known, and vice versa (Figure 1.27) (refer to McCoss, 1986 for description of methodology).

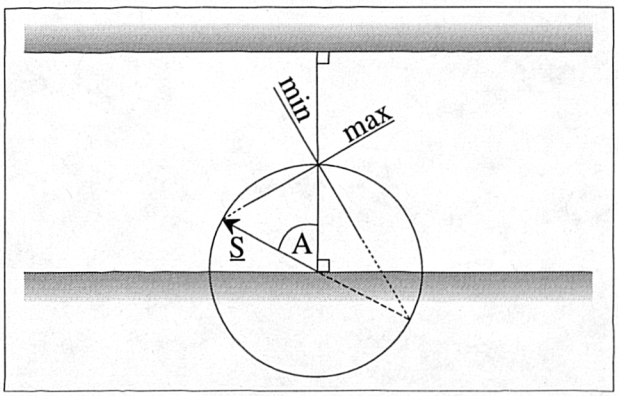

Figure 1.27. The geometrical configuration of McCoss (1986) for transpression that relates S, the angle between S and zone normal (A), and the orientations of the minimum and maximum principal strain axes of the incremental sectional strain ellipse.

By developing a deformation matrix for simultaneous simple and pure shearing, Fossen and Tikoff (1993) were able to predict unique states of strain for the geometry devised by Sanderson and Marchini (1984). Using a contoured logarithmic Flinn diagram (Figure 1.28), they demonstrated that transtensional deformation results in constrictional strain, whereas transpressional deformation results in flattening strain. This significant conclusion agrees with Sanderson and Marchini (1984), who predict S(L)-fabrics in transpressional zones, and L(S)-fabrics in transtensional zones.

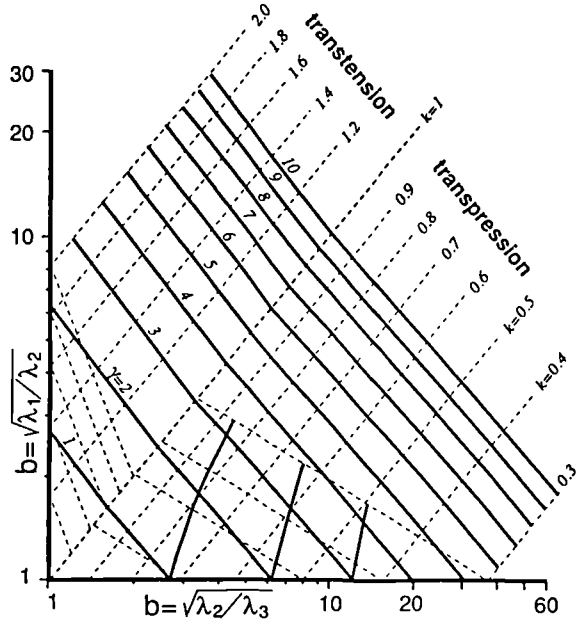

Figure 1.28. Logarithmic Flinn diagram contoured for γ (simple shear) and k (pure shear) values (from Fossen and Tikoff, 1993).

Pure shear-dominated and wrench-dominated transpression

Based on the orientation of the instantaneous stretching axes, Fossen and Tikoff (1993) defined two types of transpression: *wrench-dominated* and *pure shear-dominated* (Figure 1.29). In pure shear-dominated transpression, s_1 is vertical, while s_2 and s_3 lie in the horizontal plane, oblique to the shear (x-z) plane. Initially, the axes of the finite strain ellipsoid correspond to those of the instantaneous strain ellipsoid, but λ_2 and λ_3 progressively rotate to become parallel and perpendicular, respectively, to the shear plane at infinite strain. The difference in orientation between the finite and instantaneous strain axes is due only to the non-coaxial strain produced by the wrench component (Fossen and Tikoff, 1993; Teyssier *et al.* 1995). In contrast, during wrench-dominated transpression, s_3 and s_1 lie in the horizontal plane and oblique to the shear plane and, initially, λ_1 and λ_3 also lie in the horizontal plane. However, after a certain amount of deformation, which is dependent on the relative magnitudes of the pure shear and simple shear components (Tikoff and Teyssier, 1994), the finite strain ellipsoid records pure flattening, and eventually λ_1 switches with λ_2 and becomes

vertical (Figure 1.29b) (Fossen and Tikoff, 1993). This conclusion clearly emphasises the need to distinguish between wrench-dominated and pure shear-dominated transpression in field based kinematic analyses.

In order to distinguish quantitatively between wrench- and pure shear-dominated transpression, Fossen and Tikoff (1993) use the kinematic vorticity number (W_k), which describes the non-linear ratio of the pure and simple shear components. By 'mapping' the various combinations of the pure shear and simple shear components, Fossen and Tikoff (1993) determined the three-dimensional shape and orientation of the finite strain ellipsoid. They demonstrated that λ_1 switches with λ_2 at $W_k = 0.81$, which therefore represents the transition from pure shear- to wrench-dominated transpression. As the angle θ corresponds to a unique value of W_k (Figure 1.30), wrench-dominated transpression is defined when $1 > W_k > 0.81$ and $35° < \theta < 45°$, while for pure shear-dominated transpression $0.81 \geq W_k > 0$ (Fossen and Tikoff, 1993). Furthermore, Fossen and Tikoff (1994) derived a linear relationship between θ and α (Figure 1.31), which predicts the transition between pure shear- and wrench-dominated transpression occurs at an angle of convergence of 20°.

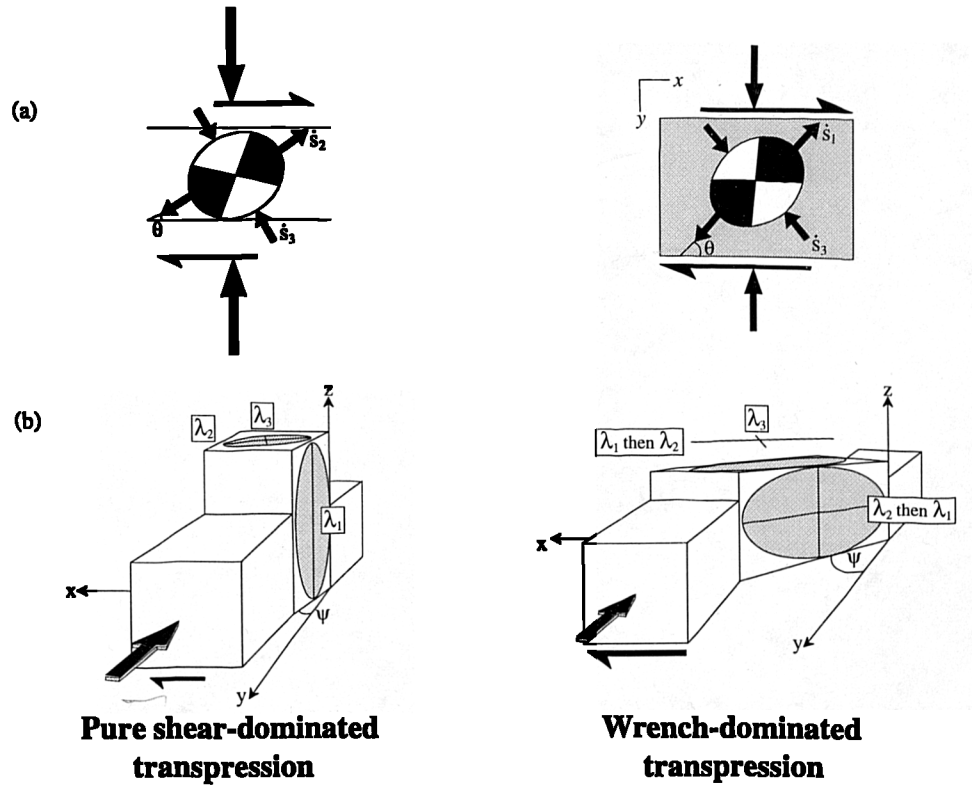

Figure 1.29. (a) Plan view of pure shear- and wrench-dominated transpressions distinguished by the orientation of instantaneous strain axes (after Tikoff and Teyssier, 1994).(b) Schematic block diagrams demonstrating the difference in the shape and orientation of the finite strain ellipsoid resulting from pure shear-dominated and wrench-dominated transpressions (after Tikoff and Teyssier, 1994).

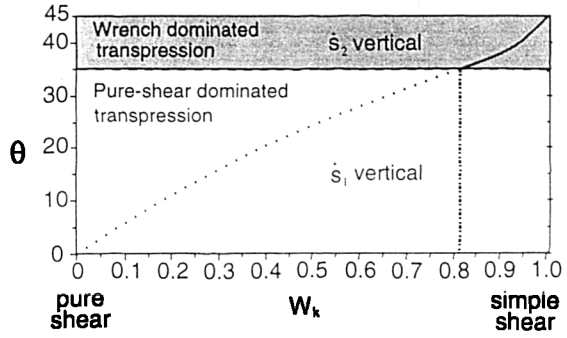

Figure 1.30. Relationship between W_k and the angle θ, showing the transition from pure shear- to wrench-dominated transpression at $W_k = 0.81$ and $\theta = 35°$ (from Tikoff and Teyssier, 1994).

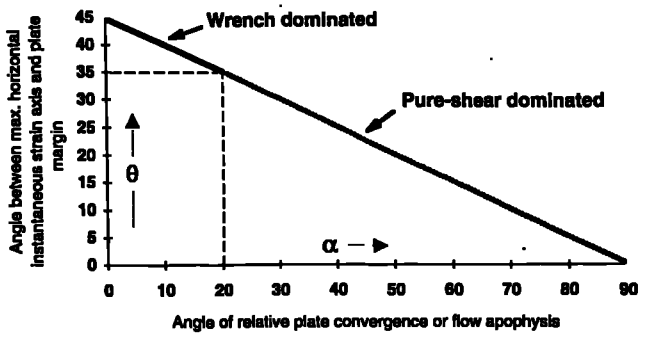

Figure 1.31. Relationship between the angle of plate convergence (α) and the angle θ, showing the transition between wrench-dominated and pure shear-dominated transpression occurs at $\alpha = 20°$ (from Tikoff and Teyssier, 1994).

Strain partitioning

In regions undergoing transpression, deformation is commonly partitioned into its strike-slip (simple shear) and contractional (pure shear) components (e.g. Oldow *et al.* 1990; Holdsworth and Strachan, 1991; Fossen *et al.* 1994; Tikoff and Teyssier, 1994; Teyssier *et al.* 1995; Jones and Tanner, 1995). In particular, the strike-slip component is often partially or wholly partitioned into discrete narrow zones dominated by simple shear, which delineate broader zones of distributed, largely coaxial deformation. Most significantly, an increase in the degree of strike-slip partitioning along localised fault zones results in an increased amount of compression (pure shear) in the diffuse zone of deformation. Therefore, with an increase in the amount of partitioning of the simple shear component, s_3 becomes increasingly orthogonal to the fault zone (Teyssier *et al.* 1995). By using a partitioning model for transpression, Tikoff and Teyssier (1994) provide a method to approximate the degree of strike-slip partitioning using the relative orientations of the plate motion vector and the maximum instantaneous shortening direction (s_3) (Figure 1.32). They concluded that kinematic partitioning is primarily controlled by relative plate motion, rather than by mechanical decoupling

generated by fault weakness, as proposed by previous authors (e.g. Zoback *et al.* 1987; Rice, 1992).

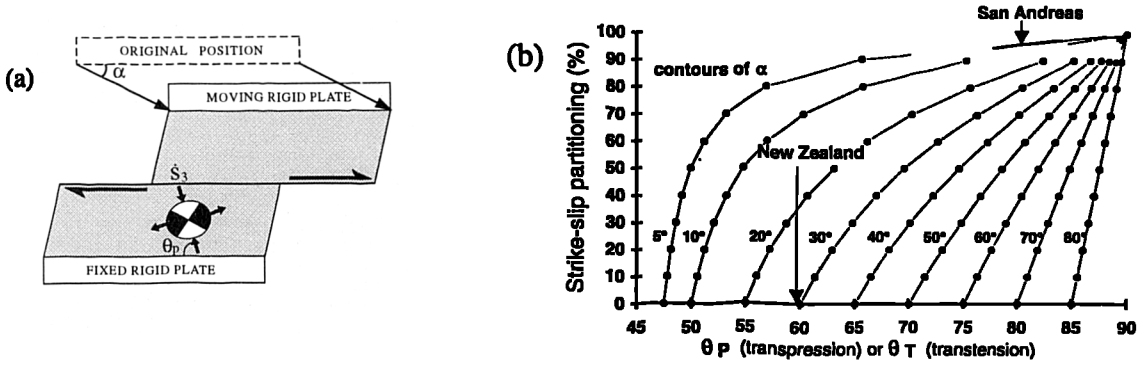

Figure 1.32. (a) Plan view of the deforming zone (grey) for strike-slip partitioned transpression. (b) Contoured graphical relationships between the angle of relative plate motion (contours of $\alpha = 5°$ to 80°), the orientations of s_3 and s_1 for transpression (θp), and the degree of strike-slip partitioning. San Andreas and New Zealand refer to examples of wrench- and pure shear-dominated transpressional faults, respectively (from Teyssier *et al.* 1995).

1.5. Nomenclature of peridotitic rocks and textures

Numerous classification schemes have been proposed to describe variably deformed and recrystallised textures preserved in peridotite xenoliths associated with kimberlites (Boullier and Nicolas, 1975) and basalts (Mercier and Nicolas, 1975; Pike and Schwarzman, 1976; Harte, 1977). Due to the similarity with fabrics observed on the seafloor and in ultramafic sections of ophiolitic complexes (Nicolas *et al.* 1980), these schemes are readily applied to peridotites from various tectonic environments. As there is a discrepancy between the conditions responsible for the formation of peridotite fabrics in these different settings, the proposed classifications place emphasis on descriptive rather than genetic elements. However, different schemes were produced in parallel, causing confusion in the literature. Therefore, for the sake of brevity and relevance to the present study, the textural terminology adopted in this work is taken from a number of publications. The principal textural types described are: *coarse granular*, *porphyroclastic*, *mylonitic* and *fluidal*, which are placed in order of increasing strain. Also, two subtypes, *equidimensional mosaic* and *equidimensional tabular*, are defined, which are used to describe the matrix fabric. For comparison, all four types and two sub-types are shown in Figure 1.33.

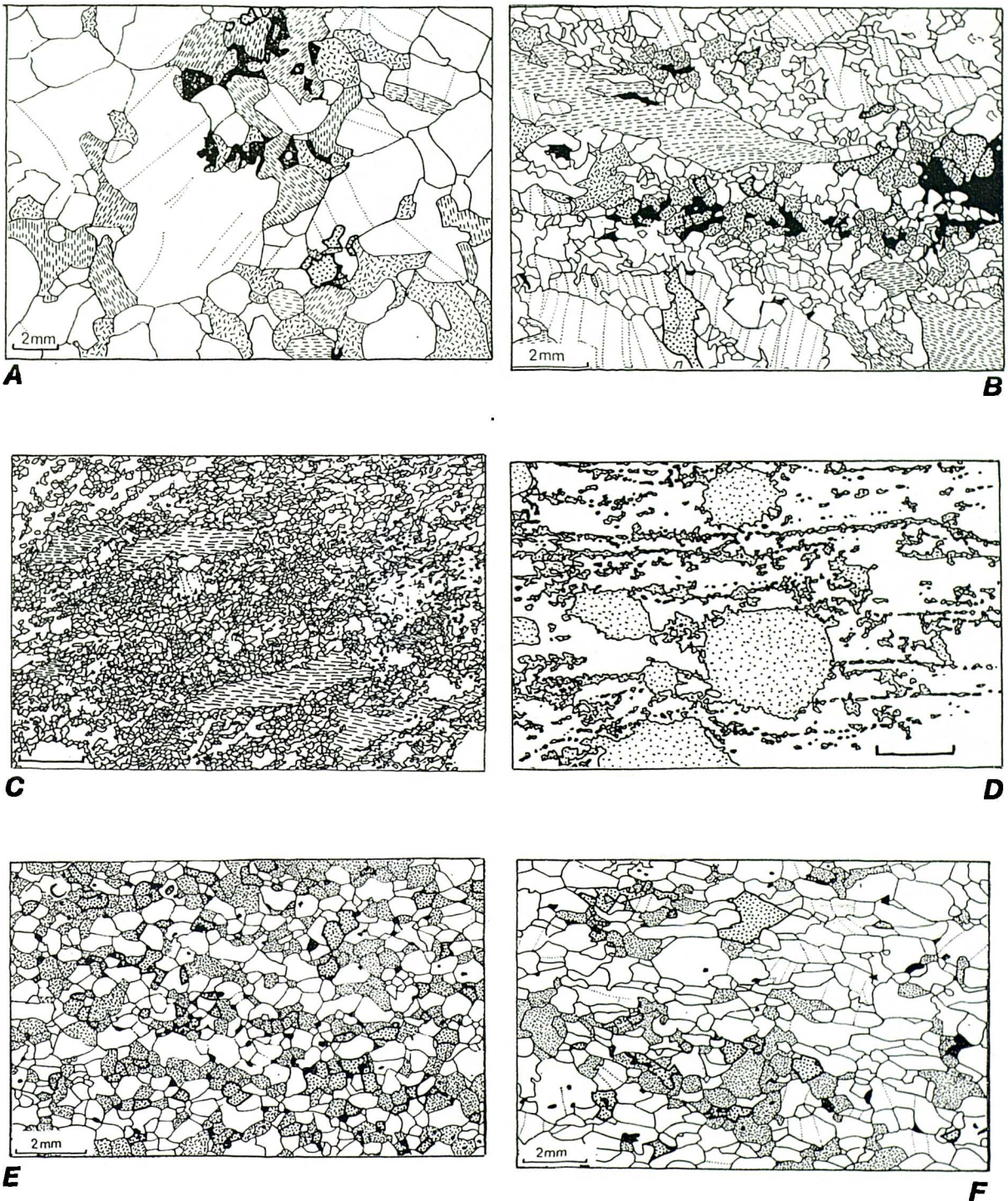

Figure 1.33. Classification of peridotite textures. A. Coarse granular texture; olivine: blank, except for dotted lines that represent kink-band boundaries. Orthopyroxene: dashes aligned parallel to the (100) plane. Clinopyroxene: random dashes. Spinel: black (from Mercier and Nicolas, 1975). B. Porphyroclastic texture. Shading scheme as above (from Mercier and Nicolas, 1975). C. Mylonitic texture. Note the more intense recrystallisation than B (redrawn from Girardeau and Mercier, 1988). D Fluidal microstructure. Olivine: blank and completely recrystallised. Orthopyroxene: dotted. (Redrawn from Mercier, 1979). E and F. Equigranular mosaic and equigranular tabular respectively. Shading scheme is the same as that used in A and B (from Mercier and Nicolas, 1975).

Coarse-granular (Figure 1.33A) (Boullier and Nicolas, 1975; or *protogranular* of Mercier and Nicolas, 1975; or *coarse* of Harte, 1977) Coarse-granular is the term used to describe a coarse-grained (2-4mm) rock that is free of porphyroclasts. These fabrics are the oldest recorded in xenoliths and are thus considered essentially pre-deformational. Crystallographic fabrics are weak, silicates show no flattening or elongation, and the rocks are devoid of any foliation or lineation. However, the constituent silicate phases may display minor deformational characteristics, such a kink banding in olivine and occasional recrystallisation along grain boundaries, which may be straight, curvilinear or slightly irregular.

Porphyroclastic (Figure 1.33B) (Boullier and Nicolas, 1975; Mercier and Nicolas, 1975; Pike and Schwarzman, 1976; Harte, 1977; Nicolas *et al.* 1980; Mercier, 1985). A rock ceases to be coarse-granular and becomes porphyroclastic at the appearance of porphyroclasts (Harte, 1977). A porphyroclast is defined as a relatively large, relict, strained grain, which is completely surrounded by significantly smaller, recrystallised, strain-free grains (neoblasts). Porphyroclastic textures are characterised by a weak foliation and/or lineation and by variably strained and kinked porphyroclasts, predominantly of pyroxene, which commonly display strong crystallographic fabrics and minor elongations. Spinel may define a lineation and characteristically possesses a 'holly-leaf' shape, which is interpreted as evidence of post-kinematic growth (Mercier and Nicolas, 1975).

Mylonitic (Figure 1.33C) fabrics are rarely described in textural classifications of xenoliths and, therefore, the transition from a porphyroclastic to a mylonitic fabrics is arbitrary. Mylonitic textures possess a strong lineation and/or foliation marked by elongate pyroxenes. They are characterised by pervasive recrystallisation, smaller matrix grain size (<0.1mm), and the presence of several generations of paleoblasts (old, strained grains) and neoblasts indicative of dynamic recrsytallisation. Olivine is normally completely recrystallised into fine-grained neoblasts, which have a heterogeneous grain size distribution (Nicolas *et al.* 1980). Evidence suggests that strong cooling is often concurrent with deformation for this textural type, as observed in lherzolite massifs and obducted ophiolites, but is not a necessary condition for their formation (Mercier, 1985).

Fluidal (Figure 1.33D) (or fluidal-mosaic type of Boullier and Nicolas, 1975; Boullier and Guegen , 1975; Harte, 1977; Mercier, 1985). The term 'fluidal' is applied to a specific mylonitic texture in which thin (<0.03mm) lamellae of intensely recrystallised, monominerallic material (<0.01mm) define a discontinuous foliation that are connected with porphyroclasts of the same material. The matrix is also very fine-grained (<0.01mm) and predominantly displays an 'equigranular mosaic' texture (see below). Fluidal microstructures are interpreted as results of very high strains

(>1000%) and are invariably correlated with superplasticity (Boullier and Nicolas, 1975; Boullier and Guegen , 1975; Drury *et al.* 1990).

Equigranular (Figures 1.33E and 1.33F) (Mercier and Nicolas, 1975; equidimensional mosaic of Pike and Schwarzman, 1976; Harte, 1977; Mercier, 1985). Equigranular textures are considered a separate type in xenoliths, but only a sub-type in this classification as they are only ever observed as a matrix fabric in high strain fabrics in this study. *Equigranular mosaic* (Figure 1.33E) is used to describe a fine, grained (<0.7mm) texture, in which all three silicate phases, olivine, enstatite and diopside, are equidimensional, of relatively constant grain size, and in which crystallographic fabrics are weak. Grain boundaries are commonly straight and converge at triple points, defining a polygonal texture. *Equigranular tabular* (Figure 1.33F) textures (Mercier and Nicolas, 1975; Harte, 1977) are also fine-grained, but differ in that they are characterised by parallel, tabular, silicate grains that define a foliation and occasionally a weak mineral lineation. Equigranular textures in xenoliths occasionally overprint porphyroclastic textures with increasing strain and are thus interpreted as the result of complete recrystallisation.

1.6. Layout of thesis

This thesis is primarily a structural and geochemical study of the serpentinite-filled faults that mark an oceanic, microplate suture zone in SW Cyprus.

- Chapter 2: geology of Cyprus and the stratigraphical terminology used, with particular reference to SW Cyprus.
- Chapter 3: geochemistry of fault zone peridotites using analyses of chrome-spinel chemistries.
- Chapter 4: field observations and structural interpretation for the 'Southern Region' of SW Cyprus. Particular attention is paid to three sets of fabrics and associated structures: initial high temperature, intermediate, and later low temperature events; all are associated with strike-slip deformation.
- Chapter 5: field observations and structural evolution of the 'Northern Region' of SW Cyprus. Reference is made to compressional tectonics.
- Chapter 6: general discussion of findings and summary of the geological evolution of SW Cyprus and implications for Cyprus.

CHAPTER TWO
PREVIOUS WORK: THE GEOLOGY OF SOUTHWEST CYPRUS.

2.1. The regional setting of Cyprus

Cyprus is a small island located in the eastern Mediterranean, 75km south of Turkey and 105km west of Syria (Figure 2.1). It covers an area of 9,250 km^2 and reaches a maximum height of 1951m at Mount Olympus in the Troodos massif. The area studied is located in the southwest and west of the island.

In Permo-Triassic palinspastic reconstructions (Wegener, 1994; Gass *et al.* 1994 and references therein), a wedge-shaped ocean, named the 'Tethys Ocean', is thought to have existed between the super-continents of Gondwanaland and Laurasia (Figure 2.2). The evolution of this ocean is divided into a Palaeozoic 'Palaeotethys', and a Mesozoic 'Neotethys'. During the Upper Permian to Triassic, continental fragments were rifted from the southern margin of Eurasia to form the Cimmerian continent (e.g. Sengör *et al.* 1984). To the SW of this continent Triassic rifting is thought to have produced Neotethys, whilst subduction beneath Eurasia consumed Palaeotethys. It is within the Neotethyan Ocean, that a number of Triassic (e.g. the Pindos and Vardar; Spray *et al.* 1984) and later Cretaceous (e.g. Baer Bassit, Hatay, Oman) oceanic complexes, including those preserved in Cyprus, were created (e.g. Robertson, 1990).

Figure 2.1. Present-day setting of Cyprus within the Eastern Mediterranean.

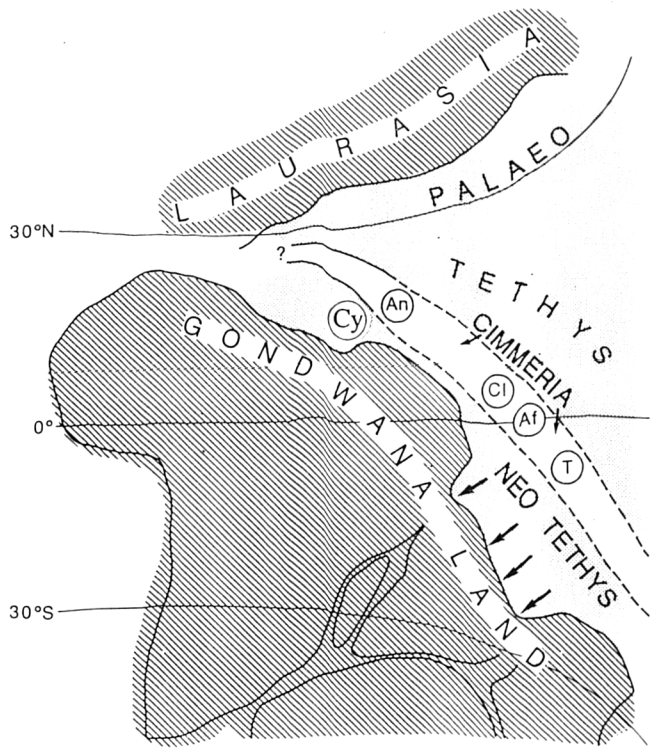

Figure 2.2. Late Triassic palaeogeographic setting of Palaeo- and Neotethys and the Cimmeria continent. An - Anatolia, CI - Central Iran, Af - Afghanistan, T - Tibet, and Cy - hypothetical location of Cyprus. Taken from Gass *et al.* (1994).

2.2. Introduction: The geological sub-division of Cyprus

Cyprus can be divided into five geologically distinct areas (Figure 2.3). These are: (1) The Troodos massif; (2) the South Troodos Transform Fault Zone (STTFZ); (3) the Kyrenia Range, (also known as the Pentadaktylos Range); (4) the Mesaoria Plain, and; (5) SW Cyprus.

2.2.1 The Troodos massif

The Troodos massif is situated in the centre of the island (Figure 2.3) and is approximately 3000km^2 in area. It consists of Upper Cretaceous ultramafic and mafic rocks (see below), which are referred to as the *Troodos Complex,* after Gass (1968). In the following text, the term 'massif' is used in a geographical context to describe the central part of the island, which comprises Upper Cretaceous rocks of the 'Troodos Complex'. Due to differential uplift centred on Mt. Olympus, the massif has been 'up-domed' to form a large, eroded anticline (Figure 2.4). The resulting concentric

outcrop pattern exposes the deepest levels of the crust and upper mantle at the highest topographic levels, whilst the stratigraphically highest, extrusive and sedimentary units crop out at the periphery of the massif (Figure 2.4; Wilson, 1959).

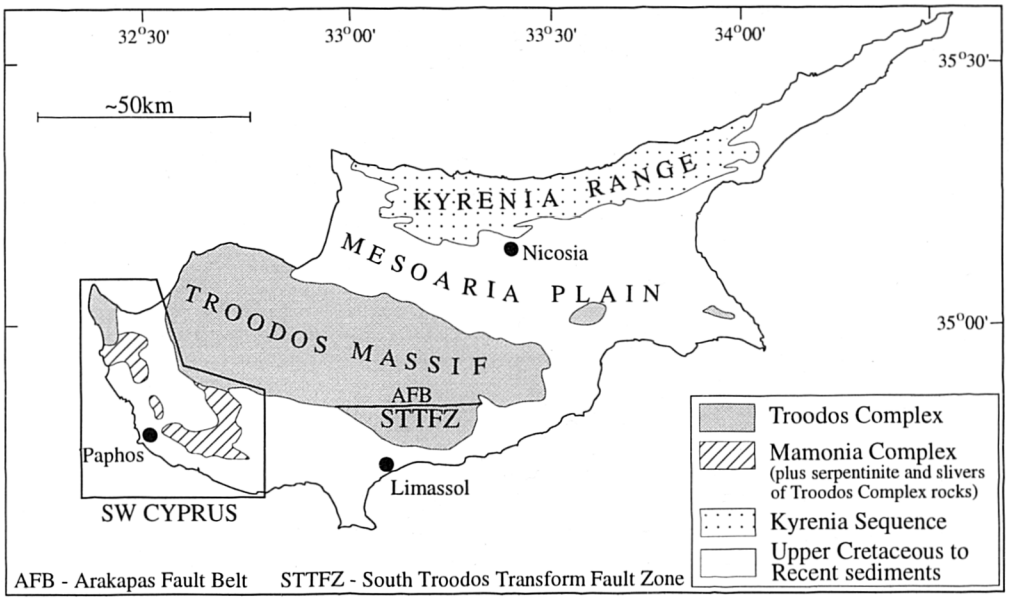

Figure 2.3. Location of the geologically distinct areas in Cyprus.

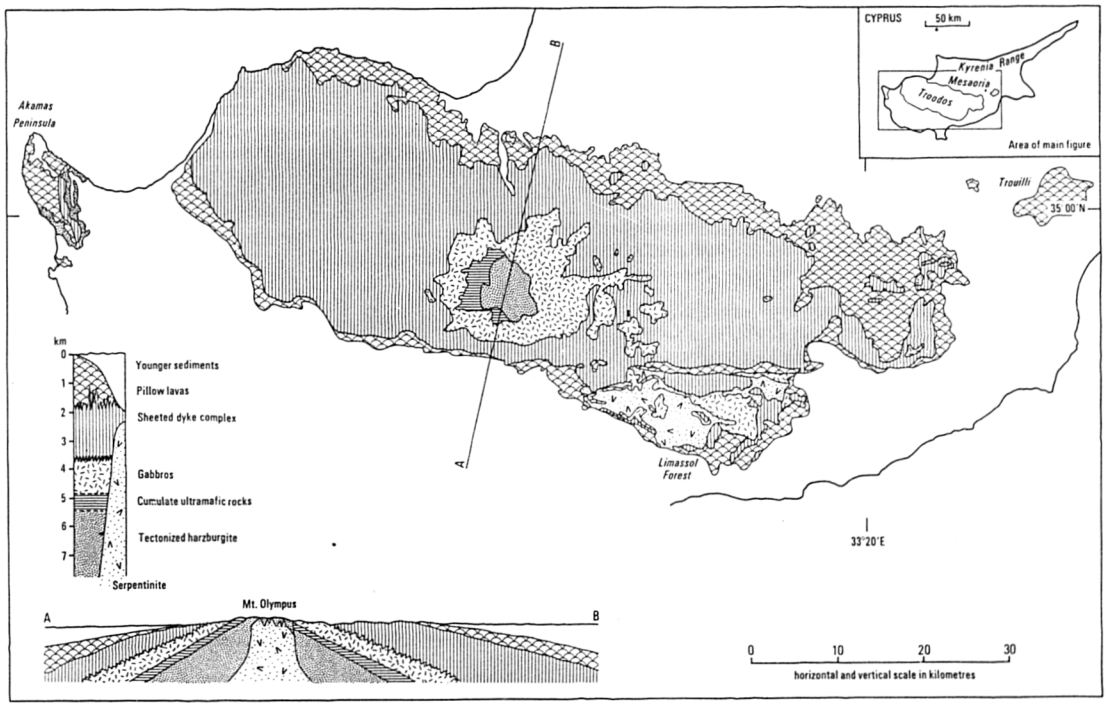

Figure 2.4. Geological map, schematic cross-section and stratigraphic sequence of the Troodos massif (from Gass, 1980).

Following the advent of plate tectonic theory and the hypothesis of sea-floor spreading (Dietz, 1961; Hess, 1962; Vine and Matthews, 1963), Gass (1968) proposed that the Troodos Complex represents a remnant of oceanic crust formed at a spreading ridge. Gass's proposal was primarily based on the structure of a sheeted dyke complex (see below) exposed in the massif, which was later supported by Moores and Vine (1971) who stated (concerning the dyke complex) "100% dykes imply....100km of extension in 100km of exposure". The only possible mechanism which has been proposed to account for such extension is seafloor spreading.

Subsequent to the definition of the term 'ophiolite' at the Geological Society of America's Penrose Conference (Anon, 1972), the rocks of the Troodos Complex were considered to represent a complete ophiolitic section as they comprise a 'distinctive assemblage of mafic and ultramafic rocks occurring in the following sequence, from base to top: ultramafic complex; gabbroic complex; mafic sheeted dyke complex, and; mafic volcanic complex' (Figures 2.4 and 2.5). Since its formation, the ophiolitic stratigraphy of the Troodos Complex has been blanketed by Upper Cretaceous to Recent sediments.

Based on geochemical evidence and analogy with other Tethyan ophiolites in the Eastern Mediterranean, the Troodos Complex formed by seafloor spreading above an intra-oceanic subduction zone within Neotethys (e.g. Pearce, 1975; Pearce *et al.* 1984) during Cenomanian to Turonian times (c. 92-90Ma; Blome and Irwin, 1985; Staudigel *et al.* 1986; Mukasa and Ludden, 1987). Whether the subduction zone dipped to the north (e.g.Macleod *et al.* 1992) or to the south (e.g. Taylor, 1990) is uncertain, but due to similarities with other Neotethyan ophiolites, Troodos was most probably underlain by a northward-dipping subduction zone (Robertson and Xenophontos, 1993; Gass *et al.* 1994).

Interpretation of gravity surveys (Gass and Masson-Smith, 1963) suggest that the Troodos Complex is approximately 20km thick and is underlain by about 10km of attenuated continental crust (Figure 2.6a). Gass and Masson-Smith (1963) proposed the uplift of Troodos occurred in response to the attempted subduction of thinned African continental crust (Figure 2.6b). However, as suggested by Murton (1986), this continental material may belong to either the North African *or* to the Eurasian continental margin. Unlike other Tethyan ophiolites, Troodos appears to be essentially *autochthonous*, i.e. it does not possess an obduction-related metamorphic aureole and it is not internally dismembered by imbricate thrust sheets as was previously proposed (e.g. Lapierre and Rocci, 1967; Biju-Duval *et al.* 1976).

Palaeomagnetic studies (Moores and Vine, 1971; Clube *et al.* 1985; Clube and Robertson, 1986) indicate a westerly-directed remnence vector in the Troodos lavas, which suggests Troodos has rotated 90° anticlockwise subsequent to its formation.

Therefore, the spreading direction was originally in a north-south orientation, which is identical to that proposed for Syrian and Turkish ophiolites (Gass, 1968; Whitechurch *et al.* 1984). Clube *et al.* (1985) demonstrate that approximately 60° of the rotation took place during Campanian-Maastrichtian times, with the rest of the rotation accommodated by the Lower Eocene.

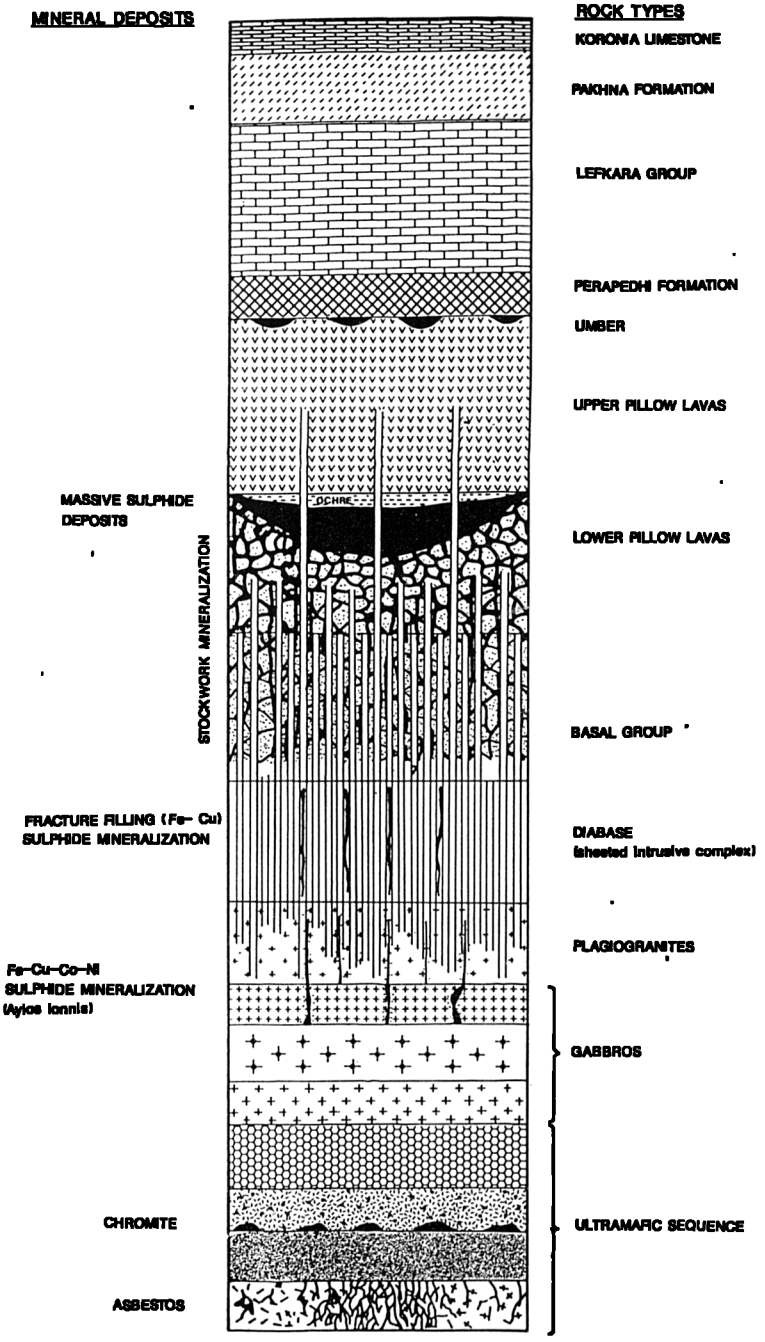

Figure 2.5. Ophiolitic stratigraphy of the Troodos Complex (after Constantinou, 1980).

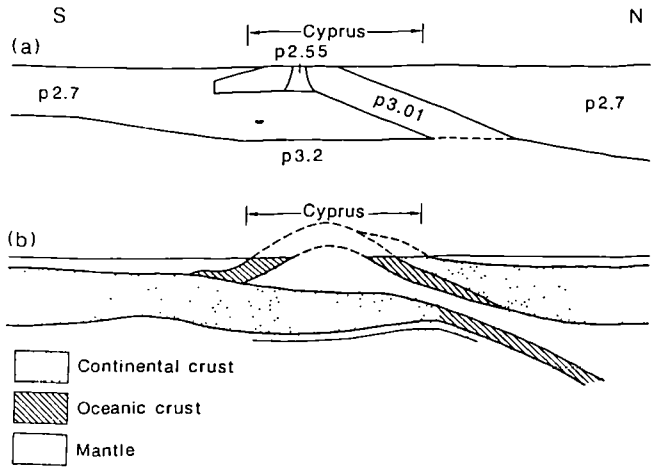

Figure 2.6. Interpretative N-S cross-section through Cyprus based on gravity data (from Gass *et al.* 1994; after Gass and Masson-Smith, 1963).

2.2.2. South Troodos Transform Fault Zone (STTFZ)

To the south and southeast of the Troodos massif is an area of disrupted ophiolitic material, which is separated from the more coherent ophiolite by an east-west striking fault, referred to as the 'Arakapas Fault Belt' (AFB) after Simonian (1975) (Figures 2.3 and 2.7). North of the fault, over a distance of 5-10km, the N-S orientation of the sheeted dyke complex in the Troodos massif progressively swings through NE-SW to E-W as the fault is approached (Figure 2.7; Wilson, 1959; Moores and Vine, 1971; Simonian, 1975; Simonian and Gass, 1978). Based on palaeomagnetic studies, the swing in trend of the dykes is attributed to the anticlockwise rotation of the Troodos massif (see above) and 'drag' along the AFB (specifically the transform fault zone to the south, see below) subsequent their formation (e.g. Clube *et al.* 1985; Clube and Robertson, 1986; Bonhommet *et al.* 1988). The fault is a site of intense brecciation of the oceanic crust and characterised by overlying volcanic rocks and clastic sediments that were not previously recognised in the Troodos massif (Moores and Vine, 1971; Simonian and Gass, 1978). Although Bear (1958) first reported the strike-slip character of the fault, it was Moores and Vine (1971) who suggested that the series of intercalated lavas and breccias were evidence for the AFB being part of a fossil oceanic fracture zone. This idea was supported by Simonian and Gass (1978), who proposed the fault was the northern margin to an east-west trending oceanic fracture zone and that the area to the south of the fault (the Limassol Forest Complex) was part of the same fossil, transform domain.

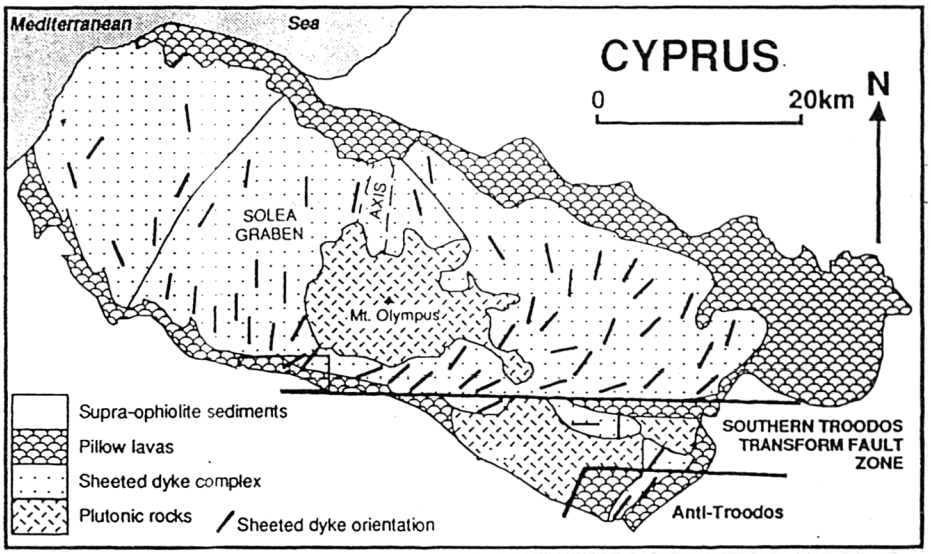

Figure 2.7. Simplified geological map of the Troodos massif, the STTFZ, and the 'Anti-Troodos' crust. Note the swing in dyke orientations in the Troodos massif with increasing proximity to the STTFZ (from MacLeod and Murton, 1993).

Detailed mapping (e.g. Murton, 1986, 1990; MacLeod, 1988, 1990; Gass *et al.* 1994) has confirmed many earlier observations, and the AFB and the Limassol Forest Complex, collectively termed the South Troodos Transform Fault zone (STTFZ), is now accepted as a major oceanic strike-slip fault zone (e.g. Murton, 1986, 1990; Macleod, 1988, 1990; Macleod and Murton, 1993, 1995). Following detailed mapping of the eastern Limassol Forest Complex, Macleod (1988, 1990) constrained the transform to at least 5km in width and discovered a fragment (~50km$^{2)}$ of *'Anti-Troodos'* crust in the southernmost exposures, which is thought to have formed at a ridge on the opposite side of the STTFZ to the main Troodos massif (Figure 2.7).

Although numerous models were proposed explaining the evolution of the STTFZ and the Troodos Complex (e.g. Murton, 1986, 1990; Macleod, 1988, 1990), the kinematic history of the transform remained a point of controversy. Both dextral and sinistral kinematic indicators have been identified throughout the STTFZ in mafic and ultramafic mylonites and in later serpentinite shear zones, which led numerous authors to suggest the transform must have reversed its sense of slip by means of ridge-jumping (e.g. Allerton and Vine, 1991; MacLeod *et al.* 1992). However, most recent studies (MacLeod and Murton, 1993, 1995) suggest the transform fault experienced regional *dextral* strike-slip displacement, whilst minor sinistral shear zones were associated with the local intrusion of mafic igneous bodies.

Using trace element geochemical analyses, Cameron (1985) recognised the lavas of the STTFZ possess a chemistry distinct from those of the main Troodos massif (Malpas *et al.* 1993). These lavas are distinguished by their extreme depletion in

HFSE and their high Mg and Si contents (i.e. suggesting a *boninitic* affinity), and are considered characteristic of the magmatism within the transform.

2.2.3. The Kyrenia Range

The Kyrenia Range (Figure 2.3) is an east-west trending, slightly arcuate, mountain range, located along the northern margin of the island. The geology of the range is dominated by thick bedded limestones and dolomites, which range in age from Permian to early Cretaceous (Moore, 1960; Ducloz, 1972). Maastrichtian sediments unconformably overlie the limestones and are interstratified with calc-alkaline volcanics (Baroz *et al.* 1980). Conglomerates, sandstones and siltstones were deposited in the mid-Miocene towards the north and south to form the Kythrea Flysch (Cleintaur *et al.* 1977). Other sediments documented in the Kyrenia Range include tectonised sandstones, *Holobia*-bearing limestones and cherts, which are all probably Mesozoic in age. Metamorphics and serpentinites are also present, but their origin and mode of emplacement is unknown.

In summary, the Kyrenia Range is interpreted as a remnant of a Mesozoic (Neotethyan) passive margin (e.g. Robertson, 1990) that was emplaced during southward-directed thrusting (Biju *et al.* 1976; Baroz. 1980) or by a combination of strike-slip and thrust tectonics (Robertson and Xenophontos, 1993). The present day north and northeasterly dips are attributed to Miocene tectonism which formed the Kythrea Flysch (Cleintaur *et al.* 1977).

2.2.4. The Mesaoria Plain

The Mesaoria Plain (Figure 2.3) is an area of lowland between the Troodos massif and the Kyrenia Range. It is separated from the Kyrenia Range by the Ovgos Fault Zone, which is interpreted as a wrench fault (North Troodos Boundary Fault; Bagnall, 1964). Geophysical observations suggest that this fault truncates the Troodos massif (Gass and Masson-Smith, 1963).

The plain is underlain by Troodos basalts, bentonitic clays (Kannaviou Formation, see section 2.1.5) and Cenozoic sediments (Cleintaur *et al.* 1977), which are overlain by over 2,500m of Miocene-Recent sediments (Cyprus Geological Survey, unpublished data).

2.2.5. Southwest (SW) Cyprus

The geology of SW Cyprus (Figure 2.3 and 2.8) is dominated by two oceanic terranes: (1) the Mamonia Complex and, (2) the Troodos Complex. The older Triassic to Lower Cretaceous Mamonia Complex represents a tectonised and collapsed, passive margin sequence. The Complex contains highly disrupted and intercalated lavas, which are predominantly alkaline in nature (see below), and shallow to deep water sediments (Swarbrick, 1979, 1980; Swarbrick and Robertson, 1980; Malpas *et al.* 1992). The younger Upper Cretaceous Troodos Complex represents supra-subduction zone oceanic crust. The Complex comprises variably disrupted igneous ophiolitic rocks, dominated by tholeiitic lavas and breccia, and its deformed sedimentary cover. Other units assigned to the Troodos Complex in SW Cyprus include intrusive basalts, dolerite and gabbro and ultramafic rocks. Both of these oceanic complexes are juxtaposed along an arcuate, serpentinite filled, suture zone. The determination of the kinematic and geochemical evolution of this fault zone is the aim of this thesis.

Both complexes and the serpentinite-filled faults are overlain by thick, relatively undeformed, essentially post-deformational Upper Cretaceous (Maastrichtian) debris flow deposits (the Kathikas Formation; Figure 2.8) and chalks (Swarbrick and Naylor, 1980; see below), and by Quaternary-Recent sediments, which record the emergence of the island of Cyprus (Robertson, 1977b).

The tectonic relationships between the five areas described above are reviewed in greater detail in Chapter 6 where they are incorporated in a regional tectonic model, which attempts to explain the Triassic to Upper Cretaceous evolution of Cyprus. The units of SW Cyprus are discussed in more detail below in section 2.2.

2.3. The geology of SW Cyprus

The first detailed work on SW Cyprus was undertaken by Turner (1971, 1973), who mapped a small area in the north of the region, and Lapierre (1972, 1975), who mapped the whole of the region. It was Lapierre who proposed that the Mamonia Complex preserved evidence of Triassic rifting, subsidence and sedimentation and that the Complex could be divided into two geologically distinct units. Using thorough field, petrographic and geochemical observations, Lapierre indicated the Mamonia lavas are alkaline, whilst the Troodos lavas are broadly tholeiitic. Furthermore she suggested the Troodos Complex formed during Upper Cretaceous "oceanisation" and that the two complexes were then juxtaposed in the Maastrichtian. Lapierre's stratigraphy was later revised by Robertson and Woodcock (1979), Swarbrick (1979), and Swarbrick and Robertson (1980) in a classification scheme that is currently

accepted (see below). The only point of controversy concerns the mode of juxtaposition of the Mamonia and Troodos terranes. Early workers envisaged *allochthonous* Triassic Mamonia sheets or "nappes" emplaced over *autochthonous* Upper Cretaceous Troodos crust, dominantly by gravity sliding mechanisms (e.g. Gass *et al.* 1960; Turner, 1971, 1973; Lapierre, 1972, 1975; Robertson and Hudson, 1974; Ealey and Knox, 1975). More recent models, based on structural field studies, favour intra-Maastrichtian strike-slip (e.g. Swarbrick, 1979, 1980, 1993) or thrust tectonism (e.g. Malpas *et al.* 1993).

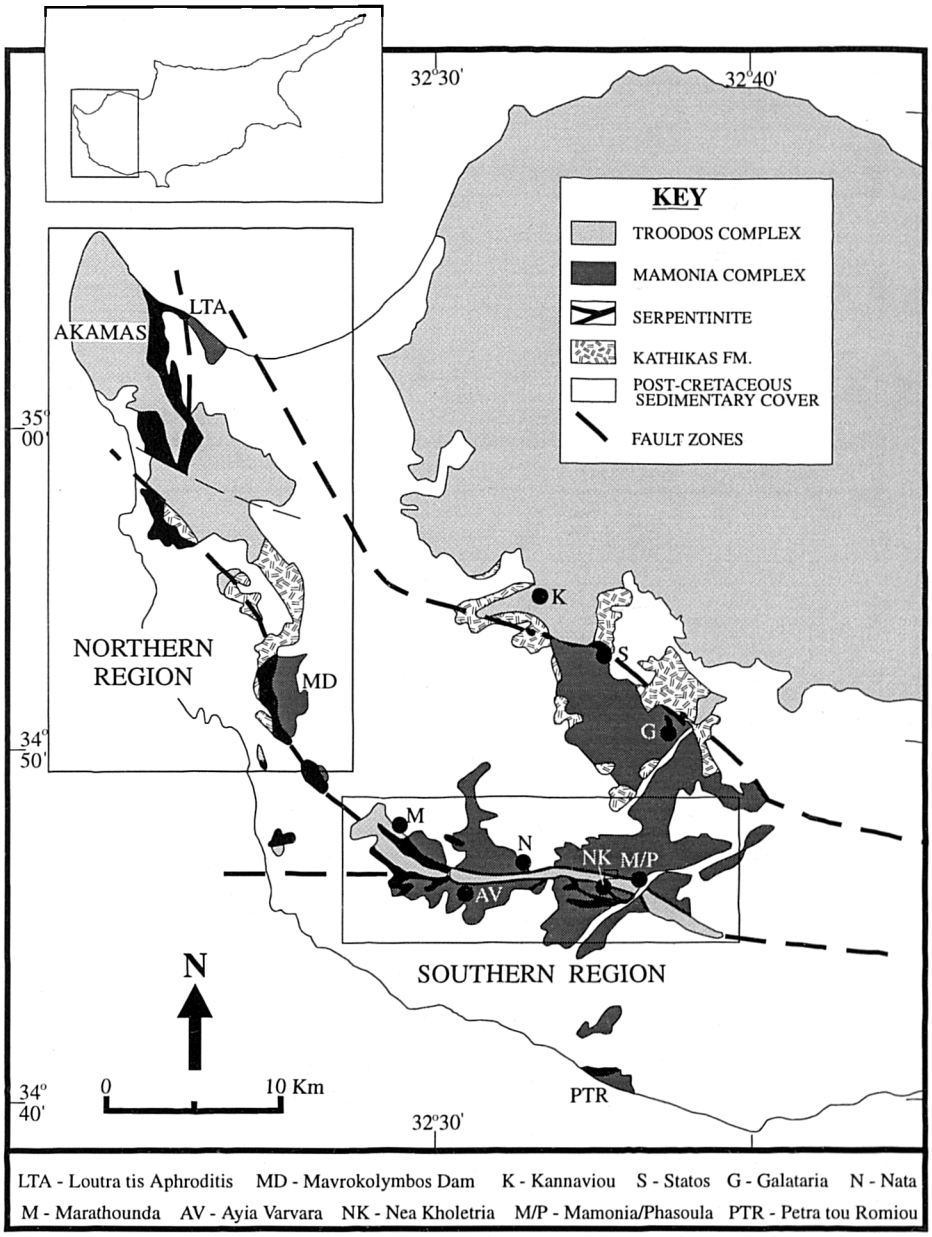

Figure 2.8. Geological map of SW Cyprus based on the maps of Swarbrick (1979). The dotted lines mark the tectonic sutures between the Mamonia and Troodos Complexes. The relative locations of the Northern and Southern Regions of SW Cyprus are shown, which are discussed below. The villages located on the map are referred to throughout this thesis.

The nomenclature and stratigraphical framework for all units referred to in the text is based on the classification of Swarbrick and Robertson (1980) (Figure 2.9). The following section is sub-divided into descriptions of four distinct units that crop out in SW Cyprus: (1) the stratigraphy of the Mamonia Complex; (2) rocks of the Troodos Complex; (3) serpentinite-filled fault zones, and; (4) post-deformational sedimentary cover.

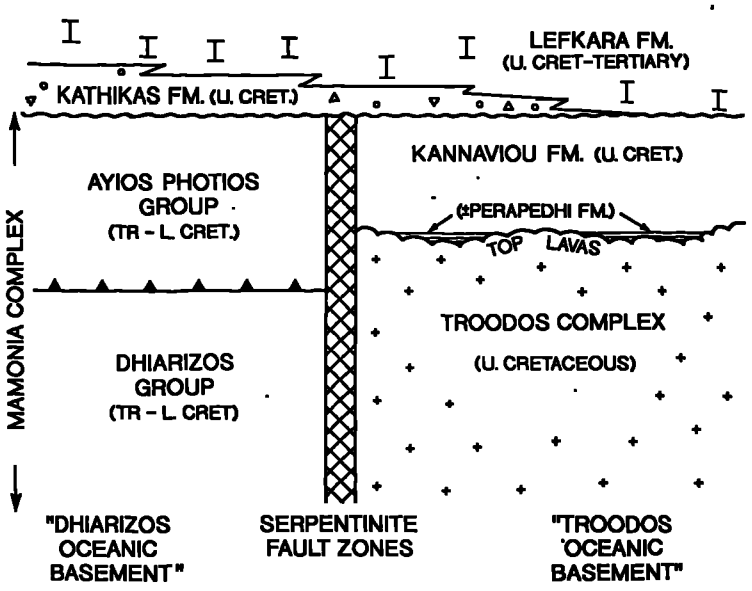

Figure 2.9. Stratigraphical summary of the units exposed in SW Cyprus (from Swarbrick, 1993).

2.3.1. Stratigraphy of the Mamonia Complex

The Mamonia Complex is named after Mamonia village, located 19km east of Paphos in the Dhiarizos valley, and comprises a number of diverse sedimentary, igneous and metamorphic units (Swarbrick and Robertson, 1980). The Complex is thought to represent a deformed Late Triassic to Mid-Cretaceous volcano-sedimentary terrain which formed in Neotethys (Malpas *et al.* 1993). The Complex is exposed throughout SW Cyprus, but it is also present in Southern Cyprus as the Moni Formation, which will be discussed in Chapter 6. The Mamonia Complex was juxtaposed with the Troodos Complex along a series of serpentinite-filled fault zones in a collisional event that ended by the latest Maastrichtian (e.g. Swarbrick, 1979, 1993; Malpas *et al.* 1993).

The stratigraphic terminology proposed by Swarbrick and Robertson (1980) is used throughout this work (Figure 2.10). This nomenclature retains the bipartite subdivision of the Mamonia Complex devised by Lapierre (1968, 1975); i.e. the volcano-sedimentary Dhiarizos Group and the continental margin-related sediments of the Ayios Photios Group. The Dhiarizos Group is subdivided into four formations

(Phasoula, Petra tou Romiou, Mavrokolymbos and Loutra tis Aphroditis) and one member (Kholetria Member of the Phasoula and Loutra tis Aphroditis Formations). The group comprises Upper Triassic lavas overlain by Upper Triassic to Lower Cretaceous sediments. The Ayios Photios Group is subdivided into three formations (Vlambouros, Marona and Episkopi) and one member (Akamas Member of the Episkopi Formation). The group consists of a variety of Upper Triassic to (at least) Lower Cretaceous siliclastic, calcareous and siliceous lutites, arenites and rudites.

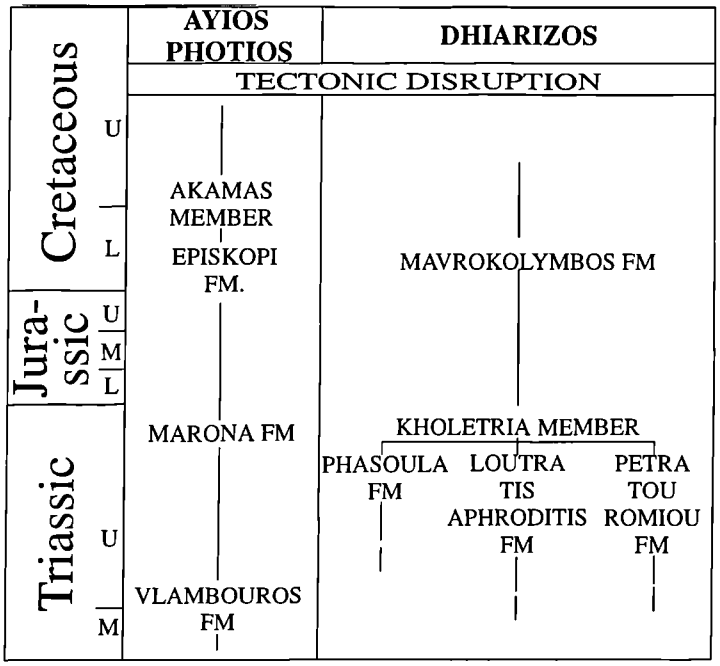

Figure 2.10. Stratigraphical framework for the Mamonia Complex (from Swarbrick, 1979).

One other unit assigned to the Mamonia Complex by Swarbrick and Robertson (1980) is the Ayia Varvara Formation, which comprises greenschist to amphibolite facies metabasic and metasedimentary material located within serpentinite-filled faults. It is assigned to the Mamonia Complex because of a spatial and interpreted genetic association with the Dhiarizos Group (e.g. Spray and Roddick, 1981; Malpas *et al.* 1992, 1993). The Ayia Varvara Formation and associated units are discussed in further detail in Chapters 3, 4 and 6.

2.3.1a The Dhiarizos Group

The Triassic to Lower Cretaceous Dhiarizos Group comprises lavas of predominantly alkaline affinity (see below) and various calcareous and siliceous shallow to deeper water sediments (Swarbrick, 1979). These units are structurally overlain by the Ayios Photios Group, but the base to the Dhiarizos Group is not preserved. As noted above,

the Group is subdivided into four main formations, namely the Phasoula, Petra tou Romiou, Mavrokolymbos and Loutra tis Aphroditis Formations, which collectively record Upper Triassic rifting, volcanism, and related sedimentation in shallow to deep waters. Deposition of hemi-pelagic and pelagic sediments into the Jurassic and Lower Cretaceous is thought to reflect deepening of the basin, related to thermal subsidence following rifting (Swarbrick, 1979).

The following text describes and summarises previous work of units assigned to the Dhiarizos Group.

The Phasoula Formation

The Phasoula Formation lavas are exposed in SW Cyprus as dominantly pillowed lava flows and less common sheet flows and associated dykes. Early workers (e.g. Lapierre, 1975; Pearce, 1975), using major elemental analyses, recognised the volcanic rocks of the Dhiarizos Group as alkali basalts and their fractionated products. However, based on immobile trace element studies on lavas from a small area located in the south of SW Cyprus, Malpas *et al.* (1993) suggested that low temperature alteration modified major elemental analyses. Using Nb/Y and Zr/TiO_2 analyses as an index for alkalinity and the degree of differentiation, Malpas *et al.* (*op cit.*) concluded that a large proportion of these rocks are in fact *tholeiitic*, with the remainder dominated by alkali basalts (plus minor ankaramites, trachybasalts, trachytes and trachytic phonolites). Malpas *et al.* (*op cit.*) provided additional data (i.e. V-Ti and Cr-Y plots, and primitive mantle-normalised plots of REE) to suggest the tholeiites possess an affinity with 'mid-ocean ridge basalts' (MORB), whilst the alkali basalts display an association with 'within-plate basalts' (WPB). In summary, the chemistries of the Phasoula lavas are analogous to extrusive material of comparable age found throughout the Eastern Mediterranean (e.g. Hawasina Formation, Oman; Lippard *et al.* 1986;). These rocks are interpreted as evidence of continental break-up, early sea-floor spreading, and ocean island development within a number of small oceanic basins along the northern margin of Gondwana, associated with the formation of Neotethys (e.g. Malpas *et al.* 1992; Gass *et al.* 1994). The volcanic rocks of the Phasoula Formation that possess tholeiitic affinity and MORB chemistry (Malpas *et al.* 1993) may represent fragments of Tethyan oceanic basement upon which ocean islands or seamounts (alkali basalts) developed.

The tholeiites consist dominantly of orange-brown weathered, pillowed flows. Individual pillows range from 20 to 50cm in diameter and are poorly amygdaloidal with variolitic margins. They are associated with detached blocks of limestone and chert belonging to the Upper Triassic Petra Tou Romiou Formation (see below) and are overlain stratigraphically by the Mavrokolymbos Formation. Locally the pillows

are hollow and some exhibit intra-pillow layering of alternating bands of chloritised basalt and zeolite, which are interpreted as evacuated lava tubes. Interpillow voids and shrinkage fractures are commonly filled with calcilutite attributed to the Kholetria Member (see below). Rarer void fillings and discontinuous interpillow beds consist of red, green or brown chert and black manganiferous chert.

The alkali basalts, which are associated with the same range of sedimentary units as the tholeiites crop out as two equally abundant types, aphyric pillow lavas and plagioclase-phyric lavas with rare sheet flows and associated dykes (Malpas *et al.* 1993). The aphyric lavas average 50 cm in diameter, weather burgundy to purple, and are variably amygdaloidal, filled with calcite and zeolite. They locally overlie tholeiitic lavas and are in turn overlain by the plagioclase-phyric type. The latter type possess a light grey weathering coloration and are easily identifiable due to their impressive porphyritic character, with plagioclase phenocrysts reaching 2cm in length. Pillows are large in this unit, ranging from 30 cm to over 1 metre.

The Petra tou Romiou (PTR) Formation

The PTR Formation crops out in SW Cyprus as large detached blocks of white recrystallised limestone. The only primary sedimentary contact preserved is with the Phasoula Formation in the Akamas region, where a block 20m in diameter rests on highly weathered lavas and fine-grained tuffs (Swarbrick, 1979). The blocks are commonly associated with the Phasoula lavas and blocks range from 5 to over 100 metres in diameter. Macrofossils, mainly corals and shell fragments, are preserved in the less recrystallised limestones. Microfossils include conodonts and foramanifera, which are preserved with algae, ooids, pisoliths and pellets (Swarbrick, 1979). PTR breccias are exposed in a number of localities and locally contain clasts of Phasoula lava, red mudstone and carbonaceous material. Large isolated blocks of PTR limestone commonly rest on other Mamonia Complex units. Field observations suggests that these blocks have reached their present locations due to movement down slope, and thus no genetic relationships are inferred.

The Loutra tis Aphroditis Formation (plus Kholetria Member)

Outcrops of the Loutra tis Aphroditis (LTA) Formation are best exposed in cliff sections in the type area, the 'Baths of Aphrodite', located along the northern coast of the Akamas Peninsula, where the maximum thickness of the formation is estimated at approximately 75km (Swarbrick, 1979). In the type area the Formation crops out sporadically as pillow lavas, lava-dominated breccias, volcaniclastic siltstones and less abundant radiolarian mudstones, which are often manganiferous. The mudstones and radiolarites are assigned to the Kholetria Member, which is more widespread

throughout SW Cyprus than the breccias and volcaniclastics. The basal contact to the LTA Formation is not exposed, whilst the upper contact is dominantly tectonic. At Petra tou Romiou, the LTA Formation is depositionally overlain by the Kannaviou Formation (see below), belonging to the Upper Cretaceous Troodos Complex. This contact relationship is unique as it is the only locality at which Kannaviou sediments overlie the Mamonia Complex. Sediments assigned to the Kholetria Member are most commonly observed as scattered outcrops within and above Phasoula lavas. The upper contact is exposed in the Phasoula area where the Member passes upwards conformably into the Mavrokolymbos Formation (see below) (Swarbrick, 1979).

Of particular note is that some breccias located in the type area contain cm-scale clasts of metamorphosed material, pegmatitic gabbro and sediment. The metamorphic material is most commonly rich in dark amphibole and white feldspar and are texturally similar to amphibolite-facies rocks assigned to the Ayia Varvara Formation (see below).

The Mavrokolymbos Formation

The Mavrokolymbos Formation comprises a thick sequence of pelagic sediments, predominantly red clay with interbeds of manganiferous siltstones, calcilutites and white radiolarian siltstones. The maximum thickness is estimated to be approximately 45m (Swarbrick, 1979). The formation overlies Phasoula lavas and the Kholetria Member, whilst the upper boundary is a low angle tectonic contact with the structurally overlying Ayios Photios Group (Figure 2.10).

The Ayia Varvara Formation

Blocks of amphibolite-facies metabasites and intercalated metasediments belonging to the Ayia Varvara Formation provide an unusual component within the fault zones of SW Cyprus. The formation crops out as a number of isolated metamorphic blocks and as more elongate units bound, in general, by serpentinite-filled fault zones. The largest unit, exposed north of Ayia Varvara, reaches a maximum length of 3.25km east-west and 870m in width north-south. The largest metamorphic blocks, which have been studied in detail (Spray and Roddick, 1981), are located at Ayia Varvara, Loutra tis Aphroditis and Phasoula. The metamorphic rocks are *always* spatially associated with Dhiarizos Group units and in some cases there is striking lithological and compositional resemblance with the intercalated lavas and sediments of the Dhiarizos Group (e.g. Swarbrick, 1979; Malpas *et al.* 1993). The metamorphic blocks are occasionally in contact with units other than serpentinite along late brittle faults, where retrogression to greenschist-facies assemblages is common.

The metasediments include grey, quartz-mica ± garnet phyllites and schists, purple phyllites, marbles and quartzites. The metabasites are more constant in terms of bulk rock composition, comprising the common amphibolite-facies assemblage:-
Amph + Plg + Ep + Apatite + Ti-Phase ± Px ± Grnt ± Bt ± Qtz ± Pyrite (Malpas *et al.* 1992).
The amphiboles commonly define a foliation and mineral lineation, which often parallel the fabric in the neighbouring serpentinite, and more importantly, adjacent peridotite mylonites (see Chapter 4). The amphiboles are calcic and of tschermakitic hornblende composition (Malpas *et al.* 1992) or edenitic or ferroan-pargasitic composition (Spray and Roddick, 1981). These amphiboles are often rimmed by actinolite, suggesting late greenschist-facies retrogression. Plagioclase feldspars are albites, andesines or oligoclase andesines (Spray and Roddick, 1981).

Geochemical studies carried out by Spray and Roddick (1981), based on immobile trace element analysis, indicate the metabasites are predominantly of tholeiitic character, but a significant proportion of samples also reflect alkalic affinities. The chemistries of the metabasites were compared to those of the Phasoula and Troodos lavas to determine possible protoliths from Cyprus for the metamorphics, but the correlation was inconclusive. However, Malpas *et al.* (1992) noted that the geochemistry of the Phasoula Formation transitional basalts was comparable to that of the metabasites. More importantly, geochemical data from the metamorphics plotted on TiO2 vs Zr and Cr vs Y plots fell into MORB fields. This association is particularly revealing as Malpas *et al.* (1993) identified MORB lavas within the Phasoula Formation, which were previously undescribed in SW Cyprus. Thus, the hypothesis that the Dhiarizos Group constitutes the protolith for the metamorphics is strengthened; tectonically intercalated lavas, of differing affinities, within the Phasoula Formation were metamorphosed, along with their associated sediments, to produce the Ayia Varvara Formation.

$^{40}Ar/^{39}Ar$ step heating analyses of hornblende separates were undertaken by Spray and Roddick (1981). The samples were taken from Ayia Varvara, Mamonia and Loutra tis Aphroditis and revealed near identical ages of between 83 to 90MY. These dates are comparable to those calculated for the formation of the Troodos massif of around 92-90Ma (Mukasa and Ludden, 1987).

Numerous models to explain the formation and mode of emplacement of the Ayia Varvara Formation have been proposed, which include:-

- Sub-ophiolitic metamorphic rocks (Woodcock and Robertson, 1977; Parrot and Whitechurch, 1978).

- Products of dynamothermal metamorphism during juxtaposition of Mamonia crust against hot Troodos crust, plus a component of shear heating along strike-slip faults (Swarbrick, 1980).
- Dynamothermal metamorphism, with or without shear heating, within an oceanic (transform?) fracture zone setting (Spray and Roddick, 1981).
- Metamorphism of Triassic ocean crust and sediments during subduction of the young Troodos crust (Malpas *et al.* 1992).

By whatever mechanism it formed, it is generally accepted that the Ayia Varvara Formation does not constitute metamorphics generated at a sole thrust of an obducted ophiolite, as is the case with all other Tethyan ophiolites (e.g. Moores *et al.* 1984). Peridotite mylonites provide new evidence presented in this thesis to further constrain the mode of formation of the metamorphics (see Chapters 3, 4 and 6).

2.3.1b The Ayios Photios Group

The Ayios Photios Group comprises clastic and carbonate sedimentary units ranging from mid-Triassic to mid-Cretaceous in age. The base of the Group is a tectonic contact above the Dhiarizos Group. The maximum reconstructed thickness of the Ayios Photios Group is about 200m (Swarbrick, 1979). The Group is subdivided into three formations, namely the Vlambouros, Marona and Episkopi Formations, based on a subdivision devised by Lapierre (1975). Overall, the Group records the progressive deepening of a basin, followed by later stabilisation of the margin. The basal, immature, clastic Vlambouros Formation was deposited rapidly on the flanks of a subsiding basin. The variation in facies indicate deposition from near-shore deltaic to deeper-water marine environments. This is succeeded by micritic limestones of the Marona Formation, which are depositionally overlain by Episkopi Formation pelagic sediments (Swarbrick, 1979).

2.3.1c. Summary and interpretation of the Mamonia Complex

The Ayios Photios and Dhiarizos Groups of SW Cyprus document the evolution of a Triassic to Lower Cretaceous oceanic marginal basin (Figure 2.11). Initial rapid deposition of immature, terrigenous material (Vlambouros Formation) at the base of the Ayios Photios Group records the uplift at the flanks of a rapidly subsidising basin during the early stages of rifting and subsidence (Swarbrick, 1979). The proposed source is a continental metamorphic terrain intruded by acid igneous bodies. An upward decrease in grain size and bed thickness reflects the deepening of the basin and an increase in pelagic sedimentation. A rising abundance of calcareous material in the Vlambouros Formation and the deposition of Marona Formation lime muds indicate

the existence of a carbonate platform on a stabilising shelf at the end of the Triassic to earliest Jurassic (Swarbrick, 1979). Continued subsidence and stabilisation of the margin led to normal pelagic sedimentation with intermittent sudden depositional events, possibly below a fluctuating CCD (Episkopi Formation) during the Jurassic and Lower Cretaceous. A change in the pattern of sedimentation in the Lower Cretaceous is indicated by shelf-derived carbonates in the Episkopi Formation and, more obviously, the progressive increase in orthoquartzites of the Akamas Member. This change is attributed to tectonic activity triggering sudden down slope movement of shelf-derived material, and may signify the onset of tectonism that caused the juxtaposition with the Dhiarizos Group, and maybe later with the Troodos Complex (Swarbrick, 1979).

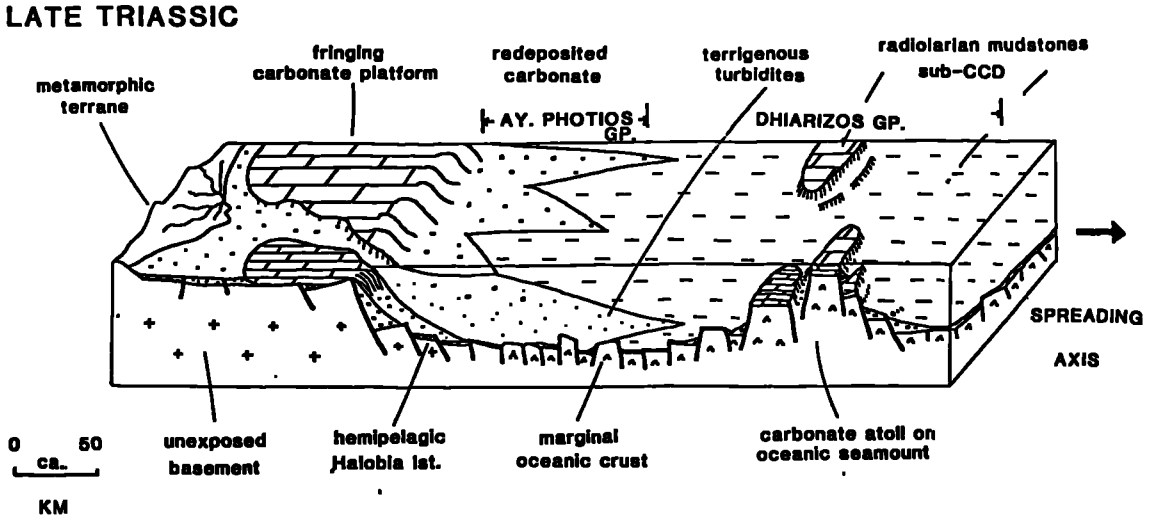

Figure 2.11. Schematic reconstruction of the Mamonia terrane in the Late Triassic (from Robertson, 1990).

The Dhiarizos Group is coeval with the Ayios Photios Group, and provides further evidence for the opening of the same basin and its evolution, though a distance away from the continental margin. Tholeiitic and alkaline chemistries of the Phasoula lavas suggest intracontinental rifting and the subsequent development of an oceanic spreading system. Vlambouros sandstones locally extend onto the lavas thus demonstrating the proximity of the Ayios Photios and Dhiarizos Groups in the Triassic (Swarbrick, 1979). Reefal limestones of the Petra tou Romiou Formation and the Kholetria Member of the Loutra tis Aphroditis Formation indicate deposition in relatively shallow, tropical waters. Their subsequent redeposition and brecciation

together with the generation of associated lava-dominated, polylithic breccias (Loutra tis Aphroditis Formation) at fault scarps, and soft sediment deformation recorded in the Kholetria Member attests to the synchroneity of tectonism, volcanism and sedimentation in an unstable, actively rifting environment. The overlying pelagic sediments of the Mavrokolymbos Formation indicate pelagic sedimentation at a distance from the volcanic centre. This unit is comparable to the Ayios Photios Episkopi Formation as it records a change in the sedimentary pattern on the continental margin.

In summary, the Ayios Photios and Dhiarizos Groups record the evolution of a small ocean basin, created by rifting in Upper Triassic times, and by thermally controlled subsidence on the basin slope and margin in the Jurassic (e.g Swarbrick, 1979).

The depositional basement to the Ayios Photios Group is not exposed as it displays a low angle tectonic contact with the underlying Dhiarizos Group (Swarbrick, 1979, 1980). Where exposed, the contact is brecciated and highly disrupted. Fold facing and vergence directions suggest emplacement of the Ayios Photios Group from the present southwest to the northeast (Robertson and Woodcock, 1979). Most workers have suggested that the juxtaposition of the allochthonous Ayios Photios Group over the essentially '*autochthonous*' Dhiarizos Group took place by gravity sliding (e.g. Robertson and Woodcock, 1979; Swarbrick, 1979, 1980). The age of this event post-dates the youngest sediments of the Ayios Photios Group, which are dated as Lower Cretaceous (Ealey and Knox, 1975) and must pre-date the juxtaposition of the Mamonia and Troodos Complexes, which is constrained by the earliest post-deformational sediments of the Maastrichtian Kathikas Formation (see below; Swarbrick and Naylor, 1980; Urquhart and Banner, 1994).

The subsequent juxtaposition of the Mamonia and Troodos Complexes took place along serpentinite-filled faults. The kinematic history of this Upper Cretaceous episode is presented in the Chapters 4, 5 and 6.

2.3.2 The Troodos Complex in SW Cyprus

Mafic and ultramafic rocks and related sedimentary cover thought to belong to the Troodos Complex are exposed throughout SW Cyprus and are tectonically intercalated with Mamonia Complex units. The largest outcrop of Troodos material outside of the main massif is located in the Akamas Peninsula, where gabbros, sheeted dyke complex, and overlying lava series have been documented (Cyprus Geological Survey Map, 1992). The lavas throughout SW Cyprus are locally overlain by umbers assigned to the Perapedhi Formation (see below) and by volcaniclastic sedimentary rocks of the

Kannaviou Formation (see below). Two pillow lava units are recognisable (Malpas *et al.* 1993). The oldest comprises small, amygdale-free pillows (15-50cm in diameter) with chilled, partly devitrified rims. Swarbrick (1979) and Malpas *et al.* (1993) noted their geochemical and petrological similarity to the 'Lower Boninites' of the STTFZ, thereby making a significant genetic relationship between the transform zone to the east with the serpentinite-filled fault zones of SW Cyprus. These 'Lower Boninites' are overlain by large, (approximately 1m diameter) light grey-green coloured pillows referred to as 'Upper Boninites', which are locally flow flattened and possess calcite and haematite interpillow fillings. Of particular importance is a sliver of Troodos material located in the southern part of SW Cyprus ('Southern Region', Figure 2.8). The unit is continuous along strike, east-west, for over 20km, but never exceeds 300m in width (Swarbrick, 1980). It is bound to the north and south by serpentinite-filled fault zones, which are in turn succeeded by the Mamonia Complex. Explaining the mode of emplacement of this sliver is of prime importance when proposing a structural model for SW Cyprus.

The serpentinite-filled fault zones commonly display dykes and sills of gabbro, dolerite, basalt, wehrlite and clinopyroxenite. Using trace element analyses, Malpas *et al.* (1993) noted that the mafic intrusives possess comparable boninitic chemistries to those exposed in the STTFZ. Furthermore, they presented field evidence to suggest intrusion and tectonism were synchronous, which is also documented in the STTFZ (e.g Gass *et al.* 1994; Macleod and Murton, 1995), thus suggesting similarities with the faults of SW Cyprus to those of the STTFZ.

2.3.2a The Perapedhi Formation

Umbers and mineralised radiolarian cherts (1-10m in thickness) of the Perapedhi Formation represent the basal part of the supra-ophiolitic sedimentary succession. They are interpreted to be deposited in hollows in the UPL at water depths estimated at 2.5km (Spooner, 1980) during the later stages of volcanic activity (Robertson, 1975, 1977c). Using radiolaria, Urquhart and Banner (1994) suggest that the Perapedhi sediments are no younger than Campanian, but previously proposed Turonian ages (e.g. Blome and Irwin, 1985) cannot be disputed. The Formation overlies UPL with no apparent hiatus or erosional gap (Constantinou and Govett, 1972; Robertson and Hudson, 1973) and they are also present as rare intercalations within the lavas. The umbers are commonly only a few metres in thickness, but reach a maximum thickness of 35m where faulting produced topographic lows (Robertson, 1975).

2.3.2b The Kannaviou Formation

The Kannaviou Formation consists of pale green-grey bentonitic clays, radiolarian mudstones, volcanogenic siltstones and sandstones, and manganiferous siltstones (Robertson, 1977c; Swarbrick, 1979). The formation locally reaches thicknesses of 300m (Robertson, 1977c), where deposition was controlled by extensional fault movement, and a maximum thickness of 750m has been recorded in western areas of SW Cyprus (Gass *et al.* 1994). Due to the absence of calcareous microfossils, Urquhart and Banner (1994) suggest that deposition may have taken place below the carbonate compensation depth. The sediments conformably overlie the Perapedhi Formation, but where the latter are absent, they rest upon both UPL and LPL, and locally on top of pillow breccias (Robertson, 1977c) and serpentinites (Malpas *et al.* 1993). Sedimentary structures include convolute and cross-laminations and channels in the sandstone interbeds.

The Kannaviou Formation is the youngest pre-deformational sediment in SW Cyprus. It is most reliably dated as Campanian on micropalaeontological grounds (e.g. Ealey and Knox, 1975; Robertson, 1977c; Urquhart and Banner, 1994), but Urquhart and Banner (1994) suggest that much of the Formation was deposited in the *later part* of the Campanian. The deposits are epiclastic and composed in the main of pumiceous debris derived from an evolved calc-alkaline source (Robertson, 1977c. 1977d). The Kannaviou Formation is generally accepted to be completely absent from the Mamonia Complex (e.g. Gass *et al.* 1994), which suggests the Mamonia and Troodos Complexes were still apart during the Campanian. An alternative suggestion is that the volcanogenic sediments were redeposited from Mamonia-related volcanics in bathymetric lows (fault-bounded? Malpas *et al.* 1993) which were occupied by Troodos lavas. However, note that Swarbrick (1979) documents one example where Kannaviou sediments overlie Mamonia Complex units (namely the Petra tou Romiou and Loutra tis Aphroditis Formations) in the Petra tou Romiou area.

2.3.3 Serpentinite

Serpentinite in SW Cyprus fills all the fault zones that mark the tectonic suture between the Mamonia and Troodos Complexes. Partially to totally serpentinised ultramafic fault rocks define an arcuate belt which passes through Loutra tis Aphroditis, Mavrokolymbos, Marathounda, Ayia Varvara and Phasoula (Figure 2.8). Another fault zone delineates the southwestern edge of the Troodos massif and can be traced through Kannaviou, Statos and Galataria. The former fault zone can be subdivided into two segments that display significantly different deformational

characteristics and contact relationships. The serpentinites in the ***Northern Region*** (Figure 2.8) are generally massive with a maximum width at outcrop of approximately 1km E-W. Contacts strike approximately N-S, with western contacts against the Troodos Complex being generally shallowly dipping, whilst eastern contacts with the Mamonia Complex are moderate to steeply dipping. This region is characterised by relatively massive serpentinite bodies and by well documented top-to-the-west thrust tectonics (Lapierre, 1972; Malpas *et al.* 1993). The ***Southern Region*** (Figure 2.8) comprises E-W trending, anastomosing, serpentinite-filled fault-zones that are dominantly sub-vertical. These faults are not restricted to the contact between the Mamonia and Troodos Complexes, commonly cross-cutting Mamonia Complex units only. The faults vary in width along their length with a maximum of over approximately 300m and minimum of less than 20m. The degree of serpentinisation and deformation along the faults is also heterogeneous, with the areas of the most intense hydration tending to coincide with zones of high strain. In contrast to the faults of the Northern Region, these fault zones preserve evidence of strike-slip and compressional motions.

The serpentinite is dominantly derived from harzburgite, but minor dunite, wehrlite, clinopyroxenite and lherzolite are also present (see Chapter 1). In SW Cyprus, the dominant serpentine minerals present are lizardite and chrysotile, which are low temperature forms of serpentine and are most common in oceanic domains. $^{18}O/^{16}O$ studies from Mount Olympus serpentinites in the Troodos massif (Wenner and Taylor, 1969, 1971) suggest temperatures during serpentinisation may have been around 100°C.

The serpentinite faults in SW Cyprus contain a number of 'exotic' units, particularly in the Southern Region, which include Troodos intrusive basalt, dolerite and gabbro dykes. They are mostly deformed, but undeformed dykes are present, occasionally in close proximity to deformed dykes. This has been cited as evidence for the synchroneity of magmatism, deformation and serpentinisation (Malpas *et al.* 1993), which is also observed along the STTFZ (Macleod and Murton, 1993). The serpentinite is also intruded by clinopyroxene-rich, peridotitic material, but this will be discussed in a Chapter 3.

Of particular importance is the genetic association of the serpentinites. Many authors (e.g. Gass, 1960; Lapierre, 1975b; Robertson and Hudson, 1974; Clube and Robertson, 1986) have argued that the serpentinites are at least in part of Troodos affinity, whilst others (e.g. Ealey and Knox, 1975) have argued otherwise. Data presented in this thesis address the controversy and describe the distribution of the different peridotite types identified (see Chapter 3).

2.3.4. Post-deformational sedimentary cover

The earliest post-deformational sediments exposed in SW Cyprus are the Upper Cretaceous Kathikas Formation debrites and the Upper Cretaceous to Tertiary Lefkara Formation pelagic chalks and marls. Younger sediments depositionally overlie the Kathikas and Lefkara Formations, and also the Mamonia and Troodos Complex rocks. However, these Tertiary to Recent deposits are not discussed in detail as this thesis concerns the Triassic to Upper Cretaceous evolution of Cyprus. The Kathikas Formation is discussed below due to its significance to Upper Cretaceous deformation in SW Cyprus and also in timing the cessation of major tectonism in the northern part of the area.

2.3.4a The Kathikas Formation

The Kathikas Formation crops out only in the Northern Region of SW Cyprus as a series of isolated wedges of sedimentary melange with a maximum thickness of 270m (Swarbrick and Naylor, 1980). The melange is a poorly sorted, matrix supported, purplish-grey breccia. Angular to poorly rounded clasts are supported in a dominantly red, argillaceous matrix. Clasts comprise 30% of the rock volume and range in size from 1mm to 6m, with a mean size of 20cm. The most common clast types are chert, shale and various sandstones, siltstones and limestones. Rarer igneous clasts include green basalts, vesicular lavas, dolerites and gabbros. Rarer still are metamorphics of the Ayia Varvara Formation, iron/manganese metalliferous sediments, serpentinite and volcanogenic sediments of the Kannaviou Formation. All clast types are derived locally in SW Cyprus, and, more specifically, most clasts belong to the Ayios Photios Group. Green lavas, vesicular basalts, pink micrite and shallow water limestones are volumetrically less important, and belong to the Dhiarizos Group. Rarer still are lavas and volcanogenic sediments derived from the Troodos Complex. The matrix is composed of >85% clay minerals. The possible sources for this argillaceous material are haematitic mudstones from both the Ayios Photios and Dhiarizos Groups of the Mamonia Complex.

Bedding is distinguished in the field by colour variations, variation in clast size and occurrence of chalk interbeds. Colour changes relate to the differing proportions of lithologies in both the clasts and matrix. This may be attributable to a change in the source area. Mean bed thickness is estimated at 3.1m (Swarbrick, 1979), but thinning up cycles are recognised within both the melange and chalk interbeds. This is interpreted as a the development of debris flows on progressively shallower slopes (Swarbrick, 1979). The chalk interbeds (<20cm thick) reflect background

sedimentation and a hiatus in deposition of debris flows. The melange matrix is poorly fossiliferous so these pelagic sediments are important as their microfossils date the Kathikas at Late Maastrichtian (Urquhart and Banner, 1994; Swarbrick and Naylor, 1980). As the Kathikas is the oldest post-deformational sediment in SW Cyprus this constrains the cessation of the major tectonics in the region.

The melange unconformably overlies the Ayios Photios Group and the Kannaviou Formation (Swarbrick, 1979). Swarbrick (1993) states that the Kathikas Formation blankets both Complexes and their serpentinite-filled faulted contacts. The melange is succeeded by pelagic Maastrichtian chalks (Robertson, 1976b), which blanket the topography remaining after Kathikas deposition.

The dominance of Ayios Photios clasts is cited as evidence for a Mamonia topographic high as provenance for the debris flows. Swarbrick (1993) proposed that this 'high' was formed by a transpressional push-up structure in the Northern Region of SW Cyprus. This explains the limited occurrence of the Kathikas Formation in this area. Swarbrick (1979) proposed the melanges were predominantly deposited from SW to NE, in a radial manner, from these Mamonia 'highs' into basin 'lows'.

The lack of serpentinite clasts in the melange may be attributable to the limited extent of serpentinite on the seafloor during the time of deposition. The substantial outcrops of serpentinite in the Northern Region at present could be due to further protrusion of serpentinite onto the seafloor after deposition of the Kathikas melange or tectonics did not expose much serpentinite on the seafloor previous to deposition.

PART TWO - GEOCHEMISTRY

CHAPTER 3
PERIDOTITE GEOCHEMISTRY AND SPATIAL RELATIONSHIPS WITH THE MAMONIA AND TROODOS COMPLEXES IN SW CYPRUS

3.1. Introduction

The aim of this chapter is to: (a) outline the spatial relationships between the serpentinites and the Mamonia and Troodos Complexes and, (b) to characterise geochemically the peridotite protoliths of the serpentinite-filled fault zones of SW Cyprus; i.e are particular ultramafic units related to the Mamonia or the Troodos Complexes? Many authors (e.g. Gass, 1960; Lapierre, 1975b; Robertson and Hudson, 1974; Clube and Robertson, 1986) have argued that the serpentinites are at least in part of Troodos affinity, whilst others have argued for an affinity with the Mamonia Complex (e.g. Ealey and Knox, 1975). In this thesis, variably serpentinised peridotites have been sampled from numerous locations, including the fault zones in the Northern and Southern Regions of SW Cyprus that delineate the suture zone that separates the Mamonia and Troodos Complexes. Additional samples were analysed from the fault zone that passes through the villages of Galataria, Kannaviou and Statos, separating the Mamonia Complex from the main Troodos massif (see Figure 3.1). Because of the heterogeneity of deformation and serpentinisation along these faults, only partially serpentinised peridotite blocks (tens of cm to 10m scale) are preserved, and it is these blocks that were used for geochemical analysis. In the following sections, field relationships are described and geochemical analyses are presented as criteria for distinguishing between the different peridotite types that crop out in SW Cyprus. Note that additional, detailed petrographic studies on specific peridotite deformational microfabrics are presented in Chapters 4 and 5.

3.2. The serpentinite fault zones

As described in Chapter 2, the serpentinite-filled fault zones of SW Cyprus are assigned to either the Southern or Northern Regions, based on their deformational characteristics (Figure 3.1). To summarise, the serpentinites in the Northern Region generally comprise a single N-S trending fault zone, which reaches a maximum width at outcrop of approximately 1km east-west. In contrast, the Southern Region is

characterised by a series of anastomosing, predominantly sub-vertical, serpentinite-filled faults that strike east-west. These faults vary in width along their length, attaining a maximum of over 300m and minimum of less than 20m. The faults bifurcate, incorporating less deformed blocks of Troodos Complex and Dhiarizos Group units, whilst the Ayios Photios Group crops out to the north and south of this faulted zone (Figure 3.2). Two main fault strands dominate in the Southern Region, which bound an elongate sliver of Troodos Complex lavas and sediments to the north and south. It is from these two main faults from which the minor fault strands are inferred to bifurcate.

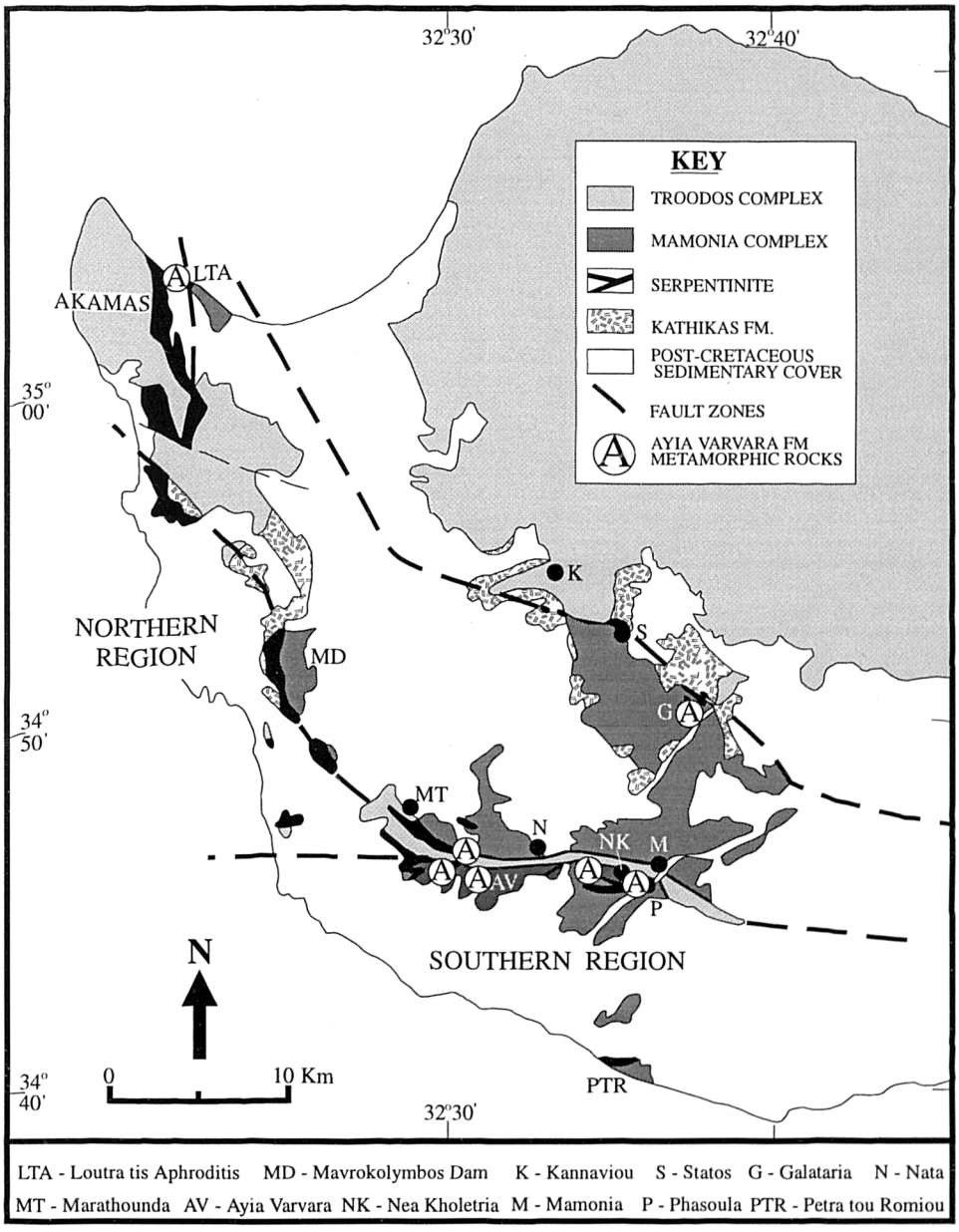

Figure 3.1. Geological map of SW Cyprus showing the locations of Ayia Varvara Formation outcrops. A detailed map of the Southern Region is shown in Figure 3.2.

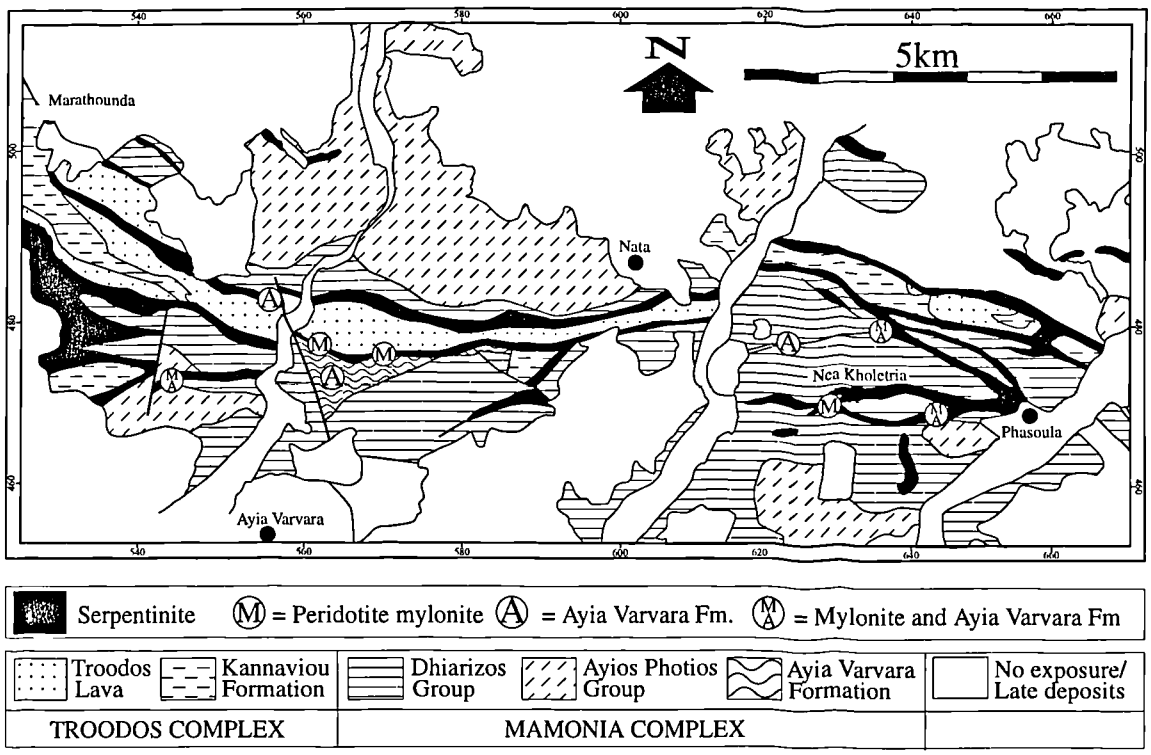

Figure 3.2. Distribution of pre-Upper Cretaceous units in the Southern Region of SW Cyprus (re-drawn after Swarbrick, 1979), showing the location of peridotite mylonites and Ayia Varvara Formation exposures. The location of the Southern Region is shown in Figure 3.1.

3.2.1. Southern Region ultramafics

Field-based observations in the Southern Region suggest that the serpentinite fault zones comprise a number of different peridotitic and minor mafic units. More importantly, the two main serpentinite belts that bound the central Troodos sliver display significantly different characteristics to the fault zones that anastomose and incorporate Dhiarizos Group units (see below). The two main serpentinite belts are dominated by variably serpentinised harzburgite and minor dunite. Harzburgite is identified by its weathered brown colouration and bronze bastite pseudomorphs after orthopyroxene, whilst dunite is easily identified by an absence of pyroxene. When sheared and serpentinised, these rocks commonly display a light blue colouration. The serpentinite faults locally contain metre-wide dykes of clinopyroxenite, wehrlite, uralitised gabbro, dolerite and basalt. Commonly, these dykes possess finer-grained and/or chilled margins, which suggest that they intruded the fault zones after the harzburgitic serpentinite host had cooled significantly. Dykes invariably strike east-west, parallel to the local fault zone boundaries, and dip steeply to vertically, parallel to the adjacent serpentinite foliation. At certain localities along the faults, 'swarms' of intrusive ultramafic and mafic dykes comprise a significant volume of the fault zone

(i.e. up to ~40%) (Figure 3.3). These areas are summarised in Table 3.1, and include outcrops mainly in the Marathounda and the Ayia Varvara areas. Malpas *et al.* (1993) suggest that the presence of the mafic dykes indicates hydrated mantle peridotites were protrusively emplaced at relatively shallow levels in the crust prior to intrusion. Furthermore, based on field observations in the Southern Region, Malpas *et al.* (1993) suggest that Troodos lavas locally erupted onto serpentinite, which cropped out on the seafloor. Evidence includes the preservation of rare, geometrically irregular contacts between serpentinite and overlying Troodos lavas. However, field work undertaken as part of this thesis could not substantiate or disprove this theory, because such a contact relationship may also have formed as a result of serpentinite protrusion from depth.

In contrast, the narrower fault strands that are in contact only with Dhiarizos Group units (i.e. those faults that are not in contact with the Troodos sliver) do ***not*** contain intrusive bodies. The unserpentinised harzburgites are similar in appearance to those from the main fault strands, except they are frequently darker in colour when weathered. However, where these rocks are intensely sheared and serpentinised they display a characteristic lime-green to olive-green colouration. Furthermore, these rocks tend to possess abundant, fine-grained (<1mm), equant dark spinels, which are readily observed in hand specimen.

Figure 3.3. Example of a mafic dyke swarm intruding a serpentinite fault zone (blue) in the Marathounda area. The widest dykes are approximately 5m wide.

Area	Grid Reference	Intrusive Lithologies
Marathounda	545 488	Wehrlite and clinopyroxenite dyke swarm
,,	543 488	Basalt and dolerite dyke swarm
Ayia Varvara	559 482	Wehrlite, clinopyroxenite and gabbro dyke swarm
,,	559 484	Heavily uralitised gabbro body (>75m diameter)
Mamonia	654 482	Wehrlite, clinopyroxenite, gabbro dykes and veins (<5m wide zone)
,,	651 478	Wehrlite, clinopyroxenite, gabbro dykes and veins (~10-20m wide zone)
Statos	630 615	Olivine-phyric gabbro body (475m E-W and max. 175m N-S)

Table 3.1. List of localities where there are volumetrically significant ultramafic and mafic intrusive units.

The serpentinite-filled faults that are in contact with Dhiarizos units also host amphibolite-facies metamorphic blocks of the Ayia Varvara Formation (Figures 3.1 and 3.2). In contact with these metamorphic units are rare outcrops of *peridotite mylonite*, which is characterised by a strong, pervasive, strike-parallel stretching lineation with or without a well-defined foliation (see Chapter 4). When pristine, these rocks are dark in colour, but where they are heavily weathered, they display a characteristic 'brick-red' or buff-brown colouration and a lineation defined by small (~1mm), bright silver minerals, which look similar to white mica. By looking at Figures 3.1, 3.2 and Table 3.2, which list the occurrences of peridotite mylonite and their field relationships within the Southern Region, it is clear that a distinct association exists between mylonites, the Ayia Varvara Formation and serpentinite. Peridotite mylonites crop out as coherent exposures (<20m in diameter), as individual blocks (<1m in length) disrupted by faulting and boudinage, and as thin 'rinds' (<30cm wide) at contacts between the Ayia Varvara Formation and serpentinite. The degree of preservation of the mylonites may be attributed to the intensity of serpentinisation, i.e. where hydration is greatest the mylonitic fabric is overprinted and destroyed by serpentinisation. Numerous outcrops of the Ayia Varvara Formation have been studied in the field and, where these units are best exposed and where serpentinisation is relatively weak, peridotite mylonites are found in contact. This observation suggests that the mylonites and metamorphics are genetically related. The inferred relationship between these two units and the Dhiarizos Group is discussed further in Chapters 4

and 6, and detailed petrographic studies of the peridotite mylonites are presented in Chapter 4.

Area	Grid Reference	Occurrence
Mamonia	649 469	~30cm-scale 'rind' around metamorphic body
Ayia Varvara	571 475	Isolated, boudinaged blocks (~50cm diameter) -contact between Ayia Varvara Fm and serpentinite
,,	560 477	<30cm wide zone along ~20m long section of contact between Ayia Varvara Fm and serpentinite
,,	551 477	10-20m outcrop, located to the ESE of an amphibolite block
Nea Kholetria	632 483	Scattered blocks (<1m) along thrust between the Dhiarizos Group, Ayia Varvara Formation and serpentinite
,,	631 468	~10-15m serpentinised block surrounded by serpentinite

Table 3.2. Summary of the occurrences of peridotite mylonites in the Southern Region.

3.2.2. Northern Region ultramafics

Compared to the Southern Region, the N-S trending suture zone between the Mamonia Complex to the east and the Troodos Complex to the west in the Northern Region displays much less complexity. The suture zone is, in general, defined by a single N-S trending, serpentinite-filled fault zone, which reaches a maximum width at outcrop of approximately 1km east-west. Where preserved, the unserpentinised protolith to much of the fault zone is invariably harzburgite with minor dunite. In contrast to the Southern Region, the Northern Region fault zones rarely contain mafic or ultramafic intrusives. An exception to this generalisation is found at the western extremity of the fault zone at Mavrokolymbos Dam, where mm to cm-scale clasts of light-grey mafic material, similar in appearance to Troodos basalt, are incorporated in a serpentinite breccia. On the south side of the valley, close to the contact with the Troodos Complex, light coloured gabbroic dykes (<50cm wide) are preserved with their chilled margins. On the north side of the valley, a sub-vertical brittle fault zone, which bounds the serpentinite exposures, contains clasts (<30cm) of highly altered clinopyroxenite and mafic material (see Chapter 5).

At Loutra tis Aphroditis, located along the north coast of the Northern Region, the ultramafic fault zone is completely exposed. Furthermore, due to coastal erosion, the rocks exposed at this locality are the most pristine found throughout SW Cyprus.

The vast majority of the rocks are clinopyroxene-bearing harzburgites. In the field, these rocks are distinguished by dark-black, partially serpentinised olivine, bronze coloured orthopyroxene bastites and minor light-blue coloured clinopyroxene. Adjacent to tectonic contacts with Ayia Varvara Formation units, the harzburgites display a pervasive sub-vertical foliation and weak, strike-parallel stretching lineation defined by deformed pyroxene grains and their finer-grained tails. This fabric parallels the amphibolite-facies metamorphic foliation in the Ayia Varvara Formation. The location of these rocks is shown in Figure 3.2.

Between 75 to 100m ESE of the northwestern contact with the Troodos Complex at Loutra tis Aphroditis, an abrupt lithological transition can be seen in the ultramafic rocks. To the SE of a poorly exposed, ~5m wide contact zone, clinopyroxene-bearing harzburgites crop out (see above) and, to the NW, wehrlites and dunites are exposed. The wehrlites are distinguished by abundant light-blue/green coloured clinopyroxene grains and dark, partially serpentinised olivine, which contrasts the lack of pyroxene in the well preserved, blue coloured dunite.

All three of these peridotite types found at Loutra tis Aphroditis (i.e. deformed clinopyroxene-bearing harzburgite, wehrlite and dunite) are described in much more detail and discussed in Chapter 5.

3.3. Peridotite petrology and geochemistry

A detailed sampling programme was undertaken in SW Cyprus in an attempt to characterise the fault zone peridotites, petrographically and geochemically, and to fingerprint their mantle protoliths. For comparative purposes, additional spinel-peridotite samples were obtained from the STTFZ and Mt. Olympus in the Troodos Massif (some Troodos samples were used courtesy of J. Freeman).

3.3.1. Petrography

Most significant about the peridotites from both Regions, which are mostly harzburgitic, was the finding that those from the Northern Region, in general, contained a higher proportion of clinopyroxene than those from the Southern Region, the STTFZ and the Troodos massif. More precisely, the harzburgites sampled from the two main fault belts in the Southern Region, which are in contact with the central Troodos Complex sliver, are clinopyroxene-poor, whilst those from fault strands bound by Dhiarizos units only are relatively clinopyroxene-rich.

Using optical microscopy, two dominant peridotite types are distinguished petrographically; those that possess red to dark coloured chrome spinels and those that

contain orange to buff-brown coloured spinels (Figure 3.4). Although the morphologies of the spinels vary, which appears to depend on the degree of deformation experienced by the host rock (see below), these two types of peridotite are associated with specific field relationships (Table 3.3).

(a)

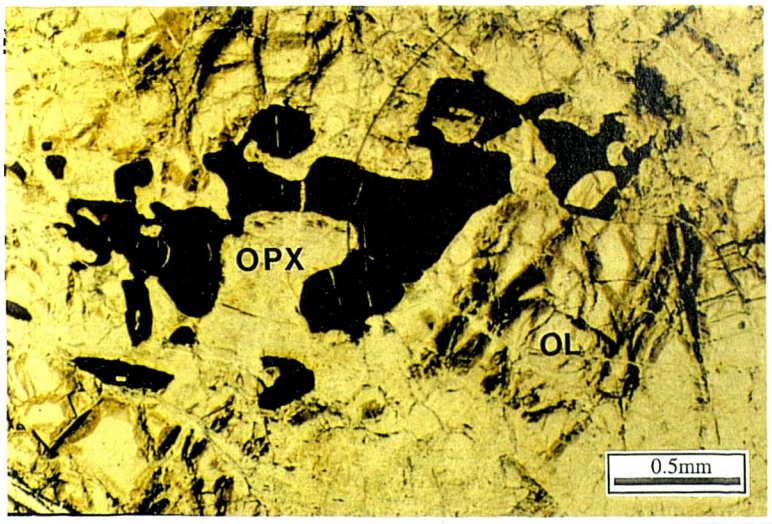

(b)

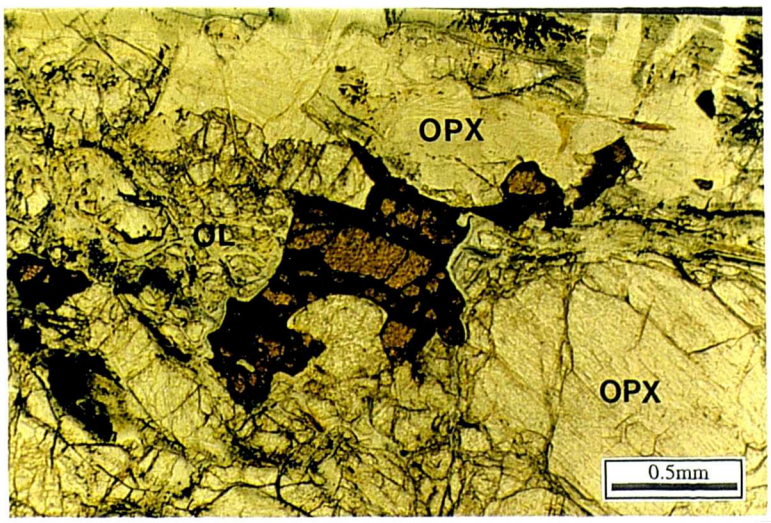

Figure 3.4. Photomicrographs of the two dominant spinel types in undeformed peridotite; (a) red-dark and, (b) orange coloured. Both examples display a typical "holly-leaf" morphology. OPX = orthopyroxene; OL = olivine.

Region	Red spinel-bearing peridotites	Orange spinel-bearing
Southern Region	Faults in contact with the Troodos Complex	Faults bound only by Dhiarizos Group units
		Faults in contact with the Ayia Varvara Formation, including peridotite mylonites
Northern Region	Wehrlites and dunites from the NW end of Loutra tis Aphroditis	Most peridotites from the Northern Region, including the cpx-harzburgites from Loutra tis Aphroditis
Troodos Massif	Harzburgites from Mt. Olympus	None

Table 3.3. Summary of the occurrences of peridotite type, defined by spinel colour.

In the least deformed samples, spinel commonly displays a "holly-leaf" morphology (Figure 3.4; *cf.* Mercier and Nicolas, 1975), which is thought to be indicative of post-kinematic growth. Furthermore, these grains are frequently associated with orthopyroxene and, to a lesser extent, clinopyroxene. On petrological grounds, clinopyroxene-orthopyroxene-spinel clusters in lherzolites, and orthopyroxene-spinel clusters in harzburgites, are thought to originate from decomposition of garnets during depressurisation (e.g. Nicolas, 1986 and references therein). This observation, combined with a lack of plagioclase and textural evidence for a cumulate origin, suggests that these rocks are of mantle origin. In contrast, samples that show evidence of high temperature deformation (i.e. peridotite mylonites; see Chapter 4) typically contain numerous small (<0.5mm), equant spinel grains. These spinels are invariably orange in colour and *no* red-coloured spinels are found in deformed peridotites. This observation and its significance is discussed further in Chapters 4 and 6.

3.3.2. Spinel Chemistry

In order to test the reliability of the sub-division of peridotite based on spinel colour, chrome spinels were analysed using an electron microprobe. As identified by previous authors, the composition of chromian spinel is a sensitive petrogenetic indicator in ultramafic rocks (Dick and Bullen, 1984; Michael and Bonatti, 1985; Bonatti and Michael, 1989). Spinel compositions from oceanic peridotites display a large

reciprocal variation of Cr and Al and a strong correlation of increasing Cr# (100Cr/(Cr + Al)) with decreasing Mg# (100Mg/(Mg^{2+} + Fe^{2+})) (Hamlyn and Bonatti, 1980; Dick and Bullen, 1984). Furthermore, an increase in Cr# in peridotites suggests an *increase* in the degree of depletion and partial melting in the mantle (Dick and Bullen, 1984).

The analytical procedure used in this thesis and a listing of the data obtained are presented in Appendix 2. In general, the spinels probed were relatively pristine with only minor alteration at their rims to magnetite, and rarer ferrit-chromite. Therefore, analyses were taken from the core of individual grains. At least three spinels were analysed in a single sample in order to identify heavily altered grains and discard them from the analysis. The analyses obtained from each sample were then averaged in order to attain a representative spinel composition for the host rock. Therefore, each point in the data sets presented below may be considered the average primary spinel composition for a single rock.

3.3.3. Results and interpretation

Figure 3.5 shows the range of spinels Cr# and Mg# values obtained from the Cyprus samples. The dashed outline represents the field occupied by abyssal peridotites determined by Dick and Bullen (1984). Using this plot, the data may be sub-divided into three main groups, the contents of which are summarised in Table 3.4:

(1) peridotites that display high Cr# values (>60), here termed *'Troodos-type'* peridotites;
(2) peridotites that possess low Cr# values (<60), referred to as *'Mamonia-type'* peridotites and ;
(3) an 'intermediate' group of peridotites (Cr# 40-60).

Individual samples within the 'intermediate' group can be independently re-assigned to either the Troodos- *or* Mamonia-types based on their field relationships or on textural grounds (e.g. colour and morphology of spinel, microstructure etc). Thus, the intermediate group is merely an artefact of the overlapping Cr# and Mg# values of peridotites associated with Troodos- and Mamonia-types (see inset, Figure 3.5).

The ***Troodos-type*** is defined by the range of values obtained from the Mt. Olympus samples. In this respect these Troodos Massif rocks are used as a geochemical reference. The range of high Cr# values (41 < Cr# < 89) are considered characteristic of the Troodos-type peridotites and are comparable to published data from the Troodos Massif (30 < Cr# <~85; Dick and Bullen, 1984).

The ***Mamonia-type*** is defined in a similar manner; peridotites that are associated only with the Mamonia Complex display low Cr# values (generally <50), which are considered characteristic of this type.

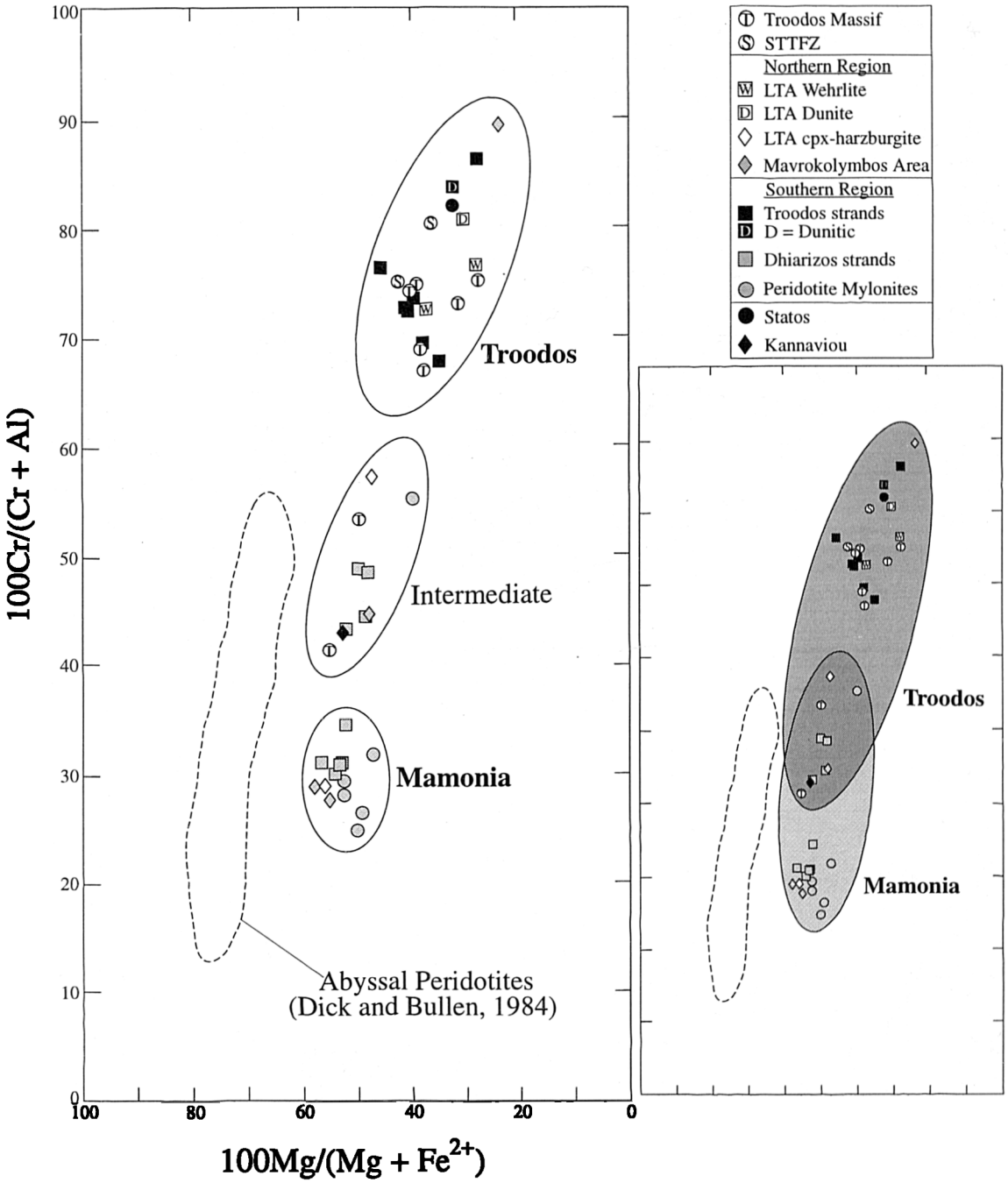

Figure 3.5. Plot of spinel Cr# against Mg# for peridotites from Cyprus (after Dick and Bullen, 1984). The plot on the right hand side is an interpretation of the data.

GROUP	CONTENTS
TROODOS-TYPE	Regional Most (6 out of 8) samples from Mt. Olympus, Troodos Massif. South Troodos Transform Fault Zone (STTFZ) samples A representative sample from the fault zone at Statos Northern Region Wehrlite and Dunite from the western end of the peridotite body at Loutra tis Aphroditis (LTA). One sample from Mavrokolymbos Dam Southern Region All samples (8) from the two main faults in contact with the Troodos sliver ("Troodos strands")
MAMONIA-TYPE	Northern Region 2 out of 4 samples from Mavrokolymbos Dam One sample from clinopyroxene-bearing harzburgite from the eastern end of the peridotite body at LTA. Southern Region Most (5 out of 9) samples from fault zones in contact with, or enclosed by, Dhiarizos Group units ("Dhiarizos strands"). Most (5 out of 6) peridotite mylonites.
INTERMEDIATE	Regional 2 out of 8 samples from Mt. Olympus, Troodos Massif*. A representative sample from the fault zone at Kannaviou*. Northern Region 1 out of 4 samples from Mavrokolymbos Dam^{+}. One sample from clinopyroxene-bearing harzburgite from the eastern end of the peridotite body at LTA^{+}. Southern Region 4 out of 9 samples from "Dhiarizos strands"$^{+}$. One peridotite mylonite^{+}.

Table 3.4. Summary of the contents of the three groups of Cyprus peridotites based on Cr# and Mg# (* = associated with Troodos-type; $^{+}$ = associated with Mamonia-type).

By assuming that the spinel compositions obtained are representative of their host fault zone chemistry, individual sections of the serpentinite-filled faults in SW Cyprus may be characterised (Figures 3.6 and 3.7). For example, the faults in the

Southern Region that bound the central Troodos Complex sliver possess high Cr# values, which suggests that the fault zone protolith is geochemically related to the Troodos Complex. Similarly, peridotites sampled from the fault zones in the Southern Region that are in contact with, or bound by, Dhiarizos Group units exhibit low Cr# values, suggestive of a Mamonia-related origin. Figures 3.6 and 3.7 show a highly idealised representation of the data and is presented as an indication of the spatial variation between the two types of fault zone protolith. The fault zones are assigned to either Mamonia- or Troodos-types based on geochemical Cr# data and also on petrological grounds (i.e. clinopyroxene content and spinel colour and morphology). However, note that certain doubt concerning the association of some fault zones still exist. This is attributed to local complexities and also to a lack of data from certain areas, for example:

- Only two peridotites were analysed from the Statos-Kannaviou serpentinite. The Statos sample displays high Cr# (81.8), whilst the Cr# from the Kannaviou peridotite is relatively low (52.7). Although, the value for the Kannaviou sample is within the range of Troodos peridotites, a genetic relationship with the Troodos Complex cannot be confirmed because the relatively low value of Cr# may suggest an affinity with the Mamonia Complex;
- Most samples (3 out of 4) analysed from the Mavrokolymbos Dam area have low Cr# values, suggesting an association with the Mamonia Complex. However, one sample, which was obtained near a thrust contact with the Troodos Complex, possesses the highest Cr# value and lowest Mg# of all the rocks studied; this sample displays phase layering, the origin of which is not understood.

Fortunately, a number of significant conclusions can be made from this study:

1. The peridotite mylonites of the Southern Region generally possess low Cr# indicative of a Mamonia association. This affinity is discussed in greater detail in Chapters 4 and 6.
2. The coastal section at Loutra tis Aphroditis (LTA) exposes two types of peridotite; the majority are clinopyroxene harzburgites, which are Mamonia-type, but a relatively small sliver of Troodos-type wehrlites and dunites crop out at the western end of the fault zone (Figure 3.6). This evidence, which is described and discussed further in Chapter 5, suggests that Mamonia and Troodos peridotites are juxtaposed within the fault zones, at least locally, in the Northern Region.
3. The wehrlite and clinopyroxenite intrusives that crop out within the fault zones of the Southern Region contain identical spinels to those observed in Troodos-type peridotites. The similar chemistry suggests that they, as well as the mafic intrusives, are of Troodos affinity.

4. Locally, zones of Mamonia-type serpentinites are preserved adjacent to Mamonia Complex rocks, along the boundaries of the two main Troodos-type fault belts (Figure 3.7). These localities are discussed further in Chapter 4.

This allocation of peridotites and their serpentinised products to Mamonia- or Troodos-types obviously bears a strong genetic connotation (see below). The following discussion aims to address and substantiate the use of these terms in describing the ultramafic rocks of SW Cyprus.

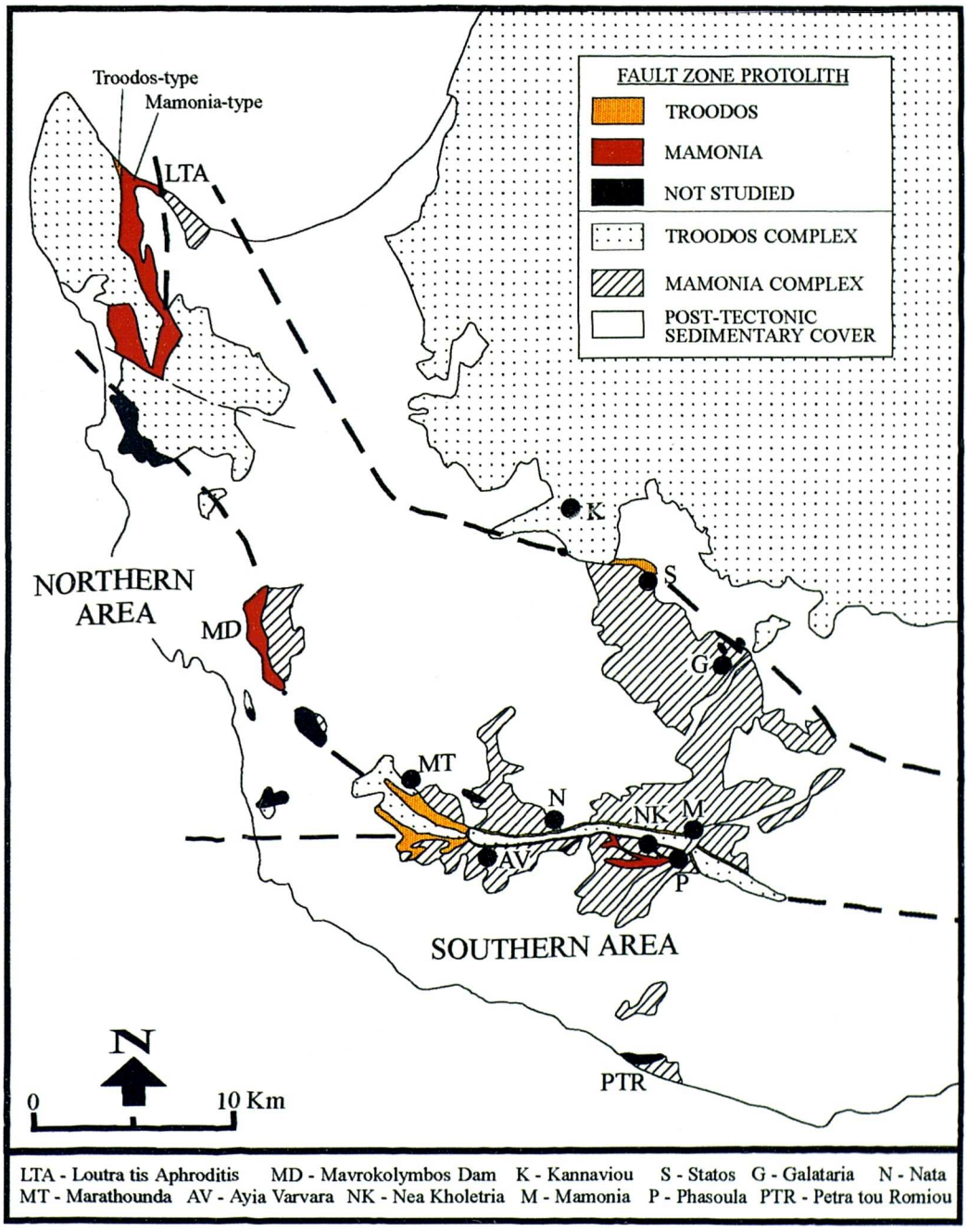

Figure 3.6. Characterisation of the serpentinite-filled fault zones in SW Cyprus based on the distribution of Troodos- and Mamonia-type peridotite protoliths.

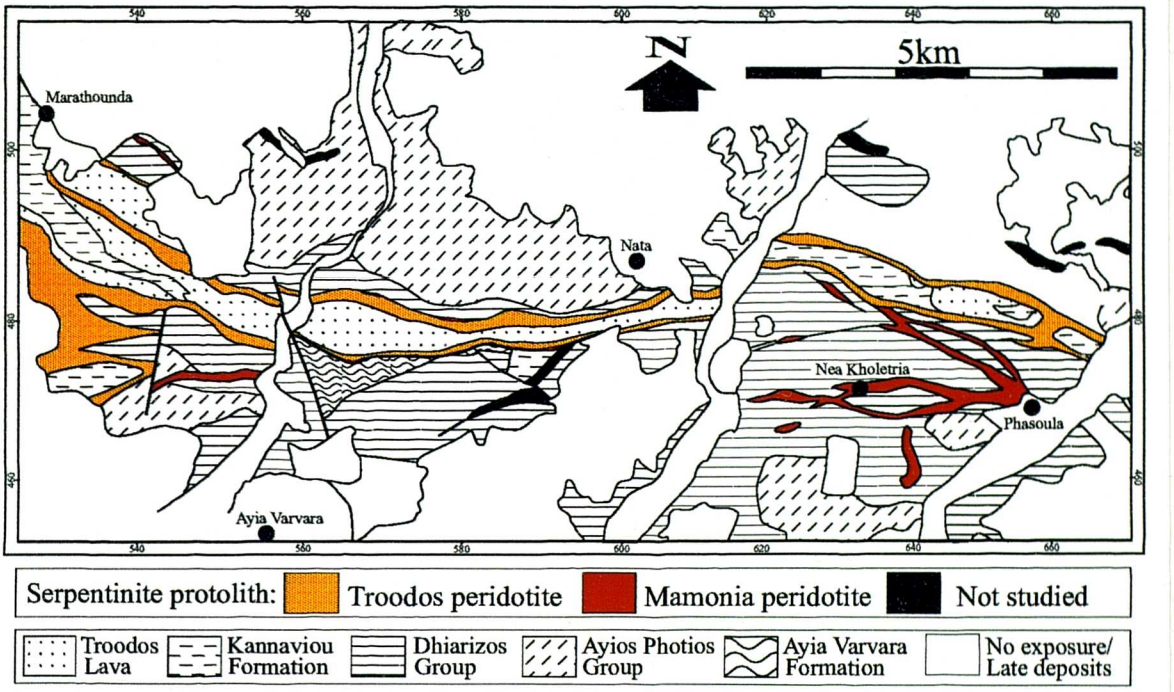

Figure 3.7. Distribution of Troodos- and Mamonia-type protoliths in the Southern Region. Note the presence of localised units of Mamonia-type serpentinites, which are situated along the boundaries of the two main Troodos-type fault belts, adjacent to Mamonia Complex rocks. These localities are discussed in Chapter 4.

3.3.4. Discussion

By examining the chemical variation of chrome spinel with changes in modal and mineral composition in a large number of oceanic and ophiolitic peridotites, Dick and Bullen (1984) classified spinel-bearing peridotites into three categories: ***Type I*** peridotites contain spinels with Cr# < 60 and are associated with abyssal peridotites formed at mid-ocean ridge spreading centres; ***Type III*** peridotites possess spinels with Cr# > 60 and are inferred to relate to sub-volcanic arc petrogenesis. ***Type II*** peridotites are intermediate between types I and III. The essential difference between Type I and Type III peridotites is thought to reflect the presence or absence of clinopyroxene in the residue at the end of melting (see below).

In their analyses, Dick and Bullen (*op cit.*) identified peridotites from the Troodos Massif, comprising mostly harzburgite and enstatite-rich dunite, as some of the most refractory examples of Type III. The range of data presented by Dick and Bullen (*op cit.*) for the Troodos Massif is comparable to that obtained for the Troodos-

type of this study, and thus the two are considered equivalent. The high degree of depletion (generally >60Cr#) that is characteristically displayed is thought to relate to melting in an arc-related oceanic environment (see below).

Dick and Bullen (*op cit.*) defined a field in Cr# and Mg# space (see Figure 3.5), which they considered representative of abyssal peridotites. The abrupt upper limit of Cr# ≈60 in these rocks, which is also the upper boundary of their Type I and the Mamonia-type of this study, suggests that the degree of melting of abyssal mantle is limited. This constraint has been attributed by numerous authors to reflect the partitioning of alumina between spinel and pyroxene, and the alumina content of these minerals at the point at which clinopyroxene disappears from the residue during melting (Dick, 1977, 1978; Dick and Fisher, 1983). Even though a significant number of abyssal peridotites contain little or no clinopyroxene, these rocks (and all Type I peridotites studied by Dick and Bullen (*op cit.*)) contain orthopyroxene rich in CaO, which suggests that the orthopyroxenes were close to saturation with respect to clinopyroxene at the end of melting. In contrast, peridotites with high Cr# spinels generally contain orthopyroxene poor in CaO and Al_2O_3, and are thus undersaturated with respect to clinopyroxene (Dick, 1977). Dick and Bullen (*op cit.*) used this as evidence to suggest the *diopside in: diopside out* phase boundary constitutes a barrier beyond which mantle melting beneath mid-ocean ridges is hindered.

The cause for the high degree of depletion of Type III peridotites, to which the Troodos-type peridotites are assigned, is thought to reflect the influx of water or hydrous melt into the mantle above a subduction zone. This hypothesis is supported by the proposed geodynamic environment for the genesis of the Troodos ophiolite above an intra-oceanic subduction zone (Pearce, 1975; Pearce *et al.* 1984). Experimental studies on mantle melting suggest that water imparts two critical effects; (1) it lowers the melting temperature by hundreds of degrees, and (2) shifts the melt composition towards pyroxene (Dick and Bullen, 1984; Bonatti and Michael, 1989, and references therein). Thus, above a subducting slab where water is introduced into the mantle wedge, pyroxene would disappear at a significantly greater rate and melting would proceed at significantly lower temperatures than under the relatively anhydrous conditions thought to exist in the mantle beneath mid-ocean ridges. The absence of clinopyroxene in the Troodos-type peridotites compared to the clinopyroxene-rich peridotites of the Mamonia-type, suggests the operation of a similar process. For example, the Mamonia-type peridotites are inferred to represent residues of relatively anhydrous partial melting in an oceanic (passive margin, mid-oceanic ridge?) environment. The Troodos-type peridotites, on the other hand, are considered products of hydrous melting above an intra-oceanic subduction zone (e.g. Pearce, 1975; Pearce *et al.* 1984). However, note that the Troodos-type samples, although

highly depleted, may not have undergone greater amounts of melting than the Mamonia-type rocks. Instead, the Troodos rocks may have experienced a more rapid disappearance of clinopyroxene during melting than those of the Mamonia-type (Dick and Fisher, 1983; Dick and Bullen, 1984).

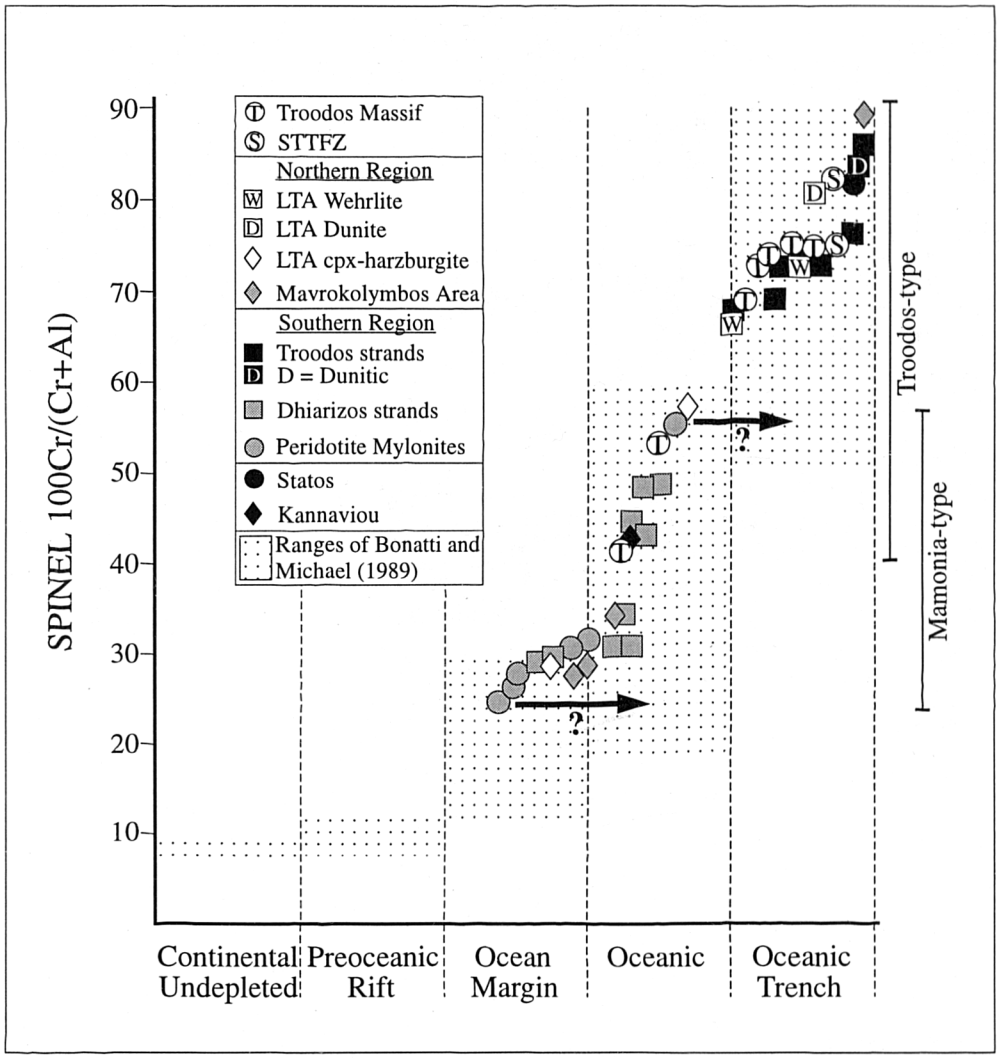

Figure 3.8. Spinel Cr# data of Cyprus peridotites plotted against inferred tectonic setting. Dotted regions are the ranges of data presented by Bonatti and Hamlyn, 1989).

By utilising a large peridotite data set and employing a variety of mineral chemical parameters (including spinel Cr#), Bonatti and Michael (1989) characterised peridotites from a variety of oceanic settings, correlating peridotite chemistry with geodynamic environment. In their study, they recognised an increase in the degree of depletion (i.e. an increase in Cr#) of spinel-bearing peridotites going from pre-oceanic rifts to passive margins to mature oceans to subduction-related oceanic trenches,. Figure 3.8. displays the range of Cr# from the Cyprus peridotites plotted against inferred tectonic setting. The dotted areas show the extent of Cr# compiled by Bonatti

and Michael (*op cit.*) for a particular tectonic setting. Going from left to right across the plot, the increase in Cr# reflects an increase in the degree of depletion and, as expected following the above discussion, the Troodos-type samples plot within the confines of the 'oceanic trench' field. In contrast, the distance of the Mamonia-type samples along the horizontal (x-) tectonic setting axis is much more conjectural. Most of the Mamonia-type data falls within the 'oceanic' field (i.e. mid-ocean ridges and fracture zones), but some of the samples have been purposely assigned in the 'ocean margin' field. This is because the volcanic and sedimentary rocks of the Mamonia Complex are thought to document continental break-up, the development of a passive margin *and* the opening of a small oceanic basin (e.g. Swarbrick, 1979, 1980; Swarbrick and Robertson, 1980). Therefore, the range of data for the Mamonia-type along the tectonic setting axis illustrates the possibility that some of these peridotites may relate to the Mamonia passive margin.

In summary, this study has recognised that two different types of peridotite exist in SW Cyprus, which are most probably genetically related to the Mamonia and Troodos Complexes. Further work beyond the scope of this study is required to establish fully their mantle evolution.

PART THREE
KINEMATIC AND TEXTURAL EVOLUTION OF THE SERPENTINITE-FILLED FAULTS OF SW CYPRUS

CHAPTER 4
KINEMATIC EVOLUTION OF THE SOUTHERN REGION

4.1. Introduction

Previous work on the regional geology of SW Cyprus (e.g. Lapierre, 1968, 1972, 1975a, 1975b; Swarbrick, 1979, 1980, 1993; Robertson and Woodcock, 1979; Swarbrick and Robertson, 1980; Malpas *et al.* 1992, 1993) and reconnaissance mapping undertaken as part of this thesis, suggest that the role of the serpentinite-filled faults is critical in explaining the tectonic evolution of the region. However, until recently detailed structural analyses of these faults were severely limited (Swarbrick, 1993; Malpas *et al.* 1993). Field observations suggest that strain is preferentially localised along the serpentinite-filled fractures, as opposed to the adjacent Mamonia and Troodos Complex rocks, in both the Southern and Northern Regions. Therefore, the structural study presented in this thesis has focused on these faults zones. This chapter deals with the faults in the Southern Region, whilst Chapter 5 concerns those in the Northern Region.

The Southern Region of SW Cyprus extends from Marathounda in the west to Mamonia in the east (Figure 4.1). Figure 4.1 summarises the areas and localities referred to in this chapter, which are shown in greater detail in Map I. The geology of the region is characterised by east-west striking, pre-dominantly sub-vertical, serpentinite-filled faults that bound and separate a sliver of Troodos Complex material from rocks of the Mamonia Complex to the north and south. Two main serpentinite-bearing fractures dominate, which are referred to as *northern* and *southern* fault zones, describing their locations with respect to the Troodos sliver. Minor faults bifurcate and anastomose from the major fault strands, incorporating less deformed lenses of mainly Dhiarizos Group material. The geochemical relationship between the serpentinites filling these faults has been discussed in Chapter 3.

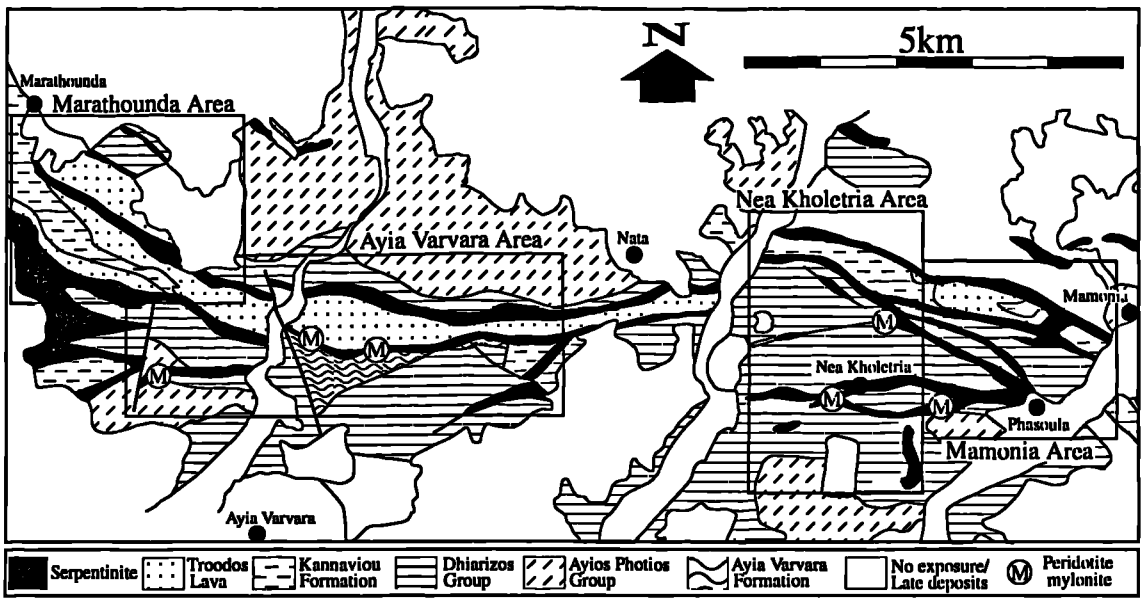

Figure 4.1. Geological map of the Southern Region (adapted after Swarbrick, 1979), showing the areas referred to in this thesis and the location of peridotite mylonite outcrops.

The serpentinite-filled fault zones characteristically crop out as approximately E-W trending, linear ridges. The most upstanding ridges are typically the least serpentinised, comprising blocks of only partially hydrated mantle peridotite (10cm to >10m diameter). In contrast, the most heavily weathered, topographically subdued scctions of the faults are ubiquitously scrpcntinised and characterised by a thoroughly pervasive, predominantly sub-vertical foliation that strikes E-W.

In general, Troodos lavas within the fault bound slivers display well preserved pillow forms and infrequent small-scale brittle faults (~1m scale), suggesting only minor tectonic disruption. However, within narrow zones (1-5m wide) immediately adjacent to the serpentinite-filled faults, the lavas occasionally display slightly ellipsoidal pillow forms and sub-vertical, brittle foliations that parallel the local fault boundaries (e.g. GR 651 483 in the Mamonia area). Throughout the Southern Region (and SW Cyprus), Kannaviou Formation sediments depositionally overlie Troodos lavas, but significantly, they are never found on top of the Mamonia Complex (Swarbrick, 1993; Gass *et al.* 1994). As the Kannaviou Formation readily weathers to grey-brown coloured swelling clays, sedimentary structures are rarely observed. However, where preserved (e.g. within the central Troodos sliver, 1km north of Nea Kholetria village at GR 641 483), bedding dips sub-vertically and strikes E-W, suggesting these sediments have been deformed.

In contrast to the Troodos Complex, the Dhiarizos Group, which crops out to the north and south of the main serpentinite belts, displays much greater evidence for tectonic disruption. Variably sized blocks (10cm to 10m-scale) of Kholetria limestone lie haphazardly in a chaotic melange of green to purple coloured lavas of the Phasoula Formation. In proximity to the serpentinite-filled faults, Dhiarizos lavas occasionally display marked elongations in high strain zones, forming ellipsoids with mean length:width ratios of 6:1 and long axes that plunge sub-horizontally to the east or west (Swarbrick, 1979). One of these zones is exposed 0.5km north of Nea Kholetria village (GR 636 478) and possesses a width at outcrop of approximately 100m N-S. About 50m to the south of this locality, Dhiarizos lavas display distinct pillow forms, which suggests deformation is localised to the vicinity of the serpentinite fault zones.

In contrast to the Dhiarizos Group, sedimentary rocks of the Ayios Photios Group typically crop out away from the serpentinite fault zones. In general, exposure of Ayios Photios Group rocks near the fault zones is sparse in the Southern Region, but where exposed, they are significantly internally disrupted.

All the above field observations suggest that strain in the Southern Region is localised to, and within the vicinity of, the serpentinite-filled fault zones. Therefore, it seems logical to study the kinematic history of the fault zones first and foremost in an attempt to unravel the tectonic history of SW Cyprus.

Structural, textural and mineralogical observations suggest that the fault zones have experienced a polyphase deformational history during the Upper Cretaceous. The faults appear to have formed zones of rheological weakness within the oceanic lithosphere, which resulted in the localisation of deformation, making the faults susceptible to reactivation. Mechanical weakness is attributed, at least in part, to the effects of hydrous fluid flux throughout the history of the fault zones.

This chapter is sub-divided into three main sections. Each section details the field relationships, structures and microfabrics characteristic of deformation at three distinct temperature conditions:-

1. Early, (Turonian to Santonian; 90-83Ma) dextral strike-slip that formed ***high temperature, (>600°C)*** peridotite mylonites. A microstructural and mineralogical chronology is detailed, which documents a switch in the dominant deformation mechanisms under changing geological conditions. Spatial and genetic relationships between serpentinite and the Dhiarizos Group and the Ayia Varvara Formation metamorphic rocks are discussed, together with similarities to units and structures in the South Troodos Transform Fault Zone.

2. Dextral transtensional/extensional deformation associated with serpentinite protrusion at relatively low temperatures ***(~100-600°C)***. *'Transitional'* serpentinite fabrics formed during this event are detailed and protrusive mechanisms discussed.
3. Late-Maastrichtian (cessation ~65Ma) sinistral transpression at ***low temperatures*** ***(≤100°C)***. Structures are interpreted to result from a *pure shear-dominated* transpression, during which a large component of strike-parallel extension took place.

4.2. High temperature deformation

The earliest deformational phase in the Southern Region is preserved as rare peridotite mylonites, which were first recognised and only briefly described by Malpas *et al.* (1993). The location of exposures of these mylonites has been described and listed in Chapter 3 (see Table 3.2)and the locations of mylonites are also shown in Figure 4.1. Outcrops of peridotite mylonite are typically found in contact with Ayia Varvara Formation metamorphic rocks, but occasionally rare isolated blocks (<15m in diameter) of mylonite are bound by serpentinite only (Nea Kholetria area, GR 631 468). The largest exposures reach 20m in diameter (Ayia Varvara area, GR 551 477), whilst the smallest occur as thin 'rinds' (>30cm wide) at contacts between the Ayia Varvara Formation and serpentinite (e.g. Mamonia area, GR 649 469; Ayia Varvara area, GR 571 475 and 560 477). At outcrop, the mylonites are identified by an intense, pervasive strike-parallel stretching lineation, with or without a foliation, which defines strong L- and LS-tectonite fabrics (Figure 4.2). When pristine, these rocks are dark in colour, but characteristically weathering accentuates the linear fabric, defining alternating bands (<1cm) of buff-brown, dark brown and occasionally 'brick-red' coloured material, which are presumably compositionally distinct. In hand specimen, the lineation is paralleled by rounded and elongate, bronze coloured orthopyroxene grains (typically ~0.5 cm in length) and by small (~1mm), silver minerals, which are similar in appearance to white mica. At the micro-scale, the mylonites preserve evidence of a textural chronology that documents deformation at high temperatures (>600°C). In thin section, these rocks are characterised by intense grain size reduction and syn-kinematic metamorphic phase changes, which are described in detail below.

Two peridotite mylonite textural end-members are defined on the basis of their microstructural characteristics: (a) high strain 'fluidal' fabrics, and (b) later amphibole-rich fabrics. Cross-cutting and overprinting relationships indicate amphibole-rich mylonites post-date the development of fluidal fabrics. Both textural types are discussed separately, but note that a complete spectrum of fabrics exist between these

end-members, suggesting that they may be products of the same progressive deformational event.

Figure 4.2. Characteristic peridotite mylonite at outcrop, displaying a strong L-tectonite fabric. No orientation is shown as this block is not in situ (Mamonia area, GR 651 468).

4.2.1. Fluidal Fabrics

The term *'fluidal'* is adopted from the existing literature concerning peridotite mylonites as there are textural similarities with fabrics preserved in ultramafic xenoliths erupted with kimberlites and basalts (Boullier and Nicholas, 1975; Boullier and Guegen , 1975; Harte, 1977; Mercier, 1985; Nicholas, 1986), and in basal peridotites associated with obducted ophiolites (Drury *et al.* 1990). As fluidal mylonites are observed in varied geotectonic environments, the application of this term is merely descriptive and has no genetic connotations.

Fluidal fabrics are characterised by large, rounded, clinopyroxene and orthopyroxene porphyroclasts supported in a fine grained (6-39μm), heavily recrystallised, polymineralic matrix (Figure 4.3a), generally displaying an equigranular mosaic texture (Figure 4.3b) (e.g. Mercier and Nicolas, 1975; Harte, 1977). The rock possesses a weak discontinuous foliation and lineation defined by recrystallised tails connected to porphyroclasts of the same material. Porphyroclasts have a bimodal

grain-size distribution; larger grains range in size from 2-5mm in diameter, as opposed to the smaller clasts which range from 0.1-0.8mm. Both appear to have been rotated, show no shape- or crystallographic-preferred orientations, and occasionally display internal deformational characteristics such as kink-banding and undulose extinction (Figure 4.3a). Orthopyroxene porphyroclasts frequently possess clinopyroxene exsolution lamellae, whilst the inverse relationship is rare. In general, porphyroclasts are rimmed or mantled by several generations of their recrystallisation and reaction products (Figure 4.3a; also see section 4.2.3).

(a)

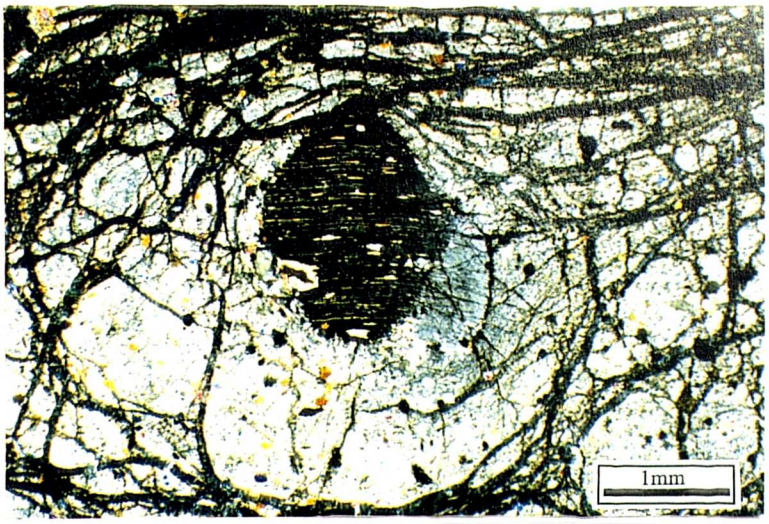

(b)

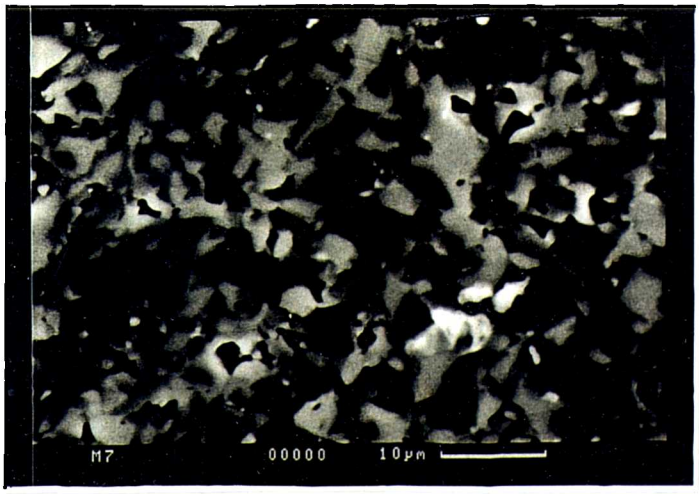

Figure 4.3a. Characteristic fluidal microstructure viewed under cross-polars. Note that the kinked orthopyroxene porphyroclast is mantled by its fine-grained recrystallisation and reaction (amphibole) products and that it possesses clinopyroxene exsolution lamellae (higher birefringence than host grain). (Sample M7I/95).

Figure 4.3b. Backscattered scanning electron micrograph showing the characteristic polymineralic, fine-grained, equigranular, mosaic-textured matrix of a fluidal mylonite. The difference in shade reflects the contrast in atomic numbers of the individual mineral grains; CPX (light grey), OPX (dark grey), AMPH (mid-grey). (Sample M7I/95)

(a)

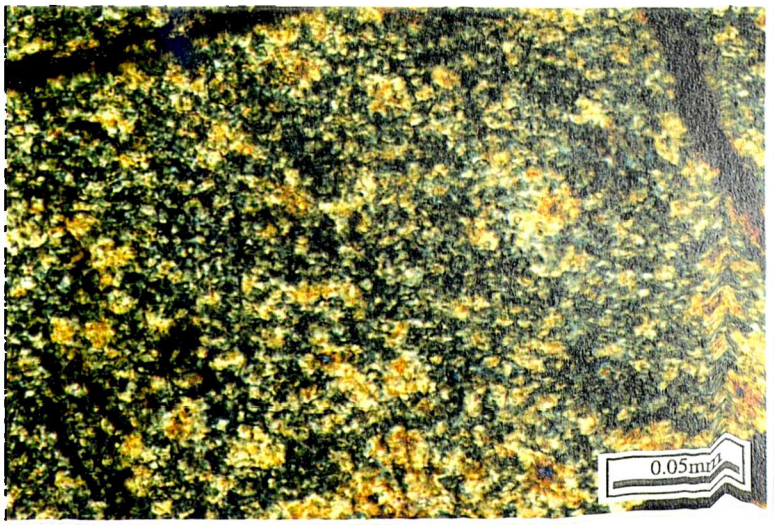

(b)

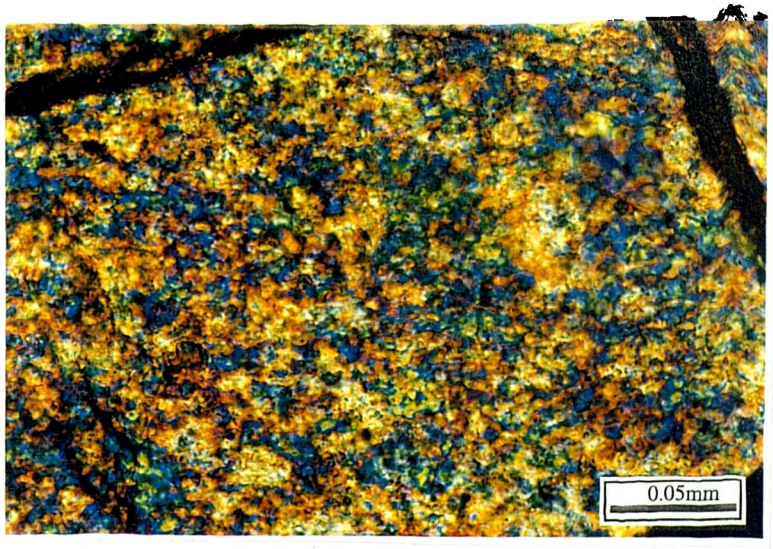

Figure 4.4. Optical micrograph showing the characteristic fine-grained microstructure of a fluidal mylonite matrix. Note the irregular, sutured grain boundaries. Cross polars without (a) and with (b) a sensitive (gypsum) plate addition. (b) The random colouration shows the lack of crystallographic-preferred orientations in these fabrics. (Sample M7II/95).

The matrix is heterogeneous in terms of grain-size and composition, and comprises olivine, clinopyroxene, orthopyroxene, amphibole and green-brown spinel in variable proportions. The variation in grain-size relates to the variable degree of recrystallisation (see section 4.2.4), which indicates heterogeneous strain on the grain scale. In general, matrix grains are equant and show little or no crystallographic-preferred orientations (Figure 4.4a and b). However, in proximity to porphyroclasts and cross-cutting shear zones, grains become elongate and define a foliation that wraps porphyroclasts and parallels shear zone boundaries (see section 4.2.4). The larger matrix grains (>20μm) display minor subgrain development, whilst the smaller grains (<20μm) appear unstrained and frequently possess irregular, sutured grain boundaries.

The mineralogical heterogeneity of these fabrics can be directly related to the mechanical breakdown of porphyroclasts; the recrystallised products define tails that are stretched out along the local flow plane away from the porphyroclast. With increasing proximity to amphibole-rich shear zones, porphyroclasts and their tails develop asymmetrical shapes, which combined with the strike-parallel stretching lineation, indicate *dextral strike-slip* (Figure 4.5). Also, in such regions, the grain size and compositional variations define a foliation and lineation. The existence of fine-grained amphibole replacing clinopyroxene in these fabrics suggests hydrous fluid was present at the earliest stages of deformation (see section 4.2.3; *cf.* Drury *et al.* 1990).

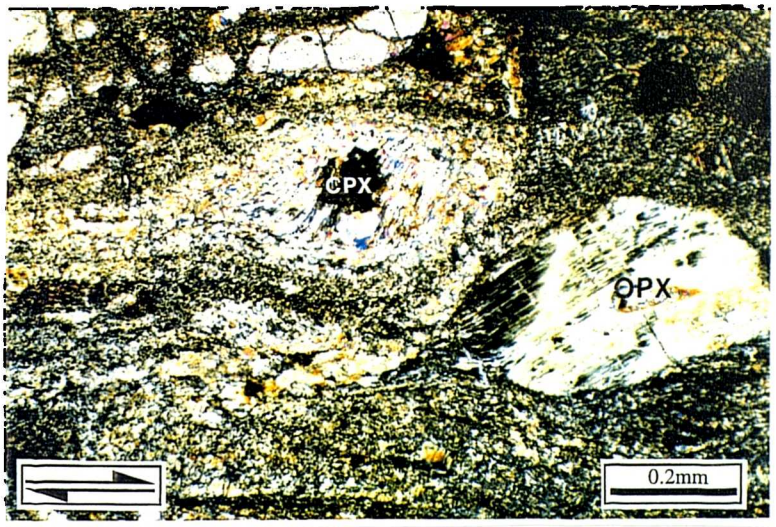

Figure 4.5. Asymmetrical porphyroclast systems developed in clinopyroxene (top) and orthopyroxene (bottom) indicating dextral shear. Note abrupt change in crystallographic-preferred orientations between the core (in extinction) and recrystallised, high birefringent mantle in the clinopyroxene porphyroclast system, which suggests the operation of migration recrystallisation (Drury *et al.* 1990). (Sample M7II/95)

4.2.2. Amphibole-bearing peridotite mylonites

Amphibole-rich peridotite mylonites cross-cut fluidal fabrics and are thus interpreted as the younger end-member. As with the fluidal sub-type, they are characterised by the presence of several generations of small neoblasts of various sizes growing at the periphery of porphyroclasts. However, these fabrics differ in that they generally lack clinopyroxene porphyroclasts, which is attributed to their replacement by amphibole, and the matrix is coarser and dominated by amphibole. Most characteristic is their strong strike-parallel stretching lineation defined mainly by elongate orthopyroxene porphyroclasts (Figure 4.6a) and an amphibole mineral lineation. Orthopyroxene porphyroclasts possess length:width ratios of up to 11:1, are often boudinaged, and frequently display internal deformational characteristics such as undulose extinction and kink-banding. They possess well developed clinopyroxene exsolution lamellae and

volumetrically subordinate spinel lamellae (see section 4.2.3) that are predominantly aligned sub-parallel to foliation. Exsolution lamellae are frequently absent as the grain boundary is approached, a feature which is attributed to local chemical re-equilibration.

(a)

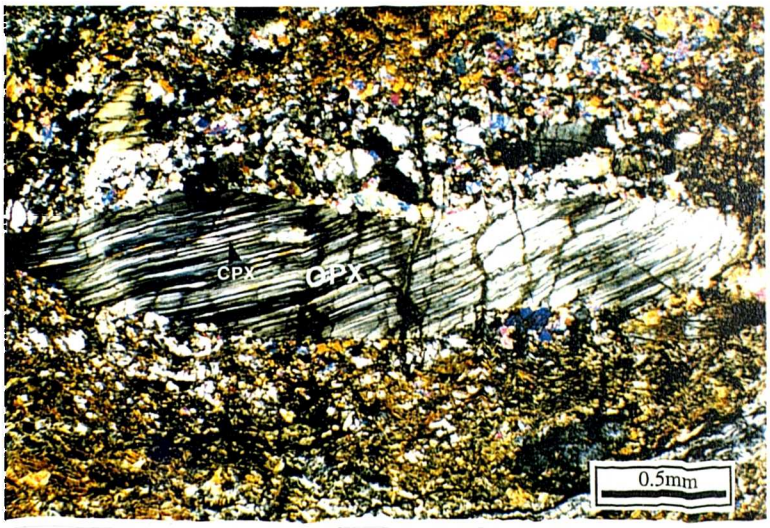

(b)

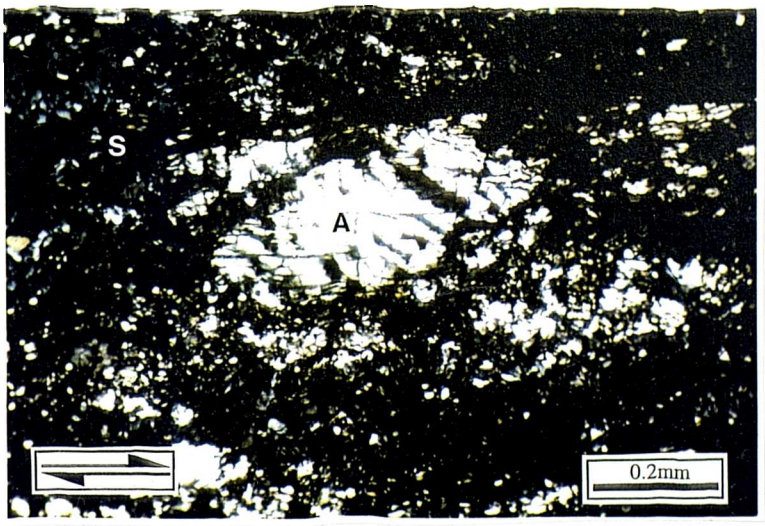

Figure 4.6a. Elongate orthopyroxene (OPX) porphyroclast in an amphibole-rich mylonite. Arrow head in the porphyroclast points to a high birefringent clinopyroxene exsolution lamellae (CPX). (Sample AV/3/95).
Figure 4.6b. Amphibole (A) paleoblast displaying undulose extinction. The dark, low birefringent matrix is post-kinematic serpentine (S). Arrows in the inset indicate dextral shear (Sample REH3/96).

As stated above, matrix olivine grains are coarser than those in the fluidal sub-type, ranging from 0.05-0.25mm in diameter. Occasionally they are elongate, with long dimensions parallel to the stretching lineation, but more commonly they are equant, possessing little or no internal deformation characteristics and planar grain boundaries. The microstructure of these rocks is dominated by amphibole-rich foliation-parallel layers (~0.4mm wide) that extend across the length of a thin section.

Amphibole exists as deformed paleoblasts (Figure 4.6b) (old strained grains) (0.1-0.75mm), possessing undulose extinction, and as recrystallised neoblasts (<150μm), both of which commonly possess well defined crystallographic- and shape-preferred orientations (Figures 4.7a and b). Thus, amphibole development is inferred to be syn-kinematic and indicates the ingress of hydrous fluid (see below; *cf.* Drury *et al.* 1990).

(a)

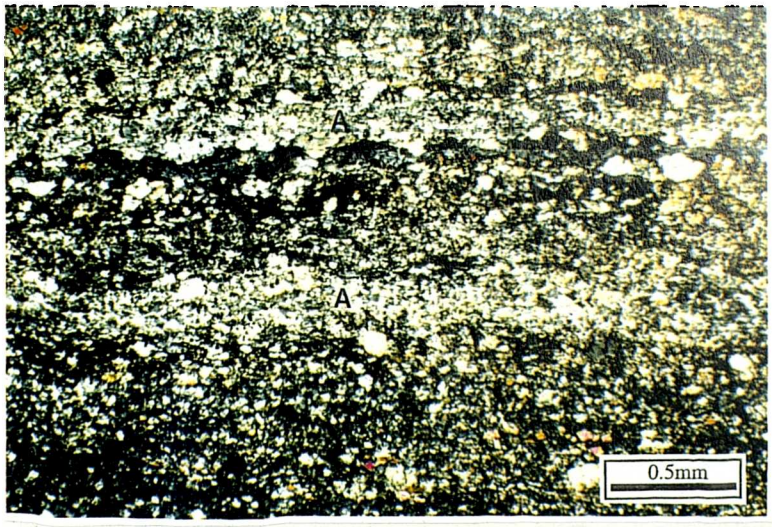

(b)

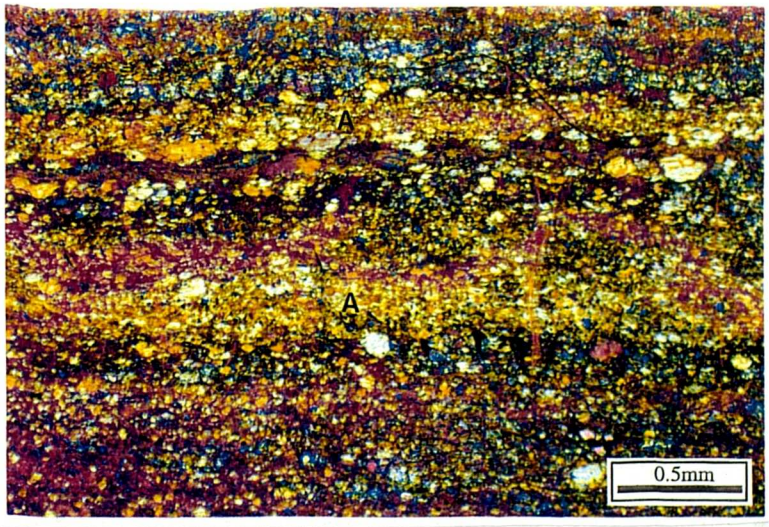

Figure 4.7. Amphibole mylonite microstructure dominated by the crystallographic- and shape-preferred orientation of amphibole; cross polars without (a) and with (b) sensitive (gypsum) plate addition. (b) Shows the well-defined crystallographic-preferred orientations within the amphibole (A) rich layers (orange) (Sample AV/16/95).

Occasionally, these mylonites are transected by foliation-parallel, ultrafine-grained (~10μm), narrow shear zones that are composed almost entirely of amphibole (Figure 4.8). These ultrafine-grained zones commonly border the coarser-grained amphibole-rich layers, which constitute tails to amphibole or clinopyroxene

porphyroclasts. Therefore, these ultrafine grain-sizes are thought to result from progressive dynamic recrystallisation of the coarser-grained layers. The ultrafine-grained zones are characterised by equant grains of amphibole that display little or no crystallographic-preferred orientations. This contrasts the strong preferred orientations observed in the coarser-grained mylonitic fabric outside of the zones.

Dextral strike-slip is again indicated by the existence of asymmetrical porphyroclast systems pre-dominantly associated with pyroxenes, but also amphibole (Figure 4.6b) and infrequently olivine, and by offsets along orthopyroxene cleavage planes (Figure 4.9).

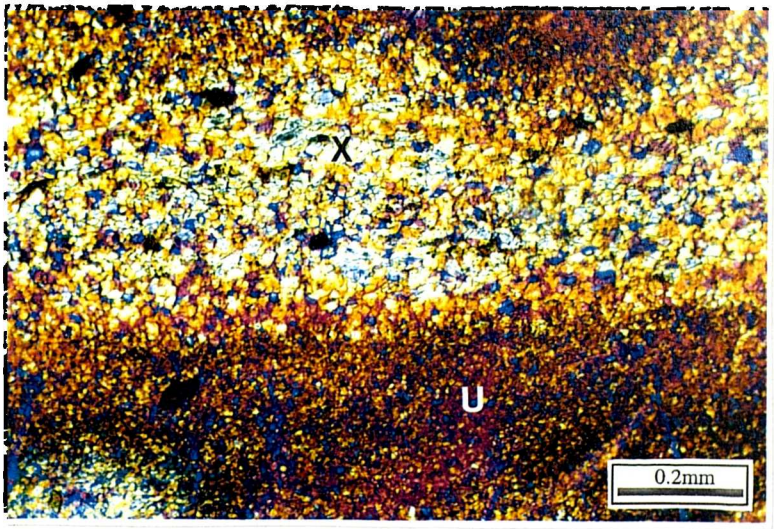

Figure 4.8. Optical micrograph (cross polars with sensitive plate addition) showing a foliation parallel shear zone comprising ~100% amphibole. Amphiboles in the coarser layer (light colours) display strong crystallographic-preferred orientations (X), whilst the crystallographic fabric within the ultrafine-grained zones (U) is much weaker (Sample M7I/95).

Figure 4.9. Offsets along orthopyroxene cleavage planes indicates dextral shear. (Sample AV/16/95).

4.2.3. Mineral chemistry

Using the chemistry of mineral phases and their recrystallised products in peridotites, a number of geological processes can be identified. Examples include metasomatic alteration by hydrous fluids and magmatic melts (Agrinier *et al.* 1993; Sen and Dunn, 1994), and chemical re-equilibration during mantle upwelling and tectonic uplift (Bonatti and Hamlyn, 1978; Hamlyn and Bonatti, 1980). Consequently, mineral chemical analysis of the SW Cyprus peridotite mylonites may be of use in constraining a model for their evolution.

The undeformed protolith of the peridotite mylonites is preserved at many locations, where it is spatially associated with Dhiarizos Group units. The protolith comprises coarse-grained (granular) (<8mm), diopside-bearing spinel harzburgites and lherzolites. The presence of orthopyroxene-spinel clusters (± clinopyroxene), combined with a lack of cumulate textures and an absence of plagioclase, suggests that these rocks are of mantle origin (see Chapter 3); on petrological grounds, clinopyroxene-orthopyroxene-spinel clusters in lherzolites, and orthopyroxene-spinel clusters in harzburgites, are thought to originate from decomposition of garnets during depressurization (e.g. Nicolas, 1986 and references therein).

Qualitative mineral chemistries were determined using a scanning electron microscope (SEM) and attached X-ray detector. The SEM used was a CamScan Series 4, which operated at 20kV. Imaging was carried out using a K.E. Electronics 4 pole solid state backscattered detector with a 10kV threshold. X-ray analyses were obtained using an Oxford Instruments Microanalytical Division (formerly Link Analytical) model AN10/25S EDS using a standard 8 micron thick Be window X-ray detector. Where necessary, the relevant spectra are presented and note that peak heights are proportional to the abundance of each element.

As observed by Sen and Dunn (1994) in experimentally metasomatised peridotites, in addition to the phases originally present (olivine, clinopyroxene, orthopyroxene and spinel), the peridotite mylonites contain amphibole and compositionally modified variants of the original phases. The variable chemistries of all these minerals is an artefact of the chemical exchange of elements such as Cr, Fe and Al between neighbouring mineralogies during metamorphism and therefore, indicates disequilibrium (Moody, 1976).

Pyroxenes

Orthopyroxene porphyroclasts invariably possess clinopyroxene and low Cr-, low Al- (high Si and Mg) spinel exsolution lamellae (Figure 4.10), whilst clinopyroxenes are generally lamellae-free. Both clinopyroxene and orthopyroxene porphyroclasts are

chemically distinct from their recrystallised products. Recrystallised orthopyroxenes are higher in Si and Ca and lower in Al, whilst clinopyroxenes are higher in Si, Mg and Al, and occasionally lower in Ca (Figures 4.11a and b).

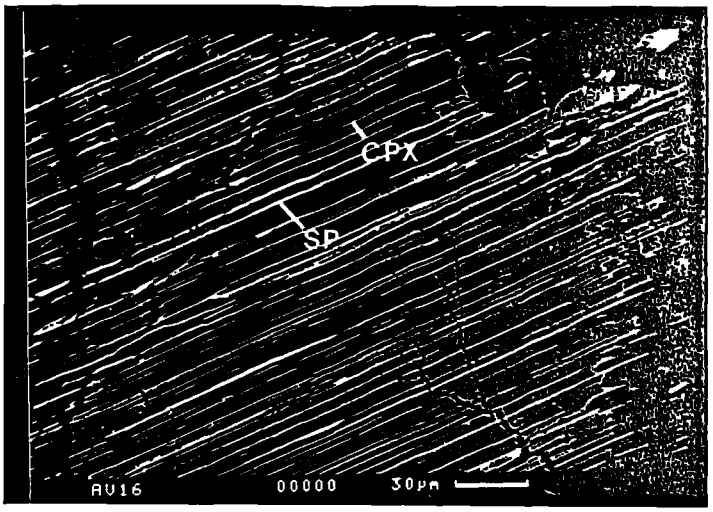

Figure 4.10. Backscattered electron image of exsolution lamellae in an orthopyroxene porphyroclast host. Spinel (SP) lamellae are much brighter than clinopyroxene (CPX) lamellae. (Sample AV/16/95).

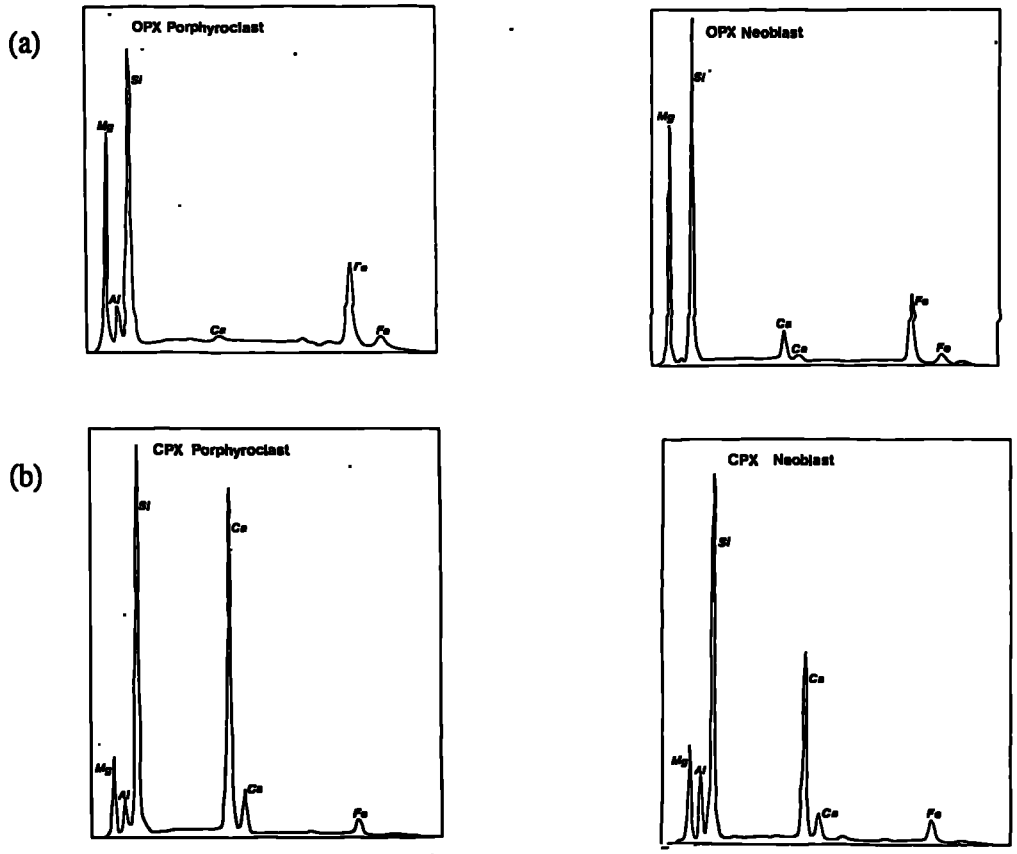

Figure 4.11. Comparative X-ray spectra for (a) orthopyroxene, and (b) clinopyroxene porphyroclast-neoblast pairs, and (c) recrystallised olivine (continued overleaf). Note that no vertical scale is given as the height of the peaks is proportional to element concentration.

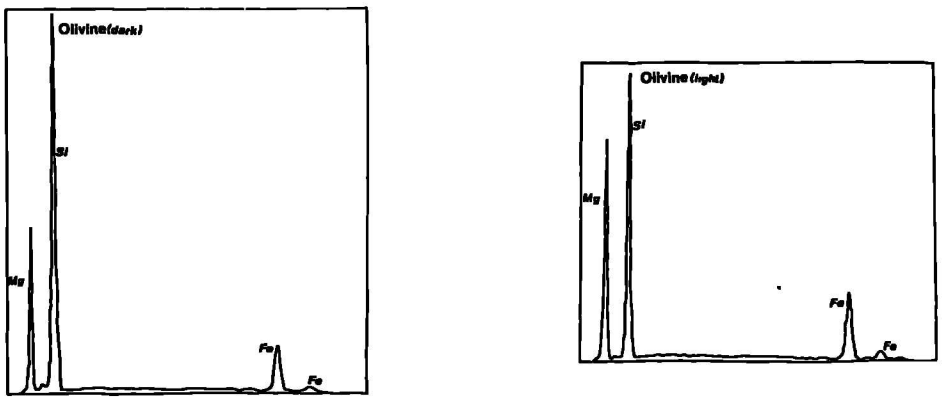

Figure 4.11. (continued) (c) Comparative X-ray spectra for recrystallised olivine grains. The olivine grains are shown in Figure 4.12

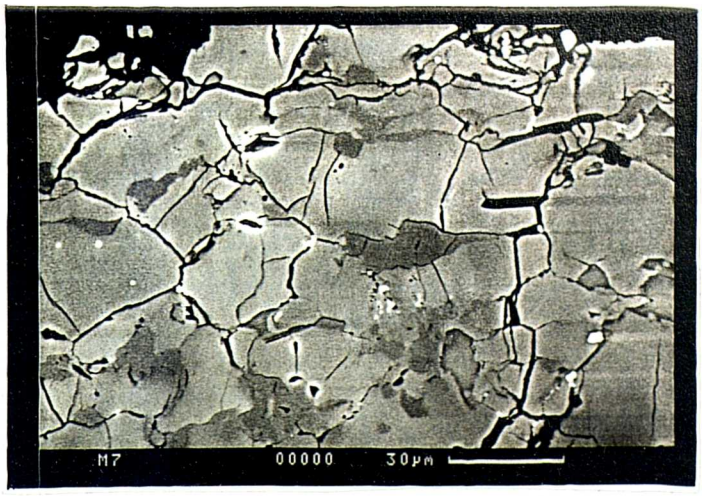

Figure 4.12. Backscattered electron micrograph of matrix olivine in a peridotite mylonite. The difference in shade between the adjacent olivine grains reflects the discrepancy in their atomic numbers and thus, their difference in composition. The dark-grey grains (Fo_{77}) possess a higher Si content than the larger, lighter-grey grains (Fo_{76}). (Sample M7/95).

Olivine

Matrix neoblastic olivine is, in general, compositionally consistent (Fo_{76-78} in fluidal mylonites and Fo_{79-80} in amphibole-rich mylonites), but micron-scale compositional heterogeneities indicate disequilibrium (e.g. Figures 4.11c and 4.12).

Spinel

In thin section, spinel is typically buff-brown in colour and rimmed by magnetite and ferrit chromite in the more serpentinised samples. In the undeformed protolith, spinel is coarse (>0.5mm), intergranular, and commonly occurs in clusters with pyroxene (see Chapter 3). However, during mylonitisation, spinel is dispersed and exists as small, anhedral grains, commonly associated with pyroxene and amphibole.

	1	2	3	4	5
Na_2O	1.019	1.111	1.13	1.15	1.172
SiO_2	53.16	50.493	47.595	50.026	50.258
K_2O	0.073	0.009	0.075	0.014	0.006
MnO	0.088	0.09	0.104	0.117	0.041
MgO	21.358	19.972	19.044	20.117	19.847
$Al2O_3$	5.59	7.614	8.439	8.202	8.316
CaO	12.682	12.865	12.206	12.46	12.71
FeO	2.711	3.121	3.311	3.584	3.12
TiO_2	0.126	0.199	0.221	0.24	0.252
NiO	0.076	0.095	0.074	0.094	0.078
Total	96.883	95.569	92.199	96.004	95.8

Table 4.1. Major (wt%) element data for amphiboles in a sample of amphibole-rich mylonite (sample AV16).

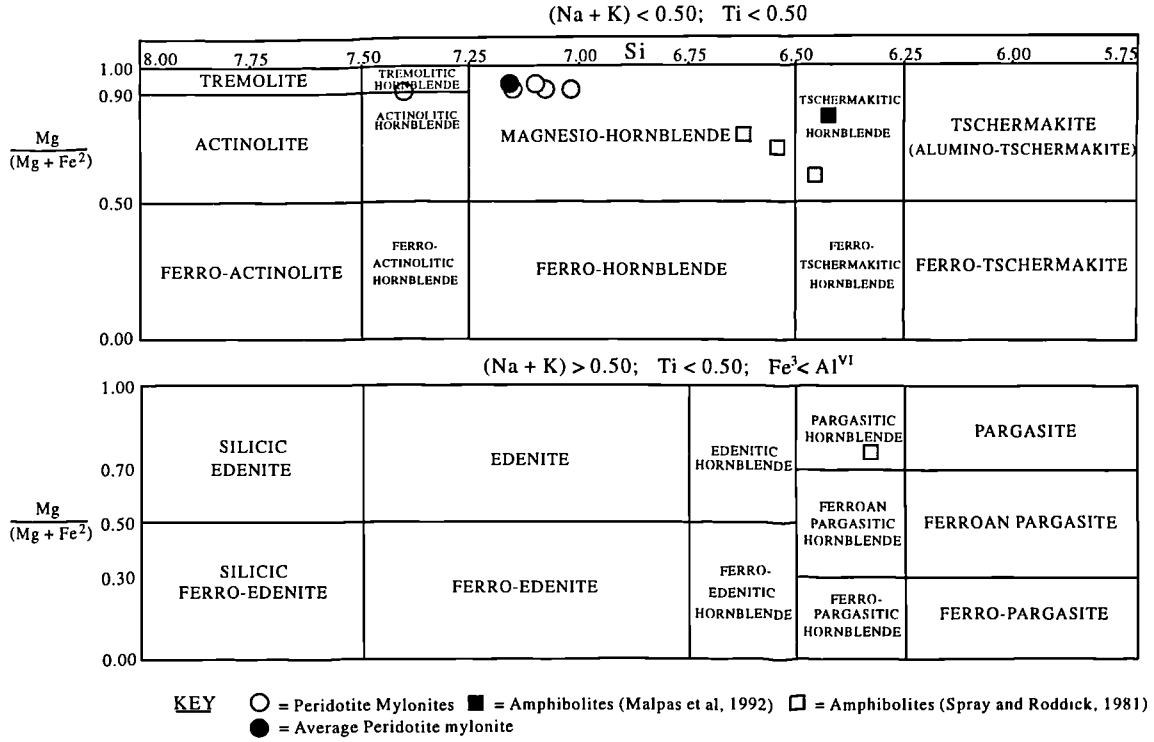

Figure 4.13. Classification of calcic amphiboles after Leake (1978). Circles show positions of amphiboles from peridotite mylonites, whilst black- and grey-squares show published data from Malpas *et al.* (1992) and Spray and Roddick (1981) respectively, for amphiboles from Ayia Varvara amphibolites.

Amphibole

The amphibole from amphibole-rich mylonites (electron microprobe analyses; Table 4.1) is calcic, of *magnesio-hornblende* composition (Figure 4.13) (after terminology devised by Leake, 1978), and possesses the average formula $[Na_{0.32}Ca_{1.92}(Mg_{4.25}Fe_{0.38}Al_{1.28})Si_{7.15}O_{23}(OH)_2]$. Amphiboles in peridotites are generally considered as records of the fluids that reacted with the host rock (Agrinier *et al.* 1993). The low Ti- and K-contents of the amphiboles suggest that the metasomatic agent was a H_2O-rich, low density fluid, rather than a volatile-rich silicate melt (see Eggler, 1987). A crustal origin for the amphibole is also inferred from the magnesio-hornblende composition, as only (Ti-)pargasites in Cr-diopside bearing peridotites are considered to form under upper mantle conditions (Dawson and Smith, 1982).

(a)

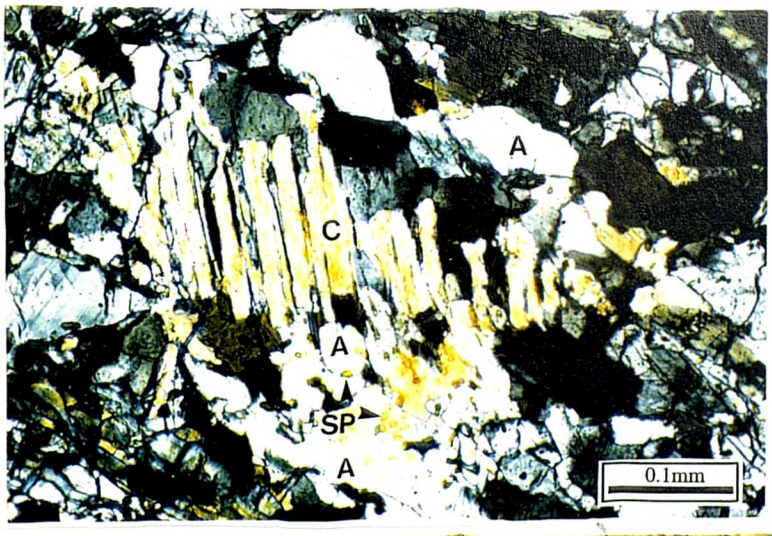

(b)

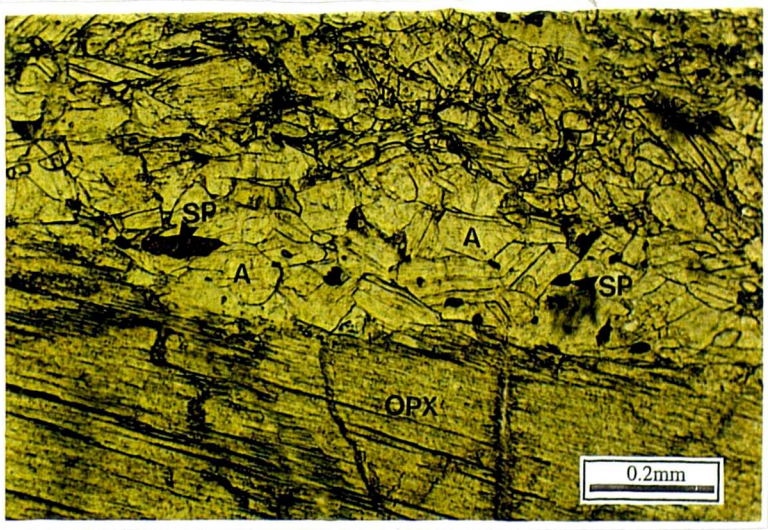

Figure 4.14a. Remnants of a clinopyroxene porphyroclast (C) rimmed by its reaction products amphibole (A) and fine-grained orange spinel (SP). (Sample AV/16/95).
Figure 4.14b. Abundant fine-grained spinel in a coarse amphibole-rich reaction rim to an orthopyroxene porphyroclast (OPX). (Sample AV/16/95).

(a)

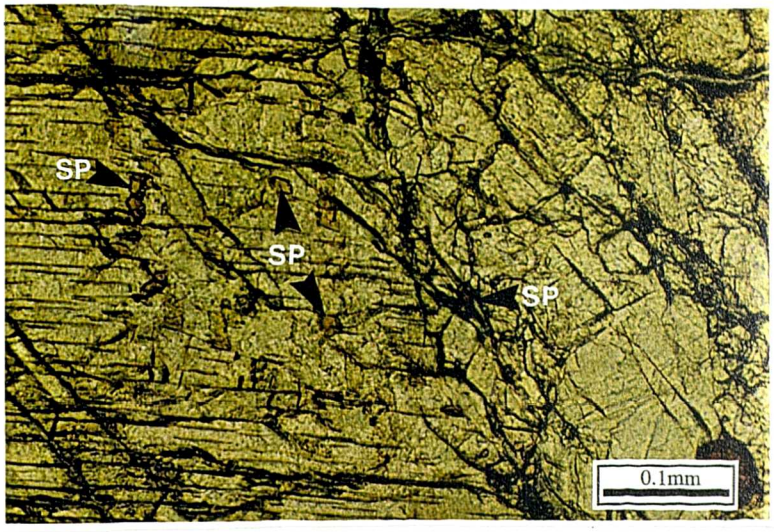

(b)

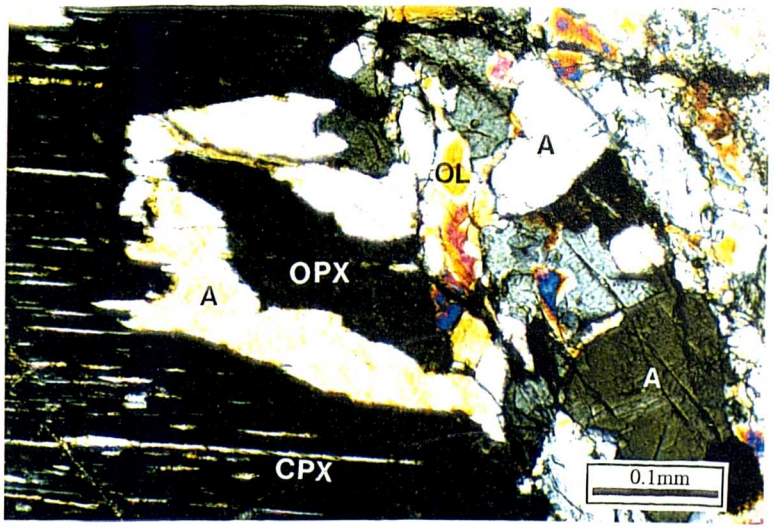

Figure 4.15. Disequilibrium texture indicating the breakdown of orthopyroxene (OPX) (+ clinopyroxene; CPX; lamellae) to spinel (SP) and amphibole (A) ± olivine (OL). PPL (a) and cross polars (b). (Sample M7I/95)

The absence of amphibole in the undeformed peridotites indicates that it was not an original phase prior to mylonitisation. The scarcity of clinopyroxene in amphibole-rich mylonites, when combined with textural observations (Figure 4.14), suggest that it is consumed in amphibole-producing reactions. The abundance of fine-grained spinel, compared to the undeformed protolith, and its association with secondary amphibole, suggest that it is also a reaction product, at least during the initial stages of amphibolitisation (Figures 4.14a and b). Orthopyroxene porphyroclasts are frequently rimmed by amphibole and spinel, and neoblasts are depleted in Al relative to parent porphyroclasts, which indicates that orthopyroxene may also be involved in the reaction (*cf.* Agrinier *et al.* 1993). However, textural observations and the abundance of orthopyroxene relative to clinopyroxene suggests

that it is less important than clinopyroxene. Whether orthopyroxene is a significant reactant or not is uncertain; the absence of clinopyroxene exsolution lamellae near orthopyroxene porphyroclast grain boundaries may be attributed to the breakdown of clinopyroxene to produce amphibole. In such a scenario, orthopyroxene is rimmed by amphibole and spinel, not because it is chemically active in the reaction, but because the grain boundary is a kinetically favourable site for diffusion and/or nucleation.

Analogies with textures indicative of the fluid-induced, incongruent breakdown of orthopyroxene to produce olivine and spinel (Reaction *A*) (Edwards and Malpas, 1995; Edwards, 1996 *pers comm.*), suggest that these rocks have undergone a similar disequilibrium process at relatively early stages in their history (Reaction *B*) (Figure 4.15).

$$(A)\ \mathrm{OPX} + \mathrm{Fluid} \rightarrow \mathrm{OL} + \mathrm{Spinel}$$
$$(B)\ \mathrm{CPX} + \mathrm{OPX} + \mathrm{Fluid} \rightarrow \mathrm{Amph} + \mathrm{Spinel} \pm \mathrm{OL}$$

However, other reaction textures are suggestive of more complex metamorphic interactions. Similar fabrics studied in detail by Agrinier *et al.* (1993) suggest spinel is involved in the generation of amphibole as both a reactant and a product:-

$$(C)\ \mathrm{Spinel\ I} + \mathrm{OPX} + \mathrm{CPX} + \mathrm{Aqueous\ fluid} \rightarrow \mathrm{Amph} + \mathrm{Spinel\ II} + \mathrm{OL}$$

Inclusions of spinel in amphibole and the undisturbed continuation of spinel exsolution lamellae across orthopyroxene porphyroclast-amphibole interfaces, indicate that *later* amphibole-producing reactions did not involve spinel. With increased modal proportions of amphibole, the amount of olivine decreases and individual olivine grains display evidence of disequilibrium (see Figures 4.11 and 4.12), suggesting that it is also involved in the production of amphibole:-

$$(D)\ \mathrm{CPX} + \mathrm{OPX} + \mathrm{OL} + \mathrm{Aqueous\ fluid} \rightarrow \mathrm{Amph}$$

A similar chronology is observed in the formation of amphibole in Red Sea peridotites; subsequent to the generation of amphibole at higher temperatures in a reaction that consumed and produced spinel (i.e. Reaction *C*), amphibole was generated at low temperatures (700-450°C) in reactions that did not involve spinel (i.e. Reaction *D*) (Agrinier *et al.* 1993).

A three-stage history is proposed for the evolution of the peridotites: (1) crystallisation of primary mineralogies under upper mantle conditions; (2) unmixing of Ca-rich pyroxene (diopside) from host Ca-poor pyroxene (enstatite); (3) recrystallisation of primary mineralogies during mylonitisation and formation of amphibole by hydrous metasomatism. Based on similar examples in the literature, this

three-stage chronology suggests that the peridotites originated at deep levels in the oceanic lithosphere (>25km), and that, subsequent to their emplacement at higher structural levels, they re-equilibrated during deformation and hydration (*cf.* Bonatti and Hamlyn, 1978; Hamlyn and Bonatti, 1980).

4.2.4. Conditions during deformation; grain size, deformation mechanisms, temperature and stress state

Grain-size

The most significant feature of these peridotite mylonites is the intense grain-size reduction involved in their formation. The undeformed protolith displays a coarse (<8mm) granular texture, which contrasts the fine-grained matrix (4-200μm) of the mylonites. This decrease in grain-size has significant implications for the resultant operative deformational mechanisms and, in turn, the rheological properties of the ultramafic fault rock. Two main grain size reducing processes have been proposed in the literature; dynamic recrystallisation (e.g. Ross *et al.* 1980; Drury *et al.* 1990; Girardeau and Mercier, 1988) and high-temperature cataclasis (*cf.* Vissers *et al.* 1995; Jaroslow *et al.* 1996). To recap, dynamic recrystallisation may take place by subgrain rotation or grain-boundary migration. Microstructural observations indicate that both recrystallisation mechanisms were operative in olivine within the fluidal mylonites; subgrain rotation for the larger paleoblasts (<39μm) keeps subgrain orientations very close to those of the parent paleoblast, and irregular, sutured grain-boundaries characterise the smaller grains (>6μm), which indicates boundary migration. As these mylonitic fabrics are dominated by fine-grained neoblasts (10-20μm), the predominant dynamic recrystallisation process of olivine in the fluidal mylonites is proposed to be migration. In contrast, many regions of the amphibole-rich mylonite matrix are characterised by equigranular, strain-free matrix grains that possess planar grain boundaries, which commonly meet at triple junctions. Such microstructures may indicate either the attainment of textural equilibrium, resulting from static recrystallisation, *or* that deformation was accommodated dominantly by diffusion-assisted grain-boundary sliding (see below).

Clinopyroxene, amphibole, and, to a lesser extent, orthopyroxene are variably strained and generally recrystallise into fine-grained aggregates with a grain size similar to that of olivine. This observation suggests that these phases may have undergone similar recrystallisation processes to olivine. However, the mylonites display microstructural evidence to suggest that high-temperature microfracture and cataclasis of pyroxene also caused grain-size reduction (*cf.* Vissers *et al.* 1995; Jaroslow *et al.* 1996). Detailed BSEM textural studies of clinopyroxene porphyroclast systems

associated with fluidal fabrics, suggest that a brittle mechanism was involved in the formation of neoblastic tails (Figure 4.16a and b). Figure 4.16b documents the brittle fracture and progressive disaggregation of a clinopyroxene porphyroclast (grey). The porphyroclast is fractured at its margins, separating clasts (~100μm in diameter) from the parent grain. These fractures are filled by amphibole (mid grey), which suggests that deformation took place in the presence of a hydrous fluid phase. With increasing proximity to the tail region, the intensity of fracturing increases, forming grains as small as 10μm. Clasts of both clinopyroxene and amphibole are then 'dragged' away from the porphyroclast where they are affected by the ductile recrystallisation processes discussed above. This process of progressive brittle fracture followed by dynamic recrystallisation results in the formation of narrow (typically <50μm in width), fine-grained, (<10μm) clinopyroxene-rich bands, which are involved in bulk ductile flow in the matrix. These bands wrap and anastomose around rigid porphyroclasts, which characterises the 'fluidal' fabric (Figure 4.16a). The presence of syn-tectonic amphibole in porphyroclast fractures and tails suggests that fluid pressures may have assisted microfracture by mechanisms such as subcritical crack propagation (e.g. Atkinson, 1982).

Deformation Mechanisms

Fine grain-sizes, polygonal recrystallised grains, an absence of crystallographic-preferred orientations and a lack of evidence for intragranular plastic deformation, are all features observed in the matrix of the fluidal mylonites, which suggest the operation of grain-size sensitive (GSS), diffusion creep deformation mechanisms. The small grain-size, resulting from a combination of dynamic recrystallisation and microfracturing of parent mineral grains, probably facilitates diffusive mass transfer processes. Diffusive mass transfer would be further assisted by the presence of a syn-tectonic fluid phase, which is suggested by the presence of amphibole. The extensive mixing of phases in the matrix (see Figure 4.3b) may be attributed to 'neighbour switching' associated with diffusion-assisted grain-boundary sliding (see Figures 3, 4 and 5 in Ashby and Verral, 1973; Vissers *et al.* 1995). However, subordinate dislocation-creep processes appear to have been operative in localised 'high strain' regions of the matrix adjacent to 'rigid' porphyroclasts and in discrete micron-scale shear zones (Figure 4.17a and b). Matrix grains in these zones display marked flattening, evidence for intragranular deformation (i.e. subgrain formation) and the development of shape- and crystallographic-preferred orientations. It is within these regions that shear strain *rate* is expected to be higher than in other areas of the matrix, thus explaining the localisation of these fabrics (Prior *et al.* 1990).

(a)

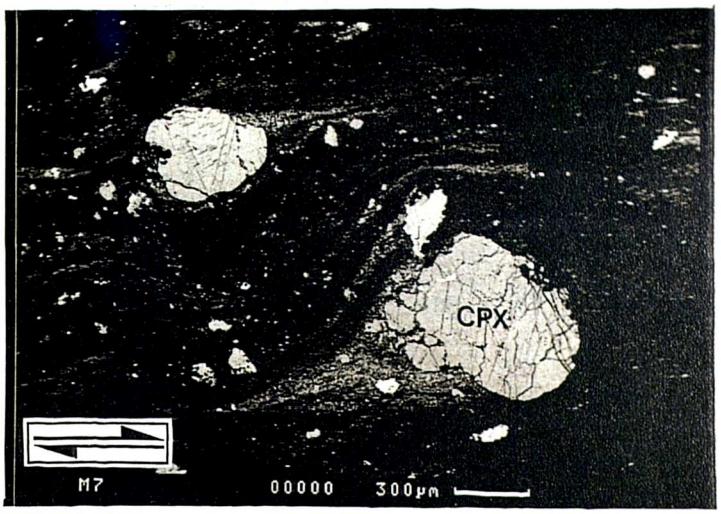

(b)

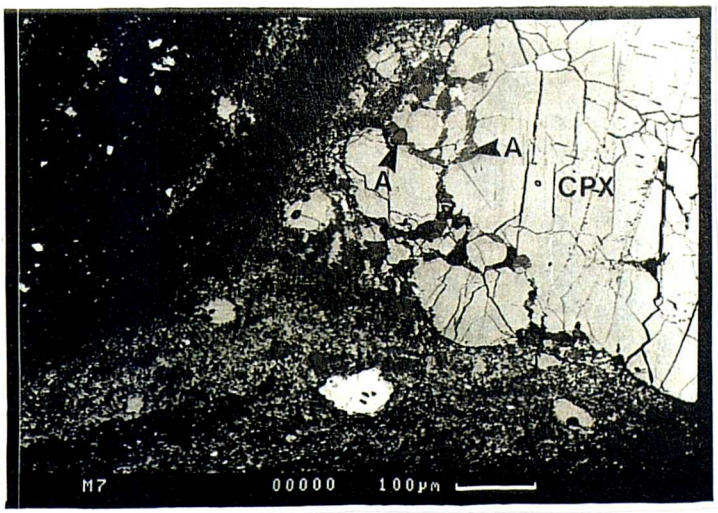

Figure 4.16. (a) Backscattered electron micrograph of clinopyroxene (CPX) porphyroclast systems in a fluidal mylonite. Arrows in inset indicate dextral shear. (b) Close up of (a). (b) Shows the fracturing process, with brittle fractures in the clinopyroxene porphyroclast (CPX; grey) filled with amphibole (A; darker). Note the increase in fracturing of the porphyroclast towards the neoblastic tail, which is rich in both clinopyroxene and amphibole. (Sample M7/95).

The intensity of crystallographic-preferred orientations, observed petrographically using a gypsum sensitive tint plate, increase substantially with increasing proximity to cross-cutting amphibole-bearing shear zones. This observation suggests a switch to grain-size insensitive (GSI) dislocation creep-dominated flow, associated with the development of amphibole-rich mylonites. These later mylonites are coarser grained, exhibiting shape- and lattice-preferred orientations, particularly in syn-kinematic amphibole (Figures 4.6b, 4.7, and 4.17), which dominates the microstructure. Amphibole commonly displays evidence for intragranular deformation, such as undulose extinction and subgrain formation, and amphibole is most abundant, it

forms monomineralic foliation-parallel layers. These observations not only suggest dislocation creep (Jaroslow *et al.* 1995; Drury *et al.* 1990; Nicolas *et al*; 1971) as the dominant mode of flow, but also that the rheology of these rocks was probably controlled by amphibole (*cf.* Drury *et al.* 1990; Vissers *et al.* 1995). However, the ultrafine-grained monomineralic foliation-parallel shear zones of amphibole, which are thought to result from the dynamic recrystallisation of the coarser layers, display microstructural evidence to suggest that they deformed by diffusion creep mechanisms. Furthermore, the relatively planar grain boundaries and lack of intragranular deformational characteristics commonly observed in olivine in these fabrics, suggests that the deformation of olivine-rich regions of the matrix was also accommodated by diffusion creep processes. On the other hand, these observations combined with their coarse grain size may be interpreted as resulting from grain growth and annealing. This is discussed in greater detail in the 'interpretation' section below. Whatever the dominant deformation mechanism operative in the amphibole-bearing mylonites was, the coarsening of these fabrics is thought to reflect a reduction in stress and/or an increase in temperature during or after deformation.

The only other deformation mechanism that may be inferred from the amphibole-rich, mylonitic microstructure is operation of the pyroxene (100)[001] slip system (Mercier, 1985). This mechanism, referred to as inversion in orthopyroxenes and twinning in clinopyroxenes, involves the formation of a clinopyroxene correctly oriented for glide and is usually represented by the development of thin (100) exsolution lamellae (e.g. Figures 4.6a and 4.10). Note that this mechanism cannot itself accommodate large deformations, and may simply be attributed to cooling.

Temperature

Estimation of the conditions during deformation in ultramafic rocks is difficult due to the restricted mineralogies concerned and their stability over a large range of pressures and temperatures. As the application of detailed geothermobarometric techniques (e.g. Fe-Mg exchange thermometers) and the identification of temperature activated olivine slip systems is beyond the scope of the present study, temperature is estimated with reference to analogous examples in the literature. An upper temperature limit of *1100°C* is inferred due to the presence of amphibole; calcic-amphibole, depending on composition (see Drury *et al.* 1990 and references therein), has an upper stability limit of between 825°C (Jaroslow *et al.* 1995) to 1100°C (Nicholas, 1986). The magnesio-hornblende composition of amphiboles from the peridotite mylonites is comparable to that of edenitic to tschermakitic hornblendes from the Ayia Varvara metamorphics (Figure 4.11: Spray and Roddick, 1981; Malpas *et al.* 1992). The amphiboles from the peridotite mylonites are higher in Si and Mg and lower in K, Al and Ti than those from

the metamorphic rocks. This difference in chemistry may be expected if the Ayia Varvara amphiboles crystallised at higher temperatures than those in the peridotite mylonites, but more realistically the difference in composition merely reflects the difference in bulk rock, protolith chemistry between these two units. Thus, calcic-amphibole chemistry may not be used as a reliable geothermometer in the Cyprus peridotites. A lower temperature limit is proposed by Jaroslow *et al* (1996), who suggest 600°C as a lower limit for plasticity in peridotites. This is supported by the absence of antigorite, which has an upper temperature limit of 510-600°C°C (Jaroslow *et al.* 1996 and references therein).

(a)

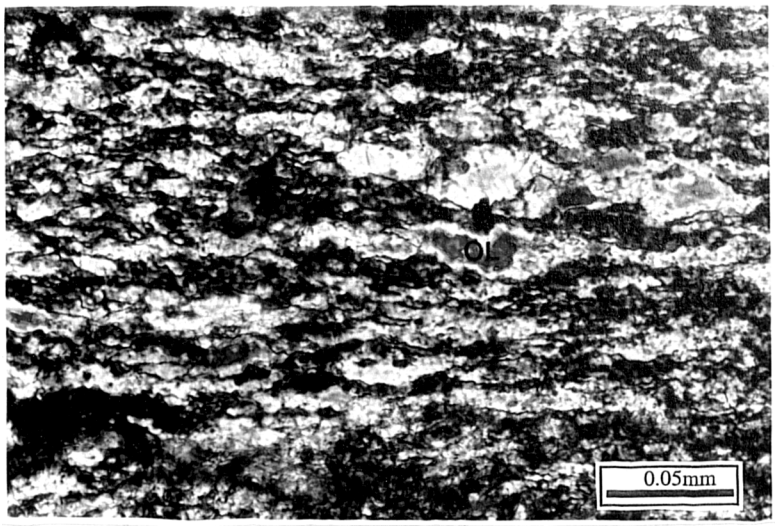

(b)

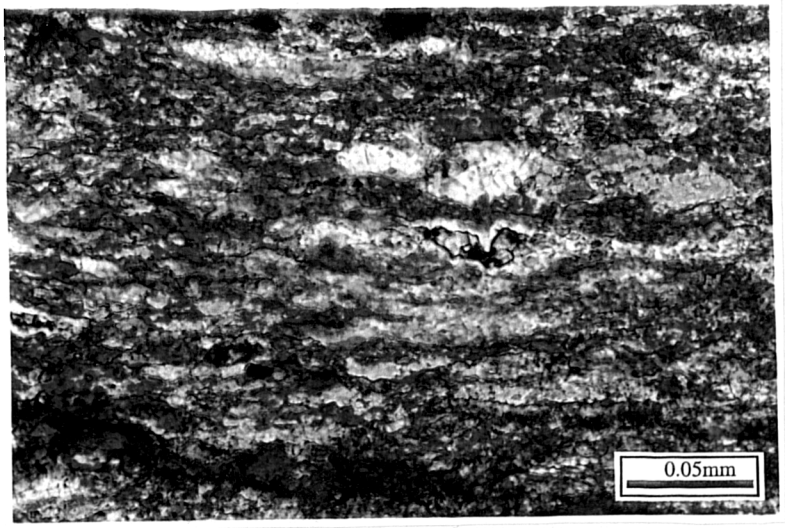

Figure 4.17. Optical micrographs of fine-grained olivine-dominated matrix in a fluidal fabric exhibiting shape- and crystallographic-preferred orientations. (a) Cross polars, and (b) with a sensitive tint plate addition. (b) Shows the well-defined crystallographic fabric of the olivines (OL), which are mainly orange. Note the irregular colouration of these grains, suggesting internal strain accumulation, and the irregular grain boundaries.

Deformation temperatures in peridotites may also be approximated using experimentally-derived flow laws for olivine. Temperature estimates calculated by this

method are merely qualitative and only useful for comparative studies. With this in mind, temperature constraints for the fluidal and amphibole-bearing mylonites are presented and discussed later in this section.

Stress state

Numerous methods are currently available in the literature for the determination of stress magnitudes associated with the formation of peridotitic deformation fabrics. Such techniques include the measurement of free dislocation densities, subgrain sizes and neoblast sizes of olivine, all of which have been demonstrated in steady-state, laboratory experiments to be dependent on stress (e.g. Nicolas, 1978; Ross *et al.* 1980; Nicolas *et al.* 1980). The olivine neoblast size palaeopiezometer, proposed by Ross *et al* (1980), is used here as it is the easiest to employ, requiring only ordinary thin sections and a calibrated micrometer eyepiece. Secondly, and more importantly, recrystallised grains are intrinsically more stable than free dislocations and subgrains, in that they are not easily altered during transient events such as might occur during emplacement or post-deformation annealing. Thirdly, unlike subgrains, recrystallised grain sizes adjust to both increasing and decreasing stress levels, at minimal strains and times, and thus record the stress history. However, caution is necessary as post-deformational recrystallisation can alter the results (e.g. Karato, 1989).

Ross *et al.* (1980) demonstrated that recrystallised grain-size in dunite deformed experimentally under 'dry' conditions is dependent only on stress (equation 1), whilst 'wet' experiments demonstrated a neoblast size that is slightly temperature-dependent.

$$(1) \qquad D(\mu m) = 137\sigma^{-1.27}$$

$$(2) \qquad D(\mu m) = 10^{3.5\pm0.7}\exp(-14.2 \pm 2.6/RT10^{-3})\sigma^{-0.82(+0.08 \text{ to } -0.09)}$$

Where D is the recrystallised grain-size and σ is differential stress (in kbar). Assumptions implicit in the application of these equations include: (1) deformation must take place under steady-state conditions (i.e. strain-rate and stress difference are constant), and (2) microstructures are generated by grain-boundary migration recrystallisation. Therefore, the results may not apply to fabrics that have experienced subgrain rotation recrystallisation mechanisms. Even though microstructural evidence for rotation recrystallisation is present in the SW Cyprus mylonites, migration recrystallisation appears to be dominant. Thus, to a certain degree, the assumptions appear valid, but note that the stress values determined must be considered only approximate due to the errors inherent in extrapolating experimentally-derived flow laws to geological conditions.

Neoblast sizes are determined as suggested by Nicolas *et al.* (1980); to obtain a representative sample, 50 to 150 olivine grains are measured in thin section at 100X, where they are in contact with other olivine crystals. Note that, measurement of olivine grain size may be hindered by post-kinematic serpentinisation, particularly in the amphibole-dominant mylonites. Therefore, heavily serpentinised regions of the matrix are avoided in the analysis.

Due to the inferred presence of syn-kinematic fluids in the SW Cyprus mylonites, the equation derived from wet dunite by Ross *et al.* (1980) should be most appropriate. As stated previously, the lack of temperature constraints in these samples makes the application of this slightly temperature-dependant equation rather too conjectural. However, Drury *et al.* (1991) propose that an *estimate* of the flow stress during deformation may be derived using the equation for dry deformation. Such stress estimates can then potentially be used to constrain the deformation temperature using a dislocation creep flow law for olivine for a range of geologically reasonable strain rates (chosen 10^{-12} to 10^{-15} s^{-1}). By substituting a maximum value for strain rate and a minimum value for the flow stress in a flow law for dry dunite, it is therefore possible to estimate the maximum value for the temperature during flow, while the minimum strain rate and maximum stress in a flow law for wet dunite provides a minimum temperature. Application of a dislocation creep flow law derived by Chopra and Paterson (1984) yield temperatures for fluidal fabrics ranging from 540 to 834°C, which is ***lower*** than the amphibole-bearing mylonites that range from 647 to 932°C (Table 4.2).

Sample	Strain rate (s^{-1})	Grain size (μm)	Flow stress (MPa)	Temperature (°C)
M7	10^{-12}	38	274	834
(fluidal-massive)	10^{-15}	8	936	568
M5	10^{-12}	21	438	803
(fluidal-lineated)	10^{-15}	4	1616	540
AV16	10^{-12}	200	74	932
(amph-bearing)	10^{-15}	45	240	647

Table 4.2. Calculated stress and temperature values.

1 Pa = 10^{-5}bar
Palaeopiezometer for mylonites - Ross *et al.* (1980)
Flow law for dry Aheim dunite (Chopra and Paterson, 1984) (see Appendix 3)
Flow law for wet Aheim dunite (Chopra and Paterson, 1984)

However, microstructural observations suggest diffusion creep was dominant in the matrix of the fluidal mylonites and thus strict application of a dislocation creep flow law may be inappropriate. Therefore, to examine this hypothesis, a diffusion creep

flow law has been applied to the fluidal samples, whilst a dislocation creep flow law is still used for amphibole bearing mylonites (Table 4.3; see Appendix 3 for equations and constants used; *cf.* Karato *et al.* 1986; Jaroslow *et al.* 1996). The results obtained are similar, except that fluidal fabrics yield *much lower* temperatures (423 to 698°C) than the amphibole-rich mylonites (709 to 906°C). This difference can be attributed to the lower activation energy for diffusion, compared to that for dislocation creep.

Sample	Strain rate (s^{-1})	Grain size (μm)	Flow stress (MPa)	Temperature (°C)
(AV16) Amph mylonite	10^{-12}	200	74	**906**
	10^{-12}	98	130	865
	10^{-12}	45	240	824
	10^{-15}	200	74	775
	10^{-15}	98	130	742
	10^{-15}	45	240	**709**
(M7) Fluidal - massive	10^{-12}	38	274	**698**
	10^{-12}	22.62	413	651
	10^{-12}	8	936	570
	10^{-15}	38	552	552
	10^{-15}	22.62		517
	10^{-15}	8	936	**458**
(M5) Fluidal - lineated	10^{-12}	21	438	**645**
	10^{-12}	11.4	721	596
	10^{-12}	4	1616	524
	10^{-15}	21	438	513
	10^{-15}	11.4	721	477
	10^{-15}	4	1616	**423**

Table 4.3. Flow stresses calculated from grain sizes and temperature values calculated using the relevant (diffusion or dislocation creep) geological flow laws for olivine at two end member strain rates (10^{-12} and $10^{-15}s^{-1}$). For each sample, a maximum estimate of temperature (bold and underlined) is constrained using the highest strain rate and the lowest flow stress (constrained using the smallest grain size). A minimum estimate of temperature (bold) is constrained using the slowest strain rate and the highest flow stress (constrained from the coarsest grain size).

Palaeopiezometer for mylonites - Ross *et al.* (1980)
Flow law for dislocation creep (AV16) (Jaroslow *et al.* 1996) (see Appendix 3)
Flow law for diffusion creep (M7 and M5) (Jaroslow *et al.* 1996).

Interpretation

The microstructural chronology preserved in the mylonites, combined with the above calculations, suggests that the transition from fluidal to amphibole-rich mylonites was accompanied by an increase in temperature, a decrease in differential stress, and a switch from diffusion-dominated to dislocation-dominated creep. However, peridotite

mylonites associated with uplift and exhumation are invariably correlated with *decreases* in temperature, *increases* in stress, and thus, *decreases* in grain-size. If the resulting reduction in grain-size is significant enough, a switch from dislocation to diffusion creep is observed (e.g. Drury *et al.* 1990; Vissers *et al.* 1995; Jaroslow *et al.* 1996). In this respect, the deformational history of the SW Cyprus peridotite mylonites is anomalous. Three main factors may account for these results:-

(1) The stress-neoblast size relationship derived by Ross *et al.* (1980) is invalid and/or the semi-quantitative extrapolation of olivine flow laws to geological conditions is unreasonable. The main problem that may arise here stems from the application of monomineralic olivine flow laws to polymineralic rocks (see point 2 below). This is especially true in the case of the amphibole-rich mylonites, in which the fault rock rheology appears to have been controlled by amphibole. Therefore, the application of an amphibole flow law would be more appropriate. Unfortunately, as no flow laws have been derived for amphibole, this hypothesis cannot be tested.

(2) If the above methodology in deriving stress and temperature estimates is assumed to be reasonable, one or more of the variables in the power law equations may be invalid. Diffusion creep is frequently associated with high strain rates and superplasticity (e.g. Ashby and Verral, 1973; Drury *et al.* 1990; Rutter and Brodie, 1987, 1988). For example, equations presented by Ashby and Verral (1973) predict strain rates during diffusion creep that are approximately an order of magnitude faster than normally expected. High strain rates are also predicted if the deforming medium is polymineralic. Based on theoretical studies, Wheeler (1993) demonstrates that the rheology of rock, deforming by a diffusion-dominated mechanism, may be drastically reduced if the rock is polymineralic relative to its monomineralic counterparts. For example, the rheology of dunite in diffusion creep is governed by the diffusion of both MgO and SiO2; which ever has the slowest rate will control the viscosity of the rock. However, in harzburgite, Wheeler (*op cit.*) indicated that strain is accommodated not only by diffusion, but also by changes in grain volumes associated with local phase transformations, which are not possible in monomineralic rocks. Wheeler (*op cit.*) demonstrated that such phase transformations may lead to rapid increases in strain rate, to such an extent that a rock such as harzburgite will only be as strong as a pure quartz rock of comparable grain size. By assuming a strain rate of 10^{-11} S^{-1}, which is an order of magnitude faster than adopted in the above equations, as predicted by Ashby and Verral (1973), the temperature estimation is increased by **55°C**, from 651°C to 706°C. Thus, the strain rate assumed appears to be crucial in the application of diffusion creep flow laws to calculate palaeotemperatures.

(3) Assuming that the calculated values for stress and temperature, although qualitative, are reasonable estimates, the unusual chronology preserved in the

mylonites may be explained by changes in conditions that occurred in SW Cyprus during deformation. There is some geological evidence linking the development of the mylonites and the event responsible for the metamorphism and ductile deformation of the Ayia Varvara Formation (see Chapter 6). The Ayia Varvara amphibolites are dated at 90-83Ma ($^{40}Ar/^{39}Ar$ geochronology; Spray and Roddick, 1981), an age that is coincident with age of formation of the Troodos massif (e.g. Blome and Irwin, 1985; Mukasa and Ludden, 1987). It seems reasonable to suggest, therefore, that the heat responsible for metamorphism of the Ayia Varvara Formation and the increase in temperature during the generation of the amphibole mylonites was supplied by the adjacent, newly formed Troodos crust (*cf.* Swarbrick, 1979; Spray and Roddick, 1981).

The coincidence between the geological evidence and the calculated estimates of temperature given above, suggest that this final interpretation is reasonable. To test this hypothesis and relate the microstructural observations to these estimates, the data shown in Table 4.3 is represented on deformation mechanism and deformation regime maps for appropriate temperatures, i.e. 600°C for fluidal mylonites and 800°C for amphibole-bearing mylonites (Figures 4.18 and 4.19). Figure 4.18a displays the rheological evolution of two fluidal mylonite fault rocks, showing how an increase in stress and a concomitant decrease in grain-size facilitates the operation of diffusion creep. Figure 4.18b shows the interpreted rheological trajectory (indicated by the black arrow) of an amphibole-bearing mylonite. In contrast to the fluidal mylonite data in Figure 4.18a, the rheological trajectory 'arrow' points towards coarser grain-sizes and a decrease in stress. This trajectory is inferred from temperature estimates combined with microstructural studies and field observations, which suggest that the matrix olivines increased in grain-size as a consequence of an increase in temperature during deformation. This trend suggests that the amphibole-rich mylonites progress towards the dislocation creep field, but note that all grain-size-stress values still plot within the diffusion creep field. The inference that diffusion creep processes were dominant in the deformation of olivine is consistent with the microstructural observation that matrix olivine grains generally display no characteristic features indicative of dislocation creep. Therefore, it is not unreasonable to suggest that, whilst amphibole experienced predominantly dislocation creep processes, diffusion creep processes may still have accommodated a large proportion of the deformation in the olivine-dominated portions of the matrix. Which mineral, and in turn which creep processes, controlled the rheology of these rocks is unknown because (a) the relative strengths of olivine and amphibole under these conditions is poorly constrained, and (b) post-kinematic serpentinisation has destroyed parts of the samples. Therefore, it is not possible to determine whether or not the amphibole- or the olivine-dominated

portions of the matrix interconnect to form weak layer microstructures, which would control the rheological properties of the fault rock (*cf.* Handy, 1994).

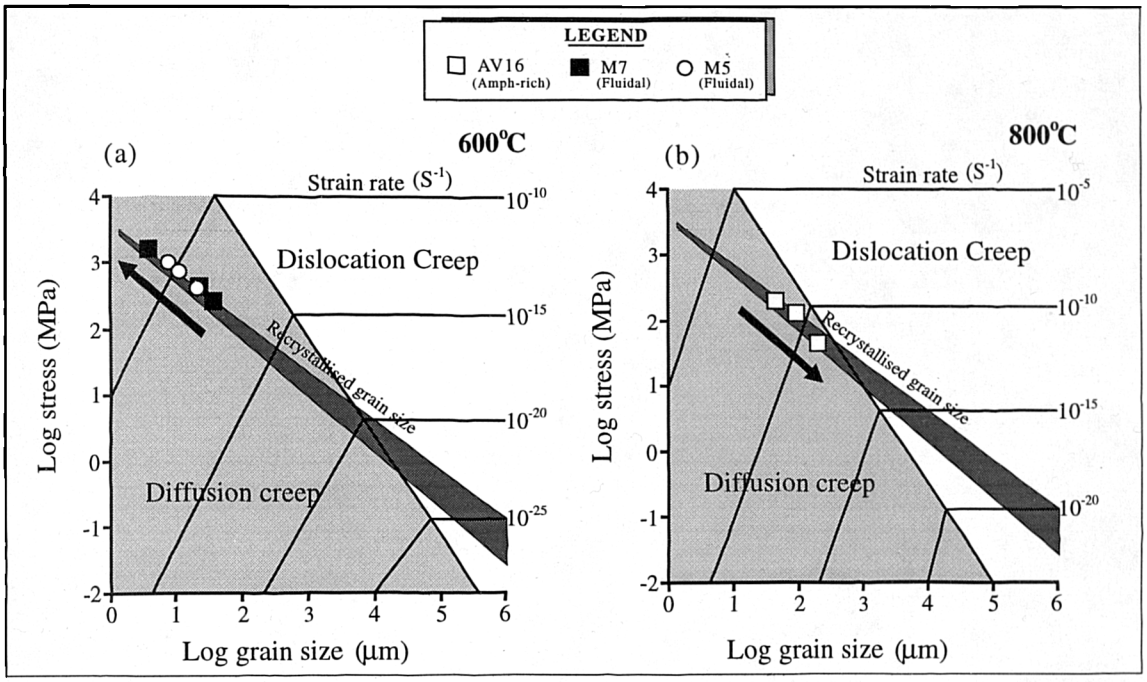

Figure 4.18. Deformation mechanism maps for olivine taken from Rutter and Brodie (1988). The dark shaded band shows the range of recrystallised grain-size vs. stress relationships constrained by Karato *et al.* (1986). (a) Rheological trajectories (indicated by black arrows) for two fluidal mylonite samples. With decreasing grain-size, the rocks move further into the diffusion creep field. (b) Rheological trajectory of an amphibole-rich mylonite. An increase in grain-size during deformation results in an evolution towards the dislocation creep field.

Figure 4.19 presents the same data on a deformation regime map taken from Handy (1989), except that here stress is fixed at a constant value and temperature (specifically, homologous temperature; $T_h = T/T_{melting}$) is a variable. The rheological trajectories (indicated by black arrows) for both mylonite types are shown. Also, the position of the undeformed protolith is plotted on this diagram (black square), which was constrained using the grain-size (8mm in diameter) from a coarse granular peridotite. This data shows that rocks comprising such coarse olivine grain-sizes are expected to accommodate deformation by dislocation creep processes. However, assuming constant temperature, a significant decrease in grain-size during the formation of a fluidal mylonite (vertical black arrows), is expected to facilitate the operation of diffusion creep processes. With decreasing temperature and decreasing grain size, the fluidal mylonites evolve towards the exponential creep and brittle failure regimes. Note that Figure 4.19 was constructed using total (or lithostatic) pressure λ ($= P_{pore}/P$) = 0, but with an increase in pore pressure the brittle failure field expands to

the right of the diagram, to higher temperatures (white arrows). Although this diagram applies only to the deformation of olivine, the cataclasis of clinopyroxene porphyroclasts may be explained by a similar process, whereby transient, grain-scale fluctuations in pore-fluid pressure facilitate microfracture.

Again the data for amphibole-rich mylonites in Figure 4.16 progresses towards the GSI, dislocation creep regime, but does not reach it, thus supporting the previous conclusion that diffusion creep may have been the dominant mode of flow in the matrix olivines. However, this is expected as both Figures 4.18 and 4.19 were constructed, at least in part, using the parameters for diffusion and dislocation creep compiled by Karato *et al.* (1986).

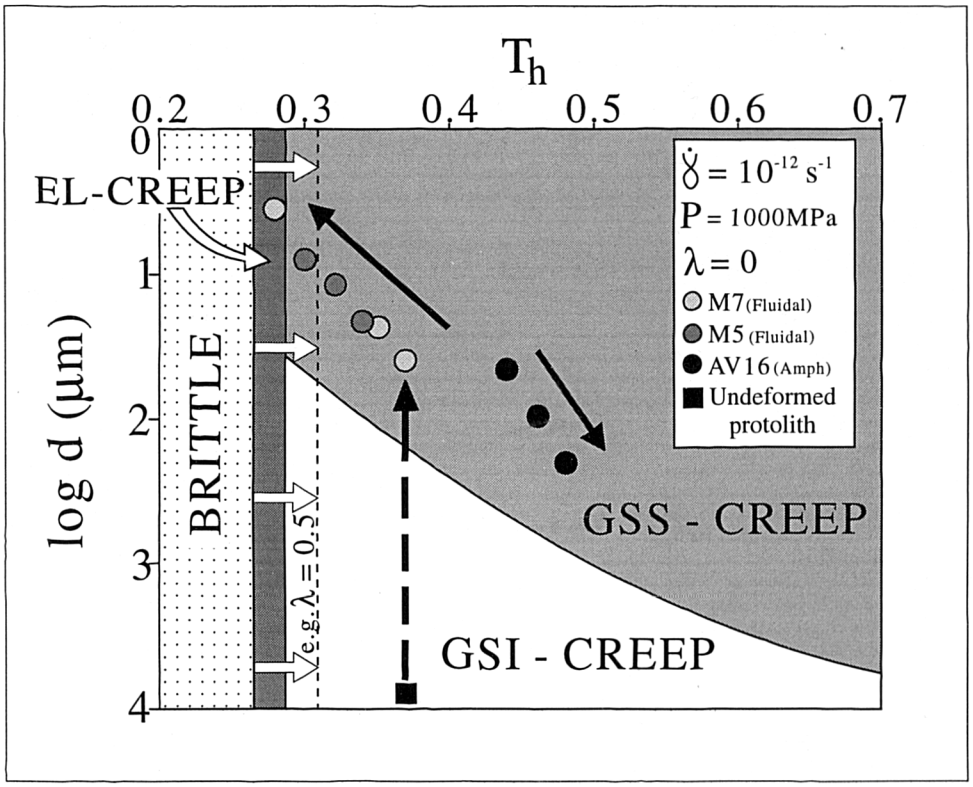

Figure 4.19. Homologous temperature (Th)-log grain-size (d) deformation regime map for hydrous dunite constructed at constant strain rate, pressure and pore pressure, taken from Handy (1989). Black arrows show the directions of the rheological trajectories for fluidal and amphibole-rich mylonites. The black square represents an undeformed peridotite which lies in the GSI field and the dashed black arrow shows its hypothetical isothermal grain-size reduction, forming a fluidal mylonite. White arrows depict a schematic expansion of the brittle failure regime to higher temperatures resulting from a hypothetical increase in pore-fluid pressure ($\lambda = 0.5$). Abbreviation EL is exponential law creep (see Handy, 1989).

4.3. Dextral transtension and serpentinite protrusion

Rare outcrops are preserved in the Southern Region that document the continued retrograde hydration and deformation of the fault zone peridotites. Fabrics associated with this event record a range of metamorphic conditions intermediate between those responsible for the formation of high temperature mylonites discussed in section 4.2 and later, low temperature (~100°C), transpressional fabrics (Section 4.4). Macroscopic-scale, kinematic analyses suggest that these 'transitional' fabrics and related structures formed during dextral transtension, which is thought to have facilitated the protrusive emplacement of serpentinite. Field evidence suggests that outcrops which display structures and fabrics relating to this event are only ever preserved at localities where later transpressional deformation was weak or absent. This observation is critical in the analysis of these outcrops because dextral faults which represent antithetic structures formed during the later sinistral tranpressional event frequently parallel the dextral transtensional structures. A summary of the example localities discussed in this section are presented in Figure 4.20.

The criteria used in the field to identify outcrops relating to this event are based on the interpretation that dextral transtension and serpentinite protrusion were coeval. At the scale of an outcrop or below, serpentinite frequently displays highly irregular contact relationships, which suggest that it *intruded* the Troodos and Mamonia Complexes at low temperatures. On a larger scale, the orientations and displacements observed along these protrusion-related faulted contacts, combined with the orientations of Troodos mafic dykes in the serpentinite, are consistent with a dextral transtensional model.

The following section is divided into two parts. The first concerns the structures and microfabrics, which preserve key evidence concerning the chronology of deformation events. The second section presents examples and interpretation of field-based kinematic analyses.

4.3.1. Deformational and microstructural chronology

Outcrops in the vicinity of Kara tou Ayiou Pati (GR 568 484) (Figure 4.21), located at the northern contact of the northern serpentinite belt in the Ayia Varvara area, preserve rare evidence of the deformational chronology in the period linking early high temperature and later low temperature deformations in the Southern Region. At outcrop, asymmetrical extensional shear bands, microfolds and sub-horizontal stretching lineations, developed in serpentinised L-tectonites, indicate dextral strike-slip (Figure 4.22). On the micro-scale, the dextral fabric is characterised by discrete foliation-parallel (*Y*-) shears and rounded to elongate orthopyroxene bastites (Figure

4.23). Their textural similarity with amphibole-rich peridotite mylonites is striking and suggests that they may be retrogressed and, at least, partially pseudomorphed equivalents. Optical microscopy, BSEM and XRD studies indicate lizardite, chlorite, magnetite and minor chrysotile ± tremolite constitute the syn-kinematic mineral assemblage (Figures 4.24 and 4.25). *Y*-shears are dominated by the localised development of coarse-grained (<0.45mm in length) chlorite laths (Figure 4.25), which display undulose extinction and strong crystallographic- and shape-preferred orientations. In contrast, fine grains (~0.04mm) of lizardite within these layers are dominantly sub-equant and display highly irregular grain boundaries and evidence of internal straining (i.e. subgrain development), suggesting the operation of dynamic recrystallisation processes. Chrome spinels are heavily altered and replaced by magnetite, which is mechanically broken down and strung out along *Y*-shears (Figure 4.23). Upper temperature limits are constrained by the existence of chlorite (450-800° C; Robinson *et al.* 1981; Wyllie, 1970), whilst the existence of deformed lizardite and chrysotile indicates deformation proceeded to low temperatures (130-185°C; Wenner and Taylor, 1971).

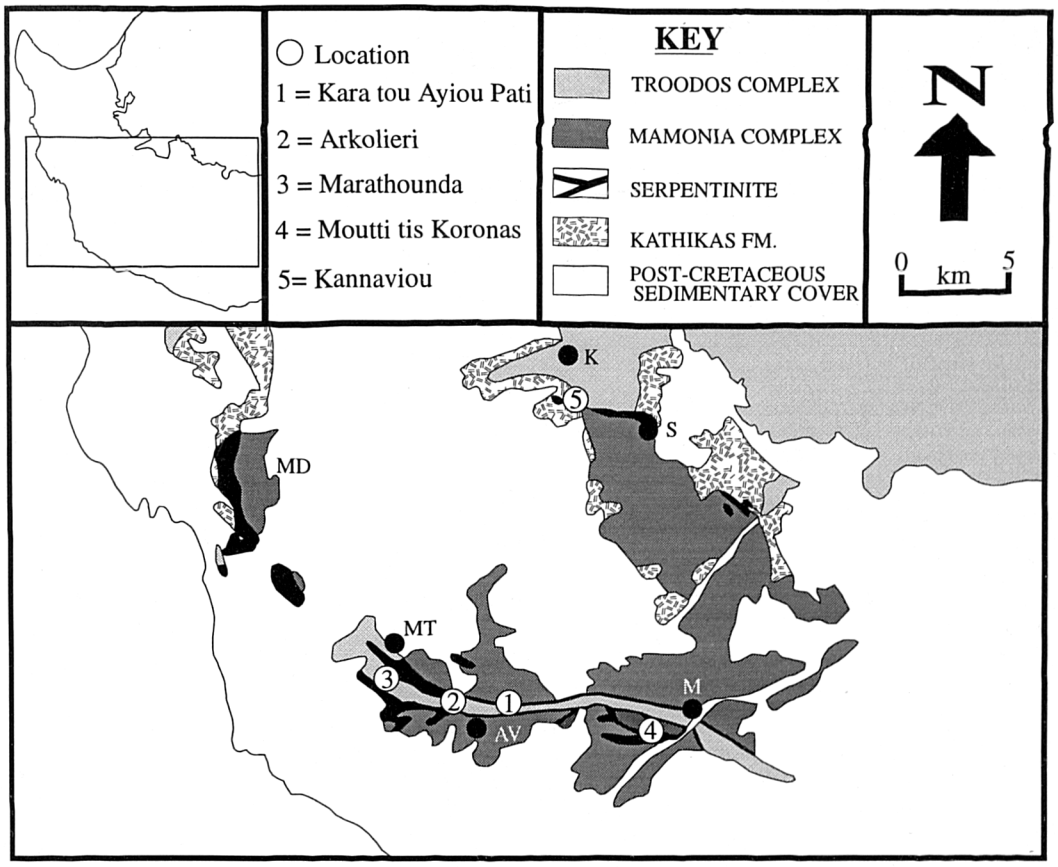

Figure 4.20. Map introducing the localities discussed in this chapter, which preserve evidence of a dextral transtensional event prior to Maastrichtian transpression (see section 4.4).

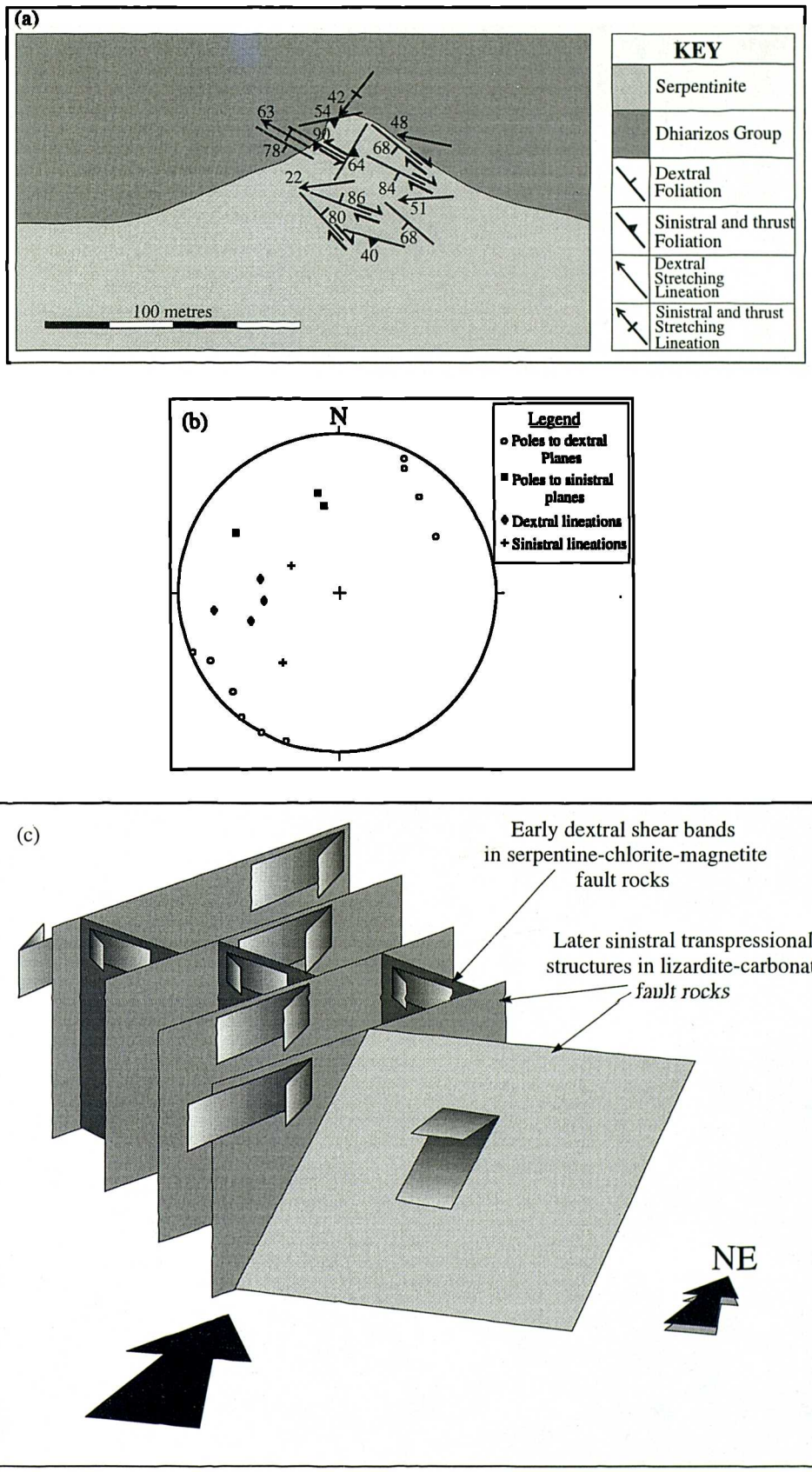

Figure 4.21. (a) Geological map of the contact exposed at Kara tou Ayiou Pati. (b) Equal area stereographic projection of data. (c) Three-dimensional interpretation of data showing the sinistral transpressive structures overprinting earlier dextral fabrics.

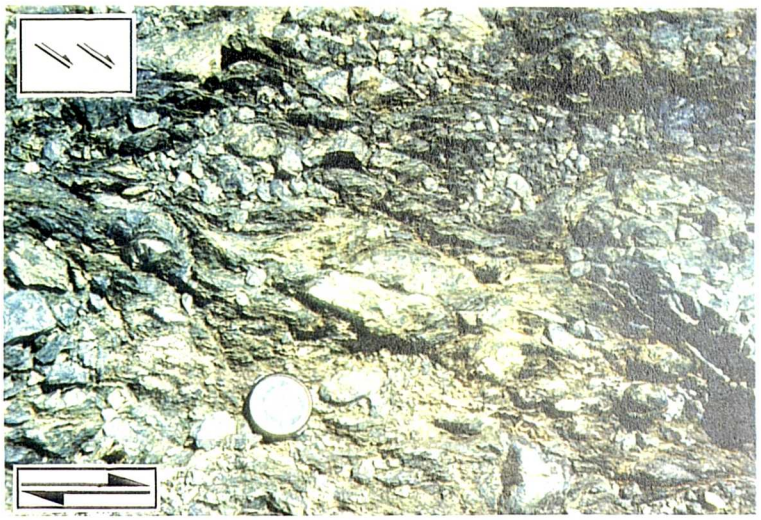

Figure 4.22. Plan view looking down onto dextral strike-slip shear bands developed in lizardite-magnetite-chlorite fault rock. Inset in the top left-hand corner shows the orientation of the shear bands.

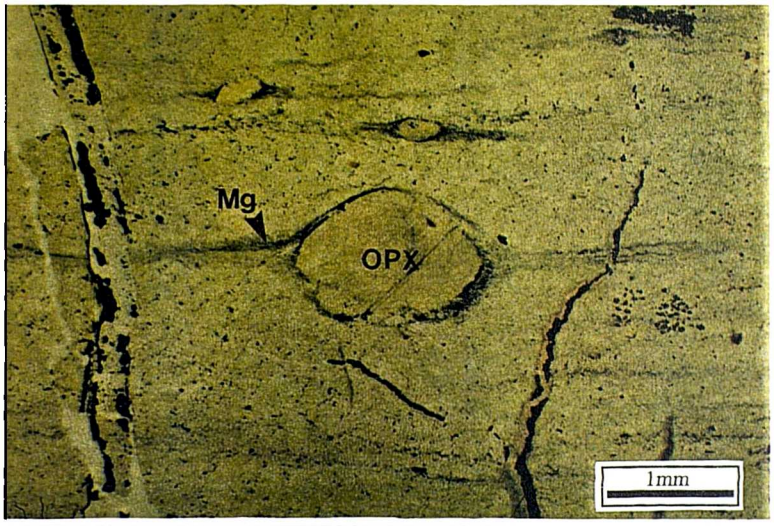

Figure 4.23. Rounded lizardite-bastite pseudomorph after orthopyroxene (OPX) located along a *Y*-shear defined by magnetite grains (Mg). (Sample BOB1/94)

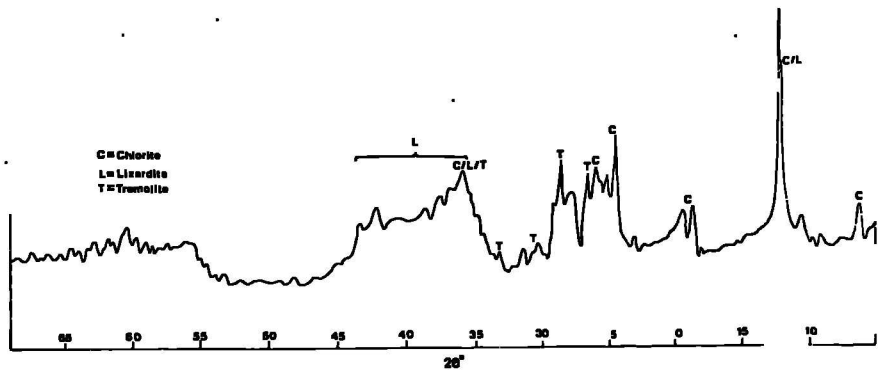

Figure 4.24. X-ray diffraction trace demonstrating the existence of chlorite and lizardite along *Y*-shears in 'transitional' deformation fabrics. Note that the presence of tremolite could not be confirmed in BSEM or optical microscopy studies.

(a)

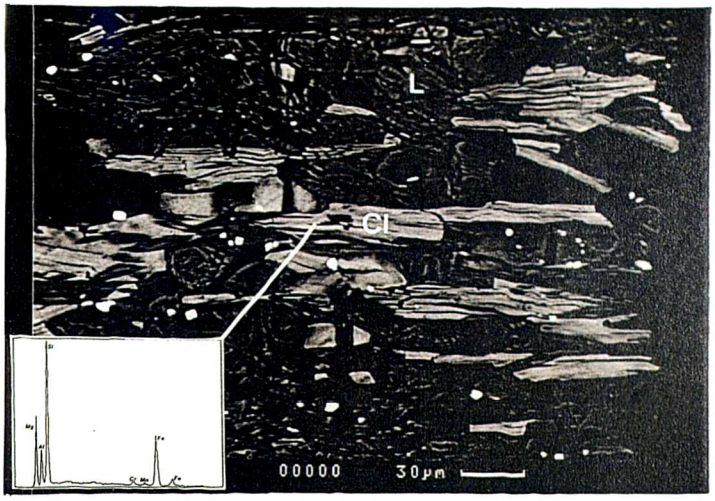

(b)

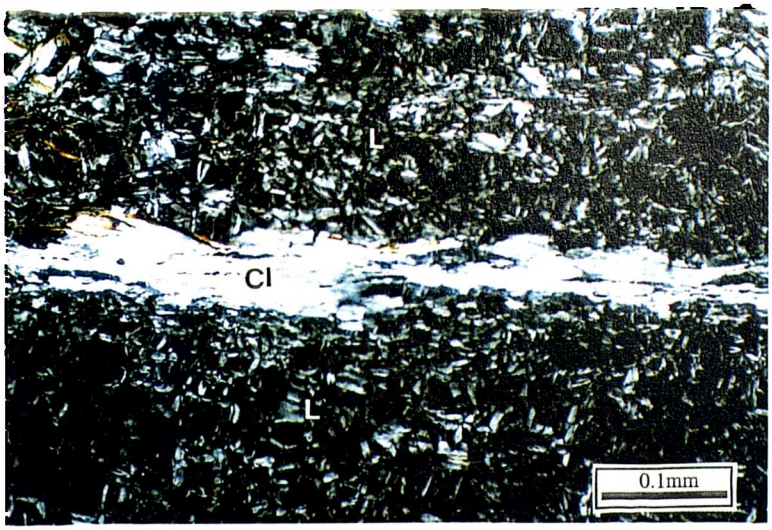

Figure 4.25. (a) Backscattered electron micrograph showing the localised development of chlorite (Cl; bright minerals) along *Y*-shears. Inset shows a LINK Analytical trace taken from a chlorite grain. (b) Optical micrograph (cross polars) of chlorite displaying undulose extinction (Cl). Note in both figures the dark coloured matrix is dominated by post-kinematic, mesh-textured lizardite serpentine (L). (Sample BOB1/94).

Two interpretations are possible to explain the development of these chlorite-bearing fabrics. Firstly, they may be products of the same progressive retrograde deformational event responsible for the development of the high temperature dextral mylonites. Alternatively, they may have resulted from the reactivation of the pre-existing mylonites. Due to the absence of fabrics that are texturally intermediate between peridotite mylonites and chlorite-bearing fabrics no definitive conclusion is possible.

At outcrop, dextral chlorite-bearing fabrics are overprinted by asymmetrical microfolds, shear bands and associated oblique-slip carbonate mineral lineations on sub-vertical foliations that indicate sinistral displacements (Figure 4.26a). Dip-slip

lineations are also present on moderately dipping surfaces, which are associated with shear bands, domino faults and displacements on fault-plane carbonate mineralisation veins that indicate thrusting of serpentinite over Dhiarizos Group material to the NE (Figure 4.26b). All these structures are developed in pervasively serpentinised lizardite-chrysotile-carbonate fault rocks which overprint, and thus post-date, the previous dextral chlorite mylonites. Due to the similarity in the style of deformation, sinistral and thrust-related structures are considered coeval. They are interpreted to have formed during the regionally recognised low temperature, sinistral transpressional event, which is discussed in detail in section 4.4.

(a)

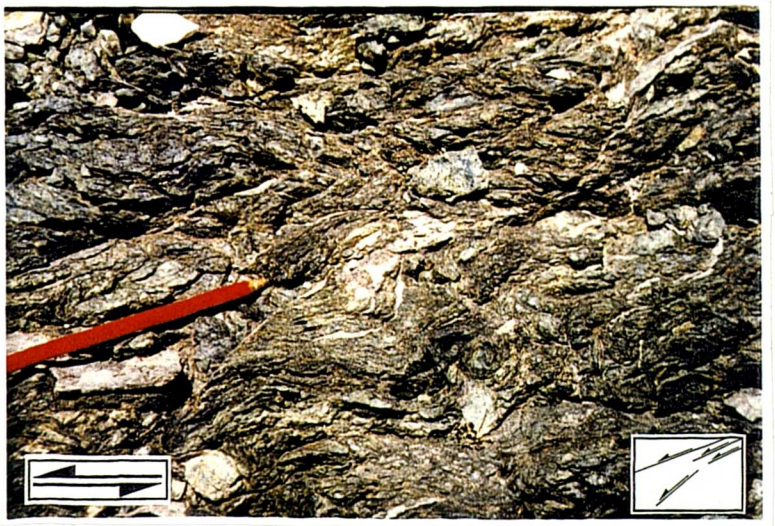

(b)

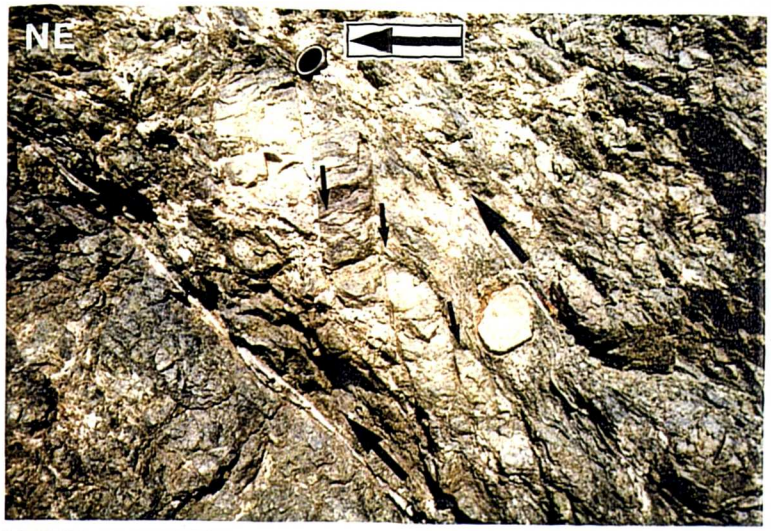

Figure 4.26. (a) Plan view looking down onto sinistral strike-slip shear bands developed in lizardite-carbonate fault rock. Pencil parallels the carbonate mineral stretching lineation. Inset in the bottom right-hand corner shows the orientation of the shear bands. (b) Antithetically rotated serpentinite blocks on a thrust fault surface. Large arrows indicate bulk, top-to-the-NE (left), reverse-slip displacement, while smaller arrows show offsets along minor antithetic faults.

4.3.2. Kinematic analyses

Macroscopic-scale kinematic analyses and field observations suggest that the protrusion of serpentinite was facilitated by a phase of dextral transtension during and/or shortly after the formation of the Troodos Complex. Evidence supporting this hypothesis is now described with reference to the following selected field examples. All of these occur in regions where the effects of later sinistral transpressive deformation are absent or minor.

4.3.2a. Arkolieri - Ayia Varvara area (GR 555 482; Locality 2, Figure 4.20)

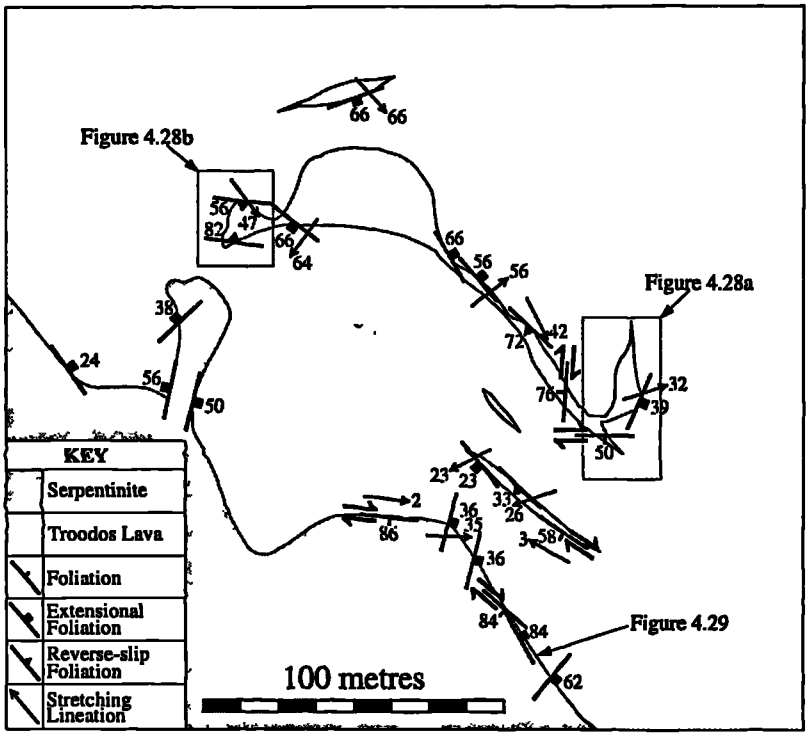

Figure 4.27. Geological map in the vicinity of Arkolieri. Note the dominance of extensional and dextral faults within the serpentinite and along its contacts. The terms 'extensional foliation' and 'reverse-slip foliation', referred to the key, represent contact-parallel foliations that display shear sense criteria and slickenfibre stretching lineations indicating extension or reverse-slip displacements, respectively.

An approximately 100m long, NW-SE striking body of serpentinite, located on the southern edge of the central Troodos sliver in the Ezousa valley, preserves pristine evidence for the tectonically facilitated protrusion of serpentinite (Figure 4.27). Most Troodos lava-serpentinite contacts in the vicinity of this serpentinite body are faulted

and locally display intrusive characteristics, which suggests that they formed during protrusion. The serpentinite body possesses a highly irregular geometry and is bound on all sides by predominantly high-angle structural contacts with Troodos Complex lavas. The southeastern end of the body is relatively tabular (Figures 4.27 and 4.28a), while the northwestern end possesses a 'mushroom'-like geometry (Figure 4.28b). Locally, lava wallrock is 'stoped' and entrained within the serpentinite, which suggests serpentinite behaved like an intruding fluid (Figure 4.29). Kinematic indicators, combined with corresponding slickenline and fibre lineations, document extension (dip-slip to oblique-slip) and dextral strike-slip. This interpretation, combined with the observation that serpentinite constitutes the up-thrown fault block at *every* contact in this area, suggests that the ultramafic material underlay at least part of the Troodos lavas in this region and that dextral transtension accompanied or facilitated protrusion.

4.3.2b. Marathounda (GR 525 495; Locality 3, Figure 4.20)

Approximately 300m SW of Marathounda village, a series of NW-SE trending serpentinite bodies crop out within Troodos lava and intrusive mafic rocks (Figure 4.30). Contact relationships with the lava demonstrate that these are isolated, protrusive bodies are contained entirely within locally brecciated Troodos crust. Contacts display two distinct strikes and corresponding kinematic indicators; E-W to ESE-WNW striking contacts (average 109/67°S) possess shallowly-plunging stretching lineations (average 39/269) and, where present, shear bands and Riedel shears indicate dextral strike-slip. NW-SE trending contacts (average 147/76°SW), on the other hand, possess steeply plunging stretching lineations (average 53/235) and kinematic indicators document oblique- to dip-slip extension. Thus, the orientations and kinematics of these structures are consistent with the hypothesis of dextral transtension during serpentinite protrusion (see inset, Figure 4.30). It is significant to note that the NW-SE strikes, that are prevalent in this area of the Southern Region fault zones, may relate to this phase of dextral transtension. Furthermore, Troodos basalt and gabbro dykes often possess similar strikes, which may suggest that deformation and Troodos magmatism are to some extent synchronous (see below).

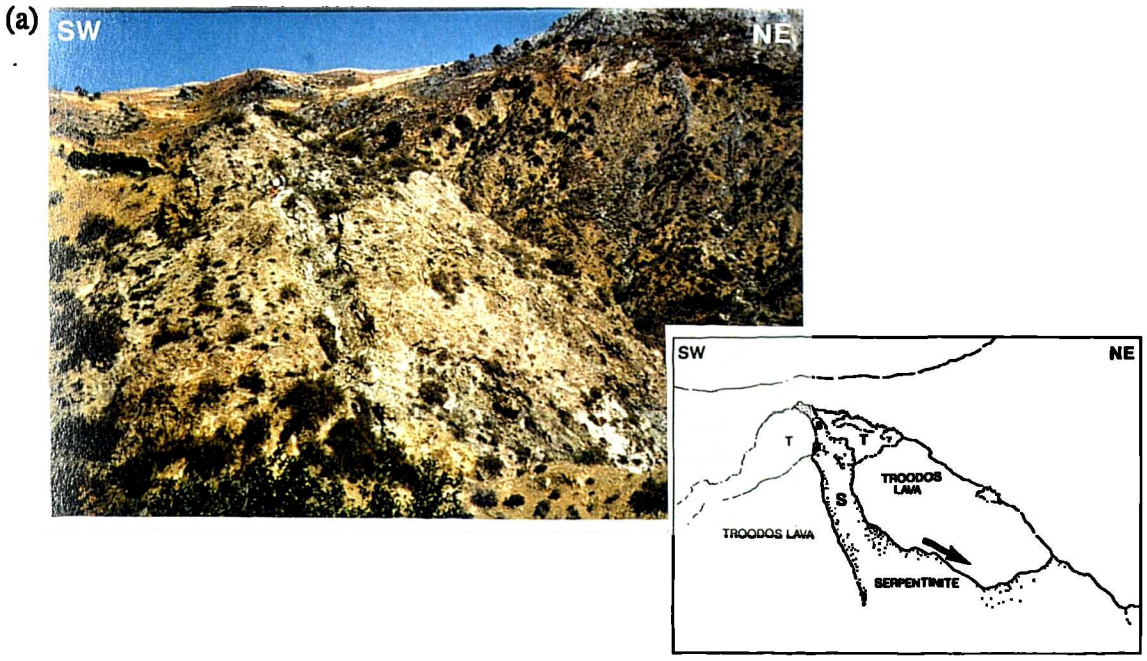

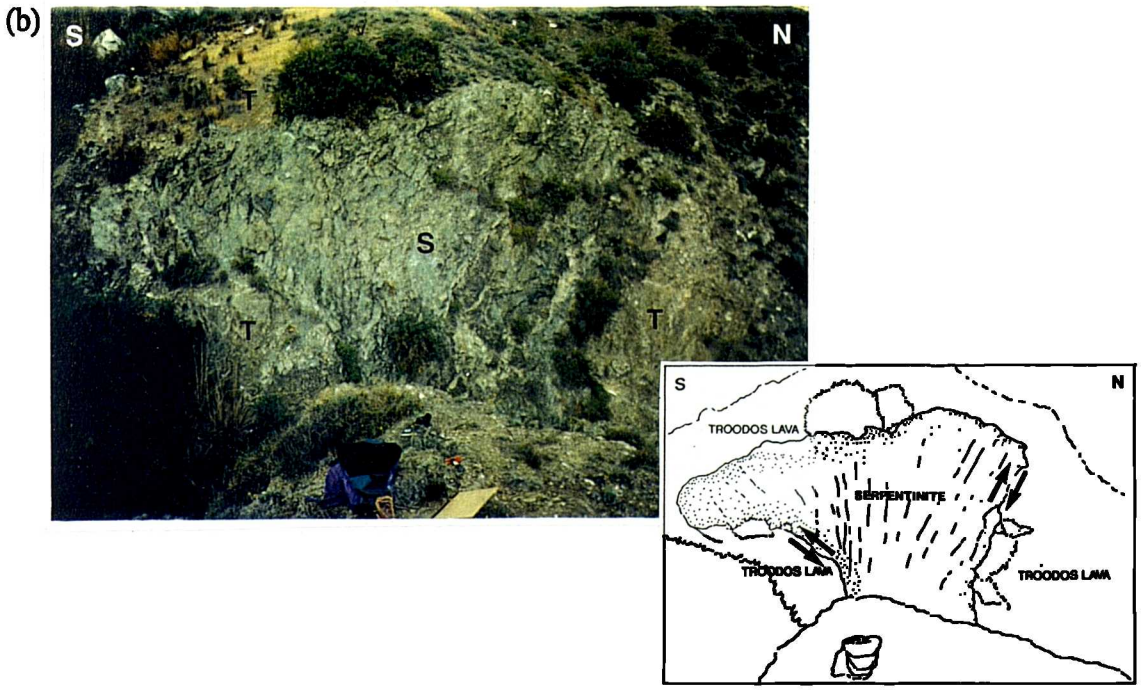

Figure 4.28. Contact relationships observed at the Arkolieri serpentinite body
(a) Southern end of the serpentinite body, displaying relatively planar contacts with Troodos lava. Note that the northeastern extensional contact shallows and exposes serpentinite beneath Troodos lava. Arrows indicate extensional displacement, downthrowing lava to the NE.
(b) The 'mushroom-like' geometry exposed at the northwestern end of the serpentinite body. Kinematic indicators suggest serpentinite has risen relative to the country-rock and 'mushroomed' against the Troodos roof.

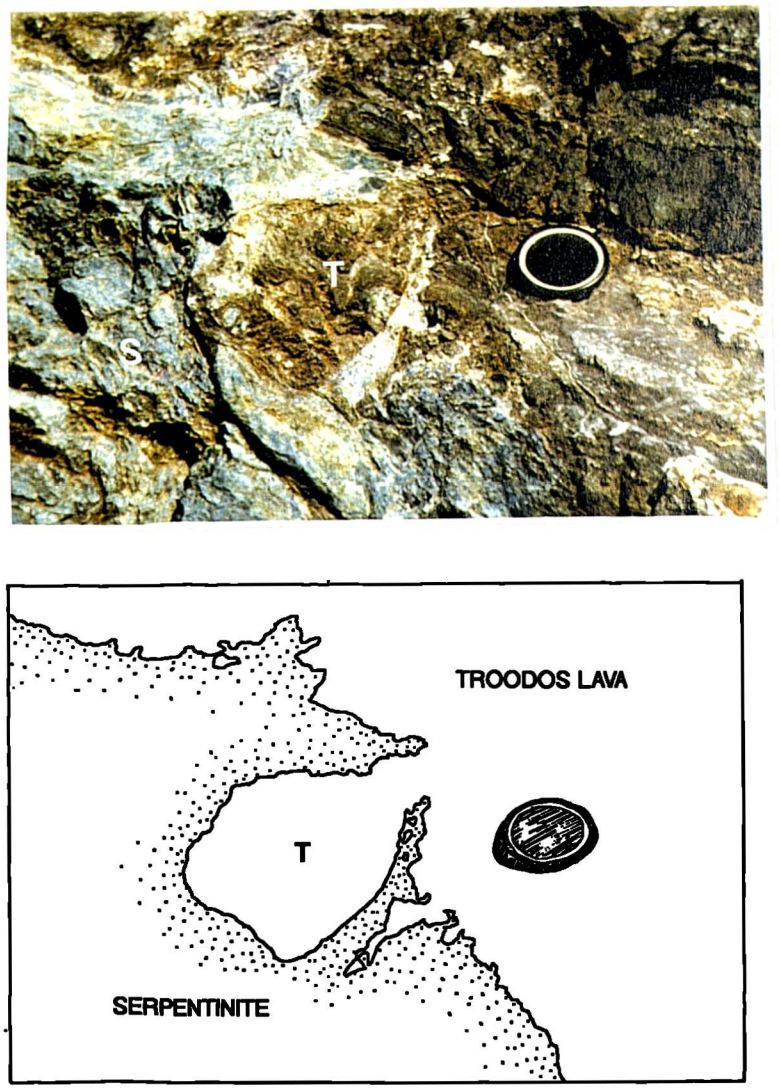

Figure 4.29. Characteristic intrusive contact relationship between Troodos lava (brown) and serpentinite (S; blue). Note the 'stoped' clast of Troodos lava (T) and the lack of any obvious baking or chilling at the contact.

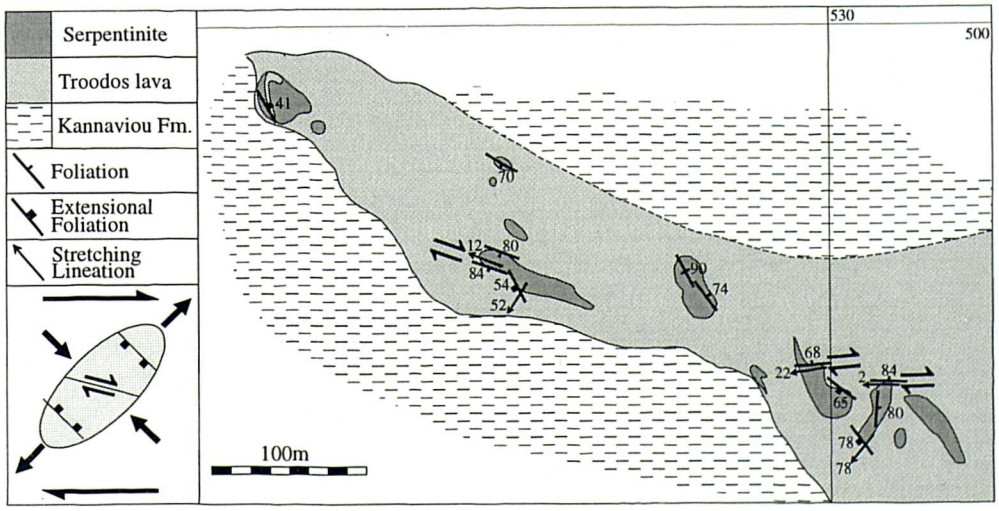

Figure 4.30. Geological map showing the isolated serpentinite bodies located with the Troodos sliver SW of Marathounda village. A hypothetical strain ellipse is presented in the bottom left hand-side of the figure.

4.3.2c. Moutti tis Koronas - Mamonia area (GR 647 470; Locality 4, Figure 4.20)

The serpentinite body, located approximately 1km west of Phasoula village in the vicinity of Moutti tis Koronas in the Dhiarizos valley, is characterised by highly irregular contacts with Phasoula lavas (Figure 4.31). Phasoula lava blocks (cm to tens of metre scale) are frequently 'stoped' and incorporated within the serpentinite at contacts that are irregular on cm to the metre scale (Figure 4.32). As seen in the previous examples, tectonic contacts and foliations strike E-W to NW-SE and kinematic indicators point to dextral strike-slip to dip-slip extension. The most spectacular contact is located at the southern edge of this serpentinite body where Phasoula lavas overlie serpentinite with a low angle tectonic contact (Figure 4.31). Extensional shear bands and Riedel shears in highly deformed serpentinite gouge along this contact indicate oblique-slip extension, down throwing lavas to the NW.

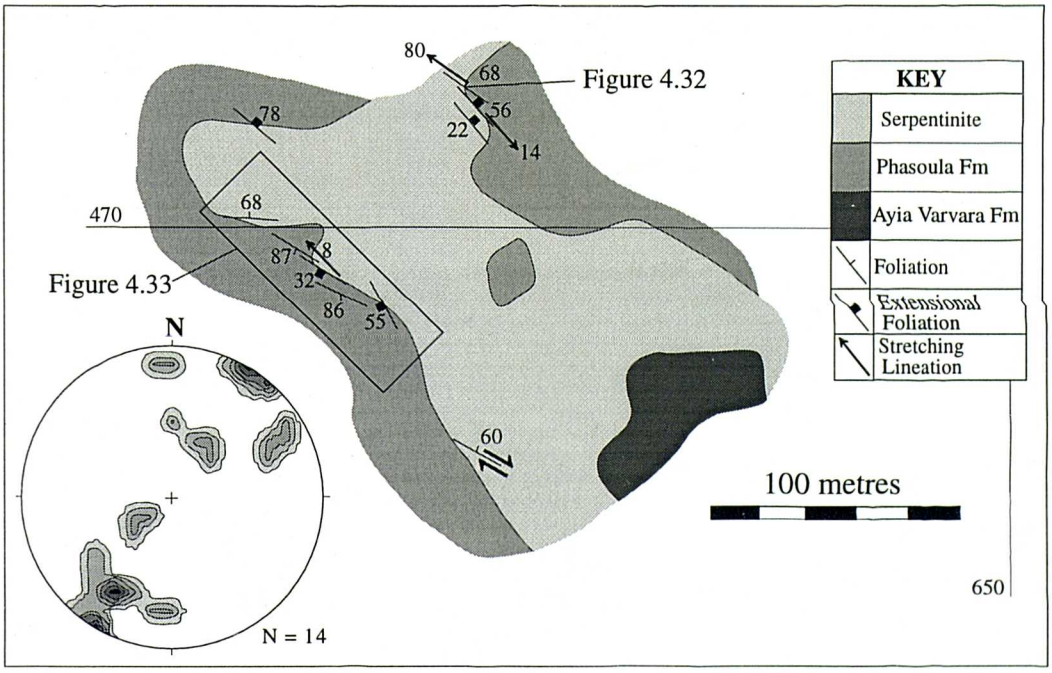

Figure 4.31. Geological map in the vicinity of Moutti tis Korona. Stereonet in the bottom left shows poles to NW-SE striking contacts and faults.

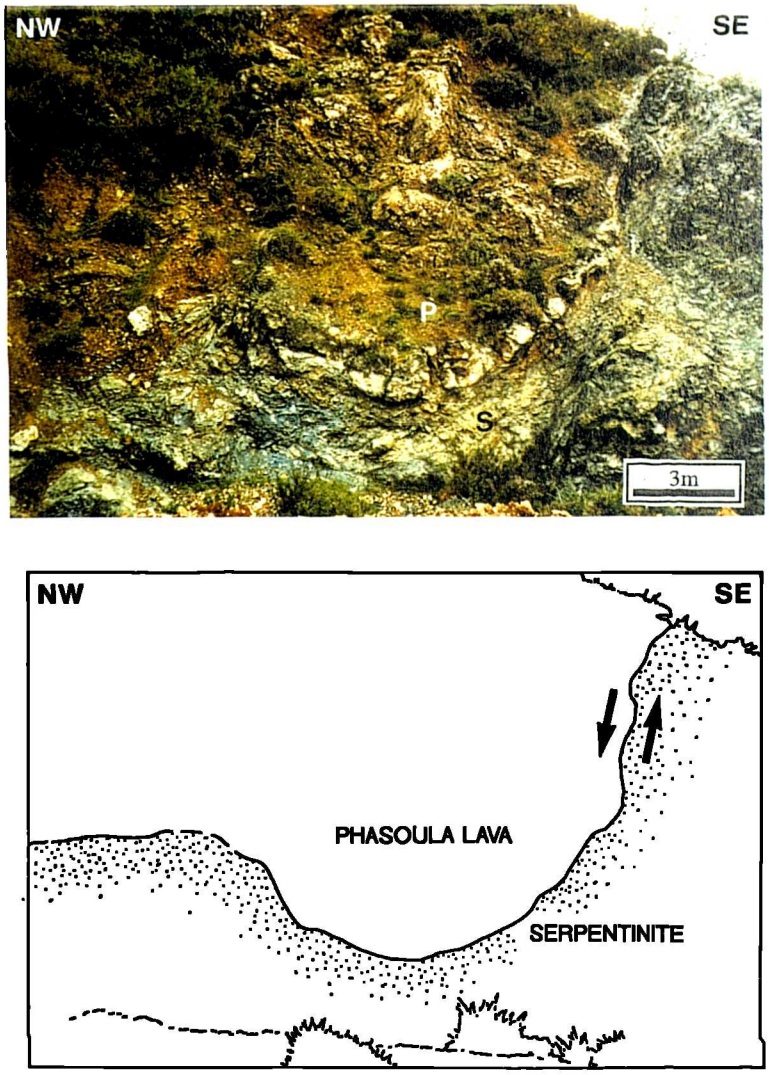

Figure 4.32. Highly irregular serpentinite (S)-Phasoula lava (P) contact. Shear sense criteria along the high-angle portion of the contact indicate Phasoula lavas are downthrown relative to serpentinite (black arrows).

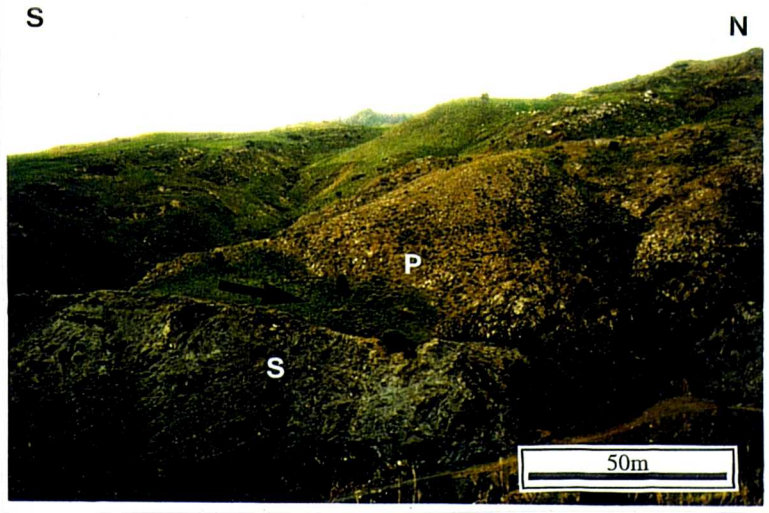

Figure 4.33. Low angle tectonic contact between Phasoula lavas (P) and serpentinite (S). Arrows indicate lavas are down thrown relative to serpentinite.

4.3.2d. Kannaviou (GR 610 635; Locality 5, Figure 4.20)

Although the serpentinites at Kannaviou and Statos have been allocated to the Northern Region by previous authors (e.g. Swarbrick, 1979) they possess structures more akin to those observed in the Southern Region. The significance of this portion of the fault zone is discussed further in Chapter 6. S of Kannaviou Village serpentinite is in contact with Troodos Complex units (Figure 4.34) and, where exposed, contacts and associated structures strike NW-SE to ESE-WNW and possess kinematic indicators that document dextral strike-slip to dip-slip extension. The most northerly contact between serpentinite and Troodos lava displays shallow plunging stretching lineations and dextral kinematic indicators. The same serpentinite body is bound at its southern end by a NW-SE striking planar extensional fault that downthrows Kannaviou sediment to the SW. Locally, sinistral faults and shear zones dominate, for example in the eastern side of the serpentinite body, but their approximate N-S strikes are consistent with a dextral model, in which they constitute an antithetic conjugate set (see inset, Figure 4.34). The correspondence of all these structures, (i.e. the similarity of strikes and dextral kinematic indicators) to those previously described in the Southern Region suggests that they may be associated with the same tectonic event. In particular, serpentinite constitutes the upthrown block at the southerly extensionally faulted contact. This relationship conforms to previous studies that propose Kannaviou sediments were deposited in extensional fault-bounded hollows (Malpas *et al.* 1993). NW-SE striking, sub-vertical, Troodos basalt dykes are located within serpentinite. The dyke orientations are consistent with a significant number observed in the Marathounda region and their existence is thought to indicate syn-deformational magmatism.

Sinistral displacements are also recorded on surfaces that possess NE-SW strikes, for example in the thin serpentinite body located within Kannaviou sediment at the western side of the map. These structures are inconsistent with their formation in a dextral transtensional regime and are therefore interpreted to relate to later sinistral deformation. Their existence in such bodies is thought to be indicative of the continued protrusion of serpentinite after the dextral event.

4.3.2e. Conclusions

Structures that are interpreted to have formed during a phase of dextral transtension can be inferred where: (a) evidence of the deformational chronology may be determined, as observed, for example, at Kara tou Ayiou Pati (GR 568 484);

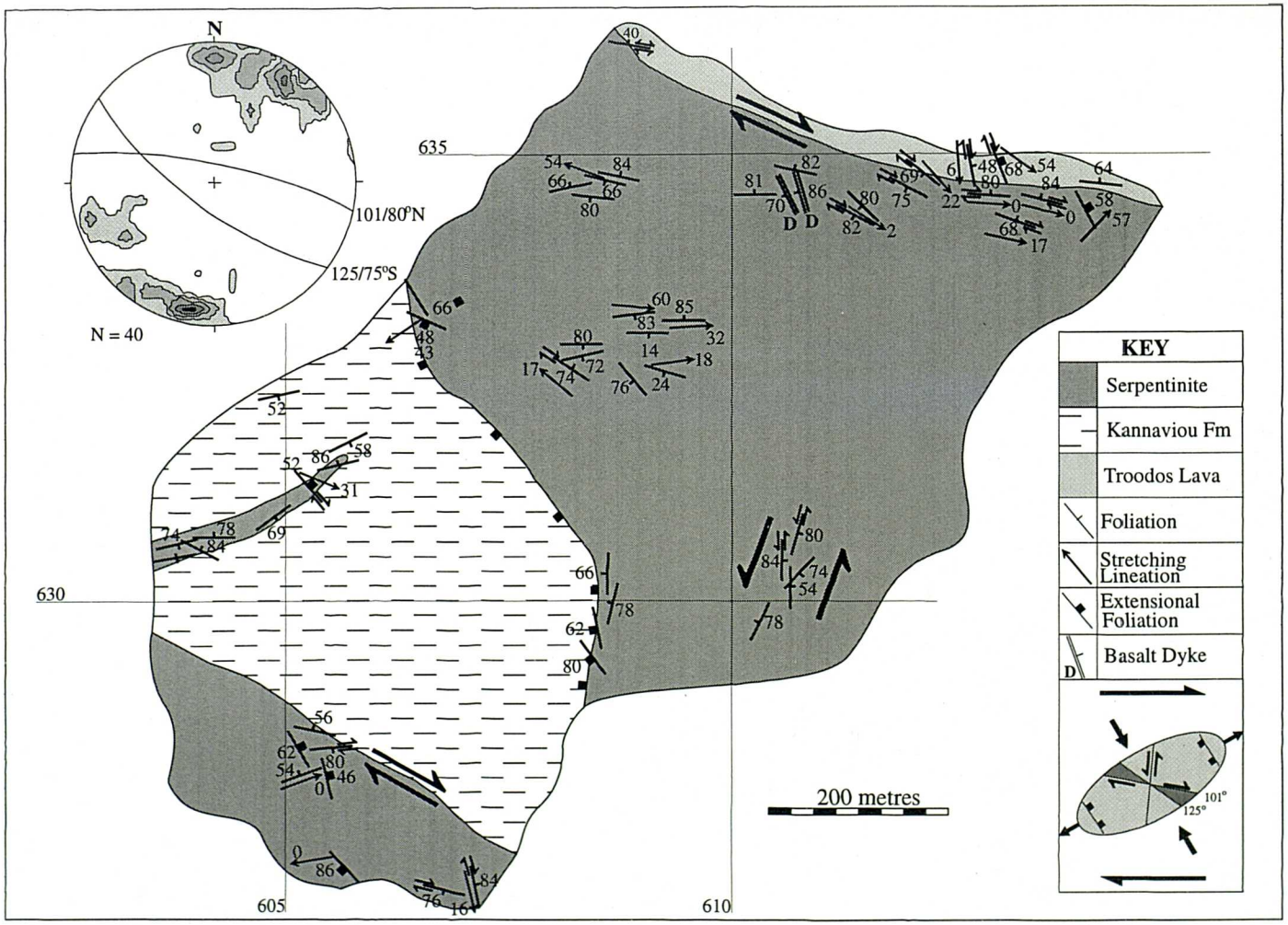

Figure 4.34. Geological map of the Kannaviou serpentinite body. The stereonet in the top-left inset shows 1% contours of poles to faults and shear zones, which indicate two dominant sets of structures exist (great circles). A hypothetical strain ellipse is presented in the bottom right hand of the figure.

(b) evidence of extensional and dextral displacements can be linked with the protrusive behaviour of serpentinite, and (c) structural evidence is present to suggest that strains resulting from the later sinistral transpressional event are low or, more favourably, absent. The reason for this distinction is due to the approximate parallelism between dextral transtensional structures and dextral faults that formed as antithetic structures during later sinistral transpression. Where sinistral transpressional strain rates were high, structures formed during the previous dextral event are expected to be reactivated or destroyed. On the other hand, where transpressional strain rates were low, protrusion of serpentinite may have been facilitated. In theory, the best field examples preserving evidence of dextral transtension would be located where the transpressional strains were efficiently partitioned. For example, the lavas within the central Troodos sliver in the Southern Region are only weakly deformed, compared to the bounding serpentinite-filled faults that are pervasively deformed and evidently highly strained. This suggests that the tranpressional strains were efficiently partitioned into the serpentinite-filled faults, thereby preserving structures within the lavas of the Troodos sliver that formed during the previous events (i.e. the protrusions at Arkolieri and Marathounda).

In summary, protrusion of serpentinite is thought to have been facilitated by a phase of dextral transtension during and/or subsequent to the formation of the Troodos Complex. The following evidence supports this hypothesis:

- Serpentinite frequently displays contact relationships analogous to those associated with magmatic intrusions. Contacts are highly irregular and blocks of Troodos and Mamonia Complex wallrock are occasionally 'stoped' and incorporated within the serpentinite. No evidence of contact metamorphism or 'baking' of the country rock is observed, which suggests serpentinite was emplaced at low temperatures.
- Kinematic indicators and orientations of protrusion-related faulted contacts are consistent with a dextral transtensional model.
- At extensionally faulted contacts with both complexes, serpentinite invariably constitutes the upthrown fault block. This observation suggests that faulting associated with protrusion may be controlled by the physical properties of serpentinite, i.e. the reduction in density and increase in volume during serpentinisation;
- Where preserved, the orientation of Troodos diabase dykes that have intruded serpentinite is consistent with their formation during dextral transtension.

4.4. Sinistral transpression

The fault zone peridotites in the Southern Region are overprinted by pervasively serpentinised, lizardite-dominated fault rocks, which have largely masked the structures and fabrics formed during the previous dextral tectonic events. Kinematic indicators within these fault rocks document synchronous strike-slip and compressional displacements, which formed during a phase of sinistral transpression at relatively low temperatures (~100°C). Macroscopic-scale kinematic analyses suggest these structures formed in response to near fault-normal compression, which resulted in the 'lateral extrusion' of fault zone material (see section 4.4.2 and Chapter 6).

As described at the beginning of this chapter, strain is heterogeneously distributed throughout the Southern Region. Field observations suggest that, on a regional-scale, tranpressional strains are predominantly localised along, and in the immediate vicinity of, the serpentinite-filled faults (i.e. within 5-50m of the fault zone). On a macroscopic-scale, low and high strain domains can be identified, which indicate that the distribution of deformation within individual faults is also heterogeneous. The complex array of faults and shear zones produced during this event appear to be preferentially developed in the zones of ultramafic material that have undergone the greatest amounts of serpentinisation. However, due to the irregularity in the distribution of deformation and serpentinisation, a systematic spatial analysis of low and high strain zones along the fault zones is not possible.

The least deformed sections are characterised by relatively massive (<10m in diameter) blocks of partially serpentinised harzburgite that are cross-cut by randomly oriented joint planes, which gives the outcrop an angular appearance (Figure 4.35). Influx of hydrous fluids along these joints has resulted in the serpentinisation of the block margins, forming characteristic kernel patterns. In Figure 4.35, the abrupt transition from the white, serpentinised kernel rim (S) to the brown, partially altered core represents the position of the serpentinisation front in the block (black arrow).

With an increase in strain and a concomitant increase in serpentinisation, the development of randomly oriented green serpentine (chrysotile) fibres on block surfaces indicates that deformation was accommodated by local translations and block rotations (Figure 4.36a). The presence of minor curved slickenfibres suggests that these rotations were locally complex. The orientation of fractures that bound these blocks, and the relative displacements recorded by serpentinite fibres, are random at all scales (Figure 4.36b and c). Figures 4.36(b) and (c) show a representative data set taken from a weakly deformed section of the northern serpentinite belt (GR 578 479), in which the deformation has been accommodated by local (< 1m-scale) translations and rotations of individual peridotite blocks. In general, the scatter displayed by these

stereonets indicates a random distribution of fracture and lineation orientations, but note that strike-slip to oblique-slip fractures dominate (~52% of total) and that sinistral faults are approximately 20% more abundant than dextral. These observations are discussed further in section 4.4.2a.

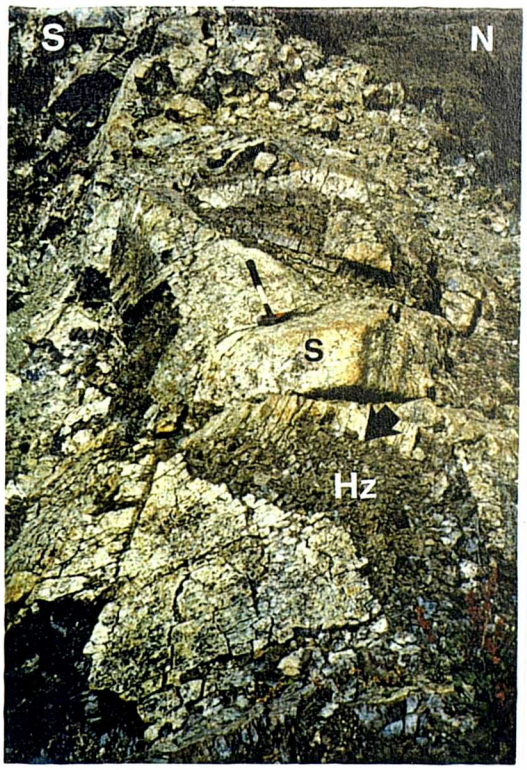

Figure 4.35. A characteristic low strain region of a fault zone, comprising blocks of partially serpentinised harzburgite (Hz; brown), cross-cut by randomly oriented joint planes. The white material that rims these blocks is serpentinised peridotite (S) (GR 653 478). The black arrow points to the position of the serpentinisation front, which defines the transition between the core (Hz) and rim (S) of a kernel structure.

With increasing strain, the undeformed blocks are offset and progressively disaggregated by cross-cutting faults and shear zones (Figure 4.37). The blocks transected by these structures are typically heavily serpentinised, preserving only pseudomorphs of the primary peridotite texture. Eventually, anastomosing networks of cm- to m-scale faults and shear zones, comprising pervasively foliated and serpentinised fault rocks, bound and separate the lesser deformed blocks. This relationship between partially to totally serpentinised blocks and cross-cutting structures characterises the majority of the serpentinite belts. The shear zones and faults are invariably sub-vertical, exhibiting relatively consistent orientations. Offsets and shear sense criteria along these structures indicate both sinistral and dextral strike-slip.

(a)

(b)

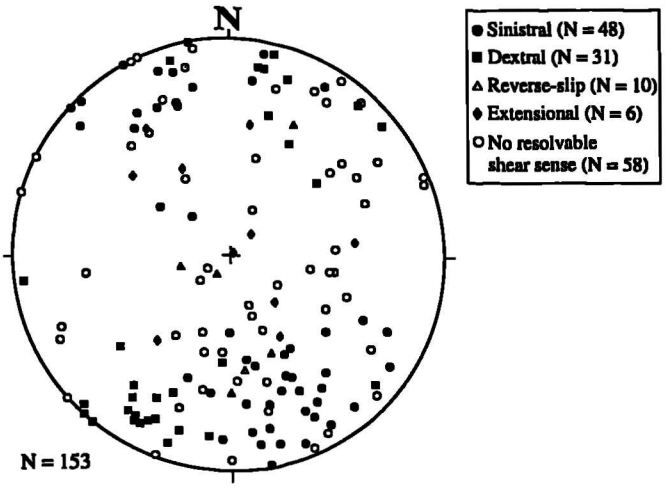

(c)

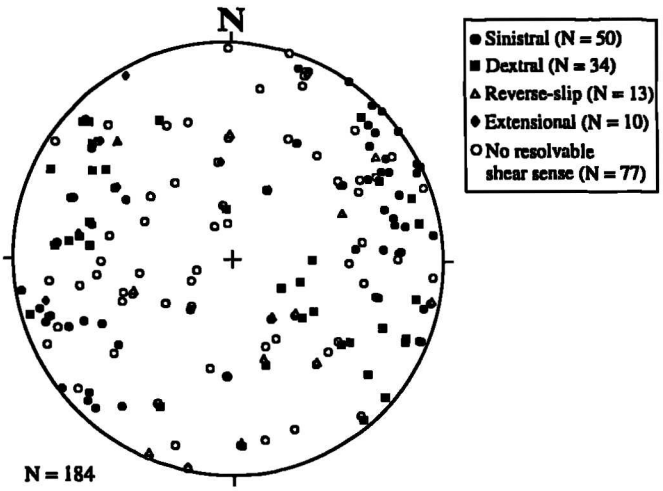

Figure 4.36. Characteristics of a weakly deformed fault zone, comprising partially serpentinised harzburgite. (a) Example of serpentine fibres (pale green) on a block surface. The blue colouration is heavily serpentinised material at block margins. (b) and (c) Stereographic projection showing the random distribution of fracture planes (b) and lineations (c). Note that sinistral and dextral fractures dominate (GR 578 479).

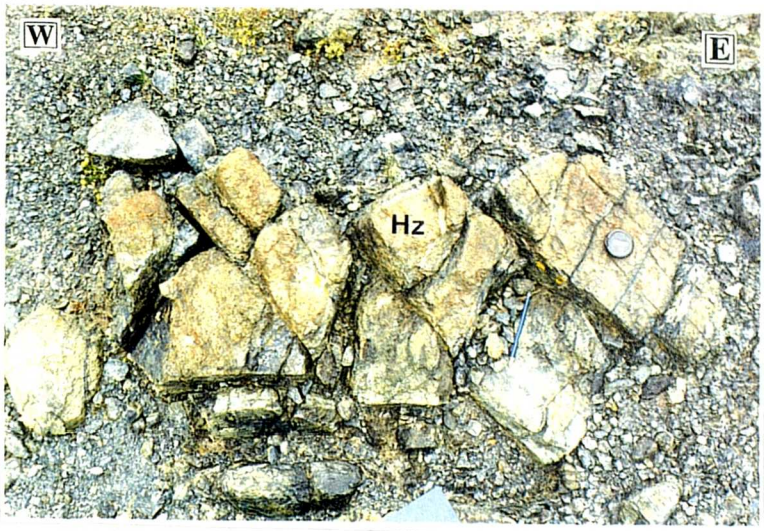

Figure 4.37. Plan view. Serpentinised harzburgite (Hz) block offset by dextral faults.

Within higher strain zones, totally serpentinised blocks, which are commonly less than 5m in diameter, are supported by an interconnected, anastomosing network of blue to green coloured, fine-grained serpentinite shear zones. With increasing strains, the shear zones widen, consuming all the peridotitic blocks (Figure 4.38; compare this with Figure 4.35). Locally, the deformation is so pervasive that the shear fabric extends over the width of a fault zone (i.e. over 70m). Fabrics associated with this high strain end-member are characterised by an intense, pervasive foliation that predominantly strikes E-W and dips sub-vertically. The foliation is deflected and offset by sub-vertical brittle and brittle-ductile, strike-slip faults and shear bands (mm- to <1m-scale offsets) that also bound and delincate lower strain lenses (mm- to 10cm-scale), defining a *'phacoidal'* fabric (Figure 4.38). These lower strain augen (or *'phacoids'*) typically possess long and short axes oriented approximately E-W and N-S, respectively. In hand specimen, the phacoids commonly display a cataclasite fabric, comprising randomly oriented, mm- to sub-mm-scale clasts of light coloured serpentinite supported in a light blue or green, fine-grained fibrous matrix. The edges of these phacoids and their bounding faults and shear zones display a variety of fault plane lineations, which invariably exhibit shallow pitch angles. The various types of lineations include polished brittle striae (i.e. ridges and grooves), serpentine fibres, and carbonate slickensides. The most highly deformed sections of the serpentinite belts, which comprise these fault rocks, are readily identified in the field as they are topographically subdued and they display characteristic light blue or olive-green to lime-green colourations. Those sections of the faults that are thought to be derived from a Troodos-related protolith frequently display blue colourations, whilst those associated with the Mamonia Complex are typically green in colour (see Chapter 3).

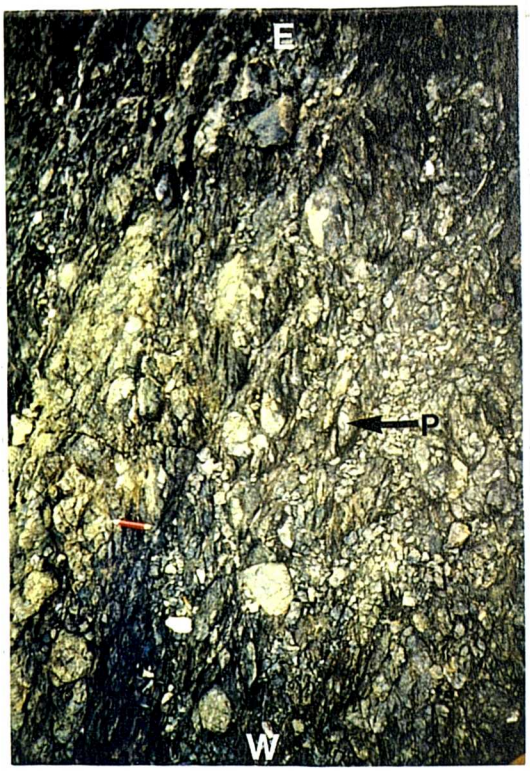

Figure 4.38. Plan view. Highly strained and intensely foliated fault rocks, displaying an E-W striking, sub-vertically dipping 'phacoidal' shear fabric (P = phacoid). Note that all the rocks are 100% serpentinised. Compare this with Figure 4.35.

The dip of foliation planes within the fault zones is typically sub-vertical and parallel to the local fault zone boundaries. However, along certain sections of the faults, tectonic contacts with the adjacent units possess shallow to moderate dips. Along these sections, the serpentinite foliation within 5-10m wide zones parallels the *contacts, but internally* within the core of fault zones foliations are sub-vertical.

The following two sections describe field evidence that suggest a phase of sinistral transpressional deformation was the last significant tectonic event that took place in the Southern Region. The first part details the fault rocks associated with this deformational phase, whilst the second concerns the macroscopic-scale field observations and kinematic analyses. Figure 4.35 shows the geographical location of areas and localities referred to in the following sections. A more detailed map (Map I) is presented in the back of this thesis.

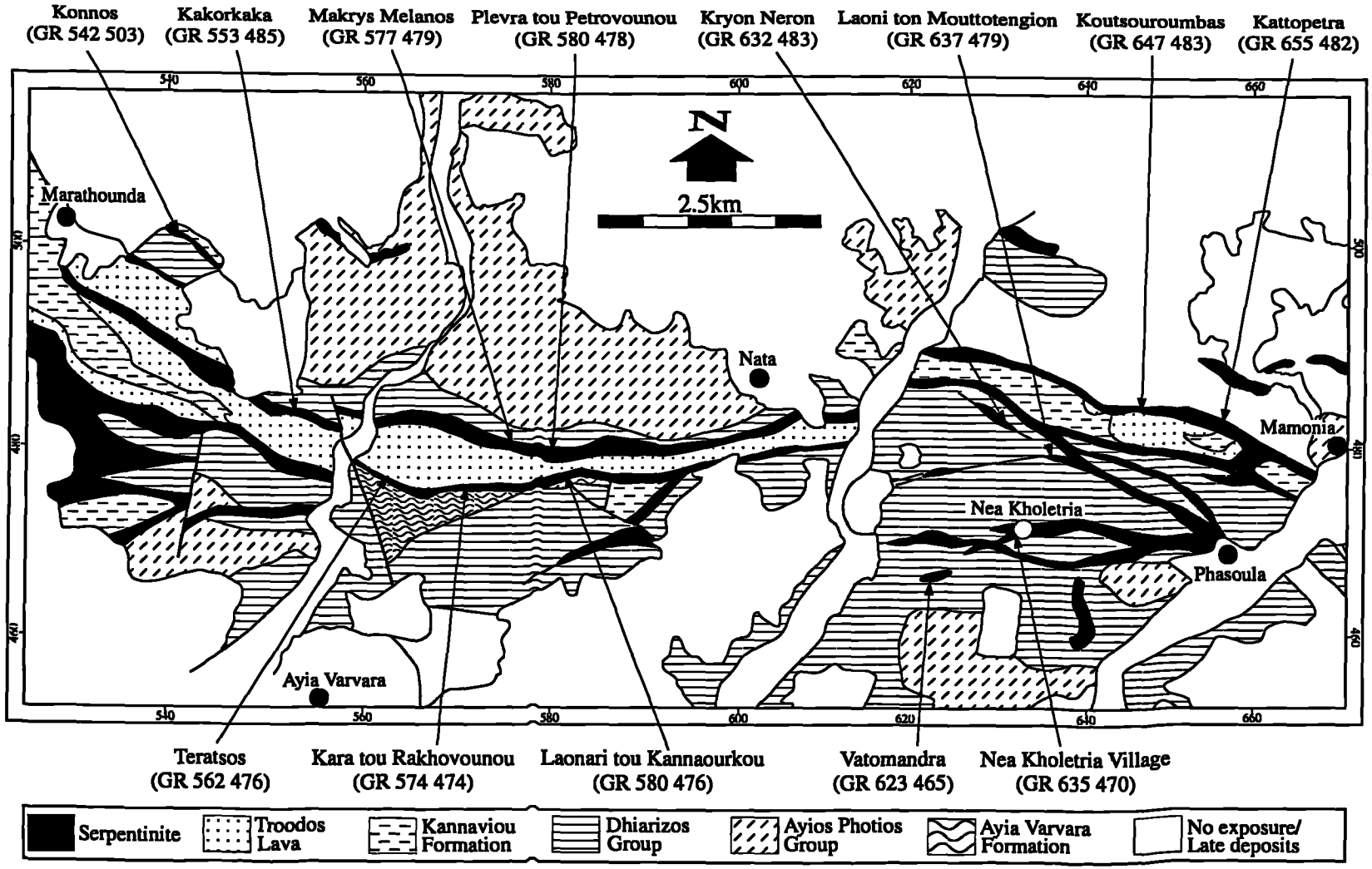

Figure 4.39. Geological map showing the localities referred to in the following sections (adapted after Swarbrick, 1979).

4.4.1. Microstructure

In hand specimen, the undeformed harzburgite protolith of the serpentinite fault rocks comprises an interlocking network of at least partially serpentinised olivine grains (<1mm) and coarser bronze orthopyroxene bastites (<1cm). Olivine grains are occasionally preserved in the cores of peridotite blocks and are identified by their 'glassy' green colour. In thin section, the olivine, which would comprise the bulk of the pristine protolith, is partially to completely serpentinised. As the serpentinisation of these rocks is essentially static (as opposed to syn-kinematic) the replacement of olivine by lizardite serpentine has produced a 'mesh' texture, which is defined by a cubic array of serpentine that rims and separates neighbouring olivine grains (Figure 4.40). Orthopyroxene is also pseudomorphed by serpentine, whilst rarer clinopyroxene is relatively resistant to serpentinisation and is typically unaltered. Spinel grains are also well preserved, with only minor alteration to magnetite along their rims. As partially serpentinised olivine is the dominant constituent of these rocks (>80%), this fabric is considered representative of the undeformed peridotites and is expected to control the rheology of these rocks.

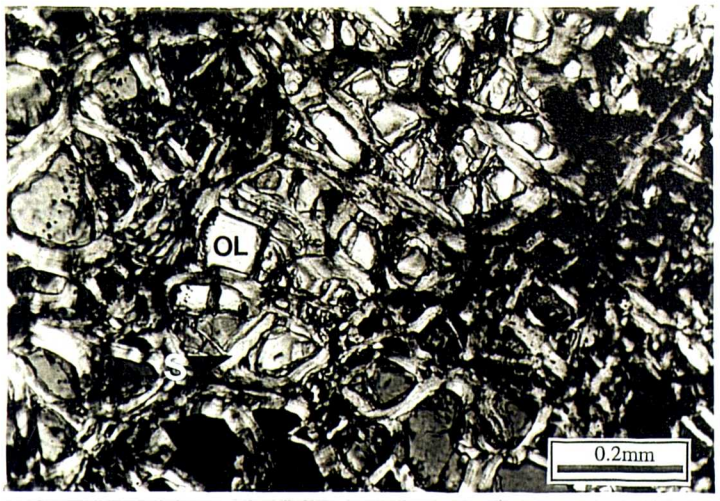

Figure 4.40. Black and white photomicrograph of a characteristic texture in an undeformed, partially serpentinised peridotite. Relict olivine grains (OL) are rimmed and pseudomorphed by lizardite serpentine (S), producing a 'mesh texture'.

In contrast, the fault rocks associated with the sinistral transpressional event are pervasively deformed and serpentinised. The typical syn-kinematic mineral assemblage comprises lizardite + Fe-oxide (magnetite) ±chrysotile ± carbonate. A number of different types of fault rocks, which exhibit a range of deformational characteristics, are interpreted to have formed during this phase of deformation. These rocks may be sub-divided into two dominant types: (a) those that display brittle

deformational characteristics on all scales, and; (b) those that display predominantly brittle-ductile characteristics. Note that many serpentinite fault rocks in SW show micro-scale evidence of brittle deformation, but at macroscopic-scales these rocks accommodate ductile flow (see below). Therefore, the sub-division in terms of deformational style is arbitrary. Both brittle and broadly ductile deformations are considered coeval for two significant reasons:

(1) structures that display brittle or ductile characteristics on all scales are geometrically and kinematically *identical.* The reason for the difference in deformational style may relate to fluctuations in stress, strain rate, pore-fluid pressure, material properties of the fault rock etc (see Chapter 6);

(2) structures which are parallel, but also exhibit contrasting deformational styles are exposed within close proximity (e.g. over <1m). For example, the contact between Troodos lavas and the southern serpentinite belt in the Mamonia area exposed at GR 654 478, is marked by a sub-vertical, highly sheared zone of essentially *ductile,* foliated, serpentinite-carbonate fault gouge (Figure 4.41). Asymmetrical shear bands and shallowly-plunging carbonate fibres in this fault rock indicate sinistral strike-slip. However, immediately to the south of, and in contact with, this sheared fault rock, the ultramafic rocks are brecciated, foliated and display characteristics of *brittle* deformation (i.e. fracturing of clasts and cataclasis). The degree of brecciation, serpentinisation and comminution of harzburgite clasts in these rocks increases noticeably with increased proximity to the ductile fault rocks at the contact. The increase in the intensity of deformation is also evident by the development of foliation in the breccias and cataclasites, which is localised to an approximately 5m wide zone adjacent to the ductile fault rocks. The parallelism between the foliation and lineations in the two fault rocks, combined with the progressive increase in the intensity of deformation towards the contact, suggests that the development of the breccias and cataclasites and the ductile fault rocks were coeval. The difference in deformational character is thought to relate to the rheological contrast between the fine-grained ductile gouge and the competent, partially serpentinised blocks of the breccia.

The following sub-sections describe the end-member *brittle* and *brittle-ductile* fault rocks associated with the transpressional event.

4.4.1a. Brittle fault rocks (breccias to cataclasites)

Fault rocks, comprising approximately 100% serpentine minerals, sometimes display brittle deformational characteristics on the scale of a hand specimen or smaller. These rocks comprise variably foliated breccias, cataclasites and gouge, which are associated with faulting along tectonic contacts and, to a lesser extent, faults that accommodate

rotation of harzburgite blocks within the serpentinite fault zones. Frequently, fault rocks that display brittle deformational characteristics on the micro-scale appear to accommodate ductile flow on the scale of a hand specimen and larger (i.e. cataclastic flow). In hand specimen, ductile flow is inferred by the presence of highly contorted, anastomosing layers, comprising finely comminuted material, which are deflected around rigid, angular to sub-angular, mm- to cm-scale clasts. At outcrop, these layers clearly parallel the sub-vertical fault zone boundaries, but in thin section, the only evidence for this 'foliation' is irregular, dark seams of amorphous to opaque material, presumably an Fe-oxide, which follow the edges of clasts (Figure 4.42). For this reason, it is reasonable to suggest that this discrete micro-scale foliation may be formed by pressure solution and the amorphous material constitutes insoluble residue.

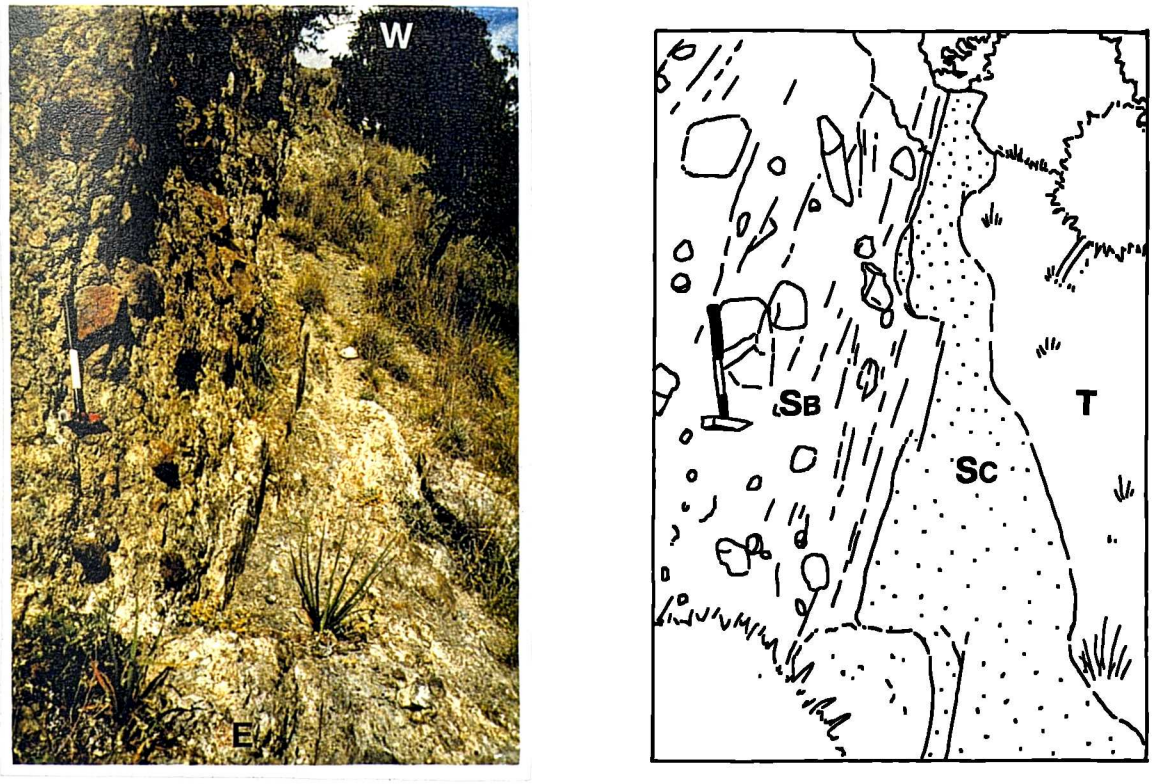

Figure 4.41. Detail of the contact between the southern serpentinite belt and Troodos lavas (T) to the north at GR 654 478. The bulk of the fault zone comprises massive, brecciated harzburgite (S_B), but the contact zone (<2m wide) is marked by foliated serpentinite-carbonate cataclasites and gouge that display characteristics of macroscopically ductile, sinistral deformation (Sc).

Commonly, contacts between serpentinite and adjacent units are heavily brecciated during tectonism as seen, for example, at Kryon Neron in the Nea Kholetria area (GR 632 484). These tectonic breccias and cataclasites comprise variable

proportions of serpentinite, country rock and carbonate clasts that locally align to form a rough foliation. The presence of carbonate as clasts and deformed veins, suggests that the influx of carbonate-rich fluids was synchronous with faulting and may have caused hydraulic fracture (i.e. pore fluid pressures > the least principal stress, σ_3).

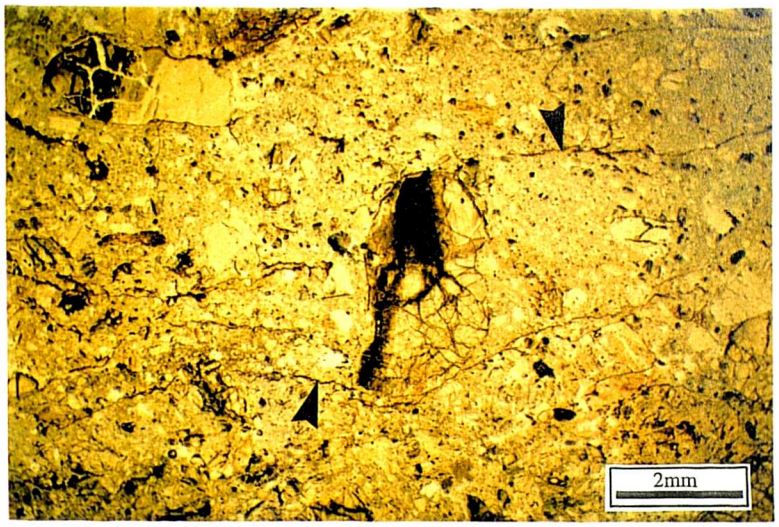

Figure 4.42. Seams of dark insoluble material (pointed to by black arrow heads) within a poorly foliated cataclasite, which are thought to result from pressure solution. Plan view cut normal to sub-vertical E-W foliation and parallel to sub-horizontal cataclastic fault plane lineation (Sample MM/CCI/94).

4.4.1b. Brittle-ductile fault rocks

The majority of the serpentinite fault rocks observed in the Southern Region display both brittle and ductile characteristics on all scales. Although many different types of fault rock exist, they can be divided into those that comprise 100% serpentine minerals and accessory phases, and those in which the microstructure is dominated by carbonate. Many of the samples studied display microstructural evidence for fluid flux during and/or after deformation.

Serpentinite fault rocks

Many tectonic contacts are marked by narrow (~5m wide) zones, comprising hard, cohesive, light-blue coloured fault rocks (e.g. Laonari tou Kannaourkou in the Ayia Varvara area; GR 581 475). At outcrop, these rocks are readily identified as they parallel contacts for many tens of metres and stand out above the surrounding units due to their resistance to weathering. Furthermore, these rocks are commonly associated with distinctive, white, fibrous serpentine (chrysotile) veins that also parallel contacts. The orientation of fibres within these veins, indicate that they are tensile and that the veins opened perpendicular to foliation and contacts (see below). In hand

specimen, the sheared fault rocks are characterised by their hard, "embrittled" shear fabric, which is defined by distinctive 10cm-scale, planar, asymmetrical brittle shears, and by the presence of numerous mm- to cm-scale holes that give the rock a deceptively fragile appearance. In thin section, the main shear planes, which are oriented between 24°-31° to foliation, are easily distinguished by strung-out aggregates of Fe-oxide (Figure 4.43a). The matrix consists of variable proportions of high birefringent, fibrous serpentine and clasts (<1mm) of serpentinite and spinel. The angularity of spinel grains, as opposed to the rounded form of serpentinite clasts, suggests that they are more competent than the surrounding serpentine matrix. Matrix fibres possess irregular grain boundaries and undulose extinction, which suggests the operation of serpentine recrystallision mechanisms. Locally, the 'holes' observed in hand specimen are present within the matrix, displaying irregularly shaped margins. They are characteristically devoid of mineralisation and elongate with long axes that parallel shear planes (Figure 4.43a). However, their mode of formation is problematic. They may represent voids created by dissolution of pre-existing material, or, alternatively, they may have formed during (or after) deformation when pore-fluid pressures were high. The latter idea is supported by the parallelism between the orientation of shear planes and holes, and by the relationship between these fault rocks and the cm-wide tensile serpentine veins discussed above. However, the presence of tensile fractures along a faulted contact, such as this one, is in itself problematic and is discussed in Chapter 6.

In most samples studied petrographically, which possessed strike-parallel stretching lineations, both sinistral and dextral offsets are present (Figures 4.43a and b). Although sinistral shear dominates in the majority of samples, the existence of these conjugate shear sets conforms with the field observations, thereby supporting the interpretation that the sinistral deformation event involved a component of strike-parallel extension (see below).

Many serpentine-dominated fault rocks are frequently rich in chrysotile veins. These veins typically exhibit chrysotile fibres oriented normal to the wall rock-vein boundary, which invariably parallels foliation, indicating that the majority are tensile. In thin section, the gradual change in optical continuity and serpentine type from the wall rock to the centre of the vein (i.e. from mesh-textured lizardite to fibrous chrysotile) indicates that these veins grew by the recrystallisation of the wall rock serpentine. Frequently, chrysotile veins contain inclusions trails of wall-derived, lizardite-rich material (Figure 4.43b). The regular arrangement of these wall-parallel trails suggests that they were incorporated into the vein during episodic opening along the vein-wall contact. This mechanism is thought to document sequential *'crack-seal'* increments and periodic fluid flux (*cf.* Ramsay, 1980). Fragments of these veins are

occasionally found as clasts within fault breccias associated with sinistral strike-slip displacements. This observation suggests that these fault rocks, which are commonly located along contacts, are prone to tectonic-'recycling' and reactivation.

(a)

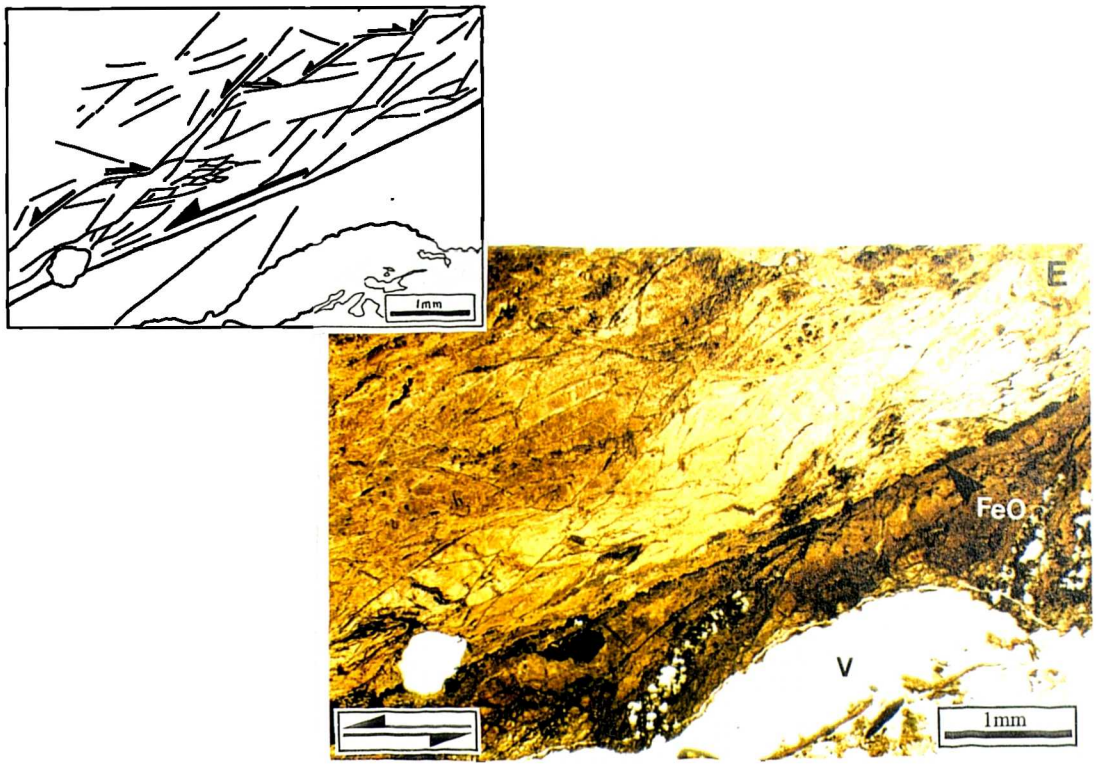

(b)

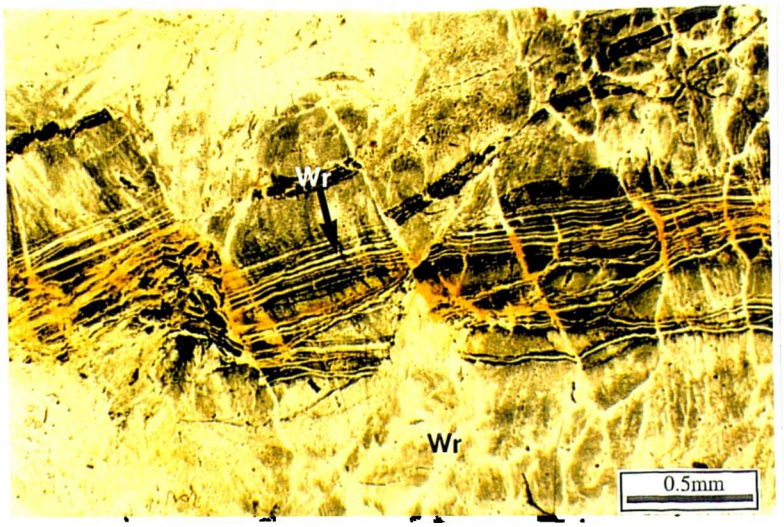

Figure 4.43. Features of brittle-ductile serpentinite fault rocks.
(a) Left-lateral, asymmetrical shear plane marked by 'strings' of Fe-oxide aggregates (FeO). Above the shear plane synthetic and antithetic shears accommodate bulk displacement (see line drawing). Note the presence of a vug (V) beneath the shear plane. (Sample AV/15/95).
(b) Inclusion trails of colourless wall rock (Wr), which parallel the vein-wall contact, located within a tensile chrysotile vein. The black material in the vein is dominantly chrysotile; this black colouration in the core and grey, 'cloudy' appearance of the material immediately adjacent is due to alteration, presumably indicating a concentration of Fe-oxide. Note the presence of later brittle, conjugate shears that offset the vein. (Sample NK/11/95).

Serpentine-carbonate fault rocks

Many tectonic contacts and shear zones are characterised by carbonate mineralisation. The displacement of carbonate veins and their occurrence along shear planes, suggest that flux of carbonate-rich fluid may have been intimately associated with the deformation of the transpressional fault rocks. The significance of this mineralisation is discussed in detail in Chapter 6.

One particular type of serpentine-carbonate fault rock characterises Troodos Complex-serpentinite contacts and it is also the dominant constituent of pervasively deformed sections of the main two serpentinite belts. At outcrop, this rock can be identified by its light-blue to grey colouration, fine grain-sizes and an intense, penetrative foliation. In hand specimen, the bulk of the fabric typically comprises incohesive, foliated gouge. Sampling of these rocks is troublesome as they are extremely friable, but fortunately, foliated, cataclasite fabrics are preserved in lower strain lenses that are more cohesive. Both rocks exhibit cross-cutting, brittle to brittle-ductile shear planes that bound lower strain, mm- to cm-scale phacoids that display foliated or random gouge and cataclasite fabrics. Shear planes and foliations are commonly marked by mm-scale carbonate veinlets, suggesting that permeability was highest along these anisotropies. Locally these veins display holes or 'vugs', which indicate pore fluid pressures were high during their development. In thin section, the curvature of the serpentinite fabric into the shear planes indicates an invariable sinistral strike-slip sense of shear (Figure 4.44). However, the presence of the tensile carbonate veinlets along these shear planes are not predicted consequences of shear fracture. This incompatibility may be explained if the carbonate veins formed subsequent to sinistral shearing. This idea is supported by the observation that veins occasionally cross-cut the gouge and cataclasite shear fabrics in the phacoids (Figure 4.44b). On the other hand, the presence of fragments of carbonate veins in some samples suggests that deformation and fluid flux may have been broadly contemporaneous. A more complete discussion is presented in Chapter 6.

The shear fractures observed in these gouge and cataclasite fault rocks are oriented approximately 15° anticlockwise from the foliation. They typically bifurcate and link up with foliation planes, forming an anastomosing network (Figure 4.44). The zones between shear planes, referred to as 'microlithons', comprise small, rounded serpentinite clasts supported in a fine-grained, fibrous serpentine matrix (Figure 4.44b). These microlithons possess a discrete foliation defined by the shape and lattice preferred orientations of fibrous serpentine and by the alignment of clasts, which display undulose extinction (Figures 4.44a and b). This minor foliation is oriented between 25-35°, commonly 30°, clockwise of the main E-W foliation (Figure 4.44c). The fibres within the serpentine matrix exhibit irregular grain boundaries and

microstructural evidence of recrystallisation, particularly with increasing proximity to shear planes, where the fibres rotate into parallelism with the shear direction.

(a)

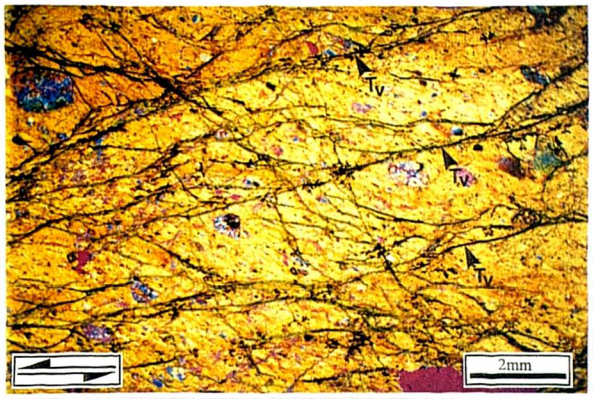

(b)

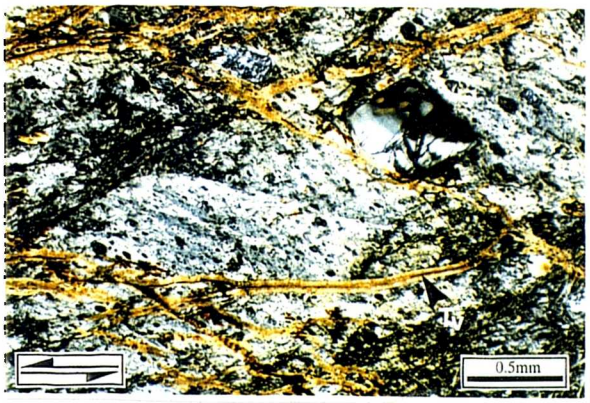

(c)

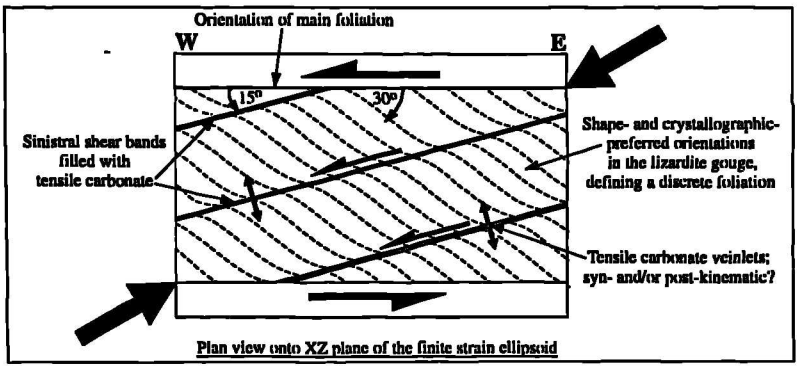

Figure 4.44 Photomicrographs of a characteristic serpentine-carbonate fault rock.
(a) Cross polars and sensitive plate addition, showing the lattice preferred orientation of fibrous serpentine (orange), which defines foliation, within the microlithons. Note the dominant sinistral shear planes defined by tensile carbonate veins (Tv). (Sample BOB/6/94).
(b) Detail of a microlithon displaying the alignment of fibrous serpentine and rounded serpentine clasts. Note that veins do not always coincide with shear planes and occasionally cross-cut the serpentinite fabric (Tv; black arrowhead), therefore at least some of these veins post-date sinistral shear.
(c) Schematic diagram showing the geometrical relationships between foliation (E-W), shear bands and microlithon foliation, with respect to the imposed sinistral shear sense. Note that the angle between shear fractures and the main foliation is half that between the microlithon foliation and the main foliation.

As stated above, the most significant feature of these rocks is the lack of antithetic shear structures, which are normally observed within other fault rocks. The geometrical arrangement of the main E-W foliation, the shear fractures, and the discrete foliation within microlithons is consistent with bulk sinistral strike-slip (Figure 4.44c). The dominance of this rock type within the main serpentinite fault zones, suggest that the bulk shear sense along these faults is sinistral.

Some fault rocks, frequently observed along high strain zones within and bordering serpentinite bodies, are dominated by carbonate, which may constitute over 80% of the rock volume. Within such rocks, carbonate, which typically comprises vein filling material, displays variable amounts of shear and tectonic disruption. However, the relative timing of veining and deformation in these rocks is not always evident. Figure 4.45 shows a characteristic example, in which veins curve into parallelism with the dominant E-W striking sub-vertical foliation. Three models are possible to explain the formation of these rocks: (1) sinistral shearing along foliation-parallel shears (*Y*-shears) took place subsequent to veining; (2) veining and deformation were contemporaneous, or; (3) the veins were not subjected to deformation at any part of their history. The first and second ideas are supported, whilst the third is discounted by microstructural evidence that suggests the foliation-parallel structures are *Y*-shears. Specifically, these shear surfaces are characterised by the presence of fine-grained, foliated serpentine fibres, which display strong shape and lattice-preferred orientations and textural evidence of dynamic recrystallisation (i.e. irregular grain boundaries and subgrain formation). This fabric contrasts the serpentinite in the relatively undeformed wall rock, which exhibits a randomly oriented fabric. Also, the intensity of Fe-oxide alteration observed along these foliation-parallel structures is normally associated with shear structures in other fault rocks. Furthermore, the intense grain-size reduction of carbonate into these *Y*-shears *may* reflect a corresponding increase in strain associated with shearing (Figure 4.45b). Note that the use of this last piece of evidence is contentious because a variation in grain-size is common in veins that form in the absence of deformation (*cf.* Ramsay and Huber, 1983). Whether veining and deformation are coeval or not is difficult to resolve, but the geometry of fabrics observed in these rocks suggests that sinistral shearing was important in their development.

4.4.1c. Discussion

The dominance of lizardite serpentine in the fault rocks that formed during sinistral transpression, suggest that deformation took place at low temperatures. Based on oxygen isotope analyses of lizardite grains sampled from the Troodos Massif and SW

Cyprus, the temperature during deformation is constrained to approximately 100°C (Margaritz and Taylor, 1974; also see Chapter 1). The fault rocks associated with this transpressional event display a range of brittle to ductile characteristics on all scales. These rocks, and the structures preserved within them, are considered to be broadly coeval as they are kinematically identical. The differences in the style of deformation that they exhibit are attributed to varying conditions (e.g. strain rate, differential stress magnitudes, pore-fluid pressures) and differing material properties. These effects are discussed further, with particular reference fault zone rheology, in Chapter 6.

(a)

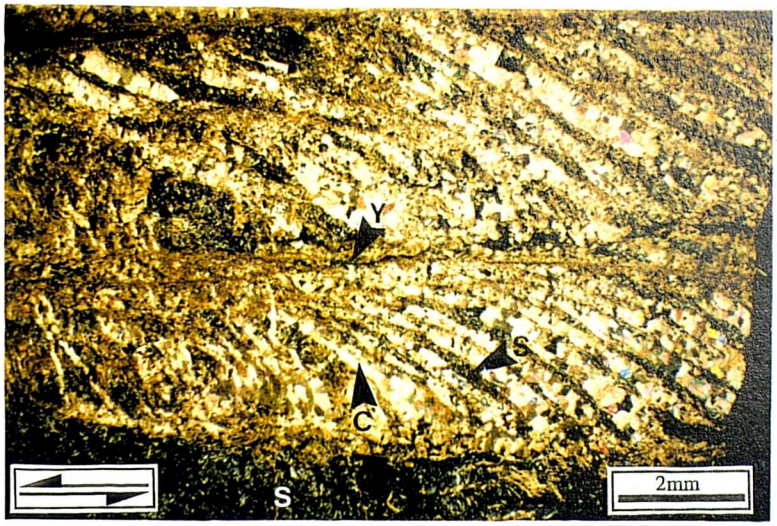

(b)

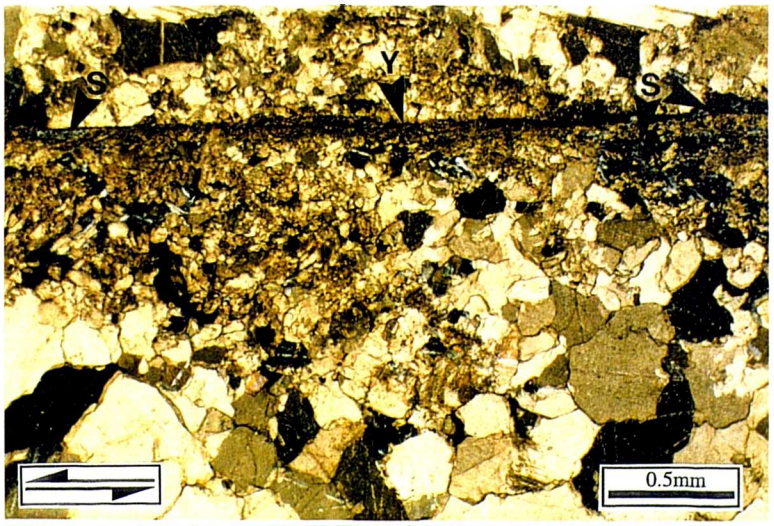

Figure 4.45. (a) Rotation (drag?) of carbonate veins (C) into foliation-parallel shear planes, or *Y*-shears (Y). Note the presence of low birefringent, serpentinite (S) 'slivers' in between carbonate vein fibres. (b) Detail of grain-size reduction into *Y*-shear plane. Note the presence of serpentinite (S) along the shear plane. The brown colouration along the shear plane is Fe-oxide (Sample NK/7/95).

The relative timing of carbonate fluid influx and deformation is difficult to resolve. Many of the fault rocks formed during the transpressional phase characteristically possess carbonate veins, which are typically concentrated along both brittle and ductile faults and foliation planes. The presence of carbonate and serpentine veins as clasts within some fault rocks suggests that at least part of this fluid flux was contemporaneous with deformation. Furthermore, considering that these rocks are pervasively serpentinised and that the degree of peridotite hydration can be directly correlated with the intensity of strain, fluids are thought to have played a significant role during deformation. This interplay between fluid and deformation is discussed in detail in Chapter 6. However, as a note of caution, microstructural observations suggest that much veining occurred after the transpressional event, which may lead to an over estimation in the extent of syn-kinematic fluid flux.

4.4.2. Macrostructure

The characteristics of the serpentinite-filled faults of the Southern Region have been described in the introduction to this section and in Chapter 3. In review, these fault zones display a variety of fault rocks, but typically they comprise blocks (<2m) of largely undeformed peridotite (generally harzburgite), bound by an anastomosing, interconnected network of totally serpentinised and sheared fault gouge and cataclasite. The structures observed within these regions are complex and are frequently difficult to interpret. However, within higher strain zones, strong fabrics and associated kinematic indicators are preserved. These high strain regions, which vary in size from mm-scale to tens of metres in width located at contacts and internally within the serpentinite belts, are readily distinguished by a preponderance of heavily foliated, serpentinite fault rocks. Phacoids within the gouge range in size from mm to tens of cms in scale and possess polished surfaces that display sub-horizontal to subordinate dip-slip brittle-striae and serpentine slickenfibres. High strain zones are also characterised by carbonate, and less common quartz, mineralisation along shear surfaces and by cm-wide tensional, contact-parallel serpentine veins that frequently extend along strike for tens of metres.

The following field examples are ordered in a traverse along the serpentinite filled faults, from east to west. They are among the most pervasively deformed sections that are exposed, which preserve structures that are thought to have formed during regional transpressional deformational. These structures record dominant *sinistral* and *compressional* displacements, which are interpreted to be coeval, and to have formed during bulk ***NNE-SSW*** to ***NE-SW*** directed shortening. The localities

discussed in this section are shown on a summary location map (Figure 4.39) and in a more detailed map (Map I).

4.4.2a. Mamonia

An exceptionally well preserved section (~1km long) of the northern serpentinite belt is located 1500m west of Mamonia village, between Koutsouroumbas (GR 647 483) and Kattopetra (GR 655 482) (Figures 4.39 and 4.46). The fault zone crops out as an approximately E-W trending, 25 to 70m-wide ridge that separates poorly exposed Dhiarizos Group rocks to the north from Troodos lavas to the south. The topographically highest parts of the ridge are typically the least serpentinised, comprising relatively undeformed harzburgite with minor clinopyroxenite and mafic intrusives. In contrast, the most pervasively deformed and serpentinised parts, which display a characteristic light-blue colouration, are topographically subdued.

The most significant feature displayed by this section of the fault zone is its distinct, NW-SE kink in strike at GR 653 482. This 'kink', which connects an E-W striking portion of the fault zone to the east with an approximately WNW-ESE portion to the west, is readily identified in the field as it the most thoroughly serpentinised part of the fault zone. Regardless of the local strike of the fault zone, where preserved, contacts are invariably sub-vertical and display shallowly-plunging, strike-parallel brittle striae and mineral fibres (carbonate and serpentine). All sections of the fault zone display sub-vertical foliations and two dominant orientations of brittle to brittle-ductile strike-slip structures; NE striking *sinistral* faults and SE striking *dextral* faults.

This fault zone also preserves evidence of the tectonic incorporation of country rock during strike-slip displacements. Along the northern contact of the serpentinite belt in particular, fault-bounded, metre-scale Phasoula lava blocks, which possess long axes that parallel the strike of the fault zone, crop out within the serpentinite, metres away from the contact with the Dhiarizos Group (Figure 4.47). These blocks are commonly cut and offset by both sinistral and dextral brittle faults, a feature that is also commonly observed in blocks of partially serpentinised peridotite.

Due its excellent exposure, this part of the fault zone was selected for detailed kinematic analysis. As the distribution of strain along the fault belt is distinctly heterogeneous, the most highly strained zones were analysed (see below). Populations of brittle to brittle-ductile faults, possessing mm- to m-scale offsets, were measured at separate localities where exposure was 100% (Figure 4.46 and 4.48). Structural measurements were preferentially taken from shear zones, comprising fine-grained serpentinite fault rocks, which were located away from perturbations associated with rigid peridotite blocks (see below). From field observations and stereonet data obtained, the following conclusions may be drawn:-

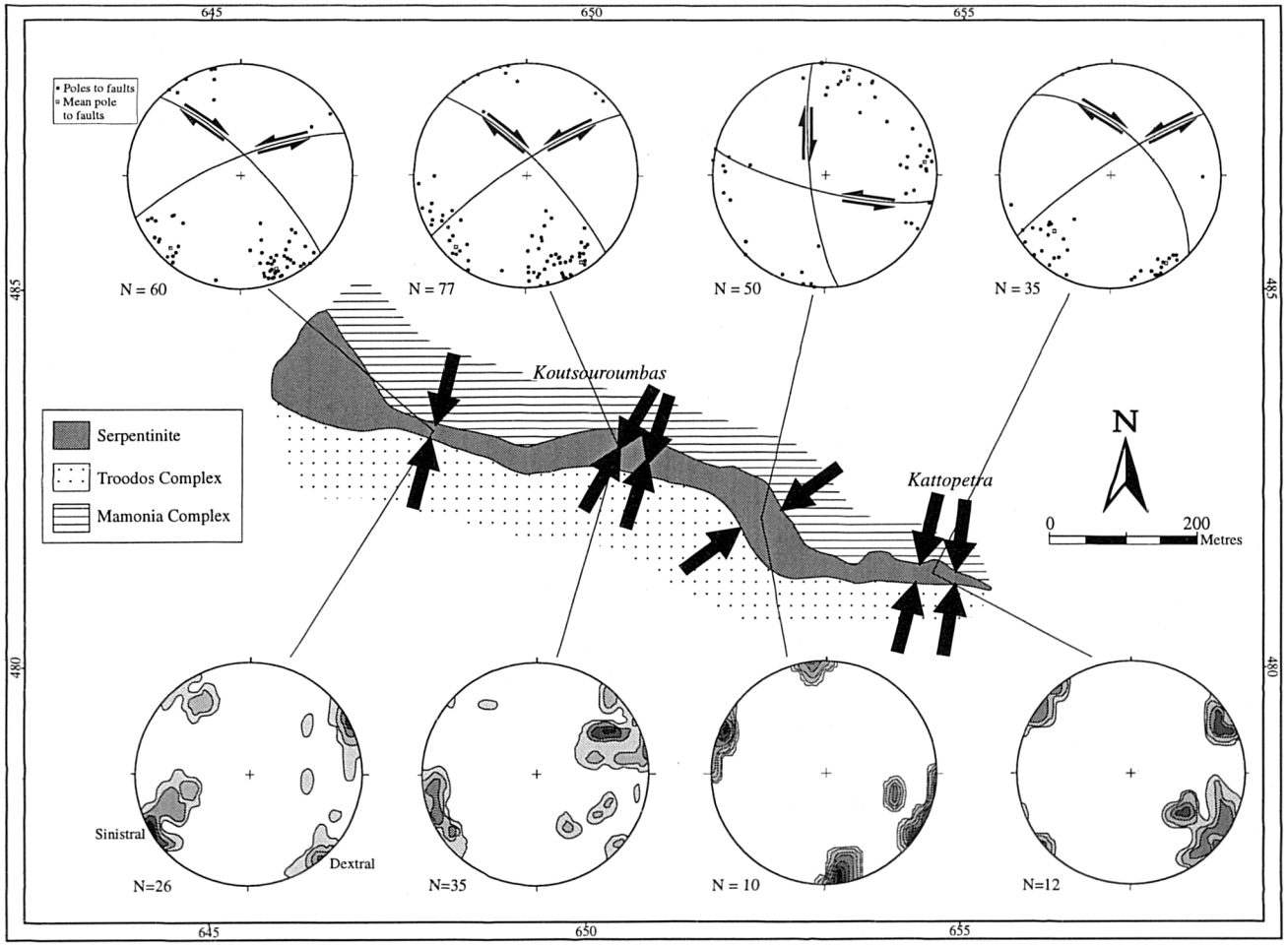

Figure 4.46. Map and data of the Mamonia fault zone. Stereonets at the top show the average orientations of conjugate strike-slip faults and shear zones. The lower stereonets display 1% area contours of strike-slip slickenlines and fibres measured on the conjugate shear planes. The black arrows show the orientations of the local maximum principal shortening directions, which are inferred to parallel the bisector of the obtuse angle of the conjugate shear pairs (see Figures 4.48 and 4.49).

- both sinistral and dextral kinematic indicators display mutually cross-cutting relationships and are therefore considered coeval and conjugate;
- sinistral kinematic indicators dominate over dextral by up to 50% (see Figure 4.48) and thus, dextral faults are considered antithetic to the dominant sense of sinistral shear;
- the direction of maximum principal shortening for each location is assumed to be coincident with the obtuse bisector of the conjugate fault sets (see explanation in Figure 4.49). At most locations the bisector of the *obtuse* angle is sub-horizontal and near orthogonal to the local fault zone boundaries, even where the strike of the fault zone swings (black arrows; Figure 4.46);
- the lack of evidence for dip-slip displacements suggests that the regional minimum principal shortening direction parallels the acute bisector of the conjugate fault sets, is sub-horizontal and near strike-parallel.

Figure 4.47. Plan view onto a Phasoula lava fault block located within the northern serpentinite belt, approximately 5-10 metres away from the contact with the Dhiarizos Group to the north. Note that the block is offset and bound by conjugate sinistral and dextral strike-slip faults, which produce symmetrical 'diamond-shaped' geometries.

Three-dimensional interpretation

Figure 4.48 displays the mean orientations of the conjugate shear planes measured in the E-W striking sections of the fault zone that are shown in Figure 4.46. From these mean planes the approximate three-dimensional orientation of the finite strain ellipsoid can be determined. The results indicate that the minimum and maximum axes of the ellipsoid are sub-horizontal and plunge towards the SSW (10/190) and WNW (6/282), respectively. Bearing in mind the serpentinite belt typically strikes 090°-270° to 108°-288° and dips sub-vertically, these orientations are approximately perpendicular and parallel to the strike of the host fault zone. Therefore, the conjugate strike-slip faults

document fault-normal shortening and strike-parallel extension (Figure 4.50). Furthermore, as sinistral faults are twice as abundant as dextral, the bulk sense of displacement along the fault zone is left lateral.

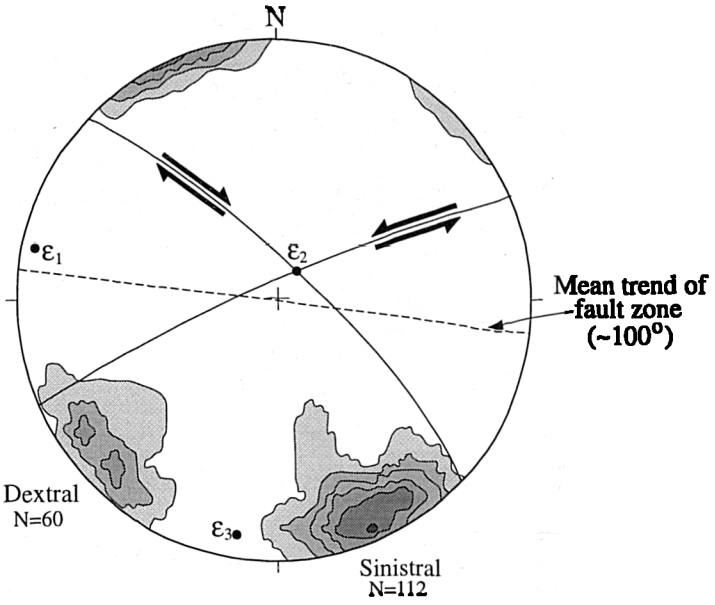

Figure 4.48. Summary stereographic projection showing a 1% area contour of the poles to sinistral and dextral strike-slip faults presented in Figure 4.46. The data shown is from E-W trending portions of the fault zone only. Note that the maximum and minimum principal shortening directions are sub-horizontal and oriented approximately NNE-SSW and ESE-WNW, respectively.

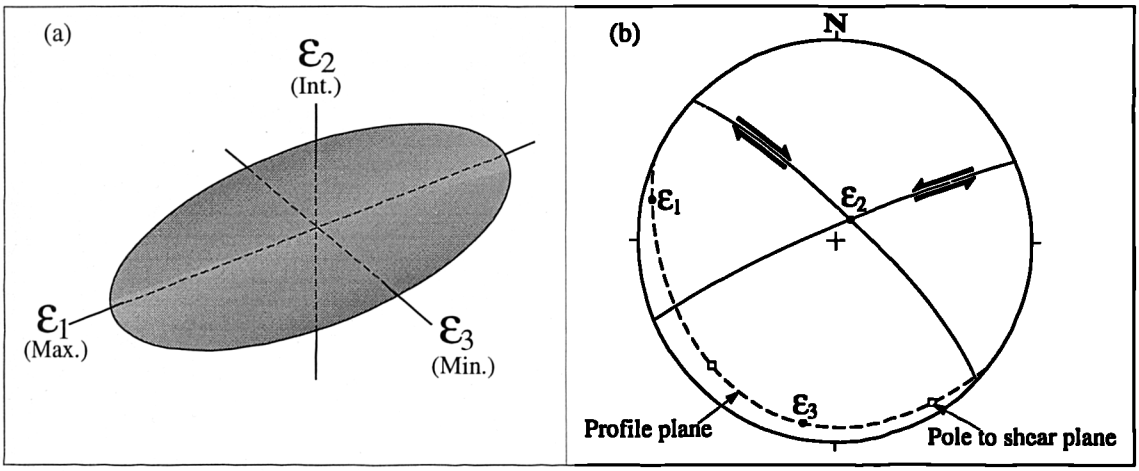

Figure 4.49. Method adopted in this thesis for determining the orientations of the maximum, intermediate and minimum principal axes of the finite strain ellipse (a) (ε_1, ε_2, and ε_3, respectively, after Hobbs *et al.* 1976). (b) The mean conjugate shear planes are plotted as great circles on a stereonet. The profile plane to these structures is constructed by drawing a great circle through the poles to the shear planes. Due to the relative displacement directions on these shear planes, the bisector of the obtuse angle is inferred to parallel the minimum axis of the finite strain ellipsoid (i.e. the maximum shortening direction), whilst the maximum axis (i.e. the maximum elongation) parallels the acute bisector.

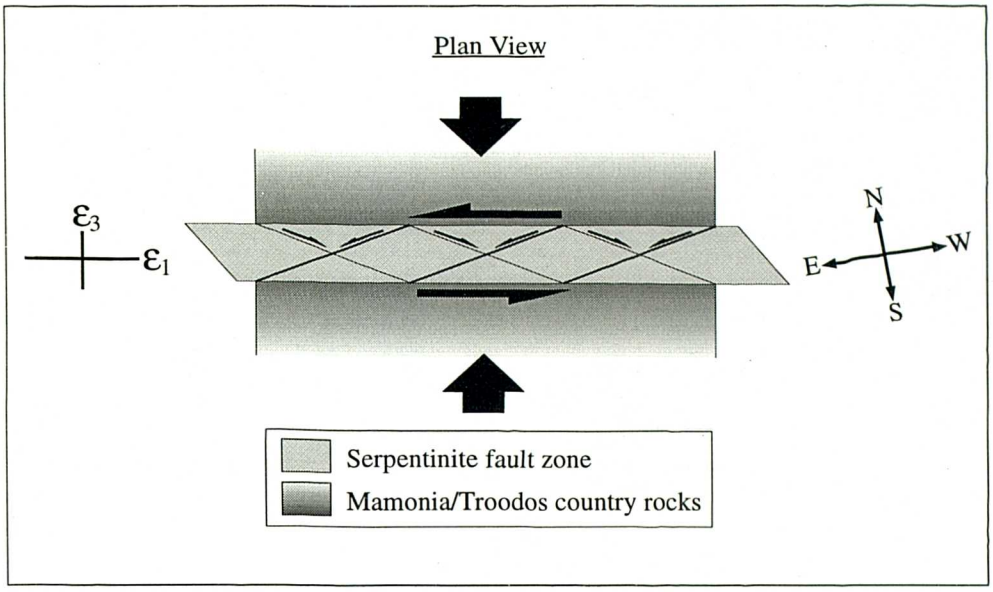

Figure 4.50. Schematic, plan view interpretation of the deformation along the Karaopetra to Koutsouroumbas fault zone. NNE-SSW directed shortening (black arrows) is accommodated by strike-parallel extension along conjugate strike-slip faults. A dominant sinistral sense of shear is inferred by the dominance of sinistral structures over dextral.

The above kinematic analyses were undertaken in the higher strain regions of the serpentinite belt because the orientations of structures are relatively consistent. Within regions of lower strain, the structural patterns produced are infinitely more complex due to the presence of material anisotropies, such as partially serpentinised peridotite blocks. The deflection of the serpentinite foliation and shear fabric around these relatively rigid blocks, suggests that there is a significant competency contrast between the macroscopically ductile serpentinite and the partially hydrated ultramafic blocks. Figure 4.36b, shows the variability in the orientation of planar structures within a weakly deformed fault zone. This data set was taken from a comparable location to the Koutsouroumbas to Kattopetra section along the northern serpentinite belt at GR 578 479. This lower strain portion of the serpentinite belt is characterised by cm- to 10m-scale blocks of variably serpentinised peridotite blocks, which are cross-cut by a brittle joints and fractures and by E-W trending serpentinite shear zones (<1m in width). As shown in Figure 4.36(b) and (c), the orientation of these structures and the relative displacements that they record is highly variable. However, note that strike-slip structures are dominant in this data set, and that sinistral faults are more abundant than dextral. This suggests that these structures may have formed during the same deformational event that produced the structural pattern observed along the fault zone between Koutsouroumbas and Kattopetra. Therefore, by removing the randomly oriented fractures, which are thought to have accommodated complex translations and rotations at block margins, a clearer kinematic interpretation of the data is possible.

Figure 4.51 shows the same data set as that used in Figure 4.36(b), except only strike-slip structures are plotted. The similarity between the orientation of sinistral and dextral faults (i.e. NE and NW striking, respectively, and steeply to sub-vertically dipping) in Figures 4.48 and 4.51 suggests that the manipulation of data in this manner is reasonable and that the strike-slip structures observed within contrasting high and low strain regions of the fault zone are contemporaneous. This is supported by the similarity in the orientation of the maximum and minimum shortening directions, i.e. approximately N-S and E-W respectively. The slight differences in the orientation of the finite strain axes may reflect the complex accommodation of deformation at a local scale within the lower strain regions.

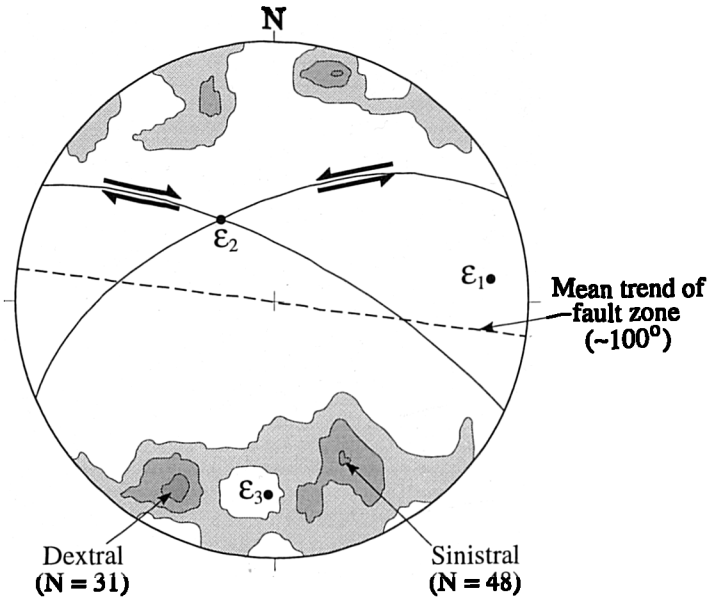

Figure 4.51. 1% area contour of poles to sinistral and dextral faults taken from a relatively undeformed section of the northern serpentinite belt at GR 578 479. This data is the same as that presented in Figure 4.36b, except all fractures that do not display strike-slip displacements have been omitted.

4.4.2b. Nea Kholetria

Nea Kholetria village

Contact relationships between serpentinite and the Dhiarizos group are excellently exposed along a 100m long road section situated within the middle of Nea Kholetria village (GR 635 470; Figure 4.39). The outcrops preserved in the road cutting show the three-dimensional geometry of tectonically intercalated slivers of serpentinite and Mamonia Complex material. Two narrow (maximum of ~30m width), approximately ESE trending, sub-vertical, serpentinite-filled faults are exposed that are separated and

bound to the north and south by intensely foliated, red Dhiarizos Group sediments (Figures 4.52 and 4.53). Isolated exposures of serpentinite, Phasoula lava and Dhiarizos sediments also crop out to the east and west of the road. Unfortunately, due to vegetation and a lack of exposure, the geometrical relationships between these units is difficult to constrain. However, the E-W linearity exhibited by serpentinite outcrops suggest that they interconnect and anastomose, bounding lenses of Dhiarizos Group material.

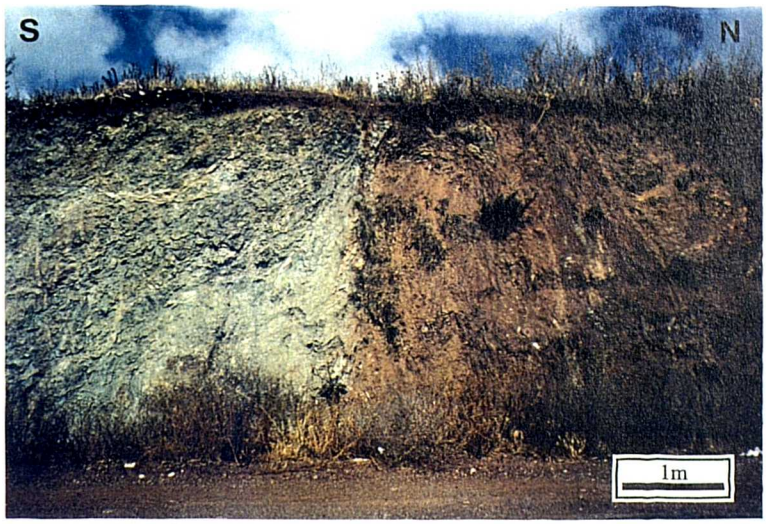

Figure 4.52. Sub-vertical contact between Dhiarizos Group sediments (red-brown) and serpentinite (light-blue) exposed on the road section through Nea Kholetria village.

The contacts exposed along the road cutting are generally sub-vertical and strike E-W to NW-SE (Figures 4.52 and 4.53). The predominance of shallowly-plunging carbonate fibres on the contacts associated with cm-scale asymmetrical shear bands in light-blue coloured serpentinite gouge indicate sinistral strike-slip. The Dhiarizos Group sediments, situated within the northernmost exposures display metre-scale folds with sub-horizontal, ESE plunging fold axes and mostly sub-vertical, ESE striking axial planes. The orientation of these folds suggests NNE-SSW shortening. The approximate parallelism between fold axes and fault strike, combined with the inference that sinistral strike-slip along E-W trending faults may have been synchronous with NNE oriented shortening associated with folding, may be used as evidence for the local partitioning of transpressional strain (*cf.* Tikoff and Teyssier, 1994; Teyssier *et al.* 1995) (Figure 4.53b).

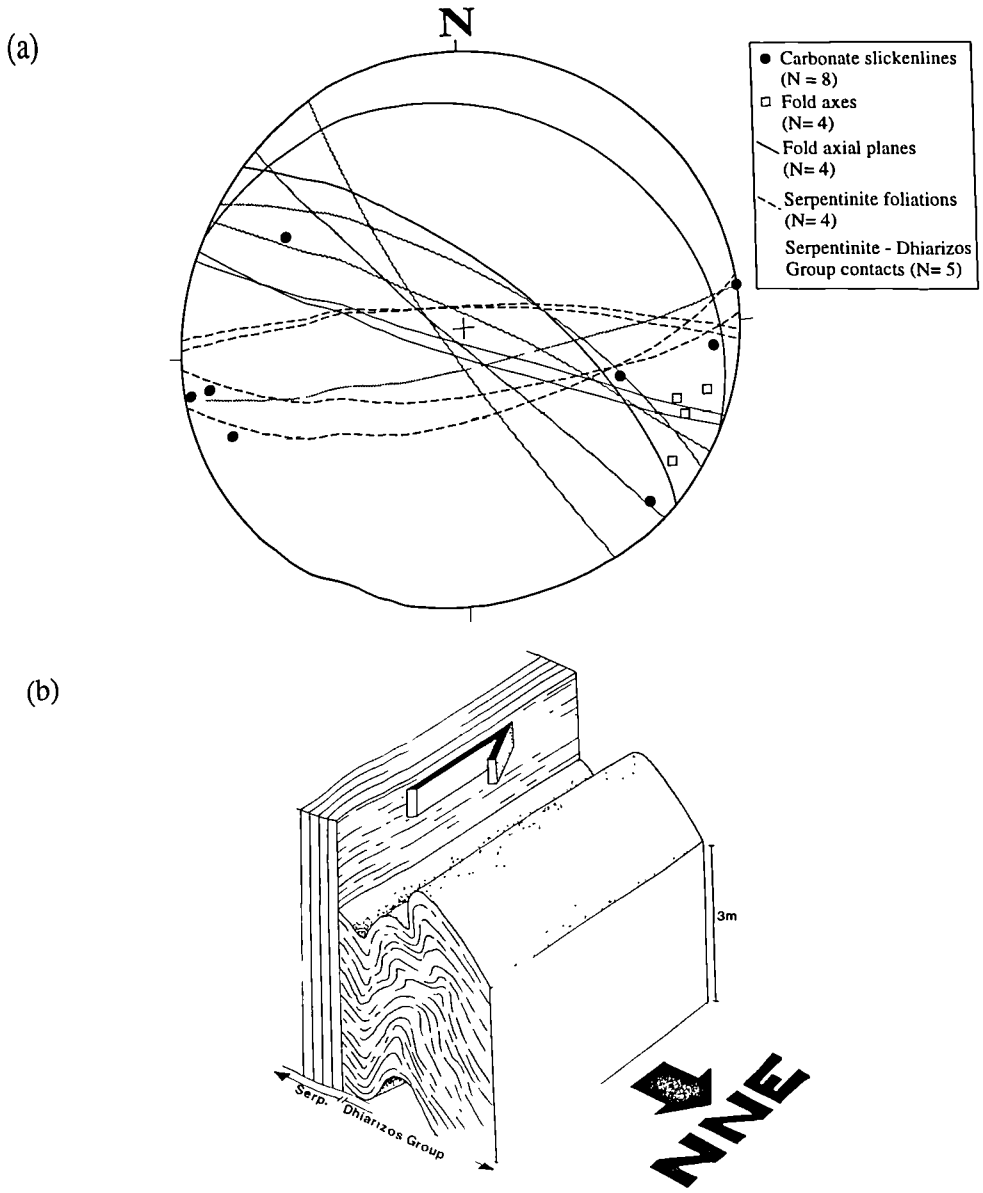

Figure 4.53. Data and interpretation of the structures exposed on the road section through Nea Kholetria village. (a) Stereographic projection of data. (b) Schematic three-dimensional interpretation. Note the approximate parallelism in strike between fold axial planes and Dhiarizos Group-serpentinite faulted contacts.

Kryon Neron (GR 632 483)

Structures associated with tectonic contacts and internal high strain zones are exposed within the serpentinite body that crops out at Kryon Neron (Figure 4.54; Figure 4.39). This unit of serpentinite trends ESE-WNW and appears to be isolated, being bound on all sides by the Dhiarizos Group. The northern contact with Dhiarizos Group units possesses moderate to steep dips and displays a kink in strike. The contact zone is heavily brecciated and marked by a metre-wide zone of cataclasite fault rock that contains variable proportions of serpentinite, Dhiarizos lava and sediment, Ayia Varvara Formation amphibolite, and exotic peridotite mylonite clasts. Brittle shears,

combined with dip- to oblique-slip slickenlines within this zone, indicate top-to-the-NE thrust displacement, placing serpentinite over the Dhiarizos Group (Stereonet (a); Figure 4.54). A thin (<5m-wide) slice of Ayia Varvara Formation, that crops out along the contact, is interpreted as a tectonic fragment incorporated along the thrust plane. Note that although this contact trends E-W, the dominant brittle foliation in the brecciated fault rocks strikes NW-SE and dips to the SW. Along a short (~10m) section of the contact, which corresponds approximately to the swing in strike, the dominant brittle foliation steepens and strikes ENE (Stereonet (b); Figure 4.54). Kinematic indicators and slickenlines within this zone record sinistral strike-slip. Immediately to the west, the contact trends NW-SE and, as to the east, displays evidence of top-to-the-NE thrust displacement. The geometrical relationships between these three sections of the contact may be explained by one of two models. One possibility is that the minor sinistral strike-slip part of the contact is a later structure that offsets the two thrusted sections (Inset (i); Figure 4.54). However, the structural continuity between these three sections and the similarity in the style of deformation suggests that they formed during the same event. Another possibility is that an irregular fault zone architecture was inherited from a previous event (i.e. dextral transtension and protrusion). In such a structural setting, bulk NE-directed shortening is expected to reactivate contacts that possess moderate southwesterly dips as thrusts, whilst (minor) sub-vertical, ENE striking sections accommodate the deformation by sinistral strike-slip (Inset (ii); Figure 4.54). In this latter model, the minor sinistral strike-slip section represents a lateral fault, which formed in response to northeasterly-directed compression.

Metre-scale shear zones are occasionally exposed internally within the serpentinite body. These high strain zones are characterised by intense carbonate mineralisation, steep to sub-vertical dips and approximately E-W strikes. One such zone is exposed within the eastern end of the serpentinite body, which displays dominant sinistral strike-slip kinematic indicators (Stereonet (c); Figure 4.54). Due to the pervasive alteration by carbonate-rich fluids these rocks exhibit a distinguishing dark-red colouration, which presumably indicates the presence of oxidised iron. A carbonate-rich fault rock sampled from this locality has been described in section 4.4.1b (Figure 4.45). As stated in the previous discussion, the relative timing of fluid flux and sinistral strike-slip is difficult to constrain, but deformation is tentatively assumed to have occurred during and/or after veining.

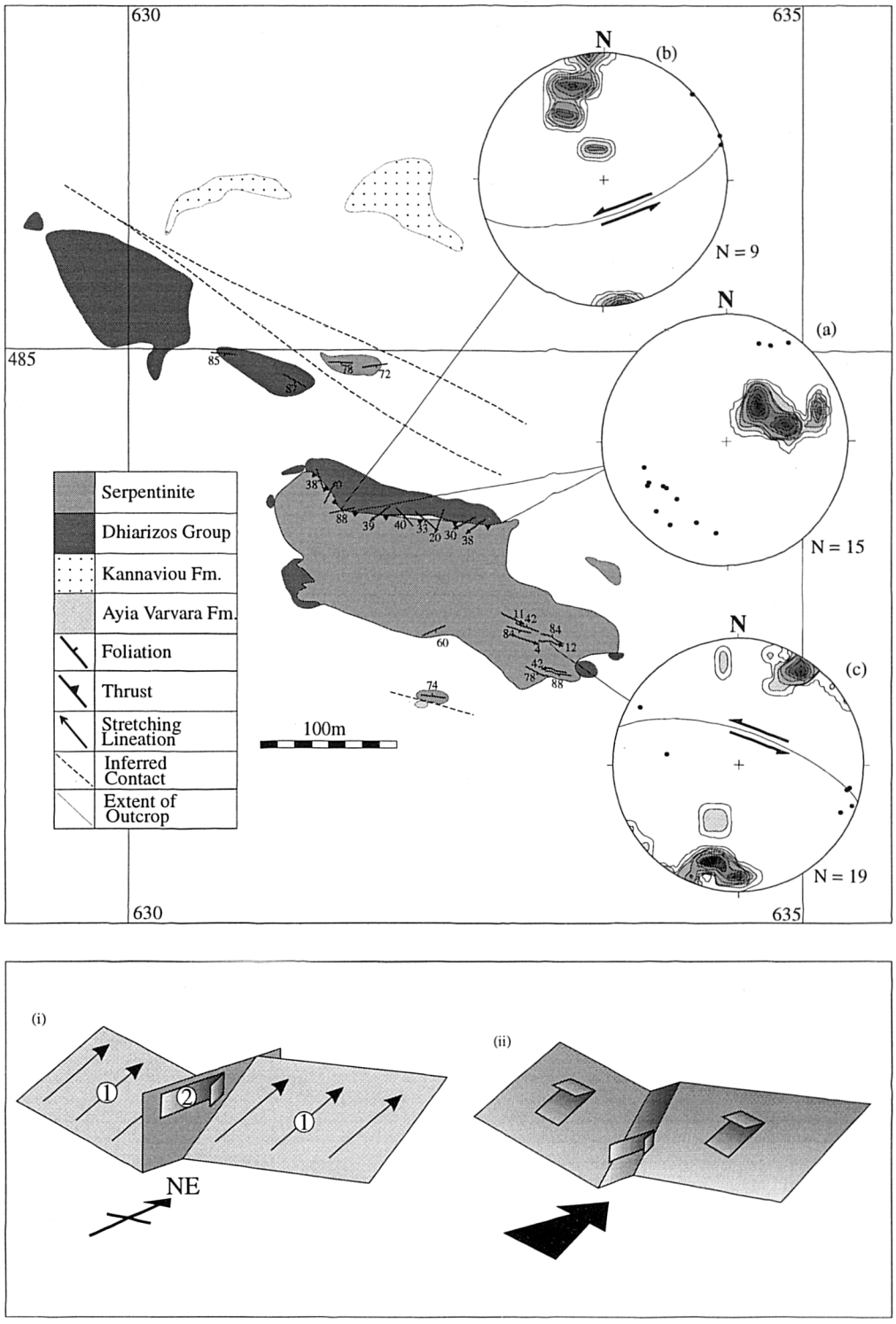

Figure 4.54. Serpentinite body exposed at Kryon Neron. Stereonet (a) displays 1% area contour of poles to thrust planes. Black dots show top-to-the-NE slickenline lineations. Stereonet (b) shows a 1% area contour of poles to sinistral foliation planes, the average orientation of foliations (great circle), and strike-slip slickenline lineations (black dots). Stereonet (c) contains a 1% area contour of poles to sinistral foliation planes, the average orientation of foliation (great circle), and carbonate fibre lineations (black dots). Insets (i) and (ii) display the two three-dimensional structural models discussed in the text.

The dominance of sinistral kinematic indicators in these discrete, E-W trending shear zones and along localised parts of the northern contact, suggest that the two deformations may be related. The assumption that northeasterly-directed thrusting and sinistral strike-slip are contemporaneous infers a sinistral transpressional model. The orientations of the thrusted contacts and strike-slip structures are broadly compatible with sub-horizontal, NE-SW oriented compression in this area.

***Vatomandra* (GR 623 465; Figure 4.39)**

The isolated serpentinite body SE of Vatomandra is located entirely within Phasoula Formation lavas and possesses a highly irregular geometry (Figure4.55a). It is approximately 160m long and oriented E-W. Contact relationships, such as stoping of lava blocks >1m in diameter, clearly indicate that serpentinite has protruded into the Dhiarizos country rock (Figure 4.55b).

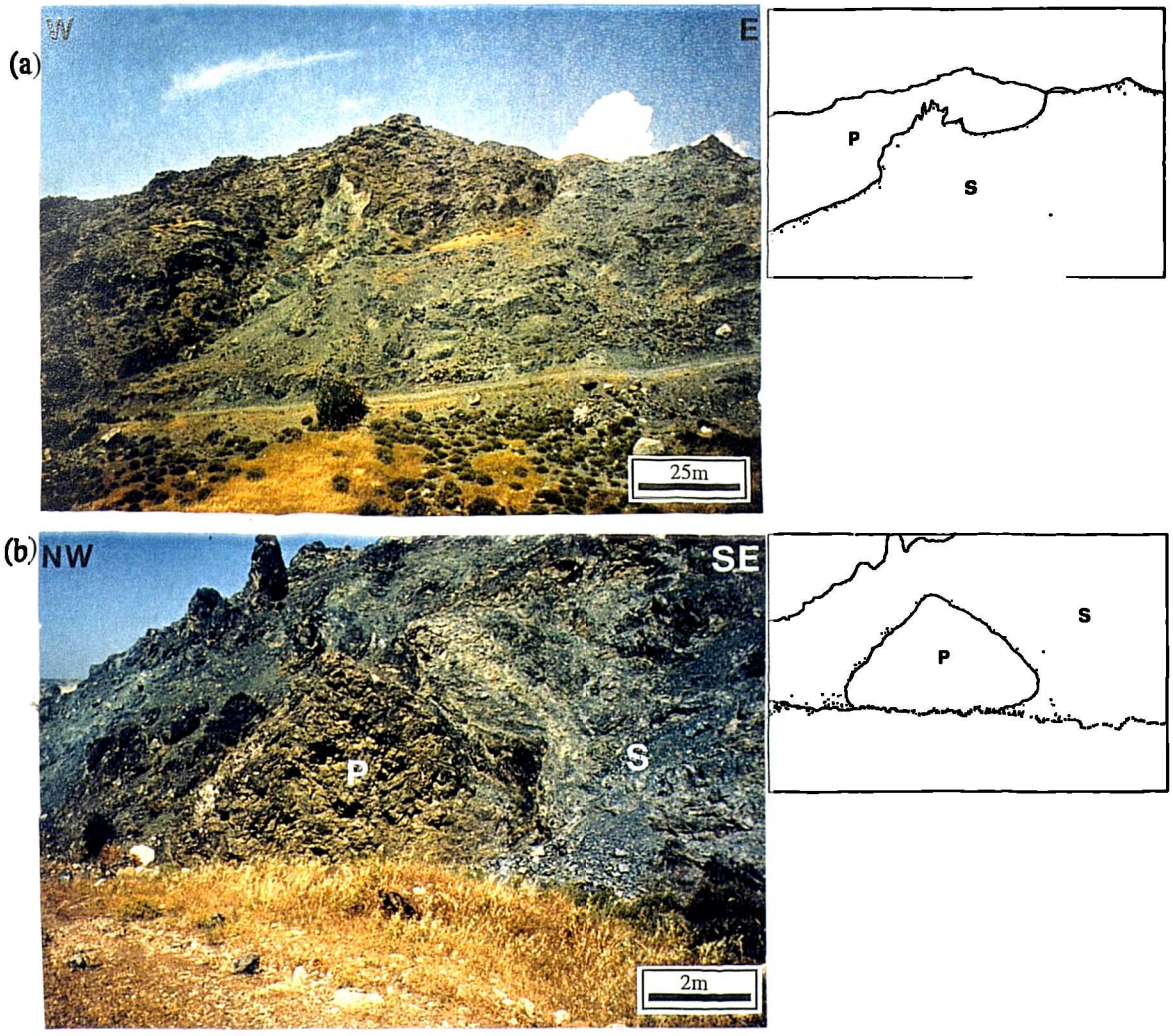

Figure 4.55. Features of the Vatomadra serpentinite body, which are suggestive of its protrusive emplacement. (a) View onto the highly irregular northern contact between serpentinite (S; blue) and Phasoula lavas (P; dark). (b) Phasoula lava block entrained within serpentinite.

Whether the protrusive emplacement of the serpentinite body at Vatomandra took place during the earlier dextral event is uncertain due to disruption during sinistral deformation. The irregularity of the northern contact is due to centimetre to metre-scale offsets along NE-SW striking sinistral, NW-SE striking dextral, and minor N-S striking extensional brittle to brittle-ductile faults (Figure 4.56a and b). Sinistral faults are slightly more abundant than dextral (5:3), but both sets are mutually cross-cutting and are therefore coeval. The obtuse bisector of the conjugate (sinistral and dextral) shear planes is inferred to represent the maximum principal shortening direction. This is supported by the near coincidence between the orientation of the obtuse bisector with the N-S strike of extensional faults (Figure 4.56c). Thus, the maximum (ε_1) and minimum (ε_3) principal axes of the finite strain ellipse in this area are inferred to be sub-horizontal and oriented 102°-282° and 012°-192°, respectively, whilst the intermediate axis is sub-vertical (Figure 4.56c). Considering the E-W trend of the fault zone, the maximum shortening direction (012°) is slightly clockwise of fault-normal (i.e. north). This, combined with the dominance of sinistral faults over dextral, is consistent with deformation during high-angle sinistral shortening (i.e. a sinistral transpression).

4.4.2c. Ayia Varvara

A number of tectonic contacts are preserved in the Ayia Varvara area (Figure 4.39), which display structures that document synchronous sinistral strike-slip and thrust displacements, suggesting that they formed during sinistral transpression. These faulted contacts, which juxtapose serpentinite against the Mamonia and Troodos Complexes, are interpreted to have formed during regional N-S to NE-SW compression. Figure 4.57 shows the geology of the area and relative positions of localities discussed in the following text. This figure also shows the locations of Kara tou Ayiou Pati and Arkolieri, which were described in section 4.3.

***Plevra tou Petrovounou* (GR 580 478)**

At Plevra tou Petrovounou (GR 578 478; Figure 4.39), the contact between the northern serpentinite belt and the Troodos Complex is exposed on the road side (Figure 4.58a). Blue serpentinite overlies Troodos lavas along a low angle tectonic contact that dips to the NE. Lineations (carbonate fibres and brittle striae) and shear sense criteria on the contact, and on subordinate shear surfaces, indicate oblique thrusting to the south, placing serpentinite over Troodos lavas. Reverse-slip along this contact is confirmed by the rotation of a sub-vertical, deformed Troodos mafic dyke.

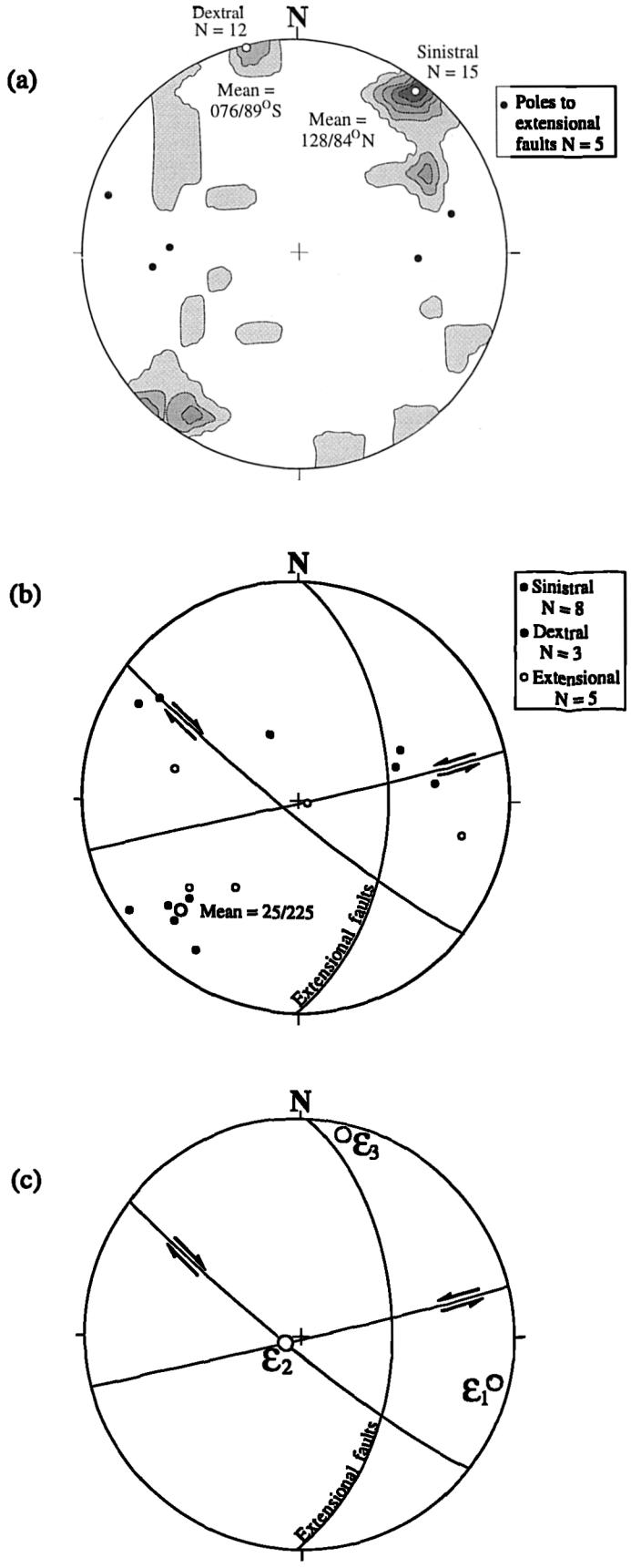

Figure 4.56. Data from the northern contact of the Vatomandra serpentinite body. (a) 1% area contours of poles to sinistral and dextral faults. Black dots represent poles to extensional faults. (b) Slickenline lineations (carbonate and serpentine fibres and brittle striae) and mean orientations of faults shown in (a). (c) Principal finite strain axes measured in the profile plane to the strike-slip conjugate shear pair.

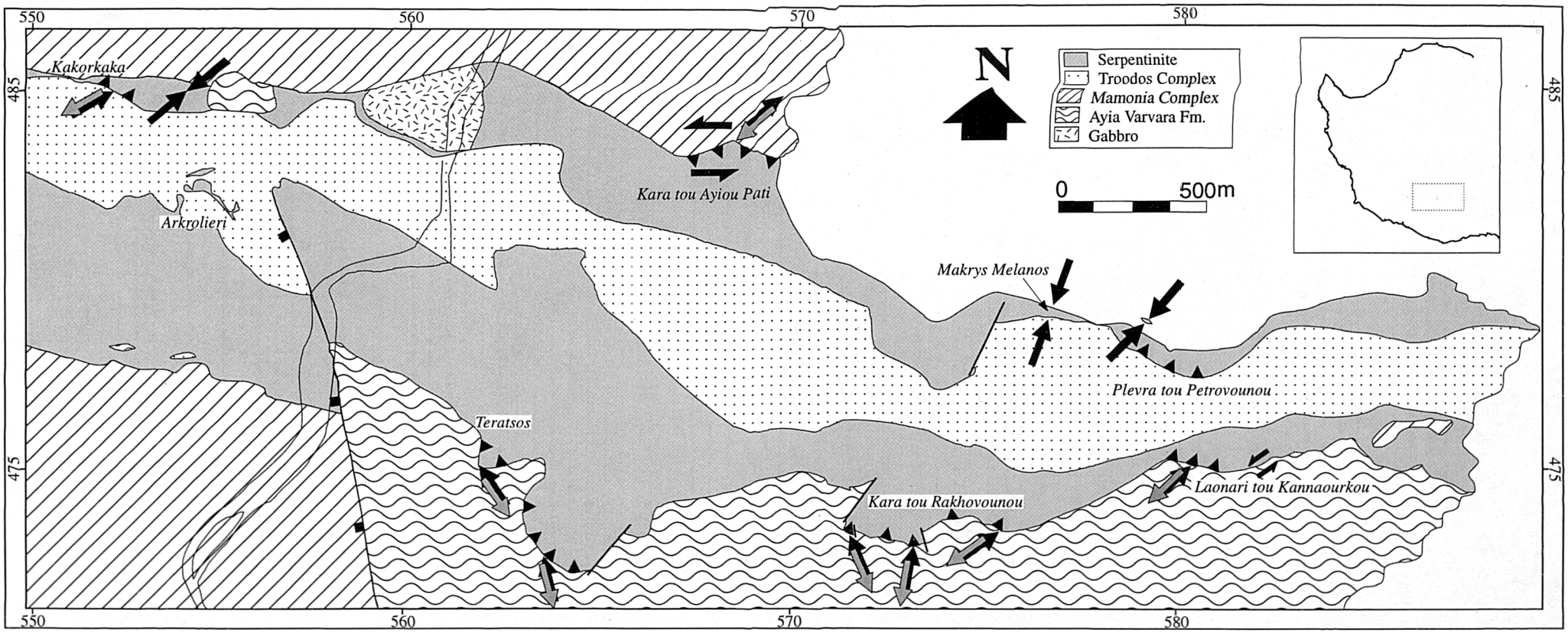

Figure 4.57. Geological map of the Ayia Varvara area showing the localities discussed in the text. Black arrows show the orientation of the maximum principal shortening directions and grey/black arrows indicate the direction of thrust displacement (see below).

The predominance of compressional deformation along this section is further supported by a back thrust which offsets the contact (Figure 4.58a). On a decimetre scale, the contact locally displays highly irregular geometries due to serpentinite cutting down into the Troodos footwall (Figure 4.58b). This relationship may be attributed to Riedel shears that cut down from the thrust plane into the Troodos lavas, or, more favourably, the thrust reactivated a previously irregular, protrusive contact. In this latter hypothesis, the contact with the lavas initially formed during the protrusion of serpentinite (i.e. during dextral transtension). The contact is envisaged to have dipped shallowly to the NE and was subsequently reactivated during sinistral transpression as a thrust.

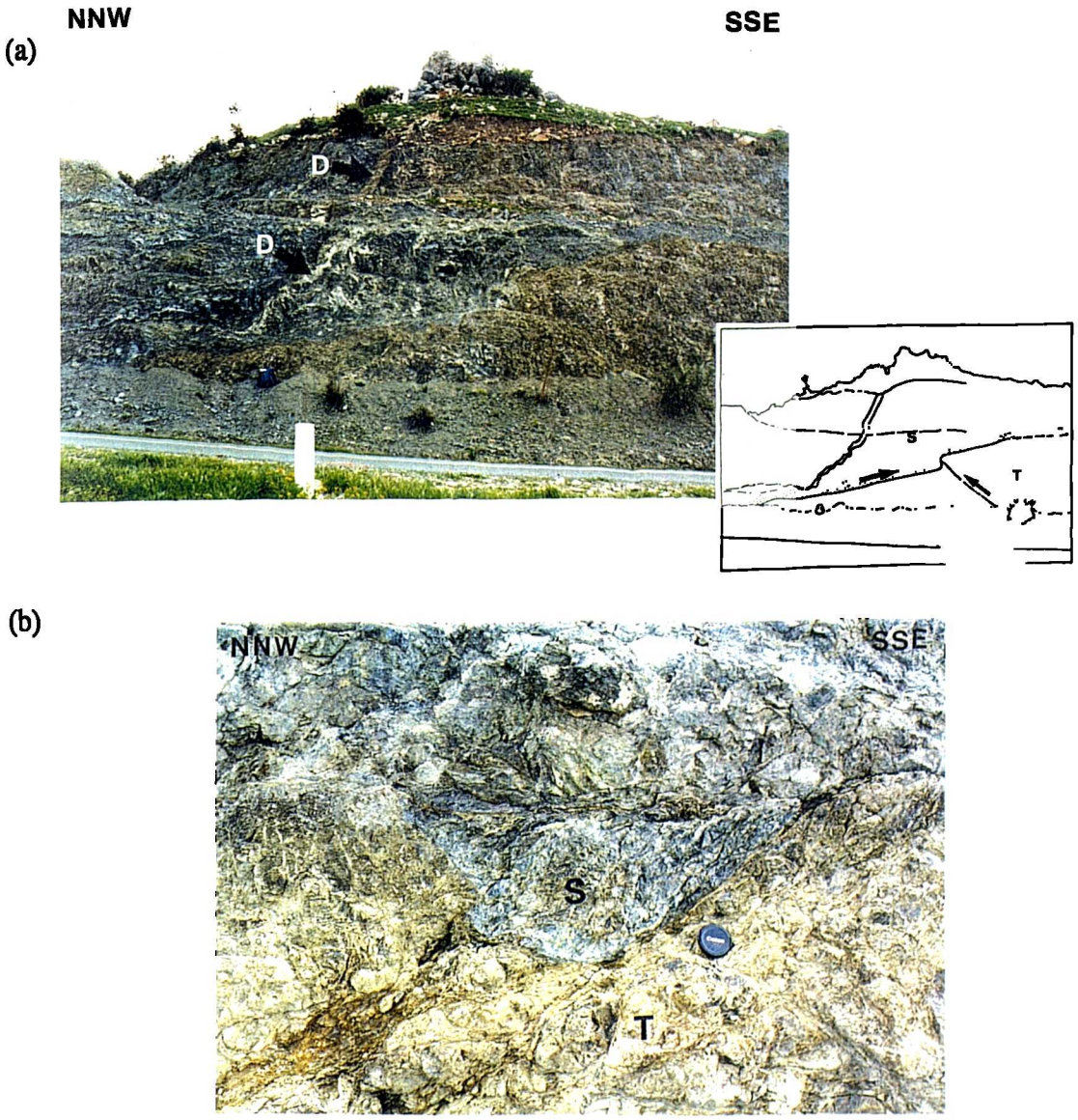

Figure 4.58. Details of the serpentinite (blue) over Troodos lava (brown) thrust contact exposed south of Plevra tou Petrovounou. (a) Note the kink in the thrust which is due to a minor offset caused by a backthrust, and the sub-vertical deformed Troodos mafic dyke (D) within the serpentinite, which rotates into the thrust. (b) Detail of thrust contact, showing blue serpentinite (S) cutting down into the grey-brown Troodos footwall (T).

Approximately 70m NE of the previous locality, a small,highly foliated, olive-green serpentinite shear zone crops out near to the unexposed contact with the Mamonia Complex on the northern side of the serpentinite belt. The colour and morphology of spinel grains preserved in lower strain blocks suggest that these serpentinites are derived from a Mamonia-related protolith (see Chapter 3). Asymmetrical extensional shear bands and shallowly-plunging slickenlines indicate both sinistral and dextral strike-slip (Figure 4.59a). Minor carbonate slickenfibres display large pitch angles on both sub-vertical (mean 122/80°NE) and moderately-dipping (mean 119/42°NE) foliation planes, which indicates subordinate dip-slip and oblique-slip displacements (Figure 4.59b). Sinistral and dextral faults are mutually cross-cutting and sinistral shear structures are slightly more dominant than dextral (12:11). Bulk displacement is inferred to be sinistral by the orientation of the maximum principal shortening direction, which is sub-horizontal and oriented a few degrees clockwise of fault-normal (Figure 4.59a and c). The dominance of the conjugate sinistral and dextral strike-slip shear bands suggests that the maximum axis of the finite strain ellipsoid is sub-horizontal, whilst the presence of northeasterly-plunging dip-slip lineations on moderately-dipping foliations is thought to reflect minor vertical thickening associated with NE-SW compression.

***Laonari tou Kannaourkou* (GR 580 476)**

At Laonari tou Kannaourkou (Figure 4.39), located at the southern contact of the southern serpentinite belt, the E-W striking serpentinite-Ayia Varvara Formation contact is well exposed. Brittle to brittle-ductile faults within a metre-wide zone of light-blue coloured fault rock (see section 4.4.1b) at the contact define heavily sheared S-C and shear band fabrics, which display ubiquitous sinistral shear senses (Figure 4.60a and b). This part of the contact (and the associated serpentinite foliation) dominantly strikes E-W and dips steeply to moderately to the north. Brittle striae and serpentine fibres on foliations and shear planes plunge shallowly to moderately to the NE, indicating sinistral strike-slip and oblique, top-to-the-SW thrusting of serpentinite over the metamorphics (Figure 4.61). Further to the east, the strike of the contact swings from E-W to NE-SW. Along this section, lineations are generally strike-parallel and shear sense criteria indicate sinistral strike-slip along fault planes that offset the contact on a metre-scale. As this latter part of the contact is relatively short (~25m long) and it connects two parallel, E-W striking sections that display structures indicative of oblique thrusting to the SW, it is interpreted as a minor sinistral transfer fault (Figure 4.61b).

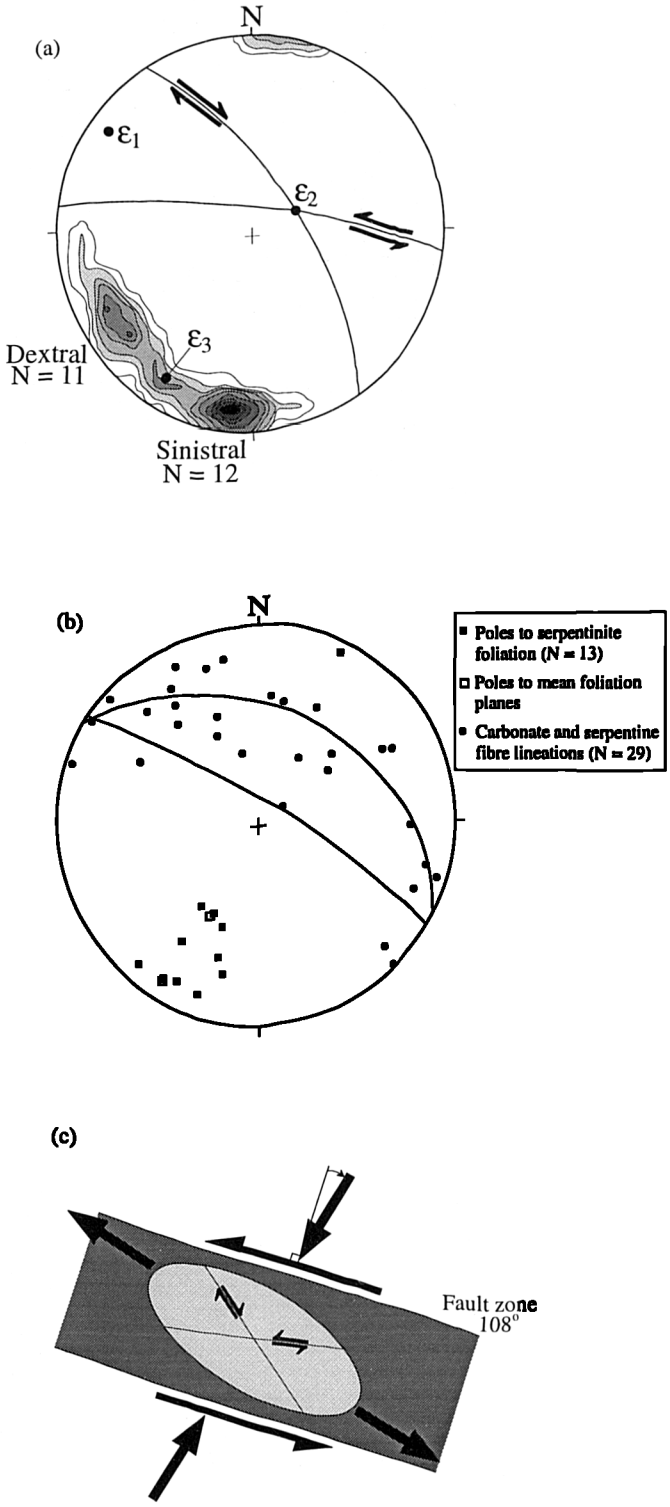

Figure 4.59. Data and interpretation of structures at Plevra tou Petrovounou. (a) Stereographic projection displaying 1% area contour of poles to sinistral and dextral shear planes, their average orientations (great circles), and the orientation of the principal finite strain axes. (b) Stereonet showing the representative orientations of foliation planes stretching lineations. Note that foliation dips sub-vertically to moderately to the NE and that some lineations plunge steeply to the NE. (c) Schematic map view showing the relative orientations of the fault zone, the finite strain ellipse, and the principal shortening axes, which support a sinistral model.

(a)

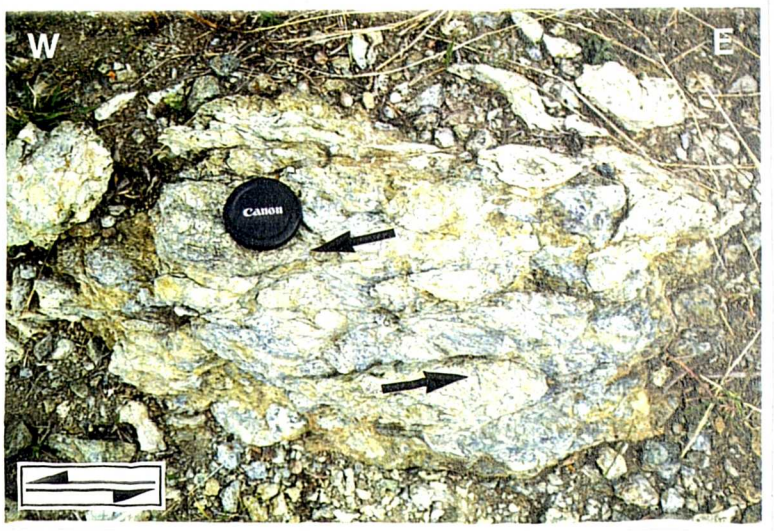

(b)

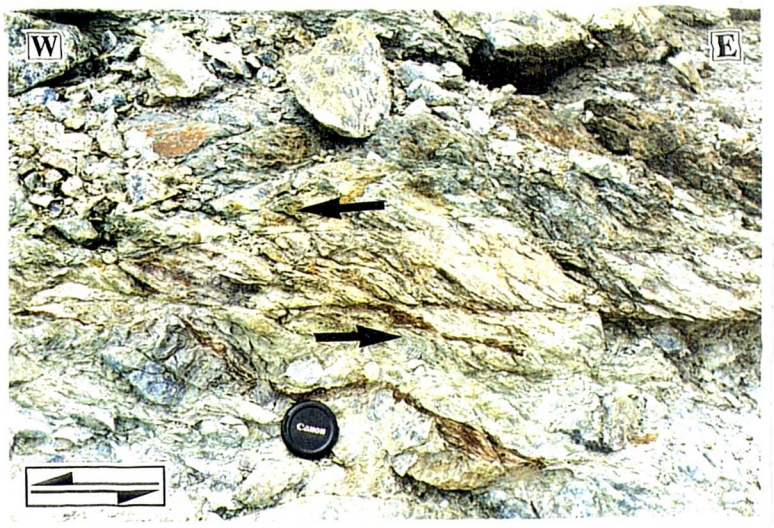

Figures 4.60. Features of the serpentinite-Ayia Varvara Formation contact at Laonari tou Kannaourkou. (a) Asymmetrical extensional shear bands within serpentinite fault rock indicating sinistral strike-slip. (b) Sinistral S-C fabric within the serpentinite fault rock.

Along moderately northerly dipping sections of the contact, the strong, amphibolite-facies fabric in the metamorphic footwall is cross-cut by steep to sub-vertically dipping brittle extensional fractures and by tensile carbonate veins, which extend down perpendicular to the contact. The orientation of these structures and the direction of opening of veins indicate that the maximum and minimum shortening directions are sub-vertical/fault-normal and sub-horizontal/strike-parallel, respectively. The orientations of veins and the principal finite strain axes suggest that the footwall was subjected to an unspecified degree of overburden and fluid-pressures were high enough to facilitate hydrofracture. High pore-fluid pressures are also inferred in the serpentinite fault rocks. The contact fault rock, which is described in detail in section 4.4.1b, is full of mm- to cm-scale 'holes', and fibres in ten centimetre-wide, tensile

chrysotile veins, which parallel the contact for tens of metres, indicate opening directions perpendicular to the fault (Figure 4.62). The relative timing of sinistral/top-to-the-SW thrusting, veining and footwall faulting is unknown. However, the presence of tensile chrysotile veins along the contacts are not predicted consequences of sinistral strike-slip or thrust faulting, and therefore, veining in the serpentinite may post-date displacement along these faults. The timing of veining and extensional fracturing in the footwall is more problematic and is described in detail below (see Teratsos to Kara tou Rakhovounou section). The interplay between faulting and fluid flow along tectonic contacts is discussed in Chapter 6.

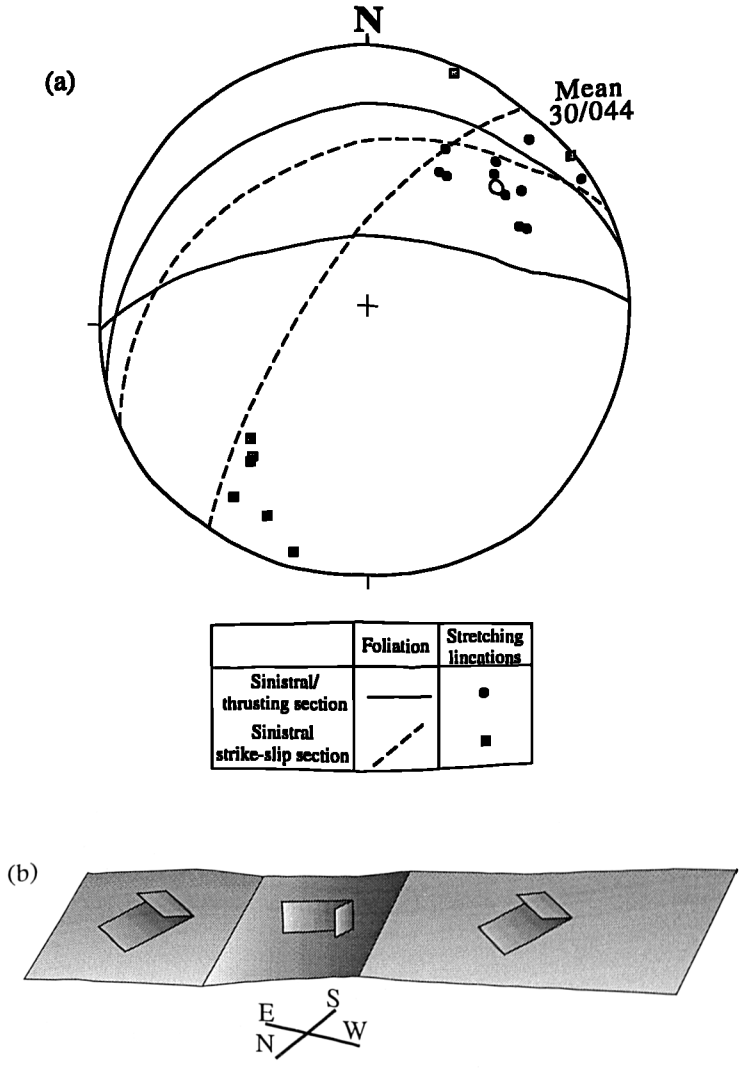

Figures 4.61. (a) Stereographic projection of data from the serpentinite-Ayia Varvara Formation contact at Laonari tou Kannaourkou. Slickenline and serpentine mineral lineations indicate sinistral strike-slip and top-to-the-SW thrust displacement along E-W striking, moderately-dipping sections of the contact (black circles and solid lines), and sinistral strike-slip along northeasterly-striking sections (grey squares and dashed lines). (b) Schematic interpretation of the data; the main sections of the faults accommodate NE-SW compression by oblique thrusting, whilst the minor northeasterly-striking section acts as a transfer fault.

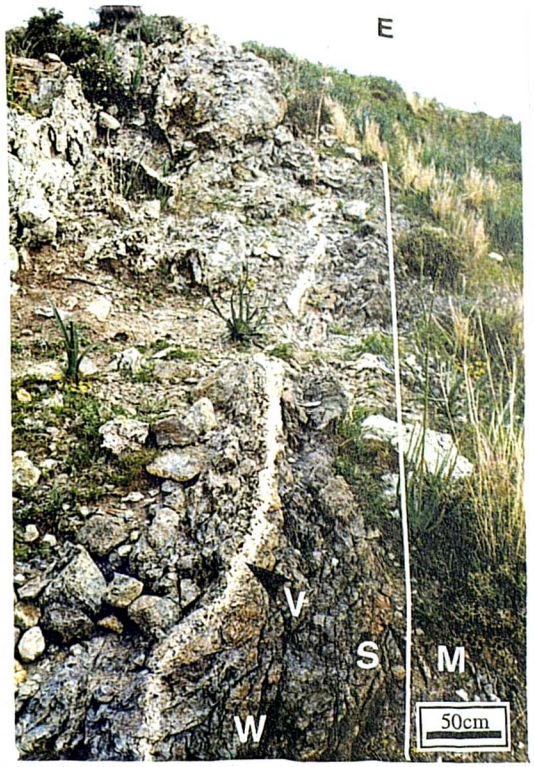

Figure 4.62. White, fibrous chrysotile vein (V) paralleling contact; the white line marks the contact between serpentinite (S) to the north and metamorphic rocks (M) to the south.

***Makrys Melanos* (GR 577 479)**

Along the northern serpentinite belt in the vicinity of Makrys Melanos (Figure 4.39), Troodos Complex lavas are juxtaposed against the serpentinites along an E-W striking contact (Figure 4.63a). This contact is high angle to sub-vertical and possesses a highly irregular geometry on a tens of metres-scale. Kinematic indicators along this section demonstrate that this architecture is due to boudinage and extension parallel to the strike of the contact, which is accommodated by shearing along two sets of strike-slip structures: NE-SW sinistral, and NW-SE striking dextral faults. At this locality, no evidence is present to suggest that one set of faults consistently cross-cuts the other and thus, they are considered synchronous and conjugate. However, sinistral faults are twice as abundant as dextral, which suggests the latter are antithetic to bulk sinistral displacement (Figure 4.63b). Figure 4.63(c) indicates that with this geometry, the bisector of the obtuse conjugate angle corresponds to the axis of maximum finite shortening (ε_3) and is oriented almost normal to the fault zone, whilst the acute bisector represents the *minimum* (ε_1) and parallels strike. Figure 4.63(d) demonstrates that ε_3 is oriented a few degrees clockwise of fault-normal, which is consistent with bulk sinistral shear, as is inferred by the dominance of sinistral faults over dextral.

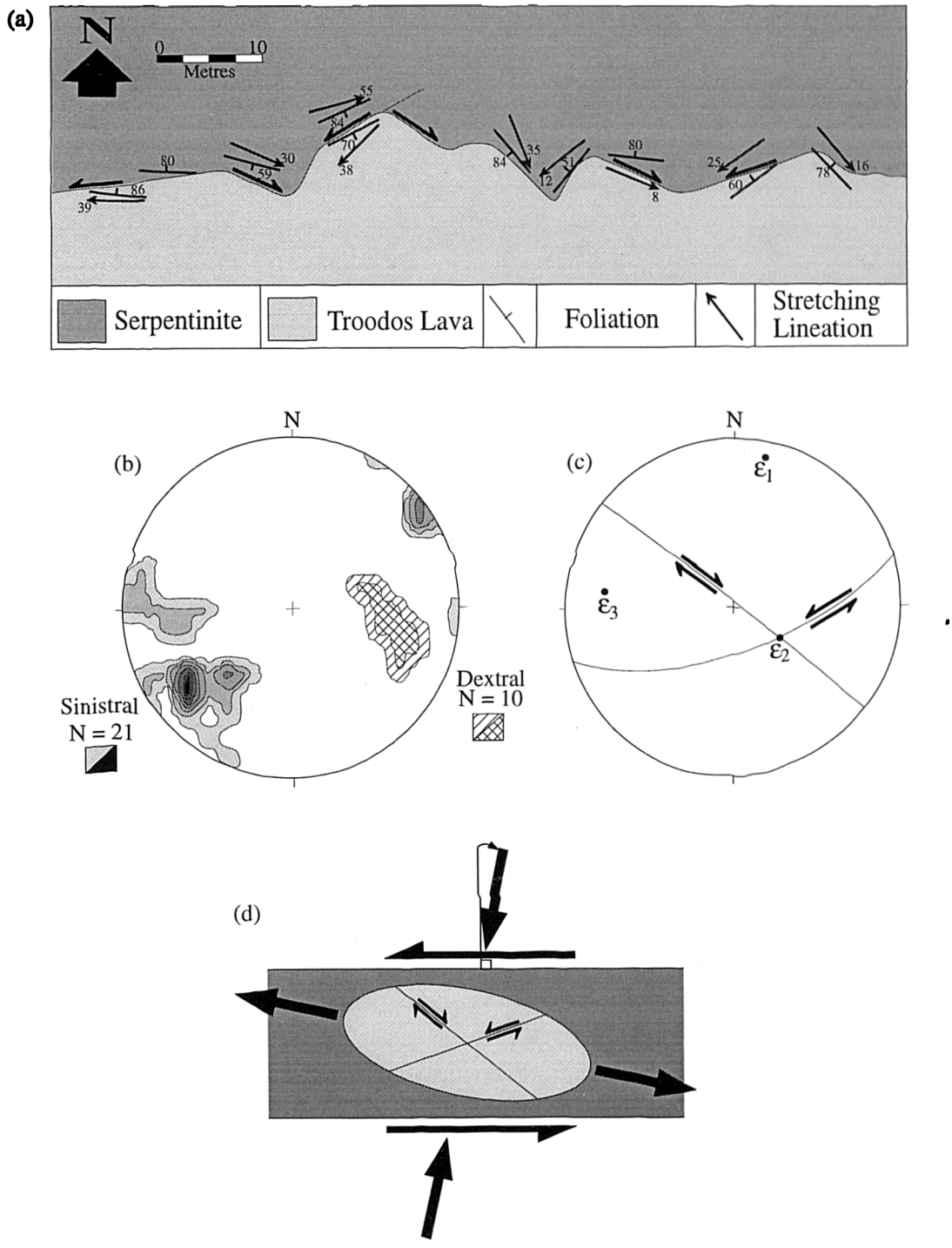

Figure 4.63. (a) Map and data of the contact at Makrys Melanos. (b) Stereographic projection showing 1% area contour of strike-slip stretching lineations. (c) Stereographic projection displaying the average orientations of conjugate strike-slip faults. The maximum and minimum principal finite shortening axes (ε_1 and ε_3, respectively) are the obtuse and acute bisectors of the conjugate faults, respectively, that lie in the profile plane. (d) Map view interpretation of data, showing the orientation of a hypothetical finite strain ellipse. Note that the principal shortening axes (arrows) are oriented a few degrees clockwise of fault-normal and fault-parallel.

***Teratsos* (GR 562 476) to *Kara tou Rakhovounou* (GR 574 474)**

Where exposed, the contact between the Southern serpentinite belt and the Ayia Varvara Formation from Teratsos to Kara tou Rakhovounou preserves evidence of the tectonic emplacement of serpentinite over the metamorphics (Figure 4.39). The contact is highly irregular on a scale of tens to hundreds of metres. The cause of this irregularity is unknown, but it may relate to the original geometry of the metamorphic body, which is thought to have been entrained within the serpentinite during dextral deformation and protrusion. Shear sense criteria and lineations within the serpentinite fault rocks at the contact indicate broadly southerly-directed tectonic transport (Figure 4.64). However, the amount and direction of dip and also the local direction of tectonic transport, varies considerably along the contact. The contact dominantly dips to the north and displays thrust geometries, whilst locally southerly-dipping sections possesses extensional geometries (Figure 4.65). Mineral lineations and brittle striae in the serpentinite hangingwall and metamorphic footwall indicate that the direction of transport varies considerably from SW to SE. The reason for this irregularity is discussed further below.

The early amphibolite-facies fabrics within the Ayia Varvara Formation, which are characterised by strong strike-parallel amphibole mineral stretching lineations, are overprinted with increasing proximity to the contact by later brittle deformation and calcic-hydrothermal alteration associated with emplacement of serpentinite. Locally the footwall is highly brecciated and transected by veins and extensional faults, which display strikes that vary considerably along the length of the contact (Figure 4.66). However, locally these faults display relatively consistent orientations and kinematic indicators, which record a concordant sense of shear sense to that observed in the overlying serpentinite fault rocks. A representative data set was taken from a well exposed section of the contact at GR 563 473 (Figure 4.67a). Fractures within the Ayia Varvara Formation along this contact display consistent northeasterly strikes and contrasting dips to the NW and SE. These faults are mutually cross-cutting and are therefore conjugate, but southeasterly-dipping faults dominate (58% of the total). Thus, bulk extensional displacement in the footwall is inferred to be top-to-the-SE, which parallels the tectonic transport direction determined from the overlying serpentinite sheet. The orientation of the principal finite strain axes in this part of the footwall may be approximated using the average orientation of the conjugate faults and their bisectors in the profile plane (Figure 4.67b and c). The maximum principal shortening axis plunges steeply, whilst the minimum plunges sub-horizontally to the NW, which is consistent with top-to-the-SE extension. As observed at Laonari tou Kannaourkou, carbonate veins extend down from the contact into the metamorphic rocks of the footwall (Figure 4.66). These veins are typically sub-vertical and are

oriented approximately perpendicular to the contact. The existence of vuggy cores to these veins indicates pore-fluid pressures were high in the footwall, which combined with the orientation of the maximum principal shortening axis, suggests that the footwall may have been overpressured (Figure 4.67c). However, this contrasts with the orientation of maximum shortening direction determined from other localities in the Southern Region, which typically plunge sub-horizontally. Two models may explain these observations: (1) extension in the footwall reflects a high degree of overburden, which resulted from the weight of the overlying serpentinite thrust sheet; (2) subsequent to thrusting resulting in vertical thickening, gravitational forces caused vertical thinning and extension. Unfortunately, no definite conclusion is possible, but the processes involved in the (2), concerning the evolution of orogenic wedges, are discussed in greater detail in Chapter 6 with reference to observations made in the Northern Region.

The variation in the direction of tectonic transport along this section of the contact may be explained by one of two models: (1) top-to-the-SE and top-to-the-SW events are diachronous, or; (2) tectonic transport to the SE and SW accommodated bulk N-S compression during the same event. In the first model, top-to-the-SE deformation is expected to have taken place during the previous dextral event, whilst southwesterly-directed thrusting occurred during sinistral transpression. However, the similarity in the style of deformation in both the serpentinite and the Ayia Varvara Formation and the gradual change in the transport direction around irregular sections of the contact favours the latter hypothesis, i.e. bulk N-S compression. For example, to the south and SW of Kara tou Rakhovounou, the direction of tectonic transport varies (from east to west) from top-to-SW, to top-to-the-SSW, to top-to-the-SE. The variation in the orientation of the contact does not appear to correlate with a systematic change in the transport direction. However, on a larger scale, these varying deformations may have accommodated regional N-S shortening. This idea is further supported by evidence of regional N-S/NNE-SSW compression in other areas (e.g. Mamonia; Plevra tou Petrovounou; Makrys Melanos) that is thought to have resulted in dominantly sinistral transpressional deformation. Also, the architecture of the fault zone prior to this deformational event is presumed to have been highly irregular, relating to serpentinite protrusion, which is expected to have a profound control on the local zone boundary displacements.

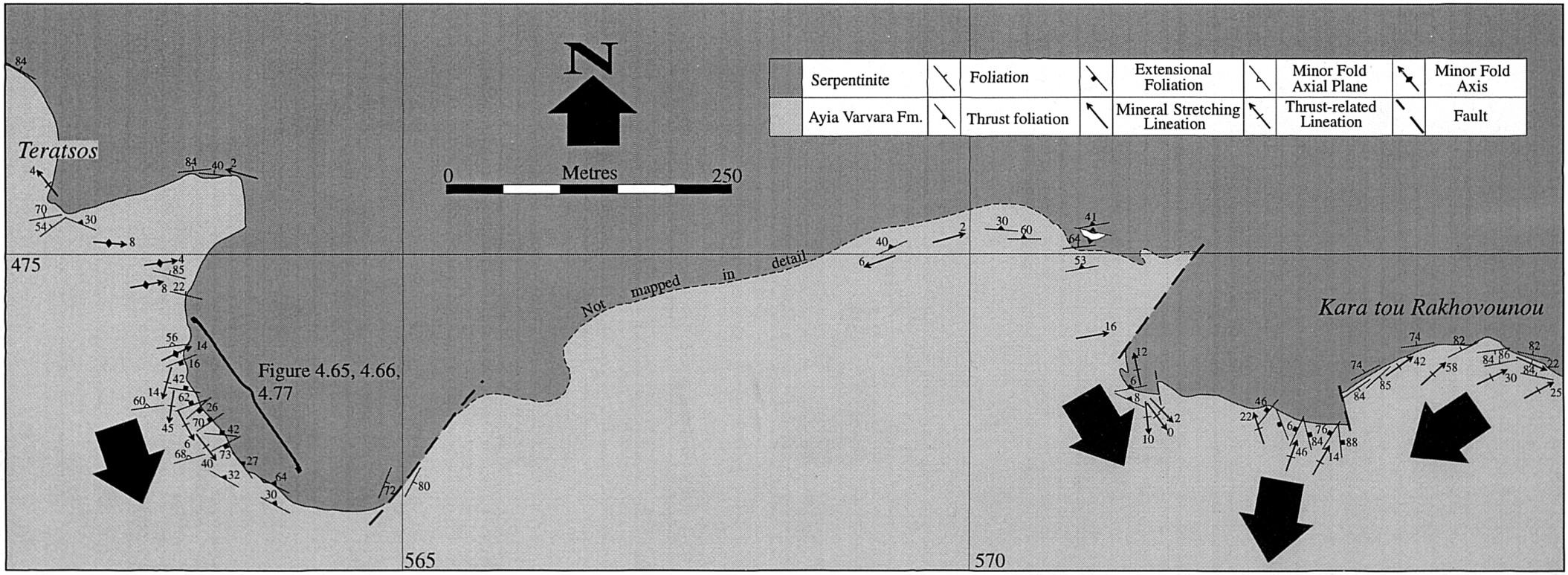

Figure 4.64. Geological map of the serpentinite-Ayia Varvara Formation contact from Teratsos to Kara tou Rakhovounou. Large black arrows indicate average lineation orientations, and thus the mean local tectonic transport direction, for each location.

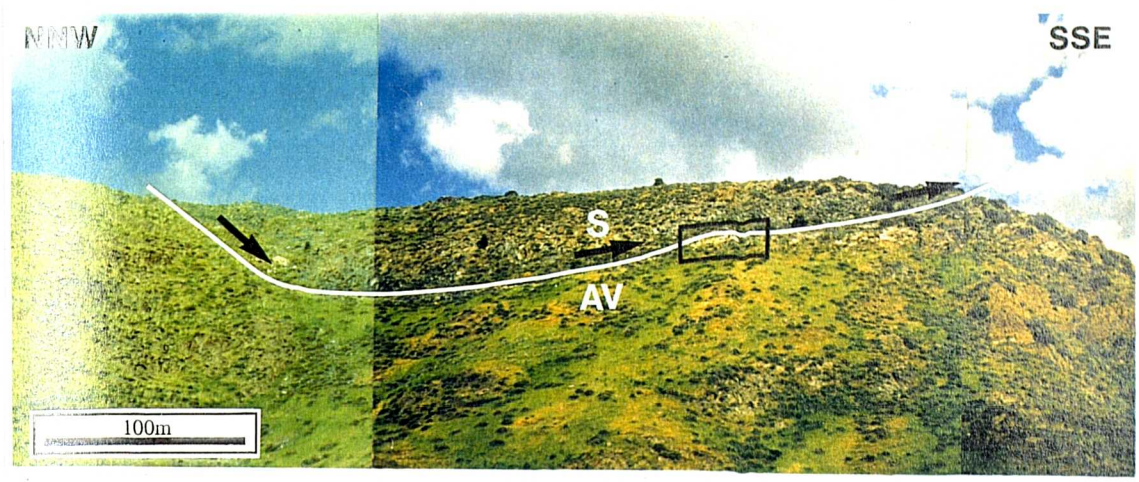

Figure 4.65. View onto a moderate to shallowly-dipping serpentinite (S)-Ayia Varvara Formation (AV) contact (GR 563 473). The black box indicates the locations of photographs and data shown in Figures 4.66 and 4.67. Note that the contact at the NNW end displays an extensional geometry.

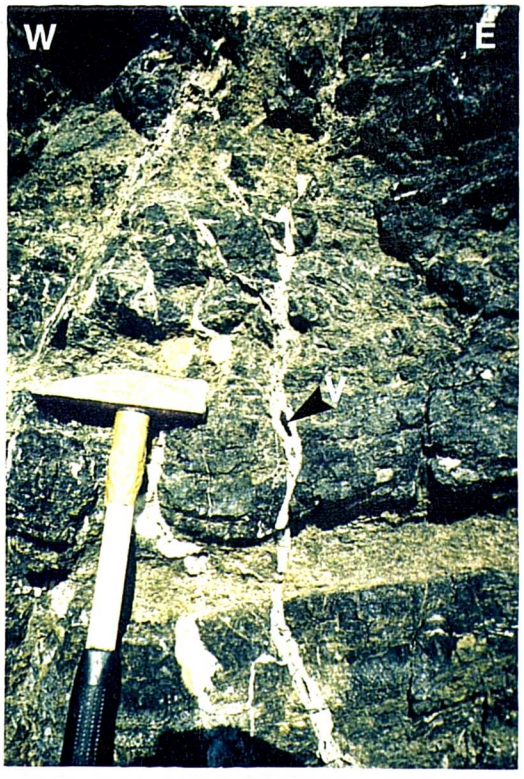

Figures 4.66. Brecciation and carbonate veining within the Ayia Varvara Formation at the contact with serpentinite. The location of these photographs is shown in Figures 4.64 and 4.65. Note the vuggy core to the vein (V), which extends down from the thrust contact. The lime-green colouration is epidote.

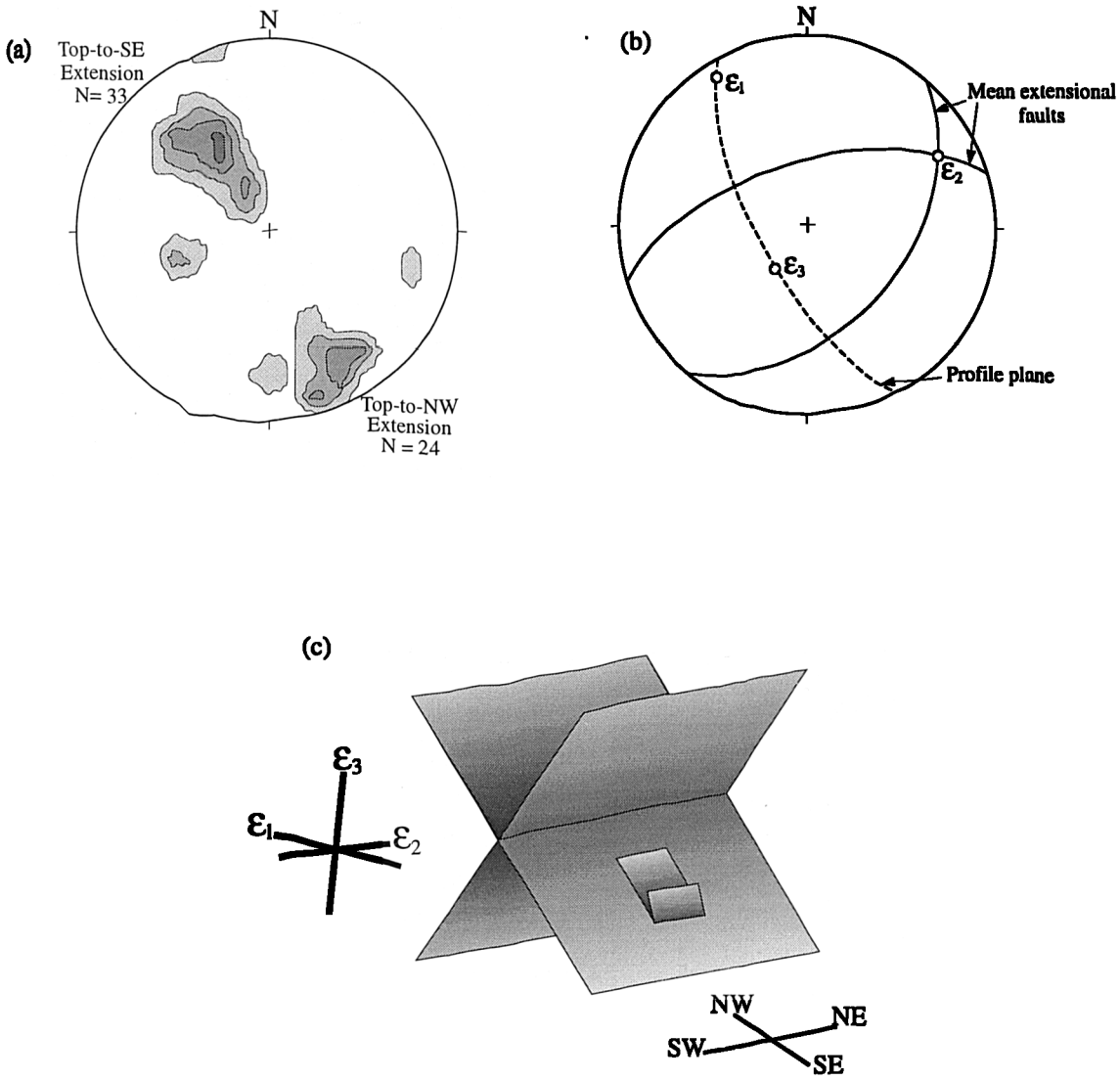

Figure 4.67. Stereographic projections of a representative data set from the Ayia Varvara Formation SE of Teratsos. The location where this data was collected is shown in Figures 4.64 and 4.65. (a). 1% area contours of poles to dip-slip, extensional fault planes, indicating extension to the SE and NW. (b) Orientations of the principal strain axes determined using the average orientations of the conjugate extensional faults shown in (a). Note that the maximum principal shortening direction if sub-vertical. (c) Schematic representation of the faults and finite strain axes in the metamorphic footwall.

Kakorkaka (GR 553 485)

In the northwestern part of the Ayia Varvara area, structures are preserved within Troodos lavas, located immediately to the south of the contact with the northern serpentinite belt, and along high strain zones that crop out internally within the serpentinite. At Kakorkaka (GR 551 486; Figure 4.39), Troodos pillow lavas are imbricated by northward-dipping, metre-scale thrusts. Oblique-slip carbonate slickensides on shear bands and S-C fabrics developed in cm-scale gouge layers along

the thrust planes indicate top-to-the-SW transport (Figure 4.68a). Approximately 300m to the east and immediately to the west of a 150m long Ayia Varvara Formation outcrop, two parallel E-W striking shear zones are exposed within the serpentinite belt (GR 554 485) These shear zones, which crop out close to the unexposed contact with the Dhiarizos Group, display a pervasive sub-vertical foliation developed in light-blue to green phacoidal gouge fabrics. They are relatively planar, 10 metre-wide features that can be traced along strike for tens of metres. They are characterised by the presence of isolated blocks (~1m long) of dark brown to maroon coloured Phasoula lava. These blocks are elongate with their long and short axes oriented sub-horizontally E-W and N-S, respectively, and are offset by brittle strike-slip faults. Both shear zones display two orientations of sub-vertical brittle to brittle-ductile faults and shear bands that are interpreted as conjugate and coeval; ESE striking sinistral and SSE striking dextral (Figure 4.68b). Strike-slip senses of shear are confirmed by the presence of shallowly-plunging brittle striae and mineral fibres (serpentine and carbonate). One shear zone is dominated by dextral kinematic indicators (i.e. brittle to brittle-ductile faults and shear bands), whilst the other displays dominant sinistral shear sense criteria, which suggests that they formed during different tectonic events. However, as observed within other serpentinite shear zones in the region, antithetic shear structures are preserved, from which an estimation of the orientation of the principal finite strain axes is possible. In both shear zones the orientations of the finite strain axes are parallel, which suggests that they are related to the same deformational event. Figure 4.68b shows the data from both the shear zones and also the orientations of the finite strain axes. Note that sinistral structures are more abundant than dextral (48:31), which infers bulk strike-slip displacement was left-lateral. The approximate parallelism between the sub-horizontal, northeasterly-plunging maximum shortening axis (ε_3) and the direction of thrust displacement in the Troodos lavas (i.e. NE-SW; Figure 4.68a), suggests that thrusting and strike-slip may have been contemporaneous. This coincidence suggests all three structures are related to the same tectonic event, during which NE-SW shortening was partitioned into separate strike-slip and compressional components; strike-slip within the serpentinite fault zones and thrusting in the Troodos Complex country rocks. The dominance of sinistral shear sense criteria in the E-W striking serpentinite belts, suggests that these structures formed during macroscopic- to regional-scale sinistral transpression.

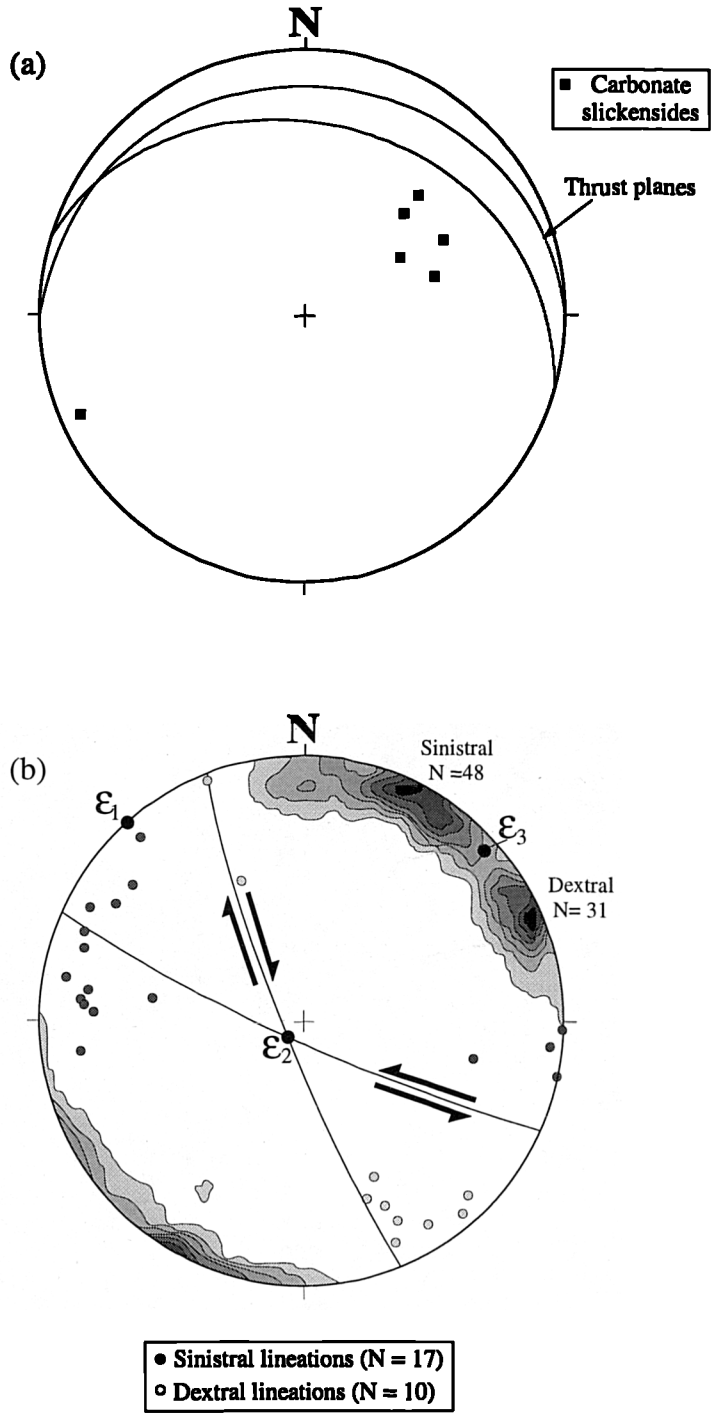

Figure 4.68. Stereographic projections displaying structural data taken from Troodos lavas and serpentinite shear zones at Kakorkaka. (a) Shows northward-dipping thrusts (great circles) in Troodos lava and carbonate slickensides that indicate top-to-the-SW displacement. (b) 1% area contour of poles to sinistral and dextral faults from both serpentinite shear zones located at GR 554 485. Great circles display the average orientations of sinistral and dextral faults. Small circles show strike-slip lineations and larger black circles represent the principal axes of the finite strain ellipse.

Ayia Varvara - summary

The structures described above that are preserved along the E-W trending serpentinite belts in the Ayia Varvara area are interpreted to have formed during a phase of sinistral transpression. The maximum shortening directions, determined from shear zones that display conjugate fault pairs, exhibit a range of azimuths from 012° at Makrys Melanos to 047° at Kakorkaka. These axes are typically oriented a few degrees clockwise of the local fault zone-normal directions which, when combined with field evidence for dominant sinistral strike-slip, is consistent with bulk sinistral deformation. Figure 4.69 displays the total data from the Ayia Varvara area taken from shear zones that contain conjugate shear pairs. The minimum finite strain axis obtained from this data indicates regional NE-SW shortening (6/046) and NW-SE extension (2/316).

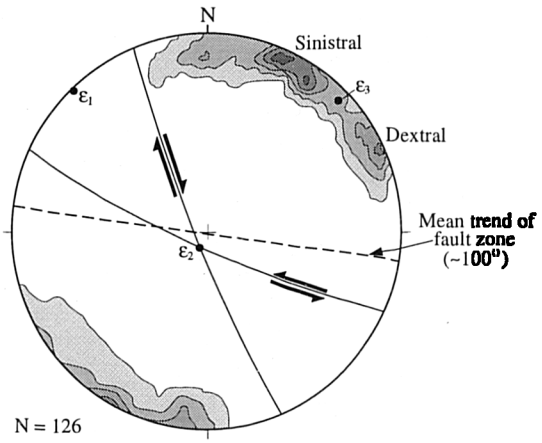

Figure 4.69. 1% area contour of poles to conjugate sinistral and dextral strike-slip faults from shear zones in the Ayia Varvara area. The orientation of the principal finite strain axes suggests NE-SW shortening and NW-SE extension.

However, the local directions of thrust transport display distinct variations. Top-to-the-SW thrusting, which is observed at Laonari tou Kannaourkou, the easternmost exposures at Kara tou Rakhovounou, and Kakorkaka, is consistent with a sinistral transpressional model. Minor top-to-the-NE thrusting associated with sinistral deformation, which is observed at Kara tou Ayiou Pati (see Section 4.3.1), is also considered as evidence for sinistral transpression. However, top-to-the-S and SE displacements typically observed along the contacts between the Ayia Varvara Formation and the southern serpentinite belt are more problematic. No definitive conclusion can be drawn, with respect to the nature of these southeasterly-directed thrusts, due to incomplete exposure along these contacts. As suggested above, they may relate to the previous dextral event, or local top-to-the-SW, -S and -SE displacements accommodated a single phase of regional N-S compression, which was imposed on an irregular fault zone architecture. In this latter hypothesis, the variability in the directions of tectonic transport and the orientations of the principal finite strain

axes, combined with the synchroneity between sinistral strike-slip and compression, suggests that the partitioning of the regional strains on a local scale is complex (see discussion).

To summarise, the predominance of sinistral shear along E-W trending fault zone boundaries and the presence of local and top-to-the-SW, and minor NE, overthrusts favours a sinistral transpressional model. Figure 4.70 shows a schematic diagram displaying the deformational characteristics of the Ayia Varvara fault zones.

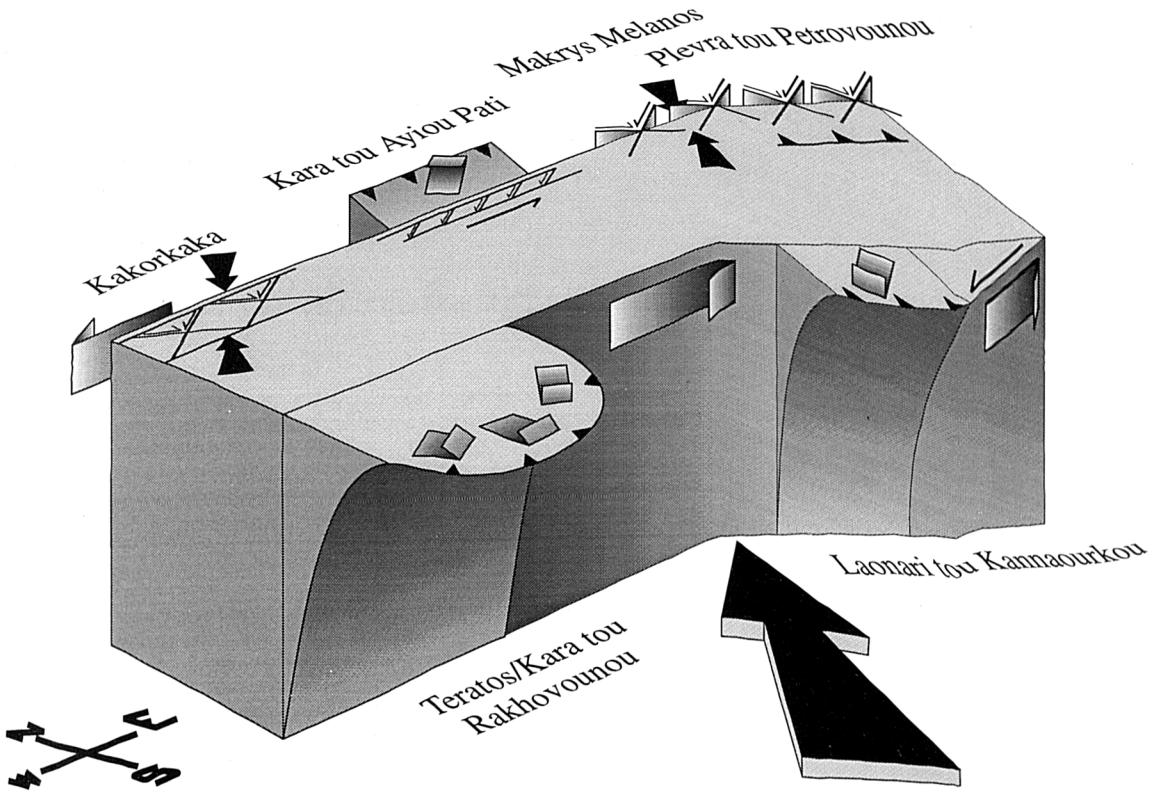

Figure 4.70. Schematic block diagram showing the deformational characteristics of the Ayia Varvara serpentinite belts. Regional NE-SW shortening across the E-W trending fault zones results in local sinistral strike-slip, top-to-the-SW thrusting and minor top-to-the-NE thrusting.

4.4.2d. Marathounda area

At Konnos, located approximately 750m east of Marathounda village (GR 542 503; Figure 4.39), a series of NW-SE trending serpentinite ridges separate Dhiarizos Group sediments to the SW from the Kannaviou Formation to the NE. These serpentinite outcrops are dominated by variably brecciated and mineralised (carbonate and quartz), serpentinite fault rocks that are cross-cut by three distinct sets of brittle faults, which display cm- to tens of metre-scale offsets: approximately E-W striking, sub-vertical sinistral faults; N-S to NW-SE striking, sub-vertical dextral faults, and; predominantly dip-slip extensional faults that possess NE-SW strikes and contrasting northwesterly and southeasterly dips (Figure 4.71a and b). The strike-slip faults are mutually cross-cutting, as are the extensional faults, which suggests that they represent conjugate pairs. The most noticeable feature of these outcrops are sub-vertical, NE-SW trending, cm-wide quartz veins and parallel, but subordinate, carbonate veins. As quartz veins cross-cut carbonate cemented serpentinite breccias, quartz mineralisation is inferred to post-date carbonate fluid flux. However, the parallelism between the two vein types suggests that they formed under a similarly oriented, if not the same, stress regime. Quartz mineralisation is rare in comparison with carbonate in SW Cyprus, but at this locality SiO_2-rich fluids are thought to be locally derived from the adjacent silicic Kannaviou sediments. The predominance of strong quartz (and minor carbonate) slickenfibres along the conjugate fault sets, suggests that veining and faulting were coeval. This assumption is supported by the orientations of all these structures, which suggest that they formed during NE-SW compression, which resulted in extension parallel to the southeasterly (129°) strike of the local fault zone boundaries (Figure 4.71c and d). Specifically:

- the maximum principal shortening direction, which is assumed to parallel the bisector of the obtuse strike-slip conjugate angle (Figure 4.71c), plunges shallowly to the NE (20/036). Similarly, the bisector of the acute angle is inferred to parallel the maximum extension direction, and is oriented 29/136, which is roughly parallel to the strike of the fault zone;
- the conjugate pair of extensional faults (mean orientations of 016/36°E and 037/53°NW) downthrow to the NW and SE;
- as all the veins are planar (i.e. they do not possess sigmoidal geometries) and they display parallel, consistent northeasterly strikes, they are considered to record coaxial strain. Fibres within these veins indicate ubiquitous NW-SE tensile opening.

The coincidence in the strike of veins, extensional faults and the orientation of the maximum principal shortening direction is consistent with the hypothesis that these

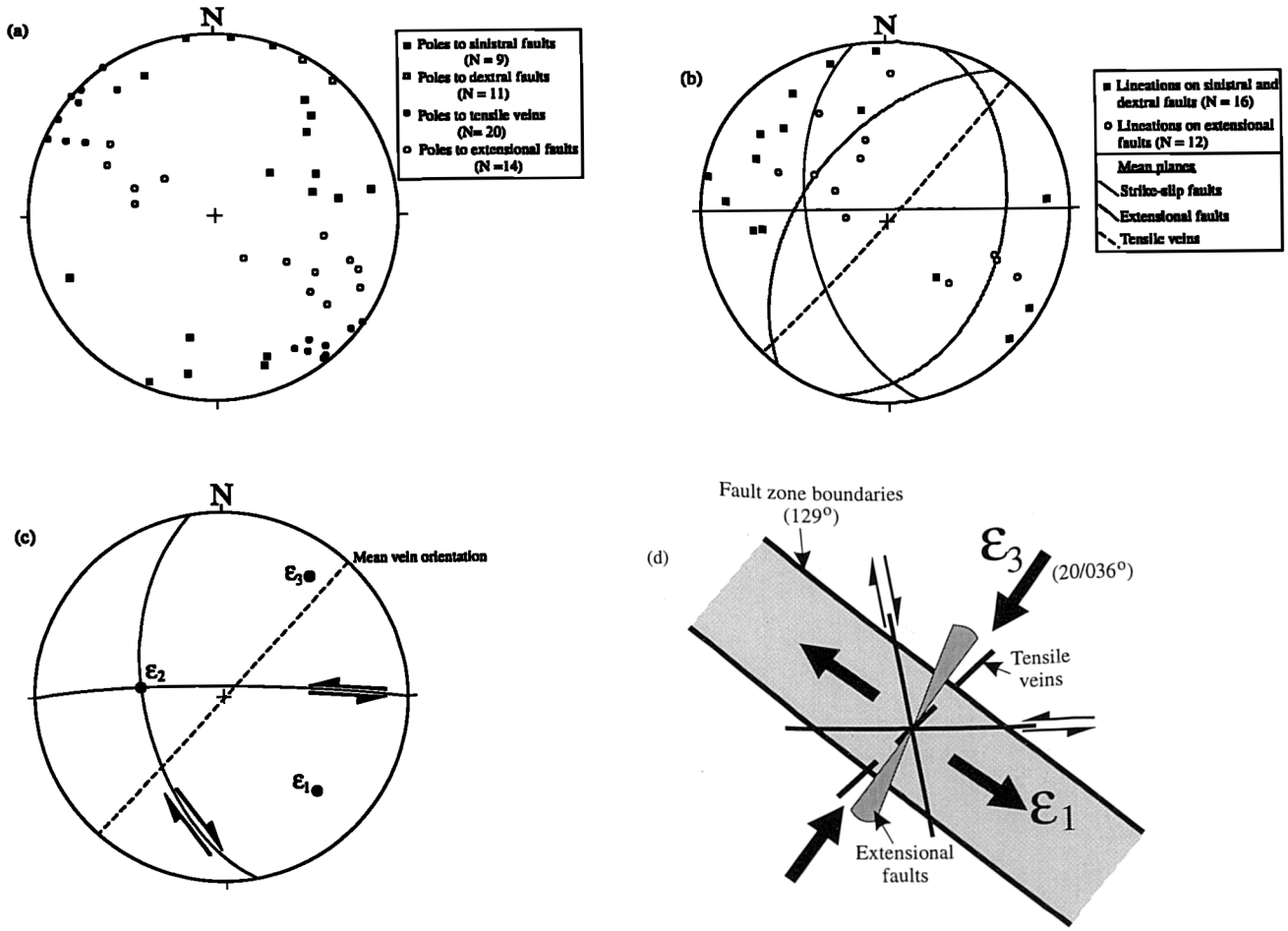

Figure 4.71. Data and interpretation of the serpentinite-filled fault zones at Konnos (GR 542 503). (a) Stereographic projection of poles to faults and veins. (b) Great circles representing the mean orientation of faults and veins shown in (a). Points show slickenfibre lineations from strike-slip and extensional faults. (c) Displays the geometrical relationship between the orientation of conjugate strike-slip faults and principal finite strain axes. (d) Schematic, plan view interpretation of the data, showing the accommodation of fault-normal shortening by extension parallel to the strike of the fault zone.

structures are contemporaneous and accommodated fault-normal shortening by strike-parallel extension. The ubiquity of vuggy cores to quartz veins and the brecciation of carbonate-cemented serpentinite breccias suggest that, during the syn-kinematic flux of both these fluids, pore-fluid pressures were high and, at least transiently, exceeded the least principal stress (σ_3) causing hydraulic fracture.

The reason for using this locality as evidence for sinistral transpression in the Southern Region may appear somewhat peculiar to the reader, especially when dextral faults are slightly more numerous than sinistral (11:9) and the maximum principal shortening direction is oriented slightly anticlockwise of fault-normal. However, what this example demonstrates is the dominance of NNE-SSW to NE-SW compression along the length of the fault zones in the Southern Region. As these fault zones typically strike E-W, NE-SW shortening is accommodated by predominantly sinistral and compression deformation in the serpentinites. In contrast, the faults at Konnos in the Marathounda area strike NW-SE, which is roughly perpendicular to the regional NE-SW shortening direction, and therefore they record bulk coaxial strains.

4.4.2e. Macroscopic transpressive strains - summary.

Although it is not possible to quantify the magnitude of strain, the bulk deformation in the Southern Region is interpreted to be regionally sinistral and transpressive based on the following observations:

- the majority of the serpentinites are enclosed within sub-vertical, fault-bounded belts, which typically display steeply dipping shear zone fabrics. Low temperature deformation in the serpentinites is accommodated by macroscopically ductile cataclastic flow and brittle/brittle-ductile fault arrays. As brittle and ductile structures are kinematically identical, they are considered to be broadly coeval;
- the faults and shear zones in the serpentinite belts form an anastomosing network of mutually cross-cutting, conjugate structures that enclose lenticular lozenges of less deformed material on all scales;
- faults and shear zones preserve numerous lineations defined by mineral slickenfibres (serpentine, carbonate and minor quartz) and brittle striae. In the higher strain zones, the majority are sub-horizontal to shallowly-plunging, and associated kinematic indicators preserve dominantly strike-slip senses of shear. In these regions, sinistral kinematic indicators dominate over dextral by up to 50%. In contrast, the interiors of the lower strain lozenges often display complex and variable orientations of slickenfibres. These lineations record the internal distortion and rotation of lozenges within the higher strain matrix of the serpentinite belts, and are thought to be of negligible regional significance;

- The lizardite-dominated serpentinites have a semi-ductile rheology, in which the obtuse (rather than the acute) angle between conjugate sets contains the axis of principal compression (*cf.* Figure 26.29 of Ramsay and Huber, 1987). In most locations (~69% of total) the bisector of the obtuse angle between conjugate fault sets is a few degrees clockwise of being orthogonal to the local zone boundaries. This is consistent with high-angle oblique sinistral shortening (i.e. pure shear-dominated sinistral transpression) (Table 4.4);
- locally, the boundaries of the serpentinite zones are defined by moderately to shallowly dipping, top-to-the-SW and, more rarely, top-to-the-NE thrusts with associated oblique or dip-slip slickenfibres. This represents small-scale partitioning of pure shear deformation, causing minor amounts of vertical thickening due to thrust stacking. The development of thrusts along the serpentinite belt margins is thought to be determined by local boundary conditions. Pre-existing, shallowly-dipping contacts are locally preserved adjacent to thrusts, which appear to have formed during serpentinite protrusion. In these areas, horizontal shortening may have been more easily accommodated by reactivation of shallowly dipping contacts as thrusts;
- there is no field evidence to indicate that large-scale partitioning of strike-slip displacements onto certain major fault strands has occurred.

Although the absence of strain markers precludes an accurate determination of the three-dimensional shape of the regional finite strain ellipsoid, the geometry and kinematics of the conjugate faults and shear zones show that the dominant direction of elongation of the finite strain ellipsoid is predominantly axial rather than vertical. There is no evidence of significant strain partitioning (i.e. into pure shear and simple shear components) on a regional scale (*cf.* Teyssier *et al.* 1995), so that the fault normal orientation of the maximum principal shortening direction appears to indicate that pure shear-dominated transpression occurred regionally along the fault zones of the Southern Region. In existing transpressional models, this orientation of the extension direction is incompatible with transpressional deformation that is pure shear-dominated (e.g. Tikoff and Teyssier, 1994; Teyssier *et al.* 1993). In confined transpression modelled by Sanderson and Marchini (1984) and Fossen and Tikoff (1993), the finite extension direction for pure shear-dominated transpression is vertical. This incompatibility between the Cyprus fault zones and pre-existing transpressional models is discussed in Chapter 6.

Locality (Grid reference)	**Fault zone trend** (+ average foliation)	**Maximum principal shortening axis** (ε_3)	**Conjugate angle**
Makrys Melanos (577 479)	097°(090°)	11/012° (CW)	120°
Plevra tou Petrovounou (580 478)	108° (116°)	17/212° (CW)	132°
Kakorkaka (553 485)	098° (110°)	6/047° (CW)	135°
Konnos; Marathounda (542 503)	129°	20/036° (ACW)	96°
Vatomandra (465 623)	~090°	5/012° (CW)	130°
Mamonia 1	108° (106°)	10/190° (ACW)	098°
Mamonia 2	108° (106°)	12/196° (-)	110°
Mamonia 3	105° (116°)	13/220° (CW)	120°
Mamonia 4	105° (090°)	14/190° (-/ACW)	105°
Mamonia 5	090° (102°)	23/182° (A/CW)	100°
Mamonia 6	090° (116°)	4/187° (A/CW)	116°
Mamonia 7	135° (135°)	14/048° (CW)	111°
Ayia Varvara area: all data	~100°	7/046° (CW)	137°
Mamonia: all data	100°	10/190° (-)	112°
Mamonia: low strain	100° (090°)	27/184° (ACW)	137°

Table 4.4. Geometrical relationships between the principal strain axes and the local trend of the fault zone at specified localities. The conjugate angle is defined as the angle, in the profile plane to the conjugate shear pair, that contains the maximum principal shortening direction. The bracketed lettering in the ε_3 column indicates whether the maximum shortening direction is clockwise (CW), anticlockwise (ACW), either anticlockwise or clockwise (A/CW), or parallel (-) to fault normal.

CHAPTER FIVE
TECTONICS OF THE NORTHERN REGION

5.1. Introduction

The Northern Region of SW Cyprus extends south from *Loutra tis Aphroditis* on the north coast, through the *Akamas* Forest, to the *Mavrokolymbos* area (Figure 5.1). The geology of this region is characterised by N-S striking, massive serpentinite bodies, which separate the Mamonia Complex in the east from the Troodos Complex to the west, along predominantly low-angle tectonic contacts. Structures observed along contacts within serpentinite and Mamonia Complex bodies suggest that adjacent units were juxtaposed during a phase of compressional tectonism in the Upper Cretaceous. Ubiquitous shear sense criteria indicate thrust transport was westerly-directed, which explains the commonly observed order of stacked units, from base to top, of Troodos Complex-serpentinite-Mamonia Complex.

This deformational event is generally considered to have caused the final juxtaposition of the Troodos and Mamonia Complexes (e.g. Swarbrick, 1979; 1980; Malpas *et al.* 1993; Gass *et al.* 1994). Based on palaeontological evidence, this event is constrained to the time period between the late Campanian to the latest Maastrichtian. The youngest pre-deformational sediment is the Kannaviou Formation, which is dated as no younger than Campanian in age (Urquhart and Banner, 1994), whilst the oldest post-deformational sediments are the Kathikas and basal Lefkara Formations, which are Maastrichtian in age (Swarbrick and Naylor, 1980; Urquhart and Banner, 1994). These latter sediments are the first to have been deposited on both the Mamonia and Troodos Complexes and also on top of their serpentinite-filled tectonic contacts (Figure 5.1). The Kathikas Formation sediments, which are unique to the Northern Region, are interpreted as local debris flow deposits derived from upthrust Mamonia Complex fault blocks, whilst the Lefkara chalks document background pelagic deposition (Swarbrick, 1979, 1980; Swarbrick and Naylor, 1980).

This chapter is sub-divided into descriptions of the tectonics within three main areas, namely: the coastal section exposed at *Loutra tis Aphroditis*; exposures preserved in the *Akamas* Forest and; the *Mavrokolymbos* area (Figure 5.1).

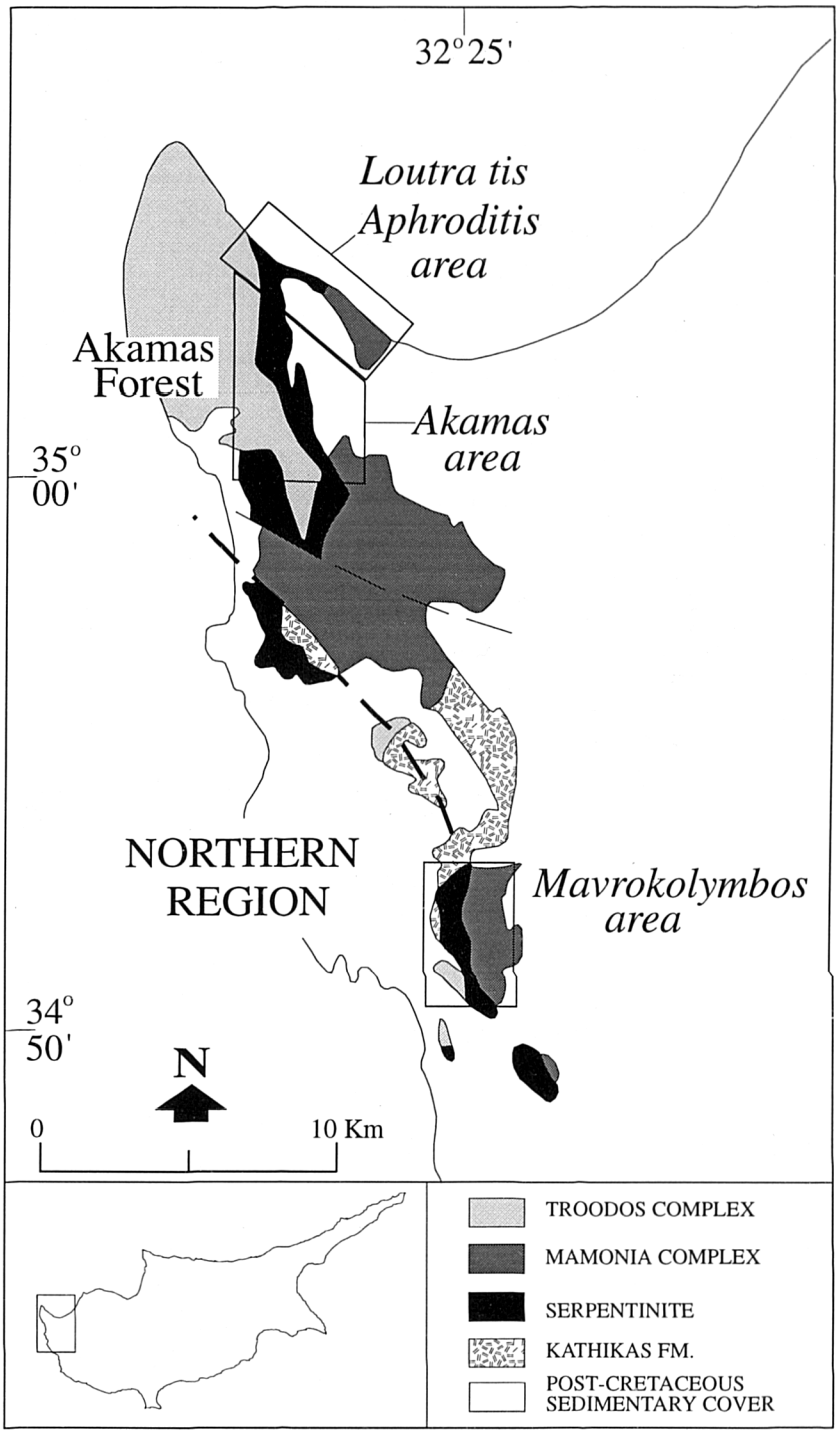

Figure 5.1. Geological map of the Northern Region of SW Cyprus.

5.2. The Loutra tis Aphroditis section

The coastal section exposed to the north of the Baths of Aphrodite tourist attraction (GR 408 794 to 390 810) is discussed separately from the Akamas area due to the preservation of additional structural and lithological complexity. As the dominant structural fabric strikes NE-SW, outcrops along this NW-SE trending coastline provide a cross-section through the structure of this area (Figure 5.2). Along this section, units of serpentinite, peridotites, Ayia Varvara Formation metamorphic rocks and unmetamorphosed Dhiarizos units are tectonically intercalated. In the following text, each unit and contact is described separately in a traverse from SE to NW along the cross-section (Figure 5.2).

5.2.1. The Loutra tis Aphroditis Formation (GR 408 794 to 406 497)

Dhiarizos sediments, assigned to the Loutra tis Aphroditis Formation (Robertson and Woodcock, 1979; Swarbrick 1979), crop out at the southeastern end of the coastal section (Figure 5.2). This package of sediments consists of lava breccias and siltstones interbedded with radiolarian mudstones. Beds in these interbedded units dip sub-vertically (stereonet (i); Figure 5.2) and display undulating 'pinch and swell' geometries due to variations in thickness (average 3-5cm thick beds). Breccias, which crop out as two isolated, probably fault-bounded exposures, comprise clasts (cm- to m-scale) of Phasoula lava and minor amphibolite set in a dark brown-maroon muddy matrix. Outcrops of breccia are typically structureless, except within metre-wide zones at their margins where they exhibit a rough disjunctive, cm- to mm-spaced, sub-vertical foliation (*cf.* Figure 13.3; Twiss and Moores, 1992). The fine-grained (mm-scale) cleavage domains within these fabrics readily weather out, accentuating discontinuous, cm-scale microlithons, comprising coarser-grained (<5cm), randomly oriented, fractured clasts. This brittle foliation, which parallels the bedding in the interbedded mudstones and siltstones, increases in intensity with proximity to the edge of the outcrop, which suggests the unexposed contacts with the adjacent sediments are faulted. The presence of sub-vertical, NE-SW striking brittle faults in these sediments and in units to the NW, which display late extensional and sinistral displacements, supports this hypothesis (see below).

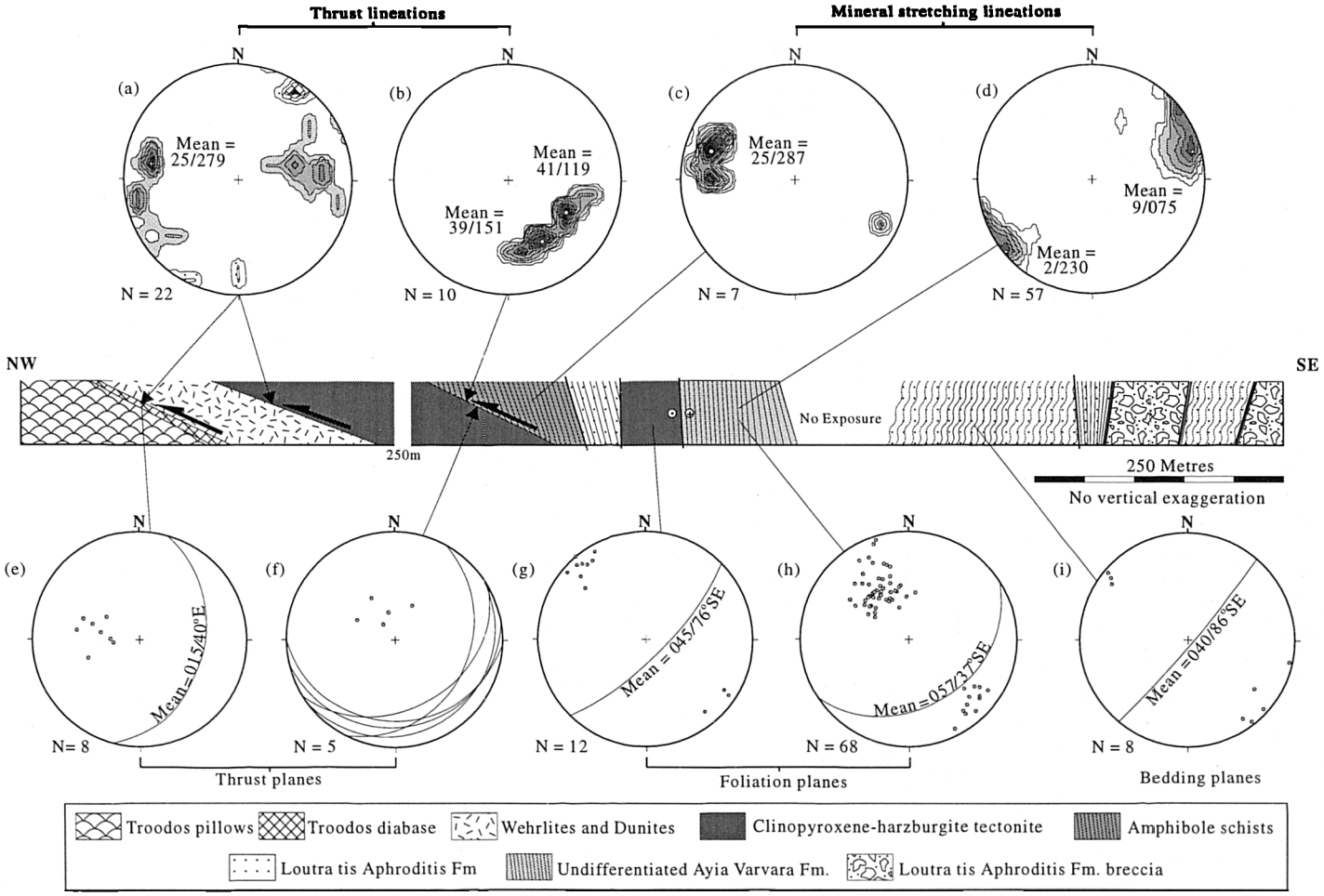

Figure 5.2. Cross-section through the Loutra tis Aphroditis area. The top stereonets display 1% area contours of lineation data, whilst the lower stereonets show the poles and mean orientations of planar data. Note that contacts, bedding and foliations generally strike NE-SW, mineral stretching lineations trend NE-SW to E-W and thrust lineations indicate variable displacements to the W and NW.

The presence of metabasic material as clasts within these breccias may be problematic. These clasts are texturally and mineralogically identical to the amphibolites of the Ayia Varvara Formation located to the NW, which have been dated as Upper Cretaceous (83-90Ma; Spray and Roddick, 1981). However, the Loutra tis Aphroditis Formation sediments are assigned to the Triassic-Lower Cretaceous Mamonia Complex (Swarbrick and Robertson, 1980). Therefore, this discrepancy provides a quandary; are these sediments Triassic or Upper Cretaceous in age? Unfortunately, as these clasts have not been dated radiometrically, no definite conclusion can be drawn. However, by analogy with brecciation of oceanic rocks along the STTFZ, the Loutra tis Aphroditis breccias may represent scarp deposits formed during extension and the formation of the Troodos Complex (*cf.* Simonian and Gass, 1978; Murton, 1986; Macleod, 1988; Gass *et al.* 1994). These possibilities are discussed further in a regional context in Chapter 6.

5.2.2. The Ayia Varvara Formation (GR 405 678 to 404 799)

The contact between the Loutra tis Aphroditis Formation and the Ayia Varvara Formation is unexposed (Figure 5.2). The Ayia Varvara Formation comprises amphibolite-facies metabasites and metasedimentary quartz-mica schists, which are intercalated and juxtaposed along NE-SW striking, sub-vertical, brittle faults. These faults are poorly exposed, but as they truncate the metamorphic fabric and they parallel better exposed brittle faults located to the NW, they are considered to be late sinistral/extensional structures (see below; sections 5.2.2b and 5.2.3). Both the metabasic and metasedimentary units possess a well defined foliation, a mineral stretching lineation (stereonets (d) and (h), Figure 5.2), and display folding on variable scales (Figures 5.3 and 5.4). In hand specimen, foliation is defined by mm- to cm-scale compositional banding and by the planar alignment of predominantly amphibole and feldspar grains in the metabasites, and by quartz and white mica in the metasediments. Foliation planes strike consistently NE-SW, but the variations in dip observed are attributed to tilting associated with cm- to m-scale, late extensional brittle faulting. The strong mineral stretching lineation observed within these rocks, which consistently plunge shallowly to the NE and SW, is defined by amphibole in the metabasites and by quartz aggregates in the metasediments. The typical mineral assemblages that constitute these L-S tectonite fabrics suggest that they formed at amphibolite-facies metamorphic conditions (~600°C; Spray and Roddick, 1981; Malpas *et al.* 1992).

5.2.2a Folding

Foliations, particularly within metasedimentary units, are folded on a mm- to m-scale. Two generations of folds are recognised; early ductile isoclines and later brittle-ductile folds (Figures 5.3 and 5.4). The earlier fold structures are typically discrete, intrafolial isoclines, which display near strike-parallel fold axes (Figure 5.3). These folds are considered to have formed during peak metamorphism (Spray and Roddick, 1981), but due to overprinting by subsequent deformation, they are far less abundant than the brittle-ductile folds and are not discussed further.

Figure 5.3. Early isoclinal, intrafolial ductile fold in banded metasediments.

The style of the later brittle folding varies considerably from folds that exhibit complex, disharmonic geometries (Figure 5.4a), to relatively simple folds that verge to SE, displaying consistent 'S'-shaped asymmetries when viewed down plunge (Figures 5.4b and c). At outcrop, asymmetrical folds appear to have formed by displacement along northwesterly-dipping ductile to brittle-ductile kink bands that transect hinge regions (Figures 5.4b and c). Whatever the style of this later folding, fold axes exhibit relatively consistent southwesterly plunge directions (28/249; Figure 5.5a), which approximately parallels the stretching lineations (2/230 and 9/075). Also, fold axial planes strike NE-SW and dip to the SE, which approximately parallels the strike of foliation (Figure 5.5b; 033/37°NW compared to 057/37°SE, respectively).

(a)

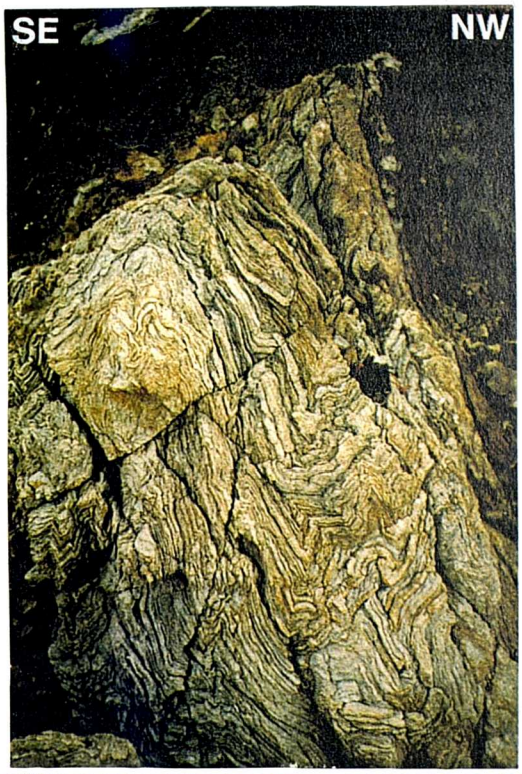

(b)

(c)

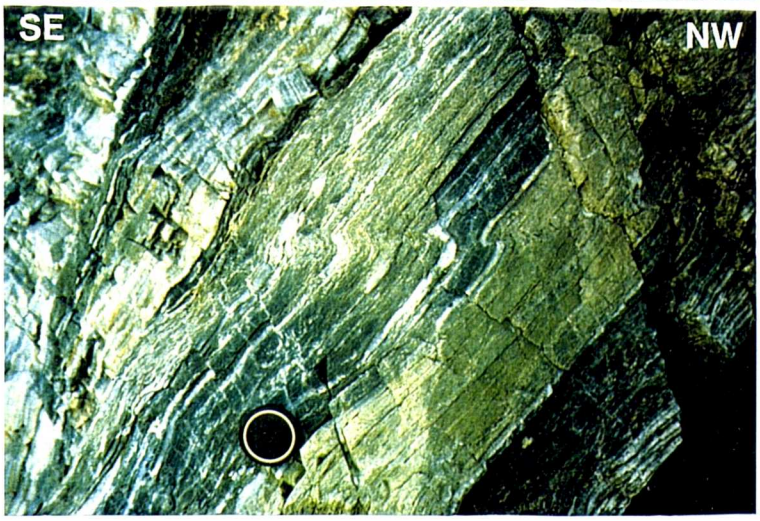

Figure 5.4. Brittle folding within metasedimentary units at Loutra tis Aphroditis. (a) Example of complex folding. (b) 'S'-shaped fold viewed to the SW, down plunge. (c) 'S'-shaped fold, displaying a kink band that transects the hinge region.

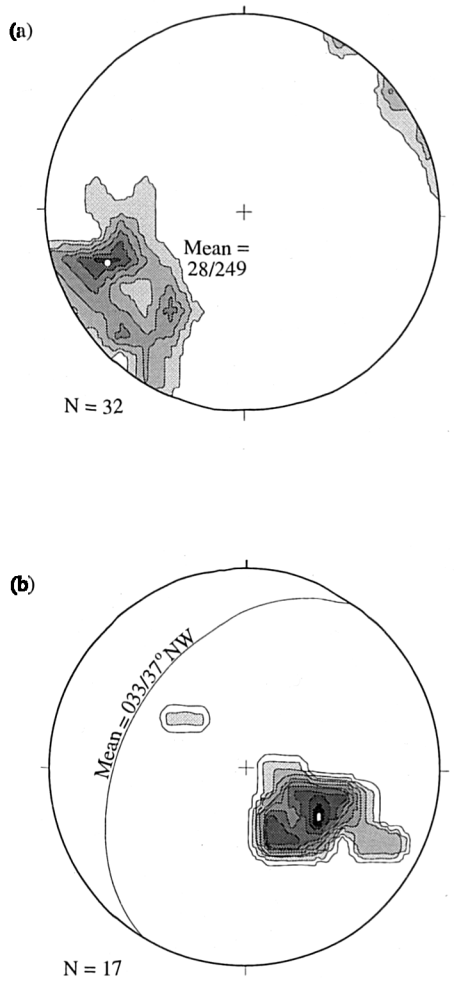

Figure 5.5. Fold data from the Ayia Varvara Formation units at Loutra tis Aphroditis. (a) Stereographic projection showing 1% area contours of fold axes and, (b) poles to fold axial planes.

Microstructure

In thin section, metasedimentary samples that contain 'S'-shaped folds preserve microstructural evidence of the deformational history experienced by these rocks. An early amphibolite-facies (Spray and Roddick, 1981), mylonitic foliation is defined by relatively coarse (up to 1mm long), stretched quartz grains, which display strong crystallographic-preferred orientations (Figure 5.6a), and by the alignment of biotite and white mica, which wrap garnet porphyroclasts. Quartz grains attain length:width ratios of 7.5:1 and are invariably strained, displaying undulose extinction, deformation bands and fine-grained, recrystallised margins. The presence of subgrains and highly irregular grain boundaries suggests that both rotation and grain boundary migration processes accommodated recrystallisation. However, note that these features may well be consequences of subsequent, lower temperature deformation (see below). This early high strain fabric is folded and fold hinges are in turn offset by high angle, predominantly westerly-dipping kink bands (Figure 5.6b). The replacement of locally

stretched garnets by chlorite (plus minor biotite and quartz), combined with the relatively high abundance of chlorite within the kink bands in comparison with the matrix, suggests that these later deformational events took place during low temperature, retrograde (chlorite-grade) metamorphic conditions (Figure 5.6c; see section 5.2.9b). With increasing proximity to kink bands, the coarse, stretched quartz grains are recrystallised to form fine, equant, grain-sizes (as small as 4μm) that display poorly defined lattice-preferred orientations (Figures 5.6a and d). The presence of subgrains and irregular grain boundaries within the kink bands suggests that both rotation and migration recrystallisation processes were operative (Figure 5.6e). The recognition of hydration reactions (e.g. the replacement of garnet by chlorite) suggests that these recrystallisation and deformation mechanisms may have been facilitated by fluids.

The predominance of reverse, top-to-the-SE displacements observed along the kink bands contrasts with asymmetrical, westerly-dipping, extensional microshears displayed in unfolded, mica and chlorite-rich portions of the matrix, which offset consistently to the NW (Figure 5.6f). Immediately adjacent to these shear bands, quartz grains display a distinct reduction in grain size and a concomitant increase in intragranular strain (i.e. the development of subgrains, irregular grain boundaries, deformation bands and undulose extinction). Evidence of this low temperature plasticity displayed by both the kink bands and shear bands, suggests that they formed contemporaneously. It is inferred that these two structures accommodated sub-horizontal, NW-SE directed shortening and shear across the anisotropic, foliated metamorphic units during the same chlorite-grade, deformational event (Figure 5.7). A 'stick-slip' model is envisaged, whereby kink bands accommodated layer-parallel shortening, whilst shear bands were consequences of foliation-parallel shear (Figure 5.7a and b; *cf.* Williams, 1987). In this model, differential motion (slip-rates) along planar anistropies (e.g. foliations) causes variations in shear strain to develop. Adjacent to regions of relatively slow strain rate (or 'stick'), zones of relative compression (kink bands) and tension (shear bands) are expected to form. The formation of top-to-the-SE kink bands and folds and top-to-the-NW shear bands in the Ayia Varvara Formation is interpreted as resulting from regional, sub-horizontal, NW-SE oriented shortening acting across pre-existing, southeasterly-dipping foliations (Figure 5.7c).

(a)

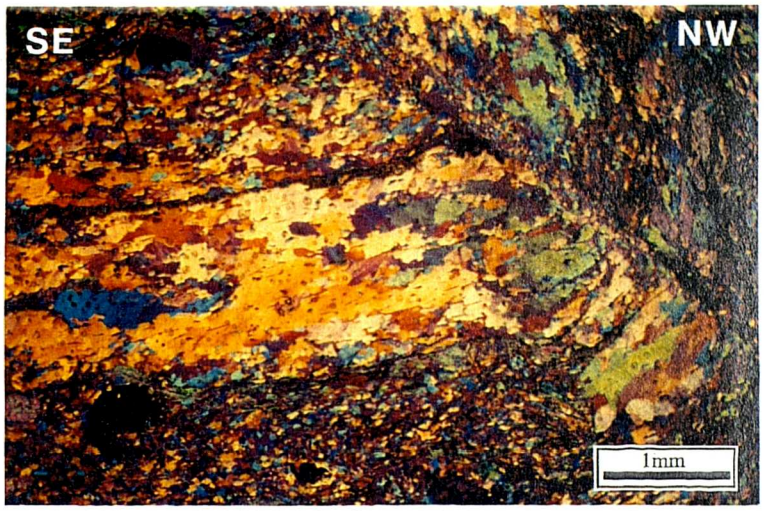

(b)

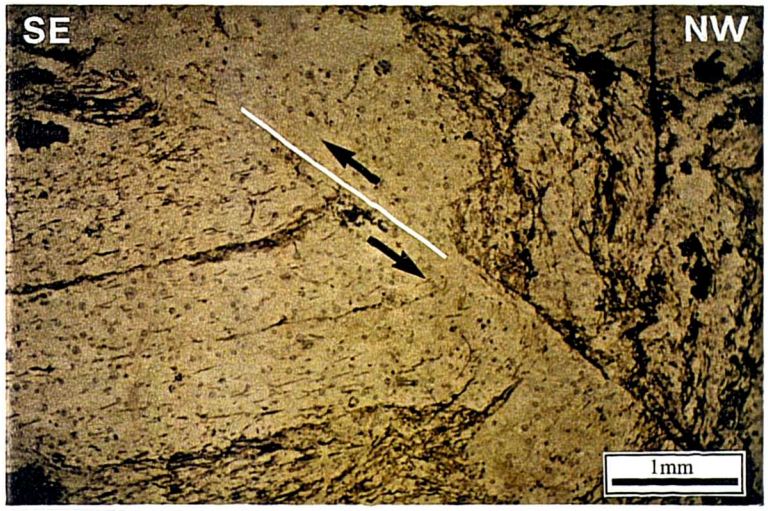

(c)

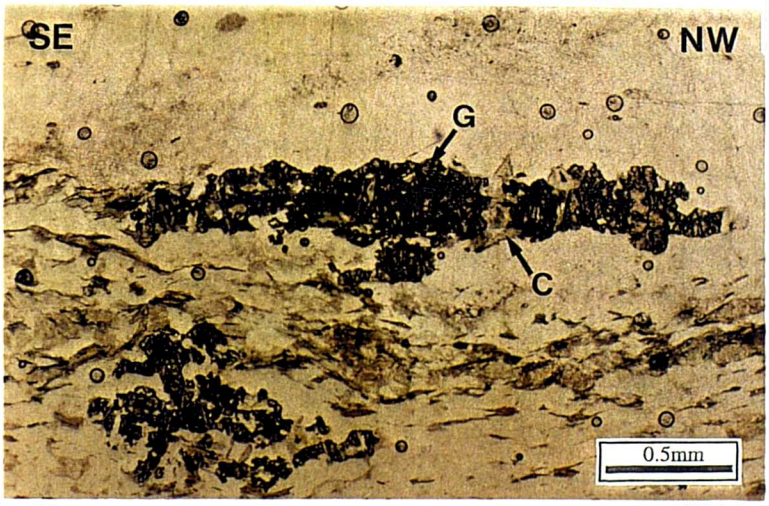

Figure 5.6. Photomicrographs taken from a metasedimentary sample containing an 'S' fold (Sample AK28/I/95). (a) Cross-polars and sensitive tint plate addition; shows the strong crystallographic-preferred orientations of the coarse, stretched quartz grains, indicated by the dominant orange colouration. Note the breakdown of this crystallographic fabric and the recrystallisation of quartz grains into the northwesterly-dipping kink band (b) Detail of the folded foliation and reverse, top-to-the-SE, offset along a kink band. (c) Stretched garnet porphyroclast (G) replaced by chlorite (C) in a pull apart. Clear regions are quartz, brown minerals are biotite.

(d)

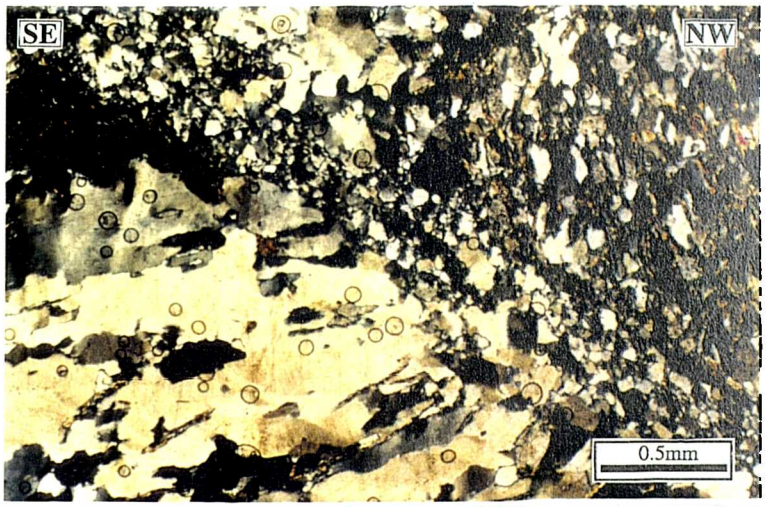

(e)

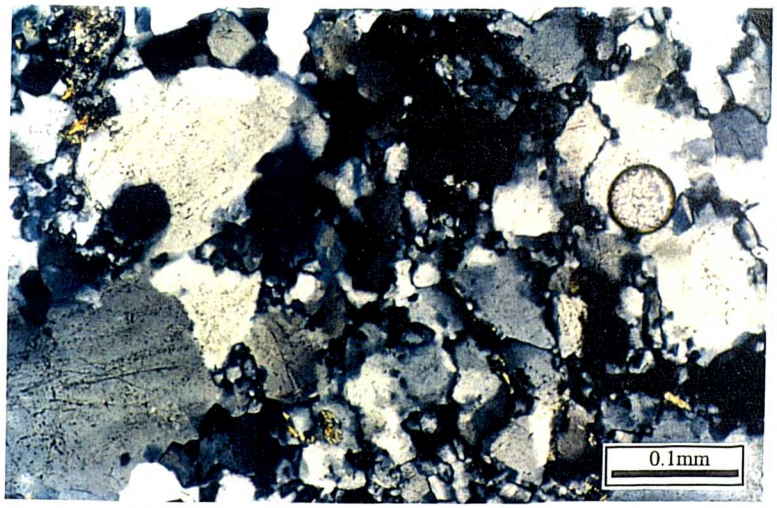

(f)

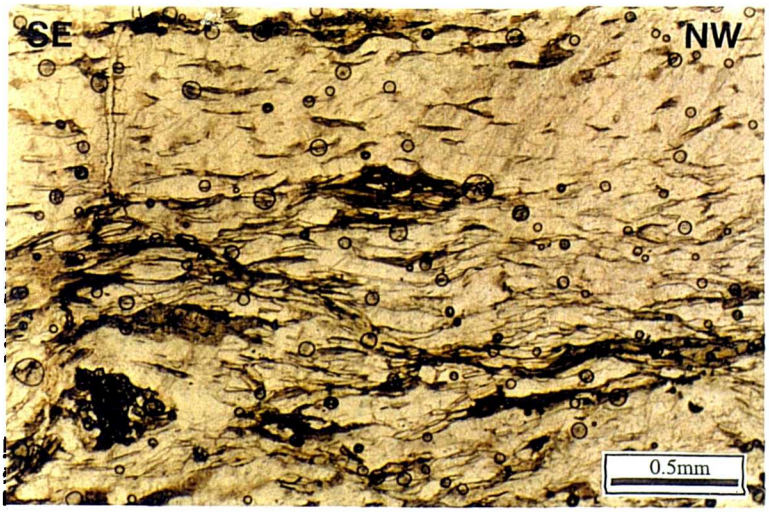

Figure 5.6. (continued). (d) Intense grain-size reduction along a kink band (Cross polars). (e) Detail of recrystallisation within a kink band. Note the presence of subgrains and irregular grain boundaries (cross polars). (f) Asymmetrical, top-to-the-NW, extensional shears along mica-rich domains of the foliation.

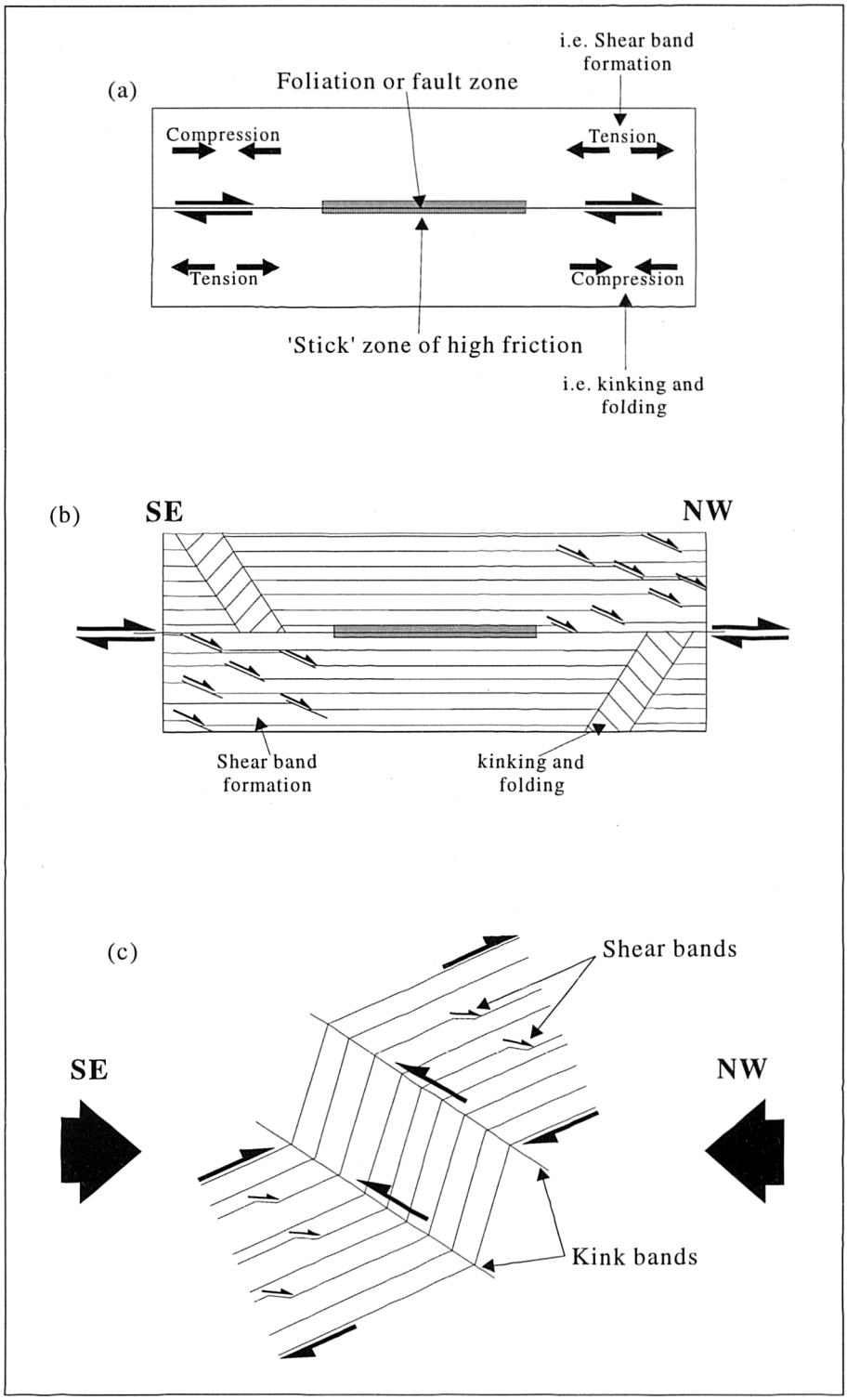

Figure 5.7. (a) Stick-slip model demonstrating how compressional and extensional structures can develop on opposite sides of a 'stick' zone of high friction (shaded) (adapted from Williams, 1987). (b) Shows the model in (a) adapted to the structures observed at Loutra tis Aphroditis. Top-to-the-SE kink bands and folds develop in zones in zones of compression, whilst top-to-the-NW shear bands form within zones of tension. (c) Summary of the structures observed at Loutra tis Aphroditis. Regional, sub-horizontal, NW-SE shortening, acting across an inclined, southeasterly-dipping foliation results in the formation of top-to-SE kink bands and folds and top-to-the-NW shear bands.

5.2.2b Late extensional faulting

Foliations and compositional banding within the metasediments and metabasites are often extensionally offset by steep to sub-vertical brittle faults (cm- to m-scale), which strike N-S to NE-SW (Figure 5.8). These faults locally disrupt kink folds, which indicates that fracturing occurred during a relatively late event. The presence of epidote and carbonate along these fractures suggests that they formed at low temperatures. The identification of late extensional faults that trend N-S to NE-SW is significant as a large number of unexposed tectonic contacts in this area, and also throughout the Northern Region, exhibit these orientations, implying that they may be related.

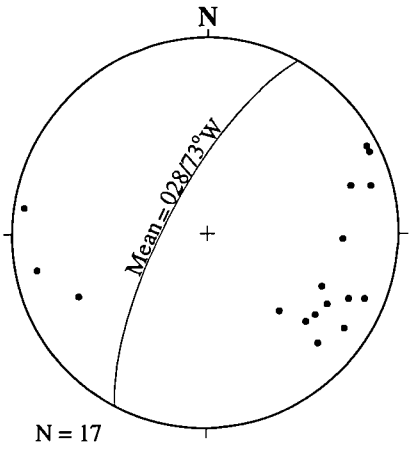

Figure 5.8. Stereographic projection showing poles to brittle extensional fractures in the Ayia Varvara Formation. Great circle represents the average orientation of fractures.

5.2.3. Clinopyroxene-harzburgite tectonite (GR 404 799)

The contact between the Ayia Varvara Formation and harzburgite (see below) (GR 404 798) is marked by a 5m wide, N-S striking, sub-vertical, olive-green coloured serpentinite fault zone. The heavily serpentinised fault gouge, which characterises this zone, displays metre-scale, sub-vertical sinistral faults with associated strike-slip carbonate and serpentine slickenfibres (Figure 5.9). However, rare carbonate fibres exhibit large pitch angles, documenting dip-slip displacements. These serpentinised fault rocks are only ever observed along tectonic contacts that bound peridotites, therefore they are thought to be derived by the hydration and deformation of the adjacent peridotitic units. The dominance of lizardite serpentine within the fault gouge infers that temperatures were low during deformation. These interpretations, combined with the observation that N-S to NE-SW trending faults cross-cut and offset all structures within this area, suggest that these fault zones are late sinistral/extensional structures.

Figure 5.9. Plan view onto sinistral faults in serpentinite fault gouge that marks the tectonic contact between the Ayia Varvara Formation and harzburgite tectonite at GR 404 798. Note that carbonate (white to light coloured) marks the shear surfaces.

The harzburgitic unit to the NW of this contact possesses a strong planar, steep to sub-vertical, S-tectonite fabric that is distinguishable at outcrop (Figure 5.10a). Foliation planes are defined by variably flattened and elongate pyroxene porphyroclasts (~0.5mm long) and by their mm-wide, recrystallised tails, which can be traced for many centimetres. This foliation has a mean trend of 045/76°SE, which parallels the strike of foliation and axial planes from the adjacent Ayia Varvara Formation (stereonet (g); Figure 5.2). In hand specimen, these rocks occasionally display a weak, strike-parallel, stretching lineation, which is defined by fine-grained tails to pyroxene porphyroclasts. Unfortunately, as these tails are typically situated symmetrically on either side of the parent porphyroclast, no consistent shear sense criteria can be determined at outcrop.

In thin section, these deformational peridotite fabrics display a recrystallised, anhydrous, syn-kinematic assemblage of olivine-orthopyroxene-clinopyroxene-spinel and they may be texturally described as porphyroclastic (Figure 5.10b; *cf.* Boullier and Nicolas, 1975; Mercier and Nicolas, 1975; Harte, 1977). The foliation that is observed at outcrop is defined by bands of pyroxene and olivine neoblasts and occasionally by stretched orthopyroxene porphyroclasts (Figure 5.10b). Pyroxene grains exhibit variable degrees of recrystallisation, reaching a minimum neoblast grain-size of 0.05mm. Olivine grains, which are heavily altered by subsequent serpentinisation, display minor elongations where preserved. Spinel is commonly altered to ferrit-chromite, but where alteration is minor, they possess a characteristic orange colour, which suggests that these rocks are related to the Mamonia Complex. This association is supported by the relatively low Cr# and high Mg# chemistries of the spinels (see

Chapter 3; samples AK24; AK27). Spinels are commonly associated with pyroxene grains (porphyroclasts and neoblasts), where they display characteristic 'holly-leaf' morphologies. This relationship may be used to infer an upper mantle origin for these peridotites (Mercier and Nicolas, 1975; see Chapter 1), which is supported by the presence of the tectonite fabric (e.g. Bonatti and Hamlyn, 1981).

These rocks are comparable to the peridotite mylonites previously described from the Southern Region, which also crop out adjacent to the Ayia Varvara Formation. However, the Loutra tis Aphroditis textures differ significantly in that they are much coarser, evidently less deformed and do not contain amphibole. The similarity and possible genetic relationship between these two peridotite deformation fabrics is discussed in section 5.2.9a and further in Chapter 6.

(a)

(b)

Figure 5.10. Details of clinopyroxene-bearing harzburgite tectonite. (a) Block displaying the sub-vertical foliation defined by fine-grained recrystallised tails to pyroxene porphyroclasts (light coloured 'strings'). (b) Photomicrograph of a characteristic peridotite cataclastic texture. Note the presence of fine-grained recrystallised pyroxenes (high birefringent minerals) preserved adjacent to the flattened orthopyroxene porphyroclast (OPX). The bulk of the low birefringent matrix is mostly post-kinematic lizardite serpentine.

5.2.4. Loutra tis Aphroditis Formation (GR 404 799)

The contact between harzburgite and Loutra tis Aphroditis sediments is again marked by variably foliated serpentinite cataclasite and gouge fault rocks. The fault zone and the foliation, defined by aligned serpentine (lizardite?) minerals, dips sub-vertically and strikes NE-SW. No pervasive structures are observed in this unit, and thus displacements along it are unresolvable. However, as these fault rocks are texturally and mineralogically analogous to those observed at the contact to the SE, which is described above, it is interpreted as a relatively late structure.

The sediments in this package are tentatively ascribed to the Loutra tis Aphroditis Formation due to similarities at outcrop, with those observed at the southeastern end of the section. This unit contains isolated outcrops of massive, white carbonate breccia and interbedded red shales and siltstones. The latter of the two displays the same sub-vertical, undulating beds as those observed to the SE of the section. Due to the poor exposure within this part of the section, the significance of these sediments is uncertain. However, as there is little evidence to suggest that these units have been metamorphosed, and they are situated between relatively high temperature peridotite tectonite and metamorphic units (see below), it is most likely that they have been emplaced into their present position along late faults, i.e. subsequent to metamorphism.

5.2.5. Amphibole-epidote-carbonate rocks (GR 403 800)

Fine-grained, green metamorphic rocks crop out to the NW of a high-angle faulted contact with the Loutra tis Aphroditis Formation. Unfortunately, this contact is poorly exposed and no kinematic information is preserved. At outcrop, these rocks possess a mineral lineation and a rough sub-vertical foliation. The mineral lineation, which is relatively constant with a mean orientation of 25/287 (Stereonet (c); Figure 5.2), is defined by the alignment of mm-long, dark green laths of amphibole. In thin section, the fabric is heavily altered and dominated by randomly oriented, colourless, fine-grained fibrous minerals. The exact composition of these fibrous minerals is uncertain, but petrographic observations suggest those that possess second order birefringence colours are amphibole (tremolite?) and/or wollastinite, whilst those that display first order colours may be serpentine (possibly antigorite). However, due to the fine grain sizes and the degree of alteration, the presence of chlorite and/or talc cannot be discounted. The mineral lineation observed in hand specimen is seen in thin section as elongate aggregates of fibrous amphibole, which exhibit lath-shaped outlines, suggesting that they are pseudomorphs after a pre-existing phase (amphibole or

clinopyroxene?). Epidote, carbonate and minor quartz are also present in significant amounts, both as vein minerals and aggregates distributed throughout the matrix. The presence of these minerals is attributed, at least in part, to calcic metasomatism associated with the emplacement and serpentinisation of the adjacent ultramafic unit. Due to their calcic and magnesian chemistry (i.e. tremolite, $\underline{Ca}_2(\underline{Mg}, Fe^{2+})_5(Si_8O_{22})(OH)_2$; wollastinite, $\underline{Ca}SiO_3$; serpentine, $\underline{Mg}_3(Si_2O_5)(OH)_4$), these metamorphic rocks may have been derived from a clinopyroxene-bearing ultramafic or mafic protolith.

5.2.6. Amphibole-carbonate-epidote unit - clinopyroxene-harzburgite tectonite contact (GR 403 800)

To the NW, the amphibole-carbonate-epidote rocks are in contact with a large body of harzburgite tectonite along a low-angle tectonic contact that dips to the SE (stereonet (f); Figure 5.2). The fault zone is characterised by highly foliated, carbonate-rich cataclasite and gouge that display dip-slip carbonate and serpentine fibres and striae that plunge to the SE. Kinematic indicators within this zone are rare, but deflections of fibres into shear planes suggest top-to-the-NW thrusting. To the NW, in the footwall to this thrust, harzburgite displays an identical steeply dipping foliation to that observed in the harzburgite tectonites to the SE. This fabric is cross-cut by low angle, thrust-related serpentinite fabrics, which indicates thrusting post-dated the fabric-forming event in the peridotites, and also by copious randomly-oriented, tensile serpentinite veins. The intensity of veining and the degree of serpentinisation decreases with increasing distance away from the contact, which suggests that fluid flux was concentrated along the contact and that the footwall was subjected to an unspecified amount of overburden.

5.2.7. Clinopyroxene-harzburgite tectonite - Dunite/wehrlite contact (GR 391 810)

The transition between harzburgite tectonites to the SE and dunites and wehrlites to the NW is constrained to a 5m-wide zone. The exact contact is difficult to pin-point, but cm-wide foliation planes within this zone, which are characterised by carbonate mineralisation, suggest that this contact is tectonic. These foliations strike ENE-WSW and dip shallowly to the SE, which approximately parallels the thrust contacts located to the NW and SE, implying that these three contacts may be related (i.e. as imbricate thrusts). Rare carbonate lineations on these planes plunge variably to the south, but no

corresponding shear sense criteria are observed and therefore, thrust displacement can only be inferred.

At outcrop, wehrlites and dunites are distinguishable from clinopyroxene-bearing harzburgite tectonites on petrological grounds and by their lack of evidence for high temperature deformation. Wehrlites contain a distinctly higher ratio of pyroxene to olivine grains than the harzburgites, with clinopyroxene comprising up to 50% or more of the rock volume. These clinopyroxene grains vary considerably in size (<1mm to >1cm in diameter), and also in orientation, displaying a relatively random fabric. The dunites are readily identified as they do not contain any pyroxenes. They are relatively fine-grained, olive-green coloured rocks, which crop out as massive, structureless units. Unfortunately, due to serpentinisation their contact relationship with the wehrlites is undetermined. In hand specimen, the dunites are relatively pristine, with sub-mm-scale, glassy green olivine grains preserved. When observed in thin section, spinels in the wehrlites and dunites are commonly altered to ferrit chromite. However, where they are preserved, spinels in the wehrlites exhibit a characteristic blood-red colouration, whilst those in the dunites are dark, which contrasts with the orange colouration of the spinels in the harzburgite tectonite. The chemistry of these spinels is also distinct; those in the wehrlites and dunites display high Cr#, whilst those in the harzburgites possess low Cr# values, which suggests that the former are related to the Troodos Complex, whereas the harzburgites are associated with the Mamonia Complex (see Chapter 3). Spinels in the wehrlites are generally coarse and display equant to sub-equant habits (Figure 5.11a), whereas spinels in dunite are equant, very abundant and commonly located at junctions between olivine grains (Figure 5.11b). These textural observations, combined with the lack of a high temperature, tectonite fabric, suggests that this package of wehrlite and dunite may be of crustal origin, which contrasts with the hypothesised mantle derivation for the harzburgites. Therefore, based on geochemical, structural and textural grounds, the tectonic boundary between the Mamonia and Troodos Complexes is constrained to the contact between the tectonite harzburgites and the wehrlite/dunite package at GR 391 810 (see section 5.2.9).

5.2.8. Dunite and Wehrlite - Troodos mafic intrusive rocks and pillow lava contact (GR 390 810)

The wehrlite/dunite unit and Troodos mafic material are juxtaposed along a carbonate-rich fault zone that strikes NNE-SSW and dips to the E (mean 015/40°E; stereonet (e); Figure 5.2). On either side of the contact, serpentinite and Troodos mafic rocks are intensely brecciated and foliated, forming cataclasite fault rocks. The presence of a

(a)

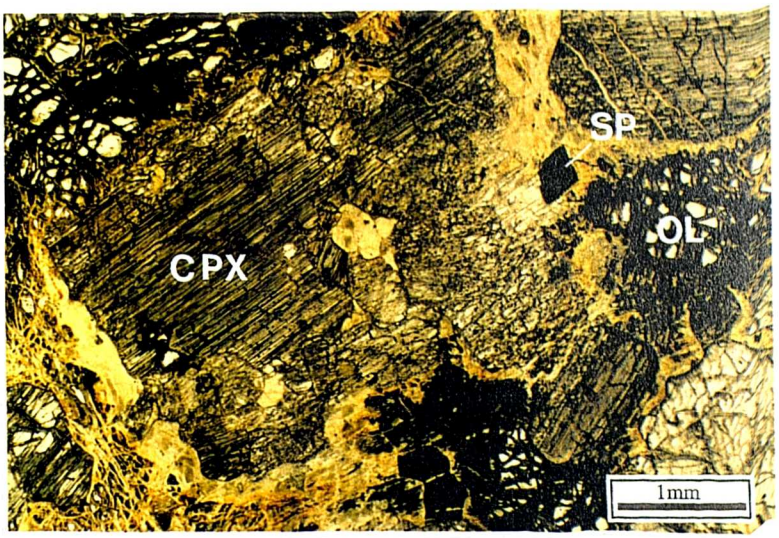

(b)

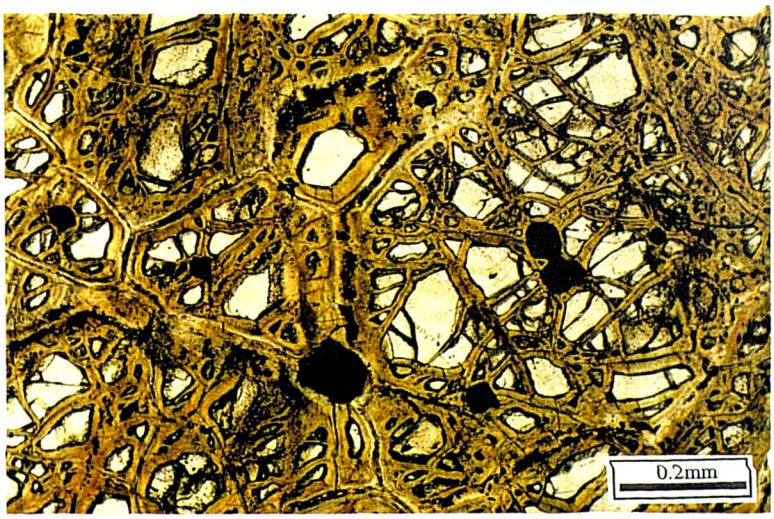

Figure 5.11. Peridotite textures observed at the northwestern end of the Loutra tis Aphroditis coastal section. (a) Wehrlite; coarse, randomly oriented clinopyroxene (CPX) and partially serpentinised olivine (OL). Note the euhedral habit of spinel (SP) (plane polarised light). (b) Dunite; equant spinel grains at junctions between partially serpentinised olivine (black = spinel; white = olivine; brown rims to olivine = serpentine; plane polarised light).

contorted, anastomosing foliation in these rocks, which parallels the contact and is defined by layers of fine-grained, comminuted material, suggest that they accommodated macroscopically ductile deformation. Foliation planes are commonly carbonate mineralised, and possess fibres and striae that dominantly plunge down dip to the east. Offsets along shear bands, with corresponding dip-slip westerly-plunging lineations (mean 25/279; stereonet (a); Figure 5.2), indicate westerly-directed thrust transport. The Troodos mafic rocks in the footwall are intensely disrupted and cross-cut by low angle thrust faults that parallel the contact. Within 20m of the contact, foliated, heavily weathered Troodos pillow lavas are identifiable. With increasing distance away from the contact, the degree of deformation decreases and intercalated

Troodos lavas and cross-cutting dykes are preserved, but no way up criteria have been determined.

5.2.9. Summary

The coastal section exposed at Loutra tis Aphroditis preserves evidence of the juxtaposition of different units with variable tectono-metamorphic histories. In all, three distinct tectonic events are identified, which include: (1) an early, high temperature event (>600°C), which involved the deformation of peridotite tectonites and the synkinematic metamorphism of the Ayia Varvara Formation (event 1 in Figure 5.12); (2) W to NW-directed thrusting of Mamonia and Troodos Complex rocks (Event 2 in Figure 5.12), and; (3) late brittle extensional/sinistral faulting along N-S to NE-SW striking faults (Event 3 in Figure 5.12).

5.2.9a. High temperature deformation (Event 1 in Figfure 5.12)

The high temperature, ductile fabrics observed in the harzburgite-tectonites and the amphibolite-facies Ayia Varvara Formation rocks clearly constitute evidence of the earliest deformational event(s) at Loutra tis Aphroditis and, more significantly, in the Northern Region. The parallelism between the strike of the foliations and the orientations of the strike-parallel stretching lineations in both of these units, suggests that they are genetically related in a manner that links the *dextral* peridotite mylonites and the metamorphic rocks in the Southern Region (see Chapter 4). Unfortunately, at Loutra tis Aphroditis, no kinematic indicators have been found that relate to the strike-parallel stretching lineation. However, due to the intensity of this lineation, particularly within the Ayia Varvara Formation, and by analogy with the high temperature rocks of the Southern Region, the bulk deformation is inferred to be strike-slip.

Based on textural similarity with examples in the literature, the porphyroclastic harzburgite tectonites are thought to have been deformed at temperatures in the region of 800-1000°C (Nicolas *et al.* 1980; Girardeau and Mercier, 1988). The ubiquity of post-kinematic serpentinisation of olivine negates the possibility of estimating the stress state and temperatures during deformation, as was undertaken with the peridotite mylonites of the Southern Region. However, the Loutra tis Aphroditis tectonite fabrics display a coarser grain-size than the Southern Region mylonites, which suggests that they formed at lower stresses and higher temperatures (i.e. >800°C; see Chapter 4).

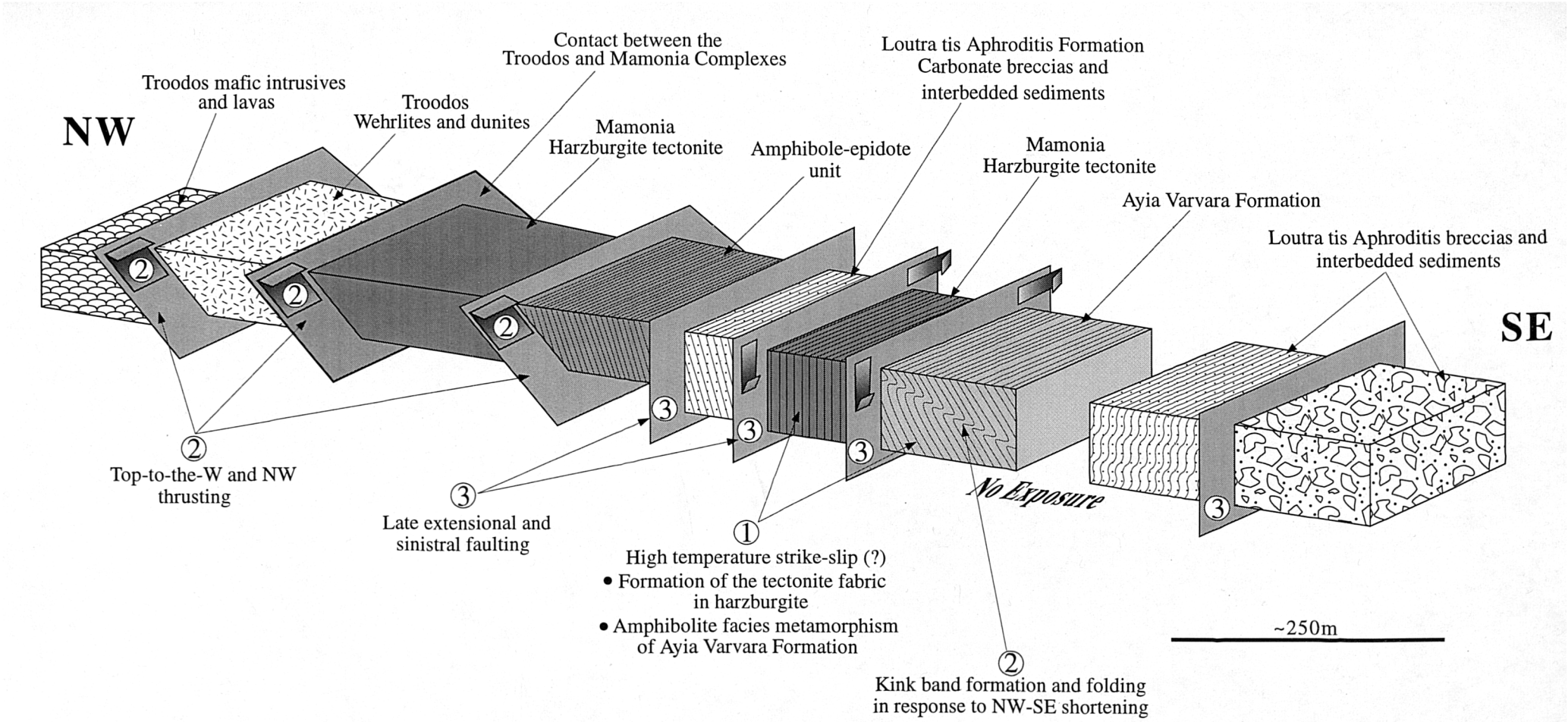

Figure 5.12. Schematic three-dimensional block diagram summarising the three main phases of deformation preserved at Loutra tis Aphroditis. The circled numbers indicate the relative ages of each event, i.e. the earliest event is 1, whilst the youngest is 3.

On the basis of mineral chemistry, previous workers (Spray and Roddick, 1981; Malpas *et al.* 1992) proposed that the peak temperature during metamorphism of the Ayia Varvara Formation throughout SW Cyprus, including Loutra tis Aphroditis, was in the region of 600°C. The obvious discrepancy between the inferred temperatures of the harzburgite tectonites and metamorphics is similar to that described in Chapter 4 for the peridotite mylonites and metamorphics in the Southern Region. The discussion raised in Chapter 4, concerning the relationship between the peridotite mylonites and the Ayia Varvara Formation is also relevant here. The difference in temperatures may be used as evidence to suggest that these two units are not genetically related. On the other hand, the heat required for the metamorphism of the Ayia Varvara Formation may have been supplied by the ambient temperature of the harzburgite tectonite. Based on a simple geothermal model of a ridge-ridge transform system, Spray and Roddick (1981) suggested that fresh igneous material at 1000°C could cause the metamorphism of the Ayia Varvara Formation at 600°C. The temperatures estimated for the peridotite mylonites in the Southern Region (600-800°C) suggest that they are too low to have caused the metamorphism alone. However, the higher temperature of the harzburgite tectonites at Loutra tis Aphroditis (~1000°C) could have caused amphibolite facies metamorphism.

An alternative hypothesis is that the heat required for metamorphism may have been supplied by the newly formed Troodos crust. Ar/Ar dating of hornblende separates from the metamorphic rocks at Loutra tis Aphroditis suggest that amphibolite facies metamorphism occurred between 83-90Ma, which is coincident with *the age of the formation of the Troodos Complex (92-90Ma; e.g.* Mukasa and Ludden, 1987). This latter model is favoured for the formation of the Ayia Varvara metamorphic rocks and peridotite mylonites in the Southern Region, due to an inferred increase in temperature during the development of amphibole-bearing mylonites (see Chapter 4). However, the peridotite tectonites at Loutra tis Aphroditis neither contain amphibole nor do they record an increase in temperature during their development. These observations, combined with their inferred high temperature (~1000°C) favours the idea that metamorphism at Loutra tis Aphroditis was primarily caused by the ambient temperature of the harzburgite tectonite.

In summary, the parallelism between the fabrics in the harzburgite tectonites and metamorphic rocks at Loutra tis Aphroditis, suggests that they formed during a phase of (strike-slip) deformation at approximately 83-90Ma (Spray and Roddick, 1981). The relevance of these fabrics and their possible association with analogous rocks observed in the Southern Region is discussed in greater detail in Chapter 6. Unfortunately, further evidence of this deformational phase is severely lacking in the

Northern Region due to the combined effects of subsequent serpentinisation and thrusting at lower temperatures (see below).

5.2.9b. Westerly-directed thrusting (Event 2 in Figure 5.12)

Structures preserved within the Ayia Varvara Formation and along tectonic contacts at the northwestern end of the section, suggest that a phase of broadly E-W compression resulted in westerly-directed thrusting, which juxtaposed both Mamonia and Troodos Complex rocks. Folding, kinking and shear band development within the Ayia Varvara Formation metamorphic rocks are interpreted to have reactivated the pre-existing amphibolite facies foliation at lower temperatures during E-W to NW-SE oriented compression. Kinematic analyses suggest that the metamorphic bodies accommodated this regional deformation by coeval top-to-the-SE shortening along northeasterly-verging folds and northwesterly-dipping (reverse-slip) kink bands, and top-to-the-NW foliation-parallel shear (thrusting) along asymmetrical shear bands. The conditions during deformation are difficult to constrain using the syn-kinematic assemblage of quartz + chlorite + white mica ± biotite. For example, chlorite may form over a wide range of metamorphic conditions in pelitic rocks, from those that develop during diagenesis at relatively low temperatures to others that are stable in high grade rocks bearing sillimanite, kyanite, andalusite and cordierite (Laird, 1988). However, textural observations suggest that these structures formed at lower temperatures than the amphibolite-facies protolith (i.e. at lower greenschist-facies).

At the northwestern end of the section, a number of units (namely, Troodos mafic rocks (dykes and lavas), ultramafic (crustal) rocks of inferred Troodos origin, Mamonia harzburgite tectonites (mantle-derived), and amphibole-carbonate-epidote metamorphic rocks) are juxtaposed across a series of sub-parallel easterly-dipping faulted contacts. The presence of dip-slip fibre lineations and brittle striae combined with top-to the-W and NW shear sense criteria along these contacts, suggest that these units were juxtaposed during west to northwesterly-directed thrusting (Figure 5.13). The dominance of lizardite serpentinite in the carbonate-rich fault rocks along these contacts implies that thrusting took place at relatively low temperatures.

Whether NW-SE shortening of the metamorphic bodies is related to the westerly-directed thrusting is difficult to ascertain. However, the similarity in the orientation of principal compression and directions of tectonic transport suggests that they may be associated. On the other hand, the lack of evidence to constrain the syn-kinematic temperature(s) poses a significant problem. For example, the chlorite-bearing fabrics in the metamorphics may have formed at higher temperatures than the thrust-related, serpentinite-carbonate fault rocks. Furthermore, the absence of primary

contacts bounding the Ayia Varvara Formation units (i.e. they are bound by *later* sinistral/extensional faults) prevents a complete kinematic interpretation of the section.

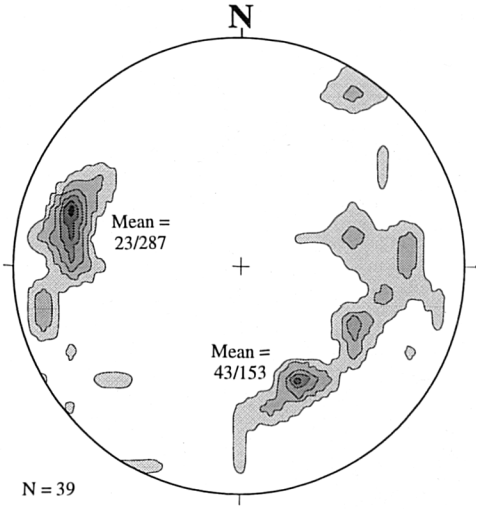

Figure 5.13. Summary top-to-the-NW thrust lineations from Loutra tis Aphroditis.

5.2.9c. Late faulting (Event 3 in Figure 5.12)

Steep to sub-vertically-dipping brittle faults, trending N-S to NE-SW, which cross-cut and bound individual units, are observed throughout the section. Late brittle extensional faulting is particularly evident within the Ayia Varvara Formation due to offsets of pre-existing compositional banding and fold structures that are interpreted to have formed during westerly-directed thrusting. Serpentinite gouge fabrics, which commonly mark tectonic contacts to the harzburgite tectonite units, document extensional *and* sinistral strike-slip displacements. The existence of both strike-slip and dip-slip mineral fibres and brittle striae along late faults may be explained by reactivation of pre-existing strike-slip faults during extension, or vice versa. The consistency in the strike and brittle style of deformation along many contacts, suggests that the juxtaposition of at least some of the units exposed along the section was accommodated by late extensional and/or strike-slip faulting. This is supported by the observation that high temperature rocks (i.e. the Ayia Varvara Formation amphibolites and harzburgite tectonites) are juxtaposed against Loutra tis Aphroditis Formation units, which do not display evidence for metamorphism. The presence of late, N-S trending faulting is observed throughout the Northern Region (see below), which, along the Loutra tis Aphroditis section appears to have resulted in at least some structural reorganisation.

5.3. The Akamas Area

The geology exposed in the Akamas Forest, from latitude 730 to 810, is characterised by N-S structural trends and predominantly low angle tectonic contacts. From east to west, the thrust stack comprises, from base to top, Troodos Complex-serpentinite-Mamonia Complex. Mamonia Complex-serpentinite contacts are poorly exposed and obscured by post-tectonic Miocene sedimentary cover. In contrast, serpentinite-Troodos Complex contacts are better exposed, and locally, the strike of these contacts and their associated structural fabric deviates substantially from the normally observed N-S orientation. These geometrical complexities are attributed to the effects of thrust tectonic processes interacting with an irregular, pre-existing fault zone architecture. The localities referred to in this section are shown in Figure 5.14.

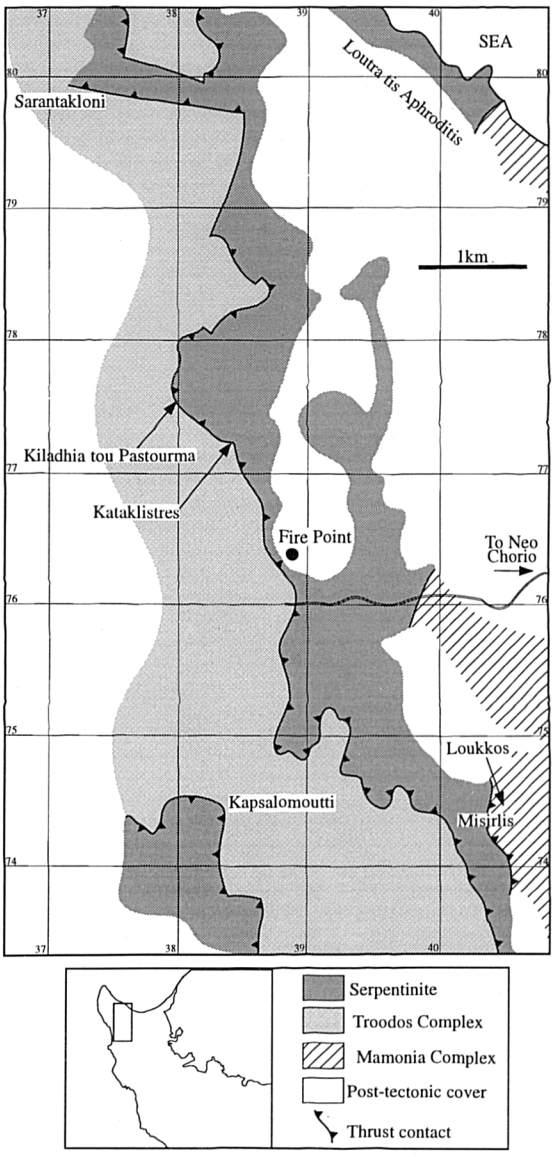

Figure 5.14. Location and geological map of the Akamas area. Adapted from the 1992 map of the Akamas-Poli area, published by the Cyprus Geological survey.

5.3.1. Mamonia Complex-serpentinite contacts

Exposure of the contact between serpentinite and the Mamonia Complex in the Akamas Forest is poor. However, in the vicinity of Misirlis (GR 403 744) and NW of Loukkos (GR 406 745), sporadic outcrops of Mamonia Complex sediments and serpentinised fault rocks preserve evidence of the juxtaposition of these two units. At Misirlis, Mavrokolymbos Formation sediments overlie serpentinite at a N-S striking, easterly-dipping (average 42°E) faulted contact. The contact zone, which is exposed for approximately 20-30m, is identified by sporadic, metre-high outcrops of extremely hard, light-blue/green serpentinite fault rock. This fault rock displays predominantly dip-slip stretching lineations (brittle striae and serpentine fibres) and is transected by cm- to ten cm-scale asymmetrical brittle faults, which indicate a top-to-the-west, thrust sense of shear, placing the Mamonia Complex over serpentinite (Figure 5.15a and b). At outcrop, these brittle faults are readily identified as they bound cm-wide layers of light coloured fibrous serpentine, which define a contorted, ductile fabric that anastomoses around rounded serpentinite clasts (1cm to sub-mm-scale). Asymmetrical extensional shear bands (mm-scale) within these layers indicate a synthetic, top-to-the-W sense of shear to the larger, bounding brittle faults, inferring mm-scale ductile flow is contemporaneous with macroscopic brittle faulting. Most distinctive of these layers is the preponderance of mm- to cm-scale 'holes', which exhibit rounded to elongate geometries (Figure 5.15b). It can be clearly demonstrated in hand specimen that these holes are formed by the dissolution of rounded serpentinite clasts. Variably altered clasts exist, from those that are relatively pristine to others that are totally 'dissolved'. The localisation of dissolution to the layers bound by brittle faults, suggests that fluid flux was concentrated preferentially through these zones. The relative timing of dissolution, fluid flux and deformation is difficult to resolve, but the presence of tensile chrysotile veins, which cross-cut, and also are cross-cut by, the top-to-the-W faults, suggests that thrusting and fluid flow were coeval.

NW of Loukkos (Figure 5.14), both the Mavrokolymbos Formation and Vlambouros Formation sandstones are exposed (GR 404 747). Within the Vlambouros Formation, located to the east of the unexposed contact, graded bedding and sole structures indicate that the beds are overturned. On bedding planes, quartz grains are slightly elongate, which defines a weak stretching lineation that plunges shallowly to the west. To the SW, interbedded mudstones, cherts and sandstones of the Mavrokolymbos Formation are folded on a metre-scale. Folds are generally upright and possess tight to isoclinal forms, depending on the competency of the folded units. Fold axes plunge shallowly to the west, while axial planes are predominantly high-angle, dipping to the north and striking ESE (Figure 5.16).

Bedding within both the Vlambouros and Mavrokolymbos units is locally variable due to folding, but generally the mean strike of bedding at this locality is E-W, which parallels the strike of fold axial planes (Figure 5.16). These observations suggest that the local compression direction was oriented N-S, which evidently contrasts with the dominant top-to-the-W thrust tectonism in the region. The relationships between folding and thrusting on a regional scale are discussed in Chapter 6.

(a)

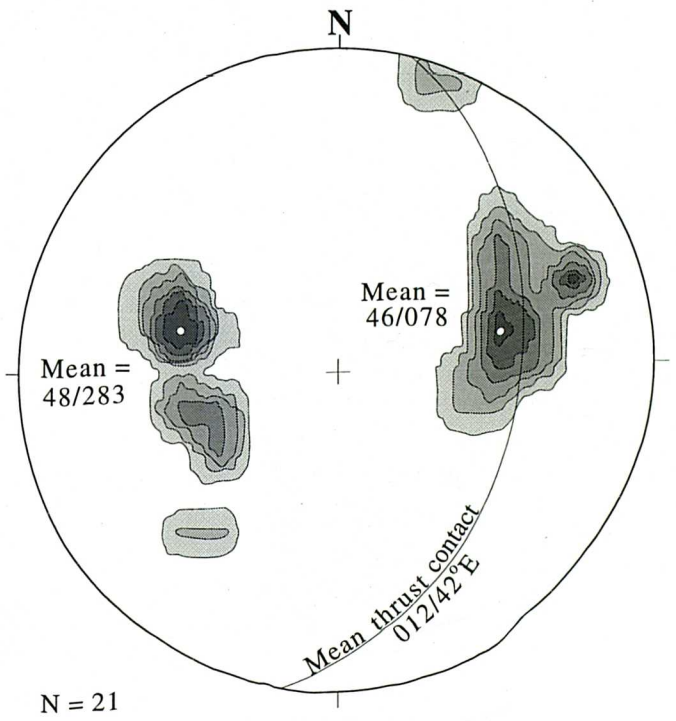

(b)

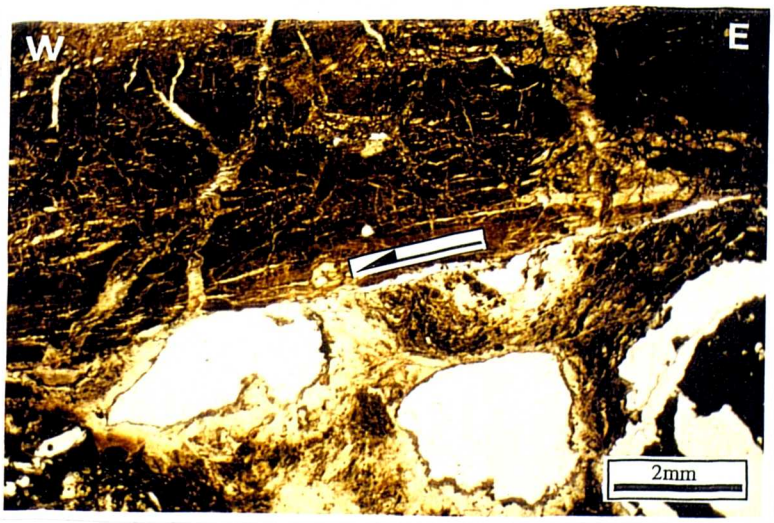

Figure 5.15. Details of the thrust contact at Misirlis. (a) 1% area contour of top-to-the-west stretching lineations (brittle striae and serpentine fibres). Great circle shows the mean orientation of the contact and contact-parallel foliations in the serpentinite. (b) Top-to-the-W, planar asymmetrical brittle fault within the serpentinite fault rock. Note the 'dissolution holes' that are located below the shear plane (Sample AK/6/95).

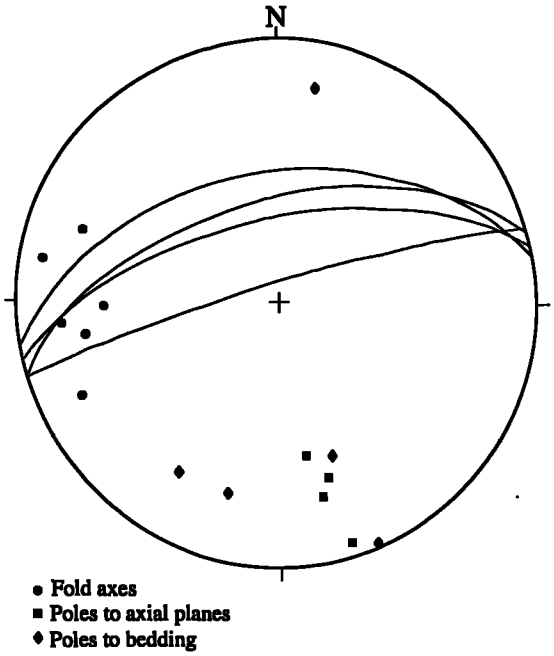

Figure 5.16. Stereographic projection of fold data from the Mavrokolymbos Formation NW of Loukkos. Note fold axial planes are steep to sub-vertical and strike E-W and fold axes plunge shallowly to the W.

5.3.2. Troodos Complex-serpentinite contacts

Throughout the Akamas Forest, variably serpentinised harzburgite bodies structurally overlie Troodos Complex rocks, which comprise tectonically disrupted and brecciated mafic intrusive rocks and lavas. The strike, dip and dip-direction of tectonic contacts between serpentinite and Troodos mafic rocks vary considerably. However, these contacts generally strike N-S, dip to the east and exhibit stretching lineations and structures indicative of westerly-directed thrust transport. The following sub-sections describe the best exposed localities in the Akamas Forest.

5.3.2a Fire point thrust (GR 388 763)

The most pristine section of contact between serpentinitè and the Troodos Complex that is preserved in the Akamas Forest is exposed to the south of the Fire Point at GR 388 763 (Figure 5.14). The contact can be seen from the E-W trending track at GR 390 760, which runs from Neo Chorio 3km to the east. The contact zone comprises an approximately 100m long, N-S trending ridge that reaches 5m in height. The contact, and the associated foliation in the serpentinite hangingwall and the brecciated Troodos mafic footwall, strikes N-S to NE-SW and dips to the east (34° to 60°E) (Figure 5.17). The contact is characterised by a 1-2m wide zone of highly sheared serpentinite fault rock, which contains abundant, mm-wide tensile carbonate veinlets

that parallel the contact and the serpentinite shear fabric (Figure 5.17b). The footwall comprises intensely brecciated mafic fault rocks, which locally exhibit fine-grained (mm-scale clasts) cataclasite fabrics. Stretching lineations along the contact, defined by brittle striae and fibres of carbonate and serpentine, are invariably dip-slip, plunging consistently to the east (mean orientation 39°/085°; Figure 5.17c). Ubiquitous mm- to cm-scale asymmetrical extensional shear bands within the serpentinite fault rock indicate top-to-the-W thrusting of serpentinite over the Troodos Complex. The microstructure of the serpentinite fault rocks typically displays brittle-ductile deformational characteristics, which define a fabric that is ductile on the scale of a hand specimen and larger. These fabrics are characterised by rounded to sub-angular, fractured clasts of serpentinite (generally <1mm in diameter) that are supported in an extremely fine-grained, fibrous serpentine (lizardite-dominated) matrix. Colour banding in this fibrous matrix defines a contorted, sub-mm-scale-spaced, ductile foliation, which is offset along brittle to brittle-ductile asymmetrical extensional shear bands, indicating dominant top-to-the-W sense of shear (Figure 5.17d). However, a significant number of faults are present on the micro-scale that indicate antithetic, top-to-the-E senses of shear (line drawing; Figure 5.17d). Both fault sets are mutually cross-cutting and are therefore interpreted as coeval, but top-to-the-W shear bands clearly dominate on a macroscopic scale as they are more abundant and they display larger offsets. The vast majority of serpentinite fault rocks at the contact are rich in foliation-parallel, tensile carbonate veins, which often constitute up to 50% of the rock volume (Figures 5.17b and e). *In thin section, the orientation of the fibres within these* tensile veins indicate that they opened perpendicular to the shear fabric. Frequently, carbonate veins cross-cut the shear fabric, indicating that much of the veining post-dates thrusting. However, the presence of dip-slip carbonate fibres, which are associated with top-to-the-W shear bands, suggest that at least some of the carbonate fluid flux was synchronous with thrusting. The effects of fluid pressures on shear fracture are discussed in Chapter 6.

Beyond 2m east of the contact, the presence of only partially serpentinised, undeformed harzburgite blocks indicates that the degree of serpentinisation and shear decreases abruptly away from the contact. Furthermore, carbonate veins, which commonly possess vuggy cores, are restricted to the serpentinite fault rock and to the diabase footwall. Veins within the footwall are high-angle to sub-vertical, E-W to ENE-WSW striking, and extend down from the contact along joint planes. These observations suggest deformation and fluid flux were localised during thrusting and that the diabase footwall was subjected to an overburden caused by the weight of the overlying harzburgite/serpentinite thrust sheet.

(a)

(b)

(c)

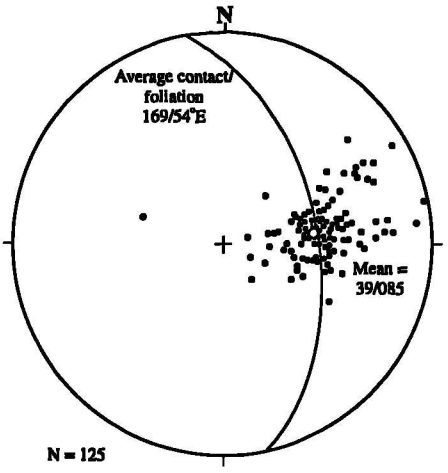

Figure 5.17. Details of the thrust contact below the Fire Point. (a) View looking north along the contact. The light coloured rocks in the hangingwall are serpentinite-carbonate fault rocks, whilst the darker coloured rocks in the footwall, beneath the overhang, are Troodos mafic breccias. The height of the ridge in the foreground is approximately 3m. (b) Close up of the serpentinite fault rock, showing the tensile carbonate veins which accentuate the shear fabric. The pencil parallels dip-slip carbonate fibres. (c) Stereographic projection showing 1% area of fault plane lineations and also the average orientation of the contact and the parallel foliation.

(d)

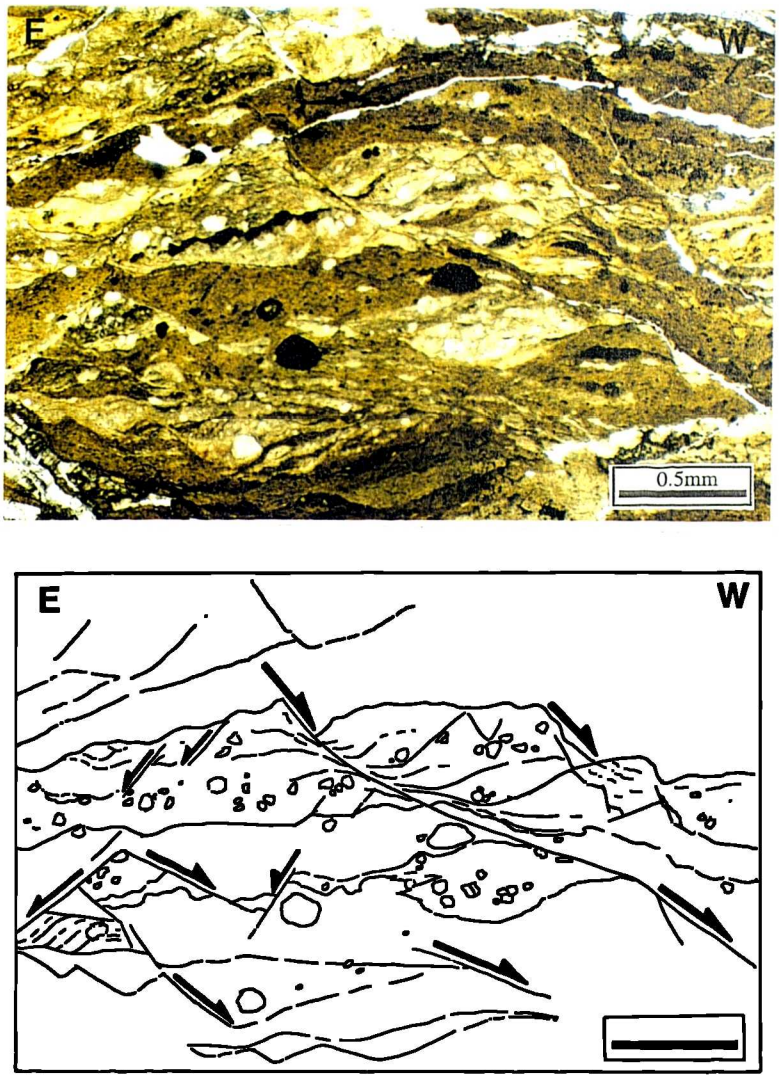

(e)

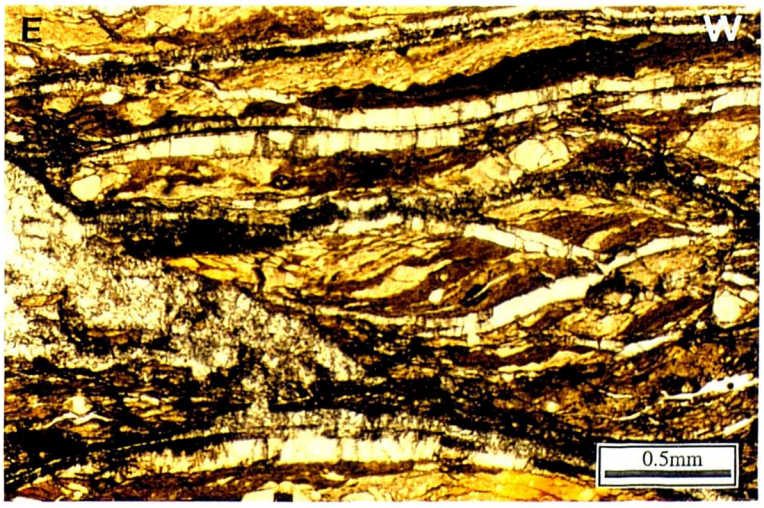

Figure 5.17. (continued) Photomicrographs of the serpentinite fault rock at the contact (Sample AK/3/95). (d) Asymmetrical, top-to-the-W (right) shear bands in the brittle-ductile serpentinite fault rock. Note the presence of minor antithetic, top-to-the-E shear bands (shown in line drawing). (e) Carbonate-rich fault rock, exhibiting abundant carbonate tensile veins (colourless) that parallel the foliation and the top-to-the-W (right) shear band fabric.

5.3.2b *Kapsalomoutti* (GR 388 746)

*To the north and NE of Kapsalomoutti, the contact between diabase and serpentinite is highly irregular (Figures 5.14 and 5.18). Where exposed, the contact between the two units is sharp, planar and carbonate mineralised. Vuggy carbonate veins extend down, perpendicular to the contact with the Troodos footwall, which comprises intensely brecciated mafic rocks. The irregularity of this section is best demonstrated by a NNE to SSW traverse and cross-section, approximately through latitude 749 (Figure 5.18b). The poorly exposed eastern contact, which strikes N-S to NE-SW and dips to the east, displays dip-slip, easterly-plunging brittle slickenlines. The contact to the west also generally strikes N-S, but in contrast here it dips to the west (30° to 53° W) and exhibits westerly-plunging lineations. To the south, the contact swings roughly 90° and trends E-W. Foliations in this part of the section display variable E-W to NE-SW strikes, north to northwesterly dips, and oblique-slip lineations. At the very western part of the contact, the swing to N-S strikes corresponds to a change back to easterly dips. Even though strikes are highly variable and the direction of dip reverses along section, azimuths of slickenlines remain relatively constant, typically plunging shallowly to the W, WNW or ENE (Figure 5.18c). Corresponding asymmetrical shear bands and fractures within serpentinite and brecciated diabase at the contact indicate broadly top-to-the-W tectonic transport (Figure 5.18c). Therefore, the opposing dips observed along this cross-section illustrate the undulating geometry of this contact. The simple cross-section in 5.18b demonstrates this contact displays a 'relief' or 'topography' in the order of 100m. This type of geometry between serpentinite thrust sheets and their footwalls is a relatively common feature of tectonic contacts in the Northern Region at *all* scales. However, the cause for this unusual geometry is not fully understood and any one of the following models is possible:*

- *the thrust contact has been folded or displaced by a series of 'blind' thrusts in the Troodos Complex footwall (Figure 5.19a);*
- *the Troodos footwall possessed a highly irregular, pre-existing, footwall architecture, over which serpentinite was thrust or, alternatively, flowed onto the seafloor subsequent to protrusion (Figure 5.19b; cf. Swarbrick, 1979, 1993).*
- *the contact cuts up and down section in response to locally-induced (i.e. gravitational) body forces. Published studies of the mechanics of thrust wedges suggest that deformation is driven by a combination of forces produced by the plate convergence and those generated within the wedge itself (Figure 5.19c; cf. Platt, 1986; Platt et al. 1989).*

Each of these hypotheses are equally viable, but unfortunately no conclusive field evidence has been found in the Akamas Forest to constrain a definitive model.

However, more detailed studies are presented in Section 5.4, which are used as evidence to suggest that thrusting in the Northern Region was largely affected by local body forces.

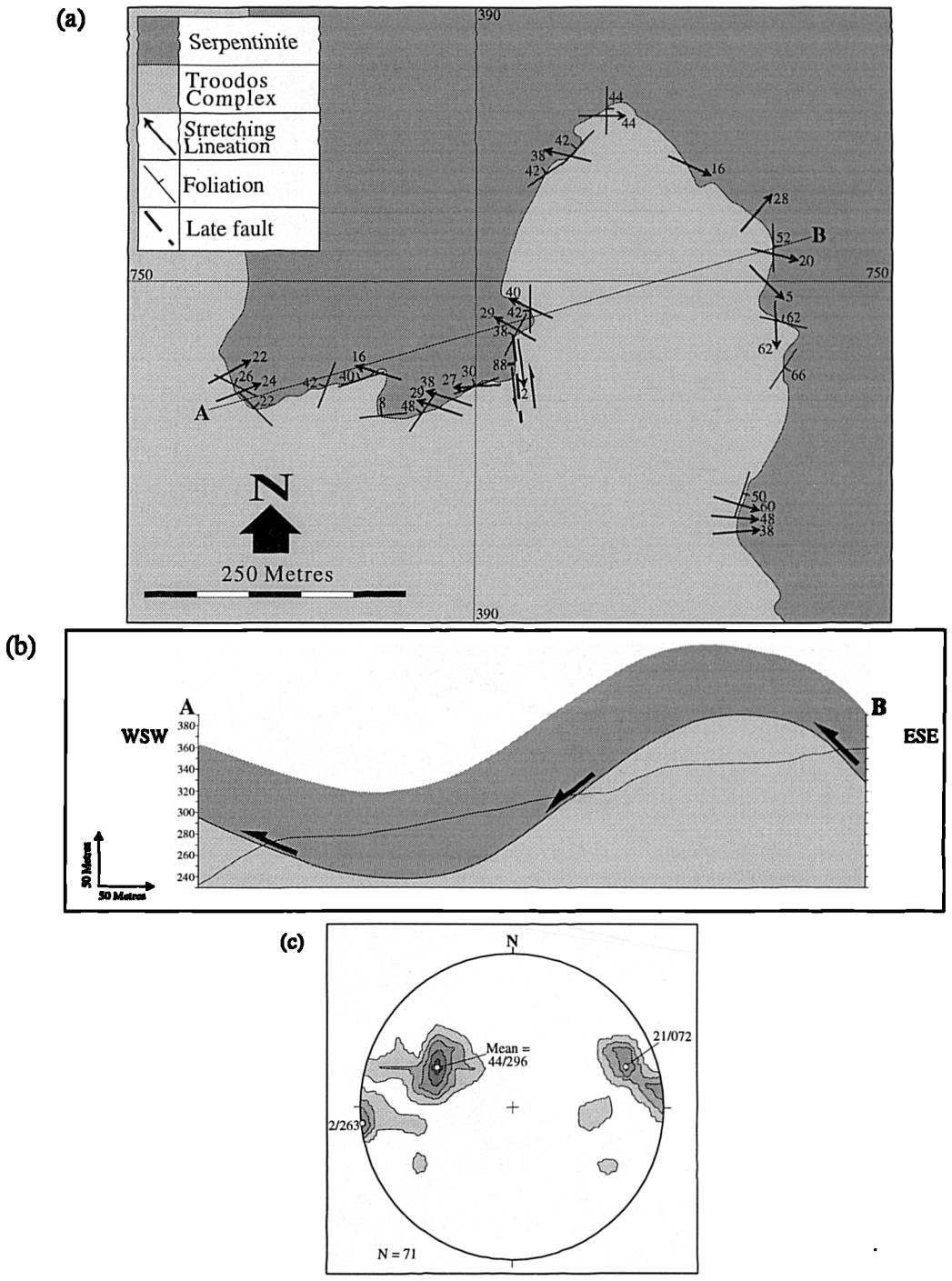

Figure 5.18. (a) Geological map, (b) cross-section, and (c) slickenfibre lineation data from the contacts exposed to the north and NE of Kapsalomoutti. (b) Shows the highly undulating geometry of the contact. (c) Shows 1% area contours of brittle striae and mineral fibre (serpentine and carbonate) lineation data from the contacts. Westerly-plunging lineations are from westerly-dipping sections of the contact, whilst easterly-plunging lineations are from easterly-dipping sections. Mean orientations indicate broadly westerly-directed tectonic transport.

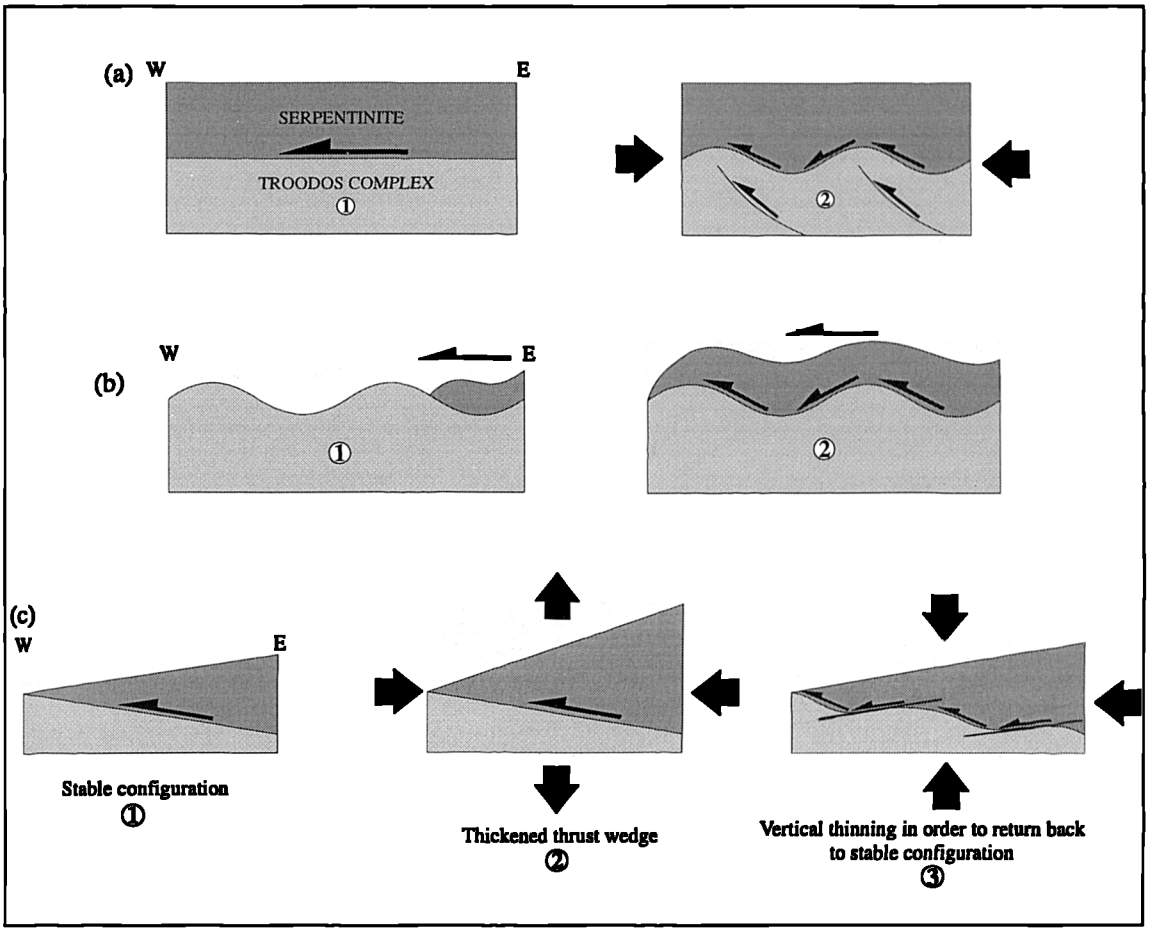

Figure 5.19. Possible models explaining the development of undulating tectonic contacts located to the N and NE of Kapsalomoutti. Circled numbers represent the order of development with 1 being the earliest. (a) Folding of the contact by blind thrusts located in the Troodos Complex footwall. (b) Thrusting or protrusion of the serpentinite hangingwall over an irregular Troodos footwall architecture. (c) Vertical thinning induced by gravitational forces subsequent to thrusting and vertical thickening. 1 - thrust wedge geometry in mechanical equilibrium; 2 - vertical thickening; 3 - vertical thinning in attempt to attain the stable configuration shown in 1. Thinning is accommodated by the basal thrust cutting down section into the Troodos footwall and also by internal deformation of the serpentinite body.

5.3.2c *Kataklistres*

Three sections of the contact, exposed in the vicinity of Kataklistres (GR 383 772) (Figure 5.14), display local deviations in strike from the dominant N-S trends commonly observed in the Akamas area (Figure 5.20). The two most southerly localities strike NW-SE and dip steeply to the NE, whilst the contact at the northern locality, situated 150m SE of Kiladhia tou Pastourma, strikes NE-SW and dips shallowly to the SE. The two southerly contacts are characterised by steep to sub-vertically dipping foliations and fault planes that possess strike-parallel slickenline and

fibre lineations. Corresponding cm- to m-scale asymmetrical shear bands and faults display consistent sinistral offsets. In contrast, dip-slip lineations and shear bands preserved within a highly foliated serpentinite and diabase fault gouge at the northern contact record top-to-the-NW thrust displacements. The parallelism in the orientation of fault plane lineations at all three locations (stereonet insets; Figure 5.20), combined with the similarity in the style of deformation, suggests that these three contacts are kinematically related. The two southerly NW-SE trending sections of the contact constitute sinistral strike-slip transfer faults or lateral ramps, whilst the northern NE-SW contact represents a northwesterly-directed thrust; all of which are interpreted to have formed in response to bulk NW-SE-directed shortening.

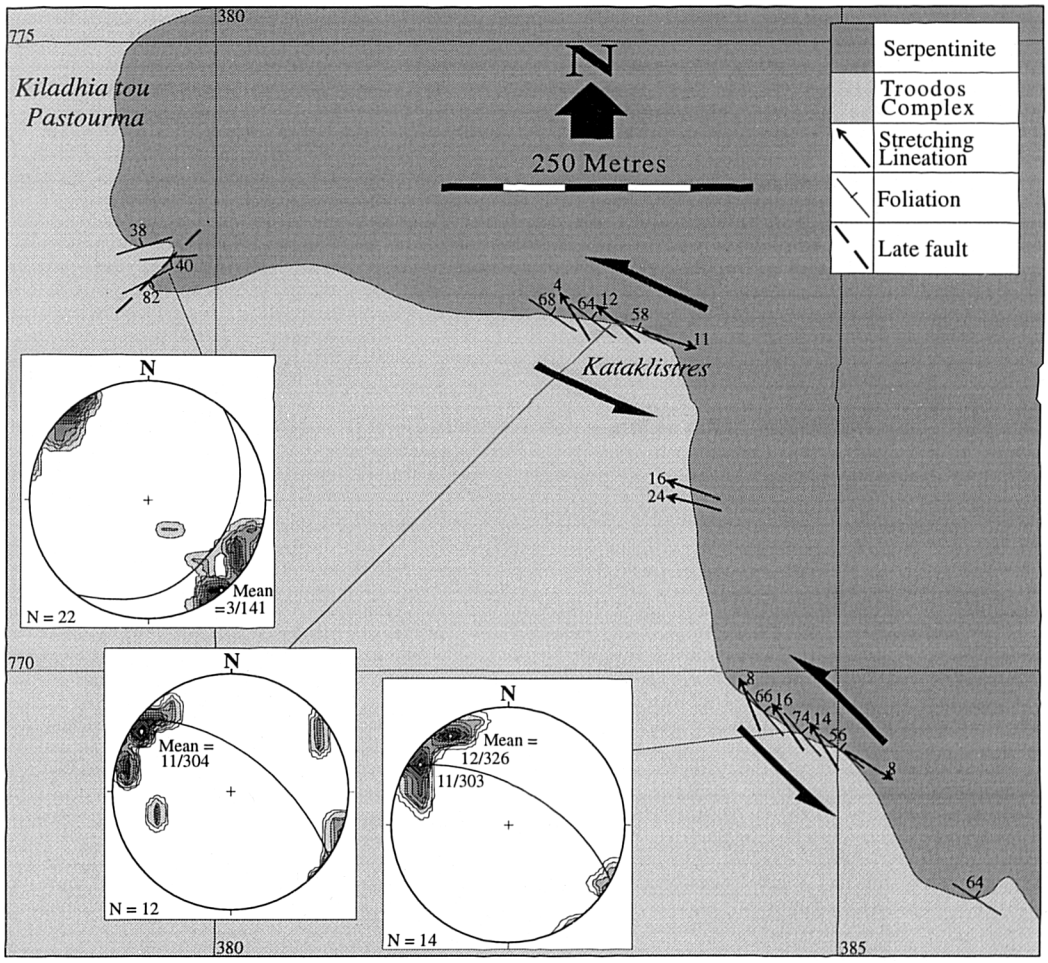

Figure 5.20. (a) Map and structural data from Kataklistres. Stereographic projections display 1% area contours of slickenline and fibre lineations. Great circles represent the average trends of faulted contacts.

5.3.2d *Sarantakloni*

The shallow to moderately-dipping contact, exposed to the north and east of Sarantakloni (GR 374 797; Figure 5.14), displays a distinct swing in strike (Figure 5.21).

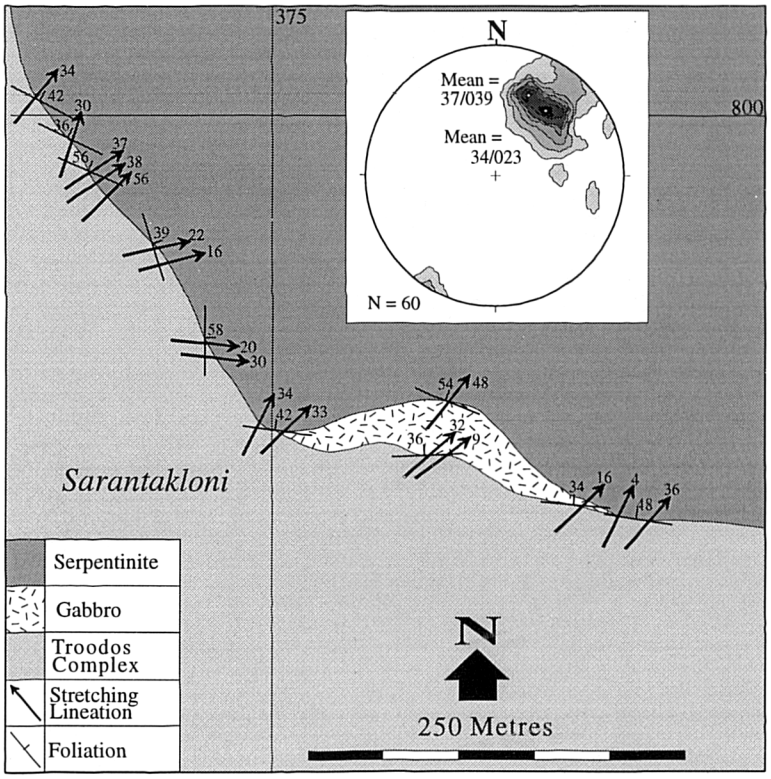

Figure 5.21. Map and data from the contact exposed at Sarantakloni. The stereographic projection shown in the inset, displays 1% area contours of brittle striae and mineral fibre lineations.

The southern section of the contact strikes approximately E-W and dips to the N, whilst the northern portion to the west trends NNW-SSE and dips to the E and NE. Along the northern segment of the contact, serpentinite overlies mafic breccias. Characteristically, the contact is distinguished by intense carbonate mineralisation and by cohesive, light blue serpentinite fault rocks. Dip-slip slickenlines and serpentine fibres preserved on foliations and shear bands indicate top-to-the-SW sense of shear. In contrast, along the southern part of the contact, which strikes E-W, serpentinite and diabase are separated by a texturally distinct sliver of gabbro. The gabbroic unit, which measures 250m E-W and 80m N-S, is bound to the north and south by sub-parallel, northerly-dipping tectonic contacts with serpentinite and mafic breccias, respectively. Both contacts are characterised by carbonate-rich cataclasite fault rocks

that comprise variable amounts of foliated serpentinite and diabase. Offsets along shear bands within these fault rocks, combined with the consistent NE-plunges of stretching lineations, indicate thrusting to the SW. The constant orientations of fault plane lineations (brittle striae and mineral fibres) and shear sense along both NW-SE and E-W sections of contact, indicate thrusting at Sarantakloni was directed to the SW (stereonet inset; Figure 5.21). Therefore, the gabbro sliver along the southern section of the contact is interpreted as a thrust slice associated with the Troodos Complex.

5.3.3. Akamas Area: summary

The outcrops exposed in the Akamas Forest preserve evidence of a phase of compressional tectonism that placed serpentinite over the Troodos Complex and the Mamonia Complex over serpentinite. Figure 5.22 demonstrates the considerable variation observed in the geometry of serpentinite-Troodos Complex contacts and also the variability in the direction of thrusting. This irregularity in the direction of tectonic transport, ranges from top-to-the-NW (mean lineation = 3/141) at Kataklistres to top-to-the-SW (mean lineation = 34/023) at Sarantakloni. The possible reasons for this variation may be attributed to one of two processes:

(1) Top-to-the-NW and top-to-the-SW thrusts formed during separate deformational events, as is suggested by Malpas *et al.* (1993). However, no cross-cutting or overprinting relationships have been found to suggest that this hypothesis is correct.

(2) Both transport directions formed in response to regional E-W shortening during a single tectonic event. In this hypothesis, the variation in shear sense and displacement direction along contacts may be consequences of one, or a combination of , three mechanisms:

- Inherent geometrical complexities of the fault zone and/or;
- Kinematic partitioning during deformation.
- The operation of specific dynamic thrust processes in evolving thrust wedges.

In the former model, an irregular fault zone architecture is thought to have existed prior to thrusting, which may have formed during the protrusive emplacement of serpentinite. When subjected to regional E-W compression, the local displacement of serpentinite is envisaged to be at least partly controlled by the pre-existing geometry of the fault zone boundaries.

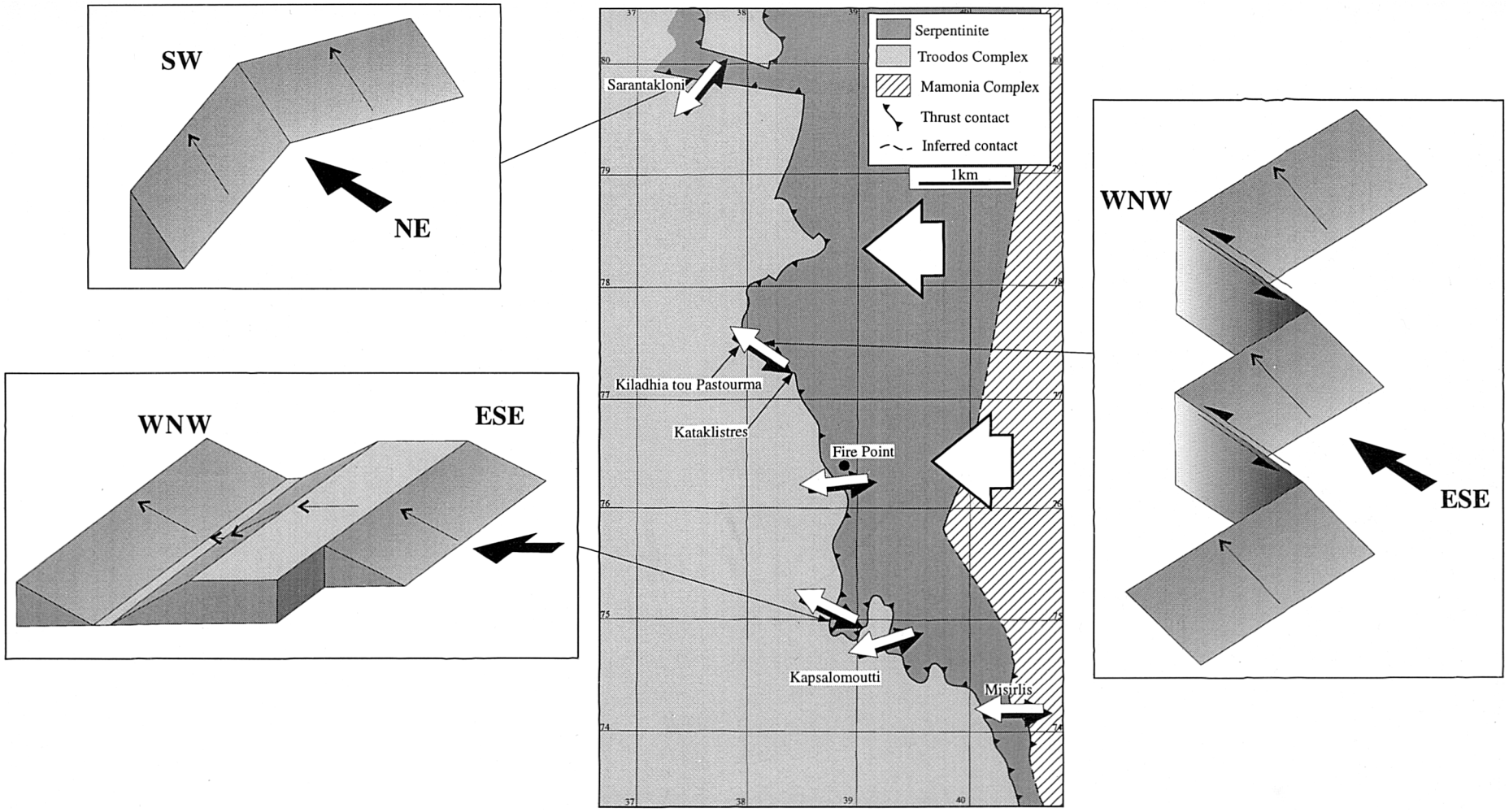

Figure 5.22. Map showing the spatial variation in thrust transport directions at serpentinite-Troodos Complex contacts in the Akamas area. The three-dimensional diagrams display the geometrical variations observed at the three sections of the contact discussed in the text. The large white arrows represent the inferred directions of regional compression.

Field evidence is present in the Akamas area which suggests that the regional strains were locally partitioned during westerly-directed thrusting. For example, the zones of sinistral strike-slip at Kataklistres may represent transfer faults or lateral structures that accommodated a minor component of strike-slip movement during thrusting. In this case, sub-vertical, NW-SE striking sections of the contact experienced strike-slip, whilst moderately-dipping, N-S trending sections accommodated the regional E-W shortening by thrusting.

An important observation made in the Akamas area is that there is a predominance of tectonic transport directions that are approximately perpendicular to the strike of the local fault zone boundaries. For example, top-to-the-W displacements are observed along the N-S trending contacts at the Fire Point and at Misirlis, and the NE-SW contacts at Kataklistres (and also at Loutra tis Aphroditis; Section 5.2) document top-to-the-NW displacements, whilst top-to-the-SW thrusting is preserved along the NW-SW contact at Sarantakloni. A similar relationship is described by Platt *et al.* (1989), who suggested that the radial distributed pattern of thrust motions around the Alpine arc were driven by local body forces. This analogy may be used as evidence to suggest that the effects of locally-induced body forces were significant during thrusting in the Akamas area. This hypothesis is favoured and is discussed in greater detail at the end of this chapter with reference to thrust wedge models and their application to explain the tectonic evolution of the Northern Region.

5.4. The Mavrokolymbos Area

Outcrops within the Mavrokolymbos area (Map II), in particular exposures within the Mavrokolymbos and Katarrakhtis Potamos valleys, display structures that document the compressional tectonics experienced by the Northern Region. Two cross-sections drawn through both of these valleys (see below) demonstrate that a stack of thrust sheets comprising, from base to top, Troodos Complex-serpentinite-Mamonia Complex, formed during top-to-the-west thrust tectonics. The unusual geometry of many thrust contacts is attributed to the operation of specific mechanical processes in the evolving thrust wedges and to the possible reactivation of a pre-existing (extensional/transtensional?), N-S striking, steeply dipping, structural architecture.

5.4.1. Mavrokolymbos valley section

The geology of the Mavrokolymbos dam section is dominated by two separate serpentinite bodies that crop out on both sides of the valley. Serpentinite consistently overlies rocks of the Troodos Complex along low angle tectonic contacts that display top-to-the-west extensional and thrust geometries. Mamonia Complex-serpentinite contacts, on the other hand, are much more variable and geometrical complexities arise due to successive events of early faulting(?), protrusion, thrusting, and late extensional faulting. The following text describes the contact relationships and structures observed along the NE-SW cross-section that is exposed on the northern side of the valley (Figure 5.24).

5.4.1a NE contact between serpentinite and the Dhiarizos Group (GR 456 578)

The serpentinite-Dhiarizos contact at the north-eastern end of the section is marked by an abrupt break of slope and a steep serpentinite fault scarp (labelled 5.4.1a in Figure 5.24). Within a few metres to the west of the contact, cm- to m-scale blocks of Dhiarizos Group lava and mudstone are enclosed within serpentinite. In general, these blocks are undeformed, and are thus interpreted as fragments of wallrock incorporated earlier into protruding serpentinite. Within a few metres west of the unexposed contact with the main outcrops of the Dhiarizos Group (mainly Mavrokolymbos Formation) (GR 456 578), a steeply-dipping (~66°E), metre-wide serpentinite shear zone is preserved that parallels the strike of the contact (Figure 5.25). This shear zone displays steeply-plunging stretching lineations and asymmetrical shear bands that indicate extension, downthrowing to the NE. Slivers of red mudstone, which are strung along the shear zone, are considered fragments of the adjacent Mavrokolymbos

Formation, situated to the east. Due to the location of this shear zone immediately adjacent to the contact, and the parallelism between these two structures, the Dhiarizos Group is inferred to have been downthrown to the NE along a steep extensional fault.

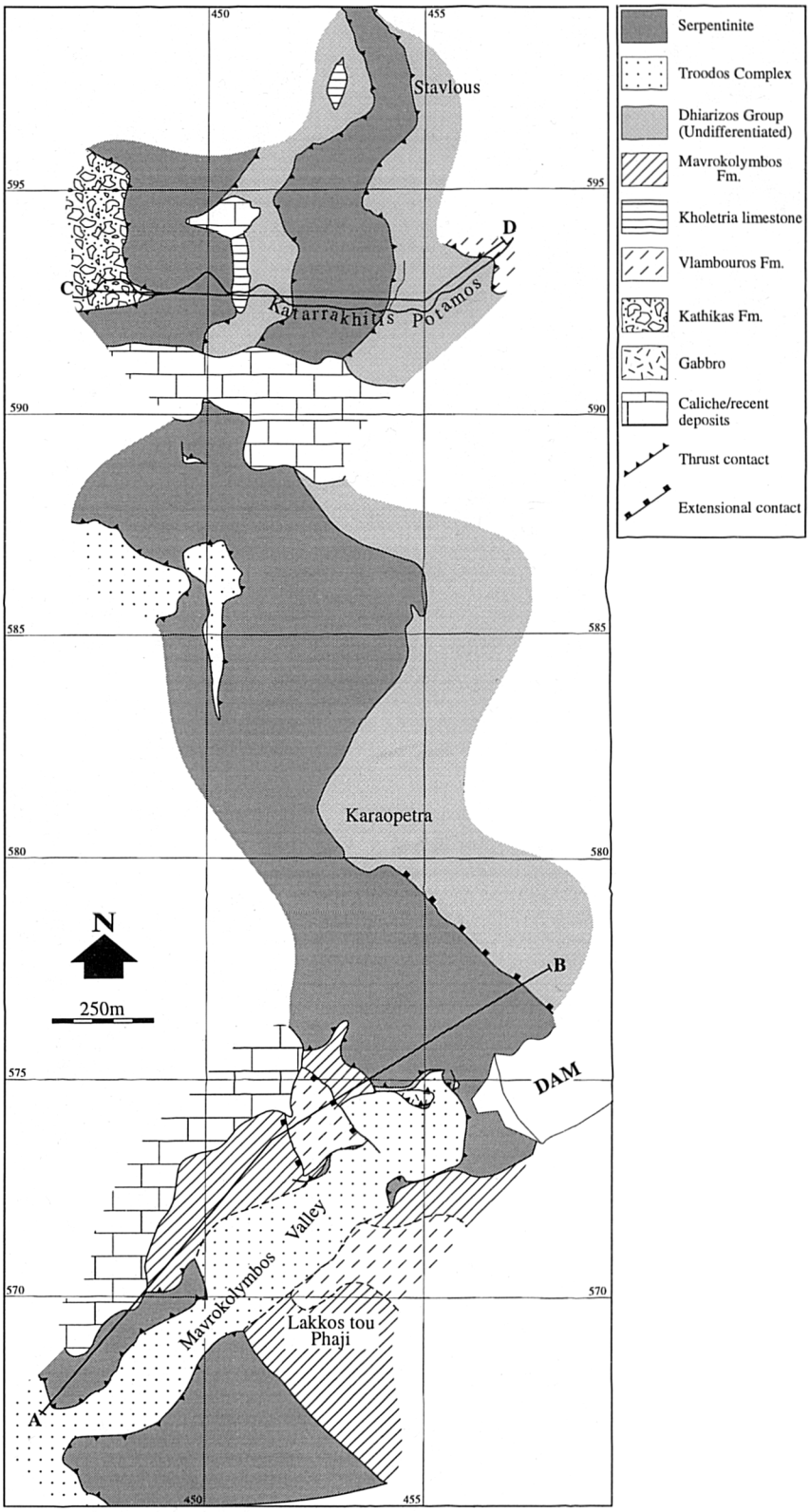

Figure 5.23. Geological map of the Mavrokolymbos area showing the locations and the approximate lines of the two cross-sections discussed in the text.

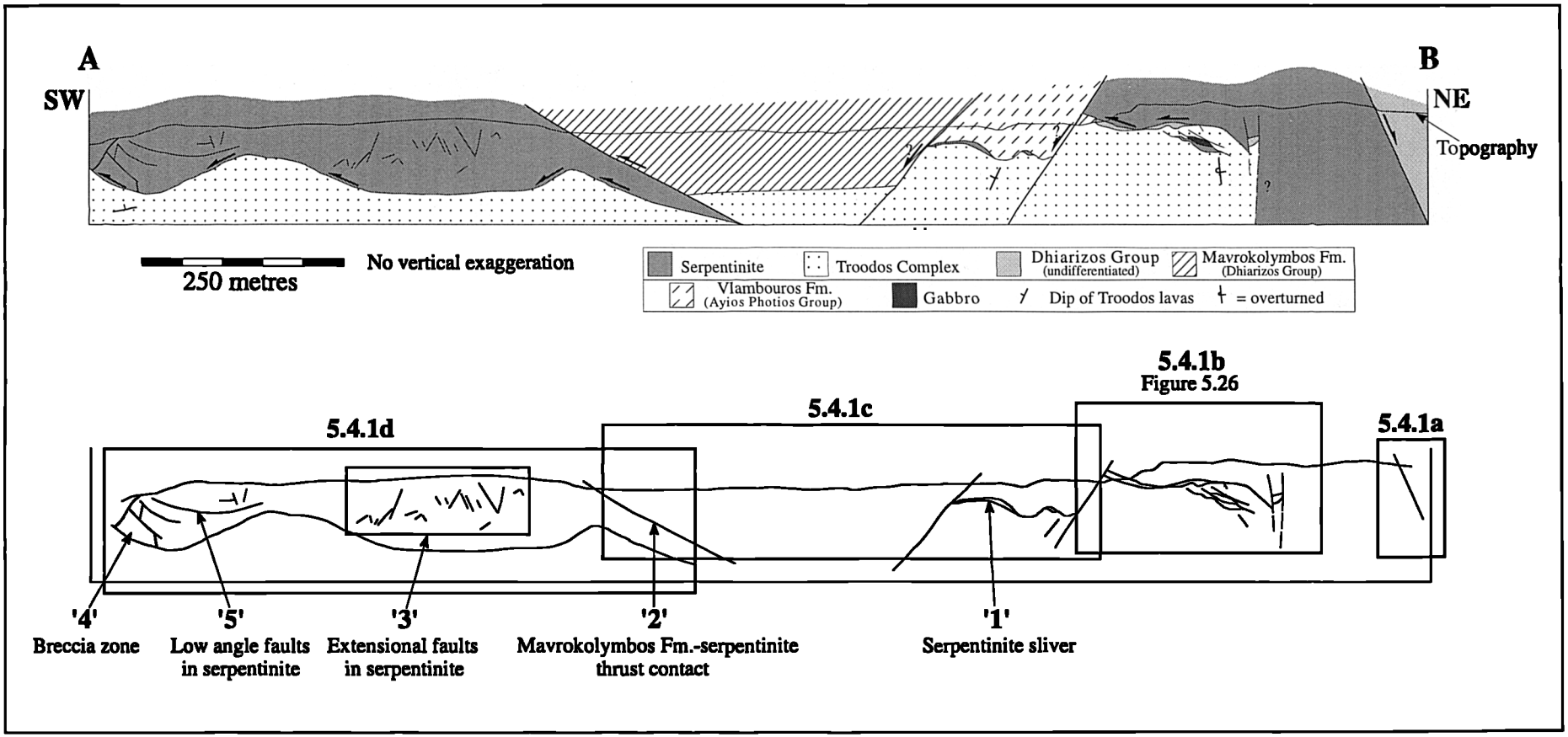

Figure 5.24. Cross-section through Mavrokolymbos valley, based on the geology exposed on the northern side of the valley. The top of the section is constrained in the field by recent caliche deposits. The line of the section is shown in Figure 5.23.

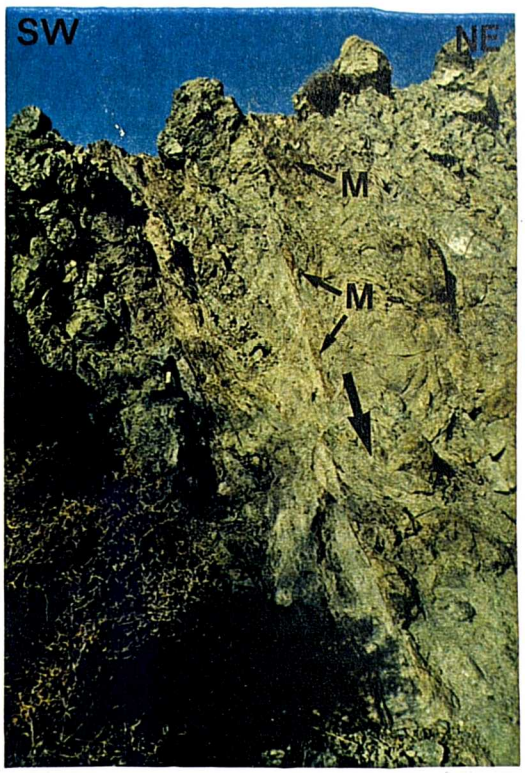

Figure 5.25. Steeply-dipping extensional serpentinite shear zone at the contact with the Dhiarizos Group. Note red slivers of mudstone (M) incorporated within the shear zone. Large arrow indicates downthrow to the NE. Scale is shown by the hammer located on the left hand-side of the shear zone.

5.4.1b NE-end of section (GR 455 475)

The geology exposed along the dam track at the northeastern end of the section is dominated by the serpentinite body. This unit is relatively massive, comprising variably serpentinised ultramafic blocks (up to 10 metres in diameter), which are transected by pervasively hydrated cm- to metre-scale fault zones. The harzburgite protolith to the serpentinites is frequently preserved in the blocks and is easily recognised by its characteristic dark-brown colouration and bright, bronze orthopyroxene bastites (mm-sized). Olivine grains, which constitute the bulk of the rock, are generally totally replaced by mesh-textured serpentine (lizardite and minor chrysotile), whilst orthopyroxenes are comonly preserved. Minor clinopyroxene grains are also present and are identified by their unaltered blue colouration. Occasionally, these blocks exhibit early, pre-serpentisation fabrics of unknown origin (e.g. mm-scale phase layering), but the rarity of these textures and the disruption that these rocks have experienced precludes a more detailed study. The harzburgite blocks are bound by

cm- to metre-scale shear zones, which comprise pervasively hydrated, light-blue serpentinite. The zones of most intense deformation are invariably the most thoroughly serpentinised. In particular, those rocks located adjacent to structural contacts are heavily foliated, light blue coloured serpentinite fault gouge and variably cohesive phacoidal mylonites. The shear zones that contain these fault rocks reach metres in width and the largest can be traced for many tens of metres.

Immediately west of the dam, along the dam track and the northern valley wall, structures and tectonic contacts are very well exposed (Figures 5.24 and 5.26). Much of the complexity observed in this part of the section is attributed to tectonic interleaving by thrusting and associated extensional faulting (GR 455 475). The structurally lowest tectonic contact between Troodos lava in the footwall and a discontinuous unit of gabbro in the hangingwall is marked by a sliver of highly serpentinised, light-blue fault rock (Figure 5.26) [note that the geometry of pillow forms at this locality indicate that the Troodos lavas are inverted and they dip steeply (~85°) to the east]. Occasionally, heavily weathered, dark green coloured rocks are preserved adjacent to the gabbroic body (GR 455 575). The origin of these green rocks is unknown due to the degree of alteration, but their colouration and brecciation is reminiscent of some Phasoula Formation lavas. Immediately above the serpentinite sliver at its western end (location 'A' in Figure 5.26), Troodos lava is preserved in situ. Therefore, based solely on its spatial relationships, whether this gabbro belongs to the Troodos or Mamonia Complex is unknown. One possible explanation is that this gabbroic unit originally intruded Troodos lavas and was subsequently disrupted during thrusting. Alternatively, it may represent a thrusted sliver of Mamonia Complex material. The association of the serpentinite sliver is also unknown, as it is far too altered at be analysed geochemically. However, of the harzburgites sampled from the valley, all but one are assigned to the Mamonia Complex. Whatever the origins of these rocks, the structural geometry exposed at this locality is considered significant. The thrust contacts between (from base to top), Troodos pillow lavas (TP1), serpentinite (S1), gabbro and Troodos lavas (TP2) are truncated by the low-angle, undulating tectonic contact, along which a thin sliver of Dhiarizos Group rocks are entrained beneath the main serpentinite thrust sheet (S2) (Figure 5.26). This observation suggests that the structurally highest thrusts, which emplaced the Dhiarizos Group sliver and the main serpentinite thrust, formed later than the lowermost thrusts (see inset in Figure 5.26).

(a)

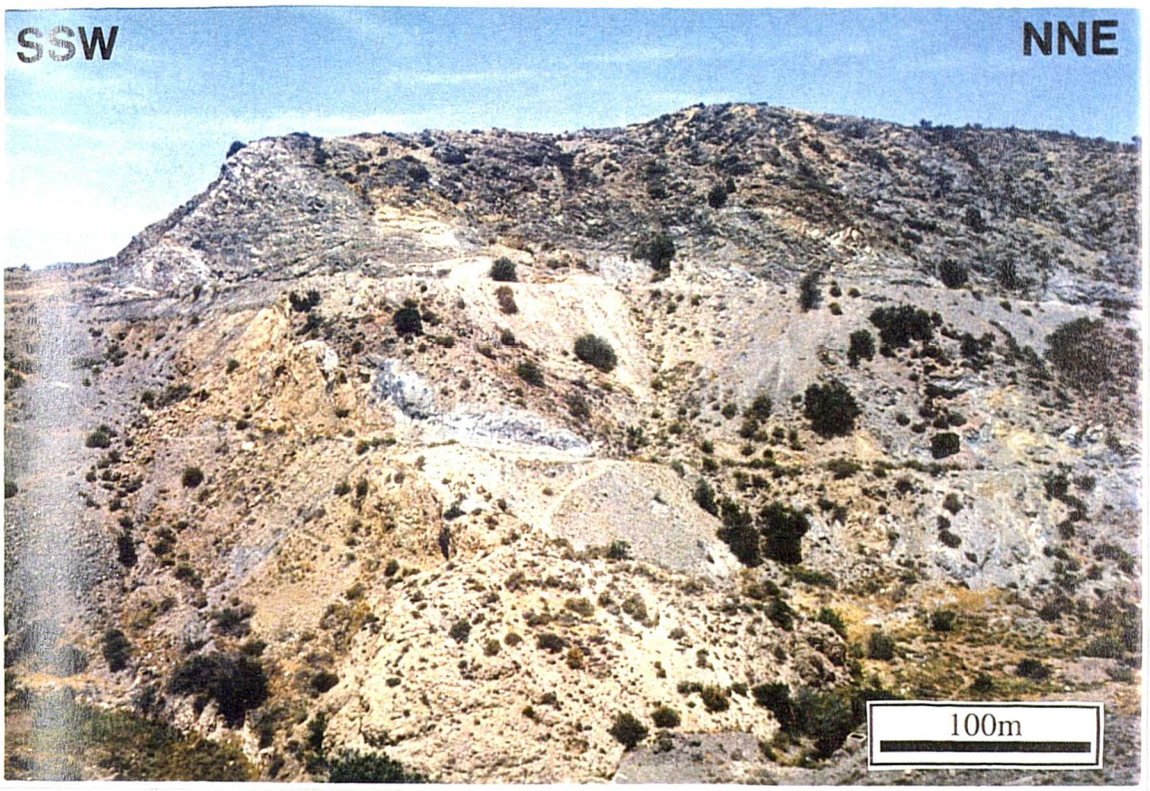

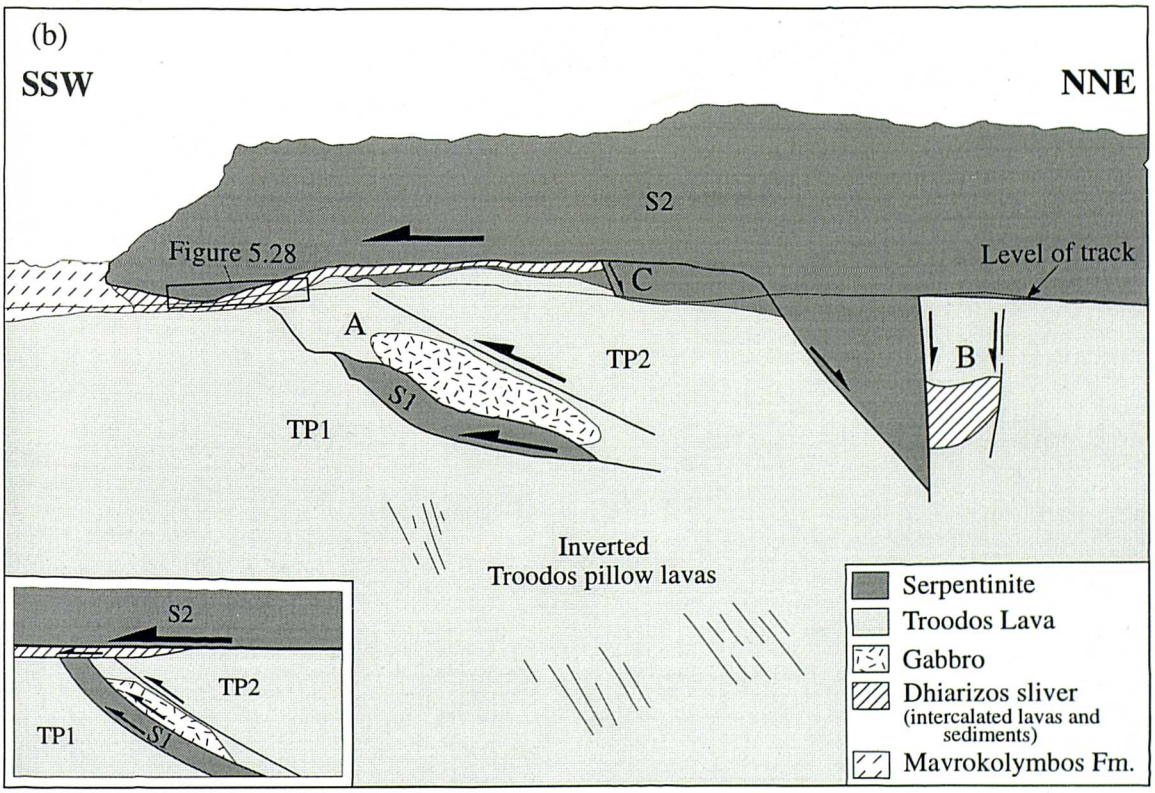

Figure 5.26. (a) Cross-section of the area exposed on the northern side of the valley, immediately to the west of the dam wall. (b) Interpretation and spatial relationships between the outcrops shown in (a). The annotations 'A', 'B' and 'C' are referred to in the text. The inset shows a schematic kinematic interpretation of the structure.

To the east, a series of sub-vertical to high-angle faults ('B' in Figure 5.26) downthrow and bound serpentinite, Troodos lavas, and Mamonia Complex units. Shear band and S-C fabrics within foliated, phacoidal serpentinite and Dhiarizos Group fault rocks, combined with dip-slip brittle striae, indicate that these structures are extensional. As these faults offset the basal tectonic contact to the main thrust sheet (S2 in Figure 5.26), they are interpreted as late, post-thrusting structures that have complicated the outcrop pattern. However, high-angle faults are exposed on the track that are cross-cut by thrust related structures (Figure 5.27). For example, at GR 455 575, a sub-vertical, 5m-wide fault zone, comprising heavily serpentinised, light-blue gouge, cross-cuts Troodos Complex lavas, but it is also truncated by the basal detachment to the main serpentinite thrust sheet (Figures 5.26 ('C') and 5.27). The serpentinite fault rocks display a characteristically chaotic, melange-like fabric and a consistent sense of shear is indeterminable. However, dip-slip fibres dominate, suggesting that the displacements along this zone were sub-vertical. The material of the fault zone is texturally analogous to rocks associated with structures found in the valley (see below) and also in the Southern Region (Chapter 4), which are interpreted as forming during serpentinite protrusion. Unfortunately, due to the intense alteration inherent with these rocks, a geochemical analysis of these rock types is not possible, but their similarity suggests that the fault zone described above may have been a protrusion-related structure.

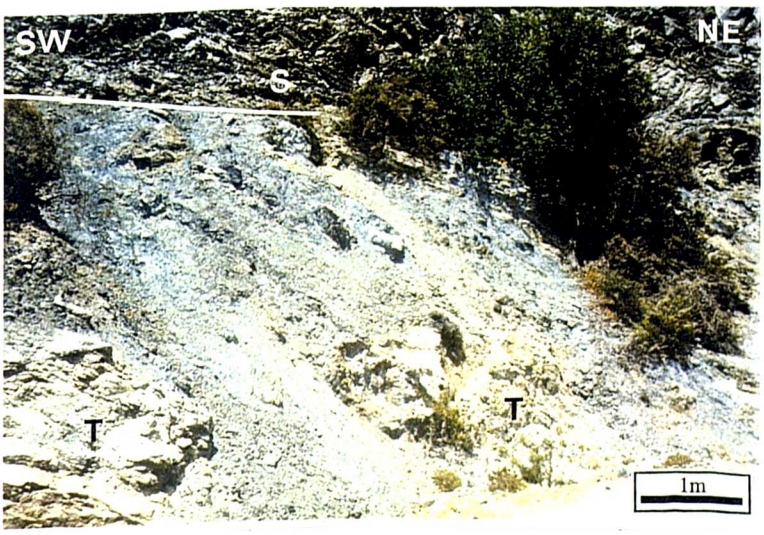

Figure 5.27. Sub-vertical, light-blue coloured serpentinite fault zone truncated by the sub-horizontal basal thrust (white line) to the main serpentinite (S) body (S2 in Figure 5.26). The location of this fault zone ('C') is shown in Figure 5.26. This fault zone cross-cuts Troodos lavas (T) and truncates the Mamonia sliver to the SW.

The structurally highest contacts in this part of the section are exposed on the dam track at GR 575 455. A detailed cross-section/field sketch constructed at this locality demonstrates that the low-angle fault-bounded slivers of Troodos lava, Dhiarizos material and serpentinite were tectonically interleaved during westerly-directed thrusting (Figures 5.28) Serpentinite overlies disrupted and intercalated *Dhiarizos Group* lavas and sediments (Figures 5.28 and 5.29a), which in turn overlie a thin sliver of serpentinite and underlying Troodos Complex lavas. The sub-horizontal, tectonic contact between serpentinite and the Dhiarizos Group is the dominant structure. Shear sense criteria along this contact, which include asymmetrical shear bands (Figure 5.29b), Riedel shears and S-C fabrics developed in serpentinite and Dhiarizos fault rocks, indicate ubiquitous top-to-the-WSW displacement. As this contact cuts up and down section on a metre-scale, it locally displays extensional and thrust geometries; therefore it is referred to as a *detachment* in the following text. The 'detachment' is characterised by pervasively foliated lavas and sediments in the footwall, a 10-20cm wide serpentinite-carbonate fault rock, and by a 10cm-wide, chrysotile vein along all exposed parts of the contact (Figure 5.29c). Petrographic studies demonstrate that the serpentinite fault rock comprises up to 70% detachment-parallel, tensile carbonate veinlets (Figure 5.29d). Fibres within these veinlets, which parallel fibres within the overlying chrysotile vein, indicate veins opened normal to the detachment. Whether both of these vein types formed during thrusting is uncertain. The formation of tensile veins, which open perpendicular to the shear direction, along tectonic contacts are not expected to be contemporaneous with faulting, and thus most veining along the Mavrokolymbos detachment is thought to post-date thrusting. However, rare top-to-the-west offsets are observed along some detachment parallel veins, suggesting that at least part of the carbonate fluid flux was coeval with thrusting. The interplay between shear fracture and fluid flow is discussed further in Chapter 6.

Evidence of fluid flux and high fluid pressures is inferred from the existence of vuggy carbonate veins along foliations and shear structures within highly deformed rocks of the Mamonia sliver. To the west of the section shown in Figure 5.28, sub-vertical, cm-wide tensile carbonate veins extend down, orthogonally from the carbonate-mineralised detachment into brecciated red Mamonia sediments (stereographic projection inset, Figure 5.28; Figure 5.29e). On the basis of strike, colour and cross-cutting relationships, at least two generations of veins are present; an earlier set, which are lighter in colour and strike NE-SW, and an later set, displaying NNE-SSW strikes. The earlier set are truncated by a 10-50cm wide zone of carbonate-rich fault rocks, whilst the later veins cross-cut these fault rocks and are truncated by the detachment (white line in Figure 5.29e). The orientation of these veins and their constituent fibres indicate that the veins opened approximately parallel

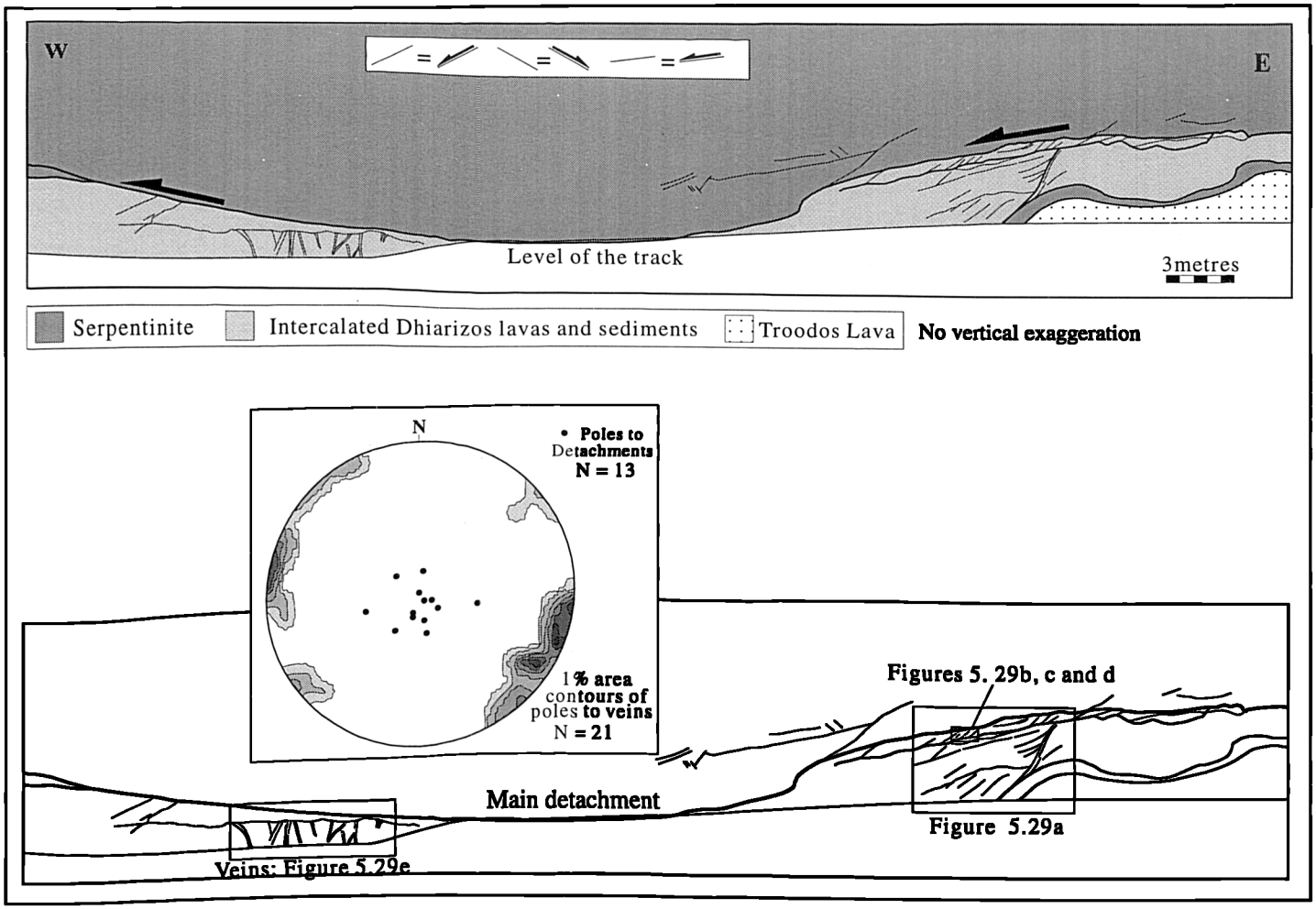

Figure 5.28. Detailed cross-section showing the contacts exposed at GR 575 455. The top section was constructed from field photographs. The bottom line drawing shows the locations of Figures 5.29a to e. The stereonet inset in the bottom diagram displays the poles to the detachment and a 1% area contour of poles to tensile veins located in the Dhiarizos Group footwall.

(a)

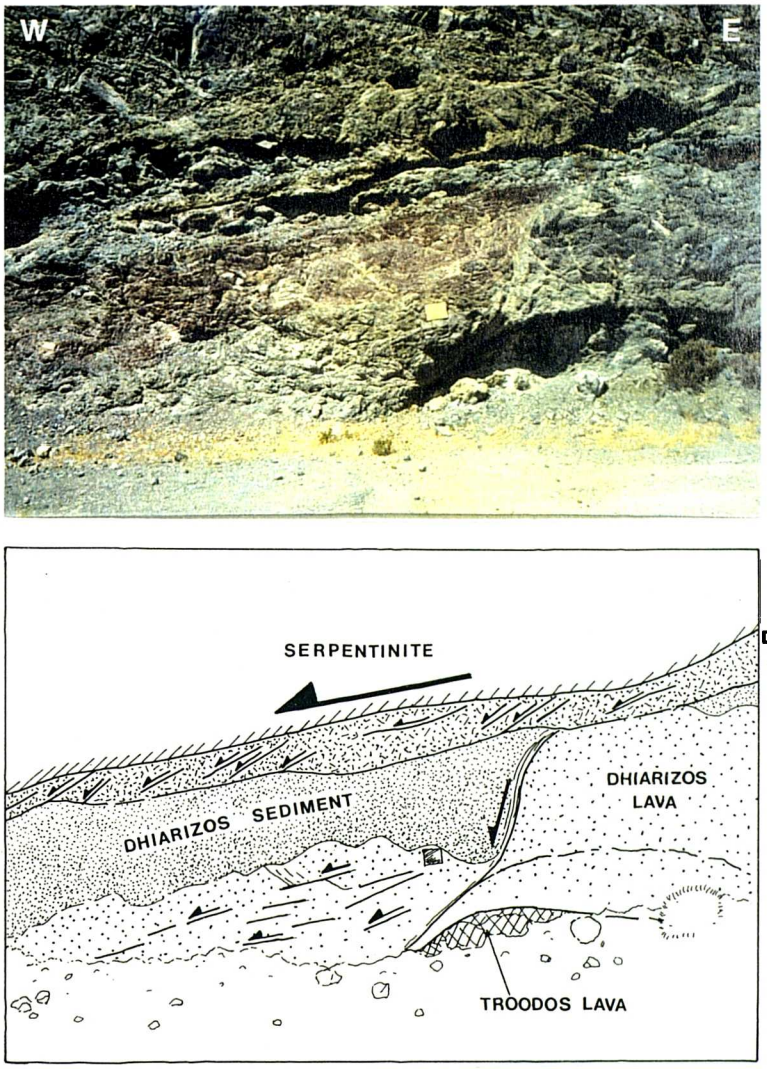

(b)

Figure 5.29. Details of the section shown in Figure 5.28. (a) Intercalated Dhiarizos units. Red sediments are juxtaposed against green lavas along a steep extensional shear zone, which is truncated by the detachment. Note that the detachment at this locality displays an extensional geometry. (b) Asymmetrical extensional shear bands indicate top-to-the-WSW displacement in foliated Dhiarizos lavas.

(c)

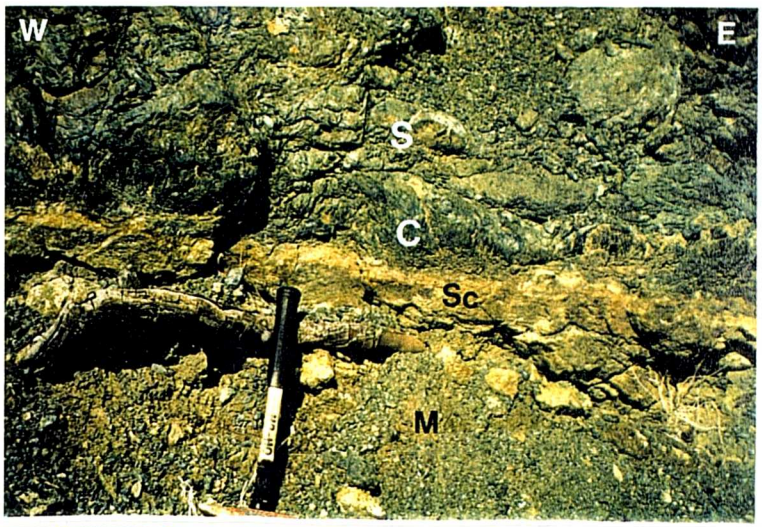

(b)

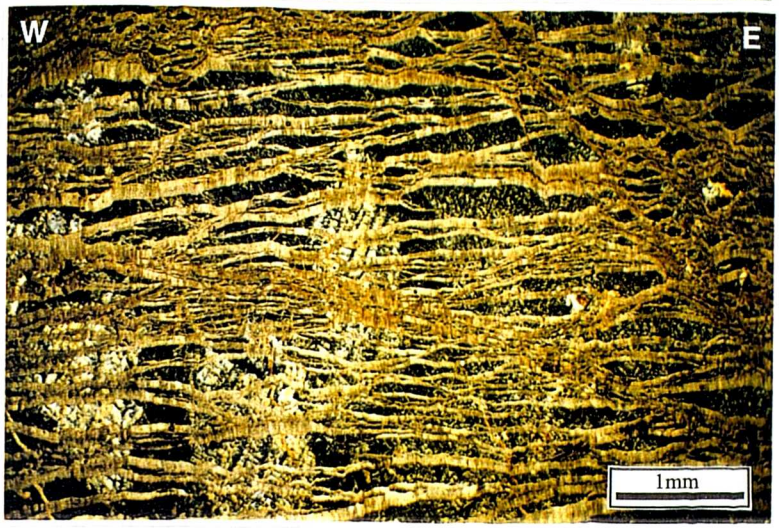

(c)

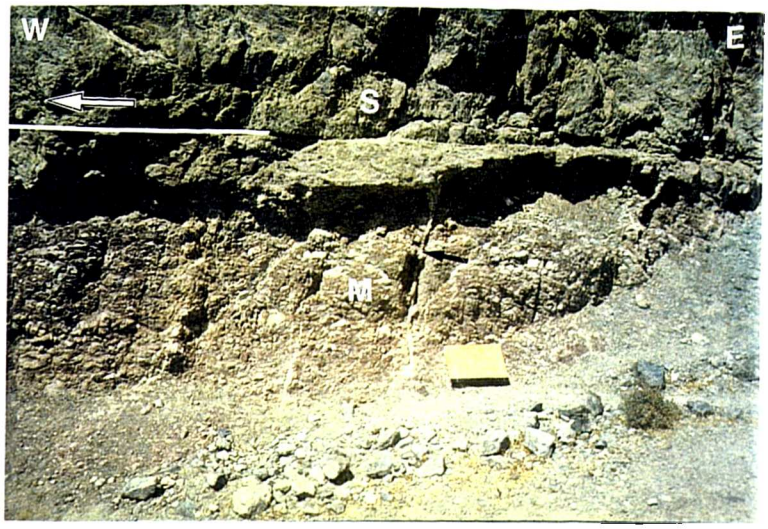

Figure 5.29. (continued). (c) serpentinite-carbonate fault rock (Sc; buff) and dark, chrysotile vein (C) along the detachment, separating serpentinite in the hangingwall (S) from the Dhiarizos sliver (M) in the footwall. The view is normal to the transport direction along the detachment. Note that the orientation of fibres within the chrysotile vein indicates opening perpendicular to the detachment. (d) Photomicrograph of the serpentinite fault rock (Sc) shown in (c). The view is parallel to that shown in (c) and the fibres within the veins indicate opening perpendicular to the detachment. (e) Brecciated red Dhiarizos sediments (M) cross-cut by sub-vertical, tensile, carbonate veins that extend down from, and are truncated by, the detachment. The arrow indicates top-to-the-WSW displacement along the contact. S = serpentinite.

to the top-to-the-west displacement direction and that the maximum principal shortening direction was sub-vertical. The cross-cutting relationships described above infer that fluid flux and thrusting were coeval, whilst the orientation of the principal strain directions suggests that the footwall was overpressured.

Due to the near 100% exposure of serpentinite along the track, the whole serpentinite body at the NE end of the section was selected for detailed kinematic analysis. The structure of this serpentinised mass is characterised by low to moderately-dipping brittle to brittle-ductile fault surfaces that display mm- to m-scale offsets. Two fault populations predominate that possess contrasting westerly and easterly dips and dip-slip slickenlines and fibres (Figure 5.30a, b and c). Shear sense criteria demonstrate that these two fault sets are extensional structures. Both fault sets are mutually cross-cutting and are thus considered coeval and conjugate. Furthermore, as westerly-dipping faults dominate over those with easterly dips by approximately 30%, bulk displacement is inferred to be top-to-the-west (Figure 5.30c). As observed within the fault zones of the Southern Region, the maximum principal shortening direction is inferred to parallel the obtuse bisector of the conjugate fault set. Thus, the maximum shortening axis plunges sub-vertically and is approximately detachment-normal (Figure 5.30d).

As stated previously, carbonate veins are observed in Dhiarizos units that extend vertically down from the detachment (Figures 5.28, 5.29e and 5.31). The presence and orientation of veins suggest that the footwall was overpressured and that maximum principal shortening direction was vertical, which is sub-parallel to that calculated in the overlying serpentinite. In contrast, shear sense criteria in the highly foliated zone directly below the detachment indicate ubiquitous top-to-the-WSW displacement. Therefore, deformation in the fault rocks immediately beneath the detachment is inferred to have been dominated by simple shear, whilst the presence of sub-vertical veins and pure shear deformation in the Dhiarizos Group sliver is thought to reflect the effects of thrust sheet loading (Figure 5.31). Based on the orientation of the principal strain axes, the overlying serpentinite thrust sheet is thought to have thinned vertically during thrusting, which was accommodated by asymmetrical extension along the conjugate fault sets. This deformation of the serpentinite sheet is interpreted as being pure shear-dominated, relating to vertical thinning, but the predominance of extensional faults that downthrow to the west documents a non-coaxial strain component, which reflects the bulk top-to-the-west displacements associated with thrusting (Figure 5.31).

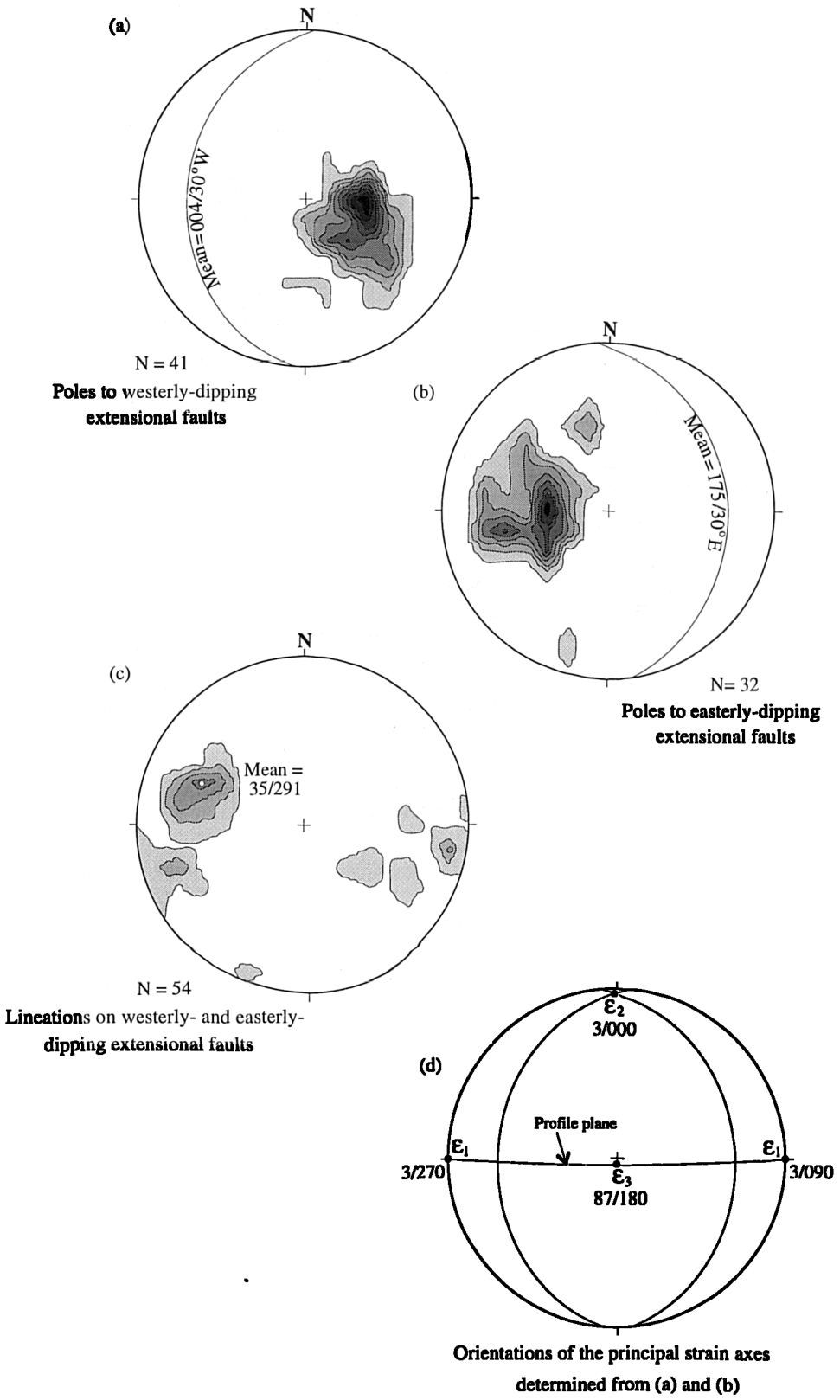

Figure 5.30. 1% area contour of fault data from the north-eastern serpentinite body. (a) Westerly-dipping extensional faults. (b) Easterly-dipping extensional faults. (c) Fibres and slickenlines on conjugate fault planes. (d) Calculation of the maximum principal shortening direction in the profile plane to the conjugate fault sets. Note that the maximum principal shortening direction plunges sub-vertically and is therefore approximately perpendicular to the sub-horizontal detachment.

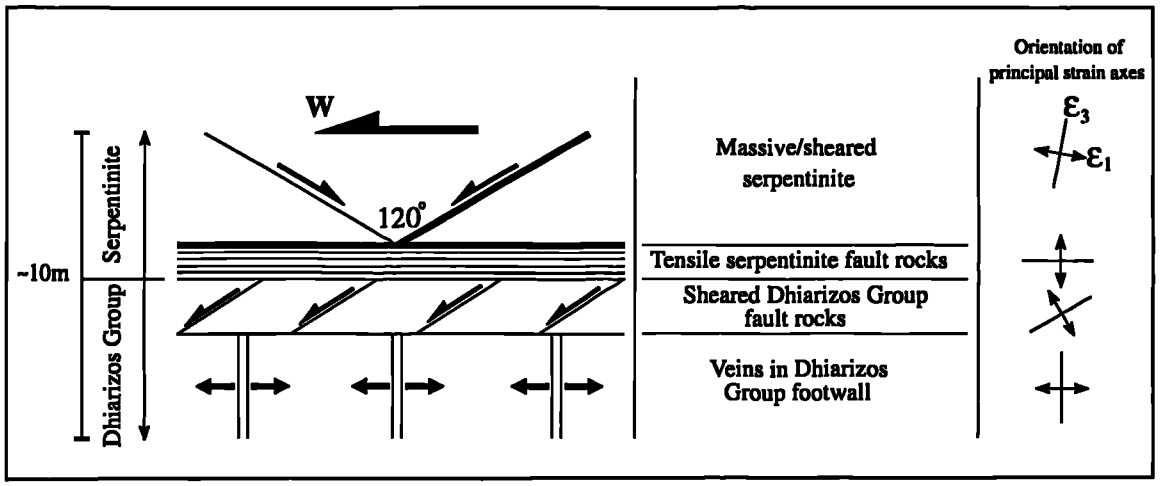

Figure 5.31. Schematic representation of deformation and fluid flow associated with the basal detachment of the northeastern serpentinite body. All structures are thought to be coeval with westerly-directed thrusting, except for tensile serpentinite fault rocks, which are interpreted to largely post-dating thrusting.

The inference that serpentinite has protruded from depth into the Troodos lavas below the serpentinite thrust sheet is indicated by the presence of serpentinite 'dykes' (Figure 5.32; GR 455 574). The dykes comprise highly serpentinised, carbonate-rich material, that are bound by sharp, sub-vertical contacts with the lava on an outcrop scale. However, locally, and on the scale of a hand specimen, the contact between the two units is highly irregular and serpentinite typically follows fractures within the lavas, suggestive of intrusive emplacement. A number of these structures, which are characterised by highly fluidised, light-blue serpentinite, crop out along the dam track as steep to sub-vertical, metre-scale features. One such structure, shown in Figure 5.27, truncates the Dhiarizos Group sliver and is in turn cross-cut by the detachment to the main serpentinite thrust sheet. These observations suggest that these structures formed prior to thrusting and most probably formed during an earlier protrusion-related, extensional, tectonic event.

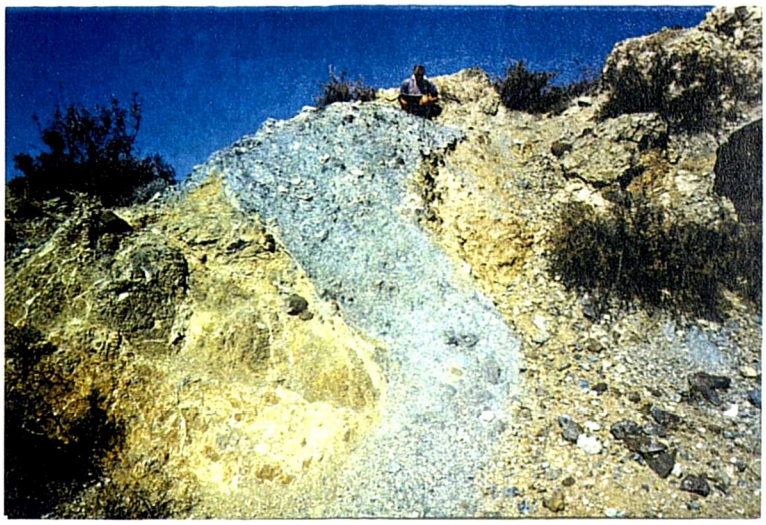

Figure 5.32. Blue serpentinite dyke protruding Troodos lava within Mavrokolymbos valley (GR 455 574).

5.4.1c Middle of the section (see Figure 5.24)

To the SW of the northeastern serpentinite body, isolated exposures of Vlambouros Formation sandstones (Ayios Photios Group) crop out between exposures of Mavrokolymbos Formation sediments (Dhiarizos Group), located to the NE and SW (see Figures 5.23, 5.24 and Map II). Occasionally (e.g. GR 452 574), Vlambouros sandstone beds display graded bedding, which indicate that they are, at least locally, overturned, but due to poor exposure the reason for this is unknown. Unfortunately, the contacts that separate the Vlambouros sandstones from the Mavrokolymbos Formation are not exposed, but the inferred contacts trend approximately N-S, which parallels much of the late extensional faulting within the region. Therefore, the Ayios Photios Group at this locality is inferred to have been down-faulted or landslipped against the Dhiarizos Group after thrusting.

A thin, sub-horizontal sliver of serpentinite, which crops out along the track (labelled '1' in Figure 5.23; GR 453 573), marks the contact between the Mamonia Complex and the underlying Troodos lavas [note that the geometry of pillow forms at this locality indicates that the Troodos lavas in the footwall are the correct way up, but they dip steeply (~65°) to the west]. The sub-horizontal attitude of the fabric in the serpentinite suggests the two Complexes were juxtaposed during thrusting. However, due to poor exposure, no definitive kinematic indicators could be found.

To the west of these outcrops, structures in Mavrokolymbos Formation sediments are occasionally exposed due to quarrying (~GR 450 571). These structures include metre-scale asymmetrical extensional faults (Figure 5.33a), folds (Figure 5.33b) and minor thrusts. Offsets of pre-existing features and the asymmetry of

westerly-verging folds, suggests top-to-the-west displacements. The form of these structures suggest that the Mavrokolymbos Formation was macroscopically ductile during deformation. Folds are locally complex, but commonly possess shallow plunges, NE-SW trends, and verge towards the WSW. Fold limbs are occasionally offset along westerly-dipping extensional faults, which are in turn locally folded, which suggests folding and extension were coeval.

(a)

(b)

Figure 5.33. Structures observed in the Mavrokolymbos Formation in the proximity of GR 450 571. SW is left on both of these figures and both views are onto vertical outcrop faces. (a) Asymmetrical extensional faults downthrowing to the SW. (b) Asymmetrical, southwesterly-verging folds.

On the south side of the valley, in the vicinity of Lakkos tou Phaji (~GR 453 569), folds are present in the Mavrokolymbos Formation. Folds exposed in sediments on, and south of the track, display variable geometries (open and upright to tight and recumbent), but no dominant sense of vergence is observed. In general, most of the fold axes plunge shallowly to the east.

Although structures exposed in the quarry near Karaopetra (GR 454 582) are located in Mavrokolymbos Formation sediments that crop out in the easternmost Dhiarizos outcrops (see Figure 5.23 and Map II), they are described here as they are thought to relate to the structures described above. This locality, which is approximately 600m north of Mavrokolymbos Dam, preserves thrusts (Figure 5.34a) and extensional faults that offset bedding and indicate tectonic transport to the WSW. In areas of complex folding (Figure 5.34b), fold axes, in general, plunge shallowly to the east (Figure 5.34c). The complexity in the fold geometries observed within these units may be explained by refolding relating to a separate deformational event. The folds at Karaopetra display geometries that appear similar to Type III style refolds of Ramsay (1967), and locally recumbent folds, which trend NE-SW are refolded across E-W- to SE-NW trending, steeply-dipping axial planes. However, previous studies concerning the folding within the Mamonia Complex indicate that fold forms, which appear geometrically similar to refold structures, are in fact due to the alternation of different fold geometries in adjacent units of contrasting competency (Robertson and Woodcock, 1979). A similar conclusion is favoured to explain the development of the fold geometries observed at Karaopetra. At this locality, the complexity is merely thought to reflect the m-scale rheological heterogeneity within this anisotropic, interbedded unit and also to the mechanical weakness of these mudrock dominated sediments.

5.4.1d. SW-end of the section

At the SW-end of the Mavrokolymbos section, the original stacking pattern that is thought to have formed during thrusting is preserved. Shear sense criteria on the low angle contact between the Mavrokolymbos Formation and serpentinite is exposed at GR 449 570 (labelled '2' in Figure 5.24). Asymmetrical shear bands and dip-slip lineations within a 30cm-wide zone of highly strained sediments and underlying foliated serpentinite gouge, indicate top-to-the-SW displacement (squares in Figure 5.35). The tectonic contact below, between the serpentinite-Troodos Complex, displays a highly irregular geometry as it cuts up and down section on a ten metre-scale Locally, light-blue coloured, foliated serpentinite fault rocks are preserved that display asymmetrical shear bands with corresponding slickenlines and carbonate fibres, which

(a)

(b)

(c)

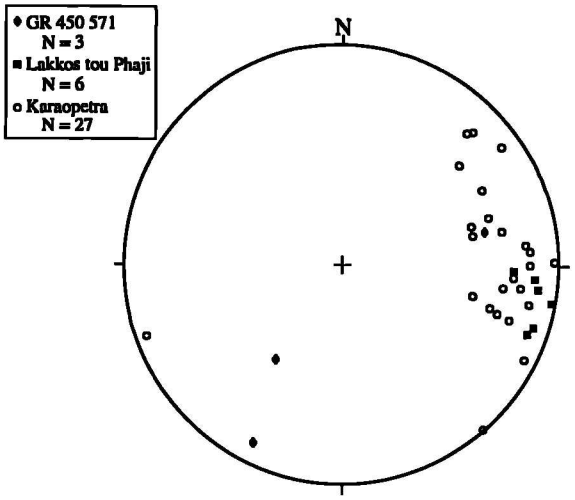

Figure 5.34. Structures within Mavrokolymbos Formation and data from Karaopetra. (a) Thrust and (b) Complex refolding (*cf.* Type III of Ramsay, 1967). (c) Stereographic projection of fold axes shown in (b) and also those measured at the localities noted above in Mavrokolymbos valley.

indicate top-to-the-WSW displacement (circles in Figure 5.35). In the footwall, Troodos lavas are brecciated and cross-cut by brittle, carbonate-mineralised shear fractures, which display cm- to ten cm-scale extensional offsets, indicating a consistent top-to-the-(W)SW sense of shear to that observed in the overlying serpentinite fault rocks [note that the geometry of pillow forms in the valley floor indicate that the Troodos lavas are the right way-up and dip shallowly (~10°W)]. This orientation contrasts with those observed up valley to the NE (see Figure 5.24 and above), suggesting a progressive steepening of the lavas, resulting in overturning (Swarbrick, 1979, 1993)

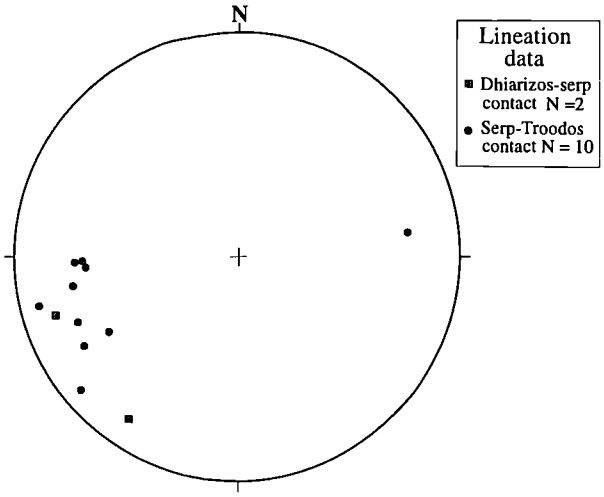

Figure 5.35. Stereographic projection of carbonate and serpentine fibre lineations on the Mavrokolymbos-serpentinite (squares) and Troodos-serpentinite contacts (circles) at the SW end of Mavrokolymbos valley. Note that contacts and foliation planes are not shown due to the variation in their orientation.

The serpentinite body, located on the northern side of the valley, crops out as a steep, 50m high, cliff face, which is cross-cut by steep to moderately-dipping, metre to ten metre-scale, brittle faults (labelled '3' in Figure 5.24). The majority of these structures are inaccessible, but metre-scale extensional offsets can be observed with the use of binoculars. The presence of both westerly and easterly-dipping faults suggests that the body has experienced vertical thinning, as was interpreted in the serpentinite body at the northeastern end of the section. However, the relative timing of these structures is largely unconstrained and they may be relatively late features.

The westernmost exposures of serpentinite are bounded by a NNW-SSE trending, 10 to 30m-wide, sub-vertical zone of highly brecciated and serpentinised ultramafic fault rock (labelled '4' in Figure 5.24). This zone comprises variably deformed clinopyroxenite, wehrlite and gabbroic dykes, which have intruded the serpentinised harzburgite host. Chilled dyke margins are found as clasts, and thus deformation is inferred to post-date intrusion. Blocks within the fault zone reach 10m

in diameter and are bound by 1m-wide shear zones, which display a brittle, foliated cataclasite fabric. Foliation within these zones is defined by the alignment of fractured serpentinite clasts and light-coloured serpentine fibres. Within the higher strain zones, the orientation of this foliation is relatively consistent, displaying NW-SE strikes and sub-vertical dips, but the orientations of serpentine fibre lineations are random and no consistent sense of displacement can be determined. Therefore, these fibres are thought to record local block rotations and translations within the host breccia fault zone. The inference that the brecciation associated with this zone is associated with westerly-directed thrusting is supported by evidence from the opposite side of the valley (GR 454 566). Here, the presence of cm-sized clasts of Troodos mafic intrusive rocks (basalt, dolerite and gabbro) in the serpentinite thrust sheets, suggests that brecciation is associated with thrusting.

To the east of this breccia zone, on the northern side of the valley, the massive serpentinite body is transected by prominent low-angle faults, which display concave upwards geometries that roughly parallel the contact with the Troodos Complex below (labelled '5' in Figure 5.24). Due to the inaccessibility of these faults, no distinct shear sense is determinable, but due to the parallelism with thrust contacts, they are interpreted to represent top-to-the-W/SW faults within the serpentinite body.

On the track at the base of the breccia zone, weathered Troodos lavas (± Kannaviou Formation sediments) are preserved. Although the contact between these two surfaces is unexposed, foliations defined by a gouge fabric within the Troodos lavas dips shallowly to the NE. These foliations approximately parallel the tectonic contact to the east, which suggests that serpentinite and the breccia zone have been thrust over the Troodos Complex. One possibility is that the breccia zone may represent an early extensional fault that was subsequently disrupted by thrusting. Alternatively, given the brittle, cross-cutting character of faults within the breccia zone, this contact may have also been reactivated as a late (extensional) fault. Unfortunately, due to the poor exposure of contacts at this locality no definite conclusion can be drawn.

5.4.2. Katarrakhtis Potamos valley section

As observed in the Mavrokolymbos cross-section, the geology of the Katarrakhtis Potamos valley is dominated by two distinct serpentinite bodies that are separated by a N-S trending sliver of Dhiarizos Group material (Figures 5.23 and 5.36; Map II). Exposure in the vicinity of this valley preserves evidence for a phase of westerly-directed thrust tectonism that formed the present day stacking pattern. A traverse and cross section from east to west, through the Katarrakhtis Potamos valley, best demonstrates the structure (Figure 5.36). The eastern contact between the Dhiarizos Group and the structurally overlying Ayios Photios Group (Vlambouros Formation) is not exposed. However, the outcrop pattern 'v's up the valley (GR 456 493), indicating that the contact dips shallowly (i.e. 20°) to the east. Where exposed along the valley floor, the Mavrokolymbos Formation strikes NW-SE and dips to the NE. Occasionally, metre-scale recumbent folds, that possess N-S-striking axial planes and gently southerly-plunging fold axes, are exposed (e.g. GR 455 592) (Stereonet (d), Figure 5.36). These metre-scale folds do not display a dominant vergence direction, but smaller-scale (<1m) folds located on the limbs to the larger folds verge to the west. The N-S striking contact between the Mavrokolymbos Formation and underlying serpentinite is well exposed north of the farm at GR 454 593. Note that this locality provides the best exposed section through a contact between serpentinite and an overlying unit belonging to the Dhiarizos Group throughout the Northern Region. The contact dips shallowly to the east and is characterised by heavily foliated and sheared Dhiarizos mudstones and lavas (average foliation = 159/32°E; stereonet (b) Figure 5.36). Carbonate and serpentine slickenfibres, and brittle slickenlines are consistently dip-slip and corresponding shear sense criteria in both units (including shear bands, S-C fabrics, vergence of asymmetrical folds and gouge fabrics) indicate uniformly top-to-the-WSW thrust displacements (Stereonet (b), Figure 5.36; Figure 5.37a).

Metre-scale irregularities in the strike of this contact are attributed to the incorporation of blocks of Dhiarizos lavas, mudstones and Kholetria limestone within the serpentinite adjacent to the contact. As suggested for similar relationships observed at the equivalent contact in the Mavrokolymbos section, these blocks are considered to have been stoped during serpentinite protrusion. Some blocks comprise carbonate cemented breccias, which contain Dhiarizos Group clasts and heavily weathered clasts that may be serpentinite. Note that the thrust contact cross-cuts these blocks in the serpentinite footwall, and thus thrusting clearly post-dates protrusion.

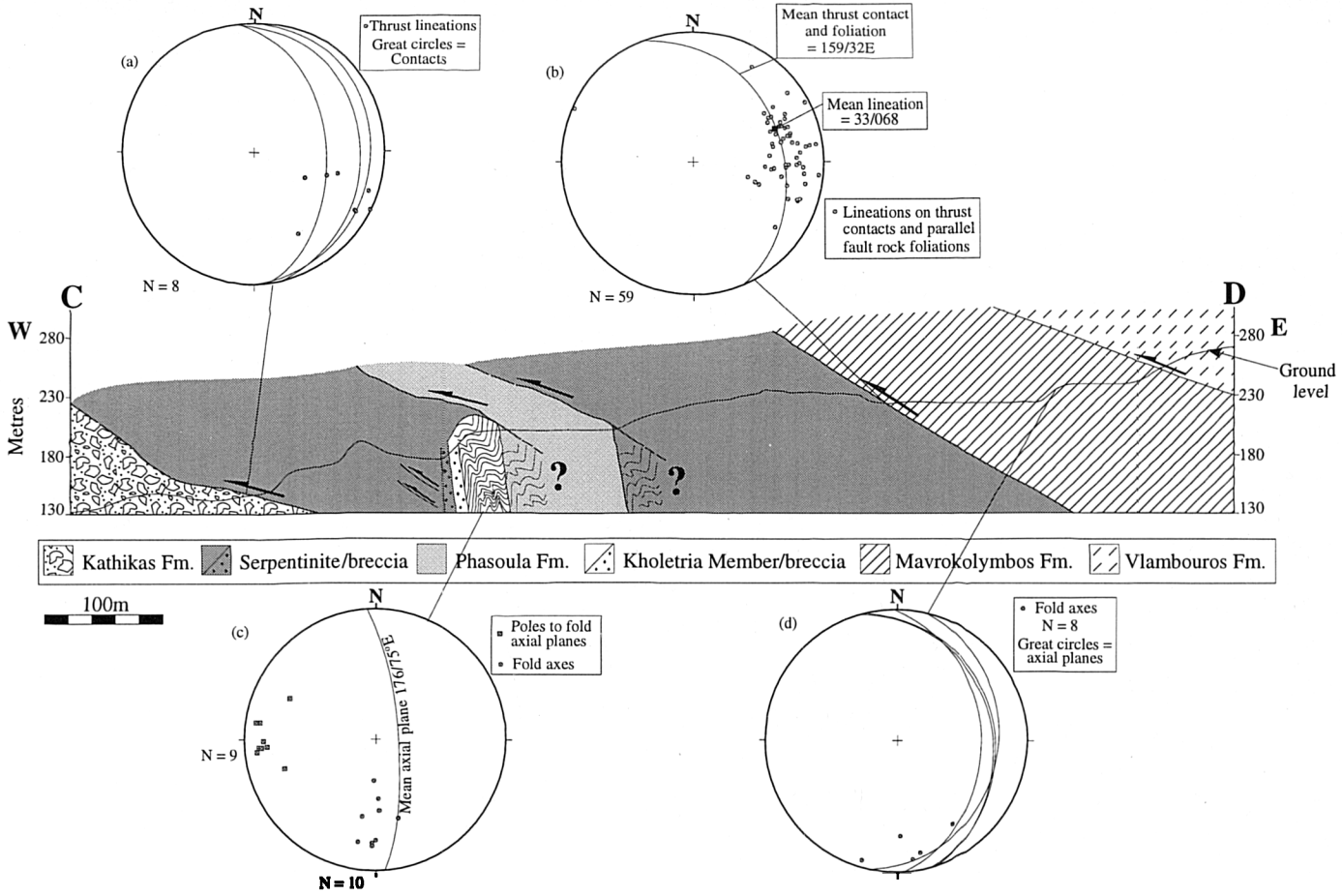

Figure 5.36. Data and cross-section through the Katarrakhtis Potamos valley. *The cross-section was constructed using observations and sketches from both* sides of the valley. Contacts placed above the line of topography have been roughly projected onto the section. (a) Orientations of brittle striae on the thrust contact, which indicates WNW-directed thrusting of serpentinite over the Kathikas Formation. (b) Lineations (brittle striae and mineral fibres) displayed by both the thrust contact and by foliations in both units (mean foliation plane shown as a great circle), indicating (south)westerly-directed thrusting of the Phasoula Formation over serpentinite. (c) Fold axes and poles to fold axial planes in Kholetria limestone block. Great circle shows the mean orientation of the axial planes. (d) Fold data from metre-scale folding of the Mavrokolymbos Formation at GR 455 592.

(a)

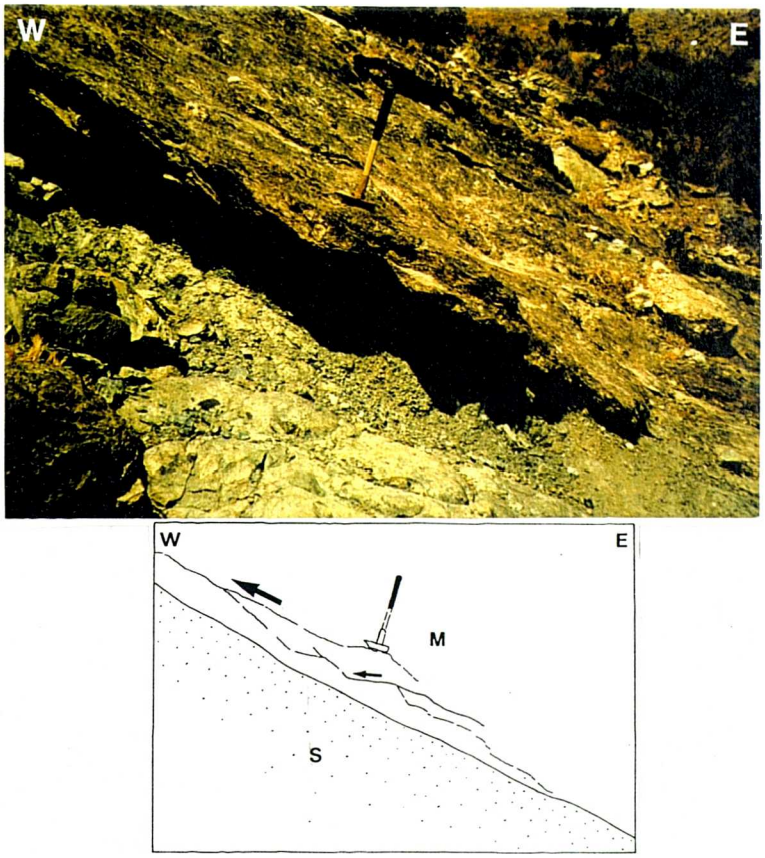

(b)

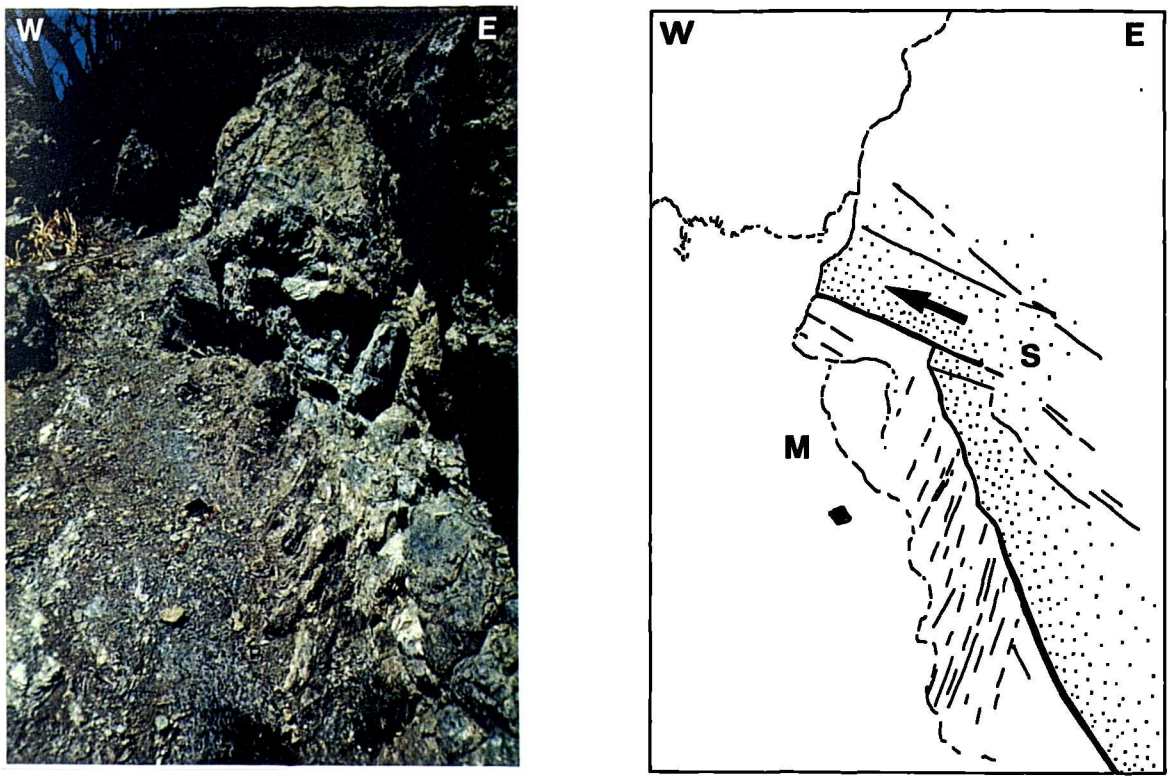

Figure 5.37. Structures from the Katarrakhtis Potamos valley cross-section. (a) Asymmetrical fault offsetting Dhiarizos Group mudstones (M; top) and serpentinite (S; below) to the west (left), indicating a westerly-directed sense of shear. (b) Example of a low angle, top-to-the-WSW thrust fault cross-cutting a sub-vertical, N-S trending contact and parallel fabrics in Dhiarizos Group mudstones (red; left) and serpentinite (blue; right) (GR 453 598).

(a)

(b)

Figure 5.37. (continued) (c) Upright folding in Kholetria limestones. Field of view is approximately 30m. (d) Thrust contact between serpentinite (hangingwall) and the Kathikas Formation debrites (red/brown breccias; footwall). Arrow indicates top-to-WNW displacement.

The easternmost contact between serpentinite and the central Dhiarizos Group sliver is poorly exposed within the valley. However, approximately 500m north of the Katarrakhtis Potamos valley, west of Stavlous, the easterly-dipping contact crops out (GR 454 598 in the south to GR 453 599 in the north). Stretching lineations along the contact vary from dip-slip on low angle sections of the contact to oblique-slip, with large pitch angles, on high angle sections and sub-vertical foliations. Kinematic indicators (S-C and shear band fabrics in foliated serpentinite gouge) associated with dip-slip lineations document top-to-the-west thrust transport, whilst structures on high angle to sub-vertical fabrics display predominantly sinistral senses of shear. Of

particular importance is the observation at one locality, where a high angle fabric in red mudstones is truncated by a low angle, top-to-the-WSW thrust contact, which suggests thrusting post-dates the formation of the sub-vertical, N-S striking fabric (Figure 5.37b; GR 453 598). An analogous geometry is observed on the south side of the valley, where the steeply dipping contact, which runs across contours in the valley floor, can be traced up slope and noticeably shallows (GR 451 592). This decrease in the dip of the contact is supported by the dominant shallow, easterly-dipping foliations within outcrops of Dhiarizos Group lavas and sediments, exposed on the track that runs to the farm in the valley.

To the east of the westernmost serpentinite-Dhiarizos Group contact, in the Katarrakhtis Potamos valley floor (GR 451 593), ten metre-scale folds are present within a large, N-S trending unit of Kholetria limestone (375m N-S and 40m E-W; Figures 5.24, 5.36 and 5.37c). These folds are typically upright, displaying open to tight forms, and some verge to the west. Fold axes plunge moderately to the south and axial planes strike N-S and dip steeply to the east (stereonet (c), Figure 5.36), which suggests that they formed in response to E-W shortening.

Immediately to the west of these folds, the contact between serpentinite and the Dhiarizos Group is obscured by a gulley. However, the serpentinite and Kholetria limestone either side of the contact are intensely brecciated in 5-10m-wide zones. This contact zone possesses vertical, N-S-striking foliations and vertically plunging slickenfibres and brittle striae, but no consistent shear sense criteria has been observed. To the west of the brecciated zone in the serpentinite, foliations dip moderately to the NE. Serpentine fibres and brittle striae on these foliation planes plunge predominantly to the east, which suggests that they represent minor thrust faults within the serpentinite. Westerly-directed thrust displacements are confirmed in higher strain zones within the serpentinite, which display shear band fabrics developed within foliated gouge and cataclasites. Looking south onto this contact, from the northern side of the valley, heavily weathered Dhiarizos lava and mudstone crop out directly above the serpentinite body. These outcrops display top-to-the-west shear sense criteria and are thus considered to be in situ. More importantly, these observations clearly demonstrate that the Dhiarizos-serpentinite contact, above the Kholetria limestone block, shallows abruptly to the west.

To the west, a low-angle, easterly-dipping tectonic contact between serpentinite and Kathikas Formation debrites is well exposed in the valley (GR 449 593; Figure 5.36d). In general, the contact is planar and displays dip-slip brittle striae, which plunge gently towards the east (stereonet (a); Figure 5.36). Within an 8cm zone adjacent to the contact, the Kathikas Formation in the footwall is intensely foliated and clasts are finely comminuted, producing a friable gouge fabric. Shear sense criteria

within this gouge layer (S-C fabrics and deflection of gouge fabric) are consistent with westerly-directed thrust transport, placing serpentinite over the Kathikas Formation. This contact relationship is unique to SW Cyprus as the Kathikas debrites typically depositionally overlie the serpentinite-filled fault zones. Thrusting of serpentinites over the Kathikas Formation, which is generally considered to be the earliest post-deformational unit in SW Cyprus, may suggest that compressional deformation continued into the latest Maastrichtian.

5.4.3. Mavrokolymbos area: summary and discussion of field relationships

The above observations suggest that the Mavrokolymbos area experienced the following three-phases of deformation:-

- An initial extensional or transtensional event during which the dominant N-S striking structural trend in the area was formed;
- Westerly-directed displacement along shallowly-dipping thrusts, which resulted in the regionally observed thrust stack development of, from, base to top, Troodos Complex-serpentinite-Mamonia Complex;
- Late extensional faulting along steeply-dipping N-S striking faults.

5.4.3a Early Extension

The dominant N-S-striking structural trend observed throughout the Mavrokolymbos area is thought to have originated during an extension or transtensional phase that pre-dated thrusting for the following reasons:

(a) The sub-vertical contacts between the central Dhiarizos Group sliver and serpentinite, observed in the Katarrakhtis Potamos valley cross-section, shallow abruptly at higher topographic levels. On an outcrop scale, this relationship is explained by the truncation of pre-existing, sub-vertical structures by low angle, thrust-related fabrics.

(b) The unusual presence of Troodos Complex mafic and ultramafic intrusive rocks within the sub-vertical, N-S striking breccia zone, which bounds the serpentinite body at the southwestern end of Mavrokolymbos valley, could be explained if this zone once underwent extension. Subsequent to intrusion, this zone has been disrupted and brecciated, possibly during thrusting.

(c) Field observations suggests that much of the protrusive emplacement of serpentinite was facilitated during a phase of extension, which mainly took place prior to thrusting. Several steeply-dipping, extensional faults that are associated with serpentinite protrusion are cross-cut by low-angle, top-to-the-west faults. Evidence

for the derivation of serpentinite from depth is demonstrated by the existence of serpentinite dykes within the Troodos Complex footwall in Mavrokolymbos valley (Figure 5.32). Although the geochemical affinity of these dykes cannot be determined due to their high degree of serpentinisation, serpentinised material of similar appearance (i.e. pervasively serpentinised, light-blue coloured, fine-grained melange) fills steeply dipping extensional faults that cross-cut Dhiarizos Group units, Troodos Complex rocks and serpentinite. These structures (e.g. Figure 5.27), which are exposed on the tracks on both sides of Mavrokolymbos valley (e.g. GR 455 575), are truncated by overlying, top-to-the-W, thrust faults, suggesting that they formed prior to thrusting.

(d) The upright folds within Kholetria limestones in the Katarrakhtis Potamos valley are thought to form during westerly-directed thrusting by 'buttressing' against pre-existing, steeply-inclined structures (see below).

The northeastern Dhiarizos Group-serpentinite contact exposed in Mavrokolymbos and Katarrakhtis Potamos valleys also preserves evidence to suggest that protrusion pre-dated thrusting. Both sections of the contact display low strain zones, in which weakly deformed blocks of Dhiarizos Group material are entrained within serpentinite. These relationships are considered as evidence for a 'stoping' mechanism during serpentinite protrusion/intrusion. Most significant of this Dhiarizos Group-serpentinite contact is that in the Mavrokolymbos valley it clearly displays extensional kinematic indicators, whilst in the Katarrakhtis Potamos valley the same contact is a thrust. The contrasting structures preserved along this contact suggests that they formed during separate tectonic events. Based on the previous observations and interpretations that suggests protrusion-related extensional structures pre-date thrusting, this contact is inferred to have initiated as an extensional structure that was subsequently reactivated as a thrust.

Malpas *et al.* (1993) propose that the dominant N-S architecture in the Mavrokolymbos area was formed during extension prior to thrusting. Alternatively, Swarbrick (1993) does not consider this phase of deformation, but suggests that the northeastern extensional faulted contact in the Mavrokolymbos valley section assisted protrusion in a transpressional 'root zone'. The observations summarised above favour the former hypothesis and a model is proposed whereby an initial phase of extension/transtension is thought to have aided protrusion of ultramafic material and to have formed the N-S striking structural trends. The timing of this event is poorly constrained, but the occurrence of extensional faults that offset lavas and intrusive mafic rocks belonging to the Troodos Complex, suggests that deformation took place subsequent to (±during) the formation of Troodos crust (i.e. post 90Ma; Mukasa and Ludden, 1987).

5.4.3b. Westerly-directed thrusting

The dominant deformational phase preserved in the Mavrokolymbos area is clearly top-to-the-west thrusting, which is documented by a variety of structures, including, low angle thrusts, associated extensional faults and westerly-verging folds. The excellent exposure of these structures within this area, particularly along the two valleys discussed above, provide an insight into the mechanisms responsible for the development and displacement of the thrust sheets throughout the Northern Region. The common occurrence of extensional structures, which typically display a synthetic sense of shear to the westerly-directed thrust contacts, are interpreted as forming during thrusting and they may be particularly useful in interpreting:
(1) the sequence of thrust stacking and,
(2) the mechanics of the thrust wedges.

Sequence of thrusting
The geometry and cross-cutting relationships between top-to-the-W/WSW structures, which are observed along the Mavrokolymbos valley section, suggest that the structurally highest faults formed generally later than the lowermost structures. This interpretation suggests that the thrust stack developed in an overstep thrust sequence (Butler, 1982). The best examples are associated within the sub-horizontal sliver of Dhiarizos material located on the Mavrokolymbos dam track at GR 575 455 (see Figures 5.25, 5.26, 5.27 and 5.38). Along this sliver, red mudstones and green lavas are intercalated and repeatedly juxtaposed along consistently, westerly-dipping extensional faults (mm to m-scale). The largest of these structures is clearly truncated by the sub-horizontal, basal detachment of the overlying serpentinite thrust sheet (Figure 5.26). The only viable way in which this geometry could have formed is by the development of asymmetrical extensional faults during westerly-directed spreading of the underlying thrust sliver, that were subsequently cross-cut by the overriding serpentinite thrust sheet (see below). Furthermore, the structurally lowermost tectonic contacts, situated directly below this section at the foot of the dam wall, also appear to be cross-cut by the serpentinite detachment. As these easterly-dipping structural contacts are traced upwards, towards the dam track, they are lost at the approximate location where the serpentinite detachment and the Dhiarizos sliver cuts down section, below the level of the track. This observation once again suggests that these lowermost thrusts are truncated by the overlying serpentinite thrust sheet, thus supporting the hypothesis that the thrust stack developed by an overstep thrust sequence (Figure 5.38).

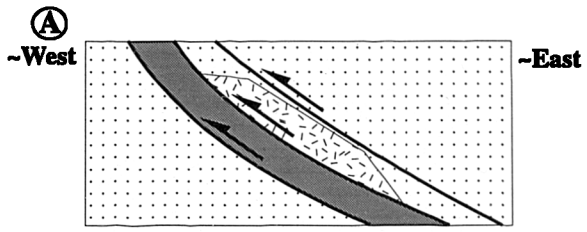

Thrusting within the Troodos Complex:
imbrication of Troodos-serpentinite-gabbro units

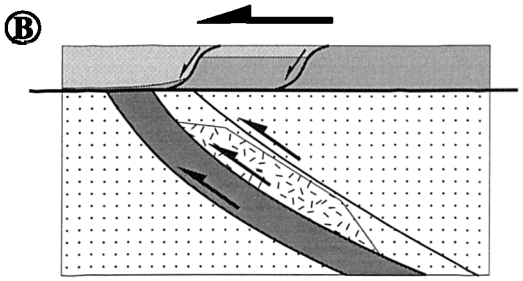

Overriding Dhiarizos Group thrust sheet:
asymmetrical top-to-the-W extension intercalates Dhiarizos units

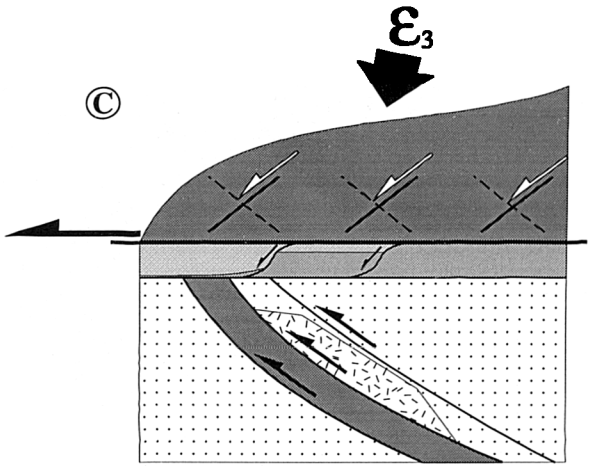

Emplacement of the main serpentinite thrust sheet:
truncation of extensional faults within the Dhiarizos sliver.
Deformation of the thrust sheet by vertical thinning and asymmetrical, top-to-the-W extension

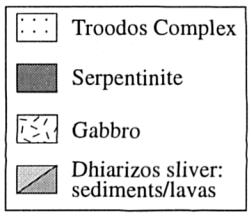

Figure 5.38. Schematic diagram explaining the stacking sequence observed at the northeastern end of the Mavrokolymbos Dam section by an overstep thrust model. Compare with Figures 5.26, 5.28 and 5.29a. Note that the main thrust contacts, from A to C, form at structurally higher levels.

Thrust mechanics

As negligible strike-slip partitioning of the compressional strain is observed, orthogonal shortening is inferred to have caused thrusting on the scale of the Mavrokolymbos area (i.e km-scale). However, the exact orientation of regional shortening is uncertain due to the differences in the direction of thrusting in the two sub-areas studied; WSW in Mavrokolymbos valley and WNW at Katarrakhtis Potamos (Figure 5.39a). There is no overprinting evidence to suggest that two different phases of thrusting occurred, as proposed by Malpas *et al.* (1993). The difference in thrust displacement direction could relate to the pre-existing structural architecture in these two areas and/or to the operation of specific dynamic processes in the evolving thrust wedges. A significant observation in this area is that NW-SE strikes dominate in the Mavrokolymbos section, whilst N-S-strikes are observed at Katarrakhtis Potamos, so that the direction of thrusting in both sub-areas is approximately perpendicular to the local strike of the fault zones (Figure 5.39b). This relationship is identical to that observed within the Akamas and Loutra tis Aphroditis areas, which is briefly described in Section 5.3. As discussed in Section 5.3, this relationship between the tectonic transport direction and the strike of the fault zone is similar to the radial, arc-normal pattern of displacements around the Alpine chain, discussed by Platt *et al.* (1989). In their interpretation, Platt *et al.* (*op cit.*) suggested that radial thrusting reflected the effect of locally generated body forces within the thrust wedge. Specifically, they proposed that the deformation was driven by the combined effects of plate convergence and gravitational forces that were generated within the wedge. In the Mavrokolymbos area, structural evidence strongly suggests that gravity tectonics were important, if not a controlling factor during thrusting. Kinematic analyses of structures within the northeastern serpentinite body in the Mavrokolymbos section suggest that the serpentinite thrust sheet deformed by asymmetrical vertical thinning, which was accommodated by predominantly top-to-the-west extensional faults synchronous with westerly-directed thrusting. This suggests that the maximum principal shortening direction was sub-vertical or steeply plunging within the serpentinite thrust sheet, and that the whole body may have been deforming by a gravity spreading mechanism. One possibility is that subsequent to vertical thickening during E-W shortening, the taper of the thrust sheet exceeded a critical value (the 'critical taper' of Davis *et al.* 1983). In order to attain a mechanically stable configuration (i.e. a geometry in which the forces controlling the mechanics of the wedge are in equilibrium) during compression, the serpentinite sheet accommodated vertical thinning by asymmetrical extension. The direction of extension is determined mainly by the direction of slope of the upper surface of the thrust wedge (Elliott, 1976; Platt, 1986; Platt *et al.* 1989). It is suggested that differences in the transport directions may have arisen due to

differences in the direction of surface slope, which in turn may have arisen due to the existence of a pre-existing, irregular footwall architecture (Figure 5.40). The presence of early, N-S trending, steeply-dipping normal faults is thought to have caused inversion and buttressing effects during westerly-directed thrusting (Figure 5.41; *cf.* Figure 24 in Butler, 1987).

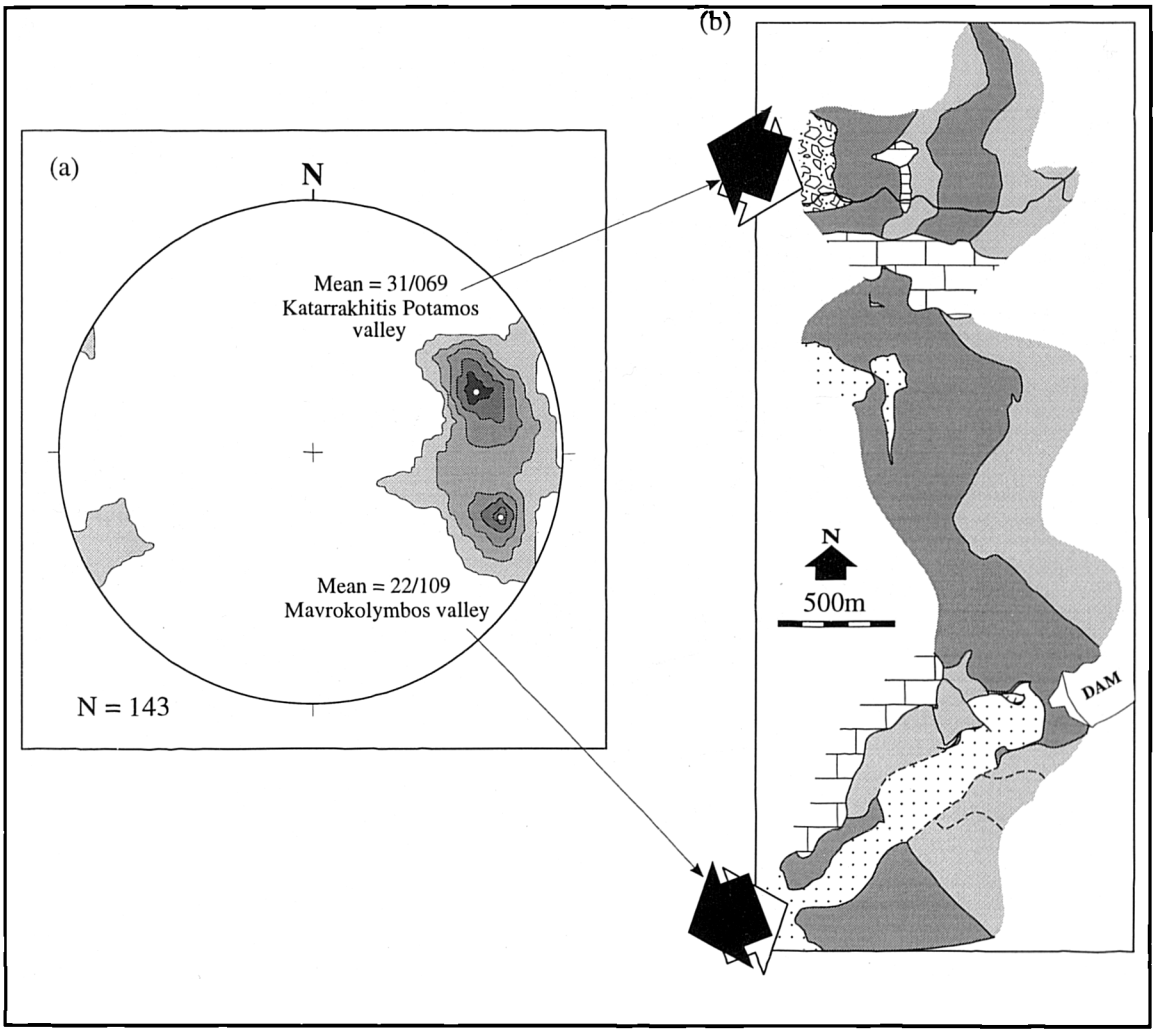

Figure 5.39. Summary of westerly-directed transport directions from the Mavrokolymbos area. (a) 1% area contour of stretching lineations (brittle striae, carbonate and serpentine fibres) taken from westerly-directed thrust contacts. (b) Mean orientations of thrust transport directions, showing top-to-the-WSW dominates in the Mavrokolymbos valley, whilst top-to-the-WNW are dominant in the Katarrakhtis Potamos valley.

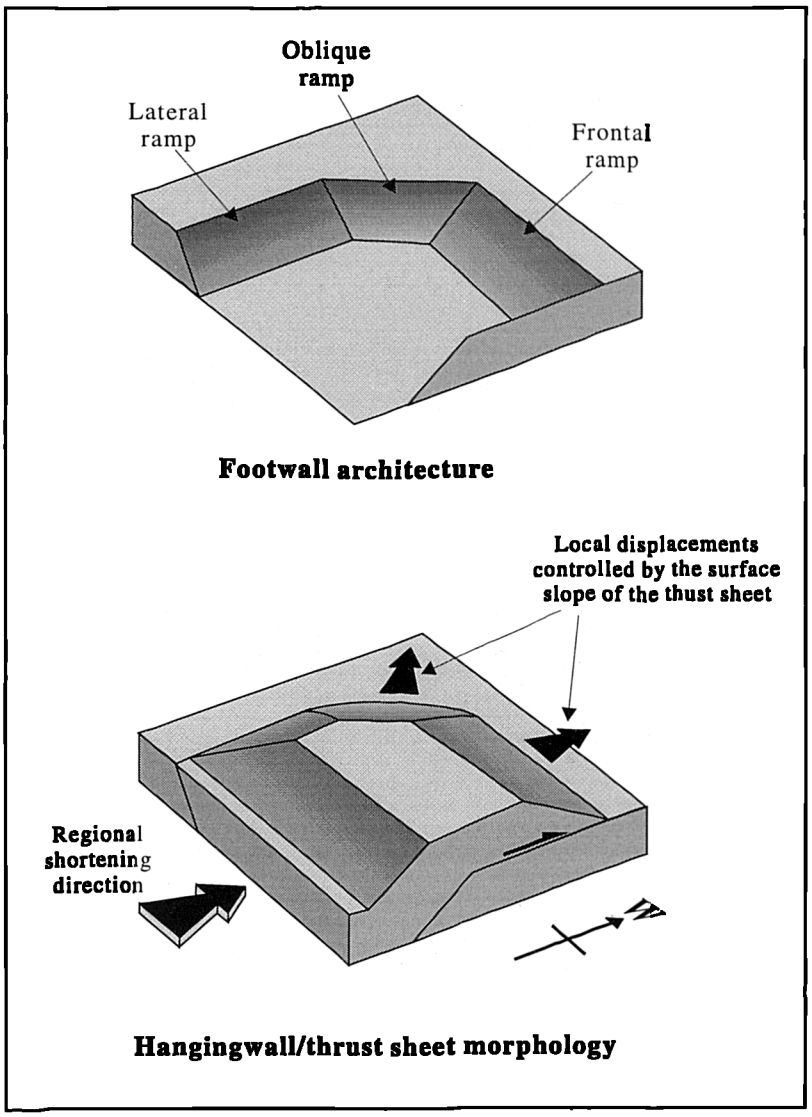

Figure 5.40. Schematic model explaining how differences in the transport direction arise due to differences in the orientation of surface slope resulting from thrusting over a pre-existing, irregular footwall architecture.

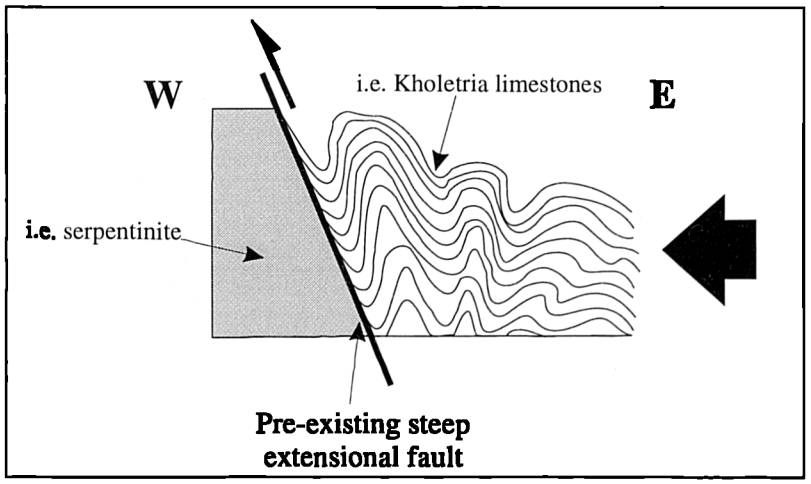

Figure 5.41. Schematic diagram showing the process of buttressing, which is considered suggestive of the inversion of normal faults during thrusting (*cf.* Butler, 1987). Compare with the folding of Kholetria limestones in Figure 5.36 and 5.37c.

Published studies of the mechanics of thrust wedges show that the deformation is also strongly influenced by the rheological properties of the wedge material and also by the mechanical strength of the basal layer (e.g. Elliott, 1976; Chapple, 1978; Platt, 1986). In the Mavrokolymbos area, serpentinite and Mamonia mudstones comprise a large volume of the thrust stack. These rocks are generally considered to be rheologically weak, a hypothesis supported by the presence of structures in these units that display characteristics of macroscopically ductile deformation. The ubiquity of top-to-the-west shear sense criteria along the basal detachment that separates the main serpentinite thrust sheet from the underlying Dhiarizos Group sliver at the northeastern end of the Mavrokolymbos section, suggests that this was a zone of localised shear strain. The intense serpentinisation and fluid flux that is evident within the fault rocks along this zone suggest that it may have been a layer of mechanical weakness during thrusting. Although some carbonate mineralisation along this contact is inferred to have taken place subsequent to thrusting, at least part of the observed fluid flux is interpreted to have been contemporaneous with top-to-the-west displacement. The evidence for high pore-fluid pressures along the detachment (i.e. vuggy veins, veins that extend down into the Dhiarizos footwall), supports the interpretation that this may have been a mechanically weak layer. The implications of, and interplay between, fluid flow and shear fracture are discussed in greater detail in Chapter 6.

5.4.3c. Folding

Folds observed within the two sections display two different orientations; easterly-plunging in the Mavrokolymbos section and southerly-plunging in the Katarrakhtis Potamos section (Figure 5.42). The N-S trending folds in the Katarrakhtis Potamos section, particularly the westerly-verging, upright folds in the Kholetria limestone block at GR 451 593, are interpreted as forming during westerly-directed compression and buttressing (Butler, 1987) against a pre-existing normal fault scarp immediately to the west. The presence of broadly E-W trending folds is more problematic. The NE-SW to E-W trending folds at Karaopetra appear to have been refolded by folds of similar orientations, but as no N-S folds are observed, no relative age relationships between different orientations of folding are evident. On the basis of fold facing and vergence directions, Robertson and Woodcock (1979) proposed that the Ayios Photios Group was emplaced towards the NE over the Dhiarizos Group by gravity sliding down the Mamonia passive margin, prior to their juxtaposition with the Troodos Complex. The easterly-plunging folds observed within the Mavrokolymbos Formation in the Mavrokolymbos area may relate to this pre-thrusting event.

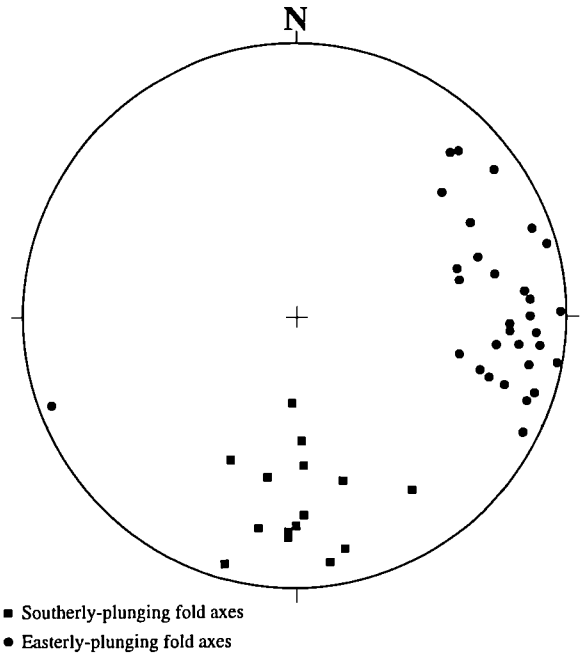

Figure 5.42. Total fold axes from Mamonia Complex sediments in the Mavrokolymbos area.

5.4.3d. Late extensional faulting

Late extensional faulting is thought to have complicated the present day outcrop pattern. For example the disrupted and poorly exposed Vlambouros Formation sandstones in the middle of the Mavrokolymbos valley section are thought to have been downfaulted or landslipped. Furthermore, considerably better exposed sub-vertical faults, located immediately to the west of Mavrokolymbos dam wall, offset thrust contacts and also all three of the major units (i.e. serpentinite and both the Mamonia and Troodos Complexes).

PART FOUR
CONCLUSIONS

CHAPTER SIX
SYNTHESIS, DISCUSSION AND CONCLUSIONS

6.1. Introduction

This chapter is sub-divided into three sections that summarise and discuss the main findings of this study:

1. Presents the findings of the present work that can be used to constrain a regional tectonic model, explaining the evolution of SW Cyprus.
2. Discusses processes leading to rheological weakening of the ultramafic fault zones in SW Cyprus at high and low temperatures.
3. Introduces a new transpressional strain model based on observations made in the Southern Region.

6.2. Summary of Upper Cretaceous tectonic events in SW Cyprus

The structural model which has emerged from this study involves the Mamonia and Troodos Complexes in SW Cyprus in three, intra-oceanic, tectonic events, which occurred during the Upper Cretaceous. These include:

- high temperature (>600°C), dextral strike-slip faulting during Turonian to Santonian times (~90-83Ma), documented by the peridotite mylonites of the Southern Region and possibly in the harzburgite tectonites at Loutra tis Aphroditis in the Northern Region (Section 6.2.1);
- dextral transtension in the Southern Region and extension (or transtension) in the Northern Region, associated with serpentinite protrusion (Section 6.2.2);
- low temperature (~100°C) sinistral transpression in the Southern Region and top-to-the-west thrusting in the Northern Region. These predominantly compressional deformations are thought to reflect the final docking of the Troodos microplate with the Mamonia Complex, which ceased by the end of the Maastrichtian (~65Ma) (Section 6.2.3).

6.2.1. Early high temperature strike-slip

The earliest deformational event in SW Cyprus is preserved in the amphibolite-facies metamorphic units of the Ayia Varvara Formation, the peridotite mylonites of the Southern Region (Section 4.2), and the cataclastic-textured peridotite tectonite fabrics exposed at Loutra tis Aphroditis (Section 5.2.3). The close spatial relationship between these three units and the Dhiarizos Group suggests that they are genetically related. Several other pieces of evidence support this conclusion:

- based on geochemical studies and field observations, the protolith for the Ayia Varvara Formation is interpreted to be the intercalated lavas and sediments of the Dhiarizos Group (e.g. Malpas *et al.* 1992, 1993);
- spinel chemistries in the deformed peridotites suggest they are associated with the Mamonia Complex (see Chapter 3);
- strike-parallel stretching lineations and inferred dextral kinematics (Spray and Roddick, 1981) in the Ayia Varvara Formation are coincident with those observed during the present study within the deformed peridotites (Sections 4.2.1 and 4.2.2), and
- the temperature of metamorphism for the amphibolites is estimated to be ~600°C and <5kbar (Spray and Roddick, 1981; Malpas *et al*, 1992), which is similar to those proposed for the peridotite mylonites (>600°C; Section 4.2.4).

Numerous geodynamic models have been proposed to explain the formation of the Ayia Varvara amphibolites, but none are generally accepted. The three most plausible possibilities are as follows:-

- Dynamothermal metamorphism at the base of an obducted ophiolite (i.e. the Troodos Massif) (Lapierre, 1972; Woodcock and Robertson, 1977).
- Metamorphism of Late Triassic oceanic lithosphere (i.e. the Dhiarizos Group) within a northward-dipping, intra-oceanic subduction zone by the overriding Troodos crust (Malpas *et al.* 1992).
- Dynamothermal metamorphism due to proximity of the newly formed Troodos crust during ridge-ridge transform movements, with or without a component of shear heating (Swarbrick, 1980; Spray and Roddick, 1981).

The lack of steep *P-T* profiles within the amphibolites (Spray and Roddick 1981; Malpas *et al.* 1992), combined with autochthoneity of the Troodos Massif (Gass *et al.* 1994), negates the proposal that the Ayia Varvara Formation represents the aureole to an obduction-related basal thrust. Whilst metamorphism within a subduction zone is possible, the hypothesis that the amphibolites and the related peridotite mylonites were generated within an oceanic transform setting is favoured due to field observations and analogies with structures observed along the South

Troodos Transform Fault Zone (STTFZ). Firstly, the fabrics discussed in Chapter 4 from the Southern Region are similar to ultramafic and mafic mylonites described from the transform (e.g. MacLeod and Murton, 1993, 1995; Gass *et al.* 1994). Secondly, kinematics within the STTFZ mylonites also indicate dextral strike-slip. Thirdly, estimated temperatures of formation of these mylonites (Murton, 1986b), coupled with the localised development of amphibole, indicate analogous conditions to those described in the mylonites of the Southern Region.

The peridotite tectonites preserved at Loutra tis Aphroditis are considered equivalent to the mylonites in the Southern Region (Section 5.2.3). The parallelism between the strike-parallel stretching lineations in the deformed peridotite units in both regions with those observed in the adjacent Ayia Varvara Formation metamorphic rocks, suggests that they may have formed during the same tectonic event. Unfortunately, no shear sense criteria has been found at Loutra tis Aphroditis, therefore dextral strike-slip, which would conclusively link these rocks to the mylonites in Southern Region, cannot be confirmed. There are also significant differences between the peridotite fabrics in both regions, which suggests that they experienced distinctly different deformational conditions. Specifically, the peridotite mylonites in the Southern Region are much finer grained and they possess amphibole. The difference in grain-size suggests that the mylonites in the Southern Region were deformed under higher flow stresses and lower temperatures than those exposed at Loutra tis Aphroditis (*cf.* Ross *et al.* 1980). The presence of amphibole in the Southern Region mylonites is thought to have resulted from the ingress of hydrous fluids during deformation. In contrast, the anhydrous mineral assemblage preserved at Loutra tis Aphroditis indicates that hydrous fluid flux did not affect these mantle rocks. From these observations, two conclusions are presented:

(1) The similarity in the geochemistry of these rocks (i.e. determined using spinel chemistries; Chapter 3), combined with their spatial relationships with the Ayia Varvara Formation, suggests that they are at least genetically related to the same tectono-metamorphic event (see below).

(2) The difference in the syn-kinematic mineral assemblage and the intensity of deformation may be explained by strain localisation within these mantle-derived rocks. Many ophiolitic complexes and ultramafic bodies preserve generations of cross-cutting shear zones that formed during progressive, reaction-related, grain-size reduction, accompanied by an increase in the degree of strain localisation (e.g. Girardeau and Mercier, 1988; Rutter and Brodie, 1988; Drury *et al.* 1990; Hoogerduijn Strating *et al.* 1993; Vissers *et al.* 1995). In these examples, coarse granular mantle peridotites are transected by a sequence of tectonite to mylonite shear zones, which record progressive decreases in temperature and concomitant

increases in flow stress. These shear zones are typically sites of localised, syn-kinematic hydration reactions, resulting from the ingress of mantle-derived magmatic fluids and later by crustally-derived hydrous fluids (e.g. Agrinier *et al.* 1993). Unfortunately, due to a lack of exposure, a similar relationship between the fabrics observed in the Southern Region and at Loutra tis Aphroditis cannot be confirmed.

In order to explain the generation of the Ayia Varvara Formation, the origin of the heat source required to cause the metamorphism must be explained. Using $^{40}Ar/^{39}Ar$ geochronolgy, Spray and Roddick (1981) determined the age of metamorphism for the Ayia Varvara Formation at 83-90Ma. These ages are coincident with the age of formation of the Troodos Complex (~92-90Ma; Mukasa and Ludden, 1987). It is possible, therefore, that the heat required for metamorphism may have been supplied by the newly formed Troodos crust. Such a model is consistent with the discrepancy between the temperatures constrained for the Ayia Varvara Formation (~600°), fluidal mylonites (~600°), and the amphibole-rich peridotite mylonites (~800°C) in the Southern Region (Section 4.2.4). The increase in temperature associated with the transition from fluidal to amphibole-rich peridotite mylonites is consistent with a syn-kinematic, contact metamorphic event that resulted from the juxtaposition of Mamonia Complex crustal and mantle rocks against young, hot Troodos crust.

An alternative heat source for metamorphism of the Ayia Varvara Formation may be supplied by the ambient temperature of the upwelling peridotite. As demonstrated by Spray and Roddick (1981), temperatures of 1000°C for the peridotite mylonites could yield a contact temperature in the region of 600°C for the amphibolites. The estimated temperature of the peridotite mylonites preserved in the Southern Region (i.e. maximum ~800°C) may not be high enough to explain the metamorphism alone. On the other hand, the Loutra tis Aphroditis harzburgite tectonites may well have been in the region of 1000°C and thus, may have caused the metamorphism. Shear heating may also be an important factor, but it is not expected to be able to generate high enough temperatures alone to cause the metamorphism (Swarbrick, 1979; Spray and Roddick, 1981).

Considering the evidence presented above, a model is favoured whereby Triassic oceanic crustal material and associated mantle rocks were involved in transform-related, dextral strike-slip faulting in proximity to the Troodos Complex in Turonian to Santonian times (~90-83Ma; Spray and Roddick, 1981). During this event, the newly formed Troodos Complex and/or hot Mamonia peridotites acted as a heat source that was responsible for the metamorphism of the Ayia Varvara Formation. The timing and nature of this event are regionally significant, as it implies that the

Mamonia and Troodos Complexes were in close proximity as early as 90-83Ma. This observation contrasts with previous published models, which propose that the two complexes were still apart by the latest Campanian (e.g. MacLeod, 1990; Murton, 1990; Robertson, 1990; Swarbrick, 1993; Malpas *et al.* 1993; Gass *et al.* 1994).

Dextral strike-slip displacements during this early event may have occurred over a longer period of time than that inferred by the Ar/Ar dates derived by Spray and Roddick (1981). These ages merely record the time at which the temperature of these rocks fell below the blocking temperature for Ar diffusion in amphibole (600-550°C) and not the cessation of metamorphism and deformation. Therefore, deformation may have initiated prior to 90Ma and continued after 83Ma.

The presence of the peridotite mylonite types observed in the Southern Region is of profound importance as they display microstructures that suggest the operation of highly efficient grain-scale deformation mechanisms (Section 6.3). Such mechanisms are generally considered to lead to fault zone weakening and are capable of accommodating very large strains (i.e. displacements of 10's to 100's of Km) (e.g. Boullier and Guegen, 1975; Girardeau and Mercier, 1988; Drury *et al.* 1990; Vissers *et al.* 1995).

6.2.2. Transtensional and extensional deformation

Evidence of dextral transtension associated with serpentinite protrusion is preserved throughout the Southern Region. As dextral and extensional faults juxtapose serpentinite against adjacent units without contact metamorphism, this phase is assumed to have occurred at much lower temperatures than the previous event. Whether this dextral deformation relates directly to the earlier episode of right-lateral strike-slip is difficult to establish, but the occurrence of rare chlorite-bearing dextral fabrics that document the down temperature evolution of the fault zones may be used as tentative evidence to suggest continuous displacement (i.e. post 83Ma).

Although substantial kinematic evidence for a corresponding deformational event is lacking in the Northern Region, the dominant N-S structural trend observed throughout the region is inferred to have been inherited from a phase of extension prior to Maastrichtian thrusting (Sections 5.3 and 5.4). The existence of steep extensional faults in the Mavrokolymbos area, interpreted to be protrusion-related structures, supports this hypothesis (Section 5.4.1b). The geometry of the structures produced during Maastrichtian thrusting are thought to have resulted to some extent from the reactivation of pre-existing, steeply-dipping extensional faults. Examples of this chronology include thrust-related structures which cross-cut sub-vertical fabrics, folding that is interpreted to have resulted from buttressing against steep, pre-existing

faults, and the inference that an irregular, pre-existing, footwall architecture influenced displacement directions during thrusting (Section 5.4.3). Based on the deformational chronology observed in both regions, the dextral transtensional deformation in the Southern Region and extension in the Northern Region are considered to be broadly coeval.

The age of this event is difficult to constrain accurately. In the Southern Region, dextral transtensional structures are predominantly associated with Troodos lavas. Therefore, transtension clearly post-dated the formation of the lavas (post 92-90Ma; Mukasa and Ludden, 1987). In comparison with the Troodos Complex igneous rocks, transtensional structures associated with the Mamonia Complex are relatively rare. However, dextral fabrics, which pre-date sinistral transpressional structures, are found in the Ayia Varvara area (e.g. Kara tou Ayiou Pati; Section 4.3.1), and protrusion-related extensional structures affecting Dhiarizos Group units are observed in the Mamonia area (e.g. Moutti tis Koronas; Section 4.3.2c). Both examples are associated with peridotites and serpentinites related to the Mamonia Complex. Therefore, it is suggested that dextral transtension in the Southern Region affected both Mamonia and Troodos Complex rocks. Furthermore, dextral trantensional structures deform serpentinites associated with both Mamonia and Troodos Complexes, which implies that both serpentinite types had been emplaced at high structural levels prior to and/or during this event. Steeply-dipping structures associated with the extensional event in the Northern Region also affect both the Mamonia and Troodos Complexes, which is consistent with the observations made in the Southern Region. Therefore, it is proposed that both complexes were juxtaposed prior to, or during, a broadly extensional event that took place after the formation of the Troodos igneous rocks. However, evidence that may be used to date the cessation of this event is poor. The youngest unit associated with dextral transtension is the Kannaviou Formation, which is bound by dextral and extensional faulted contacts in the Kannaviou area. The age of the Kannaviou sediments is poorly constrained, but they are generally considered to be no younger than Campanian in age (Urquhart and Banner, 1994). Mapping, as part of this thesis (Section 4.3.2d) and by Gass *et al.* (1994), of the contact between the main Troodos massif and the Mamonia Complex, located immediately to the SE of the Kannaviou region, suggests that the dominant NW-SE structural trend observed in this area resulted from dextral deformation. Steep NW-SE trending structures, which are associated with both the Mamonia and Troodos Complexes are correlated with analogous structures in the STTFZ (Gass *et al. op cit.*). Deformation of Troodos Complex cover sediments (e.g. Perapedhi and Kannaviou Formations) in both the Kannaviou area and the STTFZ constrain this phase of deformation to late Campanian to early Maastrichtian (see Gass *et al. op cit* for further

details from the STTFZ). Deposition of the Kannaviou Formation is thought to have been localised to bathymetric lows, which Malpas *et al.* (1993) considered to have been graben features, developed exclusively within the Troodos Complex during extensional tectonism synchronous with Troodos magmatism. This idea is modified here as transtensional and extensional structures observed in this study deform *both* Mamonia and Troodos Complex units. Kannaviou deposition is considered to be contemporaneous with, and/or post-date, transtensional deformation in the Southern Region and the Kannaviou area, and extension in the Northern Region. Therefore, this phase of broadly extensional tectonism is approximately constrained to the time period during and shortly after the Campanian.

6.2.3. Late-Maastrichtian compressional deformation

Westerly-directed thrusting in the Northern Region and pure shear-dominated sinistral transpression in the Southern Region are considered to be coeval for a number of reasons:

- The structures observed in both regions, relating to these deformations, are the most dominant and they record the last, main deformational event;
- Both have resulted in a pervasive structural overprint associated with the development of lizardite-dominated fault rocks within the serpentinite-filled fault zones. Thrust and transpressional fault rocks exhibit identical deformational characteristics and are typically associated with syn-tectonic carbonate mineralisation (Section 4.4.1 and Chapter 5);
- Neither deformational event is seen to overprint the other and both are broadly compressional in character.

This regional compressional event is thought to record the final docking of the Troodos microplate with the Mamonia Complex, which took place after the latest Campanian and prior to the late-Maastrichtian (Swarbrick and Naylor, 1980; Urquhart and Banner, 1994). The lower age is determined by the deformation of Kannaviou sediments, whilst the younger age is constrained in the Northern Region by the deposition of the Upper Maastrichtian Kathikas Formation debrites (Chapters 1 and 5). The Kathikas sediments are the first, post-tectonic unit to have been deposited across the Mamonia and Troodos Complexes and their juxtaposing serpentinite-filled fault zones (Swarbrick, 1979; 1980; Swarbrick and Naylor, 1980; Swarbrick, 1993). These debrites are restricted to the Northern Region, where they are interpreted to have been derived from the erosion of upthrust Mamonia Complex fault blocks (Swarbrick, 1979; 1980; Swarbrick and Naylor, 1980).

Compressional deformation in the Northern Region is characterised by top-to-the-west thrust tectonics, which formed the commonly observed thrust stack, from base to top, of Troodos Complex-serpentinite-Mamonia Complex. The variability in the direction of thrust transport, from top-to-the-NW to top-to-the-SW was cited as evidence of two main phases of contractional deformation of late Cretaceous age by Malpas *et al.* (1993). Based on structural observations and cross-section construction in the Mavrokolymbos and Ayia Varvara areas, Malpas *et al.* (1993). proposed a primary N and NW directed thrusting event, and later backthrusting towards the W and SW. However, an absence of cross-cutting relationships negate their arguments. As discussed in Chapter 5, the variation in top-to-the-SW, -W and -NW displacements may be explained by the combined effects of specific dynamic processes operating within the evolving thrust wedges and the reactivation of a pre-existing, irregular fault zone architecture. Gravitationally-induced body forces are thought to strongly influence or control the direction of tectonic transport, resulting in generally westerly-directed displacements that are approximately perpendicular to the local strike of the fault zone. As the variability in the direction of tectonic transport can be correlated with local deviations in the strike of the fault zones, the orientation of regional shortening may be estimated by averaging the lineation data collected throughout the Northern Region (Figure 6.1). The mean lineation orientation of 48/088° is dip-slip with respect to the predominant N-S striking, easterly-dipping contacts and foliations in the region. Field evidence suggests that there is only minor strike-slip partitioning of the compressional strains at all scales, which implies that the average thrust lineation orientation parallels the regional (10km scale) shortening direction.

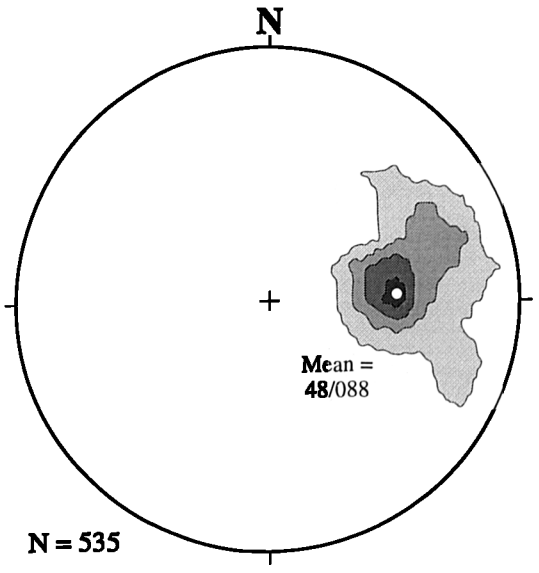

Figure 6.1. 1% area contour of all the thrust lineation data collected from the Northern Region.

The transpressional structures preserved in the serpentinite-filled fault zones in the Southern Region record a distinctly different geometric and kinematic pattern to that observed in the Northern Region. These transpressional structures are thought to have formed in response to near fault-normal shortening, which resulted in a pure shear-dominated deformation. As the maximum principal shortening directions along the E-W trending fault zones are slightly clockwise of fault-normal, bulk displacement is interpreted to be sinistral, which is supported by the dominance of sinistral strike-slip faults and shears over dextral (Section 4.4.2). The preponderance of conjugate sinistral and dextral faults along the fault zones is used as evidence to suggest that a large proportion of the pure shear component of the transpressional deformation was accommodated by strike-parallel extension (lateral extrusion). The identification of lateral extrusion during transpression is unusual and is discussed in greater detail in Section 6.4.

On a regional scale, the inferred orientations of maximum principal shortening (ε_3) vary in the Southern and Northern Regions. Figure 6.2 summarises the local directions of maximum principal shortening in the Southern Region and also the directions of thrust transport in both regions. The data and locations in the Southern Region that are shown in Figure 6.2 are presented in Table 4.4 in Chapter 4, whilst the localities in the Northern Region have been discussed in Chapter 5. The mean regional displacement directions for the Southern Region shown in Figure 6.2 as large grey arrows, have been determined using the total data from the Mamonia and Ayia Varvara areas (see Table 4.4). The equivalent displacement directions in the Northern Region are constrained from the mean orientation of thrust lineations shown in Figure 6.1. This figure shows that the compression direction in the Southern Region is oriented approximately N-S to NE-SW and thrusting is directed to the S and SW. In contrast, thrusting in the Northern Region documents local displacements to the SW, W and NW, but regional (10's of Km-scale) shortening is oriented E-W. Note that the orientation of sub-horizontal, regional (Km-scale) shortening directions also varies depending on the relative location along the fault zone. The mean shortening direction in the Mamonia-Phasoula area is oriented 10/190°, whilst to the west, the compression in the Ayia Varvara to Marathounda area is oriented NE-SW (7/046° in the Ayia Varvara area, and 043-023° for the Marathounda area). In contrast, shortening in the Northern Region is oriented E-W (48/088°). Also, northwesterly-directed thrusting is dominant in the northern part of the Akamas Forest and along the Loutra tis Aphroditis section (Section 5.2.9b). On the scale of SW Cyprus, both thrust displacement and maximum shortening directions are radially distributed along the arcuate the fault zone (Figure 6.3). This arrangement of shortening directions suggests that the serpentinite-filled fault zones of both regions were subjected to fault-normal

shortening along the whole length of the fault zone. These compressional strains were accommodated in different ways in both regions. In the Southern Region, maximum principal shortening is directed a few degrees clockwise of fault normal, which resulted in pure-shear dominated sinistral transpression accompanied by a significant component of lateral extrusion. However, in the Northern Region, orthogonal shortening resulted in predominant top-to-the-west thrusting. In the resulting model the directions of displacement are considered to be constrained by the imposed boundary conditions. Specifically, the pre-existing fault zone architecture is considered to have been an important control. Westerly-directed thrusting in the Northern Region is considered to have resulted from the partial reactivation of *steep* to *moderately-dipping*, N-S trending, extensional structures during thrusting. In contrast, near fault-normal shortening in the Southern Region acted across predominantly *sub-vertical*, E-W trending fault zones, which resulted in mainly strike-parallel displacements. Minor overthrusting at serpentinite boundaries is attributed to the reactivation of local low-angle, protrusion-related contacts. The dominant, sub-vertical structural architecture in the Southern Region is thought to have been inherited from earlier dextral strike-slip and transtension.

6.2.3a. Folding

Folds displaying various geometries and orientations are preserved within parts of the Mamonia Complex throughout SW Cyprus. In the areas studied in this thesis, folding has mainly been observed in Dhiarizos Group sediments within the Northern Region, which are located near to the serpentinite-filled fault zones. As shown in Chapter 5, two dominant orientations of folds exist; those that display shallow easterly-plunging fold axes and those that plunge to the south. In localised examples, folds that are oriented N-S clearly formed in response to E-W directed compression and westerly-directed thrusting (Section 5.4.3). For example, the folds within Kholetria limestones within Katarrakhtis Potamos valley in the Mavrokolymbos area, are thought to have resulted from localised 'buttressing' against a pre-existing steep fault zone. Another example is the westerly-verging folds in the Mavrokolymbos Formation sediments within Mavrokolymbos valley, which are associated with top-to-the-west extensional faults and thrusts. Southeasterly-verging kink folds in the Ayia Varvara Formation metamorphic blocks at Loutra tis Aphroditis may also be explained by westerly-directed (top-to-the-NW) thrusting (Section 5.2.2a). However, the relevance of the E-W trending folds is more problematic (see below).

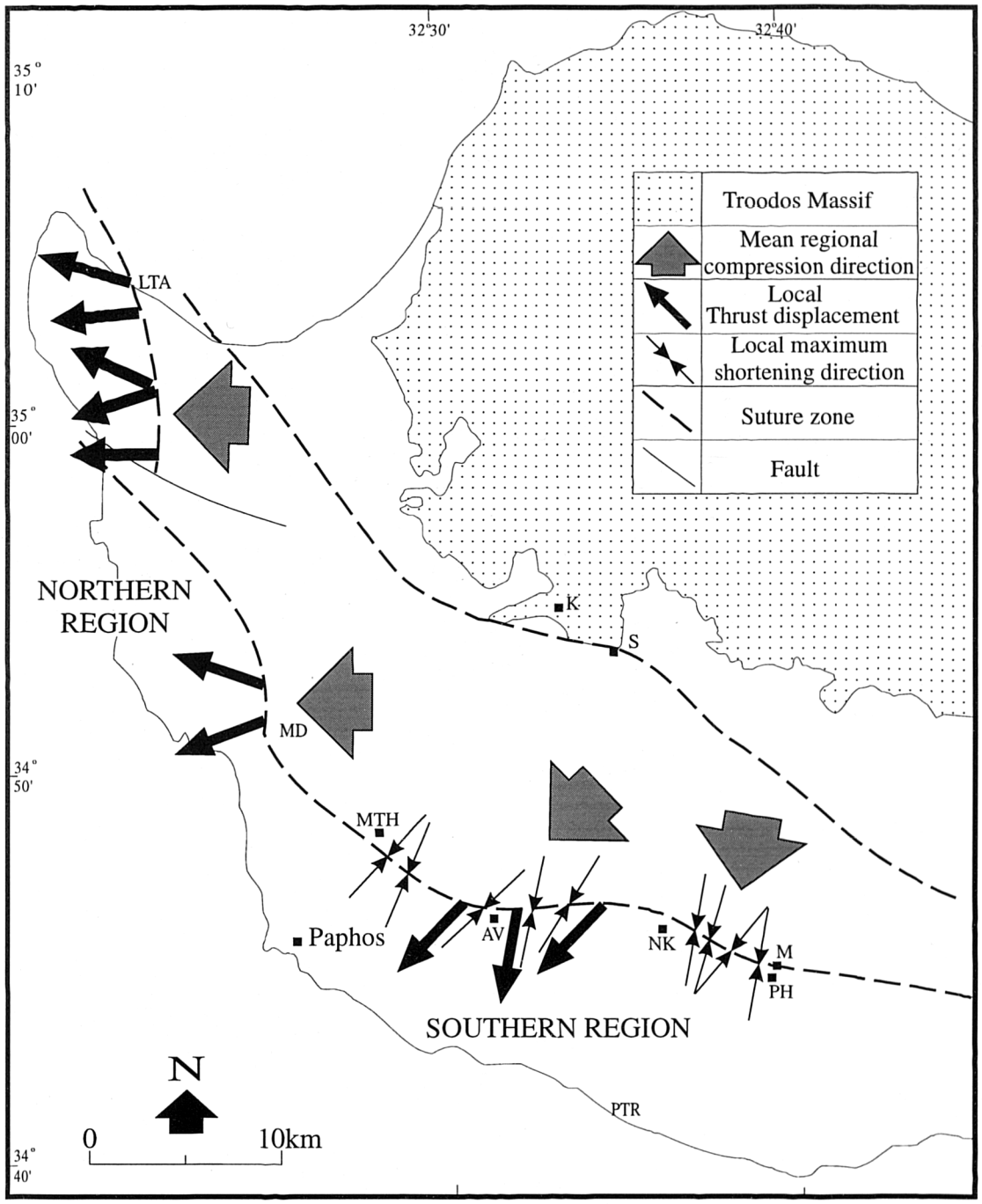

Figure 6.2. Summary map of the compressional structural data obtained from the Phasoula-Loutra tis Aphroditis fault zone. The data represented in this figure is presented in Chapters 4 and 5 (see text). The dashed lines represent the locations of the main serpentinite-filled suture zones between the Mamonia and Troodos Complexes.

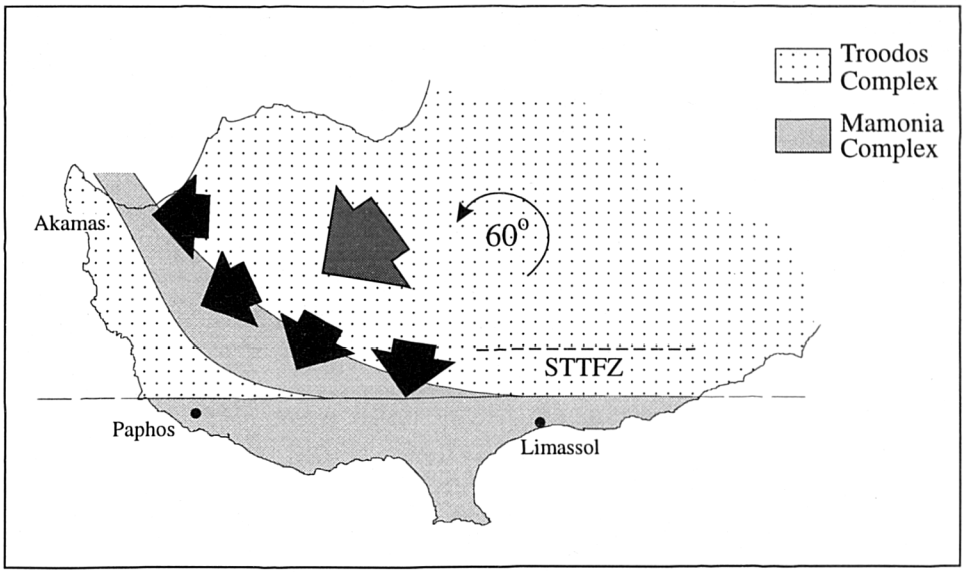

Figure 6.3. Schematic map showing the radial distribution of compression directions along the Phasoula-Loutra tis Aphroditis fault zone. The 60° anticlockwise rotation depicted for the main Troodos massif is shown here as part of this rotation is coeval with the compressional deformation (described in detail in section 6.2.4a). The relative locations of the Mamonia and Troodos Complexes is adapted from Swarbrick (1993).

Robertson and Woodcock (1979) initially provided a description of folds within the Ayios Photios Group, which mainly concerned exposures in the Southern Region, but also some localities in the Mavrokolymbos and Kannaviou areas. In their study, Robertson and Woodcock (*op cit.*) identified two dominant fold types; those that verge and face to the north, and those that face and verge to the south and west. They proposed that north facing and verging folds dominate across the suture zone and related their development to the initial emplacement of the Ayios Photios Group over the Dhiarizos Group by a gravity sliding mechanism. The development of later, south and west facing folds was attributed to the tectonism associated with the juxtaposition of the Mamonia and Troodos Complexes. Malpas *et al.* (1993) observed a similar sequence of folding, but assigned ***both*** phases of folding to the docking of the two complexes. In their interpretation, Malpas et al (*op cit.*) based their arguments on two cross-sections constructed through the Mavrokolymbos and Ayia Varvara areas. They proposed that the structures observed within these two areas preserve evidence of two phases of contractional deformation that affected both Mamonia and Troodos Complexes, which resulted in the development of folds with opposing facing and vergence directions. However, as stated in previous Chapters, the deformational chronology proposed by Malpas et al (*op cit.*) is not corroborated in this thesis. Without conclusive field evidence for refolding, or a kinematic framework with which

the easterly-plunging folds observed at Mavrokolymbos (and also those at Loukkos in the Akamas area; Section 5.3.1) may be associated, their mode of formation remains uncertain. Nevertheless, these folds are tentatively related to the initial emplacement of the Ayios Photios Group over the Dhiarizos Group prior to the Upper Cretaceous (Robertson and Woodcock, 1979).

6.2.4. Tectonic synthesis of SW Cyprus

The above summary of the Upper Cretaceous tectonic events in SW Cyprus have significant implications for the geological evolution of Cyprus. Figure 6.4 summarises the available information on the absolute and relative ages of the various units and events in the Upper Cretaceous that are considered relevant in explaining the tectonic history of SW Cyprus. The following sections briefly summarise each event documented in SW Cyprus in chronological order, which are used to constrain a geotectonic model to explain the evolution of Cyprus (Figures 6.5 and 6.6). The regional model presented, which places Cyprus in the context of the Eastern Mediterranean, is adapted from Robertson (1990). Note that no evidence is identified in SW Cyprus that may be used to refine the regional (i.e. on the scale of the Eastern Mediterranean) tectonic picture proposed by Robertson (*op cit.*). Rather, the aim of the model presented here is merely to place the findings of the present study into a previously accepted tectonic framework.

6.2.4a Cenomanian to Santonian (~92-83Ma; Figure 6.5a)

The Mamonia Complex is interpreted as a tectonically disrupted, microcontinental fragment of oceanic crust that formed within Neotethys at the northern margin of Gondwanaland. The rocks of the Mamonia Complex record the synchronous development of an oceanic spreading system and the evolution of a passive margin sequence in the Upper Triassic to mid-Cretaceous (Swarbrick, 1979, 1980; Malpas *et al.* 1993). During Cenomanian to Santonian times, the Mamonia microcontinent is considered to be in close proximity to the Troodos spreading system (Figure 6.5a). Based on geochemical evidence and analogy with other Eastern Mediterranean Tethyan ophiolites, the Troodos Complex is interpreted to have formed by seafloor spreading above a northward-dipping, intra-oceanic subduction zone within Neotethys (e.g. Pearce, 1975; Pearce *et al.* 1984; Gass *et al.* 1994 and references therein) during Cenomanian-Turonian times (*c.*92-90Ma; Blome and Irwin, 1985; Staudigel *et al.* 1986; Mukasa and Ludden, 1987). The N-S trend of the sheeted dyke complex in the main massif suggests that prior to 90° anticlockwise rotation (see below) the Troodos

spreading system was oriented E-W (Figure 6.5a). This spreading system was offset by a dextrally-slipping, magmatically active transform fault zone of at least 5km in width (the STTFZ; MacLeod and Murton, 1993; 1995). The model shown in Figure 6.5a conforms in the main with that of Robertson (1990), in the context of the relative motions of Africa and Eurasia and the palaeomagnetic data from Cyprus. The genetic relationship inferred in the present work between the peridotite mylonites, the Mamonia Complex and the STTFZ is of profound importance as it suggests that the Mamonia terrane/or microcontinent was in close proximity to the Troodos Complex as early as the Turonian (~90Ma; Spray and Roddick, 1981; Figure 6.6a). Furthermore, this suggests that the Mamonia Complex rocks were located on the overriding plate (Clube and Robertson, 1986; Robertson, 1990; Robertson and Xenophontos, 1993) and not on the subducting plate as proposed by MacLeod (1990), Murton (1990), and Malpas *et al.* (1992).

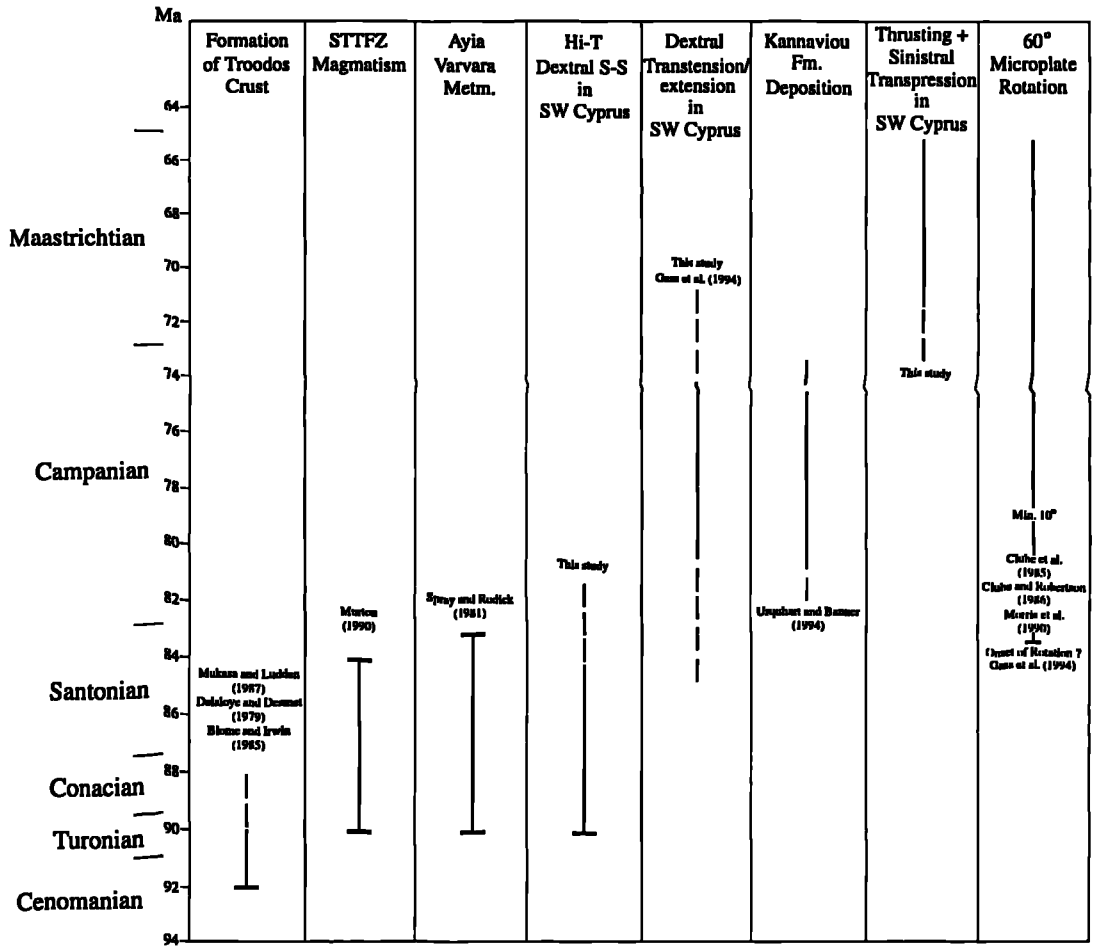

Figure 6.4. Summary of the relevant tectonic and stratigraphic events in Cyprus.

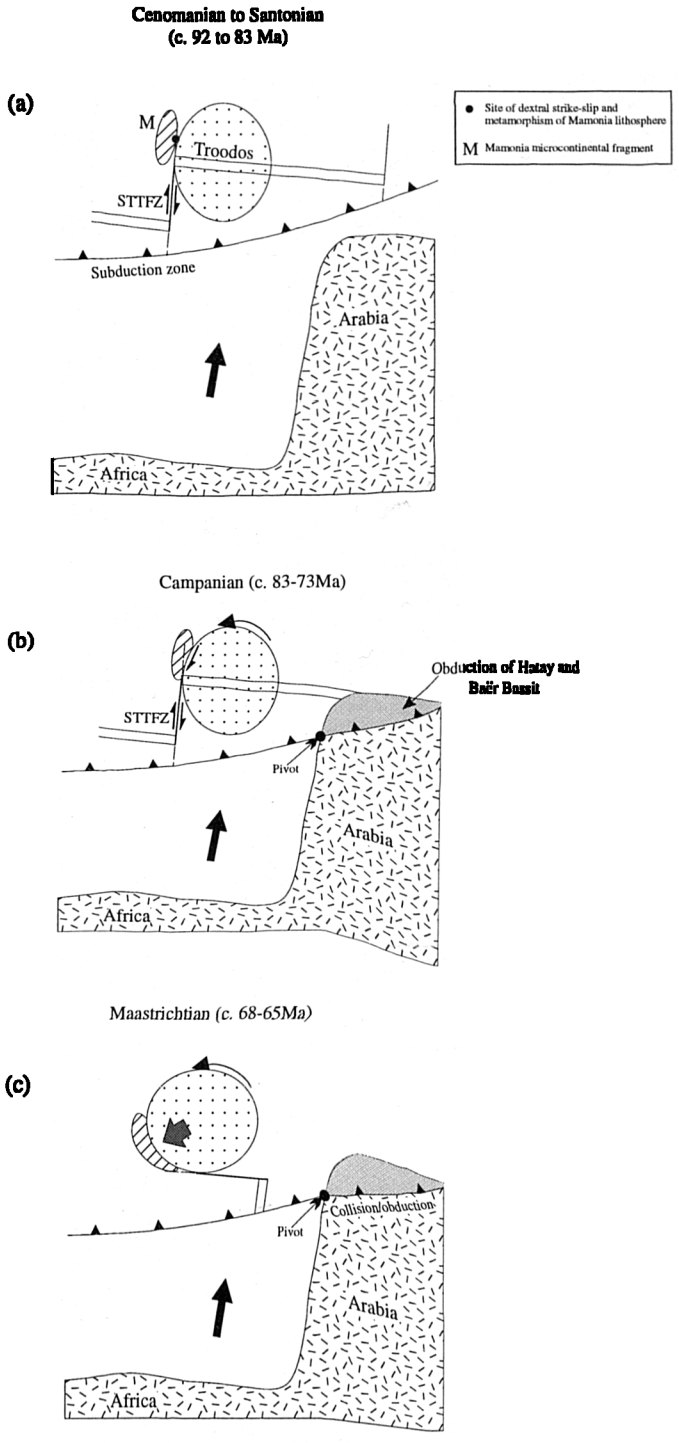

Figure 6.5. Schematic model explaining the tectonic evolution of Cyprus, adapted after Robertson (1990). (a) Cenomanian-Santonian; formation of Troodos oceanic crust above a northwardly-dipping subduction zone. The Troodos spreading system is offset by a dextrally slipping transform fault (STTFZ). The extension of transform-related faults into the nearby Mamonia microcontinent results in the syn-kinematic metamorphism of Dhiarizos group units. (b) Supra-subduction zone crust collides with the Arabian promontory to the east, resulting in the obduction of the Hatay-Baër Bassit ophiolites. Northward convergence of Africa continues, causing the Troodos microplate to pivot anticlockwise above a relict subduction zone. (c) Continued convergence causes the Troodos microplate to rotate 60° by the end of the Maastrichtian, coinciding with the compressional tectonism observed in SW Cyprus.

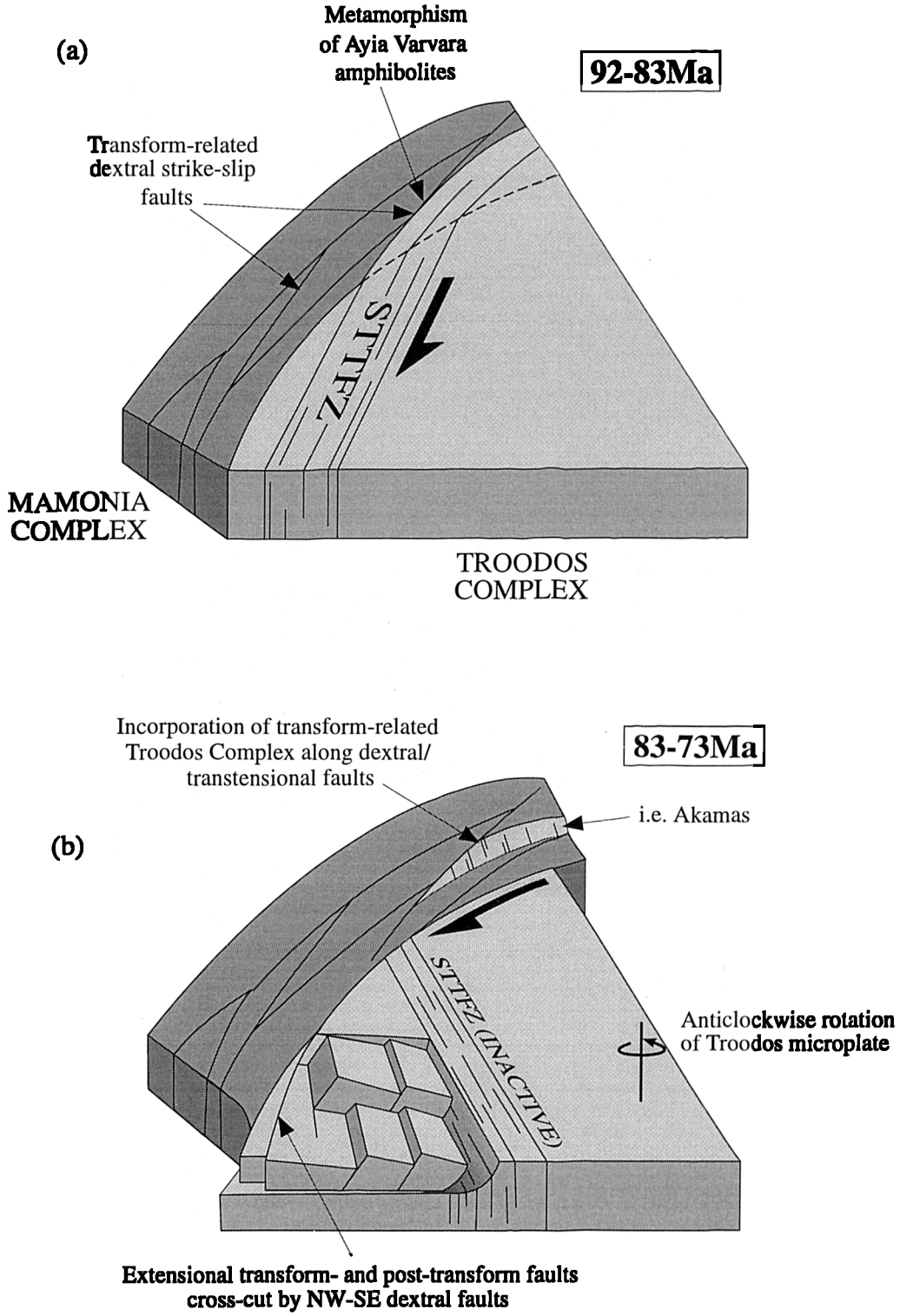

Figure 6.6. Schematic diagram showing the Cenomanian to Campanian evolution of south and west Cyprus. (a) Continuation of STTFZ-related structures into the Mamonia Complex of SW Cyprus. The proximity of fresh Troodos igneous material causes metamorphism of the parts of the Mamonia Complex crust and mantle. (b) Initiation of anticlockwise rotation and dextral transtensional tectonics causes interleaving of Mamonia and Troodos Complex rocks around the margin of the rotating Troodos microplate.

6.2.4b Campanian to early Maastrichtian (~83-72Ma; Figure 6.5b)

Palaeomagnetic studies in Cyprus suggest that subsequent to its formation, the Troodos Complex rocks of the main massif (here referred to as a *microplate*) experienced 90° anticlockwise rotation (Moores and Vine, 1971; Clube *et al.* 1985; Clube and Robertson, 1986). Based on studies of the igneous basement and the overlying sedimentary units, at least 60° of the rotation is thought to have been accommodated by the end of the Maastrichtian (*c.*65Ma), with the remaining 30° completed by the Lower Eocene (*c.*50Ma) (Clube *et al.* 1985; Clube and Robertson, 1986; Morris *et al.* 1990). Although the mechanism that caused rotation is difficult to prove, numerous authors consider rotation as a consequence of collision between the Troodos supra-subduction zone spreading system with a major promontory of the Arabian continental margin (Figure 6.5b; Clube and Robertson, 1986; MacLeod, 1988 1990; Robertson, 1990). This mechanism is supported by the coincidence between the onset of rotation in the Campanian with the obduction of the Hatay-Baër Bassit ophiolites to the present-day east of Cyprus, which is constrained to pre-Upper Campanian (Robertson, 1990 and references therein).

The regional phase of dextral transtension, which is recorded in the Southern Region and the Kannaviou area of SW Cyprus, and also along the STTFZ, is broadly coincident with the onset of microplate rotation (i.e. in the Campanian). Dextral displacements relating to tectonism associated with microplate rotation is consistent with the models proposed by numerous authors (e.g. Clube and Robertson, 1986; MacLeod, 1990; MacLeod and Murton, 1993; 1995; Gass *et al.* 1994). However, caution is noted here when correlating rotation in Cyprus to the observed tectonics. Firstly, much is still unknown about the dimensions of the rotated domain. Although all models consider the rotated microplate was small, roughly corresponding to the confines of the main massif, no conclusive palaeomagnetic data is available to confirm this assumption. As stated by Gass *et al.* (1994), the tectonic disruption experienced by the units located around the periphery of the main massif has resulted in the application of erroneous corrections and inaccurate interpretations. However, until more detailed palaeomagnetic studies are undertaken, the model presented in this thesis conforms with previous idea that the main massif is essentially the rotated microplate (Gass *et al.* 1994). Secondly, many previous authors have linked the sense of rotation of the microplate with dextral strike-slip along the STTFZ (e.g. Clube and Robertson, 1986; MacLeod, 1988, 1990; MacLeod and Murton, 1993; 1995). However, Swarbrick (1993) suggests that *anticlockwise* rotation of microplates may also be associated with *sinistral* strike-slip along bounding faults. As a note of caution, the processes linking shear sense and block rotation are infinitely more complex than a

model for Cyprus could possibly account for, due to a lack of complete exposure and palaeomagnetic data and thus, one cannot be used as evidence for the other.

Based on the stratigraphy, chemistry and petrography of sedimentary and volcanic rocks, the Troodos Complex in SW Cyprus is considered to be genetically related to the STTFZ. The features seen in the Limassol Forest, which are considered to be characteristic of the transform sequence, which are also observed in SW Cyprus, include:

(1) the presence of fault scarp breccias (e.g. near Kannaviou, Ayia Varvara, Petra tou Romiou; Loutra tis Aphroditis; Murton, 1990; Robertson, 1990);

(2) anomalously thin ophiolitic stratigraphies (e.g. the Akamas peninsula; Murton, 1990; Robertson, 1990);

(3) highly depleted, Type III boninite chemistries of lavas and mafic intrusive units (Malpas *et al.* 1987, 1993; Murton, 1987, 1990; Gass *et al.* 1994).

Therefore, the Troodos Complex fragments exposed in SW Cyprus are inferred to have been derived from a transform fault, presumably the STTFZ (e.g. Murton, 1990; Malpas *et al.* 1993; Gass *et al.* 1994). To explain the juxtaposition of Troodos with Mamonia Complex units in SW Cyprus, a model is favoured whereby tectonic slivers of STTFZ-related rocks and Mamonia units are intercalated along transform-related, dextral strike-slip faults (Figure 6.5b and 6.6b). The exact timing of this event is difficult to constrain. Based on the structural observations in SW Cyprus and their correlation with structures within the STTFZ, this tectonic interleaving may have been accommodated along early dextral faults, associated with the deformation of the peridotite mylonites, and/or along later dextral transtensional structures. The microstructures preserved within the peridotite mylonites are generally considered to be indicative of marked fault zone weakening, which may explain how tectonic slivers of transform-related Troodos Complex rocks in SW Cyprus may have been detached from the STTFZ and displaced by tens of kilometres.

As stated above, the size of the rotated domain is poorly constrained. However, based on the mapping and interpretations presented by MacLeod (1988; 1990) and Gass *et al.* (1994), the NW-SE trending structures documented in the Kannaviou area and south of the STTFZ (see Section 6.2.2) are thought to have bound the microplate (Figure 6.6b). Combined with palaeomagnetic data from the 'anti-Troodos' rocks to the south of the STTFZ (e.g Clube and Robertson, 1985), these studies suggest that the STTFZ did not accommodate any major rotational displacements, implying that the transform and the Troodos Complex rocks to the south also rotated (Figure 6.5b and c, and 6.6b).

6.2.4c Maastrichtian (~73-65Ma; Figure 6.5c)

Sinistral transpression and westerly-directed thrusting in SW Cyprus represent the last major tectonic event in SW Cyprus. This phase of broadly compressional tectonism documents the final juxtaposition between the Troodos microplate and the Mamonia Complex. The cessation of this event is constrained by the presence of the Kathikas debrites in the Northern Region, which are dated as late Maastrichtian (~65Ma; Swarbrick and Naylor, 1980; Urquhart and Banner, 1994). This phase of deformation is coincident with at least part of the 60° rotation that was completed by the end of the Maastrichtian. The dominant compressional component to this event is considered to have resulted from the broadly southwesterly-directed impingement of the Troodos microplate onto the Mamonia Complex, which may be associated with rotation. The cause of the radial distribution of displacement directions around the arcuate suture zone between the Mamonia and Troodos Complexes in SW Cyprus is considered to have resulted from gravitationally-induced body forces acting on fault zones that possessed an irregular, pre-existing architecture.

The Lefkara Formation, which stratigraphically overlies the Kathikas Formation is dated as late Maastrichtian also, and thus documents the cessation of compressional deformation. However, note that the absence of Maastrichtian to middle Palaeocene sediments of the Lefkara Formation in the Southern Region (Swarbrick, 1993) suggests that minor deformation in the Southern Region may have continued after the cessation of displacements in the Northern Region (Morse, 1996).

6.3. Fault zone weakening

There is substantial evidence to suggest that many continental and oceanic fault zones are weak (e.g. Rice, 1992; Wintsch *et al.* 1995; Jaraslow *et al.* 1996). Weakness has been inferred for many active crustal fault zones where the shear stresses that they support are substantially lower than predicted values determined by laboratory and theoretical experiments of frictional faulting. The behaviour of mechanically weak rocks and the effects of transient or longer term high pore-fluid pressures within fault zones have been cited as possible mechanisms that may facilitate weakening (e.g. Byerlee, 1990; Rice, 1992; Sleep and Blanpied, 1992; Byerlee, 1992; Wintsch *et al.* 1995).

Although many of these models may be relevant when discussing recent seismicity, they cannot explain reactivation over long time scales (i.e. >1Ma), as is observed in the ultramafic fault zones of SW Cyprus. Reactivation may be facilitated by long term weakening mechanisms, particularly in materials that cut through the main load-bearing regions of the lithosphere, e.g. the upper mantle and middle crust (Holdsworth *et al.* 1997; Figure 6.7). The ultramafic fault zones of SW Cyprus preserve evidence of two dominant deformational phases, at both high and low temperatures, which are thought to have resulted in significant weakening. These deformational events are focused in rocks that exist within the primary load-bearing region of the upper mantle. High temperature peridotite fault rocks are common constituents of deeply exhumed oceanic (Jaraslow *et al.* 1996) and continental fault zones (Rutter and Brodie, 1988; Drury *et al.* 1991; Vissers *et al.* 1995), where they are interpreted to have been deformed along major structural discontinuities that have controlled rheological behaviour on a lithospheric scale. Serpentinites are also common components of major continental (Irwin and Barnes, 1975; Dengo and Logan, 1981; Gates and Kambin, 1990; van Schalkwyk *et al.* 1993; Hoogerduijn Strating and Vissers, 1994; Moore *et al.* 1996) and oceanic fault zones (Cannat, 1993; Escartín *et al.* 1997). Therefore, the deformation observed in SW Cyprus is relevant to the rheological evolution of the oceanic *and* continental lithosphere. It is proposed that the influx of chemically active hydrous fluids during deformation in SW Cyprus has led to significant long term fault zone weakening. On the micro-scale, this has occurred due to the replacement of competent minerals and mineral frameworks by fine-grained, weaker aggregates of less competent foliated fault rocks. On a larger scale, a network of mechanically weakened faults are thought to have transected the lithosphere, forming an interconnected weak layer rheology (*cf.* Handy, 1990). The formation of this dynamic system may explain the intense strain localisation that accompanied the

deformation in Cyprus, and may also account for the reactivation over an approximately 25Ma time-scale.

Two main phases of fault zone weakening are recognised in SW Cyprus, which are discussed below:

- strain-softening and fluid-enhanced weakening at high temperatures (>600°C) within peridotite mylonites during dextral strike-slip;
- later, lower temperature (>100°C) weakening, relating to the formation of mechanically weak lizardite-chrysotile fault rocks and to the presence of transient high fluid-pressures, during the pervasive serpentinisation of mantle peridotites.

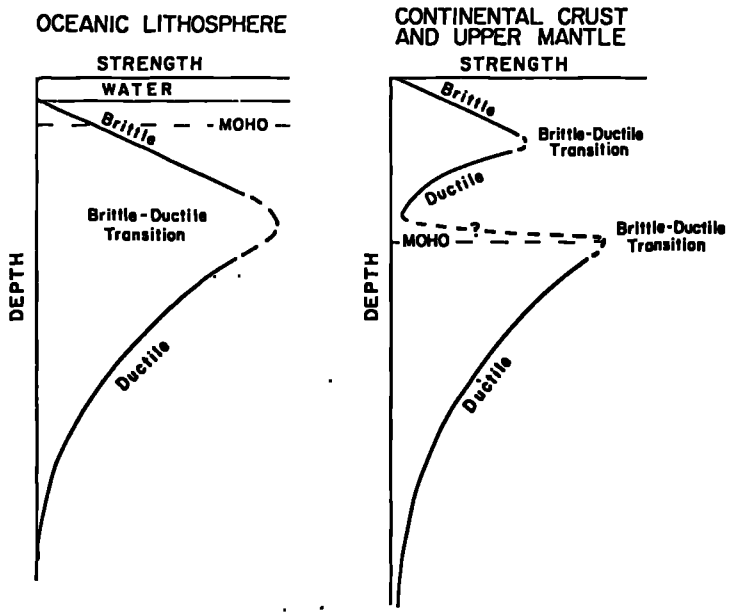

Figure 6.7. Hypothetical strength profiles for oceanic (left) and continental (right) lithosphere. Both oceanic and continental lithosphere display a main load-bearing region in the upper mantle. Continental lithosphere also exhibits a load-bearing region in the middle crust (from Molnar, 1992)

6.3.1. High temperature weakening

The deformation of coarse-grained (mm-scale grains) peridotites in the Southern Region, producing the fine-grained (μm-scale grains) fluidal and amphibole-rich mylonites is considered to be a strain-softening process. The parent ultramafic rock possesses a load-bearing framework, in which the bulk rheology is controlled by a strong, interlocking network of silicate phases dominated by olivine (*cf.* Handy, 1990). Synchronous deformation and flux of chemically active aqueous fluids is inferred to have resulted in the breakdown of this competent framework, forming localised,

interconnected shear zones of fluidal and later amphibole-rich mylonites. Both mylonite types preserve microstructural evidence for the operation and interaction of several efficient grain-scale deformation mechanisms. The resulting microstructure is dominated by fine-grained, interconnected weak layers, which control the bulk strength of the fault rock and consequently, the rheological behaviour of the host fault zone. The three main weakening mechanisms inferred are:

- grain-size reduction leading to the operation of diffusion creep;
- reaction softening caused by mineralogical phase changes;
- fluid flux facilitating intragranular and intergranular deformation mechanisms.

The intense grain-size reduction that characterises the fluidal mylonites is thought to have been sufficient to induce the operation of diffusion-controlled deformation mechanisms. Diffusion creep is favoured over dislocation creep at the low temperatures calculated (~600°C) because the activation energy for diffusion is lower than that for dislocation creep (Handy, 1989). Theoretical studies demonstrate that ultramafic shear zones deforming by diffusion creep in the oceanic lithosphere are significantly weaker than those in which deformation is accommodated by dislocation creep (Figure 6.8) (Jaraslow *et al.* 1996). This conclusion is also consistent with a model presented by Vissers *et al.* (1995) for continental lithosphere, in which the predicted flow stresses in large-scale (km-scale) shear zones deforming by diffusion creep are up to *four* orders of magnitude lower than if they were deforming by dislocation creep. The interpretation that the fluidal mylonites constituted rheological weak material is further supported by the following factors:

(1) The operation of diffusion-accommodated grain boundary sliding at high temperatures and stresses, in rocks like these which are dominated by constant microstructure, is capable of maintaining very high strains, i.e. superplastic flow (Ashby and Verral, 1973; Boullier and Gueguen, 1975; Gilotti and Hull, 1990; Drury *et al.* 1991);

(2) Diffusion-dominated deformation mechanisms are likely to be significantly faster processes in polymineralic rocks than in their monomineralic counterparts (Wheeler, 1993);

(3) The presence of fluid during deformation increases bulk and grain boundary diffusion coefficients, thereby markedly weakening rocks deforming by diffusion creep (Karato *et al.* 1986).

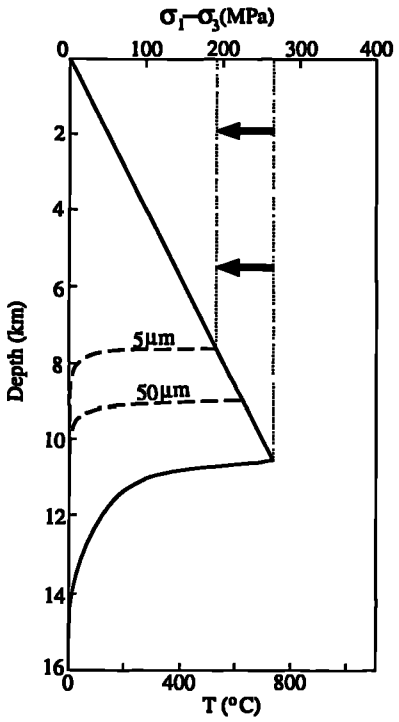

Figure 6.8. Schematic mechanical strength vs depth profile of the oceanic lithosphere. The lower portion of the solid curve is for deformation accommodated by dislocation creep, whilst the two dotted curves indicate the weakening effect of deformation accommodated by diffusion creep at the indicated grain-sizes. The upper line represents the brittle strength based on Byerlee's law for frictional sliding and the lower curve represents the ductile strength of the mantle assuming an olivine composition (after Jaraslow *et al.* 1996).

Based on the extrapolation of constitutive flow laws for olivine, the development of coarser-grained (<0.25mm) amphibole-rich mylonites is inferred to have taken place at higher temperatures (~800°C) and at lower stresses than the formation of the earlier fluidal mylonites (~600°C). This increase in grain-size might be expected to lead to strain hardening through a transition from diffusion creep to dislocation creep (Karato, 1989). However, the localisation of deformation accompanying the development of these amphibole-dominated shear zones suggests weakening, which is attributed to the interplay between a number of grain-scale processes. Firstly, although olivine grains within these fabrics are significantly coarser than those in the fluidal mylonites, they are sufficiently fine-grained to be expected to deform by diffusion creep processes (see deformation mechanism and regime maps in section 4.2.4). Secondly, weakening of these rocks is thought to reflect the replacement of pyroxene by amphibole, i.e. reaction softening. These reactions are related to the influx of aqueous fluids that may also lead to additional weakening effects, e.g. enhancing diffusive mass transfer and hydrolytic weakening etc (Karato *et al.* 1986). Initial deformation of amphibole is accommodated by crystal-plastic deformation mechanisms. Dynamic recrystallisation processes induce decreases in

grain-size, which results in the development of localised, ultrafine-grained, shear zones that are composed almost entirely of amphibole. These ultrafine-grained, monomineralic zones are characterised by equant grains that define only a weak crystallographic fabric, suggesting that deformation was accommodated by diffusion creep. Similar textural relationships observed in other peridotite mylonites are considered to be suggestive of phenomenological superplasticity (*cf.* Drury *et al.* 1991; Vissers *et al.* 1995). Previous studies concerning the deformation of amphibole at high temperatures suggest that it is very strong and resistant to deformation (Mercier, 1985). However, the observations and interpretations presented above clearly indicate that this is not necessarily the case, calling for more detailed studies on the deformation and rheological behaviour of amphibole-dominated rocks.

6.3.2. Low temperature weakening

Based on mineralogical and microstructural observations, hydrous fluids penetrated the ultramafic fault rocks in SW Cyprus throughout their deformational history. Initially, hydration reactions produced amphibole (see above) and later chlorite (see Section 4.3.1), but at lower temperatures serpentinisation reactions dominated (see Sections 4.3, 4.4 and Chapter 5). Serpentinites in SW Cyprus are deformed by transtensional structures, indicating serpentinisation began prior to and/or during the Campanian (see Section 6.2).

The phase of broadly compressional deformation in the Maastrichtian, which resulted in sinistral transpression in the Southern Region and westerly-directed thrusting in the Northern Region, is characterised by a pervasive overprint by thoroughly serpentinised fault rocks. These macroscopically ductile fault rocks typically comprise massive to foliated cataclastic gouge, dominated by lizardite-chrysotile serpentine minerals, transected by networks of brittle to brittle-ductile fractures and shear bands. The intensity of strain localisation and the correlatable increase in the degree of serpentinisation accompanying this event is consistent with fault zone weakening processes. Mechanical weakening on all scales is thought to result from two dominant mechanisms:-

- Experimental studies demonstrate that lizardite-dominated serpentinites are at least three times weaker than other crustal rocks (Reinen *et al.* 1994). The replacement of olivine-dominated peridotites in SW Cyprus by lizardite-chrysotile serpentinites clearly constitutes a reaction softening process.

- Fractures on all scales in the serpentinite-filled fault zones are filled by fibrous carbonate and chrysotile, suggesting the presence of high fluid pressures during deformation and the operation of fluid-assisted deformation mechanisms.

6.3.2a Weak fault rocks

Previous experimental work shows that lizardite and chrysotile serpentinites are significantly weaker than other lithospheric rocks (Reinen *et al.* 1994; Moore *et al.* 1996). At room temperature, fault gouges that are composed of lizardite and chrysotile have coefficients of friction ($\mu \approx 0.2$-0.3; Reinen *et al.* 1994; Moore *et al.* 1996), which are significantly lower than that of the parent olivine-dominated rocks ($\mu \approx 0.73$ for dunite; Escartín *et al.* 1996). Thus, the conversion of peridotite to serpentinite constitutes an unequivocal reaction softening process. Unfortunately, most studies on serpentinite deformation merely concern frictional and load-bearing behaviour and do not discuss mechanisms by which these rocks deform. However, of the few studies presented in the literature, microstructural observations of naturally and synthetically deformed serpentinite suggest that lizardite-chrysotile serpentinites are expected to deform by ductile, stable-sliding over a wide range of geological conditions (Dengo and Logan, 1987; Gates and Kambin, 1990). This conclusion is supported by field and microstructural observations of the serpentinite fabrics in SW Cyprus, which suggest that they deformed by macroscopically ductile flow. Recent microstructural studies and volumetric strain analyses by Escartín *et al.* (1996) suggest that both brittle (localised) and ductile (distributed) deformation in serpentinites is accommodated by *non-dilatant* shear along micro-scale fractures that form parallel to the (001) cleavage. As stated by Escartín *et al.* (*op cit.*), upper crustal fault zones in which the bulk rheology is controlled by non-dilatant microcracking, as opposed to general frictional processes described by Byerlee's Law or by single crystal plasticity (e.g. Wintsch *et al.* 1985), are expected to be significantly weakened because the effects of dilatancy hardening are suppressed. The conclusion by Escartín *et al.* (*op cit.*) that serpentinite fault rocks deform by macroscopically ductile cataclastic flow accommodated by non-dilatant micro-scale fracturing is consistent with the textural and field observations of the SW Cyprus fabrics.

An important implication from the above review is that the fault zones in SW Cyprus may have accommodated macroscopic ductile flow under relatively low shear stresses in a deformation(s) that accumulated negligible volumetric strains. These assumptions imply that the host fault zone may have exhibited stable-sliding behaviour and aseismic creep rather than stick-slip and seismic failure. The presence of this type of fault rock along some portions of major crustal fault zones may explain why those

portions display localised steady-state creeping behaviour (e.g. Dengo and Logan, 1987).

6.3.2b. Fluid pressure

For some time, geologists have realised that high fluid pressures impart a significant effect during faulting (e.g. Hubbert and Rubey, 1959; Phillips, 1972; Sibson *et al.* 1975; Sibson, 1990). To explain the apparent weakness of major crustal fault zones, the presence of near lithostatic fluid pressures has been proposed (Byerlee, 1990; Rice, 1992; Sleep and Blanpied, 1992).

Fluids have clearly played a substantial role in the development and deformation of the serpentinite fault rocks in SW Cyprus. These rocks are characteristically pervasively serpentinised, documenting the flux of large volumes of aqueous fluids that led to the ubiquitous hydration of the peridotite protolith. As the degree of serpentinisation can be correlated with the intensity of deformation, fluid flux is considered to be syn-kinematic. The serpentinite fault rocks commonly display both tensile veins and brittle to brittle-ductile shear fractures with fibrous infills. Tensile veins infilled with carbonate, chrysotile, and lesser quartz, typically lie parallel to tectonic contacts, foliations and the shear fabric within the fault rocks. Occasionally, veins cross-cut the deformation fabrics, indicating that some veining took place subsequent to faulting. However, the common occurrence of mineralised fault plane lineations, the presence of veins as clasts, and fault rocks that are rich in deformed and mechanically re-worked carbonate, suggests that fluid flux and faulting were broadly contemporaneous. As emphasised in Chapters 4 and 5, the localisation of tensile veins along shear fractures is unusual. The prevalence of both tensile and shear fracture types may be attributed to their diachronous development by changing stress and fluid pressure conditions during the same progressive deformational event (Figure 6.9; Phillips, 1972; Etheridge, 1983; Etheridge *et al.* 1984; Reynolds and Lister, 1987; Moore, 1989; Byerlee, 1990; Rice, 1992; Sleep and Blanpied, 1992). Deformation accommodated dominantly by shear fracture is thought to take place when differential stresses are relatively high ($(\sigma_1-\sigma_3) \geq 8T$; where T is the tensile strength of the rock; Phillips, 1972; Etheridge, 1982). The production of transiently high fluid pressures and a lowering of the differential stresses ($(\sigma_1-\sigma_3) < 8T$) causes a transition to deformation dominated by hydraulic extensional shear fracture or tensile failure. As deformation in the serpentinites involved cataclasis and displacements along brittle to brittle-ductile shear fractures, this suggests that conditions of relatively high differential stresses prevailed. It is assumed that tensile fractures and veining occurred due to an increase in fluid pressure. As a result, extensional shear or tensile fractures could

propagate (i.e. $(\sigma_1-\sigma_3) \leq 8T$) under the same stress conditions that had previously allowed shear fractures to develop under lower fluid pressure conditions ($(\sigma_1-\sigma_3) \geq 8T$).

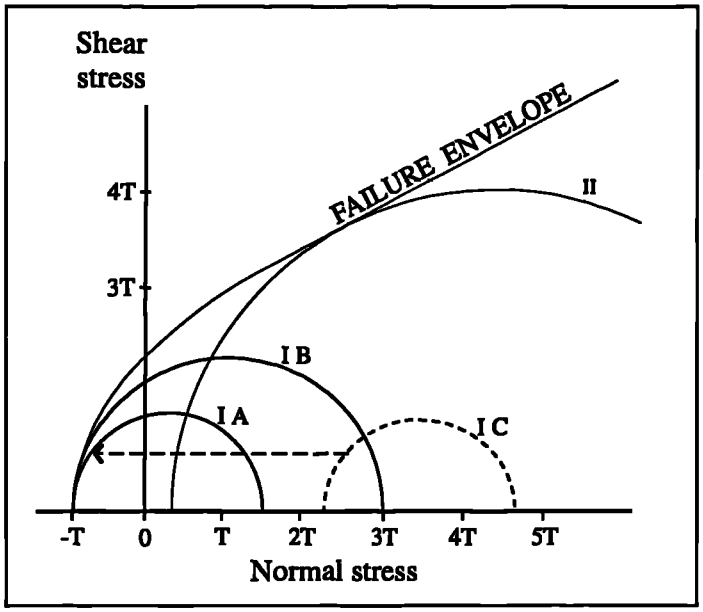

Figure 6.9. Coulomb-Griffith failure envelope and stress circles for tensile failure (IA), maximum deviatoric stress for tensile failure (IB), and shear failure (II). Circle IC represents non-failure stress conditions that can result in tensile failure by increasing fluid pressure, which decreases effective stress, as indicated by the movement of the stress circle to the left (from Reynolds and Lister, 1987).

A possible mechanism of generating episodic high fluid pressure in a fault zone is by the influx of overpressured fluids from depth, where fluid pressures are generally considered to approach lithostatic values (e.g. Rice, 1992). Alternatively, episodic seismic failure mechanisms proposed and adapted by a number of authors (e.g. Sibson *et al.* 1975; Sibson; 1981; Rice, 1992; Sleep and Blanpied, 1992) may be applicable. In these models, a cyclic process is envisaged whereby progressive, interseismic creep compacts the fault zone, increasing the pore-fluid pressures, ultimately resulting in seismic failure and slip at relatively low shear stresses. A similar model is favoured to explain the development of both shear fractures and tensile fracture associated with fluid flux in the serpentinite fault rocks in SW Cyprus. An adaptation to these models is required because, as discussed above, these faults contain a sufficient volume of lizardite-chrysotile fault rocks to control the bulk rheology of the host fault zone, which are expected to exhibit aseismic steady-state creep. The shear fractures are expected to have formed during the predominant steady-state creep of the fault zone. During this deformation fluid pressures are thought to have been low enough to inhibit

hydrofracture, but high enough to reduce the effective stresses, facilitating macroscopically ductile cataclastic flow. The presence of tensile veining documents transient increases in fluid pressure to values higher than the least principal stress, which may have resulted from *creep compaction* (*cf.* Sleep and Blanpied, 1992) of the lizardite-chrysotile fault rocks, at least on microscopic- to macroscopic-scales. As shown in examples from décollements in accretionary prisms (e.g. Moore, 1987), tensile failure and fluid flow might be expected to follow pre-existing anisotropies in the fault rocks, such as the previous shear fractures, which would therefore explain the localisation of tensile veins along foliations, tectonic contacts and the shear fabrics in SW Cyprus.

The serpentinite-filled fault zones are characteristically sites of localised fluid flux, particularly within the most intensely deformed regions. This correlation is to be expected because fluid flow during ductile deformation within a fault zone can result in a large increase in dynamically maintained permeability (Etheridge *et al.* 1983). Consequently, a reduction in the effective confining pressure due to high pore-fluid pressure is expected to further increase permeability (Etheridge *et al.* 1984). Furthermore, a strong material anisotropy is commonly observed within serpentinite fault gouge, defined by the alignment of (001) shear microfractures parallel to fault zone boundaries (Hoogerduijn Strating and Vissers, 1995; Escartín *et al.* 1997). Escartín *et al.* (*op cit.*) suggest that the development of these non-dilatant microfractures in a preferred orientation will also favour the confinement of fluids within serpentinite-filled fault zones.

6.4. Transpression in the Southern Region: implications on quantitative transpressional modelling

Using the field evidence and observations described in Chapter 4, the lizardite-chrysotile fault rocks of the Southern Region are thought to have been deformed during a phase of sinistral transpression in the Maastrichtian. Bulk deformation in this region is interpreted to be transpressive based on the inference that sub-vertical fault zones with predominantly strike-parallel lineations and coeval minor thrust faults formed in response to high-angle oblique sinistral shortening, i.e. a pure shear-dominated transpression (Harland, 1971; Fossen and Tikoff, 1993; Tikoff and Teyssier, 1994). Although the absence of adequate strain markers precludes an accurate determination of the three-dimensional shape of the regional finite strain ellipsoid, the geometry and kinematics of the conjugate faults demonstrate that the long axis of the finite strain ellipsoid parallels the E-W striking, fault zone boundaries. Unusually, the transpression is thought to have resulted in extension parallel to the strike of the fault zone, which is referred to here as "*lateral extrusion*". Lateral extrusion is defined as 'a stretch in the horizontal direction that causes a deformation zone to lengthen relative to the undeformed rocks that comprise the zone margins' (Jones *et al.* 1997). In existing transpressional models, however, the presence of extension parallel to the fault zone boundaries is apparently incompatible with transpressional deformation that is demonstrably pure shear-dominated (e.g. Fossen and Tikoff, 1993; Tikoff and Teyssier, 1994; Teyssier *et al.* 1995; see Chapter 1). In *confined* transpression, as modelled by Sanderson and Marchini (1984) and subsequent workers, the finite extension direction for pure shear-dominated transpression should be vertical. This is because these models consider homogeneous transpression in a vertical zone that is *laterally* and *basally* confined, so that the component of shortening across the zone is compensated solely by vertical extension (Figure 6.10a). However, by removing the boundary conditions imposed by Sanderson and Marchini (1984), Jones *et al* (1997) demonstrate that no specific geometrical relationship between the orientation of the finite strain axes and the zone boundaries exists for *unconfined transpression* (Figure 6.10b). Specifically, Jones *et al.* (*op cit.*) consider deformation in a zone that is not laterally or basally confined, so that material can move into or out of the zone parallel to its length, and the zone can thicken or thin vertically. This new model is consistent with the original concept of transpression of Harland (1971), who envisaged transpressional and transtensional strains as general tectonic consequences arising from the oblique motion of lithospheric plates. By expanding the mathematical definition of transpression to incorporate the effects of lateral extrusion, Jones *et al.* (1997) illustrated a more generalised model for describing three-dimensional non-coaxial

deformation. Their work provides a numerical and conceptual model for describing bulk deformation in crustal regions in which evidence for lateral extrusion has been recognised (e.g. Harland, 1971; Tapponier and Molnar, 1976; Molnar and Tapponier, 1977; Dewey *et al.* 1986). Unconfined transpressional deformation may be factorised into three end-member plane strain components, namely: wrench simple shear; pure shear in the XY plane (lateral stretch); and pure shear in the YZ plane (vertical stretch) (Figure 6.11). These biaxial strains can be viewed as the apices of a "*strain triangle*" for unconfined transpression (or transtension). The edges of the triangle represent a limited range of deformations between two end-member strain components. For instance, the three edges of the triangle correspond to triaxial pure shear (*cf.* Reches, 1978); non-coaxial, biaxial lateral extrusion (*cf.* Dias and Ribeiro, 1994); and the triaxial confined transpressional strain of Sanderson and Marchini (1984). The interior of the triangle represents a full spectrum of homogeneous, constant volume, transpressional deformation.

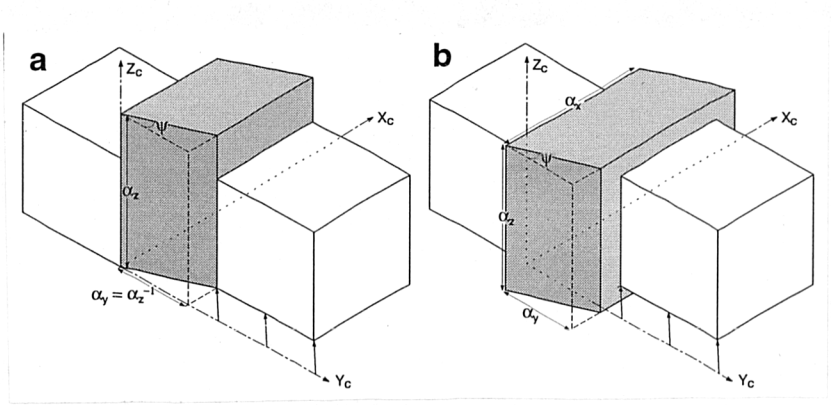

Figure 6.10. Transpressional geometries, showing the constant volume, homogeneous deformation of a unit cube (shaded). (a) Transpression zone which is laterally and basally confined: horizontal shortening perpendicular to the zone, α_y, is balanced by upward vertical thickening, α_z (based on Figure 1 of Sanderson and Marchini, 1984). α_x = lateral stretch = 1. (b) Vertically and laterally unconfined transpression zone. Horizontal shortening across the zone is balanced by both upward and downward vertical thickening and lateral shortening (taken from Jones *et al.* 1997). The zones of deformation are shaded, whilst the undeformed rocks on either side are unshaded. α_x, α_y, and α_z are the stretches of the unit cube parallel to the Cartesian axes, X_c, Y_c and Z_c. ψ is the angular shear strain.

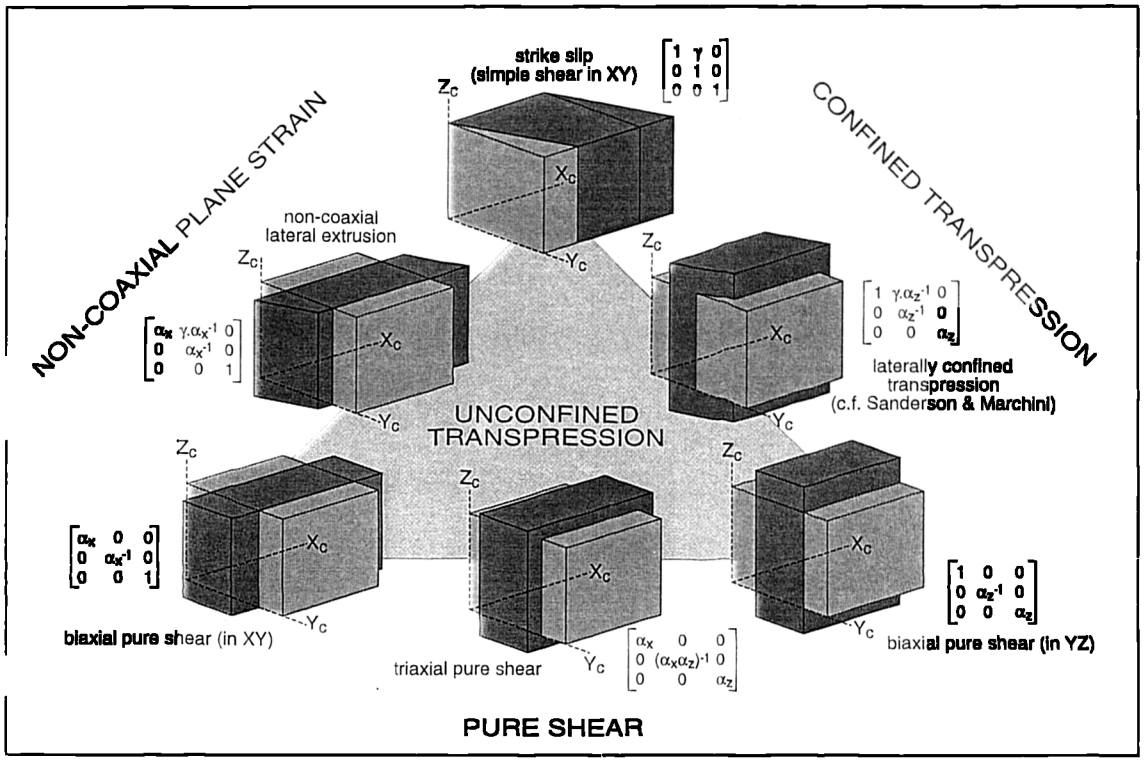

Figure 6.11. Schematic diagram showing how unconfined transpression, as defined by Jones *et al.* (1997), may be described using three plane strain components, which constitute the apices of a 'strain triangle'. The interior of the triangle represents the full spectrum of homogeneous constant volume, unconfined transpressional deformation (taken from Jones *et al.* 1997).

During unconfined transpression, the orientation and in particular, the geometry (k-value) of the finite strain ellipsoid depends not only upon the amount of shortening across the zone and the amount of strike-parallel to the zone, but also upon the ratio of vertical to lateral stretch. The contoured Flinn diagrams shown in Figure 6.12 demonstrate that the shape of the finite strain ellipsoid varies considerably depending on the ratio of simple shear (γ) to orthogonal stretch (α_y) during constant volume, homogeneous, unconfined transpression. Each plot shows the possible strain geometries for a different ratio of these two parameters, with (a) representing 100% confined transpression (*cf.* Figure 2 of Sanderson and Marchini, 1984), and (b) to (e) representing increasing proportions of lateral stretch. The progressive rotation of γ contours and thus, all possible ellipsoid geometries, towards the k=1 line reflects the fact that when orthogonal shortening is balanced by 100% lateral extrusion, the deformation is a plane strain. The marked difference in each of these graphs emphasises that the amount of lateral extrusion has a significant effect on the resultant *shape* of the finite strain ellipsoid. Therefore, strain geometries measured in the field

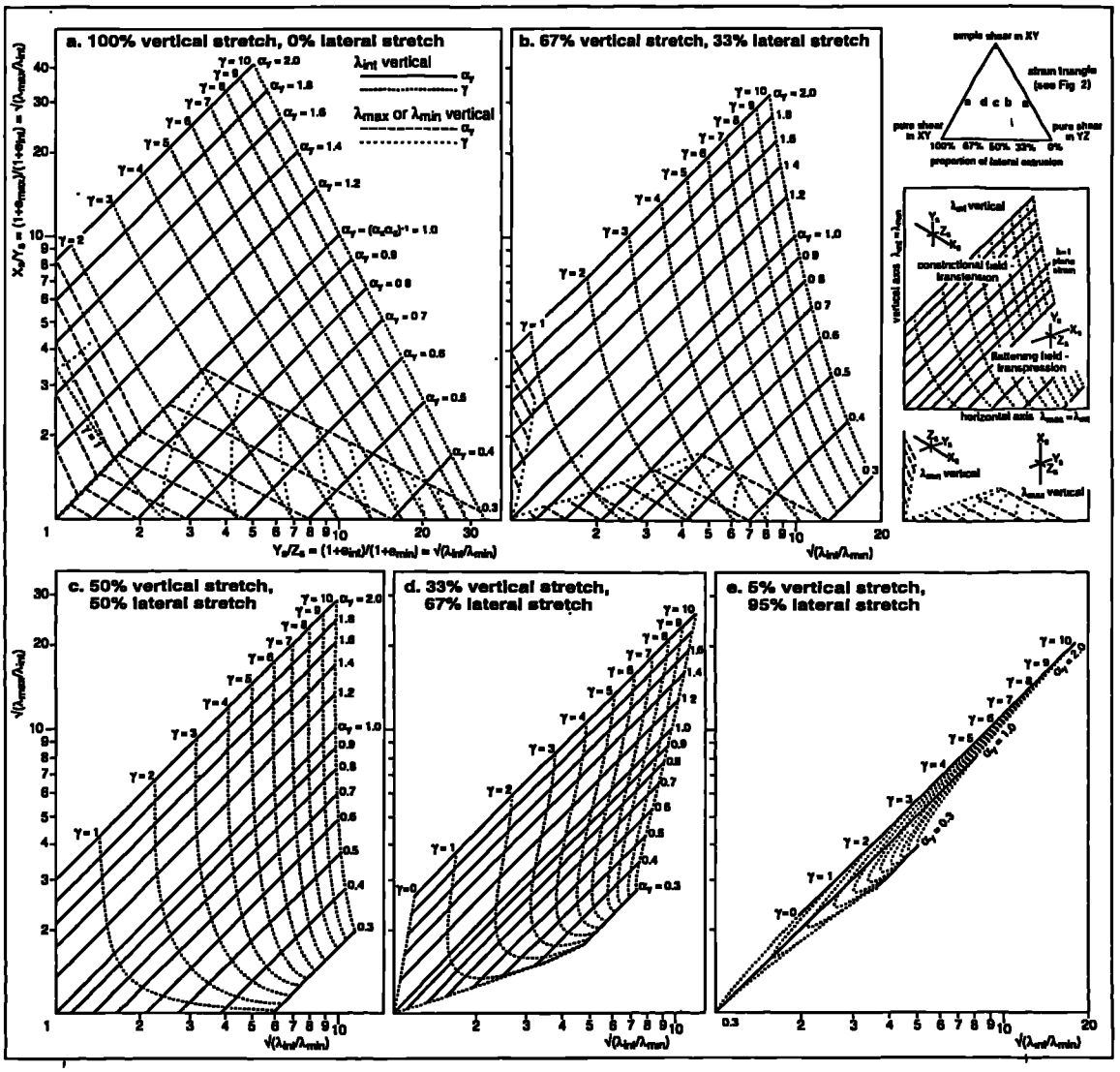

Figure 6.12. Series of contoured Flinn diagram plots showing the shape of the finite strain ellipsoid produced by constant volume, unconfined transpression (and transtension) for a range of values of simple shear (γ) and orthogonal stretch (α_y). X_s, Y_s and Z_s are the principal axes of the finite strain ellipsoid such that $X_s>Y_s>Z_s$ (taken from Jones *et al.* 1997). See text for discussion.

cannot generally be interpreted in terms of any single pair of unique values of γ and α_y. On the other hand, the plots shown in Figure 6.13 demonstrate that the degree of lateral extrusion has negligible effects on the *orientation* of the finite strain ellipsoid. This is illustrated by the similar form of each plot with an increasing percentage of lateral to vertical stretch, from (a) to (c), which is shown schematically in the inset diagrams which depict the orientation of the XY plane of the finite strain ellipsoid

(cleavage) for a specific zone boundary displacement. The conclusion that the ratio of lateral to vertical stretch has little effect on the orientation of the finite strain ellipsoid, suggests that the application of simple geometrical constructions, such as that proposed by McCoss (1986), to determine the *direction* of regional displacement vectors is reasonable. However, as shown in Figure 6.12, the use of previous models (e.g. Sanderson and Marchini, 1984; McCoss, 1986; Fossen and Tikoff, 1993) to determine the *magnitudes* of transpressional strain may be fundamentally flawed if a significant component of lateral extrusion has occurred.

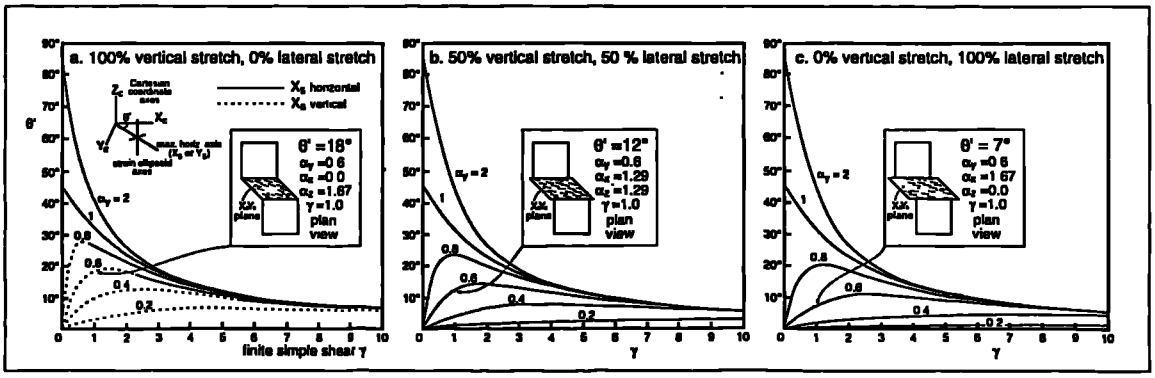

Figure 6.13. Plots showing the orientation of the long axis of the finite strain ellipsoid in the horizontal plane (θ') for a range of values of simple shear (γ) and orthogonal stretch (α_y) (taken from Jones *et al.* 1997). See text for discussion.

By considering displacement vectors for points at the deformation zone boundaries it is possible to visualise the necessary kinematic displacements required to balance the strain geometrically across a transpressional zone (Figure 6.14). During transpression in which there is a component of lateral extrusion, there is a kinematic requirement that some material is displaced with an opposing sense of shear to the dominant simple shear component acting across the whole zone. This is shown in Figure 6.14b by the diverging pattern of displacement vectors. This would account for the formation of dextral faults and shear zones during sinistral-dominated transpression within the serpentinite belts of the Southern Region.

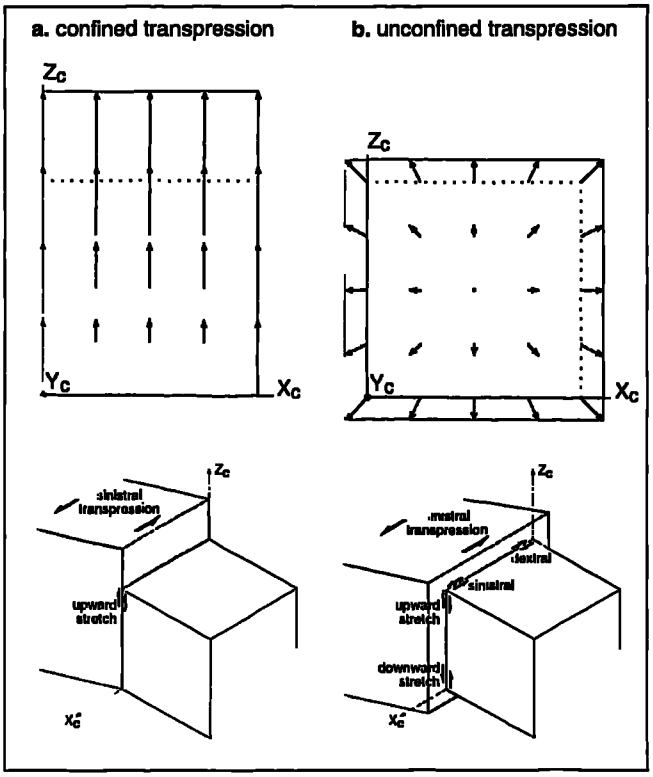

Figure 6.14. Schematic displacement vectors for points lying along the deformation zone boundary, i.e. X_cZ_c plane in Figure 6.10. (a) The confined transpressional configuration of Sanderson and Marchini (1984), where orthogonal shortening (α_y) is balanced entirely by vertical displacement towards the upper free surface. Note that the zone is basally confined and is effectively pinned along the X_c-axis. (b) Unconfined transpression in which orthogonal shortening (α_y) is balanced by both lateral extrusion and vertical thickening. The pin-point is shown here to be in the centre of the zone boundary, although this position is expected to vary (taken from Jones *et al.* 1997)

Special boundary conditions may be required in order for lateral extrusion to occur in transpressional zones. Three features of the serpentinite-filled faults of the Southern Region may explain why material was extruded laterally:

(1) The pre-existing serpentinite-filled suture zone may have possessed an irregular geometry that included lateral 'free surfaces', so that NNE-SSW shortening would have lead to the lateral movement of material along strike, infilling previously "barren" parts of the fault zone (Figure 6.15). An irregular architecture could be inherited from complex, pre-existing fault zone geometries that include numerous promontories and embayments (*cf.* Harland, 1971; Mckenzie, 1972; Dewey and Burke, 1973). Alternatively, an irregular fault zone architecture may have resulted

from the non-uniform distribution of serpentinite protrusions in some parts of the fault zone and not others. For example, a series of serpentinite bodies may have been emplaced diapirically (Figure 6.15ai), or as is inferred from field observations, may have been protrusively emplaced along extensional fractures during the earlier dextral transtensional event (Figure 6.15aii). Isolated serpentinite bodies are well documented along oceanic fracture zones (e.g. Bonatti and Crane, 1984), forearcs (e.g. Keen *et al.* 1984), and mid-ocean ridge-parallel highs (e.g. Bonatti, 1976). The existence of several irregular intrusive units of serpentinite throughout less deformed parts of the Southern Region (e.g. Vatomandra, Nea Kholetria area; Section 4.4.2b) suggests that this may an important factor.

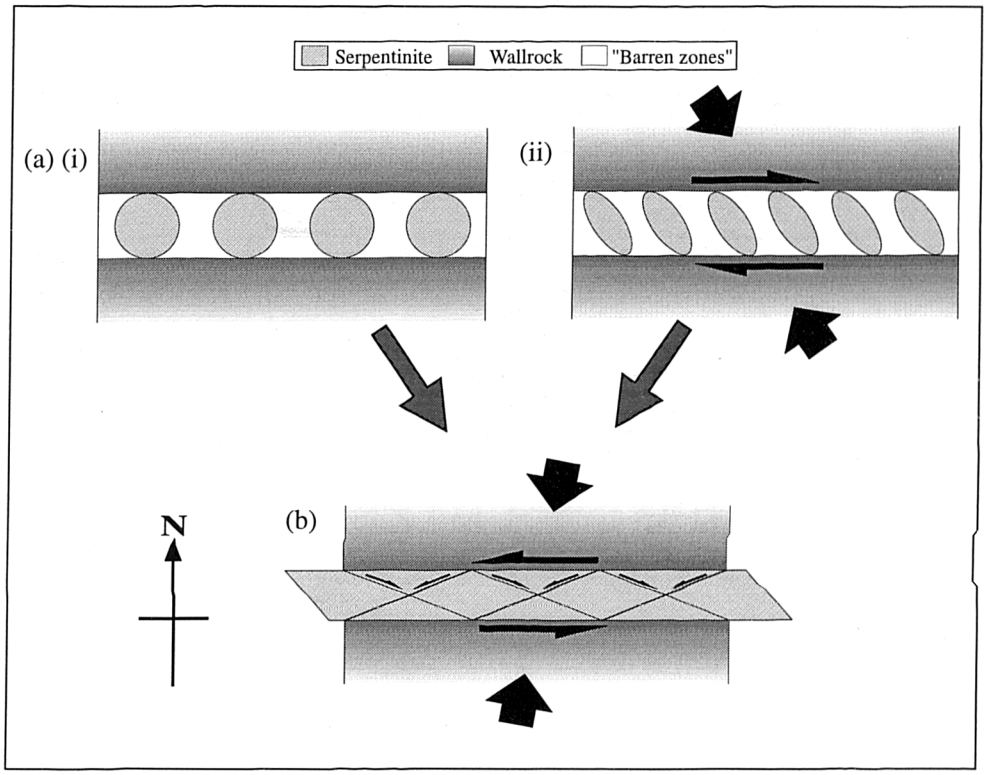

Figure 6.15. Schematic representation of lateral extrusion of fault zone material facilitated by the existence of an irregular fault zone architecture, caused by the non-uniform distribution of serpentinite as diapirs (a) or protrusions localised along tensile fractures formed dextral transtension. The unshaded areas in (a) and (b) may be considered as lateral free surfaces or "barren zones" into which serpentinite might be displaced. (c) The geometrical configuration observed during and after transpression and lateral extrusion. Plan view, i.e. onto the X_cY_c plane in Figure 6.10.

(2) The upward mobility of serpentinite that allowed vertical thickening, may have been hindered by a large amount of overburden or the presence of a strong "cap rock". Evidence of an unspecified degree of overburden during transpression is provided by the identification of overpressured rocks in the footwall to thrusts in

the Ayia Varvara area. Also in the Ayia Varvara area at Arkolieri (Section 4.3.2a), the presence of an isolated serpentinite protrusion that has "mushroomed" against the overlying Troodos "roof" also suggests that vertical ascent has been prevented.

(3) Laboratory experiments demonstrate that lizardite-chrysotile serpentinites are demonstrably weak when compared to most other crustal rocks and that they tend to deform in a ductile manner (e.g. Dengo and Logan ,1981; Gates and Kambin, 1990; Moore *et al.* 1996). Such a low strength material would be relatively mobile in comparison to the wall rocks, and would therefore be easily moved laterally along faults during deformation.

It is thought that all of the above three factors may have lead to the occurrence of unconfined transpressional deformation in the serpentinite-filled fault zones. It is concluded that a critical phase of structural analysis is recognising the relative contributions of regional strain, displacement boundary conditions and fault zone rheology in controlling the local strains and the displacement field.

6.5. Final Conclusions

- Field, microstructural and geochemical studies undertaken as part of this study have identified evidence of three tectonic events of Upper Cretaceous age, which involved both the Mamonia and Troodos Complex rocks of SW Cyprus.

- The earliest deformational event is documented by peridotite mylonites, which are interpreted as fragments of Mamonia Complex mantle deformed at high temperatures (>600°C) within a transform-related, dextral strike-slip fault zone during Turonian to Santonian times (~90-83Ma). The microstructures preserved in these mylonites suggest that during their formation, heat was supplied by the newly formed Troodos Complex, which acted as a heat source causing amphibolite-facies metamorphism of Mamonia Complex crustal rocks.

- Dextral transtension and extension of approximately Campanian age (*c.* 83-73Ma) is interpreted to have facilitated the low temperature protrusion of mantle-derived serpentinites associated with both the Mamonia and Troodos Complexes. The formation of a steep fault zone architecture is thought to have influenced displacement patterns during subsequent compressional reactivation.

- The final juxtaposition of the two complexes took place during a phase of compressional deformation that ceased by the end of the Maastrichtian (~65Ma). Compression is envisaged to have resulted from the impingement of the Troodos microplate on the Mamonia Complex along an arcuate suture zone, producing a radial distribution of displacements. Top-to-the-west thrusting in the Northern Region is thought to have been controlled by gravitationally-induced body forces that developed within the evolving thrust wedges. Synchronous compression in the Southern Region resulted in pure shear-dominated sinistral transpression. During this transpressional deformation, shortening was accommodated by the dominant lateral extrusion of fault zone material, which is considered to have arisen from the compression of a laterally 'unconfined' fault zone.

- It is proposed that intense grain-size reduction and flux of chemically active hydrous fluids throughout the deformational history of the SW Cyprus fault zones led to significant long term weakening. Microstructural observations suggest that the operation of efficient grain-scale deformation mechanisms at both high and low temperatures facilitated weakening, accounting for the observed reactivational history of the fault zones over a *c.*25Ma timescale. It is concluded that faults zones that contain similar rock types to those preserved in SW Cyprus (i.e. peridotite mylonites and serpentinites) are expected to strongly influence the rheological strength of the lithosphere.

REFERENCES CITED IN THE TEXT

Agrinier, P., Mevel, C., Bosch, D. and Javoy, M., 1993. Metasomatic hydrous fluids in amphibole peridotites from Zabargad Island (Red Sea). *Earth and Planetary Science Letters*, **120**, 187-205.

Allen, C.R., 1968. The tectonic environments of seismically active and inactive areas along the San Andreas fault system. In: *Proceedings of the Conference on Geologic Problems of the San Andreas Fault System*, Stanford University Press, Palo Alto, CA., 1968, 70-82.

Allerton, S. and Vine, F.J., 1991. Spreading evolution of the Troodos ophiolite, Cyprus. *Geology*, **19**, 637-640.

Ashby, M.F. and Verral, R.A., 1973. Diffusion-accommodated flow and superplasticity, *Acta Metallurgica,* **21**, 149-161.

Anonymous, 1972. Penrose feld conference on ophiolites. *Geotimes*, **17**, 24-25.

Atkinson, B.K., 1982. Subcritical crack-propogation in rocks: theory, experimental results and applications. *Journal of Structural Geology*, **4**, 281-290.

Aumento, F., 1970. Serpentine mineralogy of the ultrabasic intrusions in Canada and the Mid-Atlantic Ridge, *Geological Survey of Canada Papers,* **69-53**, pp51.

Aumento, F., Loncarevic, B.D. and Ross, D.I., 1971. Hudson Geotraverse: geology of the Mid-Atlantic Ridge at 45°N. *Philosophical Transactions of the Royal Society of London.*, **A268**, pp23-650.

Aumento, F. and Loubat, H., 1971. The Mid-Atlantic near 45°N; serpentinised ultramafic intrusions. *Canadian Journal of Earth Science*, **8**, 631-663.

Bagnall, P.S., 1964. Wrench faulting in Cyprus. *Journal of Geology*, **72**, 327-345.

Bailey, S.W., 1984. XRD identification of the polytypes of mica, serpentine, and chlorite. In: *Clays and Clay Minerals,* **v. 36**, Nc. 3, 193-213.

Barber, D.J., 1985. Regimes of plastic deformation - processes and microstructures: an overview. In: Wenk, H.,-R. (ed.), *Prefferred orinentation in deformed metals and rocks: an introduction to modern texture analysis.* Academic Press, New York.

Baroz, F., 1980. Volcanism and continent-island arc collision in the Pentadaktylos Range, Cyprus. In Panayiotou, A. (ed.), *Ophiolites, Proceedings of the International Ophiolite Symposium Cyprus 1979.* Cyprus Geological Survey Department, 73-85.

Baroz, F. Desmet, A. and Lapierre, H., 1976, Les traits dominants de la geologie de Chypre. *Bull. Soc. Geol. Fr.* **18**, 429-437.

Bear, L.M., 1958. Wrench fault zones in Cyprus. *Cyprus Geological Survey Department Annual Report.*

Behrman, J. H., 1987. A precautionary note on shear bands as kinematic indicators. *Journal of Structural Geology*, **9**, 659-666.

Berthé, D., Choukroune, P. and Jegouzo, P., 1979. Orthogneiss, mylonite and non-coaxial deformation of granites: the example of the South Armorican Shear-zone. *Journal of Structural Geology*, **1**, 31-42.

Biju-Duval, B. Lapierre, H. and Letouzey, J., 1976, Is the Troodos Massif (Cyprus) allochthonous? *Bull. Soc Geol. France*, **18**, 1347-1356.

Bishopp, D.W,. 1952, Some new features of the geology of Cyprus. 19th International. Geological Congress, **17**, 13-18.

Blome, C.D. and Irwin,W.P., 1985. Equivalent radiolarian ages from ophiolitic terrains of Cyprus and Oman. *Geology*, **13**, 401-404.

Bogolepov, V.G., 1969. Problem of serpentinisation of ultrabasic rocks, *International Geological Revue*, **12**, 421-432.

Bonatti, E., 1973. Origin of offsets of the Mid-Atlantic Ridge in fracture zones. Journal of Geology, **81**, 144-186.

Bonatti, E., 1976. Serpentinite protrusions in the oceanic crust. *Earth and Planetary Science Letters*, **32**, 107-113.

Bonatti, E., 1978. Vertical tectonism in oceanic fracture zones. *Earth and Planetary Science Letters*, **37**, 369-379.

Bonatti, E., Emiliani, C., Ferrara, J., Honnorez, J. and Rydell, H., 1974. Ultramafic-carbonate breccias from the equatorial mid Atlantic ridge. *Marine Geology*, **16**, 83-102.

Bonatti, E. and Crane, K., 1984. Oceanic Fracture Zones. *Scientific American,* **250**, 36-47.

Bonatti, E. and Hamlyn, P.R., 1978. Mantle uplifted block in the western Indian Ocean. *Science*, **201**, 249-252.

Bonatti, E. and Hamlyn, P.R., 1981. Oceanic ultramafic rocks. In: Emiliani, C. (ed.),*The Sea*, **7**, , 241-283. J. Wiley and Sons, New York.

Bonatti, E. and Honnorez, J., 1976. Sections of the Earth's crust in the equatorial Atlantic. *Journal of Geophysical Research,* **84**, 4104-4116.

Bonatti, E. and Michael, P.J., 1989. Mantle peridotites from continental rifts to ocean basins to subduction zones. *Earth and Planetary Science Letters*, **91**, 297-311.

Bonhommet, N., Roperch, P. and Calza, F., 1988. Palaeomagnetic arguments for block rotations along the Arakapas fault (Cyprus). *Geology*, **16**, 422-425.

Bottinga, Y. and Javoy, M., 1973. Comments on oxygen isotope geothermometry, *Earth and Planetary Sciencel Letters*, **20**, 250-265.

Boullier, A.M. and Guegen, Y., 1975. SP Mylonites: Origin of Some Mylonites by Superplastic Flow. *Contributions to Mineralogy and Petrology*, **50**, 93-104.

Boullier A.M. and Nicolas A., 1975. Classification of textures and fabrics of peridotite xenoliths from South African Kimberlites. In: Ahrens (ed.), Physics and Chemistry of the Earth, **9**, 97-105. Oxford: Pergamon.

Bowen, N.L. and Tuttle, O.F., 1948. The system M_gO-SiO_2-H_2O. *Geological Society of America Bulletin*, **60**, 439-460.

Bowin, C.O., Nalwalk, A.J. and Hersey, J. B., 1966. Serpentinized peridotite from the north wall of the Puerto Rico Trench. *Geological Society of America Bulletin*, **77**, 257-270.

Brace, W. F., 1961. Dependence of fracture strength of rocks on grain size. *Bull. Earth Miner. Sci. Exp. Stn. Pa. State Univ.*, **79**, 99-103.

Brodie, K.H. and Rutter, E.H., 1985: On the relationship between deformation and metamorphism, with special relationship to the behavoir of basic rocks. - In: A.B. Thompson & D.C. Rubie(eds.), *Advances in Physical Geochemistry*, 4, Springer-Verlag, 138-179.

Butler, R.W.H., 1982. The terminology of structures in thrust belts. *Journal of structural Geology*, **4**, 239-245.

Butler, R.W.H., 1987. Thrust sequences. *Journal of the Geological Society, London*, **144**, 619-634.

Byerlee, J., 1990. Friction, overpressure and fault normal compression. *Geophysical Research Letters*, **7**, 2109-2112.

Byerlee, J., 1992. The change in orientation of subsidiary shears near faults containing pore fluid under high pressure. *Tectonophysics*, **211**, 295-303.

Cameron, W.E., 1985. Petrology and origin of primitive lavas from the Troodos ophiolite, Cyprus. *Contributions to Mineralogy and Petrology*, **89**, 239-255.

Campbell, I.H., 1975. Direct evidence of present-day serpentinization in the Jimberlana Intrusion, Western Australia. *Geological Magazine*, **112**, 77-80.

Cannat, M., 1993. Emplacement of mantle rocks in the seafloor at mid-ocean ridges. *Journal of Geophysical Research*, **98**, 4163-4172.

Carlson, C., 1984. Depositional facies of sedimentary serpentinite: selected examples from the Coast Ranges, California. In: *SEPM Field Trip Guidebook No. 3. 1984 Mid-Year Meeting, San Jose, California,* 73-126.

Casey, M., 1980. Mechanics of shear zones in isotropic dilatant materials. *Journal of Structural Geology*, **2**, 143-147.

Cerney, P., 1967. Comments on serpentinization and related metasomatism. *American Mineralogist*, **53**, 1377-1385.

Chapple, W.M., 1978. Mechanics of thin-skinned fold and thrust belts. *Geological Society of America Bulletin*, **89**, 1189-1198.

Christensen, N., 1972. The abundance of serpentinites in the ocean crust. *Journal of Geology*, **80**, 709-719.

Chopra, P.N. and Paterson, M.S., 1984. The role of water in the deformation of dunite. *Journal of Geophysical Research*, **89**, 7861-7876.

Cleintaur, M.R. Knox, G.J. and Ealey, P. J., 1977, The geology of Cyprus and its place in the East-Mediterranean framework. *Geologie en Mijonbouw*, **56**, 66-82.

Clube, T.M. M. Creer, K.M. and Robertson, A.H.F., 1985, Palaeorotation of the Troodos microplate, Cyprus. *Nature*, **317**, 522-525.

Clube, T.M.M. and Robertson, A.H.F., 1986, The palaeorotation of the Troodos microplate, Cyprus, in the Late Mesozoic-Early Cenozoic plate tectonic framework of the Eastern Mediterranean. *Surv. Geophys.* **8**, 375-437.

Coleman, R.G., 1971, Petrologic and geophysical nature of serpentinites, *Geological Society of America Bulletin*, **82**, 897-918.

Coleman, R.G. and Keith, T.E., 1971. A chemical study of serpentinisation - Burro Mountain, California, *Journal of Petrology*, **12**, 311-328.

Condie, K.C. and Madison, J.A., 1969. Compositional and volume changes accompanying progressive serpentinization of dunites from the Webster-Addie ultramafic body, North Carolina. *American Mineralogist*, **54**, 1173-1179.

Constantinou, G., 1980. Metallogenesis associated with Troodos Ophiolite. In: Panayiotou, A. (ed.), *Proceedings of the International Ophiolite Symposium, Cyprus 1979,* Cyprus

Constantinou, G. and Govett, G.J.S., 1972. Genesis of sulphide deposits, ochres and umbers of Cyprus. *Transactions of the Institute of Mining and Metallurgy (section B)*, **81**, 634-646.

Cowan, D.S. and Mansfield, C.F. 1970. Serpentinite flows on Joaquin Ridge, Southern Coast Ranges, California. *Geological Society of America Bulletin*, **81**, 2615-2628.

Cox, A., Doell, R. Whitechurch, H. Juteau, T. and Montigny, R., 1984, Role of the Eastern Mediterranean ophiolites (Turkey, Syria, Cyprus) in the history of Neo-Tethys. *In*: Dixon, J.E. and Robertson, A.H.F. (eds), *The Geological Evolution of the Eastern Mediterranean*, Geological Society of London Special Publication, **17**, 301-317.

Cox, A., Doell, R,R. and Thompson, G., 1964. Magnetic properties of serpentinite from Mayaguez, Puerto Rico. In: Burk, C. A., ed., *A Study of Serpentinite (the AMSOC core hole near Mayaguez, Puerto Rico.* Natl. Res. Council, pub. **1188**, pp175.

Davis, D., Suppe, J. and Dahlen, F.A., 1983. Mechanics of fold-and-thrust belts and accretionary wedges. *Journal of Geophysical Research*, **88**, 1153-1172.

Dawson, J.B. and Smith, J.V., 1982. Upper-mantle amphiboles: a review. *Mineralogical magazine*, **45**, 35-46.

Deer,W.A., Howie,R.A., and Zussman, J. 1962. Rock Forming Minerals, Vol. 3, Sheet silicates: John Wiley and Sons,Inc., New York.

Deer, W.A., Howie, R.A. and Zussman, J., 1966. An introduction to the rock forming minerals, Wiley and Sons, Inc., New York.

Delaloye, M. and Desmet, A., 1979. Nouvelles donées radiométriques sur les pillow-lavas du Troodos (Chypre). *Paris, Académie des Sciences Comptes Rendus*, **288**, 461-464.

Dengo, C.A. and Logan, J.M., 1981. Implications of the mechanical and frictional behaviour of serpentinite to seismogenic faulting. *Journal of Geophysical Research*, **86**, 10771-10782.

Dewey, J.F. and Burke, K.C.A., 1973. Tibetan, Variscan and Precambrian basement reactivation: products of continental collision. *Journal of Geology*, **18**, 683-692.

Dewey, J.F., Hempton, M.R., Kidd, W.S.F., Saroglu, F. and Sengor, A.M.C., 1986. Shortening of continental lithosphere: the neotectonics of Eastern Anatolia - a young collision zone. In: Coward, M.P. and Ries, A.C. (eds.), *Collision Tectonics.* Geological Society of London Special Publication, **19**, 3-36.

de Wit, M.J. Dutch, S., Klingfield, R., Allen, R. and Stern, C., 1977. Deformation, serpentinisation and emplacement of a dunite complex, Gibbs Island, South Shetland Islands: Possible fracture zone tectonics. *Journal of Geology*, **85**, 745-762.

Dias, R. and Ribeiro, A., 1994. Constriction in a transpressive regime: an example in the Iberian branch of the Ibero-Armorican arc. *Journal of Structural Geology*, **11**, 1543-1554.

Dick, H.J.B., 1977. Partial melting in the Josephine Peridotite I: The effect on mineral composition and it's consequences for geobarometry and geothermometry. *American Journal of Science,* **227**, 801-832.

Dick, H.J.B., 1978. Mineralogy of abyssal peridotites from the far South Atlantic Caribbean and Equitorial Atlantic. *Abs. with Progr. Geol. Soc. Am.*, **10**, 388pp.

Dick, H.J.B. and Fisher, R.L., 1983. Mineralogic studies of the residues of mantle melting. *Proceedings of the third International Kimberlite Conference* (publ. abstract in Terra Cognita 2:242 (1982)) Developments in Petrology Series, Elsevier.

Dick, H.J.B. and Bullen, T., 1984. Chromian spinel as a petrogenic indicator in abyssal and alpine-type peridotites and spatially associated lavas. *Contributions to Mineralogy and Petrology*, **86**, 54-76.

Dickinson, W.R., 1966. Table Mountain serpentinite extrusion in California Coast Ranges. *Geological Society of America Bulletin*, **77**, No. 7, 451-472.

Dietrich, V. and Peters, T., 1971. Regionale verteilung der Mg-phyllosilikate in den serpentiniten des Oberhalbsteins, Schweiz. Min. Pet. Mitt., **51**, 331-349.

Dietz, R.S., 1961. Continent and ocean basin evolution by spreading of the sea-floor. *Nature*, **190**, 854-857.

Drury,M.R., Hoogerduijn Strating,E.H., and Vissers,R.L.M., 1990. Shear zone structures and microstructures in mantle peridotites from the Voltri Massif, Ligurian Alps, N.W. Italy. *Geologie en Mijnbouw*, **69**, 3-17.

Drury,M.R. and Urai,J.L., 1990. Deformation-related recrystallization processes. *Tectonophysics*, **172**, 235-253.

Drury, M.R., Vissers, R.L.M., Van der Wal, D. and Hoogerduijn Strating, E.H., 1991. Shear localization in upper mantle peridotites. *Pure and Applied Geophysics,* **137**, 439-460.

Ducloz, C., 1972, The geology of the Bellapais-Kythrea area of the central Kyrenia range. *Bulletin of the Geological Survey of Cyprus*, **6**, 75pp.

Dungan, M., 1977. Metastability in serpentine-olivine equilibria. *American Mineralogist*, **62**, 1018-1029.

Du Rietz, T. 1935. Peridotites, serpentines and soapstones of northern Sweden. Geol. Fören. Stckholm Förh., **57**, 133-260.

Ealey, P.J. and Knox, G.J., 1975. The pre-Tertiary rocks of SW Cyprus. *Geologie en Mijnbouw*, **54**, 85-100.

Edwards, S.J. and Malpas, J., 1995. Multiple origins for mantle harzburgites: examples from the Lewis Hills, Bay of Islands ophiolite, Newfoundland. *Canadian Journal of Earth Sciences*, **32**, 1046-1057.

Eggler, D.H., 1987. Solubility of major and trace elements in mantle metasomatic fluids. Experimental Constraints, In: *Mantle metasomatism*, Menzies, M.A. and Hawkesworth, C.J. (eds.), Academic Press, London, 21-39

Elliot, D., The motion of thrust sheets. *Journal of Geophysical Research*, **81**, 949-963.

Engel, C. G. and Fischer, R. L., 1969. Lherzolite, anorthosite, gabbro and basalt dredged from the Mid-Indian Ocean Ridge. *Science*, **166**, 1136-1141.

Engel, C. G. and Fisher, R. L., 1975. Granitic to ultramafic rock complexes of the Indian Ocean Ridge System, western Indian Ocean. *Geological Society of America Bulletin*, **86**, 1553-1578.

Escartín, J., Hirth, G. and Evans, B., 1997. Non-dilatant brittle deformation of serpentinites: Implications for Mohr-Coulomb theory and the strength of faults. *Journal of Geophysical Research*, (in press).

Etheridge, M.A., 1983. Differential stress magnitudes during regional deformation and metamorphism: Upper bound imposed by tensile fracturing. *Geology*, **11**, 231-234.

Etheridge, M.A., Cox, S.F., Wall, V.J. and Vernon, R.H., 1984. High fluid pressures during regional metamorphism and deformation: Implications for mass transport and deformation mechanisms. *Journal of Geophysical Research*, **89**, 4344-4358.

Evans, B.W. and Frost, B.R., 1975. Chrome-spinel in progressive metamorphism - a preliminary analysis, *Geochimica Cosmochimica Acta*, **39**, 959-972.

Evans, B.W., Johannes, W., Otterdoom, H. and Trommsdorff, V., 1976. Stability of chrysotile and antigorite in the serpentine multisystem. *Schweizerische Mineralogische und Petrographische Mitteilungen*, **56**, 79-93.

Fisher, R.L. and Engel, C.G., 1969. Ultramafic and basaltic rocks dredged from the near-shore flank of the Tonga Trench. *Geological Society of America Bulletin,* **80**, 1373-1378.

Fossen,H. and Tikoff,B., 1993. The deformation matrix for simultaneous simple shearing, pure shearing and volume change, and its application to transpression-transtension tectonics. *Journal of Structural Geology*, **15**, 413-422.

Fowler, C.M.R., 1990. The Solid Earth, An Introduction to Global Geophysics. Cambridge University Press, 472pp.

Friedman, M., 1975. Fracture in rock. *Reviews of Geophysics and Space Physics*, **13**, 352-358.

Fryer, P., Ambos, E.L. and Hussong, D.M., 1985. Origin and emplacement of Mariana forearc seamounts. *Geology*, **13**, pp774-777.

Fryer, P. and Fryer, G.J., 1987. Origins of non-volcanic seamounts in a forearc environment. In: Keating,B.H.; Fryer,P.; Batiza,R.; and Bochlert,G.W.,eds., Seamounts, Islands and Atolls: *Geophysical Monograph*, **43**, American Geophysical Union, 61-69.

Fryer, P., 1992. Mud volcanos of the Marianas. *Scientific American*, **266**, No. 2, 46-52.

Fryer,P. et al., 1989. Plumbing the Pacific sinks. *Nature*, **339**, 427-428.

Gass, I.G., 1960, The geology and mineral resources of the Dhali area. *Cyprus Geological Survey Memoirs*, **4**, 116pp.

Gass, I.G., 1968. Is the Troodos massif of Cyprus a fragment of Mesozoic oceanic floor? *Nature*, **220**, 39-42.

Gass, I.G., 1980. The Troodos Massif: Its role in the unravelling of the ophiolite problem and its significance in the understanding of constructive margin processes. In: Panayiotou, A. (ed.), *Ophiolites: Proceedings of the International Symposium, Cyprus, 1979*. Cyprus Geological Survey Department, 23-35.

Gass, I.G. and Masson-Smith, D., 1963, The geology and gravity anomalies of the Troodos Massif, Cyprus. *Philosophical Transactions of the Royal Society of London*, **A255**, 417-467.

Gass, I.G., MacLeod, C.J., Murton, B.J., Panayiotou, A., Simonian, K.O. and Xenophontos, C., 1994. The Geology of the Southern Troodos Transform Fault Zone. Cyprus Geological Survey Department, Memoir No.9, 218pp.

Gates, A.E. and Kambin, R.C., 1990. Comparison of the natural deformation of the State-Line Serpentinite, U.S.A., with experimental studies. *Tectonophysics*, **182**, pp249-258.

Gealey, W.K., 1977. Ophiolite obduction and geological evolution of the Oman Mountains and adjacent areas. *Geological Society of America Bulletin*, **88,** 1183-1191.

Gilotti, J.A. and Hull, J.M., 1990. Kinematic stratification in the hinterland of the central Scandinavian Caledonides. *Journal of Structural Geology,* **15**, 629-646.

Girardeau, J. and Mercier, J.-C.C., 1988. Petrology and texture of the ultramafic rocks of the Xigaze ophiolite (Tibet): constraints for the mantle structure beneath slow-spreading ridges. *Tectonophysics*, **147**, 33-58.

Green, D.H., 1961. Ultramafic breccias from the Musa Valley, Eastern Papua. *Geological Magazine*, **98**, No. 1, 1-25.

Gresens, R.L., 1967. Composition-volume relationships of metasomatism. *Chemical Geology*, **2**, 47-65.

Guggenheim, S. and Eggleton, R.A., 1985. Modulated 2:1 layer silicates: Review, systematics and predictions. *American Mineralogist*, **72**, 724-738.

Hamlyn, P.R. and Bonatti, E., 1980. Petrology of mantle-derived ultramafics from the Owen Fracture Zone, northwest Indian Ocean: Implications for the nature of the oceanic upper mantle. *Earth and Planetary Science Letters*, **48**, 65-79.

Handy,M.R., 1989. Deformation regimes and the rheological evolution of fault zones in the lithosphere: the effects of pressure, temperature, grainsize and time. *Tectonophysics*, **163**, 119-152.

Handy, M.R., 1994. Flow laws for rocks containing two non-linear viscous phases: a phenomenological approach. *Journal of Structural Geology*, **16**, 287-301.

Harland,W.B., 1971. Tectonic Transpression in Caledonian Spitsbergen. *Geological Magazine*, **108**, 27-42.

Hanmer, S. and Passchier, C. W., 1991. Shear sense indicators: a review. Geological survey of Canada, Paper 90-17, 1-71.

Harte,B., 1977. Rock nomenclature with particular relation to deformation and recrystallisation textures in olivine-bearing xenoliths. *Journal of Geology*, **85**, 279-288.

Harte, B., Cox, K. G. and Gurney, J. J., 1975. Petrography and geological history of upper mantle xenoliths from the Matsoku kimberlite pipe. In: *Physics and Chemistry of the Earth*, **9**, Ahrens, L. H., Dawson, J. B., Duncan, A. R. and Erlank, A. J., Eds. Pergamon, Oxford, 477-506.

Hébert, R., Bideau, D. and Hekinian, R., 1983. Ultramafic and mafic rocks from the Garret transform fault near 13°30'S on the East Pacific Rise: Igneous petrology. *Earth and Planetary Science Letters*, **65**, 107-125.

Hess, H. H., 1955a. Serpentines, orogeny, and epeirogency. *Geological Society of America Special Paper*, **62**, pp391-407.

Hess, H. H., 1955b. The oceanic crust. *Journal of Marine Research*, **14**, No. 4, 423-439.

Hess, H.H., 1962. History of the Ocean Basins. In: *Petrologic Studies* (Buddington Volume), Geological Society of America, Boulder, Colorado, 599-620.

Hess, H. H., 1965. Mid-ocean ridges and tectonics of the sea-floor. In: Whittard, W. F. and Bradshaw, R., eds., *Submarine Geology and Geophysics*, Colston Res. Symp., 17th, Bristol, England, Proc.: Butterworths, London, 317-333.

Hobbs, B.E., 1981. The influence of metamorphic environment upon the deformation of minerals. *Tectonophysics*, **78**, 335-383.

Hobbs, B.E., Means, W.D. and Williams, P.F., 1976. An outline of structural geology, Wiley and Sons, 571pp.

Holdsworth, R.E. and Strachan R.A., 1991. Interlinked system of ductile strike slip and thrusting formed by Caledonian sinistral transpression in northeasten Greenland. *Geology*, **19**, 510-513.

Holdsworth, R.E., Bailey, W.R., Imber, J., Butler, C.A. and Lloyd, G., 1997. The structural role played by fluids during reactivation of mid-crustal and upper mantle fault zones. Extended abstract, *Geofluids 2 '97; Second International Conference on Fluid Evolution, Migration and Interaction in Sedimentary Basins and Orogenic Belts,* (in press).

Hoogerduijn Strating, E.H., Rampone, E., Piccardo, G.B., Drury, M.R. and Vissers, R.L.M., 1993. Subsolidus emplacement of mantle peridotites during incipient oceanic rifting and opening of the Mesozoic Tethys (Votri Massif, NW Italy). *Journal of Petrology*, **34**, part 5, 901-927.

Hoogerduijn Strating, E.H. and Vissers, R.L.M., 1994. Structures in natural serpentinite gouges. *Journal of Structural Geology*, **16**, No. 9, 1205-1215.

Hostetler, P.B., Coleman, R.G., Mumpton, F.A. and Evans, B.W., 1966. Brucite in Alpine serpentinites, *American Mineralogist*, **51**, 75-98.

Hubbert, M.K. and Rubey, W.W., 1959. Role of fluid pressure in the mechanics of overthrust faulting. *Geological Society of America Bulletin*, **70**, 115-166.

Huggins, C.W. and Shell, H.R., 1965. Density of bulk chrysotile and massive serpentine. *American Mineralogist*, **50**, 1058-1067.

Irwin, W.P. and Barnes, I., 1975. Effect of geologic structure and metamorphic fluids on seismic behaviour of the San Andreas fault system in Central and Northern California. *Geology*, **3**, 713-716.

Jackson, E.D., Green, H.W.II and Moores, E.M., 1975. The Vourinos Complex, Greece: cyclic units of lineated cumulates overlying harzburgite tectonite. *Geological Society of America Bulletin*, **86**, 390-398.

Janecky,D.R. and Seyfried,W.E., 1986. Hydrothermal serpentinization of peridotite within the oceanic crust: Experimental investigations of mineralogy and major element chemistry. *Geochimica et Cosmochimica Acta*, **50**, 1357-1378.

Jaroslow,G.E., Hirth,G. and Dick, H.J.B., 1996. Abyssal peridotite mylonites: implications for grain-size sensitive flow and strain localization in the oceanic lithosphere. *Tectonophysics*, **256**, 17-37.

Johannes,W., 1968. An experimental investigation of the system MgO-SiO_2-H_2O-CO_2. *American Journal of Science*, **267**, 1083-1104.

Jones, R.R., Holdsworth, R.E. and Bailey, W., 1997. Lateral extrusion in transpression zones: the importance of boundary conditions. *Journal of Structural Geology*, (in press).

Jones,R.R. and Tanner,G.P.W., 1995. Strain partitioning in transpression zones. *Journal of Structural Geology*, **17**, 793-802.

Karato, S., 1989. Grain growth kinetics in olivine aggregates. *Tectonophysics*, **168**, 255-273.

Karato,S., Paterson,M.S., and Fitzgerald,J.D., 1986. Rheology of synthetic olivine aggregates: Influence of grain size and water. *Journal of Geophysical Research*, **91**, 8151-8176.

Karson, J.A. and Dewey, J.F., 1978. Coastal Complex, western Newfoundland: An early Ordovician oceanic fracture zone. *Geological Society of America Bulletin*, **89**, 1037-1049.

Karson, J.A. and Dick, H.J.B., 1983, Tectonics of ridge-transform intersections at the Kane fracture zone. *Marine Geophysical Researches*, **6**, 51-98.

Knipe,R.J., 1989. Deformation mechanisms - recognition from natural tectonites. *Journal of Structural Geology*, **11**, 127-146.

Korytkova, E.N. and Makarova, T.A., 1971. Experimental study of the serpentinization of olivine. *Dokl. Akad. Nauk USSR*, **196**, 144-145.

Korytkova, E.N., Makarova, T.A. and Kosulina, G.I., 1972, Experimental serpentinization of olivine, *International Geological Review*, **14**, 1074-1078.

Laird, J., 1988. Chlorites: Metamorphic Petrology. In: Bailey, S.W. (ed.), Hydrous Phyllosilicates (exclusive of micas), *Reviews in Mineralogy*, **19**, 405-447.

Lapierre, H,. 1968. Decouverte d'une serie volcano-sedimentaire probablement d'age cretace superieur au Sud-Ouest de la l'ile de Chypre. *C. R. Acad. Sc. Paris.* **266**, 1817-1820.

Lapierre, H., 1972. Les formations sedimentaries et eruptives des nappes de Mamonia et leurs relations avec le Massif du Troodos. (Chypre occidentale). *Mem. Soc. Geol. France*, **123**, 132pp.

Lapierre, H., 1975a. Les formations sedimentaires et eruptives des nappes de Mamonia (Chypre), *C. R. Acad. Sci. Paris*, **d276**, 32-35.

Lapierre, H., 1975b. Les formations sedimentaires et eruptives des nappes de Mamonia et leurs relation avec le Massif de Troodos (Chypre occidentale). *Soc. Geol. Fr. Mem.* **123:** 132pp.

Lapierre, H. and Rocci, G., 1967. Le massif pluto-volcanique basique de Kellaki, (Chypre). I - Etude petrographique et structurale. *Sciences de la Terre*, **12**, 145-181.

Lapierre, H. and Rocci, G.M,. 1976. Le valcanisme alcalin du sud-ouest de Chypre et la probleme de l'ouverture des regions Tethysiennes au Trias. *Tectonophysics*, **30**, 299-313.

Lauder, W.R., 1965. The geology of Dun Mountain, Nelson, New Zealand. Part 2. The petrology and structure and origin of the ultrabasic rocks. *New Zealand Journal of Geology and Geophysics*, **8**, 475-504.

Leake, B.E., 1978. Nomenclature of Amphiboles. *The Canadian Mineralogist*, **16**, 501-520.

Lippard, S.J., Shelton, A.W. and Gass, I.G., 1986. The ophiolite of northern Oman. *Geological Society London Memoirs*, **11**, 178pp.

Lloyd, G.E. and Knipe, R.J., 1992. Deformation mechanisms accommodating faulting of quartzite under upper crustal conditions. *Journal of Structural Geology,* 127-142.

Lockwood, J.P., 1971. Sedimentary and gravity slide emplacement of serpentinite. *Geological Society of America Bulletin*, **82**, 919-936.

Logan, J.M., Friedman, H., Higgs, N.G., Dengo, C. and Shimamoto, T., 1979. Experimental studies of simulated gouge and their application to studies of natural fault zones. *United States Geological Survey Open-file Report*, **79-1239**, 305-343.

MacDonald, A.H. and Fyfe, W.S.,1985. Rate of serpentinization in seafloor environments. *Tectonophysics*, **116**, 123-135.

MacLeod, C.J., 1988. Tectonic evolution of the Eastern Limassol Forest Complex, Cyprus. *Unpublished Ph.D. thesis*, Open University, 231pp.

MacLeod, C.J., 1990. Role of the Southern Troodos Transform Fault in the rotation of the Cyprus microplate: Evidence from the Eastern Limassol Forest Complex. In: Malpas, J., Moores, E., Panayiotou, A. & Xenophontos, C. (eds.), *Ophiolites. Oceanic Crustal Analogues*, Proc. 'Troodos 87' Symposium. Cyprus Geological Survey Department, 75-86

MacLeod, C.J., Robertson, A.H.F., Allerton, S., Browning, P., Gass, I.G., Taylor, R.N., Vine F.J. and Xenophontos, C., 1992. Comment on ' Tectonic evolution of the Troodos ophiolite within the Tethyan framework' by Y. Dilek, P. Thy, E.M. Moores & T.W. Ramsden. *Tectonics* (in press).

MacLeod, C.J. and Murton, B.J., 1993. Structure and Tectonic evolution of the Southern Troodos Transform Fault Zone, Cyprus. In: Prichard, H.M., Alabaster, T., Harris, N.B.W. & Neary, C.R. (eds.), *Magmatism and Plate Tectonics*. Geological Society of London Special Publication, 141-176.

MacLeod, C.J. and Murton, B.J., 1995. On the sense of slip of the southern Troodos transform fault zone. *Geology*, **23**, 257-260.

Maltman, A.J,. 1978. Serpentinite textures in Anglesey, North Wales,United Kingdom. *Geological Society of America Bulletin*, **89**, 972-980.

Malpas, J., Xenophontos, C. and Williams, D., 1992. The Ayia Varvara Formation of SW Cyprus: a product of complex collisional tectonics. *Tectonophysics*, **212**, 193-211

Malpas, J., Calon, T. and Squires, G., 1993. The development of a late Cretaceous microplate suture zone in S.W. Cyprus. In: Prichard, H.M., Alabaster, T., Harris, N.B.W. & Neary, C.R. (eds.), *Magmatism and Plate Tectonics*. Geological Society of London Special Publication, 177-195.

Margaritz, M. and Taylor, H.P., 1974. Oxygen and hydrogen isotope studies of serpentinization in the Troodos Ophiolite Complex, Cyprus, *Earth and Planetary Science Letters*, **23**, 8-14.

Martin, B. and Fyfe, W.S., 1970. Some experimental and theoretical observations on the kinetics of hydration reactions with particular reference to serpentinization. *Chemical Geology*, **6**, 185-195.

McCoss, A.M., 1986. Simple Constructions for deformation in transpression/transtension zones. *Journal of Structural Geology*, **8**, 715-718.

Mckenzie, D.P., 1972. Active tectonics of the Mediterranean Region. *Geophys. J.*, **18**, 1-32.

Mercier, J.C., 1985. Olivine and Pyroxenes, in: Preferred orientation in deformed rocks: An introduction to modern texture analysis.Academic Press, inc. 407-430.

Mercier, J.C. and Nicholas, A., 1975. Textures and fabrics of upper-mantle peridotites as illustrated from xenoliths from basalts. *Journal of Petrology*, **16**, 454-487.

Michael, P.J. and Bonatti, E., 1985. Peridotite composition from the North Atlantic: Regional and tectonic variations and implication for partial melting. *Earth and Planetary Science Letters*, **73**, 91-104.

Middleton, G.V. and Hampton, M.A., 1973. Subaqueous sediment transport and deposition in sediment gravity flows. In: Stanley, D.D. and Swift, D.J.P. (eds.), *Marine sediment transport and environmental management.* John Wiley & Sons, New York, 197-218.

Molnar, P., 1992. Brace-Goetze Strength Profiles, The Partitioning of Strike-slip and Thrust Faulting at Zones of Oblique Convergence, and the Stress-Heat Flow Paradox of the San Andreas Fault. In: *Fault Mechanics and Transport Properties of Rocks*, Academic Press Ltd., 435-459.

Molnar, P. and Tapponier; P., 1977. Relation of the tectonics of eastern China to the India-Eurasia collision: Application of slip-line field theory to large-scale continental tectonics. *Geology*, **5**, 212-216.

Moody, J.B., 1976. Serpentinisation: a review, *Lithos*, **9**, 125-138.

Moore, J.C., 1989. Tectonics and hydrogeology of accretionary prisms: role of the décollement zone. *Journal of Structural Geology*, **11**, 95-106.

Moore, T.A., 1960. The geology and minaeral resources of the Astromerilis-Kormakiti areas.*Geological Survey of Cyprus Memoirs*,**6**, 66pp.

Moore, D.E., Summers, R. and Byerlee, J.D., 1989. Sliding behaviour and deformation textures of heated illite gouge. *Journal of Structural Geology*, **11**, 329-342.

Moore, D.E. and Byerlee, J.D., 1991. Comparative geometry of the San Andreas fault, California, and laboratory fault zones. *Geological Society of America Bulletin*, **103**, pp762-774.

Moore, D.E, Lockner, D.A., Summers, R., Shengli, Ma. and Byerlee, J.D., 1996. Strength of chrysotile-serpentinite gouge under hydrothermal conditions: Can it explain a weaker San Andreas Fault? *Geology*, **24**, 1041-1044.

Moores, E.M., 1969. Petrology and structure of the Vourinos Ophiolite Complex, Northern Greece. *Geological Society of America Special Paper,* **118**, pp74.

Moores, E.M. and Vine, F.J., 1971. The Troodos Massif, Cyprus, and other ophiolites as oceanic crust: Evaluation and implications. *Philosophical Transactions of The Royal Society of London*, ser. A, v. **268**, 443-465.

Moores, E.M., Robinson, P.T., Malpas, J. and Xenophontos, C., 1984. Model for the origin of the Troodos massif, Cyprus, and other mideast ophiolites. *Geology*, **12**, 500-503.

Morris, A., Creer, K.M. and Robertson, A.H.F., 1990. Palaeomagnetic evidence for Clockwise rotations related to dextral shear along the Southern Troodos Transform Fault (Cyprus). *Earth and Planetary Science Letters*, **99**, 250-262.

Morse, T., 1996. Biostratigraphical Constraints (Calcareous Nannofossils) on the Lower Cretaceous to Lower Miocene evolution of SW Cyprus. *Unpubl. Ph.D. Thesis*, University of Durham.

Mukasa, S.B. and Ludden, J.N., 1987 Uranium-lead ages of plagiogranite from the Troodos ophiolite, Cyprus, and their tectonic significance. *Geology*, **15**, 825-828.

Mumpton, F.A. and Thompson, C.S., 1975. Mineralogy and origin of the Coalinga asbestos deposit, *Clays and Clay Minerals*, **23**, 131-144.

Murton, B.J., 1986. Anomalous oceanic lithosphere formed in a leaky transform fault: evidence from the Western Limassol Forest Complex, Cyprus. *Journal of the Geological Society of London*, **143**, 207-258.

Murton, B.J., 1986b. The tectonic evolution if the Western Limassol Forest Complex, Cyprus,. *Unpubl. Ph.D. thesis*, Open University, 332pp.

Murton, B.J., 1990. Was the Southern Troodos Transform Fault a victim of microplate rotation? In: Malpas, J., Moores, E., Panayiotou, A. & Xenophontos, C. (eds.), *Ophiolites. Oceanic Crustal Analogues*, Proc. 'Troodos 87' Symposium. Cyprus Geological Survey Department, 87-98.

Nicolas, A., 1978. Stress estimates from structural studies in some mantle peridotites. *Philosophical Transactions of the Royal Society of London*, **288**, 49-57.

Nicolas, A., 1986. Structure and petrology of peridotites: Clues to their geodynamic environment. *Reviews of Geophysics*, **24**, 875-895.

Nicolas, A., Bouchez, J.L., Boudier, F. and Mercier, J.C., 1971. Textures, structures and fabrics due to solid state flow in some European lherzolites. *Tectonophysics*, **12**, 55-86.

Nicolas, A. and Poirer, J.P., 1976. *Crystalline Plasticity and Solid State Flow in Metamorphic Rocks*. J. Wiley and Sons, pp144.

Nicolas, A., Boudier, F. and Bouchez, J.-L., 1980. Interpretation of peridotite structures from ophiolitic and oceanic environments. *American Journal of Science*, **280**, 192-210.

O'Hanley, D.S., 1992. Solution to the volume problem in serpentinization. *Geology*, **20**, 705-708.

O'Hanley, D.S., 1991. Fault-controlled phenomena associated with hydration and serpentine recrystallization during serpentinisation. *Canadian Mineralogist*, **29**, 21-35.

O'Hanley, D.S. and Dyar, M.D., 1993. The composition of lizardite and the formation of magnetite in serpentinites. *American Mineralogist,* **78**, 391-404.

O'Hanley, D.S. and Offler, R., 1992. Characterization of multiple serpentinization, Woodsreef, New South Wales. *Canadian Mineralogist*, **30**, 1113-1126.

Oldow,J.S., Bally,A.W. and Av., Lallement,H.G., 1990. Transpression, orogenic float, and lithospheric balance. *Geology,* **18**, 991-994.

Page, N.J., 1968. Chemical differences between the serpentine "polymorphs". *American Mineralogist*, **53**, 201-215.

Parrot, J.F. and Whitechurch, H., 1978. Subductions antérieures au charriage nord-sud de la croûte Tethysienne: facteur de métamorphisme de séries sédimentaires et volcaniques liées aux assemblages ophiolitiques Syro-Turcs, en schistes verts et amphiboles. *Rev. Géol. Dyn.*, **20**, 153pp.

Passchier, C.W. and Simpson, C., 1986. Porphyroclast systems as kinematic indicators. *Journal of Structural Geology*, **8**, 831-843.

Paterson, M.S., 1978. Experimental rock deformation - The Brittle field. Berlin, Springer-Verlag. 254pp.

Pearce, J.A., 1975. Basalt geochemistry used to investigate past tectonic environments on Cyprus. *Teconophysics*, **25**, 41-67.

Pearce, J.A., Lippard, S.J. and Roberts, S., 1984. Characteristics and tectonic significance of supra-subduction zone ophiolites. In: Kokelaar, B.P. & Howells, M.F. (eds.), *Marginal Basin Geology*. Geological Society of London Special Publication, **16**, 77-94.

Petit, J.P., 1987. Criteria for the sense of movement on fault surfaces in brittle rocks. *Journal of structural Geology*, **9**, No. 5/6, 597-608.

Phillips, W.J., 1972. Hydraulic fracturing and mineralization. *Journal of the Geological Society of London*, **128**, 337-359.

Pike, J.E. and Schwarzman, E.C., 1977. Classification of textures in ultramafic xenoliths. *Journal of Geology*, **85**, 49-61.

Platt, J.P., 1986. Dynamics of orogenic wedges and the uplift of high-pressure metamorphic rocks. *Geological Society of America Bulletin*, **97**, 1037-1035.

Platt, J.P. and Vissers, R.L.M., 1980. Extensional structures in anisotropic rocks. *Journal of Structural Geology*, **2**, 397-410.

Platt, J.P., Behrmann, J.H., Cunningham, P.C., Dewey, J.F., Helman, M., Parish, M., Shepley, M.G., Wallis, S and Weston, P.J., 1989. Kinematics of the Alpine arc and the motion history of Adria. *Nature*, **337**, 158-161.

Prichard, H.M., 1979. A petrogrphic study of the process of serpentinisation in ophiolites and the ocean crust. *Contributions to Mineralogy and Petrology*, **68**, 231-241.

Prinzhofer, A. and Nicolas, A., 1980 The Bogata Peninsula: A possible oceanic transform fault. *Journal of Geology*, **88**, 387-398.

Prior, D.J., Knipe, R.J. and Handy, M.R., 1990. Estimates of the rates of microstructural changes in mylonites. In: Knipe, R.J. and Rutter, E.H. (eds.), *Deformation Mechanisms, Rheology and Tectonics*, Geological Society Special Publication No. 54, 309-319.

Raleigh, C.B. and Paterson, M.S., 1965. Experimental Deformation of Serpentinite and its Tectonic Implications. *Journal of Geophysical research*, **70**, 3965-3985.

Ramsay, J.G., 1967. "Folding and Fracturing Rocks". McGraw Hill Book Co., New York, 568pp.

Ramsay, J.G., 1980a. Shear zone geometry: a review; *Journal of Structural Geology*, **2**, 83-99.

Ramsay, J.G., 1980b. The crack seal mechanism of rock deformation. *Nature*, **284**, 135-139.

Ramsay, J.G. and Graham, R.H., 1970. Strain variations in shear belts. *Canadian Journal of Earth Science*, **7**, 786-813.

Ramsay, J.G. and Huber, M.I., 1983. The Techniques of Modern Structural Geology, Volume 1: Strain Analysis. Academic Press Inc. (London) Ltd. 307.

Ramsay, J.G. and Huber M.I., 1987. The Techniques of Modern Structural Geology, Volume 2: Folds and Fractures. Academic Press Inc. (London) Ltd. 307-700.

Reches, Z., 1978. Analysis of faulting in three-dimensional strain field. *Tectonophysics*, **47**, 109-129.

Reinen, L.A., Weeks, J.D. and Tullis, T.E., 1991. The frictional behaviour of serpentinite: implications for aseismic creep on shallow crustal faults. *Geophysical Research Letters*, **18**, No. 10, 1921-1924.

Reinen, L.A., Weeks, J.D. and Tullis, T.E., 1994. The frictional behaviour of lizardite and antigorite serpentinites: experiments, constitutive models, and implications for natural faults. *Pageoph.*, **143**, No1/2/3, pp317-358.

Reynolds, S.J. and Lister, G.S., 1987. Structural aspects of fluid-rock interactions in detachment zones. *Geology*, **15**, 362-366.

Rice, J.R., 1992. Fault stress states, pore pressure distributions, and weakness of the San Andreas Fault. In: *Fault Mechanics and Transport Properties of Rock* (Evans, B. and Wong, T. F. eds.) 475-503, Academic Press Ltd., 1992.

Riedel, W., 1929. Zur mechanik geologischer Brucherscheinungen. *Zbl. Mineral. Geol. Palaeont.*, Abt., **1929B**, 354-368.

Robertson, A.H.F., 1975. Cyprus Umbers: basalt-sediment relationships on a mesozoic ocean ridge. *Journal of the Geological Society of London*, **131**, 511-531.

Robertson, A.H.F., 1976b. Pelagic chalks and calciturbidites from the Lower Tertiary of the Troodos Massif, Cyprus. *Journal of Sedimentary Petrology*, **46**, 1007-1016.

Robertson, A.H.F, 1977a. The origin and diagenesis of cherts from Cyprus. *Sedimentology*, **24**, 11-30.

Robertson, A.H.F., 1977b. The Moni Melange, Cyprus,: an olistostrome formed at a destructive plate margin. *Journal of the geological society of London*, **133**, 447-466.

Robertson, A..H.F, 1977c. The Kannaviou Formation, Cyprus: volcaniclastic sedimentation of a late Cretaceous volcani arc.*Journal of the geological society of London*, **134**, 269-292.

Robertson, A.H.F., 1977d. The Tertiary uplift history of the Troodos Massif, Cyprus. *Geological Society of America Bulletin*, **88**, 1763-1772.

Robertson, A.H.F., 1990. Tectonic evolution of Cyprus. In: Malpas, J., Moores, E., Panayiotou, A. & Xenophontos, C. (eds.), *Ophiolites. Oceanic Crustal Analogues*, Proc. 'Troodos 87' Symposium. Cyprus Geological Survey Department, 235-250.

Robertson, A.H.F. and Hudson,J.D., 1973. Cyprus umbers: chemical precipitates on a Tethyan ocean ridge. *Earth and Planetary Science Letters*, **18**, 93-101.

Robertson, A.H.F. and Hudson, J.D., 1974. Pelagic sediments in the Cretaceous and Tertiary history of the Troodos Massif, Cyprus. *Spec. Publ. Internat. Assoc. Sediment.* **1**, 403-436.

Robertson, A. and Woodcock, N.H., 1979a. The Mamonia Complex, south west Cyprus: the evolution and emplacement of a Mesozoic continental margin. *Geological Society of America Bulletin,*(in press in 1979-80).

Robertson, A. and Woodcock, N.H..,1979b. Evidence for the emplacement direction of allochthonous rocks in southern Cyprus. *Proc. 6th Coll. on Geology Aegean Region. Ismir,* (in press in 1979-80)

Robertson, A. and Xenophontos, C., 1993, Development of concepts concerning the Troodos ophiolite and adjacent units in Cyprus. *From* Prichard, H. M. Alabaster, T. Harris, N. B. W. and Neary, C. R. (eds), *Magmatic Processes and Plate Tectonics,* Geological Society Special Publication No. **76**, 85-119.

Robinson, P., Spear, F.S., Schumaker, J.C., Laird, J., Klein, C., Evans, B.W. and Doolan, B.W., 1981. Phase relations of Metamorphic Amphiboles: natural occurrence and theory. In: Veblen, D. (ed.), Amphiboles: Petrology and Experimental Phase Relations. *Reviews in Mineralogy*, 9B. Mineralogical Society of America, 1-211.

Rona, P. A., Widenfalk, L. and Boström, K., 1987. Serpentinized ultramafics and hydrothermal activity at the Mid-Atlantic Ridge crest near 15°N. *Journal of Geophysical Research*, **92**, No. B2, 1417-1427.

Ross, J.V., Lallemant, H.G., and Carter, N.L., 1980. Stress dependence of recrystallized-grain and subgrain size in olivine. *Tectonophysics*, **70**, 39-61.

Rovetta, M.R., Holloway, J.R. and Blacic, J.D., 1986. Solubility of hydroxyl in natural quartz annealed in water at 900°c and 1.5GPa. *Geophysical Research Letters*, **13**, 145-148.

Rutter, E.H., 1983. Pressure solution in nature, theory and experiment. *Journal of the Geological Society of London,* **140**, 725-740.

Rutter, E.H., 1986. On the nomenclature of mode of failure transitions in rocks. *Tectonophysics*, **122**, 381-387.

Rutter, E.H., and Brodie,K.H., 1987. Experimental " syntectonic" dehydration of serpentinite under conditions of controlled pore water pressure. *Journal of Geophysical Research*, **93**, 4907-4932.

Rutter E.H. and Brodie, K.H., 1988. The role of tectonic grain size reduction in the rheological stratification of the lithosphere. *Geologische Rundschau*, **77**, 295-308.

Rutter, E.H., Maddock, R.H., Hall, S.H. and White, S.H., 1986. Comparative microstructures of natural and experimentally produced clay-bearing fault gouges. *Pure and Applied Geophysics,* **124**, 3-30.

Sanderson, D.J. and Marchini, W.R.B., 1984. Transpression. *Journal of Structural Geology*, **6**, 449-458.

Sanford, R.F., 1981. Mineralogical and chemical effects of hydration reactions and applications to serpentinization. *American Mineralogist*, **66**, 290-297.

Schmid, S.M. and Handy, M.R., 1991. Towards a Genetic Classification of Fault Rocks: Geological Usage and Tectonophysical Implications. In: Muller, D.W., McKenzie, J.A. and Weissert, H. (eds.), "*Controversies in Modern Geology: Evolution of Geological Theories in Sedimentology, Earth History and Tectonics*", Academic Press Ltd.

Scholz, C.H., 1977. ransform fault systems of California and New Zealand: similarities in their tectonic styles. *Journal of the Geological Society of London*, **133**, 215-229.

Selfridge, G.C., 1935. An X-ray and optical investigation of the serpentine minerals. *American Mineralogist,* **21**, 463-503.

Sen, C. and Dunn, T., 1994. Experimental modal metasomatism of a spinel lherzolite and the production of amphibole-bearing peridotite. *Contributions to Mineralogy and Petrology*, **119**, 422-432.

Sengör, A.M.C., Yilmaz, Y. and Sungurlu, O., 1984. Tectonics of the Mediterranean Cimmerides: nature and evolution of the western termination of Palaeo-Tethys. In: Dixon, J.E. and Robertson, A.H.F.(cds.), *The Geological Evolution of the Eastern Mediterranean*, Geological Society of London Special Publication, **17**, 77-112.

Sibson; R.H., 1981. Fluid flow accompanying faulting: field evidence and models. In: Simpson, D.W. and Williams, P.G. (eds.), *Earthquake Prediction: an International Review*. American Geophysical Union, Maurice Ewing Series, **4**, 593-603.

Sibson, R.H., 1990. Conditions for fault-valve behavoir. In: Knipe, R.J. and Rutter, E.H. (eds.), *Deformation Mechanisms, Rheology and Tectonics*, Geological Society Special Publication, **54**, 15-28.

Sibson, R.H., Moore, J.M. and Rankin, A.H., 1975. Seismic pumping - a hydrothermal fluid transport mechanism. *Journal of the Geological Society of London*, **131**, 653-659.

Simonian,K. O., 1975, The geology of the Arakapas Fault Belt area, Troodos Massif, Cyprus. PhD thesis, Open University, Milton Keynes.

Simonian, K.O. and Gass, I.G.,1978. Arakapas fault belt, Cyprus: a fossil transform fault. *Geological Society of America Bulletin*, **89**, 1220-1230.

Sleep, N.H. and Blanpied, M.L., 1992. Creep, compaction and the weak rheology of major faults. *Nature*, **359**, 687-692.

Smith, J.V. and Durney, D.W., 1992. Experimental formation of brittle structural assemblages in oblique divergence. *Tectonophysics*, **216**, 235-253.

Spooner, E.T.C., 1980. Cu-pyrite mineralization and seawater convection in oceanic crust: The ophiolite ore deposits of Cyprus. *Geological Society of Canada Special Paper,* **20**, 685-704.

Spray, J.G. and Roddick, J.C., 1981. Evidence for Upper Cretaceous transform fault metamorphism in West Cyprus. *Earth and Planetary Science Letters*, **55**, 273-291.

Staudigel, H., Gillis, K. and Duncan, R., 1986. K/Ar and Rb/Sr ages of caledonites from the Troodos ophiolite, Cyprus. *Geology*, **14**, 72-75.

Stuart-Smith, P.G., 1990. The emplacement and fault history of the Coolac Serpentinite, Lachlan Fold Belt, southeastern Australia. *Journal of Structural Geology*, **12**, No. 5/6, 621-638.

Swanson, M.T., 1988. Pseudotachylyte-bearing strike-slip duplex structures in the Fort Foster Brittle Zone, S. Maine. *Journal of Structural Geology*, **10**, 813-828.

Swarbrick, R.E., 1979, The sedimentology and structure of SW Cyprus its relationship to the Troodos Complex. PhD thesis, University of Cambridge.

Swarbrick, R.E., 1980, The Mamonia Complex of SW Cyprus, a Mesozoic continental margin and its relationship to the Troodos Complex. In: Panayioutou A. ed., Ophiolites Proceedings, International Ophiolite Symposium, Cyprus, 1979, 86-92.

Swarbrick, R.E.,1993. Sinistral strike-slip and transpressional tectonics in an ancient ocean setting: the Mamonia Complex, southwest Cyprus. *Journal of the Geological Society, London*, **150**, 381-392.

Swarbrick, R.E. and Naylor, M.A., 1980. The Kathikas melange, SW Cyprus: late Cretaceous submarine debris flows. *Sedimentology*, **27**, 63-78.

Swarbrick, R.E. and Robertson, A.H.F., 1980, Revised stratigraphy of the Mesozoic rocks of southern Cyprus. *Geological Magazine*, **117**, 547-563.

Tanaka, H., 1992. Cataclastic lineations. *Journal of Structural Geology*, **14**, 1239-1252.

Tapponier, P. and Molnar, P., 1976. Slip-line field theory and large scale continental tectonics. *Nature*, **264**, 319-324.

Taylor, R.N., 1990. Geochemical stratigraphy of the Troodos extrusive sequence: temporal development of a spreading centre magma chamber. In: Malpas, J., Moores, E.M., Panayiotou, A. and Xenophontos, C. (eds.), *Ophiolites. Oceanic Crustal Analogues*. Cyprus Geological Survey Department, 173-184.

Tchalenko,J.S., 1970. Similarities between shear zones of different magnitudes. *Geological Society of America Bulletin.* **81**, 1625-1640.

Teyssier,C., Tikoff,B., and Markley,M., 1995. Oblique plate motion and continental tectonics. *Geology,* **23**, 447-450.

Thayer, T.P., 1960. Some critical differences between alpine-types and stratiform peridotite-gabbro complexes. Internat. Geol. Congr. 21st, Copenhagen, Proc., Pt. 13, pp247-259.

Thayer, T.P., 1966. Serpentinization considered as a constant volume metasomatic process. *American Mineralogist*, **51**, 685-710.

Tikoff,B. and Teyssier,C., 1994. Strain modelling of displacement-field partitioning in transpressional orogens. *Journal of Structural Geology*, **16**, 1575-1588.

Thompson, G. and Melson, W.G., 1972. The petrology of oceanic crust across fracture zones in the Atlantic Ocean: Evidence of a new kind of seafloor spreading. *Journal of Geology*, **80**, 526-538.

Turner, W.M., 1971. The geology of Polis-Kathikas area, Cyprus. *Unpubl. Thesis , Univ. Albuquerque*, New Mexico.

Turner, W.M., 1973. The Cyprian Gravity Nappe and the Autochthonous Basement of Cyprus. In: *Gravity and Tectonics*. John Wiley & Sons, New York, 287-301.

Twiss, R.J. and Moores, E.M., 1992. Structural Geology. W.H. Freeman and Company, New York.

Urquhart, E. and Banner, F.T., 1994. Biostratigraphy of the supra-ophiolite sediments of the Troodos Massif, Cyprus: the Cretaceous Perapedhi, Kannayiou, Moni and Kathikas Formations. *Geological magazine*, **131**, 499-518.

Van Schalkwyk, J.F., de Wit, M.J., Roering, C. and van Reenen, D.D., 1993. Tectono-metamorphic evolution of the simatic basement of the Pietersburg greenstone belt relative to the Limpopo Orogeny: evidence from serpentinite. *Precambrian Research,* **61**, 67-88.

Vine, F.J. and Matthews, D.H., 1963. Magnetic anomalies over oceanic ridges. *Nature*, **199**, 947-949.

Vissers, R.L.M., Drury, M.R., Hoogerduijin Strating, E.H., Spiers, C.J. and van der Wal, D., 1995. Mantle shear zones and their effect on lithosphere strength during continental breakup. *Tectonophysics*, **249**, 155-171.

Weijermars, R., 1991. The role of stress in ductile deformation. *Journal of Structural Geology*, **13**, 1061-1078.

Wenner, D.B. and Taylor, H.P., 1969. δD and δO^{18} studies in serpentinization of ultramafic rocks [abs.]: Geol. Soc. America Abs. with Programmes, Atlantic City, 234-235.

Wenner, D.B. and Taylor, H.P., 1971. Temperatures of serpentinization of ultramafic rocks based on O^{18}/O^{16} fractionation between co-existing serpentine and magnetite, *Contributions to Mineralogy and Petrology*, **32**, 165-185.

Wenner, D.B. and Taylor, H.P., 1973. Oxygen and hydrogen isotope studies of the serpentinization of ultramafic rocks in oceanic environments and continental ophiolite complexes, *American Journal of Science*, **273**, 207-239.

Wenner, D.B. and Taylor, H.P., 1974. D/H and O^{18}/O^{16} studies of serpentinization of ultramafic rocks, *Geochemica Cosmochimica Acta*, **38**, 1255-1286.

Wheeler, J., 1993. Importance of Pressure Solution and Coble Creep in the Deformation of Polymineralic Rocks. *Journal of Geophysical Research*, **97**, 4579-4586.

White, S.H., Burrows, S.E., Carreras, J., Shaw, N.D., and Humphreys,F.J., 1980. On mylonites in ductile shear zones, *Journal of Structural Geology*, **1**, 175- 187.

Whitechurch, H. Juteau, T. and Montigny, R., 1984. Role of the Eastern Mediterranean ophiolites (Turkey, Syria, Cyprus) in the history of Neo-Tethys. *In*: Dixon, J.E. and Robertson, A.H.F. (eds), *The Geological Evolution of the Eastern Mediterranean*, Geological Society of London Special Publication, **17**, 301-317.

Whittaker, E.J.W. and Wicks, F.J., 1970. Chemical differences among the serpentine "polymorphs" - A discussion. *American Mineralogist,* **55**, 1025-1047.

Whittaker, E.J. and Zussman, J, 1956. The characterization of the serpentine minerals by X-ray diffraction, *Mineralogical Magazine*, **31**, 107-126.

Whittaker, E.J. and Zussman, J, 1971. The serpentine minerals, *in* Gard. J. A. (Ed), *The electron-optical investigation of clays*, Mineralogical Society, London, 159-191.

Wicks, F.J., 1969. X-ray and optical studies of serpentine minerals, *D.Phil. Dissertation*, Oxford University, Oxford, England.

Wicks, F.J., 1979. Mineralogy, chemistry and crystallography of chrysotile asbestos. *Min. Assoc. Canada, Short Course*, dB., **4**, 35-78.

Wicks, F.J. and Plant G., 1979. Electron microprobe and X-ray microbeam studies of serpentine textures. *Canadian Mineralogist*, **17**, 785-830.

Wicks, F.J. and Whittaker, E.J.W.,1975. A reappraisal of the structures of the serpentine minerals, *Canadian Mineralogist*, **13**, 227-243.

Wicks, F.J., Whittaker, E.J.W. and Zussman, J., 1977. An idealized model for serpentine textures after olivine. *Canadian Mineralogist*, **15**, 446-458.

Wicks, F.J. and Zussman, J., 1975. Microbeam X-ray diffraction patterns of the serpentine minerals. *Canadian Mineralogist*, **13**, 244-258.

Wintsch, R.P., Christofferson, R. and Kronenberg, A.K., 1995. Fluid-rock reaction weakening of fault zones. *Journal of Geophysical Research*, **100**, 13021-13032.

Williams, H., 1973. Bay of Islands map-area, Newfoundland. *Canada Geological Survey Paper*, **72-34**, pp7.

Williams, H.R., 1987. Stick-slip model for kink band formation in shear zones and faults. *Tectonophysics*, **140**, 327-331.

Williams, P.F., Goodwin, L.B., and Ralser, S., 1994. Ductile Deformation Processes. in, Hancock, P.L., ed., *Continental Deformation,* Pergamon Press, Oxford, 1-27.

Wilcock, W.S., Purdy, G.M. and Solomon, S.C., 1990. Microearthquake evidence for extension across the Kane transform fault. *Journal of Geophysical Research*, **95**, 15,439-15,462.

Woodcock, N.H. and Robertson, A.H.F., 1977. The origins of ophiolite related metamorphic rocks of the Tethys. *Geology*, **5**, 373-376

Wyllie, P.J., 1970, Magmas and volatile components. *American Mineralogist*, **64**, 469-500.

Zoback, M.D., Zoback, M.L., Mount, V.S., Suppe, J., Eaton, J.P., Healy, J.H., Oppenheimer, D., Reasenberg, P., Jones, L., Raleigh, C.B., Wong, I.G. Scotti, O. & Wentworth., 1987. New evidence on the state of stress on the San Andreas fault system. *Science*, **238**, 1105- 1111.

APPENDICES

APPENDIX 1: X-RAY DIFFRACTION (XRD) STUDIES

Quantitative XRD analyses of mineral mixtures are based on measurements of peak intensities (or peak height). The peak intensity of a mineral in a mixture is mainly dependant on concentration and the mass absorption coefficients of the mineral and mixture (Büttner and Saager, 1982). In this respect, the strongest peaks are used for quantitative XRD analyses.

Specimens for XRD analysis were prepared by adding acetone to a rock powder and the mixture ground into a slurry in an agate mortar, which was then smeared onto a glass slide. All analyses presented in this thesis were made on a Philips 3kw PW1130 X-ray generator/diffractometer under the following conditions:-

Radiation: CuKα at 45kv and 25 milliamps
Divergence slit: 1°
Receiving slit: 0.1°
Scatter slit: 1°

D-spacings were calculated and intensities estimated from the peak heights. Results were compared to charts in the *Mineral Powder Diffraction File - Data Book*, (published by the International Centre for Diffraction Data, 1601 Park Lane, Swarthmore, PA 19081, USA).

As stated previously, the serpentine 'polymorphs' are extremely diverse and complex, and one of the three main types (i.e. chrysotile) may be further subdivided (i.e. into ortho-, clino- and para-chrysotile) due to intricate crystallographic complexities. Also, as many minerals associated with serpentine and the different serpentine minerals themselves produce coincident peaks it is often troublesome identifying which types are present. However, as suggested by Büttner and Saager (1982) and by Prichard (1979) the presence or absence of certain peaks as well as their form are more indicative of the polytypes present than their relative positions (Figure 1).

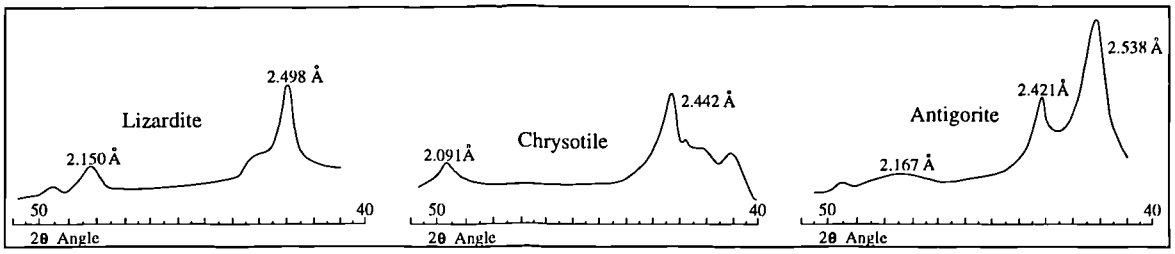

Figure 1. Characteristic X-ray diffractometer traces of the three main serpentine minerals (after Prichard, 1979).

APPENDIX 2:
ELECTRON MICROROBE ANALYSES OF CHROME SPINELS

Major and selected trace elements in spinels were analysed at the Electron Probe Unit, Edinburgh University, using a Camebax wavelength-dispersive electron microprobe. The probe was calibrated using natural and artificial standards. Peak count times of 30 seconds were used for all elements. The data was corrected using the PAP program and formulae were calculated assuming 32 oxygens.

Tables A1 and A2 display the data collected during two visits to Edinburgh in 1995 and 1996. The Cr# and Mg# values calculated are presented in Chapter 3.

	MG	AL	SI	NA	CR	V	CA	TI	MN	FE2+	FE3+	NI	ZN	TOTAL	Mg	Fe	Mg#	Mg#Av.	Cr	Al	Cr#	Cr#Av.
3131	10.085	20.021	0.045	0.039	45.835	0.296	0.001	0.077	0.327	19.433	4.059	0.019	0.243	100.480	6.051	15.11456	28.5889	27.61047	31.36079	10.59935	74.73947	75.02074
3132	9.446	19.097	0.047	0.020	45.065	0.290	0.021	0.077	0.349	19.544	4.081	0.062	0.280	98.379	5.6676	15.20089	27.15865		30.83395	10.11018	75.30738	
3133	9.536	19.951	0.047	0.023	46.219	0.280	0.046	0.063	0.327	20.443	3.887	0.046	0.189	101.057	5.7216	15.90011	26.46229		31.62353	10.56229	74.96245	
3134	10.033	20.208	0.041	0.016	47.093	0.278	0.010	0.078	0.327	19.675	2.771	0.067	0.132	100.730	6.0198	15.30278	28.23205		32.22153	10.69835	75.07366	
1941	16.681	36.868	0.013	0.019	21.226	0.135	0.006	0.055	0.151	8.543	5.146	0.101	0.227	89.170	10.0086	6.644556	60.10032	55.11184	14.52305	19.51835	42.66291	41.21708
1942	17.370	43.921	0.030	0.019	23.726	0.146	0.000	0.065	0.163	12.002	1.879	0.106	0.225	99.651	10.422	9.334889	52.75122		16.23358	23.25229	41.11237	
1943	17.593	43.362	0.041	0.004	23.701	0.143	0.020	0.072	0.145	11.370	2.190	0.111	0.198	98.947	10.5558	8.843333	54.41377		16.21647	22.95635	41.39725	
1944	17.402	43.216	0.000	0.023	23.666	0.144	0.011	0.093	0.177	11.568	2.124	0.093	0.200	98.717	10.4412	8.997333	53.71393		16.19253	22.87906	41.44323	
1945	17.684	43.577	0.019	0.007	23.954	0.127	0.018	0.073	0.190	11.452	2.225	0.115	0.217	99.657	10.6104	8.907111	54.36349		16.38958	23.07018	41.53492	
1946	17.876	44.864	0.043	0.026	22.336	0.127	0.008	0.083	0.154	11.134	1.843	0.098	0.182	98.773	10.7256	8.659778	55.3283		15.28253	23.75153	39.15178	
2691	12.360	18.942	0.039	0.011	44.508	0.231	0.006	0.065	0.241	13.808	3.506	0.036	0.128	93.879	7.416	10.73956	40.847	40.22016	30.45284	10.02812	75.22757	74.11529
2692	12.277	18.991	0.045	0.022	44.683	0.235	0.021	0.060	0 279	14.007	3.463	0.043	0.156	94.282	7.3662	10.89433	40.33946		30.57258	10.05406	75.25255	
2693	13.008	21.650	0.024	0.026	47.093	0.255	0.021	0.063	0 291	15.272	2.490	0.004	0.127	100.323	7.8048	11.87822	39.65245		32.22153	11.46176	73.76167	
2694	13.091	22.727	0.024	0.004	46.665	0.238	0.000	0.060	0.248	15.559	2.135	0.061	0.209	101.020	7.8546	12.10144	39.3595		31.92868	12.03194	72.63019	
2695	13.238	21.448	0.475	0.005	46.516	0.241	0.000	0.058	0.274	14.755	3.159	0.046	0.200	100.416	7.9428	11.47611	40.9024		31.82674	11.35482	73.70446	
4011	12.812	22.627	0.034	0.023	45.977	0.243	0.000	0.077	0.322	15.663	2.242	0.033	0.207	100.258	7.6872	12.18233	38.68838	31.37231	31.45795	11.979	72.4221	72.95331
4012	11.778	23.265	0.036	0.000	45.369	0.249	0.007	0.075	0.312	17.410	1.652	0.043	0.249	100.445	7.0668	13.54111	34.29169		31.04195	12.31676	71.59333	
4013	7.803	19.541	0.167	0.028	44.986	0.291	0.021	0.065	0.470	22.459	3.759	0.022	0.503	100.115	4.6818	17.46811	21.13688		30.77989	10.34524	74.84449	
2671	12.696	21.402	0.030	0.027	48.321	0.287	0.017	0.068	0.276	15.755	1.373	0.053	0.214	100.521	7.6176	12.25389	38.33432	38.92508	33.06174	11.33047	74.47644	74.76888
2672	12.845	21.640	0.051	0.000	48.239	0.272	0.008	0.052	0.306	15.697	1.681	0.050	0.185	101.028	7.707	12.20878	38.69796		33.00563	11.45647	74.23318	
2673	13.000	20.701	0.032	0.011	49.620	0.259	0.003	0.060	0.288	15.205	1.144	0.060	0.215	100.598	7.8	11.82611	39.74297		33.95053	10.95935	75.59701	
2881	13.063	24.295	0.032	0.011	43.342	0.247	0.013	0.067	0.284	15.740	3.516	0.055	0.197	100.860	7.8378	12.24222	39.03283	38.3574	29.65505	12.86206	69.74851	68.89632
2882	12.875	25.126	0.043	0.028	42.902	0.237	0.000	0.062	0.265	16.107	2.728	0.052	0.271	100.696	7.725	12.52767	38.14313		29.354	13.302	68.81564	
2883	12.865	25.703	0.024	0.023	42.505	0.246	0.004	0.058	0.243	16.264	2.514	0.050	0.279	100.777	7.719	12.64978	37.89624		29.08237	13.60747	68.1248	
ZYCT-111	16.700	36.973	0.036	0.016	31.145	0.166	0.015	0.048	0.167	12.146	2.708	0.092	0.136	100.349	10.02	9.446889	51.47202	49.72789	21.30974	19.57394	52.12285	53.26229
ZYCT112	15.752	35.779	0.039	0.008	31.665	0.178	0.007	0.040	0.221	13.186	2.740	0.074	0.194	99.883	9.4512	10.25578	47.95865		21.66553	18.94182	53.35371	
ZYCT113	16.029	34.827	0.000	0.016	32.032	0.169	0.000	0.045	0.201	12.488	3.328	0.078	0.168	99.380	9.6174	9.712889	49.75301		21.91663	18.43782	54.31031	
T1951	12.940	26.043	0.034	0.018	41.506	0.249	0.018	0.062	0.249	16.216	3.223	0.045	0.199	100.801	7.764	12.61244	38.10282	37.71014	28.39884	13.78747	67.31767	66.92224
T1952	12.671	26.064	0.030	0.016	41.035	0.271	0.010	0.085	0.269	16.545	3.302	0.074	0.192	100.563	7.6026	12.86833	37.13851		28.07658	13.79859	67.04828	
T1953	12.869	26.526	0.032	0.019	40.562	0.272	0.000	0.077	0.279	16.274	3.311	0.046	0.183	100.450	7.7214	12.65756	37.88909		27.75295	14.04318	66.40077	
MM33941	14.485	19.932	0.043	0.001	49.504	0.257	0.001	0.052	0.222	13.058	3.471	0.123	0.085	101.235	8.691	10.15622	46.1129	45.54067	33.87116	10.55224	76.24622	76.2082
MM33942	14.522	20.095	0.053	0.022	49.169	0.259	0.011	0.083	0.221	13.036	3.535	0.038	0.068	101.113	8.7132	10.13911	46.21821		33.64195	10.63853	75.97467	
MM33943	14.008	19.777	0.049	0.000	49.549	0.243	0.000	0.077	0.243	13.592	2.909	0.059	0.067	100.572	8.4048	10.57156	44.29091		33.90195	10.47018	76.40371	
M21	12.371	25.423	0.056	0.027	43.228	0.227	0.003	0.057	0.293	16.757	1.451	0.038	0.139	100.069	7.4226	13.03322	36.286	37.93959	29.57705	13.45924	68.72585	69.39898
M22	11.867	25.646	0.047	0.019	42.429	0.268	0.011	0.050	0.306	17.453	1.548	0.060	0.269	99.973	7.1202	13.57456	34.40582		29.03037	13.57729	68.13415	
M23	13.749	23.469	0.071	0.016	45.195	0.250	0.013	0.048	0.245	13.987	1.672	0.038	0.092	98.846	8.2494	10.87878	43.12695		30.92289	12.42476	71.33694	
35-941	13.777	20.754	0.047	0.000	48.960	0.290	0.010	0.060	0.285	14.151	2.488	0.043	0.119	100.985	8.2662	11.00633	42.89109	42.32533	33.49895	10.98741	75.30162	74.93717
35-942	13.570	21.175	0.041	0.039	48.059	0.285	0.015	0.078	0.256	14.426	2.424	0.055	0.141	100.565	8.142	11.22022	42.05096		32.88247	11.21029	74.57566	
35-943	13.600	21.003	0.030	0.020	48.583	0.300	0.010	0.062	0.232	14.468	2.370	0.053	0.139	100.872	8.16	11.25289	42.03393		33.241	11.11924	74.93423	
ZYC91	12.053	16.463	0.051	0.004	53.068	0.305	0.007	0.068	0.270	16.086	2.293	0.042	0.121	100.830	7.2318	12.51133	36.62944	36.28102	36.30968	8.715706	80.64269	80.22347
ZYC92	11.933	16.973	0.045	0.005	52.628	0.307	0.010	0.048	0.276	16.411	2.300	0.060	0.123	101.121	7.1598	12.76411	35.93572		36.00863	8.985706	80.02925	
ZYC93	11.977	16.901	0.024	0.008	52.304	0.282	0.008	0.050	0.285	16.229	2.535	0.055	0.117	100.776	7.1862	12.62256	36.2779		35.78695	8.947588	79.99848	
MD4-1	18.645	49.977	0.047	0.000	17.095	0.119	0.004	0.090	0.161	10.924	1.913	0.093	0.149	99.218	11.187	8.496444	56.83456	57.82361	11.69658	26.45841	30.65544	28 83343
MD4-2	19.408	53.136	0.036	0.036	14.002	0.093	0.011	0.073	0.127	10.367	1.986	0.141	0.159	99.576	11.6448	8.063222	59.0866		9.580316	28.13082	25.40447	
MD4-3	18.811	50.052	0.026	0.003	16.948	0.093	0.001	0.097	0.139	10.704	2.041	0.135	0.166	99.216	11.2866	8.325333	57.54966		11.596	26.49812	30.4404	
MV8-1	18.471	51.630	0.017	0.016	14.774	0.128	0.011	0.052	0.148	11.338	2.118	0.125	0.203	99.032	11.0826	8.818444	55.68853	55.11274	10.10853	27.33353	26.99779	27 62778
MV8-2	18.407	50.820	0.120	0.012	16.057	0.124	0.000	0.063	0.129	11.570	2.207	0.118	0.224	99.850	11.0442	8.998889	55.10229		10.98637	26.90471	28 99461	
MV8-3	18.206	50.893	0.036	0.008	15.094	0.135	0.010	0.038	0.146	11.497	2.285	0.159	0.244	98.752	10.9236	8.942111	54.98721		10.32747	26 94335	27.70927	
MV8-4	18.175	51.146	0.030	0.009	14.496	0.124	0.000	0.062	0.155	11.624	2.602	0.139	0.284	98.845	10.905	9.040889	54.67292		9.918316	27 07729	26 80944	
MTH6-1	13.301	22.780	0.056	0.000	45.651	0.259	0.015	0.048	0.261	14.950	2.674	0.062	0.116	100.173	7.9806	11.62778	40.69995	40.6693	31.23489	12 06	72 14452	72 36473
MTH6-2	13.441	22.447	0.041	0.000	46.466	0.287	0.000	0.062	0.261	14.976	2.894	0.066	0.118	101.059	8 0646	11.648	40.91089		31.79253	11.88371	72 79137	

Table A1 Spinel data 1995 analyses

MTH6-3	13.366	22.902	0.032	0.009	45.927	0.266	0.007	0.050	0.258	15.213	3.020	0.057	0.163	101.271	8.0196	11.83233	40.39707		31.42374	12.12459	72.15831	
L2-1	17.956	47.675	0.024	0.047	18.447	0.160	0.004	0.063	0.168	11.350	2.433	0.097	0.197	98.620	10.7736	8.827778	54.96348	53.30764	12.62163	25.23971	33.33647	30.88045
L2-2	19.955	54.330	0.024	0.013	15.674	0.154	0.017	0.050	0.121	11.000	2.016	0.144	0.161	103.659	11.973	8.555556	58.32364		10.72432	28.76294	27.15893	
L2-3	11.111	43.449	0.385	0.019	16.047	0.147	0.057	0.047	0.168	11.765	0.000	0.092	0.162	83.448	6.6666	9.150556	42.14791		10.97953	23.00241	32.30989	
L2-4	18.481	49.404	0.047	0.012	17.744	0.169	0.007	0.052	0.142	11.353	2.542	0.137	0.161	100.252	11.0886	8.830111	55.66926		12.14063	26.15506	31.70234	
L2-5	18.267	49.820	0.017	0.001	16.438	0.168	0.003	0.048	0.137	11.329	2.362	0.143	0.144	98.878	10.9602	8.811444	55.43393		11.24705	26.37529	29.89461	
NK14-1	18.097	47.392	0.036	0.034	18.726	0.140	0.017	0.090	0.120	11.168	2.523	0.111	0.177	98.629	10.8582	8.686222	55.55652	56.50555	12.81253	25.08988	33.80399	31.03822
NK14-2	18.577	48.571	0.028	0.023	17.625	0.147	0.004	0.065	0.163	10.747	2.998	0.099	0.184	99.231	11.1462	8.358778	57.14541		12.05921	25.71406	31.92525	
NK14-3	18.780	51.585	0.041	0.042	15.053	0.134	0.003	0.065	0.148	11.012	2.339	0.122	0.178	99.502	11.268	8.564889	56.81472		10.29942	27.30971	27.38543	
AK27-1	18.944	41.204	0.188	0.035	32.603	0.179	0.021	0.085	0.209	11.760	2.527	0.048	0.193	107.998	11.3664	9.146667	55.41054	47.27591	22.30732	21.81388	50.55918	57.18167
AK27-2	12.088	26.381	0.205	0.050	35.982	0.197	0.007	0.128	0.225	14.499	0.982	0.043	0.198	90.986	7.2528	11.277	39.14128		24.61926	13.96641	63.80415	
AK24-1	18.821	50.432	0.039	0.019	15.667	0.087	0.007	0.070	0.147	10.425	2.336	0.109	0.185	98.344	11.2926	8.108333	58.20648	55.93284	10.71953	26.69929	28.64742	28.86571
AK24-2	18.367	50.988	0.043	0.022	15.013	0.125	0.000	0.063	0.155	11.305	2.354	0.141	0.198	98.774	11.0202	8.792778	55.62112		10.27205	26.99365	27.56436	
AK24-3	17.934	49.374	0.026	0.008	16.675	0.100	0.013	0.070	0.152	11.799	2.485	0.149	0.230	99.015	10.7604	9.177	53.97093		11.40921	26.13918	30.38535	
S11-1	11.075	15.709	0.030	0.031	54.350	0.265	0.003	0.128	0.303	17.633	1.527	0.039	0.169	101.263	6.645	13.71456	32.63824	32.35739	37.18684	8.316529	81.72327	81.83175
S11-2	10.885	15.382	0.024	0.005	54.001	0.274	0.010	0.102	0.285	17.781	2.051	0.043	0.123	100.967	6.531	13.82967	32.07655		36.94805	8.143412	81.94024	
S11-3	11.045	15.970	0.043	0.022	53.824	0.288	0.007	0.120	0.333	17.658	1.708	0.032	0.172	101.221	6.627	13.734	32.54752		36.82695	8.454706	81.32863	
M5-1	17.850	50.177	0.021	0.004	13.942	0.104	0.011	0.033	0.145	12.119	4.606	0.145	0.336	99.494	10.71	9.425889	53.18861	52.47547	9.539263	26.56429	26.42195	28.00758
M5-2	17.339	48.293	0.017	0.000	15.706	0.106	0.018	0.038	0 186	12.465	4.522	0.122	0.296	99.109	10.4034	9.695	51.76233		10.74621	25.56688	29.59321	
M5-3	17.029	46.937	0.015	0.044	16.481	0.102	0.000	0.038	0.190	12.711	5.159	0.145	0.320	99.171	10.2174	9.886333	50.8234		11.27647	24.849	31.21474	
AV16-1	17.483	47.653	0.021	0.000	16.789	0.134	0.010	0.045	0.163	12.159	4.198	0.121	0.222	98.997	10.4898	9.457	52.58889	52.79281	11.48721	25.22806	31.28728	30.93878
AV16-2	17.599	48.025	0.041	0.000	16.377	0.124	0.013	0.047	0.174	12.041	4.265	0.102	0.195	99.001	10.5594	9.365222	52.99674		11.20532	25.425	30.59028	
AV16-3	17.989	49.348	0.032	0.020	14.356	0.118	0.007	0.040	0.146	11.625	4.899	0.121	0.228	98.927	10.7934	9.041667	54.41575		9.822526	26.12541	27.32431	

Table A1 Spinel data 1995 analyses

	MG	CA	V	FE	AL	TI	MN	CO	SI	CR	NI	ZN	CR"	AL"	MG"	FE"	CR#	CR#AV.	MG#	MG#AV.
1 NK13I	13.867	0.023	0.233	17.808	22.016	0.065	0.241	0.066	0.033	46.089	0.164	0.11	31.53458	11.65553	8.3202	12.4656	73.01343	72.5759	40.02829	41.10172
2 NKI3II	14.188	0.013	0.226	17.134	22.414	0.054	0.21	0.053	0.068	45.833	0.151	0.117	31.35942	11.86624	8.5128	11.9938	72.54817		41.51249	
3 NK13III	14.253	0.003	0.241	17.035	22.773	0.065	0.22	0.059	0.032	45.686	0.137	0.108	31.25884	12.05629	8.5518	11.9245	72.16609		41.76438	
4 MTH14I	13.929	0.011	0.252	16.474	21.373	0.049	0.236	0.068	0.05	47.979	0.139	0.123	32.82774	11.31512	8.3574	11.5318	74.36705	73.48434	42.01979	39.52131
5 MTH14II	13.505	0.003	0.263	16.735	20.935	0.044	0.291	0.089	0.065	48.713	0.12	0.141	33.32995	11.08324	8.103	11.7145	75.04517		40.8881	
6 MTH14III	12.303	0.037	0.277	19.03	23.421	0.038	0.264	0.089	0.065	44.456	0.101	0.232	30.41726	12.39935	7.3818	13.321	71.04079		35.65605	
7 MMKK94I	14.532	0.006	0.258	17.349	27.477	0.081	0.219	0.047	0.054	39.746	0.156	0.128	27.19463	14.54665	8.7192	12.1443	65.15045	67.70995	41.79165	34.84359
8 MMKK94II	13.729	0.009	0.262	18.073	27.776	0.102	0.239	0.069	0.054	39.587	0.142	0.157	27.08584	14.70494	8.2374	12.6511	64.81296		39.4351	
9 MMKK94III	10.63	0.011	0.295	22.406	23.394	0.125	0.323	0.093	0.055	43.056	0.132	0.31	29.45937	12.38506	6.378	15.6842	70.40213		28.90917	
10 MMKK94IV	10.75	0	0.303	22.3	23.305	0.095	0.33	0.092	0.032	43.041	0.097	0.253	29.44911	12.33794	6.45	15.61	70.47424		29.23844	
11 MTH5I	16.465	0	0.155	14.513	36.611	0.075	0.194	0.073	0.04	31.636	0.166	0.165	21.64568	19.38229	9.879	10.1591	52.75835	48.70735	49.30108	49.81216
12 MTH5II	16.176	0.015	0.169	14.97	38.729	0.06	0.189	0.075	0.04	28.84	0.199	0.312	19.73263	20.50359	9.7056	10.479	49.04196		48.08418	
13 MTH5III	16.585	0.014	0.17	14.275	36.362	0.087	0.194	0.065	0.02	31.986	0.193	0.162	21.88516	19.25047	9.951	9.9925	53.20244		49.89596	
14 MTH5IV	17.222	0	0.163	13.644	44.134	0.051	0.151	0.091	0.042	22.602	0.194	0.291	15.46453	23.36506	10.3332	9.5508	39.82666		51.96741	
15 MM3094I	11.309	0.021	0.234	20.934	13.798	0.184	0.302	0.063	0.042	53.542	0.09	0.095	36.634	7.304824	6.7854	14.6538	83.37501	83.54327	31.6495	32.2834
16 MM3094II	11.629	0.018	0.232	20.367	13.943	0.199	0.308	0.08	0.05	53.656	0.089	0.081	36.712	7.381588	6.9774	14.2569	83.25927		32.8591	
17 MM3094III	11.568	0.016	0.234	20.743	13.341	0.166	0.342	0.093	0.054	54.176	0.091	0.122	37.06779	7.062882	6.9408	14.5201	83.99552		32.34161	
18 PP11I	17.478	0.008	0.127	13.641	41.73	0.087	0.177	0.08	0.007	26.132	0.275	0.152	17.87979	22.09235	10.4868	9.5487	44.73063	42.85706	52.34109	52.70783
19 PP11II	17.64	0.004	0.13	13.552	43.359	0.08	0.173	0.088	0.027	24.297	0.295	0.163	16.62426	22.95476	10.584	9.4864	42.00271		52.73438	
20 PP11III	17.729	0.011	0.111	13.45	43.217	0.077	0.129	0.056	0.039	24.054	0.298	0.186	16.458	22.87959	10.6374	9.415	41.83785		53.04801	
21 MMPP94I	14.155	0.008	0.229	15.742	20.153	0.062	0.199	0.059	0.069	49.832	0.143	0.065	34.09558	10.66924	8.493	11.0194	76.16602	86.08334	43.52617	27.69869
22 MMPP94II	4.085	0.034	0.396	33.614	3.536	0.139	1.204	0.203	0.138	57.338	0.078	0.175	39.23126	1.872	2.451	23.5298	95.44562		9.43389	
23 MMPP94III	6.439	0.01	0.445	31.167	3.267	0.12	0.428	0.073	0.08	57.907	0.088	0.051	39.62058	1.729588	3.8634	21.8169	95.81722		15.04422	
24 MMPPIV	14.078	0.02	0.233	16.133	19.487	0.068	0.213	0.075	0.077	50.208	0.151	0.091	34.35284	10.31665	8.4468	11.2931	76.90449		42.79049	
25 AK10IIA	12.473	0.006	0.271	18.119	22.31	0.049	0.294	0.07	0.044	46.948	0.11	0.209	32.12232	11.81118	7.4838	12.6833	73.11578	72.51852	37.10895	37.25195
26 AK10IIB	12.778	0.011	0.283	18.001	23.288	0.047	0.306	0.098	0.015	45.596	0.053	0.267	31.19726	12.32894	7.6668	12.6007	71.67467		37.82805	
27 AK10IIC	12.456	0.006	0.271	18.321	22.47	0.044	0.291	0.105	0.018	46.452	0.093	0.171	31.78295	11.89588	7.4736	12.8247	72.76511		36.81885	
28 AV1095I	14.917	0	0.187	18.598	34.883	0.021	0.21	0.095	0.007	30.51	0.22	0.22	20.87526	18.46747	8.9502	13.0186	53.06002	55.24102	40.7405	39.82824
29 AV1095II	14.5	0.015	0.205	18.83	33.857	0.041	0.239	0.097	0.03	31.874	0.168	0.223	21.80853	17.92429	8.7	13.181	54.88794		39.76052	
30 AV1095III	14.19	0.001	0.207	19.037	32.006	0.015	0.265	0.107	0.025	33.885	0.164	0.218	23.18447	16.94435	8.514	13.3259	57.77511		38.98369	
31 L4I	18.469	0.008	0.124	14.154	48.841	0.055	0.115	0.074	0.054	17.73	0.317	0.16	12.13105	25.857	11.0814	9.9078	31.93386	34.41402	52.79572	52.21659
32 L4II	18.07	0.006	0.138	13.831	47.526	0.073	0.179	0.079	0.043	19.133	0.308	0.176	13.091	25.16082	10.842	9.6817	34.22321		52.82673	
33 L4III	17.737	0.006	0.116	14.25	46.211	0.064	0.148	0.06	0.026	20.422	0.254	0.173	13.97295	24.46465	10.6422	9.975	36.35229		51.61807	
34 L4IV	17.872	0.017	0.152	14.354	46.641	0.089	0.148	0.055	0.048	19.558	0.319	0.176	13.38179	24.69229	10.7232	10.0478	35.14671		51.62582	
35 ANDRADITE	0.074	32.062	0.006	27.251	1.667	0.08	0.425	0.034	35.015	0.048	0.009	0.006	0.032842	0.882529	0.0444	19.0757	3.587844		0.232216	
36 NK9I	18.351	0.016	0.123	14.402	49.893	0.048	0.157	0.063	0.034	15.919	0.302	0.177	10.89195	26.41394	11.0106	10.0814	29.19632	29.27754	52.20273	52.52679
37 NK9II	18.597	0.02	0.139	14.174	50.021	0.047	0.148	0.087	0.025	15.973	0.313	0.192	10.92889	26.48171	11.1582	9.9218	29.21336		52.93264	
38 NK9III	18.395	0.003	0.132	14.297	49.713	0.056	0.136	0.088	0.013	16.036	0.351	0.216	10.972	26.31865	11.037	10.0079	29.42293		52.44501	
39 NK5I	16.204	0.016	0.179	15.229	37.266	0.058	0.214	0.07	0.036	30.185	0.206	0.149	20.65289	19.72906	9.7224	10.6603	51.14387	48.3822	47.69927	48.07335
40 NK5II	16.865	0	0.149	14.923	41.513	0.05	0.162	0.093	0.022	25.25	0.226	0.137	17.27632	21.97747	10.119	10.4461	44.01185		49.20472	
41 NK5III	16.327	0.005	0.16	15.488	38.388	0.057	0.164	0.075	0.014	29.418	0.234	0.181	20.12811	20.32306	9.7962	10.8416	49.75903		47.46727	
42 NK5IV	16.417	0.024	0.161	15.292	39.01	0.036	0.156	0.077	0.043	28.556	0.217	0.168	19.53832	20.65235	9.8502	10.7044	48.61406		47.92212	
43 NK19I	17.321	0.002	0.145	13.555	41.976	0.06	0.173	0.078	0.012	26.034	0.267	0.149	17.81274	22.22259	10.3926	9.4885	44.49255	43.14073	52.27377	52.10695
44 NK19II	17.366	0.017	0.127	13.766	42.619	0.061	0.177	0.087	0.017	24.441	0.22	0.203	16.72279	22.563	10.4196	9.6362	42.56702		51.95305	
45 NK19III	17.354	0.018	0.13	13.679	43.072	0.082	0.179	0.096	0.038	24.495	0.257	0.208	16.75974	22.80282	10.4124	9.5753	42.36262		52.09404	
46 NK17I	18.762	0.002	0.126	13.189	50.817	0.057	0.135	0.062	0.022	15.785	0.34	0.208	10.80026	26.90312	11.2572	9.2323	28.64534	29.92327	54.94131	54.00198
47 NK17II	18.253	0.007	0.132	13.887	48.82	0.07	0.143	0.062	0.038	17.451	0.284	0.136	11.94016	25.84588	10.9518	9.7209	31.59939		52.97711	
48 NK17III	18.597	0.007	0.151	13.531	49.713	0.058	0.103	0.095	0.022	16.115	0.344	0.208	11.02605	26.31865	11.1582	9.4717	29.52508		54.08751	
49 AK16I	10.91	0	0.235	21.125	16.108	0.257	0.287	0.101	0.041	52.122	0.077	0.156	35.66242	8.527765	6.546	14.7875	80.70213	80.54465	30.68414	30.35387
50 AK16II	11.168	0.01	0.229	20.981	15.991	0.253	0.339	0.073	0.031	51.662	0.095	0.122	35.34768	8.465824	6.7008	14.6867	80.67759		31.33045	
51 AK16III	10.38	0.017	0.243	21.733	16.419	0.249	0.326	0.079	0.032	51.635	0.095	0.128	35.32921	8.692412	6.228	15.2131	80.25422		29.04702	
52 AK13I	10.071	0.008	0.268	23.448	20.101	0.202	0.352	0.137	0.063	45.865	0.106	0.241	31.38132	10.64171	6.0426	16.4136	74.67649	76.37214	26.90838	28.05223
53 AK13II	10.475	0.02	0.246	22.331	17.443	0.2	0.335	0.089	0.045	49.53	0.077	0.166	33.88895	9.234529	6.285	15.6317	78.58584		28.67676	
54 AK13III	10.522	0.02	0.24	22.547	19.413	0.219	0.306	0.059	0.05	47.188	0.101	0.216	32.28653	10.27747	6.3132	15.7829	75.85408		28.57156	

Table A2 Spinel data 1996 analyses

55	MV1I	16.768	0.008	0.119	14.845	41.043	0.09	0.195	0.087	0.086	26	0.215	0.184	17.78947	21.72865	10.0608	10.3915	45.01599	44.39608	49.19153	48.48111
56	MV1II	16.484	0.015	0.115	15.663	42.186	0.097	0.163	0.098	0.016	24.73	0.231	0.272	16.92053	22.33376	9.8904	10.9641	43.10491		47.42574	
57	MV1III	16.519	0.014	0.107	14.84	41.032	0.089	0.173	0.07	0.015	26.047	0.234	0.234	17.82163	21.72282	9.9114	10.388	45.06733		48.82607	
58	M7AI	18.968	0.009	0.125	14.028	54.625	0.034	0.126	0.103	0.027	10.912	0.385	0.191	7.466105	28.91912	11.3808	9.8196	20.51961	24.75619	53.68201	49.98089
59	M7AII	17.019	0.007	0.107	16.933	49.109	0.047	0.168	0.071	0.04	15.515	0.281	0.199	10.61553	25.99888	10.2114	11.8531	28.99276		46.27977	
60	M7BIII	16.941	0.033	0.123	16.903	47.387	0.056	0.141	0.092	0.036	17.045	0.329	0.22	11.66237	25.08724	10.1646	11.8321	31.73468	26.43336	46.20966	49.15589
61	M7BIV	18.257	0	0.103	15.301	51.729	0.064	0.168	0.054	0.029	12.651	0.395	0.177	8.655947	27.38594	10.9542	10.7107	24.01635		50.56197	
62	M7BIV2	18.318	0	0.119	15.27	52.287	0.038	0.145	0.064	0.022	12.462	0.357	0.196	8.526632	27.68135	10.9908	10.689	23.54904		50.69604	
63	M7CV	17.671	0.013	0.081	15.965	50.004	0.034	0.137	0.096	0.04	13.966	0.293	0.248	9.555684	26.47271	10.6026	11.1755	26.52265	31.75238	48.68469	47.12855
64	M7CVI	16.797	0.008	0.118	17.195	45.241	0.085	0.199	0.106	0.035	20.543	0.249	0.269	14.05574	23.95112	10.0782	12.0365	36.98211		45.5724	
65	494I	8.351	0.011	0.18	22.474	9.442	0.116	0.436	0.104	0.038	60.213	0.067	0.193	41.19837	4.998706	5.0106	15.7318	89.17961	89.18834	24.15632	23.71244
66	494II	7.69	0.022	0.21	23.189	9.369	0.118	0.407	0.118	0.034	60.105	0.056	0.333	41.12447	4.960059	4.614	16.2323	89.23704		22.13342	
67	494III	8.566	0.012	0.179	22.207	9.482	0.111	0.434	0.13	0.034	60.273	0.051	0.192	41.23942	5.019882	5.1396	15.5449	89.14838		24.84759	
68	BOB9I	16.121	0.004	0.167	15.537	39.669	0.075	0.166	0.079	0.016	27.443	0.188	0.195	18.77679	21.00124	9.6726	10.8759	47.20393	44.60198	47.07205	47.76624
69	BOB9II	16.344	0.024	0.174	15.998	41.363	0.068	0.177	0.069	0.021	25.736	0.236	0.244	17.60884	21.89806	9.8064	11.1986	44.57156		46.68603	
70	BOB9III	16.887	0	0.144	14.743	42.971	0.055	0.151	0.051	0.025	24.107	0.174	0.19	16.49426	22.74935	10.1322	10.3201	42.03044		49.54064	
71	CHROMITITE894I	9.677	0.006	0.181	21.091	7.815	0.138	0.341	0.058	0.042	62.183	0.07	0.062	42.54626	4.137353	5.8062	14.7637	91.13746	91.0094	28.22668	30.24824
72	CHROMITITE894II	11.209	0.006	0.172	18.679	8.087	0.137	0.266	0.032	0.032	62.549	0.094	0.059	42.79668	4.281353	6.7254	13.0753	90.90584		33.96547	
73	CHROMITITE894III	9.811	0	0.157	21.043	7.979	0.136	0.339	0.057	0.047	62.309	0.057	0.087	42.63247	4.224176	5.8866	14.7301	90.98489		28.55258	

Table A2 Spinel data 1996 analyses

APPENDIX 3; FLOW LAWS USED FOR OLIVINE

Power law equations used to constrain temperatures in Table 4.2 are in the form (Chopra and Paterson, 1984):-

$$\varepsilon = A\,\sigma^{n}\,e^{-Q/RT}$$

Where ε is the strain rate, A (s^{-1} MPa^{-n}) is a pre exponential factor, σ (MPa) is differential stress, n is the stress exponent, Q (kJ mol^{-1}) is the apparent activation energy, R is the gas constant (8314.5 kJ mol^{-1} $°C^{-1}$), and T is the absolute temperature (°K). Errors are quoted as ± 2 standard deviations (i.e. 95% confidence limits).

Flow law for dry Aheim dunite:-

$$\varepsilon = 10^{4.46\pm0.18}\,\sigma^{3.60\pm0.22}\exp\frac{-(535\pm33\text{kJ mol}^{-1})}{RT}$$

Flow law for wet Aheim dunite:-

$$\varepsilon = 10^{2.62\pm0.18}\,\sigma^{4.48\pm0.31}\exp\frac{-(498\pm38\text{kJ mol}^{-1})}{RT}$$

Flow law used for both dislocation and diffusion creep regimes used to constrain temperatures in Table 4.3 (Karato *et al.* 1986; Jaroslow *et al.* 1996):-

$$\varepsilon = A\exp(-Q/(RT))\,\sigma^{n}d^{m}$$

Where ε is strain rate, A is an empirical constant, Q is the activation energy for flow, R is the gas constant, T is the absolute temperature, is the flow stress and d is grain size. Parameters for olivine flow laws are as follows:-

	Dislocation creep	Diffusion Creep
A (s^{-1} MPa^{-n} $(\mu m)^{-m}$)	2.4×10^{5}	1.8×10^{7}
Q (kJ mol^{-1})	540	315 ± 35
n	3.5	1
m	0	-3

Parameters for dislocation creep are taken from Chopra and Patterson (1984). Parameters for diffusion creep are taken from Hirth and Kohlstedt (1995a).

KEY

SYMBOLS			
	Foliation		Extensional cont act
	Synform axis		Solid contact
	Antiform axis		Inferred contact
	Thrust contact		Limit of outcrop
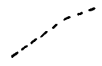	Road		Fault plane lineation (slickenline)

LITHOLOGIES			
Ca	Quaternary to recent deposits	Kf	Kathikas Formation
S	Serpentinite	W	Wherlite & Clinopyroxenite
Tc	Troodos Complex	K	Kannaviou Formation
Dz	Dhiarizos Group (undifferentiated)	Mv	Mavrokolymbos Format on
Ph	Phasoula Formation Lavas	Kh	Kholetria Member
Vl	Vlambouros Formation	Av	Ayia Varvara Formation
G	Gabbro		